frontiers
RESEARCH TOPICS

REBUILDING CEREBELLAR NETWORK COMPUTATIONS FROM CELLULAR NEUROPHYSIOLOGY

Hosted by
Egidio D'Angelo

frontiers in
CELLULAR NEUROSCIENCE

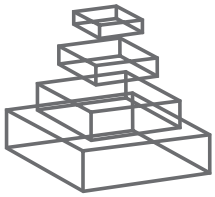

frontiers

Cover image provided by Ibbl sarl, Lausanne CH

ISSN 1664-8714
ISBN 978-2-88919-075-1
DOI 10.3389/978-2-88919-075-1

ABOUT FRONTIERS

Frontiers is more than just an open-access publisher of scholarly articles: it is a pioneering approach to the world of academia, radically improving the way scholarly research is managed. The grand vision of Frontiers is a world where all people have an equal opportunity to seek, share and generate knowledge. Frontiers provides immediate and permanent online open access to all its publications, but this alone is not enough to realize our grand goals.

FRONTIERS JOURNAL SERIES

The Frontiers Journal Series is a multi-tier and interdisciplinary set of open-access, online journals, promising a paradigm shift from the current review, selection and dissemination processes in academic publishing.
All Frontiers journals are driven by researchers for researchers; therefore, they constitute a service to the scholarly community. At the same time, the Frontiers Journal Series operates on a revolutionary invention, the tiered publishing system, initially addressing specific communities of scholars, and gradually climbing up to broader public understanding, thus serving the interests of the lay society, too.

DEDICATION TO QUALITY

Each Frontiers article is a landmark of the highest quality, thanks to genuinely collaborative interactions between authors and review editors, who include some of the world's best academicians. Research must be certified by peers before entering a stream of knowledge that may eventually reach the public - and shape society; therefore, Frontiers only applies the most rigorous and unbiased reviews.
Frontiers revolutionizes research publishing by freely delivering the most outstanding research, evaluated with no bias from both the academic and social point of view.
By applying the most advanced information technologies, Frontiers is catapulting scholarly publishing into a new generation.

WHAT ARE FRONTIERS RESEARCH TOPICS?

Frontiers Research Topics are very popular trademarks of the Frontiers Journals Series: they are collections of at least ten articles, all centered on a particular subject. With their unique mix of varied contributions from Original Research to Review Articles, Frontiers Research Topics unify the most influential researchers, the latest key findings and historical advances in a hot research area!
Find out more on how to host your own Frontiers Research Topic or contribute to one as an author by contacting the Frontiers Editorial Office: researchtopics@frontiersin.org

REBUILDING CEREBELLAR NETWORK COMPUTATIONS FROM CELLULAR NEUROPHYSIOLOGY

Hosted By:
Egidio D'Angelo, University of Pavia, Italy

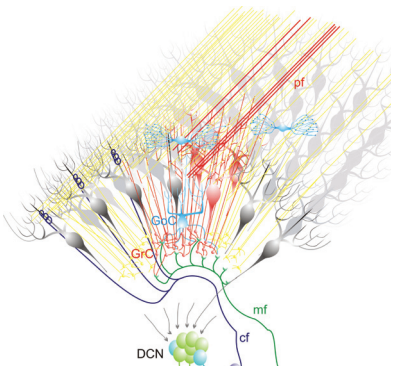

Taken from D'Angelo E (2010). Rebuilding cerebellar network computations from cellular neurophysiology. *Front. Cell. Neurosci.* 4:131. doi: 10.3389/fncel.2010.00131

This Research Topic is centered around the attempt to understand network activity of the brain by combining experimental and modeling techniques. A surprisingly rich set of new observations is emerging about the functions of the olivo-cerebellar cortical modules. This Research Topic will consider the critical elements of new emerging knowledge achieved using *in vitro* and *in vivo* techniques and the computational attempts at functional circuit reconstruction.

Table of Contents

frontiers in
CELLULAR NEUROSCIENCE

EDITORIAL ARTICLE
published: 04 November 2010
doi: 10.3389/fncel.2010.00131

Rebuilding cerebellar network computations from cellular neurophysiology

Egidio D'Angelo*

Department of Physiology, University of Pavia, Pavia, Italy
**Correspondence: dangelo@unipv.it*

This schematic drawing shows the most relevant connections within a cerebellar module. The mossy fibers contact granule cells (GrC) and deep cerebellar nuclei (DCN) cells which, in turn, receive inhibition from the same common set of Purkinje cells (PC). Moreover, the interior olive (IO) cells emit climbing fibers that contact DCN cells and Purkinje cells (PC), which also project to the same DCN cells. An activate group of GrCs is in (red), while others (yellow) are laterally inhibited by the GoCs. The active GrCs excite the overlaying PCs (dark red) according to a vertical organization pattern (Bower and Woolston, 1983). The PCs inhibit DCN neurons which in turn inhibit the IO neurons. Note that, within a cerebellar module, different circuit elements communicate in closed loops. The mossy fibers contact granule cells and DCN cells which, in turn, receive inhibition from the same common set of Purkinje cells. Moreover, the IO cells emit climbing fibers that contact DCN and PC, which also project to the same DCN cells.

The cerebellum has traditionally provided an ideal case for investigating the relationship between cellular neurophysiology and circuit functions, because of the limited number of neuronal types and the regular organization of its internal network (**Figure 1**). The Motor Learning Theory (Marr, 1969; Albus, 1971), which proposed the first computational model of cerebellar function, was inspired by morphological determinations of the number of neurons and synapses but accounted for only very limited knowledge on functional properties of the cerebellar circuitry. In recent years, in association with remarkable developments of physiological technologies, important achievements at the cellular level have suggested that the original view needs to be revisited (Rokni et al., 2008). The papers in this special issue are focused on the relationship between cellular properties and circuit responses, which hold the key to control spike timing and long-term synaptic plasticity (Hansel et al., 2001; De Zeeuw and Yeo, 2005; D'Angelo and De Zeeuw, 2009; D'Angelo et al., 2009) and eventually cerebellar functioning.

In the cerebellum, inputs are conveyed through a double system formed by the mossy fibers and the climbing fibers. These inputs converge onto Purkinje cells, which eventually inhibit the DCN, representing the sole output of the circuit (**Figure 1**). Despite the wealth of available information, outstanding issues remain open about the spatial organization of granular layer activity, the discharge of Purkinje cells and deep cerebellar neurons, the mechanisms of circuit inhibition, the forms of long-term synaptic plasticity and their relationship with behavior. These aspects are covered by the papers in this special issue combining a careful literature review with significant original data.

Signals coming into the cerebellum through the mossy fibers are first processed in the granular layer network. The mossy fibers show complex firing patterns, ranging from frequency-modulated discharges to short bursts (van Kan et al., 1993; Chadderton et al., 2004; Rancz et al., 2007; Arenz et al., 2008; Prsa et al., 2009). With the intervention of the inhibitory circuits and synaptic plasticity, mossy fiber activity is transformed into new spatio-temporally organized spike sequences for further processing in Purkinje cells (Mitchell and Silver, 2003; Nieus et al., 2006; Mapelli and D'Angelo, 2007; D'Angelo, 2008; D'Angelo et al., 2009). Then, granule cell spikes propagate through the ascending axon and along the parallel fibers. Despite the wealth of information on single cell properties, the spatio-temporal organization of activity in the granular layer network remains largely to be determined.

In this special issue, it is shown that afferent mossy fiber signals are differentially filtered and amplified depending on the intensity of local inhibition and on several receptor- and channel-dependent properties (Mapelli and D'Angelo, 2007; Mapelli et al., 2010a,b). These results lend support to the emerging concept that the granular layer performs complex transformations on the mossy fiber input by generating new spatio-temporal pattern with the aid of local circuitry and synaptic plasticity. These temporal patterns are likely to integrate with repetitive and coherent activity enhancing responses in the theta band (Pellerin and Lamarre, 1997; Hartmann and Bower, 1998; Courtemanche et al., 2009). These observations are integrated through the first realistic large-scale computational reconstruction of the granular layer providing a direct link between molecular, cellular, and network properties in the cerebellar network (Solinas et al., 2010).

These papers also contribute to sheds light on the mechanisms of transmission from granular layer to Purkinje cells and molecular layer interneurons. This process has been the object of debate, in which evidence for spots-like or beam-like activation has been contrasted (Rokni et al., 2007). Here, it is suggested that native bursts are amplified along the vertical transmission line, thereby generating activity spots (Mapelli et al., 2010b). Then, the effect of bursts along the parallel fibers is filtered, probably through molecular layer interneurons (Bower, 2010), generating weaker and frequency-independent responses. This effect was proposed to explain the "spot vs. stripe" controversy, since spots would easily emerge following burst transmission generated following punctuate stimulation.

The Purkinje cells receive inputs both from parallel fibers and climbing fibers originating from the inferior olive. The inferior olive itself is an oscillator (Llinas and Yarom, 1981a,b; Chorev et al., 2007; Khosrovani et al., 2007; Van Der Giessen et al., 2008), which can produce theta-frequency patterns influencing Purkinje cells and inhibitory interneurons of the molecular layer (Barmack and Yakhnitsa, 2008). Although much less numerous than parallel fibers, the climbing fibers exert a powerful effect on the Purkinje cells eliciting the complex spikes. The complex spike has been variously interpreted as a signal carrying either an error or an instruction for

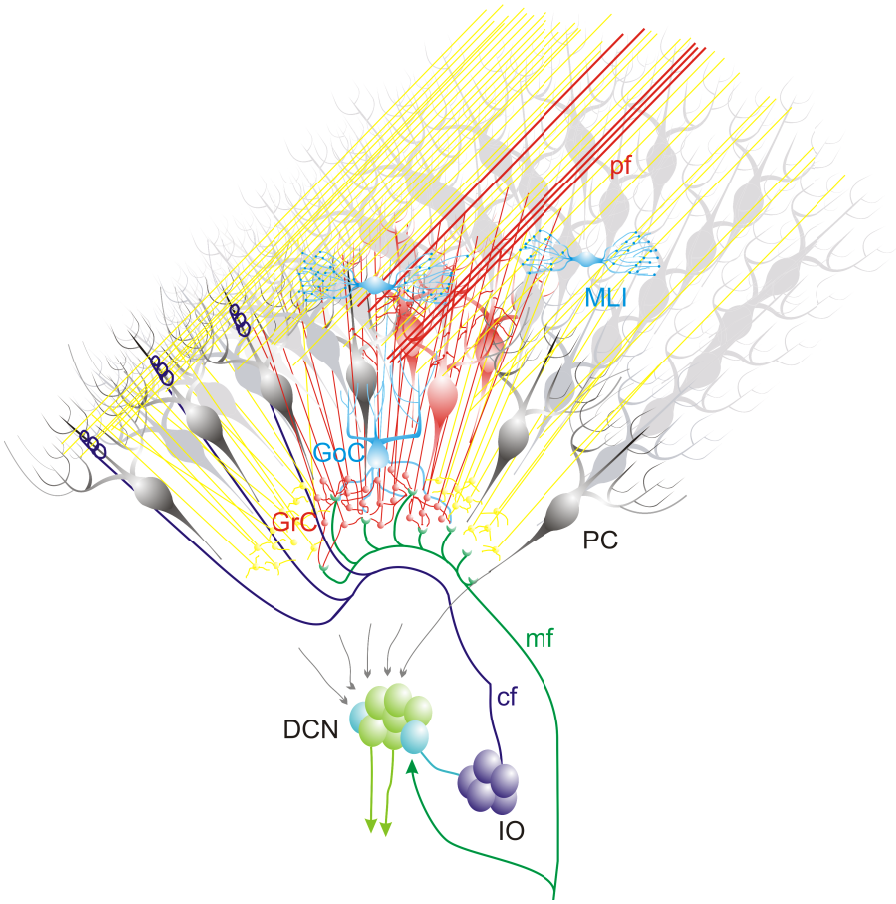

FIGURE 1 | Functional organization of the olivo-cerebellar system: a dynamic view.

generating synaptic plasticity at the parallel fiber – Purkinje cell synapse (Ito and Kano, 1982; Ito et al., 1982). Moreover, it has recently been demonstrated that both the climbing fiber and the parallel fiber inputs may influence the bistable transition of Purkinje cells between UP and DOWN states (Loewenstein et al., 2005; Jacobson et al., 2008), at least in anesthetized animals (Schonewille et al., 2006). Both the mechanisms of olive activation and of climbing fiber control of plasticity are incompletely understood. Moreover, it is still debated which kind of coding is used by Purkinje cell and how molecular layer inhibition could control it.

In this special issue, the Purkinje cell processing mechanisms have been considered. Purkinje cells are spontaneously active and their discharge is modulated by the activity coming from the granular layer and the inferior olive. It was recently shown that the molecular layer can sustain synchronous gamma band (30–80 Hz) and high-frequency (100–200 Hz) oscillations entraining the Purkinje cells (de Solages et al., 2008; Middleton et al., 2008). Purkinje cells were proposed to act as perceptrons (Brunel et al., 2004) and to process spike pauses (Steuber et al., 2007), and may live in a bistable UP–DOWN state (Loewenstein et al., 2005). Here, it is proposed that, in Purkinje cells, regulation of firing precision seems a more creditable coding strategy than frequency modulation (Rokni et al., 2009). Moreover, superposition of UP/DOWN states can engage specific groups of Purkinje cells. Interestingly, the mossy fiber input can play a critical role in determining both the spike-to-spike variability and the UP/DOWN state of Purkinje cells, generating a complex blend of dynamics on multiple time-scales. Purkinje cell synchrony and the repercussion of PC firing on DCN neurons have been investigated *in vivo* (Jorntell and Ekerot, 2006; Baumel et al., 2009; Bengtsson and Jorntell, 2009) and novel information on PC functioning has been provided through the development of genetically expressed fluorescent proteins in these neurons (Akemann et al., 2009).

The cells of DCN consists of diverse neuronal populations with distinct integrative properties (Uusisaari et al., 2007) and generate the sole cerebellar output. Both mossy fibers and to a lesser extent climbing fibers make collateral connections on to neurons of the DCN. DCN neurons also inhibit the IO cells regulating their coupling. IN DCN cells, intrinsic dynamics generate silent pauses, and possibly rebound excitation, producing alternating phases of activity. The DCN, in addition to act as a "relay station" between cerebellar mossy fiber input and cerebellar output to premotor areas, either directly or via the cerebellar cortex may also act as the substrate of motor memory storage (Raymond et al., 1996; Aizenman et al., 1998; Aizenman and Linden, 2000; Ito, 2006). It has been hypothesized that the synchronous oscillations in the Purkinje

cell activities together with plasticity at the mossy fiber – DCN and the Purkinje cell – DCN synapses form the main mechanistic tools to control the activity in the DCN output neurons (De Zeeuw et al., 2008). A critical issue is that the convergence of Purkinje cell inhibition on DCN neurons remains to be demonstrated. Here, the discharge of DCN neurons *in vivo* is considered under the effect of harmaline (Baumel et al., 2009). Harmaline induced a rhythmic firing pattern of short bursts on a quiescent background at about 8 Hz, while other neurons become quiescent for long periods (seconds to minutes). The major effect harmaline was carried indirectly by the inhibitory Purkinje cells (PCs) activated by the IO, so that the DCN response profile was probably determined by the number of concurrently active PCs, their firing rate and the level of synchrony occurring in their transitions between continuous firing and quiescence.

These papers suggest an extension of anatomical observations toward a dynamic view of the cerebellar circuit. **Figure 1** shows that the entire olivo-cerebellar system is organized in modules (Voogd et al., 2003; Apps and Hawkes, 2009; Glickstein et al., 2009). The intricate set of connections makes sense under specific hypothesis for network dynamics. Once a MF bundle discharges, it activates a groups of granule cells, while others are laterally inhibited by the Golgi cells. The active granule cells could be coordinated into low-frequency oscillations (Courtemanche et al., 2009; Solinas et al., 2010) and excite the overlaying PCs according to a vertical organization pattern upon arrival of specific afferent signals (Bower and Woolston, 1983). The parallel fibers can also activate PCs on the low-frequency band due to the intense low-pass filtering caused by molecular layer interneurons (Santamaria et al., 2007; Mapelli et al., 2010b). Eventually, the PCs can entrain the DCN-IO-PC system into coherent low-frequency oscillations (Jacobson et al., 2008; Rokni et al., 2009). The hypothesis is that certain inhibitory interneurons on the DCN are inhibited, releasing electrical coupling groups of IO neurons and causing their coherent subthreshold oscillation. The oscillations generated by the IO along the sagittal axis (climbing fiber-mediated) may collide with that conveyed by the cerebral cortex and diffusing along the transverse axis (parallel fiber-mediated), causing local resonance at the intersection of the parallel fiber and climbing fiber signals. DCN neurons may finally transfer temporal patterns resulting from strong correlations in PCs state transitions, while largely ignoring the timing of simple spikes from individual PCs (Baumel et al., 2009). PC correlations occur also in high-frequency bands (Akemann et al., 2009; Bengtsson and Jorntell, 2009). The Purkinje cell synapses are sites of plasticity, including the renown parallel fiber – Purkinje cell LTD (Hansel et al., 2001). At odd with the original predictions of the motor learning theory, the rearrangement of the network during learning may critically involve reversible LTP/LTD both at parallel fiber – Purkinje cell synapses (Ohtsuki et al., 2009) and at mossy fiber – granule cells synapses (Solinas et al., 2010). The impact of plasticity on behavior is addressed by reviewing the effect of mutations in the pf-PC mechanisms on VOR and eye-blink conditioning reflex (Boele et al., 2010). Finally, the impact of cerebellar learning and computation at the system level is critically considered by comparing the feed-forward and feed-back controller hypothesis (Frens and Donchin, 2009).

REFERENCES

Aizenman, C. D., and Linden, D. J. (2000). Rapid, synaptically driven increases in the intrinsic excitability of cerebellar deep nuclear neurons. *Nat. Neurosci.* 3, 109–111.

Aizenman, C. D., Manis, P. B., and Linden, D. J. (1998). Polarity of long-term synaptic gain change is related to postsynaptic spike firing at a cerebellar inhibitory synapse. *Neuron* 21, 827–835.

Akemann, W., Middleton, S. J., and Knopfel, T. (2009). Optical imaging as a link between cellular neurophysiology and circuit modeling. *Front. Cell. Neurosci.* 3:5. doi: 10.3389/neuro.03.005.2009.

Albus, J. (1971). The theory of cerebellar function. *Math. Biosci.* 10, 25–61.

Apps, R., and Hawkes, R. (2009). Cerebellar cortical organization: a one-map hypothesis. *Nat. Rev. Neurosci.* 10, 670–681.

Arenz, A., Silver, R. A., Schaefer, A. T., and Margrie, T. W. (2008). The contribution of single synapses to sensory representation in vivo. *Science* 321, 977–980.

Barmack, N. H., and Yakhnitsa, V. (2008). Functions of interneurons in mouse cerebellum. *J. Neurosci.* 28, 1140–1152.

Baumel, Y., Jacobson, G. A., and Cohen, D. (2009). Implications of functional anatomy on information processing in the deep cerebellar nuclei. *Front. Cell. Neurosci.* 3:14. doi: 10.3389/neuro.03.014.2009.

Bengtsson, F., and Jorntell, H. (2009). Climbing fiber coupling between adjacent purkinje cell dendrites in vivo. *Front. Cell. Neurosci.* 3:7. doi: 10.3389/neuro.03.007.2009.

Boele, H. J., Koekkoek, S. K., and De Zeeuw, C. I. (2010). Cerebellar and extracerebellar involvement in mouse eyeblink conditioning: the ACDC model. *Front. Cell. Neurosci.* 3:19. doi: 10.3389/neuro.03.019.2009.

Bower, J. M. (2010). Model-founded explorations of the roles of molecular layer inhibition in regulating purkinje cell responses in cerebellar cortex: more trouble for the beam hypothesis. *Front. Cell Neurosci.* 4: 27. doi: 10.3389/fncel.2010.00027.

Bower, J. M., and Woolston, D. C. (1983). Congruence of spatial organization of tactile projections to granule cell and Purkinje cell layers of cerebellar hemispheres of the albino rat: vertical organization of cerebellar cortex. *J. Neurophysiol.* 49, 745–766.

Brunel, N., Hakim, V., Isope, P., Nadal, J. P., and Barbour, B. (2004). Optimal information storage and the distribution of synaptic weights: perceptron versus Purkinje cell. *Neuron* 43, 745–757.

Chadderton, P., Margrie, T. W., and Hausser, M. (2004). Integration of quanta in cerebellar granule cells during sensory processing. *Nature* 428, 856–860.

Chorev, E., Yarom, Y., and Lampl, I. (2007). Rhythmic episodes of subthreshold membrane potential oscillations in the rat inferior olive nuclei in vivo. *J. Neurosci.* 27, 5043–5052.

Courtemanche, R., Chabaud, P., and Lamarre, Y. (2009). Synchronization in primate cerebellar granule cell layer local field potentials: basic anisotropy and dynamic changes during active expectancy. *Front. Cell Neurosci.* 3:6. doi: 10.3389/neuro.03.006.2009.

D'Angelo, E. (2008). The critical role of Golgi cells in regulating spatio-temporal integration and plasticity at the cerebellum input stage. *Front. Neurosci* 2, 35–46. doi: 10.3389/neuro.01.008.2008.

D'Angelo, E., and De Zeeuw, C. I. (2009). Timing and plasticity in the cerebellum: focus on the granular layer. *Trends Neurosci.* 32, 30–40.

D'Angelo, E., Koekkoek, S. K., Lombardo, P., Solinas, S., Ros, E., Garrido, J., Schonewille, M., and De Zeeuw, C. I. (2009). Timing in the cerebellum: oscillations and resonance in the granular layer. *Neuroscience* 162, 805–815.

de Solages, C., Szapiro, G., Brunel, N., Hakim, V., Isope, P., Buisseret, P., Rousseau, C., Barbour, B., and Lena, C. (2008). High-frequency organization and synchrony of activity in the purkinje cell layer of the cerebellum. *Neuron* 58, 775–788.

De Zeeuw, C. I., Hoebeek, F. E., and Schonewille, M. (2008). Causes and consequences of oscillations in the cerebellar cortex. *Neuron* 58, 655–658.

De Zeeuw, C. I., and Yeo, C. H. (2005). Time and tide in cerebellar memory formation. *Curr. Opin. Neurobiol.* 15, 667–674.

Frens, M. A., and Donchin, O. (2009). Forward models and state estimation in compensatory eye movements. *Front. Cell. Neurosci.* 3:13. doi: 10.3389/neuro.03.013.2009.

Glickstein, M., Sultan, F., and Voogd, J. (2009). Functional localization in the cerebellum. *Cortex*.

Hansel, C., Linden, D. J., and D'Angelo, E. (2001). Beyond parallel fiber LTD: the diversity of synaptic and non-synaptic plasticity in the cerebellum. *Nat. Neurosci.* 4, 467–475.

Hartmann, M. J., and Bower, J. M. (1998). Oscillatory activity in the cerebellar hemispheres of unrestrained rats. *J. Neurophysiol.* 80, 1598–1604.

Ito, M. (2006). Cerebellar circuitry as a neuronal machine. *Prog. Neurobiol.* 78, 272–303.

Ito, M., and Kano, M. (1982). Long-lasting depression of parallel fiber-Purkinje cell transmission induced by conjunctive stimulation of parallel fibers and climbing fibers in the cerebellar cortex. *Neurosci. Lett.* 33, 253–258.

Ito, M., Sakurai, M., and Tongroach, P. (1982). Climbing fibre induced depression of both mossy fibre responsiveness and glutamate sensitivity of cerebellar Purkinje cells. *J. Physiol.* 324, 113–134.

Jacobson, G. A., Rokni, D., and Yarom, Y. (2008). A model of the olivo-cerebellar system as a temporal pattern generator. *Trends Neurosci.* 31, 617–625.

Jorntell, H., and Ekerot, C. F. (2006). Properties of somatosensory synaptic integration in cerebellar granule cells in vivo. *J. Neurosci.* 26, 11786–11797.

Khosrovani, S., Van Der Giessen, R. S., De Zeeuw, C. I., and De Jeu, M. T. (2007). In vivo mouse inferior olive neurons exhibit heterogeneous subthreshold oscillations and spiking patterns. *Proc. Natl. Acad. Sci. U.S.A.* 104, 15911–15916.

Llinas, R., and Yarom, Y. (1981a). Electrophysiology of mammalian inferior olivary neurones in vitro. Different types of voltage-dependent ionic conductances. *J. Physiol.* 315, 549–567.

Llinas, R., and Yarom, Y. (1981b). Properties and distribution of ionic conductances generating electroresponsiveness of mammalian inferior olivary neurones in vitro. *J. Physiol.* 315, 569–584.

Loewenstein, Y., Mahon, S., Chadderton, P., Kitamura, K., Sompolinsky, H., Yarom, Y., and Hausser, M. (2005). Bistability of cerebellar Purkinje cells modulated by sensory stimulation. *Nat. Neurosci.* 8, 202–211.

Mapelli, J., and D'Angelo, E. (2007). The spatial organization of long-term synaptic plasticity at the input stage of cerebellum. *J. Neurosci.* 27, 1285–1296.

Mapelli, J., Gandolfi, D., and D'Angelo, E. (2010a). Combinatorial responses controlled by synaptic inhibition in the cerebellum granular layer. *J. Neurophysiol.* 103, 250–261.

Mapelli, J., Gandolfi, D., and D'Angelo, E. (2010b). High-pass filtering and dynamic gain regulation enhance vertical bursts transmission along the mossy fiber pathway of cerebellum. *Front. Cell. Neurosci.* 4:14. doi: 10.3389/fncel.2010.00014.

Marr, D. (1969). A theory of cerebellar cortex. *J. Physiol.* 202, 437–470.

Middleton, S. J., Racca, C., Cunningham, M. O., Traub, R. D., Monyer, H., Knopfel, T., Schofield, I. S., Jenkins, A., and Whittington, M. A. (2008). High-frequency network oscillations in cerebellar cortex. *Neuron* 58, 763–774.

Mitchell, S. J., and Silver, R. A. (2003). Shunting inhibition modulates neuronal gain during synaptic excitation. *Neuron* 38, 433–445.

Nieus, T., Sola, E., Mapelli, J., Saftenku, E., Rossi, P., and D'Angelo, E. (2006). LTP regulates burst initiation and frequency at mossy fiber-granule cell synapses of rat cerebellum: experimental observations and theoretical predictions. *J. Neurophysiol.* 95, 686–699.

Ohtsuki, G., Piochon, C., and Hansel, C. (2009). Climbing fiber signaling and cerebellar gain control. *Front. Cell. Neurosci.* 3:4. doi: 10.3389/neuro.03.004.2009.

Pellerin, J. P., and Lamarre, Y. (1997). Local field potential oscillations in primate cerebellar cortex during voluntary movement. *J. Neurophysiol.* 78, 3502–3507.

Prsa, M., Dash, S., Catz, N., Dicke, P. W., and Thier, P. (2009). Characteristics of responses of Golgi cells and mossy fibers to eye saccades and saccadic adaptation recorded from the posterior vermis of the cerebellum. *J. Neurosci.* 29, 250–262.

Rancz, E. A., Ishikawa, T., Duguid, I., Chadderton, P., Mahon, S., and Hausser, M. (2007). High-fidelity transmission of sensory information by single cerebellar mossy fibre boutons. *Nature* 450, 1245–1248.

Raymond, J. L., Lisberger, S. G., and Mauk, M. D. (1996). The cerebellum: a neuronal learning machine? *Science* 272, 1126–1131.

Rokni, D., Llinas, R., and Yarom, Y. (2007). Stars and stripes in the cerebellar cortex: a voltage sensitive dye study. *Front. Syst. Neurosci.* 1:1. doi: 10.3389/neuro.06/001.2007.

Rokni, D., Llinas, R., and Yarom, Y. (2008). The morpho/functional discrepancy in the cerebellar cortex: looks alone are deceptive. *Front. Neurosci.* 2, 192–198. doi: 10.3389/neuro.01.036.2008.

Rokni, D., Tal, Z., Byk, H., and Yarom, Y. (2009). Regularity, variability and bi-stability in the activity of cerebellar purkinje cells. *Front. Cell. Neurosci.* 3:12. doi: 10.3389/neuro.03.012.2009.

Santamaria. F., Tripp, P. G., and Bower, J. M. (2007). Feedforward inhibition controls the spread of granule cell-induced Purkinje cell activity in the cerebellar cortex. *J. Neurophysiol.* 97, 248–263.

Schonewille, M., Khosrovani, S., Winkelman, B. H., Hoebeek, F. E., De Jeu, M. T., Larsen, I. M., Van der Burg, J., Schmolesky, M. T., Frens, M. A., and De Zeeuw, C. I. (2006). Purkinje cells in awake behaving animals operate at the upstate membrane potential. *Nat. Neurosci.* 9, 459–461; author reply 461.

Solinas, S., Nieus, T., and D'Angelo, E. (2010). A realistic large-scale model of the cerebellum granular layer predicts circuit spatio-temporal filtering properties. *Front. Cell Neurosci.* 4:12. doi: 10.3389/fncel.2010.00012.

Steuber, V., Mittmann, W., Hoebeek, F. E., Silver, R. A., De Zeeuw, C. I., Hausser, M., and De Schutter, E. (2007). Cerebellar LTD and pattern recognition by Purkinje cells. *Neuron* 54, 121–136.

Uusisaari, M., Obata, K., and Knopfel, T. (2007). Morphological and electrophysiological properties of GABAergic and non-GABAergic cells in the deep cerebellar nuclei. *J. Neurophysiol.* 97, 901–911.

Van Der Giessen, R. S., Koekkoek, S. K., van Dorp, S., De Gruijl, J. R., Cupido, A., Khosrovani, S., Dortland, B., Wellershaus, K., Degen, J., Deuchars, J., Fuchs, E. C., Monyer, H., Willecke, K., De Jeu, M. T., and De Zeeuw, C. I. (2008). Role of olivary electrical coupling in cerebellar motor learning. *Neuron* 58, 599–612.

van Kan, P. L., Gibson, A. R., and Houk, J. C. (1993). Movement-related inputs to intermediate cerebellum of the monkey. *J. Neurophysiol.* 69, 74–94.

Voogd, J., Pardoe, J., Ruigrok, T. J., and Apps, R. (2003). The distribution of climbing and mossy fiber collateral branches from the copula pyramidis and the paramedian lobule: congruence of climbing fiber cortical zones and the pattern of zebrin banding within the rat cerebellum. *J. Neurosci.* 23, 4645–4656.

Received: 24 September 2010; accepted: 27 September 2010; published online: 04 November 2010.

*Citation: D'angelo E (2010). Rebuilding cerebellar network computations from cellular neurophysiology. Front. Cell. Neurosci. **4**:131. doi: 10.3389/fncel.2010.00131*

frontiers in
CELLULAR NEUROSCIENCE

REVIEW ARTICLE
published: 06 July 2009
doi: 10.3389/neuro.03.004.2009

Climbing fiber signaling and cerebellar gain control

Gen Ohtsuki*[1,2]*, Claire Piochon*[1] *and Christian Hansel*[1,2]*

[1] *Department of Neurobiology, University of Chicago, Chicago, IL, USA*
[2] *Department of Neuroscience, Erasmus University Medical Center, Rotterdam, The Netherlands*

Edited by:
Egidio D'Angelo, University of Pavia, Italy

Reviewed by:
Masao Ito, RIKEN, Japan
David Linden, Johns Hopkins University, USA

****Correspondence:***
Christian Hansel, The University of Chicago, Department of Neurobiology, 947 E. 58th Street/J243, Chicago, IL 60637, USA.
e-mail: chansel@bsd.uchicago.edu

The physiology of climbing fiber signals in cerebellar Purkinje cells has been studied since the early days of electrophysiology. Both the climbing fiber-evoked complex spike and the role of climbing fiber activity in the induction of long-term depression (LTD) at parallel fiber-Purkinje cell synapses have become hallmark features of cerebellar physiology. However, the key role of climbing fiber signaling in cerebellar motor learning has been challenged by recent reports of forms of synaptic and non-synaptic plasticity in the cerebellar cortex that do not involve climbing fiber activity, but might well play a role in cerebellar learning. Moreover, cerebellar LTD does not seem to strictly require climbing fiber activity. These observations make it necessary to re-evaluate the role of climbing fiber signaling in cerebellar function. Here, we argue that climbing fiber signaling is about adjusting relative probabilities for the induction of LTD and long-term potentiation (LTP) at parallel fiber synapses. Complex spike-associated, dendritic calcium transients control postsynaptic LTD and LTP induction. High calcium transients, provided by complex spike activity, do not only favor postsynaptic LTD induction, but simultaneously trigger retrograde cannabinoid signaling, which blocks the induction of presynaptic LTP. Plasticity of the climbing fiber input itself provides additional means to fine-tune complex spike associated calcium signaling and thus to adjust the gain of heterosynaptic climbing fiber control. In addition to dendritic calcium transients, climbing fiber activity leads to the release of the neuropeptide corticotropin-releasing factor (CRF), which facilitates LTD induction at both parallel fiber and climbing fiber synapses.

Keywords: calcium, cerebellum, climbing fiber, corticotropin releasing factor, long-term depression, long-term potentiation, parallel fiber, Purkinje cell

INTRODUCTION

The first detailed characterization of excitatory synaptic responses to climbing fiber stimulation resulted from intracellular Purkinje cell recordings performed in anaesthetized cats by Eccles, Llinas and Sasaki, working at the time at the Australian National University in Canberra (Eccles et al., 1964, 1966). Stimulation of the climbing fiber input, or the contralateral inferior olive (from which climbing fibers originate) led to an all-or-none 'giant' or 'complex' spike, composed of an initial fast action potential, followed by smaller spikelets superimposed on a sustained depolarization (Eccles et al., 1966). In the mature cerebellum, this massive, excitatory response pattern results from the activity of only one climbing fiber input (Ramón y Cajal, 1911) that remains after a period of developmental elimination of surplus climbing fibers, which in rats occurs during the first 3 weeks of postnatal life (Crépel et al., 1976).

The characteristic complex spike provides a hallmark feature of cerebellar physiology, particularly because of its seemingly invariant nature (for review, see Schmolesky et al., 2002). Another hallmark feature is the role assigned to climbing fiber activity in cerebellar motor learning. It is widely assumed that long-term depression (LTD) at parallel fiber-Purkinje cell synapses, a type of synaptic plasticity that requires co-activation of the parallel fiber and the climbing fiber input, provides the cellular correlate of forms of motor learning. Climbing fiber activity results in large, widespread calcium transients in Purkinje cell dendrites (Miyakawa et al., 1992; Ross and Werman, 1987), which are required for the induction of cerebellar LTD (Konnerth et al., 1992).

More recent observations suggest that the role of climbing fiber signaling is more complex than that of an invariant 'teacher' signal contributing to LTD induction and, therefore, to cerebellar motor learning. Here, we will discuss recent evidence showing that climbing fiber synapses onto cerebellar Purkinje cells show forms of plasticity as well. Moreover, we will review recent observations on types of synaptic and non-synaptic cerebellar plasticity that do not depend on climbing fiber signaling, suggesting that motor learning is not exclusively linked to climbing fiber activity. Rather, a picture emerges, in which the presence or absence of climbing fiber activity influences induction probabilities for various types of plasticity, thus orchestrating Purkinje cell output patterns and cerebellar gain control.

THE COMPLEX SPIKE: SIGNATURE OF CLIMBING FIBER ACTIVITY

Climbing fiber synaptic transmission onto Purkinje cells is very powerful and reliable, resulting from the large number of synaptic contact sites formed by an individual climbing fiber input (Palay and Chan-Palay, 1974) as well as from the high probability of release at each climbing fiber terminal (Dittman and Regehr, 1998; Hashimoto and Kano, 1998; Silver et al., 1998). Climbing fiber synapses contact spines on the primary Purkinje cell dendrite,

whereas parallel fiber synapses contact spines on secondary and tertiary dendritic branches (Strata and Rossi, 1998). Whereas parallel fiber stimulation causes a graded excitatory postsynaptic potential (EPSP) in Purkinje cells, climbing fiber activity is monitored in somatic recordings as an all-or-none complex spike (Eccles et al., 1964, 1966), characterized by a fast sodium spike that is followed by typically two to three spikelets riding on top of a depolarization plateau (**Figure 1**). Purkinje cell complex spikes occur at low frequencies around 1 Hz, but can reach frequencies up to 11 Hz when nociceptive stimulation is applied (Ekerot et al., 1987). Each complex spike can be associated with high-frequency firing of spikes in the climbing fiber itself, which can reach frequencies up to 500 Hz (Maruta et al., 2007). In Purkinje cell dendrites, climbing fiber activation evokes calcium spikes, which have been characterized in early intradendritic recordings (Llinas and Sugimori, 1980). For a long time, however, the origin of the different somatically recorded complex spike components remained unclear (as discussed in Schmolesky et al., 2002). Recent somato-dendritic double-patch recordings demonstrate that dendritically recorded calcium spikes show no obvious relation to the number and occurrence of spikelets within the simultaneously recorded complex spike (Davie et al., 2008). These observations suggest that the typical, somatically recorded complex spike waveform is locally generated, whereas in the dendrite, climbing fiber activity evokes isolated calcium spikes. Simultaneous somatic and dendritic patch-clamp recordings from our lab are shown in **Figure 1**. In the soma, climbing fiber stimulation evokes complex spikes (black traces). In contrast, the dendritic recordings (blue traces) obtained at distances of about 75 µm (**Figure 1A**) and 100 µm (**Figure 1B**) from the soma, respectively, reveal local climbing fiber responses, which do not show

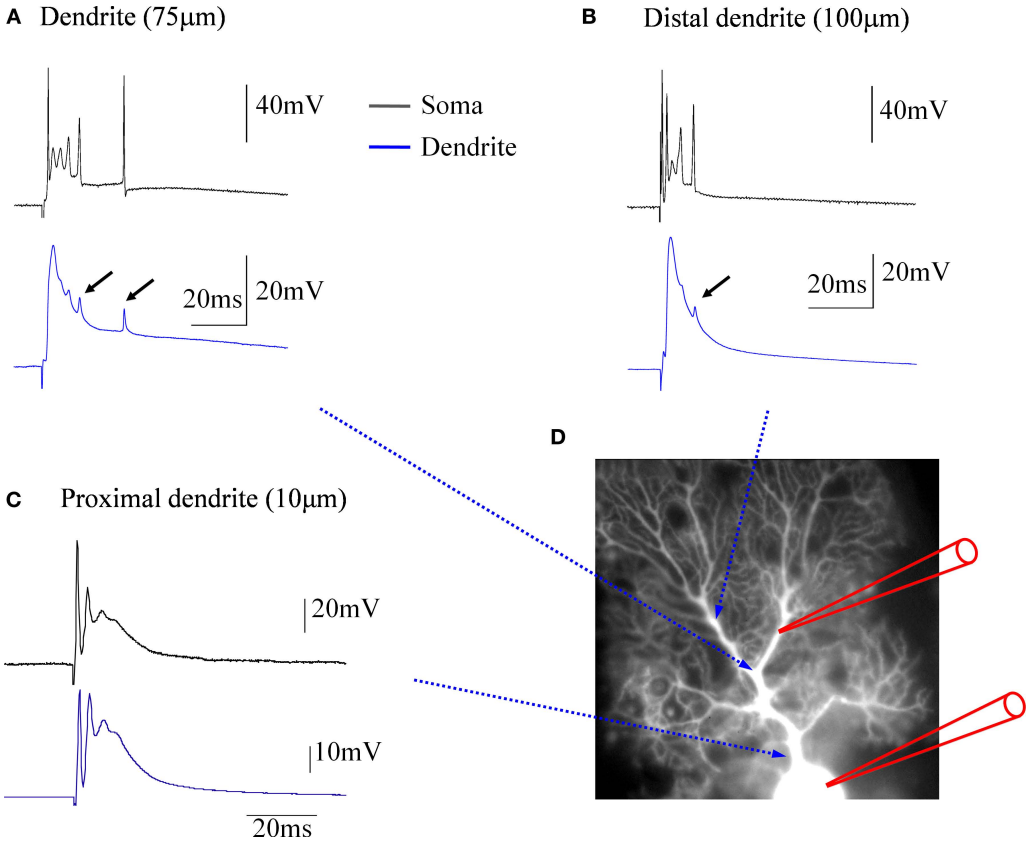

FIGURE 1 | Climbing fiber responses monitored by simultaneous double patch-clamp recordings from the soma and dendrites of cerebellar Purkinje cells. (A) Paired recordings from the soma (black trace) and the dendrite (blue trace). The dendritic patch electrode was located at about 75 µm distance from the soma. **(B)** In this recording, which was obtained from a different Purkinje cell, a more distal location (ca. 100 µm) was selected for the dendritic patch electrode. Small arrows in **(A)** and **(B)** point towards small, delayed spikelets seen in the dendritic recordings, that likely reflect sodium action potentials generated in the axon (see corresponding, but larger spikes in the somatic recordings), which passively spread into the dendrite. **(C)** At a far more proximal location (ca. 10 µm), the dendritic recording resembles the complex spike recorded in the soma, but already at this distance an attenuation of the initial, fast sodium spike can be seen. **(D)** Recording configuration of the experiments. This picture was assembled for illustration purposes only. The recordings were obtained from cerebellar slices prepared from P28-35 Sprague-Dawley rats. Slices were perfused with standard ACSF (as described in Coesmans et al., 2004) bubbled with 95% O_2 and 5% CO_2. The recordings were performed at near-physiological temperature (31–34°C) using an EPC-10 amplifier (HEKA Electronics, Germany). Currents were filtered at 3 kHz, digitized at 10 kHz, and acquired using Fitmaster software. The recording electrodes were filled with a solution containing (in mM): 9 KCl, 10 KOH, 120 K gluconate, 3.48 $MgCl_2$, 10 HEPES, 4 NaCl, 4 Na_2ATP, 0.4 Na_3GTP, and 17.5 sucrose (pH 7.25). Patch electrodes used for somatic recordings had electrode resistances of 3–4 MΩ, and patch electrodes used for dendritic recordings had electrode resistances of 7–10 MΩ. For climbing fiber stimulation, glass pipettes were used that were filled with ACSF.

the spikelets that are characteristic for the somatically recorded complex spike. An exception to this are small spikelets that occasionally occur during the late stages of the dendritic climbing fiber response (**Figures 1A,B**: arrows). These spikelets coincide with late, higher amplitude spikes seen in the somatic recordings. In Purkinje cells, sodium action potentials are initiated in the axon, and passively spread into the dendrite, where their amplitude decreases with increasing distance from the soma (Stuart and Häusser, 1994). The small spikelets seen in our dendritic recordings likely represent those attenuated sodium spikes.

CLIMBING FIBER ACTIVITY EVOKES DENDRITIC CALCIUM TRANSIENTS

Climbing fibers form so-called 'en passant' synapses with their target Purkinje cells, whose number and distribution along the axis of the Purkinje cell primary dendrite allow for excitatory action throughout the dendritic tree. The most obvious consequence of this unusually tight synaptic contact formed by a single climbing fiber input is a large, widespread calcium transient that accompanies complex spikes (Miyakawa et al., 1992; Ross and Werman, 1987). Climbing fiber-evoked calcium transients not only can be recorded in the primary dendrites (an example of a calcium transient recorded in a primary dendrite spine is shown in **Figure 2**), but also in secondary and tertiary branches (Miyakawa et al., 1992; Ross and Werman, 1987). Such 'out-of-territory' calcium signaling has also been described in cerebellar Purkinje cells of mormyrid fish (Han et al., 2007), in which the separation of climbing fiber and parallel fiber input territories is even more pronounced. The dendritic tree of these cells is palisade-shaped, with a horizontal dendrite (contacted by the climbing fiber input), and vertical dendrites (contacted by parallel fibers) that show a much lower degree of branching as compared to their mammalian counterparts. Climbing fiber stimulation results in calcium transients in both the horizontal dendrite and the vertical dendrites (Han

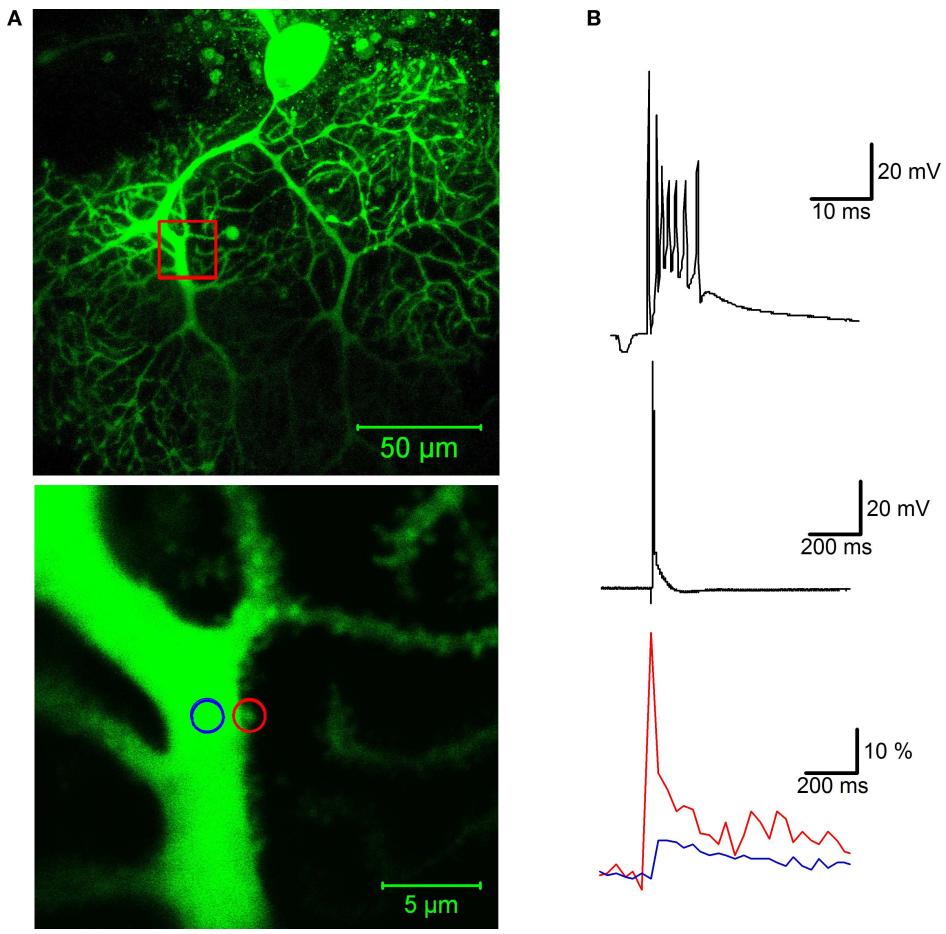

FIGURE 2 | Calcium signaling in a dendritic spine evoked by climbing fiber activity. (A) Top: A rat Purkinje cell (P36) was filled through the patch pipette with the fluorescent calcium indicator Oregon Green BAPTA-2 (200 µM). The red box indicates the magnification area. Calcium transients were recorded in a spine (red circle) and in the shaft (blue circle) of the primary dendrite using a Zeiss LSM 5 Exciter confocal microscope and a ×63 Zeiss Apochromat objective (bottom picture). **(B)** Climbing fiber stimulation evokes a complex spike shown at two different time scales (top), which is associated with a large calcium transient monitored in the spine (red trace), and a smaller transient in the shaft (blue trace; bottom). The calcium traces represent averages of 10 transients (acquired at 30 s delays), and are displayed as normalized fluorescence changes ($\Delta F/F$). For image acquisition and analysis we used ZEN software (Carl Zeiss MicroImaging, Thornwood, NY, USA). Patch-clamp recording details are described in **Figure 1**.

et al., 2007). In both mammalian and mormyrid Purkinje cells, calcium influx associated with dendritic calcium spikes is partially mediated by P/Q-type voltage-dependent calcium channels (Han et al., 2007; Usowicz et al., 1992; Watanabe et al., 1998), suggesting that these channels provide the regenerative component needed for the spatial spread of the calcium signal. In spines contacted by parallel fibers, coincident parallel fiber and climbing fiber activity results in supralinear calcium transients (Wang et al., 2000). These spine calcium signals are largest when the parallel fiber activation precedes climbing fiber activation by 50–200 ms, and depend on calcium release from IP_3-sensitive calcium stores when the parallel fiber input is weakly activated (Wang et al., 2000). Stronger parallel fiber stimulation results in the activation of more parallel fibers. In this scenario, supralinear calcium signaling is not restricted to individual spines and is mediated by the activation of voltage-dependent calcium channels (Wang et al., 2000). A similar enhancement in dendritic calcium signaling at parallel fiber input sites has been found in mormyrid Purkinje cells upon parallel fiber and climbing fiber stimulation (Han et al., 2007). These observations show that calcium transients evoked by climbing fiber activity do not only invade the parallel fiber input territory, but that they contribute to a local amplification of calcium transients at parallel fiber input sites, even in spines located on distal branchlets that are contacted by parallel fibers (Wang et al., 2000). This is a remarkable finding, as the climbing fiber input itself only contacts spines on the primary dendrite (Strata and Rossi, 1998). The amplitude of the climbing fiber-evoked calcium transient itself also depends on the state of the membrane potential. Synaptic activity of the climbing fiber or the granule cell input can shift the membrane potential to an 'UP' state, while inhibitory inputs can cause a transition towards a 'DOWN' state (Loewenstein et al., 2005; but see Schonewille et al., 2006). Dendritic climbing fiber-evoked calcium transients are smaller following a 'DOWN' state (Rokni and Yarom, 2009). If these bidirectional state transitions occur *in vivo*, 'UP' states could provide an optimal time window for enhanced dendritic calcium signaling.

GLUTAMATERGIC TRANSMISSION AT CLIMBING FIBER SYNAPSES: NEW PLAYERS IN SIGHT

Excitatory postsynaptic currents (EPSCs) at climbing fiber synapses are largely mediated by the activation of AMPA receptors (Konnerth et al., 1990; Llano et al., 1991; Perkel et al., 1990) that contain GluR2 subunits and are therefore not permeable to calcium (Hollmann et al., 1991). In the following, we will focus on two additional types of glutamate receptors, whose contribution to climbing fiber signaling (and potential role in calcium signaling) has only recently been fully appreciated: N-methyl-D-aspartate (NMDA) receptors and metabotropic glutamate receptors.

NMDA RECEPTORS

At many types of excitatory synapses, NMDA receptors provide a major source of calcium influx and are therefore considered as key players in synaptic plasticity (Bliss and Collingridge, 1993). Purkinje cells, in contrast, were until recently assumed to lack functional NMDA receptors. Both NR1 and NR2 subunits are required to form functional NMDA receptors. In Purkinje cells, NR1 subunits are expressed at all ages, from birth throughout adulthood, as consistently shown by numerous morphological studies (Monyer et al., 1992, 1994; Moriyoshi et al., 1991; Petralia et al., 1994). During the first postnatal week in rodents, a juvenile form of the NR2 subunit (the NR2D subtype) has clearly been demonstrated in Purkinje cells (Momiyama et al., 1996). However, during this period the resulting NMDA receptors do not contribute to synaptic transmission at parallel fiber or climbing fiber inputs (Lachamp et al., 2005; Llano et al., 1991). In mature Purkinje cells, in situ hybridization and immunohistochemical studies reached contradicting conclusions regarding the expression of NR2 subunits (Monyer et al., 1994; Watanabe et al., 1994; Yamada et al., 2001; but see Akazawa et al., 1994; Thompson et al., 2000). As no NMDA currents were detected in whole-cell patch-clamp recordings (Farrant and Cull-Candy, 1991; Konnerth et al., 1990; Llano et al., 1991), the notion became widely accepted that Purkinje cells lack functional NMDA receptors.

Recently, this question has been re-examined in older animals (>8-week-old mice) using more selective pharmacological tools (NBQX instead of CNQX as an AMPA receptor antagonist) and a new generation of antibodies. It now appears in the light of these more recent results (Piochon et al., 2007; Renzi et al., 2007) that mature Purkinje cells express functional NMDA receptors from the end of the third postnatal week on, which contain NR2A and/or NR2B subunits. These NMDA receptors are activated by climbing fiber stimulation and contribute to the complex spike waveform, by influencing the number and timing of spikelets, as well as the afterdepolarization plateau (Piochon et al., 2007). Thus, in mature Purkinje cells, functional NMDA receptors are expressed at climbing fiber synapses, and might well contribute to climbing fiber-evoked calcium signaling.

METABOTROPIC GLUTAMATE RECEPTORS

Similar to parallel fiber burst stimulation, climbing fiber stimulation can evoke a slow excitatory current that is triggered by the activation of type 1 metabotropic glutamate receptors (mGluR1) and can be significantly enhanced when glutamate uptake is blocked (Dzubay and Otis, 2002). Such mGluR1-mediated potentials are also evoked by climbing fiber stimulation in the presence of an mGluR agonist in the bath, suggesting agonist binding and a widespread, dendritic calcium transient as key triggers for this type of slow excitatory signaling (Yuan et al., 2007). In this scenario, climbing fiber activity could facilitate mGluR1 potentials well beyond the climbing fiber input territory, providing that the climbing fiber-evoked calcium signal coincides with sufficiently high local glutamate transients. A related phenomenon has been described earlier, in which parallel fiber activation elicits mGluR1 potentials when the climbing fiber input was stimulated up to 90 s prior to the parallel fiber input (Batchelor and Garthwaite, 1997). Adding the calcium chelator EGTA to the recording electrode abolished the slow potentials, while they could be triggered when substituting photolytic calcium uncaging for climbing fiber stimulation. The examples provided in these studies (Batchelor and Garthwaite, 1997; Yuan et al., 2007) show that calcium signaling is required to trigger mGluR1 potentials. Recent evidence suggests that this calcium sensitivity results from the involvement of TRPC cation channels that mediate the slow, excitatory conductances. Both TRPC1 (Kim et al., 2003) and TRPC3 channels (Hartmann et al., 2008) have been suggested to

mediate the slow current. TRPC channels open in response to G-protein-coupled receptor activation and/or the occurrence of calcium surges. This activation pattern principally enables TRPC channels to mediate capacitive calcium entry after release of calcium from intracellular stores (Montell et al., 2002). However, the calcium transient associated with slow, mGluR1 potentials is not blocked in Purkinje cells obtained from TRPC1$^{-/-}$ or TRPC3$^{-/-}$ mice (Hartmann et al., 2008). These observations suggest that mGluR1 potentials might be triggered by calcium surges, but that significant components of the associated calcium influx are not contributed by TRPC channels.

These novel findings are crucial for the present discussion of the consequences of climbing fiber signaling for cerebellar plasticity and function, because mGluR1 potentials significantly enhance complex spike associated calcium transients (Yuan et al., 2007), and might therefore facilitate the induction of parallel fiber LTD. It has been suggested that such an increase in the LTD induction probability occurs when mGluR1 potentials are enhanced after blockade of glutamate transporters (Brasnjo and Otis, 2001). However, the cause for the enhanced probability of LTD induction remains unclear. Both TRPC channels (but see Hartmann et al., 2008) and IP_3-mediated calcium release from internal stores could contribute to more pronounced calcium signaling. Moreover, a stronger mGluR1 activation would also result in enhanced PKC activation. All of these factors could enhance the LTD induction probability. Despite of these remaining uncertainties with regard to the type of TRPC channels involved and the origin of the calcium signal associated with slow excitatory potentials, new aspects of mGluR1 signaling at climbing fiber synapses emerge. First, mGluR1-triggered potentials can be evoked by climbing fiber signaling, and second, these slow potentials enhance calcium signaling and are likely to facilitate LTD induction.

PLASTICITY OF CLIMBING FIBER-PURKINJE CELL SYNAPSES

Marr-Albus-Ito models of cerebellar motor learning describe the parallel fiber input to Purkinje cells as the site in the cerebellar network at which the learning events take place (Albus, 1971; Ito, 1984; Marr, 1969). In these classic models, the climbing fiber plays a crucial role as well, but is seen as a 'teacher' that signals errors and disturbances in sensomotoric function, rather than an additional site of information storage. The long prevailing dogma of the 'invariant' climbing fiber response resulted from the high probability of release at climbing fiber terminals (Dittman and Regehr, 1998; Hashimoto and Kano, 1998; Silver et al., 1998), as well as the all-or-none character of climbing fiber signaling (Eccles et al., 1966). These features make climbing fiber transmission both extremely reliable and forceful, and distinguish it from transmission at most other types of central nervous system synapses.

Nevertheless, synaptic plasticity exists at climbing fiber synapses as well: LTD of climbing fiber EPSCs (recorded in voltage-clamp mode) can be induced using low-frequency (5 Hz, 30 s) climbing fiber stimulation (Carta et al., 2006; Hansel and Linden, 2000). In current-clamp mode, LTD is associated with an alteration in the complex spike waveform (Hansel and Linden, 2000), a reduction in the complex spike afterhyperpolarization (Schmolesky et al., 2005), and a long-term depression of climbing fiber evoked calcium transients (Weber et al., 2003). **Figure 3** illustrates two crucial aspects of climbing fiber LTD: climbing fiber tetanization leads to a reduction in the amplitude of the slow spikelets that make up the late component of a complex spike (**Figure 3A**), and the associated calcium transients (**Figure 3B**). Climbing fiber LTD is postsynaptically induced and expressed (Shen et al., 2002). The biochemical cascade for the induction of climbing fiber LTD shares elements with the LTD induction cascade at parallel fiber synapses: at both types of synapses, a postsynaptic calcium surge, activation of mGluR1 receptors, and activation of protein kinase C (PKC) are required for LTD induction (Hansel and Linden, 2000). Climbing fiber LTD induction is also PKA-dependent (Schmolesky et al., 2007), which has not been tested for parallel fiber LTD yet.

It remains to be determined whether climbing fiber plasticity can play a similar role in motor learning as assumed for parallel fiber LTD. However, the reduction of calcium transients accompanying climbing fiber LTD (Weber et al., 2003) has a significant effect on the LTD induction probability at parallel fiber synapses (Coesmans et al., 2004) and might therefore provide a critical component of cerebellar gain control (see below).

DEVELOPMENTAL CLIMBING FIBER PLASTICITY

Climbing fiber synaptic plasticity has also been observed in the developing cerebellum, where it might play a role in the activity-dependent elimination of surplus climbing fibers, and the stabilization of the remaining 'winner' climbing fiber input. This pruning process is typically completed at the end of the third postnatal week (Crépel et al., 1976; Lohof et al., 1996). Recent studies suggest that long-term potentiation (LTP) and LTD can be observed at climbing fiber synapses during postnatal development (Bosman et al., 2008; Ohtsuki and Hirano, 2008). In P4-11 Purkinje cells, pairing of climbing fiber stimulation and Purkinje cell depolarization leads to LTP at 'large' climbing fiber inputs, which are sufficiently strong to evoke spike firing in Purkinje cells, but induces LTD at 'small' climbing fiber inputs (Bosman et al., 2008). As multiple climbing fiber inputs share innervation fields on Purkinje cell dendrites (Scelfo et al., 2003; Sugihara, 2005), it is conceivable that LTP and LTD at developing climbing fiber synapses reflect a direct synaptic competition of neighbouring climbing fiber inputs, at the end of which the potentiated input is stabilized and becomes the 'winner', whereas the depressed synaptic inputs are eventually eliminated (Bosman et al., 2008). The LTP described in this study is calcium-dependent, but does not require the activation of NMDA receptors. The potentiation is mediated by an increase in the single channel conductance of AMPA receptors, suggesting a postsynaptic induction and expression mechanism (Bosman et al., 2008). Another study also described that in postnatal development (P5-9), climbing fiber stimulation leads to LTP at strong climbing fiber inputs, and LTD at weak climbing fiber inputs (Ohtsuki and Hirano, 2008). In this study, however, LTP and LTD were accompanied by changes in the paired-pulse depression ratio and alterations in the frequency of asynchronous EPSCs, indicating that both types of plasticity are presynaptically expressed. LTP (but not LTD) induction requires a postsynaptic calcium transient, suggesting the involvement of a retrograde messenger (Ohtsuki and Hirano, 2008). Whether or not the different observations made in these two studies can be explained by slight differences in the stimulation protocols (for example, the second study applied unpaired

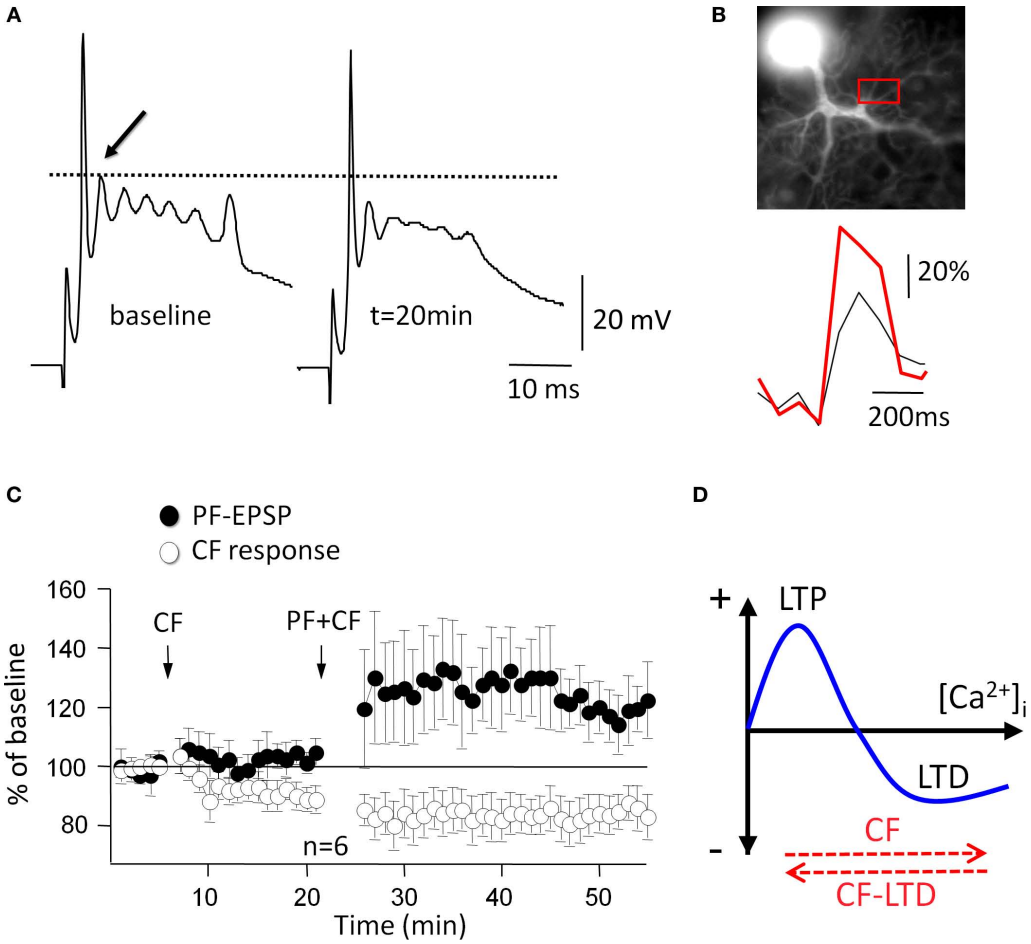

FIGURE 3 | Climbing fiber LTD affects bidirectional parallel fiber plasticity. **(A)** A 5-Hz climbing fiber tetanization for 30 s evokes climbing fiber LTD, which is monitored here as a reduction in the amplitude of the first slow spike component (arrow). **(B)** Climbing fiber LTD is accompanied by a reduction in complex spike-associated calcium transients (red trace: before climbing fiber tetanization). Calcium transients were recorded in the region of interest (red box). Fluorescence signals were monitored using a cooled CCD camera (Quantix, Roper Scientific), and the calcium indicator dye Oregon Green BAPTA-2 (200 μM). **(C)** After induction of climbing fiber LTD (open dots; CF stimulation at 5 Hz, 30 s), subsequent application of the parallel fiber LTD protocol (PF + CF stimulation at 1 Hz, 5 min) induces LTP instead (closed dots). **(D)** 'Inverse' calcium thresholds in the cerebellum: a higher calcium threshold has to be reached for LTD than for LTP induction. Climbing fiber stimulation contributes calcium to reach this higher threshold, whereas climbing fiber LTD lowers the amplitude of this calcium transient (red arrows). **(A)**, **(C)** and **(D)** are modified from Coesmans et al. (2004). Copyright 2004 by Elsevier. **(B)** is modified from Weber et al. (2003). Copyright 2003 by the National Academy of Sciences, USA.

climbing fiber stimulation) remains to be determined. Despite of the existing discrepancies, both Bosman et al. (2008) and Ohtsuki and Hirano (2008) show that bidirectional climbing fiber plasticity exists during postnatal development. These forms of climbing fiber plasticity might be critically involved in the elimination of surplus climbing fibers.

PARALLEL FIBER PLASTICITY UNDER HETEROSYNAPTIC CLIMBING FIBER CONTROL

The classic Marr-Albus-Ito theories of cerebellar motor learning suggest that synaptic plasticity at parallel fiber synapses (the learning site) depends on activity at the heterosynaptic climbing fiber synapses (the instructor site). In agreement with this theoretical framework, Masao Ito and colleagues described in the early 1980s a form of LTD at parallel fiber synapses that is induced following paired parallel fiber and climbing fiber activity (Ito and Kano, 1982; Ito et al., 1982). As first suggested by Albus (Albus, 1971), parallel fiber LTD provides an attractive candidate mechanism for cerebellar motor learning, as it is expected to result in a disinhibition of the target cells of inhibitory Purkinje cell projections in the deep cerebellar nuclei (DCN) or vestibular nuclei.

Parallel fiber LTD induction depends on activation of the mGluR1/PKC signaling cascade (for review see Hansel and Bear, 2008) and activation of the α isoform of calcium/calmodulin-dependent kinase II (αCaMKII; Hansel et al., 2006). Climbing fiber signaling triggers dendritic calcium transients and contributes to parallel fiber LTD induction (Konnerth et al., 1992) by activating these induction cascades. Co-activation of parallel fiber and climbing fiber inputs causes

supralinear calcium signaling in parallel fiber spines (Wang et al., 2000), thus providing a coincidence detection mechanism that might be required to reach a critical calcium threshold for LTD induction. A somewhat puzzling observation has been that strong parallel fiber activation on its own can trigger parallel fiber LTD in the absence of climbing fiber activity (Eilers et al., 1997; Hartell, 1996). Similarly, climbing fiber stimulation can be replaced by somatic depolarization (Linden et al., 1991). These findings suggest that climbing fiber activity indeed facilitates LTD induction by amplifying local calcium transients, but that there is no specific requirement for climbing fiber-evoked calcium signals. This conclusion is supported by recent recordings from cerebellar Purkinje cells of mormyrid fish (introduced above). Parallel fiber stimulation alone at enhanced stimulus strength (increase in the pulse duration) can induce parallel fiber LTD. When the climbing fiber is co-stimulated, however, a lower stimulus strength (as applied to monitor test responses before and after tetanization) is sufficient for LTD induction (Han et al., 2007). These observations suggest that parallel fiber LTD can be induced in the absence of climbing fiber activity, which might nevertheless have an important role in facilitating the induction process.

The impact of climbing fiber signaling on parallel fiber plasticity becomes more obvious when taking LTP into consideration. Both pre- and postsynaptically expressed types of LTP have been described at parallel fiber synapses (Lev-Ram et al., 2002; Salin et al., 1996). LTP can be induced when applying the same low-frequency/low-intensity parallel fiber stimulation protocol used for LTD induction, when climbing fiber stimulation is omitted (Lev-Ram et al., 2002). Just like LTD, this form of LTP is postsynaptically induced and expressed (Coesmans et al., 2004; Lev-Ram et al., 2002) and might therefore function as a reversal mechanism for LTD. LTP induction depends on lower calcium transients than LTD induction (Coesmans et al., 2004; **Figure 3D**), and requires the activation of protein phosphatases PP1, PP2A and PP2B (Belmeguenai and Hansel, 2005). Therefore, at the level of calcium signaling and kinase/phosphatase activation requirements, cerebellar bidirectional synaptic plasticity seems to be governed by induction rules that provide a mirror image of those described at glutamatergic synapses in hippocampal and neocortical pyramidal cells (Jörntell and Hansel, 2006). Moreover, a unique motif in cerebellar plasticity is the heterosynaptic control of parallel fiber plasticity by the climbing fiber input. The efficacy of this control function becomes obvious when looking at the consequences of LTD at the climbing fiber input itself (Hansel and Linden, 2000). Climbing fiber LTD is accompanied by a reduction in complex spike-associated calcium transients (Weber et al., 2003). This reduction in calcium signaling is sufficiently strong to reverse the polarity of parallel fiber plasticity after previous climbing fiber LTD induction (Coesmans et al., 2004). This metaplastic interaction is illustrated in **Figure 3C**: when climbing fiber LTD is induced first, subsequent application of the parallel fiber LTD induction protocol results in LTP induction instead. The most likely explanation for this sign reversal is that climbing fiber LTD reduced the activity-dependent calcium signal below the threshold for LTD induction (**Figure 3D**).

In addition to its role in postsynaptic parallel fiber plasticity, climbing fiber signaling also affects a form of presynaptic parallel fiber LTP that results from brief parallel fiber tetanization (e.g. 8 Hz for 15 s; Salin et al., 1996). Presynaptic parallel fiber LTP is induced by activation of adenylyl cyclase I (Storm et al., 1998), production of cAMP and the subsequent activation of cAMP-dependent protein kinase (PKA; Chen and Regehr, 1997; Salin et al., 1996). More recent observations show that climbing fiber-evoked calcium signaling can trigger the release of endocannabinoids from Purkinje cell dendrites (Brenowitz and Regehr, 2003), which bind to CB1 receptors at parallel fiber terminals and suppress LTP induction by interfering with the adenylyl cyclase/PKA cascade (Van Beugen et al., 2006). It has been suggested that endocannabinoid signaling facilitates the induction of postsynaptic LTD (Safo and Regehr, 2005). The inhibitory action of CB1 receptor activation on presynaptic LTP might well contribute to this facilitation of LTD, assuming that activity-dependent postsynaptic alterations are often accompanied by presynaptic changes. In this scenario, climbing fiber-evoked calcium transients do not only promote postsynaptic LTD, but in addition provide a 'safety lock' mechanism that prevents that presynaptic LTP and postsynaptic LTD occur at the same time (Van Beugen et al., 2006). Under some conditions, coincident parallel fiber activity and retrograde endocannabinoid signaling might even promote the induction of a presynaptic form of LTD (Qiu and Knöpfel, 2009), thus aligning pre-and postsynaptic changes. These recent reports show that the climbing fiber input heterosynaptically affects four forms of parallel fiber plasticity: postsynaptic LTD, postsynaptic LTP, presynaptic LTP, and presynaptic LTD.

THE OTHER CLIMBING FIBER SIGNAL: CORTICOTROPIN-RELEASING FACTOR

The complex spike-associated calcium transients in Purkinje cell dendrites are certainly the best characterized contribution of climbing fiber signaling to cerebellar plasticity. However, it should not be overlooked that climbing fiber activity can additionally result in the release of the neuropeptide corticotropin-releasing factor (CRF) from climbing fiber terminals (Barmack and Young, 1990; Tian and Bishop, 2003). CRF can bind to type 1 and/or type 2 CRF receptors expressed in Purkinje cells. Whereas type 2 CRF receptors are not expressed in spines, type 1 receptors, which are G-protein coupled and lead to the activation of adenylyl cyclase/PKA and PKC pathways (Grammatopoulos et al., 2001), are located in the dendrite across from parallel fiber terminals, and in non-synaptic regions (Swinny et al., 2003). CRF signaling has been shown to be critically involved in parallel fiber LTD induction as the CRF receptor antagonists α-helical CRF-(9-41) (α-h CRF) and astressin prevent LTD (Miyata et al., 1999). Type-1 CRF receptors are not expressed in the dendrite across from climbing fiber terminals (Swinny et al., 2003), and yet climbing fiber LTD is blocked, too, in the presence of astressin (Schmolesky et al., 2007), suggesting that diffusion to adjacent receptors is sufficient. It is possible that CRF signaling facilitates LTD induction at both climbing fiber and parallel fiber synapses by activating the PKC signaling cascade and, at least in the case of climbing fiber LTD, the PKA signaling cascade (Schmolesky et al., 2007). These results show that the climbing fiber input exerts a control function over parallel fiber plasticity not only through the calcium transients associated with complex spike activity, but also by the activity-dependent release of the neuropeptide CRF (**Figure 4**). Moreover, it seems that the same factors involved in parallel fiber LTD (here: high calcium, CRF receptor activation) promote LTD at the climbing fiber input as well.

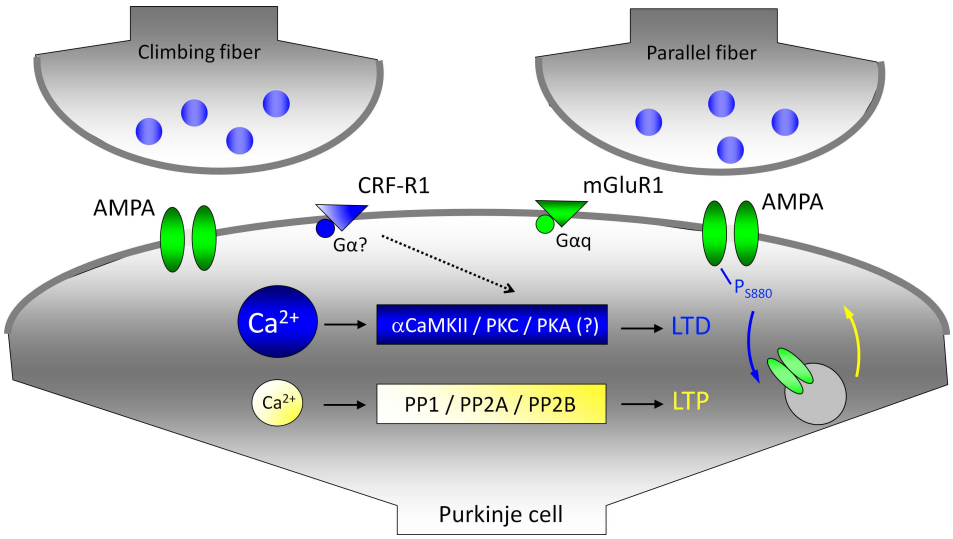

FIGURE 4 | Climbing fiber activity facilitates LTD induction at parallel fiber synapses. For simplicity, climbing fiber and parallel fiber terminals are shown to contact the same postsynaptic compartment. The LTD induction cascade is shown in blue: large calcium transients promote the activation of αCaMKII and PKC. A PKC-mediated phosphorylation of the AMPA receptor subunit GluR2 triggers the internalization of GluR2 subunits. The LTP cascade is shown in yellow: lower calcium transients promote phosphatase activation (only PP2B is directly calcium-regulated). Eventually, GluR2 subunits are delivered to the membrane. Climbing fiber activity facilitates LTD induction by elevating the overall calcium transient (calcium sources are not shown), and by releasing the neuropeptide CRF. CRF binding to type 1 CRF receptors (CRF-R1) facilitates the activation of PKC and PKA. The activation of PKA is a required step for the induction of climbing fiber LTD. It has not been determined yet, whether the same holds true for parallel fiber LTD.

IS CLIMBING FIBER SIGNALING INVOLVED IN CEREBELLAR MOTOR LEARNING?

Numerous studies using genetically modified mice suggest a correlation between parallel fiber LTD and cerebellar motor learning (De Zeeuw and Yeo, 2005). However, LTD has never been demonstrated during motor learning in behaving animals. It has indeed been claimed that parallel fiber LTD might not be involved in motor learning at all, based on the observation that motor learning (eyeblink conditioning) is intact when parallel fiber LTD is pharmacologically inhibited (Welsh et al., 2005). Even if LTD is involved in motor learning, the contribution of the climbing fiber input remains unclear, as LTD can be induced in the absence of climbing fiber activity, as long as the parallel fiber input is sufficiently active (Eilers et al., 1997; Han et al., 2007; Hartell, 1996). Moreover, when reviewing recent developments in cerebellar plasticity research, it becomes obvious that several types of plasticity that have been characterized do not require climbing fiber activity for induction. This holds true for presynaptic LTP (Salin et al., 1996) and postsynaptic LTP (Lev-Ram et al., 2002). Climbing fiber activity is only required for the induction of LTD at both climbing fiber (Hansel and Linden, 2000) and parallel fiber inputs (Ito and Kano, 1982; Ito et al., 1982) as well as for rebound potentiation at interneuron – Purkinje cell synapses (Kano et al., 1992). While climbing fiber activity-dependent parallel fiber LTD has been the predominant model for cerebellar motor learning, these more recently discovered types of plasticity could well be involved in cerebellar learning as well, but are independent of climbing fiber activity.

So what is the role of parallel fiber plasticity, and specially climbing fiber activity-dependent parallel fiber plasticity, in cerebellar motor learning? To slightly clear the fog, it might be useful to take a step back and have a look at the evidence at hand. Granule cells provide massive excitatory input to Purkinje cells via ascending granule cell axons on the one hand, and parallel fiber synapses on the other. These two sets of granule cell input, however, seem to play different roles in cerebellar processing and gain control. Synapses of the ascending axons do not show forms of long-term plasticity (Sims and Hartell, 2006). In contrast, there is a high degree of pre-and postsynaptic plasticity at parallel fiber synapses, but about 85% of these synapses are functionally silent (Isope and Barbour, 2002). It has therefore been suggested that granule cells predominantly activate Purkinje cells through the hardwired ascending axon input, while the parallel fiber input allows for acquired control using fine-tuned recruiting of parallel fiber synapses (Rokni et al., 2008). These observations suggest a high degree of functional specialization of the two different sets of synaptic contacts provided by granule cells, and support the view that the parallel fiber system plays a key role in cerebellar adaptations. But under what conditions does parallel fiber plasticity occur, and what are its functional consequences? A very elegant study has been provided by Jörntell and Ekerot, who showed that parallel fiber receptive fields in adult cats can be bidirectionally modified after parallel fiber stimulation *in vivo* (Jörntell and Ekerot, 2002). Paired parallel fiber and climbing fiber stimulation causes a long-term decrease in the receptive field size of Purkinje cells, while unpaired parallel fiber stimulation causes a lasting increase. While this study provides an example of plasticity of sensory inputs to cerebellar Purkinje cells, without immediately obvious consequences for motor control, there are three aspects that are highly relevant for the present discussion. First, the stimulus

protocols applied suggest that both LTD (paired stimulation) and LTP (unpaired stimulation) phenomena contribute to the decrease and increase, respectively, of the receptive field sizes. If so, this study demonstrates that LTD and LTP are involved in a form of cerebellar learning that can be monitored *in vivo*. Second, this study elegantly shows that LTD and LTP can perfectly complement each other in cerebellar information storage, without the need to classify one as the 'learning' mechanism and the other as a tool used for 'extinction' or 'reversal'. In other words, in some types of cerebellar learning, depression and potentiation simply provide two sides of the same coin, allowing for bidirectional adaptations. Third, this study clearly demonstrates that climbing fiber activity exerts a crucial function in the control of bidirectional cerebellar plasticity. This latter observation is in line with the widespread notion that enhanced climbing fiber activity precedes cerebellar learning, acting as an 'error detector', or as a 'teacher' (for review see Simpson et al., 1996). In this view, climbing fiber activity signals the need for adjusting the gain values of cerebellar sensory inputs and/or motor output control.

CONCLUSION

In a recent paper published in *Frontiers in Neuroscience*, Rodolfo Llinas and Yosef Yarom review the histology and physiology of the cerebellar cortex, concluding that 'the cerebellum should be regarded as a control machine rather than a learning machine' (Rokni et al., 2008). We do not agree with this assessment. In our view, the cerebellum certainly acts as a control machine, but on top of that the cerebellum (particularly the cerebellar cortex) provides a giant switchboard for associative learning. Currently, the existing evidence does not seem to allow for a definite conclusion. Our more learning-biased view results from close inspection of the cerebellar circuitry and its capacity for information storage based on both *in vitro* and *in vivo* studies (see also Hansel et al., 2001; Jörntell and Hansel, 2006). Parallel fiber to Purkinje cell synapses are perfect candidate locations for the storage of motor memories, because of their ability to bidirectionally adjust synaptic gain both pre- and postsynaptically. Although not strictly required, elevated climbing fiber activity facilitates the induction of parallel fiber LTD by enhancing dendritic calcium signals and by releasing the neuropeptide CRF from climbing fiber terminals. Climbing fiber activity also suppresses presynaptic LTP by triggering the release of endocannabinoids from Purkinje cell dendrites. The complexity of this 'orchestration' of parallel fiber plasticity by the climbing fiber input shows after induction of LTD at the climbing fiber input itself: the accompanying reduction in complex spike-associated calcium transients shifts the relative probabilities for the induction of LTD and LTP, respectively, at the parallel fiber input. Plasticity residing at the parallel fiber synapses is likely complemented by additional types of cerebellar plasticity, such as plasticity at inhibitory synapses onto Purkinje cells, and intrinsic plasticity mechanisms found in several types of neurons within the cerebellum. It remains to be seen how the cerebellum puts these features to use, but its underlying circuitry seems very well suited for activity-dependent information storage and learning.

ACKNOWLEDGMENTS

We would like to thank Qionger He for invaluable comments on the manuscript. The authors were supported by a Japanese Society for the Promotion of Science fellowship JSPS 02714 to G.O., a National Institute of Neurological Disorders and Stroke grant NS-62771 to C.H., and a Netherlands Organization for Scientific Research grant NWO-ALW 817-02-013 to C.H.

REFERENCES

Akazawa, C., Shigemoto, R., Bessho, Y., Nakanishi, S., and Mizuno, N. (1994). Differential expression of five N-methyl-D-aspartate receptor subunit mRNAs in the cerebellum of developing and adult rats. *J. Comp. Neurol.* 347, 150–160.

Albus, J. S. (1971). A theory of cerebellar function. *Math. Biosci.* 10, 25–61.

Barmack, N. H., and Young, W. S. (1990). Optokinetic stimulation increases corticotropin-releasing factor mRNA in inferior olivary neurons of rabbits. *J. Neurosci.* 10, 631–640.

Batchelor, A. M., and Garthwaite, J. (1997). Frequency detection and temporally dispersed synaptic signal association through a metabotropic glutamate receptor pathway. *Nature* 385, 74–77.

Belmeguenai, A., and Hansel, C. (2005). A role for protein phosphatases 1, 2A, and 2B in cerebellar long-term potentiation. *J. Neurosci.* 25, 10768–10772.

Bliss, T. V. P., and Collingridge, G. L. (1993). A synaptic model of memory: long-term potentiation in the hippocampus. *Nature* 361, 31–39.

Bosman, L. W., Takechi, H., Hartmann, J., Eilers, J., and Konnerth, A. (2008). Homosynaptic long-term synaptic potentiation of the 'winner' climbing fiber synapse in developing Purkinje cells. *J. Neurosci.* 28, 798–807.

Brasnjo, G., and Otis, T. S. (2001). Neuronal glutamate transporters control activation of postsynaptic metabotropic glutamate receptors and influence cerebellar long-term depression. *Neuron* 31, 607–616.

Brenowitz, S. D., and Regehr, W. G. (2003). Calcium dependence of retrograde inhibition by endocannabinoids at synapses onto Purkinje cells. *J. Neurosci.* 23, 6373–6384.

Carta, M., Mameli, M., and Valenzuela, C. F. (2006). Alcohol potently modulates climbing fiber – Purkinje neuron synapses: role of metabotropic glutamate receptors. *J. Neurosci.* 26, 1906–1912.

Chen, C., and Regehr, W. G. (1997). The mechanism of cAMP-mediated enhancement at a cerebellar synapse. *J. Neurosci.* 17, 8687–8694.

Coesmans, M., Weber, J. T., De Zeeuw, C. I., and Hansel, C. (2004). Bidirectional parallel fiber plasticity in the cerebellum under climbing fiber control. *Neuron* 44, 691–700.

Crépel, F., Mariani, J., and Delhaye-Bouchaud, N. (1976). Evidence for a multiple innervation of Purkinje cells by climbing fibers in the mature rat cerebellum. *J. Neurobiol.* 7, 567–578.

Davie, J. T., Clark, B. A., and Häusser, M. (2008). The origin of the complex spike in cerebellar Purkinje cells. *J. Neurosci.* 28, 7599–7609.

De Zeeuw, C. I., and Yeo, C. H. (2005). Time and tide in cerebellar memory formation. *Curr. Opin. Neurobiol.* 15, 667–674.

Dittman, J. S., and Regehr, W. G. (1998). Calcium dependence and recovery kinetics of presynaptic depression at the climbing fiber to Purkinje cell synapse. *J. Neurosci.* 18, 6147–6162.

Dzubay, J. A., and Otis, T. S. (2002). Climbing fiber activation of metabotropic glutamate receptors on cerebellar Purkinje neurons. *Neuron* 36, 1159–1167.

Eccles, J. C., Llinas, R., and Sasaki, K. (1964). Excitation of cerebellar Purkinje cells by the climbing fibres. *Nature* 203, 245–246.

Eccles, J. C., Llinas, R., and Sasaki, K. (1966). The excitatory synaptic action of climbing fibres on the Purkinje cells of the cerebellum. *J. Physiol.* 182, 268–296.

Eilers, J., Takechi, H., Finch, E. A., Augustine, G. J., and Konnerth, A. (1997). Local dendritic Ca2+ signaling induces cerebellar long-term depression. *Learn. Mem.* 3, 159–168.

Ekerot, C. F., Oscarsson, O., and Schouenborg, J. (1987). Stimulation of cat cutaneous nociceptive C fibres causing tonic and synchronous activity in climbing fibres. *J. Physiol.* 386, 539–546.

Farrant, M., and Cull-Candy, S. G. (1991). Excitatory amino acid receptor-channels in Purkinje cells in thin cerebellar slices. *Proc. R. Soc. Lond. B Biol. Sci.* 244, 179–184.

Grammatopoulos, D. K., Randeva, H. S., Levine, M. A., Kanellopoulou, K. A., and Hillhouse, E. W. (2001). Rat cerebral cortex corticotropin-releasing hormone receptors: evidence for

receptor coupling to multiple G-proteins. *J. Neurochem.* 76, 509–519.

Han, V. Z., Zhang, Y., Bell, C. C., and Hansel, C. (2007). Synaptic plasticity and calcium signaling in Purkinje cells of the central cerebellar lobes of mormyrid fish. *J. Neurosci.* 27, 13499–13512.

Hansel, C., and Linden, D. J. (2000). Long-term depression of the cerebellar climbing fiber – Purkinje neuron synapse. *Neuron* 26, 473–482.

Hansel, C., Linden, D. J., and D'Angelo, E. (2001). Beyond parallel fiber LTD: the diversity of synaptic and non-synaptic plasticity in the cerebellum. *Nat. Neurosci.* 4, 467–475.

Hansel, C., De Jeu, M., Belmeguenai, A., Houtman, S. H., Buitendijk, G. H., Andreev, D., De Zeeuw, C. I., and Elgersma, Y. (2006). αCaMKII is essential for cerebellar LTD and motor learning. *Neuron* 51, 835–843.

Hansel, C., and Bear, M. F. (2008). LTD – Synaptic depression and memory storage. In J. D. Sweatt (Ed.), Molecular Mechanisms of Memory. Vol. [4] of *Learning and Memory: A Comprehensive Reference*, 4 vols, J. Byrne, ed. (Oxford, Elsevier), pp. 327–366.

Hartell, N. A. (1996). Strong activation of parallel fibers produces localized calcium transients and a form of LTD that spreads to distant synapses. *Neuron* 16, 601–610.

Hartmann, J., Dragicevic, E., Adelsberger, H., Henning, H. A., Sumser, M., Abramowitz, J., Blum, R., Dietrich, A., Freichel, M., Flockerzi, V., Birnbaumer, L., and Konnerth, A. (2008). TRPC3 channels are required for synaptic transmission and motor coordination. *Neuron* 59, 392–398.

Hashimoto, K., and Kano, M. (1998). Presynaptic origin of paired-pulse depression at climbing fiber-Purkinje cell synapses in the rat cerebellum. *J. Physiol.* 506, 391–405.

Hollmann, M., Hartley, M., and Heinemann, S. (1991). Ca2+ permeability of KA-AMPA-gated glutamate receptor channels depends on subunit composition. *Science* 252, 851–853.

Isope, P., and Barbour, B. (2002). Properties of unitary granule cell to Purkinje cell synapses in adult rat cerebellar slices. *J. Neurosci.* 22, 9668–9678.

Ito, M., Sakurai, M., and Tongroach, P. (1982). Climbing fibre induced depression of both mossy fibre responsiveness and glutamate sensitivity of cerebellar Purkinje cells. *J. Physiol.* 324, 113–134.

Ito, M., and Kano, M. (1982). Long-lasting depression of parallel fiber-Purkinje cell transmission induced by conjunctive stimulation of parallel fibers and climbing fibers in the cerebellar cortex. *Neurosci. Lett.* 33, 253–258.

Ito, M. (1984). The Cerebellum and Neural Control. New York, Raven Press.

Jörntell, H, and Ekerot, C. F. (2002). Reciprocal bidirectional plasticity of parallel fiber receptive fields in cerebellar Purkinje cells and their afferent interneurons. *Neuron* 34, 797–806.

Jörntell, H., and Hansel, C. (2006). Synaptic memories upside down: bidirectional plasticity at cerebellar parallel fiber-Purkinje cell synapses. *Neuron* 52, 227–238.

Kano, M., Rexhausen, U., Dreessen, J., and Konnerth, A. (1992). Synaptic excitation produces a long-lasting rebound potentiation of inhibitory synaptic signals in cerebellar Purkinje cells. *Nature* 356, 601–604.

Kim, S. J., Kim, Y. S., Yuan, J. P., Petralia, R. S., Worley, P. F., and Linden, D. J. (2003). Activation of TRPC1 cation channel by metabotropic glutamate receptor mGluR1. *Nature* 426, 285–291.

Konnerth, A., Llano, I., and Armstrong, C. M. (1990). Synaptic currents in cerebellar Purkinje cells. *Proc. Natl. Acad. Sci. U.S.A.* 87, 2662–2665.

Konnerth, A., Dreessen, J., and Augustine, G. J. (1992). Brief dendritic calcium signals initiate long-lasting synaptic depression in cerebellar Purkinje cells. *Proc. Natl. Acad. Sci. U.S.A.* 89, 7051–7055.

Lachamp, P., Balland, B., Tell, F., Baude, A., Strube, C., Crest, M., and Kessler, J. P. (2005). Early expression of AMPA receptors and lack of NMDA receptors in developing rat climbing fibre synapses. *J. Physiol.* 564, 751–763.

Lev-Ram, V., Wong, S. T., Storm, D. R., and Tsien, R. Y. (2002). A new form of cerebellar long-term potentiation is postsynaptic and depends on nitric oxide, but not cAMP. *Proc. Natl. Acad. Sci. U.S.A.* 99, 8389–8393.

Linden, D. J., Dickinson, M. H., Smeyne, M., and Connor, J. A. (1991). A long-term depression of AMPA currents in cultured cerebellar Purkinje neurons. *Neuron* 7, 81–89.

Llano, I., Marty, A., Armstrong, C. M., and Konnerth, A. (1991). Synaptic- and agonist-induced excitatory currents of Purkinje cells in rat cerebellar slices. *J. Physiol.* 434, 183–213.

Llinas, R., and Sugimori, M. (1980). Electrophysiological properties of in vitro Purkinje cell dendrites in mammalian cerebellar slices. *J. Physiol.* 305, 197–213.

Loewenstein, Y., Mahon, S., Chadderton, P., Kitamura, K., Sompolinsky, H., Yarom, Y., and Häusser, M. (2005). Bistability of cerebellar Purkinje cells modulated by sensory stimulation. *Nat. Neurosci.* 8, 202–211.

Lohof, A. M., Delhaye-Bouchaud, N., and Mariani, J. (1996). Synapse elimination in the central nervous system: functional significance and cellular mechanisms. *Rev. Neurosci.* 7, 85–101.

Marr, D. (1969). Theory of cerebellar cortex. *J. Physiol.* 202, 437–470.

Maruta, J., Hensbroek, R. A., and Simpson, J. I. (2007). Intraburst and interburst signaling by climbing fibers. *J. Neurosci.* 27, 11263–11270.

Miyakawa H., Lev-Ram, V., Lasser-Ross, N., and Ross, W. N. (1992). Calcium transients evoked by climbing fiber and parallel fiber synaptic inputs in guinea pig cerebellar Purkinje neurons. *J. Neurophysiol.* 68, 1178–1189.

Miyata, M., Okada, D., Hashimoto, K., Kano, M., and Ito, M. (1999). Corticotropin-releasing factor plays a permissive role in cerebellar long-term depression. *Neuron* 22, 763–775.

Momiyama, A., Feldmeyer, D., and Cull-Candy, S. G. (1996). Identification of a native low-conductance NMDA channel with reduced sensitivity to Mg2+ in rat central neurones. *J. Physiol.* 494, 479–492.

Montell, C., Birnbaumer, L., and Flockerzi, V. (2002). The TRP channels, a remarkably functional family. *Cell* 108, 595–598.

Monyer, H., Sprengel, R., Schoepfer, R., Herb, A., Higuchi, M., Lomeli, H., Burnashev, N., Sakmann, B., and Seeburg, P. H. (1992). Heteromeric NMDA receptors: molecular and functional distinction of subtypes. *Science* 256, 1217–1221.

Monyer, H., Burnashev, N., Laurie, D. J., Sakmann, B., and Seeburg, P. H. (1994). Developmental and regional expression in the rat brain and functional properties of four NMDA receptors. *Neuron* 12, 529–540.

Moriyoshi, K., Masu, M., Ishii, T., Shigemoto, R., Mizumo, N., and Nakanishi, S. (1991). Molecular cloning and characterization of the rat NMDA receptor. *Nature* 354, 31–37.

Ohtsuki, G., and Hirano, T. (2008). Bidirectional plasticity at developing climbing fiber-Purkinje neuron synapses. *Eur. J. Neurosci.* 28, 2393–2400.

Palay, S. L., and Chan-Palay, V. (1974). Cerebellar Cortex. New York, Springer.

Perkel, D. J., Hestrin, S., Sah, P., and Nicoll, R. A. (1990). Excitatory synaptic currents in Purkinje cells. *Proc. R. Soc. Lond. B Biol. Sci.* 241, 116–121.

Petralia, R., Yokotani, N., and Wenthold, R. (1994). Light and electron miscroscope distribution of the NMDA receptor subunit NMDAR1 in the rat nervous system using a selective anti-peptide antibody. *J. Neurosci.* 14, 667–696.

Piochon, C., Irinopoulou, T., Brusciano, D., Bailly, Y., Mariani, J., and Levenes, C. (2007). NMDA receptor contribution to the climbing fiber response in the adult mouse Purkinje cell. *J. Neurosci.* 27, 10797–10809.

Qiu, D. L., and Knöpfel, T. (2009). Presynaptically expressed long-term depression at cerebellar parallel fiber synapses. *Pflugers Arch.* 457, 865–875.

Ramón y Cajal, S. (1911). Histologie du système nerveux de l'homme et des vertébrés, Vol. II. Paris, Maloine.

Renzi, M., Farrant, M., and Cull-Candy, S. G. (2007). Climbing fibre activation of NMDA receptors in Purkinje cells of adult mice. *J. Physiol.* 585.1, 91–101.

Rokni, D., Llinas, R., and Yarom, Y. (2008). The morpho/functional discrepancy in the cerebellar cortex: looks alone are deceptive. *Front. Neurosci.* 2, 192–198.

Rokni, D., and Yarom, Y. (2009). State-dependence of climbing fiber-driven calcium transients in Purkinje cells. *Neuroscience.* doi: 10.1016/J.Neuroscience.2008.12.044. [Epub ahead of print].

Ross, W. N., and Werman, R. (1987). Mapping calcium transients in the dendrites of Purkinje cells from the guinea-pig cerebellum in vitro. *J. Physiol.* 389, 319–336.

Safo, P. K., and Regehr, W. G. (2005). Endocannabinoids control the induction of cerebellar LTD. *Neuron* 48, 647–659.

Salin, P. A., Malenka, R. C., and Nicoll, R. A. (1996). Cyclic AMP mediates a presynaptic form of LTP at cerebellar parallel fiber synapses. *Neuron* 16, 797–803.

Scelfo, B., Strata, P., and Knöpfel, T. (2003). Sodium imaging of climbing fiber innervation fields in developing mouse Purkinje cells. *J. Neurophysiol.* 89, 2555–2563.

Schmolesky, M. T., Weber, J. T., De Zeeuw, C. I., and Hansel, C. (2002). The making of a complex spike: ionic composition and plasticity. *Ann. N. Y. Acad. Sci.* 978, 359–390.

Schmolesky, M. T., De Zeeuw, C. I., and Hansel, C. (2005). Climbing fiber synaptic plasticity and modifications in Purkinje cell excitability. *Prog. Brain Res.* 148, 81–94.

Schmolesky, M. T., De Ruiter, M. M., De Zeeuw, C. I., and Hansel, C. (2007). The neuropeptide corticotropin-releasing factor regulates excitatory transmission and plasticity at the climbing fibre – Purkinje

cell synapse. *Eur. J. Neurosci.* 25, 1460–1466.

Schonewille, M., Khosrovani, S., Winkelman, B. H., Hoebeek, F. E., De Jeu, M. T., Larsen, I. M., Van den Burg, J., Schmolesky, M. T., Frens, M. A., and De Zeeuw, C. I. (2006). Purkinje cells in awake behaving animals operate at the upstate membrane potential. *Nat. Neurosci.* 9, 459–461.

Shen, Y., Hansel, C., and Linden, D. J. (2002). Glutamate release during LTD at cerebellar climbing fiber – Purkinje cell synapses. *Nat. Neurosci.* 5, 725–726.

Silver, R. A., Momiyama, A., and Cull-Candy S. G. (1998). Locus of frequency-dependent depression identified with multiple-probability fluctuation analysis at rat climbing fiber-Purkinje cell synapses. *J. Physiol.* 510, 881–902.

Simpson, J. I., Wylie, D. R., and De Zeeuw, C. I. (1996). On climbing fiber signals and their consequence(s). *Behav. Brain Sci.* 19, 384–398.

Sims, R. E., and Hartell, N. A. (2006). Differential susceptibility to synaptic plasticity reveals a functional specialization of ascending axon and parallel fiber synapses to cerebellar Purkinje cells. *J. Neurosci.* 26, 5153–5159.

Storm, D. R., Hansel, C., Hacker, B., Parent, A., and Linden, D. J. (1998). Impaired cerebellar long-term potentiation in type I adenylyl cyclase mutant mice. *Neuron* 20, 1199–1210.

Strata, P., and Rossi, F. (1998). Plasticity of the olivocerebellar pathway. *Trends Neurosci.* 21, 407–413.

Stuart, G., and Häusser, M. (1994). Initiation and spread of sodium action potentials in cerebellar Purkinje cells. *Neuron* 13, 703–712.

Sugihara, I. (2005). Microzonal projection and climbing fiber remodeling in single olivocerebellar axons of newborn rats at postnatal days 4–7. *J. Comp. Neurol.* 487, 93–106.

Swinny, J. D., Kalicharan, D., Blaauw, E. H., Ijkema-Paassen, J., Shi, F., Gramsbergen, A., and van der Want, J. J. (2003). Cotricotropin-releasing factor receptor types 1 and 2 are differentially expressed in pre- and postsynaptic elements in the post-natal developing rat cerebellum. *Eur. J. Neurosci.* 18, 549–562.

Thompson, C. L., Drewery, D. L., Atkins, H. D., Stephenson, F. A., and Chazot, P. L. (2000). Immunohistochemical localization of N-methyl-D-aspartate receptor NR1, NR2A, NR2B and NR2C/D subunits in the adult mammalian cerebellum. *Neurosci. Lett.* 283, 85–88.

Tian, J. B., and Bishop, G. A. (2003). Frequency-dependent expression of corticotropin releasing factor in the rat's cerebellum. *Neuroscience* 121, 363–377.

Usowicz, M. M., Sugimori, M., Cherksey, B., and Llinas, R. (1992). P-type calcium channels in the somata and dendrites of adult cerebellar Purkinje cells. *Neuron* 9, 1185–1199.

Van Beugen, B. J., Nagaraja, R. Y., and Hansel, C. (2006). Climbing fiber-evoked endocannabinoid signaling heterosynaptically suppresses presynaptic cerebellar long-term potentiation. *J. Neurosci.* 26, 8289–8294.

Wang, S. S. H., Denk, W., and Häusser, M. (2000). Coincidence detection in single dendritic spines mediated by calcium release. *Nat. Neurosci.* 3, 1266–1273.

Watanabe, M., Mishina, M., and Inoue Y. (1994). Distinct spatiotemporal expressions of five NMDA receptor channel subunit mRNAs in the cerebellum. *J. Comp. Neurol.* 343, 513–519.

Watanabe, S., Takagi, H., Miyasho, T., Inoue, M., Kirino, Y., Kudo, Y., and Miyakawa, H. (1998). Differential roles of two types of voltage-gated Ca^{2+} channels in the dendrites of rat cerebellar Purkinje neurons. *Brain Res.* 791, 43–55.

Weber, J. T., De Zeeuw, C. I., Linden, D. J., and Hansel, C. (2003). Long-term depression of climbing fiber-evoked calcium transients in Purkinje cell dendrites. *Proc. Natl. Acad. Sci. U.S.A.* 100, 2878–2883.

Welsh, J. P., Yamaguchi, H., Zeng, X. H., Kojo, M., Nakada, Y., Takagi, A., Sugimori, M., and Llinas, R. R. (2005). Normal motor learning during pharmacological prevention of Purkinje cell long-term depression. *Proc. Natl. Acad. Sci. U.S.A.* 102, 17166–17171.

Yamada, K., Fukaya, M., Shimizu, H., Sakimura, K., and Watanabe, M. (2001). NMDA receptor subunits GluRepsilon1, GluRepsilon3 and GluRzeta 1 are enriched at the mossy fiber-granule cell synapse in the adult mouse cerebellum. *Eur. J. Neurosci.* 13, 2025–2036.

Yuan, Q., Qiu, D. L., Weber, J. T., Hansel, C., and Knöpfel, T. (2007). Climbing fiber-triggered metabotropic slow potentials enhance dendritic calcium transients and simple spike firing in cerebellar Purkinje cells. *Mol. Cell. Neurosci.* 35, 596–603.

Conflict of Interest Statement: The authors declare that the research was conducted in the absence of any commercial or financial relationships that could be construed as a potential conflict of interest.

Received: 11 March 2009; paper pending published: 31 March 2009; accepted: 09 June 2009; published online: 06 July 2009.
Citation: Ohtsuki G, Piochon C and Hansel C (2009) Climbing fiber signaling and cerebellar gain control. Front. Cell. Neurosci. (2009) ***3****:4. doi:10.3389/neuro.03.004.2009*

frontiers in
CELLULAR NEUROSCIENCE

ORIGINAL RESEARCH ARTICLE
published: 10 August 2009
doi: 10.3389/neuro.03.007.2009

Climbing fiber coupling between adjacent Purkinje cell dendrites *in vivo*

***Fredrik Bengtsson*[1]* and *Henrik Jörntell*[1,2]**

[1] *Division for Neuroscience, Lund University, Lund, Sweden*
[2] *Neuronano Research Center, Lund University, Lund, Sweden*

Edited by:
Egidio D'Angelo, University of Pavia, Italy

Reviewed by:
Yosef Yarom, Hebrew University, Israel
Egidio D'Angelo, University of Pavia, Italy

***Correspondence:**
Fredrik Bengtsson, Department for Experimental Medical Science, Division for Neuroscience, Lund University, BMC F10, Tornavägen 10, SE-221 84 Lund, Sweden.
e-mail: fredrik.bengtsson@med.lu.se

Climbing fiber discharges within the rat cerebellar cortex have been shown to display synchrony, especially for climbing fibers terminating in the same parasagittal bands. In addition, Purkinje cells which have the smallest rostrocaudal separation also seem to have the highest degree of synchrony. But this has so far only been investigated for distances down to 250 μm. In the present study, we wanted to investigate whether Purkinje cells that are located immediately next to each other display a particularly pronounced synchrony in their climbing fiber discharges. To this end, we used a previously undescribed type of electrophysiological recording, a single electrode, loose patch, dual dendritic recording, from pairs of adjacent Purkinje cells in the decerebrated, non-anesthetized cat. From each recorded dendrite, this technique provided well isolated, unitary calcium spikes, which we found to have a spontaneous activity that was essentially identical with the pattern of spontaneous climbing fiber discharges. By calculating the coupling in firing between the adjacent dendrites, we found that most climbing fiber responses occurred independently of each other and that the probability of coupled discharges was less than 8%. These values are comparable to those obtained in previous studies for Purkinje cells located within the same parasagittal band and show that climbing fiber coupling within a microzone exists also in non-rodent mammalian species. However, since the degree of synchrony of climbing fiber discharge was not particularly pronounced in adjacent Purkinje cells, it seems unlikely that climbing fiber synchrony has pronounced systematic regional variations within the same microzone.

Keywords: climbing fibers, synchrony, electrotonic coupling, Purkinje cells, inferior olive

INTRODUCTION

Inferior olivary (IO) neurons are connected to each other with gap junctions (Llinas et al., 1974), which makes them electrotonically coupled (Devor and Yarom, 2002; Llinas and Yarom, 1981; Placantonakis et al., 2006). The coupling provides a mechanism by which IO neurons may become synchronized in their output. This has been shown to occur in numerous studies in which the synchrony of climbing fiber (CF) discharges have been investigated with recordings of CF responses in Purkinje cells (PCs) of the cerebellar cortex (De Zeeuw et al., 1997; Flusberg et al., 2008; Lang et al., 1999; Ozden et al., 2008; Welsh et al., 1995). Interestingly, the synchronization has been reported to preferentially occur in narrow sagittal bands (De Zeeuw et al., 1997; Lang et al., 1999) suggesting that synchronization may primarily be a property of the IO neurons that project to the same microzone of the cerebellar cortex.

Microzones are extremely narrow sagittal bands of the cerebellar cortex, which can extend over several folia. A microzone is defined as an area in which the PCs receive CF input activated from exactly the same peripheral receptive field (Andersson and Oscarsson, 1978; Ekerot et al., 1991). They run primarily in the parasagittal direction, but can be interleaved in patterns that are not purely parasagittal (Ekerot et al., 1991). The morphological underpinnings of the microzonal organization are that individual IO cells diverge to innervate 5–10 PCs which all are located in a very narrow sagittal band (Sugihara et al., 2001) and that different IO neurons projecting the same microzone can be found in the same small part of the IO (Garwicz et al., 1996; Sugihara et al., 2007).

Importantly, the PCs of a single microzone innervates the same restricted area of the cerebellar nucleus (Apps and Garwicz, 2005; Garwicz and Ekerot, 1994; Garwicz et al., 1996), which has a motor output that is functionally specific to the CF receptive field of the afferent PCs (Ekerot et al., 1995; Jorntell and Ekerot, 1999). Therefore, the microzones, together with their corticonuclear target cells and olivocerebellar afferent neurons, may be regarded as the smallest functional units of the cerebellum, which has been termed microcomplexes (see Apps and Garwicz, 2005).

Interestingly, within a microzone, PCs with the smallest rostrocaudal separation also seem to have the highest degree of synchrony. This is true at least down to distances of 250 μm, which is the resolution defined by the physical constraints of the multi-electrode arrays used to obtain the data (Lang et al., 1999; Sugihara et al., 2007). Since anatomical studies suggest that the most closely located IO neurons have the highest chance of providing the most closely spaced olivocortical terminations within the microzone (Garwicz et al., 1996; Sugihara et al., 2007), it is thus possible that the highest degree of CF synchronization may be found for adjacent PCs. The correlation between (several) adjacent PCs was also studied in two recent papers describing PC dendritic calcium transients

using optical methods (Flusberg et al., 2008; Ozden et al., 2008). However, in these studies the temporal resolution was limited to 50–256 ms. Hence, many additional mechanisms in addition to the gap junction couplings may account for the observed synchrony. Here we use the higher temporal resolution that can be achieved in electrophysiological recordings of two adjacent PC dendrites to limit our analysis to the time window during which gap junction coupling may occur. Another purpose of our study was to investigate if the IO neuron synchrony observed in rodents is demonstrable also in the cat.

MATERIALS AND METHODS

PREPARATION

Adult cats were prepared as previously described. Briefly, following an initial anesthesia with propofol (Diprivan® Zeneca Ltd, Macclesfield Cheshire, UK), the animals were decerebrated at the intercollicular level and the anesthesia was discontinued. The animals were artificially ventilated and the end-expiratory CO_2, blood pressure and rectal temperature were continuously monitored and maintained within physiological limits. Mounting in a stereotaxic frame, drainage of cerebrospinal fluid, pneumothorax and clamping the spinal processes of a few cervical and lumbar vertebral bodies served to increase the mechanical stability of the preparation. Our EEG recordings were characterized by a background of periodic 1–4 Hz oscillatory activity, periodically interrupted by large-amplitude 7–14 Hz spindle oscillations lasting for 0.5 s or more. These forms of EEG activities are normally associated with deep stages of sleep. The pattern of EEG activity and the blood pressure remained stable, also on noxious stimulation, throughout experiments.

RECORDINGS AND STIMULATION

The initial delineation of the forelimb area of the C3 zone in the cerebellar anterior lobe and the continuous monitoring of the general condition in the sensitive mossy fiber-to-granule cell-to-parallel fiber pathway were performed as described previously.

In vivo patch clamp recordings, loose patch (Stuhmer et al., 1983) and whole cell recordings, were made from PC dendrites in the upper 2/3 of the superficial molecular layer accessible from the surface with patch pipettes pulled to 6–14 MOhm (potassium-gluconate based internal solution) on a Sutter micropipette puller (P-97, Sutter Instruments Co., USA). Loose patch dendritic recordings were obtained on a routine basis as a result of failed attempts to obtain giga-Ohm seals on PC dendrites (for more details on our standard methods to obtain *in vivo* patch clamp recordings, see Jorntell and Ekerot, 2006). Non-invasive patch recordings in the current clamp mode has previously been demonstrated to provide a reasonable reflection of the major transmembrane potentials (Mason et al., 2005). The present analysis was confined to rare cases in which two distinct dendritic spikes could be detected in the recordings. The example of the morphologically recovered PC (**Figure 1**) was obtained from an intracellular PC dendritic recording in the whole cell mode in which the recording solution contained 1.5% neurobiotin (see Bengtsson and Jorntell, 2009; Jorntell and Ekerot, 2006). Extracellular metal electrode recordings (exposed metal tips 3–15 μm) were also made from PCs in the PC layer.

The IO was accessed with a tungsten-in-glass electrode inserted through the vermis at a perpendicular angle relative to the stereotaxic horizontal plane, just caudal to the primary fissure. This electrode was then used to stimulate the IO. The position of the electrode was confirmed to have an appropriate location within the IO as thresholds for evoking CF responses in the C3 zone (measured with surface ball electrodes) always were below 20 μA.

ANALYSIS

Using home-made software and the Data Translation 3010 A/D-board, all recordings were continuously sampled and digitized at 100 kHz. Off-line analysis of dendritic spike times was made in another home-made program.

For calculations of spike-coupling, one of the two spikes recorded were set as the trigger. The software then identified the relative times of the other spike over a 2-s time window that straddled the trigger spike. When the two spikes coincided or nearly coincided, the time was determined by close inspection of the trace. Typically, when spikes partly overlapped in time, the start point of a spike was still easy to identify by a distinct break of the normal time course of the other spike (**Figure 1E**). The procedure was repeated for every trigger spike encountered and a frequency distribution histogram of the spike times of non-trigger spike was created. From these histograms, we subtracted the baseline activity. The remaining number of spikes in time bins 0.0–4.9 and 5.0–9.9 ms were summed and divided by the number of trigger spikes and the result was considered the spike coupling.

All data are given as mean ± standard error of the mean (SEM).

All experiments were approved in advance by the local Swedish Animal Ethics Committee.

RESULTS

PROPERTIES OF DOUBLE LOOSE PATCH DENDRITIC PURKINJE CELL RECORDINGS

In the present study, we used single patch clamp electrodes to obtain double loose patch dendritic recordings in the current clamp mode from two different PCs simultaneously. Double loose patch dendritic recordings were only obtained in preparations that were highly mechanically stable. Double loose patch recordings were typically obtained as a side effect of failed attempts to establish a giga-Ohm seal on a single PC dendrite, and seemed to be facilitated by the application of negative pressure in the patch clamp electrode. However, double loose patch dendritic recordings were extremely rare to get and those we report represent a set obtained during a long series of investigations dedicated to obtain whole cell recordings from interneurons (Jorntell and Ekerot, 2003) and PC dendrites.

The seal resistance of the double loose patch dendritic recordings were 190 ± 44 MOhm ($N = 7$). Although the membrane resistance of PC dendrites *in vivo* has not been reported, our preliminary data indicate that it is typically well below 40 MOhm. In other words, the seal resistance in the loose patch dendritic recordings were at least five times higher than the membrane input resistance. Under such conditions it has been shown that steady-state and dynamic changes in transmembrane potential can be recorded, although the potentials are attenuated in amplitude and a minor additional

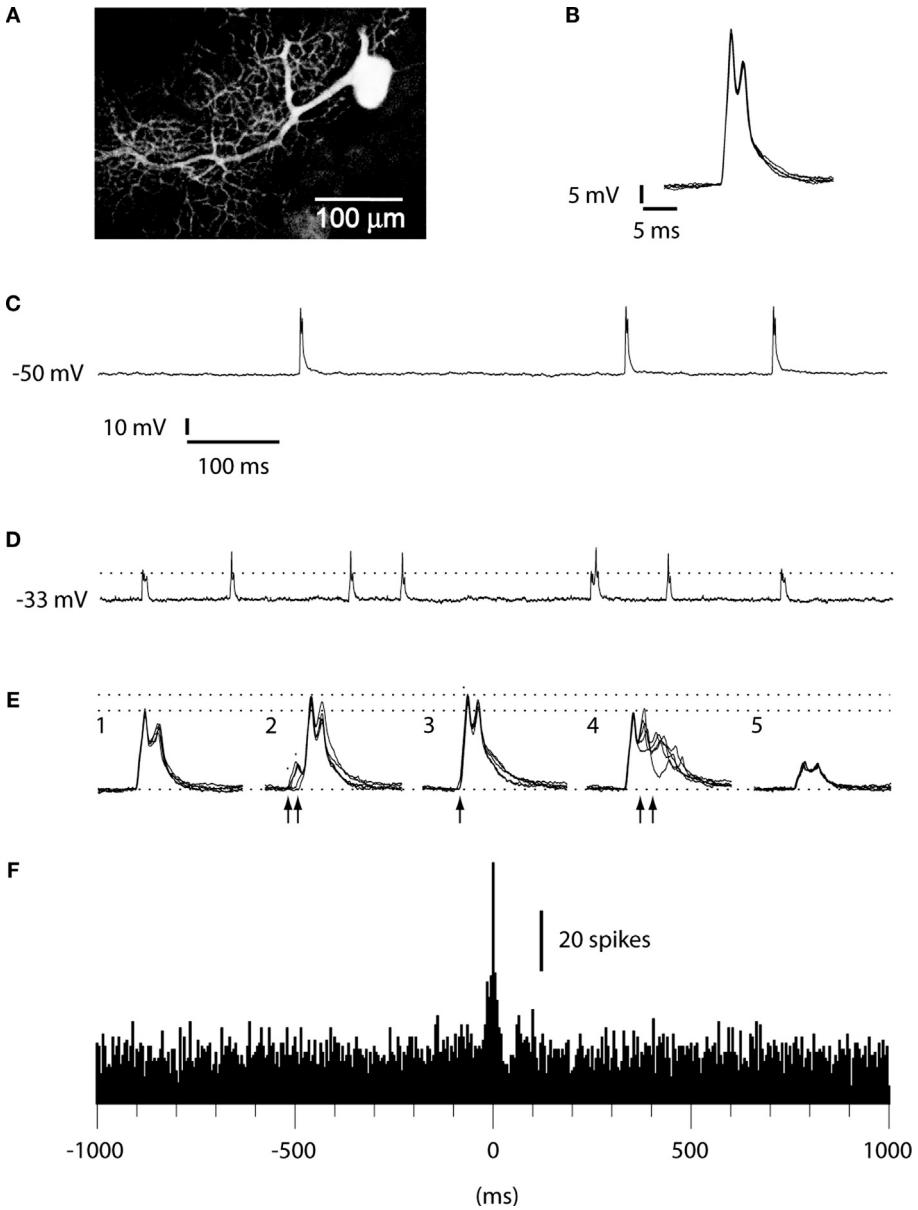

FIGURE 1 | Intradendritic versus loose patch dendritic recordings. (A) PC dendrite and soma, partially reconstructed after recording in the whole cell (intracellular) mode with neurobiotin in the pipette solution. **(B)** Superimposed dendritic spikes from the intracellular recording. Membrane potential, recorded with 0 pA bias current, as in **(C)**. **(C)** Long sweep illustrating the constant amplitude of the dendritic spike. **(D)** Long sweep of a double loose patch dendritic recording. Dashed line indicates the peak amplitude of the smaller of the units. Calibrations as in **(C)**. **(E)** Superimposed dendritic spikes. The dashed lines indicate the peak amplitudes of the largest unit in isolation and during coincident activation with the smaller unit, respectively. (E1 and E5) Superimposed spikes of the two dendritic spike units in isolation. (E2) Recorded response when the onset of the small unit (arrows) barely preceded the large unit. (E3) Recorded response when the small and large units coincided in time. (E4) Recorded response when the small unit was activated after the larger unit. **(F)** Histogram of cross-correlated activity with the spike times of the larger unit serving as the 'trigger' against which the relative spike times of the smaller unit were plotted. Bin width: 5 ms.

time constant is added to the recorded signal (Mason et al., 2005). According to the data of (Mason et al., 2005), the recorded DC potential with a ratio between the seal and membrane resistance of 5 should be in the range of 60–90% of the actual membrane potential. In our double loose patch dendritic recordings the DC potential was -35 ± 7 mV ($N = 7$), which corresponded to more than half of the membrane potential recorded intracellularly in the dendrites under whole cell mode (−50 to −52 mV).

According to the data of (Mason et al., 2005, Equation 4 in that paper), the additional time constant obtained in loose patch recordings is also determined by the relationship between the membrane resistance and the seal resistance. In cases like ours, with the seal resistance being five times higher than the membrane resistance, the time constant of the recorded signal would be expected to increase by 20% as compared to the signal that would have been recorded in the whole cell mode. This is a marginal change which

is compatible with the observation that for the larger of the two dendritic spikes recorded the time-course was not obviously different from the dendritic spikes recorded in the whole cell mode (**Figures 1, 3 and 4**).

However, for the smaller dendritic spike in the pair, the attenuation was more obvious, with a partial obliteration of the spikelets on top of the dendritic spike (see below). Since the amplitude of the smaller spike was much smaller than the larger spike, we may assume that the seal resistance with the former may actually be much lower than the seal resistance with the latter. According to (Mason et al., 2005), the time constant of the recording will increase to double that of the cell when the seal resistance and cell resistance decreases to unity. This would then suggest that the seal resistance (and DC potential) we recorded were dominated by the interaction between the electrode and the larger of the two dendritic units whereas the seal resistance with the smaller of the two units was much lower, which can explain the lower amplitude of the spikelets in the latter.

COMPARISON WITH INTRACELLULAR DENDRITIC RECORDINGS

To verify that the double loose patch dendritic recordings were from the dendrites of two independent PCs, we compared their activity with that of PC dendrites recorded intracellularly and with that of CF responses in somatic PC recordings. During the course of the collection of the data reported here, we have obtained approximately 100 intracellular PC dendritic recordings, which will be described in detail in a separate paper under preparation. However, since they are an important tool to demonstrate that the dual dendritic loose patch recordings really represented the activity of two independent PC dendrites, we report some of their basic characteristics here. The spontaneous activity of intracellularly recorded PC dendrites was dominated by the spontaneously active and relatively stereotyped slow spikes, often with 1–2 spikelets riding on the top (**Figure 1**). Comparison with previous *in vitro* studies indicates that these spikelets were most likely calcium spikes whereas the underlying 'spike' was likely the CF EPSP (Callaway et al., 1995). Importantly, in all intracellular dendritic recordings we obtained with the whole cell technique, the amplitude of the spontaneous dendritic spikes was similar and there were no partial or intermediate-sized events (**Figure 1C**).

The double loose patch dendritic recordings differed from the intracellular recordings by showing spikes of two different amplitudes (**Figure 1D**). Importantly, when these spikes coincided in time, the resulting spike simply represented the sum of the two events, which made it possible to separate the two units even when they occurred exactly at the same time (**Figure 1E**). This circumstance made it possible to construct cross-correlograms of the activity of the two spikes (**Figure 1F**)

All dendritic recordings used in the present study were obtained in the upper 2/3 of the molecular layer and were hence free from somatic sodium spikes, which are known to propagate passively from the soma up to the most proximal parts of the proximal dendrites (Stuart and Hausser, 1994).

COMPARISON OF THE ACTIVITY OF THE SPONTANEOUS DENDRITIC SPIKES WITH CLIMBING FIBER RESPONSES

The spontaneous activity of dendritic spikes, recorded in whole cell mode and in dual dendritic-attached mode, was in principle identical to that of the complex spikes recorded extracullarly in the PC layer (**Figure 2**). All three types of recordings were characterized by a low spontaneous firing frequency, an extremely broad distribution of interspike intervals and a near complete absence of interspike intervals shorter than 50 ms. The shortest interspike intervals recorded were 52 ± 1.6 ms ($N = 14$) for loose patch dendritic recordings and 56 ± 2.8 ms ($N = 12$) for complex spikes recordings, again very similar values (all data based on 400–4000 spike intervals). Mean unitary firing frequency for the loose patch dendritic recordings was 2.8 ± 0.13 Hz and 2.7 ± 0.14 Hz for the complex spikes ($P = 0.46$ students *t*-test). We compared these values with those obtained from extracellular recordings of molecular layer interneurons (cf. Ekerot and Jorntell, 2001, 2003; Jorntell and Ekerot, 2002). For this type of unit, the average spontaneous firing frequency was considerably higher (14.2 ± 3.4 Hz, $N = 10$) and at

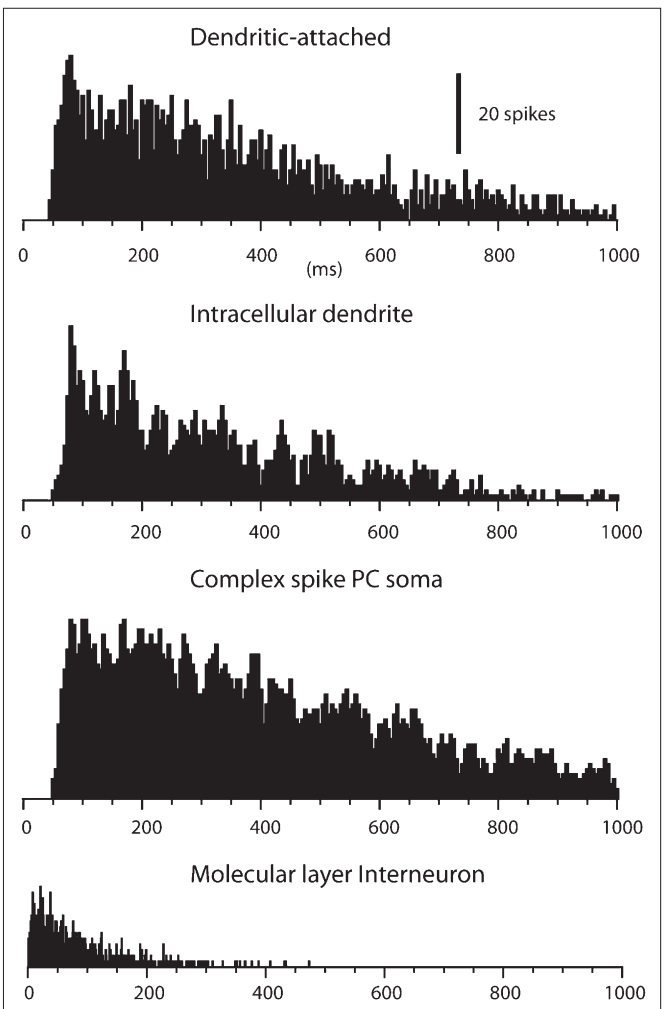

FIGURE 2 | Spike interval-frequency histograms for dendritic and complex spikes. From the top, this figure shows the spike interval-histograms of a single unit dendritic spike, extracted from a double loose patch dendritic recording, of a dendritic spike in an intradendritic recording, and of a complex spike in a PC soma recorded extracellularly with a metal electrode. For comparison, the lowermost histogram plots the spike interval distribution of a molecular layer interneuron. Bin widths, 5 ms, except in lowermost histogram, which has a bin width of 1 ms.

least 50% of the interspike intervals were shorter than 50 ms in all cases. Hence we conclude that the spikes that can be recorded in loose patch dendritic and intracellular recordings are likely to correspond to the CF response of the PC dendrite.

DENDRITIC SPIKES ARE EVOKED BY CLIMBING FIBERS IN AN ALL-OR-NONE FASHION

In addition, we also investigated the activation of dendritic spikes using electrical stimulation within the IO. In the population of the dendritic recordings, electrical stimulation in the IO evoked spike responses with a single threshold. In addition, IO stimulation always evoked the dendritic spike in an all-or-none fashion ($N = 53$, Intracellular and loose patch dendritic recordings). This is shown for a double loose patch dendritic recording in **Figure 3**. Importantly, in the three cases tested for the double loose patch dendritic recordings, the threshold for the two dendritic spikes were identical (with 5 μA resolution), in line with the suggestion that IO neurons projecting to adjacent parts of the cerebellar cortex is located nearby each other in the IO.

COUPLING BETWEEN DENDRITIC SPIKE PAIRS

Figure 4 illustrates the cross-correlograms and the calculated coupling between two dendritic units recorded simultaneously in a single-electrode double loose patch dendritic recording. This method differs somewhat from previous investigations, which focused on CF synchrony within ±1 ms of the 'master' cell (Lang et al., 1999; Sugihara et al., 2007). Instead, in order to provide a more complete measure of coupling, where the discharge of one IO cell leads the discharge of an adjacent IO cell, we measured the probability with which the discharge of one IO cell was followed by a discharge in its putative neighbor within a time window of 0–10 ms (**Figure 4C**). This can be motivated by the fact that the time constant of the electrotonic coupling between IO neurons and the long duration of the IO action potential result in that the peak depolarization in an IO neuron is reached in the order of 5–10 ms after the occurrence of the spike in the coupled neuron (Devor and Yarom, 2002; Llinas and Yarom, 1981). From our recordings, we found that most of the spike couplings between a pair of dendritic spikes were observed at about 2–7 ms, whereas the number of exact coincidences (i.e. at 0–1 ms) was comparatively much lower (in the order of 10% of the total number of the spikes that were defined as triggered by the other dendrite's spike). Mean baseline activity was subtracted and the sum of the remains in the two bins (**Figure 4C**) were divided by the number of 'trigger' spikes. Measured in this way, the coupling between adjacent dendritic spikes was $7.7 \pm 0.9\%$ ($N = 14$).

It can be noted that in this case, the spikes tended to be activated in an oscillatory pattern (**Figure 4B**). Such patterns were not observed for all dendritic pairs (cf. **Figure 1C**) and were not analyzed further.

DISCUSSION

Using a not previously described type of recording, the single-electrode double loose patch dendritic recording, we investigated the degree of CF coupling in pairs of adjacent PC dendrites. We found that the coupling was not particularly strong, less than 8% of the CF discharges of one dendrite were coupled to the CF discharges of an adjacent dendrite. These values were essentially similar to those found for PC pairs located within 250–500 μm in the same sagittal axis of rodents (Lang et al., 1999). Hence, the findings indicate that spike coupling between IO neurons exist in

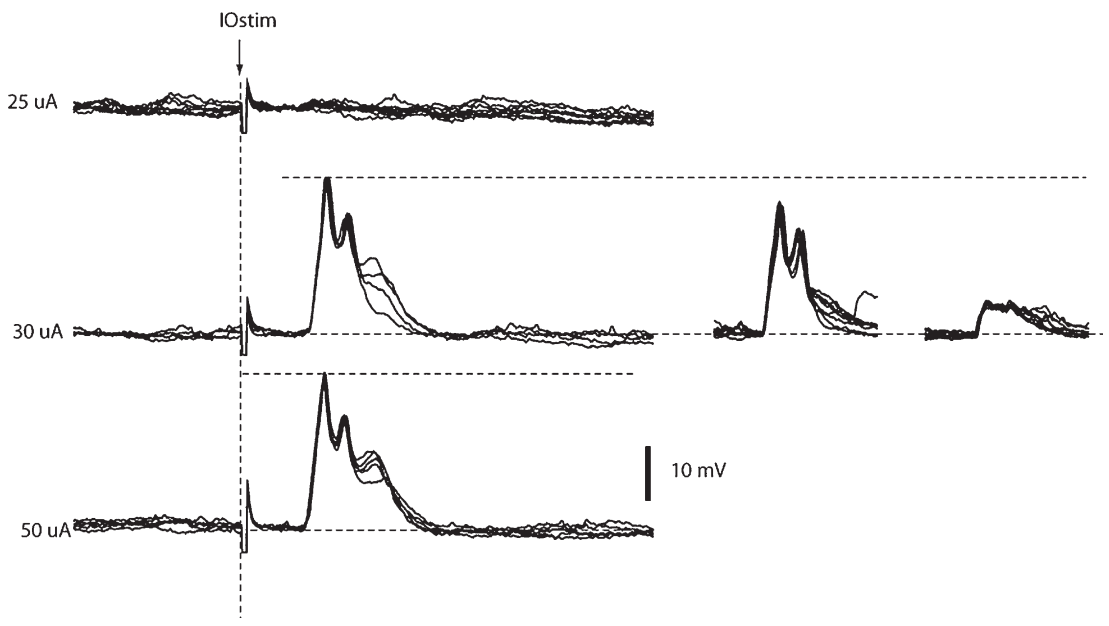

FIGURE 3 | IO stimulation activates the dendritic spikes in an all-or-none fashion. From top to bottom, the responses evoked in a double loose patch dendritic recording by increasing stimulation intensities in the inferior olive (IOstim). Inset to the right, the spontaneous responses of the individual unitary dendritic spikes superimposed. Note that the peak amplitude of the response evoked by IOstim represented the sum of the two unitary dendritic spikes, showing that both dendritic spikes were activated by the stimulation.

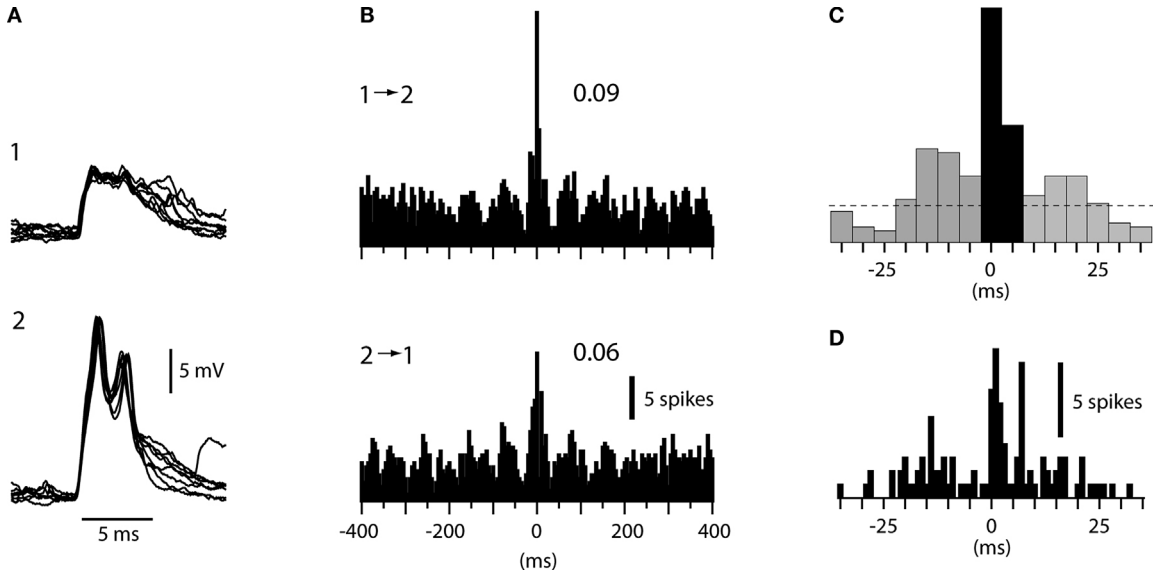

FIGURE 4 | Coupling between dendritic spikes in paired loose patch dendritic recordings. (A) Superimposed dendritic spikes of the two dendritic units. **(B)** Cross-correlograms of the spontaneous activity of the two dendrites. In the upper histogram, the spike times of dendrite 2 relative to the occurrence of the dendritic spike 1 was plotted. The reverse relationship was plotted in the lower histogram. Numbers indicate degree of coupling. Bar calibration applies to **(B)** and **(C)**. **(C)** Close-up of the upper histogram in **(B)** illustrating the bins that were used for the analysis of the spike coupling (black bars). Dashed line indicates the mean background activity. Note that the first bin includes all spike intervals of 0.0–4.9 ms, the second includes all spike intervals between 5.0–9.9 ms etc. **(D)** For comparison, the same histogram with 1 ms bin width.

the non-anesthetized, decerebrated cat but do not support that adjacent PCs are substantially more coupled than more remotely located PCs within the same microzone.

The double loose patch dendritic recordings we report here are likely to be closely related to loose patch clamp recordings. In the latter type of recording, a tight seal between the electrode and the recorded unit allows measurement of its transmembrane potential, the accuracy of which depends on the ratio between the seal resistance and the resistance of the recorded cell (Mason et al., 2005). Due to the comparatively small dimensions of distal, spiny dendrites, we believe that patch clamp recordings is most likely to be primarily obtained from the smooth stem dendrites, which ascend nearly all the way up to the upper end of the molecular layer. Since PCs are extremely flat (the transverse dimension being in the order of 10 μm, see Ito, 1984; Sugihara et al., 1999) their packing density in the transverse direction also becomes very high. Hence, it is likely that the stem dendrites of two adjacent PCs may at least for a part of their course be located in very close proximity to each other. Our paired loose patch dendritic recordings, which were obtained on rare occasions during failed attempts to establish a giga-Ohm seal on a PC dendrite, presumably reflect situations when the patch electrode happened to be located in a site where two stem dendrites were co-localized. The maintained suction in the patch electrode presumably resulted in the attraction of both of these stem dendrites and a partial access to both membrane surfaces.

The configuration of the spikes recorded was compatible with them being dendritic calcium spikes: for the biggest of the two units, the appearance was very similar to calcium spikes recorded from PC dendrites in the whole cell (intracellular) mode (**Figure 1**). For the smaller unit of the pair, the basic time course was also similar, but there was a reduction of the spikelets riding on top of the spike – this can be explained by the fact that in the loose patch mode an additional time constant is added to the recorded signal, and this time constant is increased as the seal resistance on the cell is decreased (Mason et al., 2005). We believe that the larger unit simply reflected the dendrite which was located closer to the electrode whereas the smaller unit recorded was located at a larger electrical distance.

The other spiking unit of the molecular layer, the interneurons, could essentially be excluded as a source of the recorded signals already on basis of the discrepancy in spike duration/configuration (Jorntell and Ekerot, 2003), but additional analysis of the patterns of spontaneous activity strengthened this conclusion (**Figure 2**). Also the fact that the response latency time and response reliability on IO stimulation was very different from those reported from interneurons (Jorntell and Ekerot, 2002, 2003), exclude the possibility that some of our recordings were from interneurons. In addition, since the level of spontaneous activity and the interspike-interval distributions of dendritic spikes and complex spikes recorded from PCs were essentially identical, it is most likely that all of the signals we recorded in the loose patch dendritic mode were due to CF activation of dendritic spikes. Since CF inputs *in vivo* always transmit to the PC (for example, sensory activation can drive the CF response of a single PC with 100% security at a response latency time coefficiency of variation of 0% (at 1 ms resolution); Jorntell et al., 1996), the dual dendritic signals must also have reflected input from two different CFs.

The point with the single-electrode double loose patch dendritic recordings was that they described the CF activity of two adjacent PC dendrites, which could correspond to the activity of

two adjacent neurons in the IO. Anatomical evidence supports the notion that within a microzone, more closely located PCs tend to be innervated by more closely located IO neurons (Garwicz et al., 1996; Sugihara et al., 2007). Such recordings should therefore be well suited to study the coupling of CF activity.

Although we used a similar method but a different time window in comparison to previous studies (De Zeeuw et al., 1997; Flusberg et al., 2008; Lang, 2001, 2002; Lang et al., 1999) the values of CF synchrony are at least roughly comparable. In their analysis of CF synchrony De Zeeuw et al. (1997) used several different time frames and showed that for a time window of ±10 ms, the calculated level of CF synchrony was about two times higher than for a time window of ±1 ms. We measured spikes that followed the trigger spike at up to +10 ms and our values may therefore be considered as being similar to the values obtained from previous studies.

An important difference between this and previous electrophysiological studies was that we focused on spike coupling, i.e. when one CF discharge coincides with or precedes the CF discharge in another PC. Previous works have instead focussed on coincidence within ±1 ms of a 'master' cell (i.e. the 'trigger'-spike of our cross-correlograms) (Lang et al., 1999), or an even wider time window that *straddles* the spike onset of the 'master' cell (De Zeeuw et al., 1997). We believe that the distinction could be important, since discharges in one CF that is driven by the electrotonic coupling between IO neurons can only occur after the discharge of the 'master' CF. Due to the long duration of the IO neuron action potential (the fast sodium spike is followed by a calcium plateau of substantial amplitude and duration; Llinas and Yarom, 1981) and the time constant in the electrotonic coupling, the peak depolarisation (approx. 2 mV) in an IO neuron is reached in the order of 5–10 ms after the occurrence of the spike in the coupled neuron (Devor and Yarom, 2002; Llinas and Yarom, 1981; Long et al., 2002). For spike discharges that coincides exactly or slightly precedes the 'master' cell, the reason for the synchrony could be a shared drive rather than direct coupling through gap junctions. Among the numerous factors that could contribute to both spike synchrony and spike coupling, there are four main alternatives (**Figure 5**).

1. Gap junctions: provide a means by which the membrane potential of one cell influences the membrane potentials of its coupled neighbors. However, the resistance is high (5 GOhm) and the signal that passes through is low-pass filtered. Hence, a full spike in one IO neuron suffices to give a few mVs of depolarization in its coupled neighbor with a substantially reduction of its rise-time and time-course (Devor and Yarom, 2002; Llinas and Yarom, 1981; Long et al., 2002). Hence, the coupling mediated by gap junctions should be relatively weak and impose a certain delay on the spike coupling. Nevertheless, in mice with a knocked-out gene expression of the gap junction component, spike synchrony (at ±1 ms) has been reported to be substantially reduced (Marshall et al., 2007).
2. Excitatory afferent input: Evoked excitatory afferent input to the IO can drive CF responses in all of the PCs of a microzone within a few 100's of a μs with a near 100% fidelity (e.g. Jorntell et al., 1996). Blocking spontaneously active excitatory synapses in the IO enhances synchrony within the microzone (Lang, 2001, 2002).

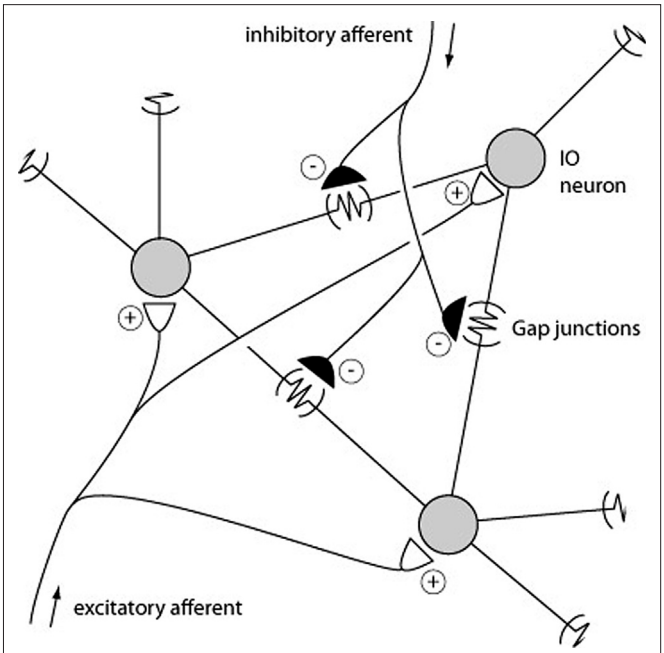

FIGURE 5 | Schematic description of mechanisms that could promote CF synchrony. Three IO neurons and their gap junction couplings are illustrated. 'Half' junctions extending towards the outer edges indicate that the gap junction couplings include additional IO neurons that are not depicted. Also illustrated are the excitatory and inhibitory afferents. Some inhibitory afferents terminate specifically on the sites of gap junctions (De Zeeuw et al., 1989).

3. Inhibitory afferent input: the parasagittal specificity of the CF synchrony has been shown to be under the control of inhibitory input (Lang, 2002), possibly due to the inhibitory projection from the deep cerebellar nuclei (DCN) to the IO (Bengtsson and Hesslow, 2006). This can be understood as a consequence of the fact that the passive electrotonic spread is normally limited to pairs of neighboring IO neurons (Devor and Yarom, 2002), but that a release from inhibition may increase the excitability of the IO neurons and thereby the electrotonic spread within the IO. Conversely, this mechanism could under normal levels of inhibition ensure that the highest degree of synchrony is limited to the IO neurons with the shortest electrotonic distances.
4. Subthreshold intrinsic oscillatory activity: This is an intrinsic form of activity that is set up by the membrane conductances of the IO neurons. It appears to drive episodes of subthreshold oscillations in the membrane potential that may coordinate the spike generation in neighboring IO neurons if the oscillations are in phase. Some studies have indicated that these oscillations disappear when gap junctions are blocked or non-existent (Placantonakis et al., 2006), although contrary evidence exists (De Zeeuw et al., 2003; Long et al., 2002). Oscillatory activity in IO neurons has been described also *in vivo* (Chorev et al., 2007; Khosrovani et al., 2007).

CF synchrony has been suggested to be an important way to elicit timed movements (Welsh et al., 1995). However, in the system studied here, which contributes to the voluntary control of limb, paw and digit movements (Ekerot et al., 1995; Jorntell

and Ekerot, 1999), CF activation is severely depressed during such movements (Apps et al., 1997; Gibson et al., 2004; Horn et al., 2004). Furthermore, at least in this system, each DCN cell is contacted by 100's of PCs from the same microzone (Garwicz and Ekerot, 1994; Palkovits et al., 1977). If the output of a microzone is summed in the DCN, a substantial cortical influence on the DCN activity may require concerted actions of a higher number of PCs than could be achieved with the relatively low degree of spike coupling found here (even more so if the CF activation is depressed during movement). However, synchronization of CF activity within a microzone may be an important mechanism to achieve coordinated learning. Since both PCs and their afferent inhibitory interneurons are subjected to CF dependent forms of parallel fiber synaptic plasticity, it may be important to have a synchronized CF disharge within the microzone in order for the cells to learn to respond to parallel fiber inputs that are activated under similar circumstances. This in turn, may be a requirement to provide a sufficient coordination of the PC simple spikes so that the output of the microzone may provide a substantial modulation of the DCN output.

ACKNOWLEDGEMENTS

This work was supported by SENSOPAC (an Integrated Project funded by the EU under FP6, IST-028056-SENSOPAC), the Swedish Medical Research Council (project no. K2005-04X-14780-03A and K2006-04X-08291-19-3), the Segerfalk Foundation, the Swedish Medical Society.

REFERENCES

Andersson, G., and Oscarsson, O. (1978). Climbing fiber microzones in cerebellar vermis and their projection to different groups of cells in the lateral vestibular nucleus. *Exp. Brain Res.* 32, 565–579.

Apps, R., Atkins, M. J., and Garwicz, M. (1997). Gating of cutaneous input to cerebellar climbing fibres during a reaching task in the cat. *J. Physiol.* 502(Pt 1), 203–214.

Apps, R., and Garwicz, M. (2005). Anatomical and physiological foundations of cerebellar information processing. *Nat. Rev. Neurosci.* 6, 297–311.

Bengtsson, F., and Hesslow, G. (2006). Cerebellar control of the inferior olive. *Cerebellum* 5, 7–14.

Bengtsson, F., and Jorntell, H. (2009). Sensory transmission in cerebellar granule cells relies on similarly coded mossy fiber inputs. *Proc. Natl. Acad. Sci. U.S.A.* 106, 2389–2394.

Callaway, J. C., Lasser-Ross, N., and Ross, W. N. (1995). IPSPs strongly inhibit climbing fiber-activated [Ca2+]i increases in the dendrites of cerebellar Purkinje neurons. *J. Neurosci.* 15, 2777–2787.

Chorev, E., Yarom, Y., and Lampl, I. (2007). Rhythmic episodes of subthreshold membrane potential oscillations in the rat inferior olive nuclei *in vivo*. *J. Neurosci.* 27, 5043–5052.

De Zeeuw, C. I., Chorev, E., Devor, A., Manor, Y., Van Der Giessen, R. S., De Jeu, M. T., Hoogenraad, C. C., Bijman, J., Ruigrok, T. J., French, P., Jaarsma, D., Kistler, W. M., Meier, C., Petrasch-Parwez, E., Dermietzel, R., Sohl, G., Gueldenagel, M., Willecke, K., and Yarom, Y. (2003). Deformation of network connectivity in the inferior olive of connexin 36-deficient mice is compensated by morphological and electrophysiological changes at the single neuron level. *J. Neurosci.* 23, 4700–4711.

De Zeeuw, C. I., Holstege, J. C., Ruigrok, T. J., and Voogd, J. (1989). Ultrastructural study of the GABAergic, cerebellar, and mesodiencephalic innervation of the cat medial accessory olive: anterograde tracing combined with immunocytochemistry. *J. Comp. Neurol.* 284, 12–35.

De Zeeuw, C. I., Koekkoek, S. K., Wylie, D. R., and Simpson, J. I. (1997). Association between dendritic lamellar bodies and complex spike synchrony in the olivocerebellar system. *J. Neurophysiol.* 77, 1747–1758.

Devor, A., and Yarom, Y. (2002). Electrotonic coupling in the inferior olivary nucleus revealed by simultaneous double patch recordings. *J. Neurophysiol.* 87, 3048–3058.

Ekerot, C. F., Garwicz, M., and Schouenborg, J. (1991). Topography and nociceptive receptive fields of climbing fibres projecting to the cerebellar anterior lobe in the cat. *J. Physiol.* 441, 257–274.

Ekerot, C. F., and Jorntell, H. (2001). Parallel fibre receptive fields of Purkinje cells and interneurons are climbing fibre-specific. *Eur. J. Neurosci.* 13, 1303–1310.

Ekerot, C. F., and Jorntell, H. (2003). Parallel fiber receptive fields: a key to understanding cerebellar operation and learning. *Cerebellum* 2, 101–109.

Ekerot, C. F., Jorntell, H., and Garwicz, M. (1995). Functional relation between corticonuclear input and movements evoked on microstimulation in cerebellar nucleus interpositus anterior in the cat. *Exp. Brain Res.* 106, 365–376.

Flusberg, B. A., Nimmerjahn, A., Cocker, E. D., Mukamel, E. A., Barretto, R. P., Ko, T. H., Burns, L. D., Jung, J. C., and Schnitzer, M. J. (2008). High-speed, miniaturized fluorescence microscopy in freely moving mice. *Nat. Methods* 5, 935–938.

Garwicz, M., Apps, R., and Trott, J. R. (1996). Micro-organization of olivocerebellar and corticonuclear connections of the paravermal cerebellum in the cat. *Eur. J. Neurosci.* 8, 2726–2738.

Garwicz, M., and Ekerot, C. F. (1994). Topographical organization of the cerebellar cortical projection to nucleus interpositus anterior in the cat. *J. Physiol.* 474, 245–260.

Gibson, A. R., Horn, K. M., and Pong, M. (2004). Activation of climbing fibers. *Cerebellum* 3, 212–221.

Horn, K. M., Pong, M., and Gibson, A. R. (2004). Discharge of inferior olive cells during reaching errors and perturbations. *Brain Res.* 996, 148–158.

Ito, M. (1984). The Cerebellum and Neural Control. New York, Raven Press.

Jorntell, H., and Ekerot, C. F. (1999). Topographical organization of projections to cat motor cortex from nucleus interpositus anterior and forelimb skin. *J. Physiol.* 514(Pt 2), 551–566.

Jorntell, H., and Ekerot, C. F. (2002). Reciprocal bidirectional plasticity of parallel fiber receptive fields in cerebellar Purkinje cells and their afferent interneurons. *Neuron* 34, 797–806.

Jorntell, H., and Ekerot, C. F. (2003). Receptive field plasticity profoundly alters the cutaneous parallel fiber synaptic input to cerebellar interneurons *in vivo*. *J. Neurosci.* 23, 9620–9631.

Jorntell, H., and Ekerot, C. F. (2006). Properties of somatosensory synaptic integration in cerebellar granule cells *in vivo*. *J. Neurosci.* 26, 11786–11797.

Jorntell, H., Garwicz, M., and Ekerot, C. F. (1996). Relation between cutaneous receptive fields and muscle afferent input to climbing fibres projecting to the cerebellar C3 zone in the cat. *Eur. J. Neurosci.* 8, 1769–1779.

Khosrovani, S., Van Der Giessen, R. S., De Zeeuw, C. I., and De Jeu, M. T. (2007). *In vivo* mouse inferior olive neurons exhibit heterogeneous subthreshold oscillations and spiking patterns. *Proc. Natl. Acad. Sci. U.S.A.* 104, 15911–15916.

Lang, E. J. (2001). Organization of olivocerebellar activity in the absence of excitatory glutamatergic input. *J. Neurosci.* 21, 1663–1675.

Lang, E. J. (2002). GABAergic and glutamatergic modulation of spontaneous and motor-cortex-evoked complex spike activity. *J. Neurophysiol.* 87, 1993–2008.

Lang, E. J., Sugihara, I., Welsh, J. P., and Llinas, R. (1999). Patterns of spontaneous purkinje cell complex spike activity in the awake rat. *J. Neurosci.* 19, 2728–2739.

Llinas, R., Baker, R., and Sotelo, C. (1974). Electrotonic coupling between neurons in cat inferior olive. *J. Neurophysiol.* 37, 560–571.

Llinas, R., and Yarom, Y. (1981). Electrophysiology of mammalian inferior olivary neurones *in vitro*. Different types of voltage-dependent ionic conductances. *J. Physiol.* 315, 549–567.

Long, M. A., Deans, M. R., Paul, D. L., and Connors, B. W. (2002). Rhythmicity without synchrony in the electrically uncoupled inferior olive. *J. Neurosci.* 22, 10898–10905.

Marshall, S. P., van der Giessen, R. S., de Zeeuw, C. I., and Lang, E. J. (2007). Altered olivocerebellar activity patterns in the connexin36 knockout mouse. *Cerebellum* 1–13.

Mason, M. J., Simpson, A. K., Mahaut-Smith, M. P., and Robinson, H. P. (2005). The interpretation of current-clamp recordings in the cell-attached patch-clamp configuration. *Biophys. J.* 88, 739–750.

Ozden, I., Lee, H. M., Sullivan, M. R., and Wang, S. S. (2008). Identification and clustering of event patterns from *in vivo* multiphoton optical recordings of neuronal ensembles. *J. Neurophysiol.* 100, 495–503.

Palkovits, M., Mezey, E., Hamori, J., and Szentagothai, J. (1977). Quantitative histological analysis of the cerebellar nuclei in the cat. I. Numerical data on

cells and synapses. *Exp. Brain Res.* 28, 189–209.

Placantonakis, D. G., Bukovsky, A. A., Aicher, S. A., Kiem, H. P., and Welsh, J. P. (2006). Continuous electrical oscillations emerge from a coupled network: a study of the inferior olive using lentiviral knockdown of connexin36. *J. Neurosci.* 26, 5008–5016.

Stuart, G., and Hausser, M. (1994). Initiation and spread of sodium action potentials in cerebellar Purkinje cells. *Neuron* 13, 703–712.

Stuhmer, W., Roberts, W. M., and Almers, W. (1983). The loose patch clamp. In Single Channel Recording, B. Sakmann and E. Neher, eds (New York, Plenum Press), pp. 123–132.

Sugihara, I., Marshall, S. P., and Lang, E. J. (2007). Relationship of complex spike synchrony bands and climbing fiber projection determined by reference to aldolase C compartments in Crus IIa of the rat cerebellar cortex. *J. Comp. Neurol.* 501, 13–29.

Sugihara, I., Wu, H., and Shinoda, Y. (1999). Morphology of single olivocerebellar axons labeled with biotinylated dextran amine in the rat. *J. Comp. Neurol.* 414, 131–148.

Sugihara, I., Wu, H. S., and Shinoda, Y. (2001). The entire trajectories of single olivocerebellar axons in the cerebellar cortex and their contribution to cerebellar compartmentalization. *J. Neurosci.* 21, 7715–7723.

Welsh, J. P., Lang, E. J., Suglhara, I., and Llinas, R. (1995). Dynamic organization of motor control within the olivocerebellar system. *Nature* 374, 453–457.

Conflict of Interest Statement: The authors declare that the research was conducted in the absence of any commercial or financial relationships that could be construed as a potential conflict of interest.

Received: 18 March 2009; paper pending published: 10 April 2009; accepted: 11 July 2009; published online: 10 August 2009.
*Citation: Bengtsson F and Jörntell H (2009) Climbing fiber coupling between adjacent Purkinje cell dendrites in vivo. Front. Cell. Neurosci. **3**:7. doi: 10.3389/neuro.03.007.2009*

frontiers in
CELLULAR NEUROSCIENCE

REVIEW ARTICLE
published: 20 July 2009
doi: 10.3389/neuro.03.005.2009

Optical imaging as a link between cellular neurophysiology and circuit modeling

Walther Akemann, Steven J. Middleton and Thomas Knöpfel*

Laboratory for Neuronal Circuit Dynamics, RIKEN Brain Science Institute, Wako, Japan

Edited by:
Egidio D'Angelo, University of Pavia, Italy

Reviewed by:
Timothy J. Ebner, University of Minnesota, USA
Egidio D'Angelo, University of Pavia, Italy

****Correspondence:***
Thomas Knöpfel
Laboratory for Neuronal Circuit Dynamics, RIKEN Brain Science Institute, 2-1 Hirosawa, Wako-shi, Saitama 351-0198, Japan.
e-mail: tknopfel@brain.riken.jp

The relatively simple and highly modular circuitry of the cerebellum raised expectations decades ago that a realistic computational model of cerebellar circuit operations would be feasible, and prove insightful for unraveling cerebellar information processing. To this end, the biophysical properties of most cerebellar cell types and their synaptic connections have been well characterized and integrated into realistic single cell models. Furthermore, large scale models of cerebellar circuits that extrapolate from single cell properties to circuit dynamics have been constructed. While the development of single cell models have been constrained by microelectrode recordings, guidance and validation as these models are scaled up to study network interactions requires an experimental methodology capable of monitoring cerebellar dynamics at the population level. Here we review the potential of optical imaging techniques to serve this purpose.

Keywords: optical imaging, cerebellum, calcium probes, voltage probes, genetically encoded probes

INTRODUCTION

The cerebellar cortex, the deep cerebellar nuclei and the inferior olive form the three main hubs of the cerebellar circuit. Each of these components of the olivo-cortico-nuclear circuit involves a relatively modest number of cell types, with synaptic connectivity within and between the hubs being highly parallel and modular. To date, the electrophysiological properties of most cerebellar cell types have been characterized in detail, resulting in data that has allowed the construction of compartmental conductance-based single cell models. Thus, for most cerebellar cell types, a digital representative already exists, that faithfully implements its active membrane properties and the transformation of synaptic inputs into spiking outputs. It is these cellular models which are in turn used as the foundations to computationally rebuild the cerebellar circuit (for review see Medina and Mauk, 2000). In order for these models to generate realistic data when scaled up to the network level, additional parameters such as functional connectivity and population dynamics must be incorporated, however much of this information is either conflicting or missing.

It should be stressed here that functional connectivity cannot be derived from anatomical information only. One particular example related to cerebellar circuitry where a discrepancy between anatomical and functional connectivity became an issue, involves the synapses between granule cells and Purkinje cells. It is well established anatomically that granule cell axons form synapses with Purkinje cells, via the ascending axons entering the molecular layer, and also following bifurcation as the parallel fibers contact with Purkinje cell dendrites (see Huang et al., 2009 and references cited therein). However, it is still under debate as to, whether granule cells influence the firing of Purkinje cells predominantly via the ascending axon synapses or via the parallel fiber system. With this in mind, optical imaging data combines both structural and functional information and therefore is, at least in principle, well suited in resolving such issues (For further discussion on these issues see: Cohen and Yarom, 1998; Coutinho et al., 2004; Vranesic et al., 1994).

Whilst there remains a significant lack of detailed information related to functional connectivity between major cerebellar neuronal populations, "educated guesswork-based" network models have been constructed, with emerging circuit properties that can replicate experimental observations. However, since these cerebellar circuit models are based on connectivity assumptions, their power of prediction is somewhat limited. This problem can be ameliorated not only by providing better information about functional connectivity but also by validating experimentally the dynamics that emerge from circuit modeling. Here we review the potential of optical imaging methodologies to serve these purposes. This focused review does not cover systems other than the cerebellum, and highlights how optical imaging has been applied in the context discussed above.

"INTRINSIC" OPTICAL IMAGING

Optical imaging most often refers to imaging modalities based on fluorescent probes that transform network activity into optical signals. There are, however, approaches that use "intrinsic" optical signals that correlate with neuronal activity. These methods rely on changes in light absorption and scattering or tissue autofluorescence, negating the need for exogenous application of chemical dyes (Chance et al., 1962; Coutinho et al., 2004; Reinert et al., 2004, 2007; Rossini et al., 1991). None of these "intrinsic" optical imaging methods have been extensively used in the cerebellum to obtain information that is relevant for construction of large scale circuit models. An exception is perhaps FAD (flavin adenine dinucleotide) green autofluorescence imaging, which has been used to investigate the metabolic consequences of synaptic excitation and inhibition (Gao et al., 2006), the functional connectivity in the mossy fiber-granule cell-Purkinje cell pathway and the topology of climbing fiber projections *in vitro* and *in vivo* (Coutinho et al., 2004; Reinert et al., 2004, 2007). Imaging based on hemodynamic events

used extensively for studying changes in cerebrocortical neuronal activity (Vanzetta et al., 2005) has yet to be successfully exploited for the cerebellum. There are optical imaging approaches other than those covered in this review, most notably are the exciting advances in application of second harmonic generation microscopy to monitor cerebellar electrical activity (Sacconi et al., 2008).

CLASSICAL CALCIUM IMAGING

Fluorescent calcium indicators can be added to the internal solution of glass electrodes used for intracellular recordings. Filling cells with such calcium sensitive dyes allows for measurements of calcium dynamics at the single cell level with excellent sensitivity and spatio-temporal resolution. There are, however, only a few cases where single cell calcium imaging data were used to fine-tune realistic computational models of cerebellar neurons. Examples include the optically determined localization of calcium channels in Purkinje cells, granule cells and deep cerebellar nuclei (Gall et al., 2005; Knöpfel et al., 1991; Muri and Knöpfel, 1994; Tank et al., 1988) and the corresponding compartmental models (De Schutter and Bower, 1994a,b; Diwakar et al., 2009; Quadroni and Knöpfel, 1994). Whilst calcium imaging in single cells has not led to useful constraints for circuit models, calcium imaging of large populations of cerebellar neurons at single cell resolution could potentially provide information that is not readily accessible by microelectrode techniques.

The most widely used calcium imaging approach to investigate activity in intact circuits is based on staining with membrane permeable calcium indicator dyes (that become impermeable and trapped following intracellular cleavage of a lipophilic side group), which also allows for the simultaneous sampling of many single cells (Ikegaya et al., 2004; Kerr et al., 2005). In the cerebellum, this AM dye technology when combined with cutting edge optical systems and specific staining protocols (Garaschuk et al., 2006) has proven successful to permit the monitoring of CF activities of several Purkinje cells in the living, and even, freely moving rodent cerebellum (Engelbrecht et al., 2008; Sullivan et al., 2005). It should be noted however, that AM calcium based imaging *in vivo* has been demonstrated only in the molecular layer with staining of parallel fibers, interneurons and Purkinje cells (e.g. Sullivan et al., 2005). Functional imaging of deeper circuit elements (like granule cells and Golgi cells) has not yet been clearly demonstrated and is, according to some investigators, hampered by excessive light scattering in the cerebellar granule cell layer (Sullivan et al., 2005).

Taken together, calcium imaging techniques in the cerebellum *in vivo*, are still being methodologically refined, but it is anticipated these techniques have a high potential to provide experimental data by which network simulations can be constrained and validated in the near future.

CLASSICAL VOLTAGE IMAGING

In contrast to calcium imaging, which is limited by the temporal precision of the calcium signals themselves, voltage sensitive dyes bind to the plasma membrane, where their fluorescence is modulated directly by changes in membrane potential, allowing faithful optical reporting of electrical signals with very rapid kinetics, including single action potentials. Indeed, cerebellar voltage sensitive dye imaging was demonstrated over a decade ago, enabling the activity of single cerebellar Purkinje cells to be imaged in cultured neurons (Staub et al., 1994), see **Figure 1**.

The promise of resolving single action potentials from acute cerebellar slices however, was only achieved when dyes were intracellularly applied via patch pipettes (Zhou et al., 2008). Of course the rationale behind using imaging over conventional electrophysiology, is that theoretically, optical approaches would permit the electrical activity of large populations of neurons to be monitored, at single cell resolution in intact tissue. However to date this has not

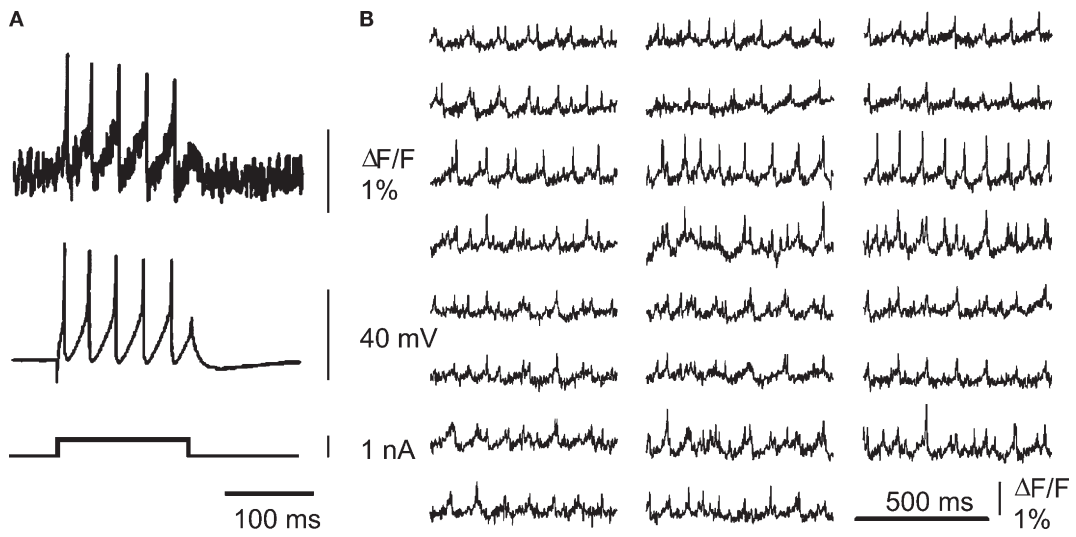

FIGURE 1 | Voltage sensitive dye imaging in cerebellar slice cultures. Cerebellar cultures containing granule cells and Purkinje cells were stained with the voltage sensitive dye di-4-ANEPPS. **(A)** Optical voltage signal (upper trace) and simultaneous microelectrode recording from a Purkinje cell during injection of a current pulse (lower trace). **(B)** Simultaneous optical recording of spontaneous spiking activity of several Purkinje cells. For methodological details see Staub et al. (1994).

yet proven feasible. The reason that success with voltage sensitive dye imaging has been limited, involves their main drawback, in that, they (when exogenously applied) stain tissue indiscriminately (including the membranes of all neurons and glial cells within the tissue). The implications this has for recording of optical activity is that signals of interest from specific morphologically identified neurons are diluted by a large background of stained cells within the tissue, meaning that in reality signals are too small to allow for isolation of specific cellular responses.

Despite the outlined drawbacks, voltage sensitive dyes have proven useful for monitoring network activity, in which the imaged signals reflect summations over many cells. In some cases these compound optical signals have been dissected by pharmacological means, allowing them to be attributed to specific cellular subpopulations. This approach has been used to isolate parallel fiber action potentials, and to characterize their transverse propagation through the molecular layer and their excitation of Purkinje neurons (Cohen and Yarom, 1998; Vranesic et al., 1994). Whilst the dream scenario of classical voltage sensitive dyes providing a tool to monitor the activity of many hundreds of neurons (or whole networks) simultaneously at single cell resolution still seems far away, their ability to monitor population responses has already been successfully exploited. This is a particularly pertinent property when one considers computational modeling of neuronal structures such as the cerebellum, since more detailed single-cell electrophysiology recordings are readily available characterizing specific cellular behaviors. The forte of optical voltage imaging is that by varying the spatial scale, activity of whole networks can be recorded, demonstrating the spatial extent over which, and with what temporal precision, areas within a given network can synchronize, with the added advantage that these data can be gathered non-invasively (i.e. without altering intracellular ionic compositions that are associated with patch-clamping).

It is well-established that neuronal networks, including those residing within the cerebellar cortex generate oscillatory activity (Middleton et al., 2008; Niedermeyer, 2004; Soteropoulos and Baker, 2006; Timofeev and Steriade, 1997), and these have been shown in cerebrocortical regions to be associated with the temporal coding of various features of sensory stimuli (Canolty et al., 2006; Gray et al., 1989; Womelsdorf et al., 2007). However when considering the precise, spatio-temporal patterning and propagation of these rhythms, conventional microelectrode techniques become impractical. To this end, voltage dye imaging has been successfully used to study network dynamics in the inferior olive (IO) *in vitro*. In this study of Rodolfo Llinas and co-workers, IO local electrical stimulation was used to reset the phase of subthreshold oscillations and entrain a large population of IO neurons. Whilst intracellular recordings demonstrated that individual cells display membrane potential oscillations, optical imaging was used to reveal that at the network level, such stimulation produced oscillations which clustered in to coherent populations comprising hundreds of neurons (Leznik et al., 2002; Llinas et al., 2002). Notably these population responses were used to validate and interpret the behavior of computational simulations of the IO network (Llinas et al., 2002).

More recently, voltage imaging was used to elucidate the spatial expression of cerebellar high frequency oscillations (Middleton et al., 2008). Nicotinic receptor activation in the cerebellum is associated with generation of high frequency network oscillations, which field potential recordings reveal to be a mixture consisting of classical gamma band oscillations (40 Hz), co-existing with very fast oscillations (VFOs, 80–160 Hz). Optical signals however, accurately localize the changes in membrane potential, demonstrating that gamma frequency rhythms are confined predominantly to the Purkinje cell layer and distal white matter, whilst VFO peak power originates in the granule cell layer and diffusely throughout the white matter (see **Figure 2**).

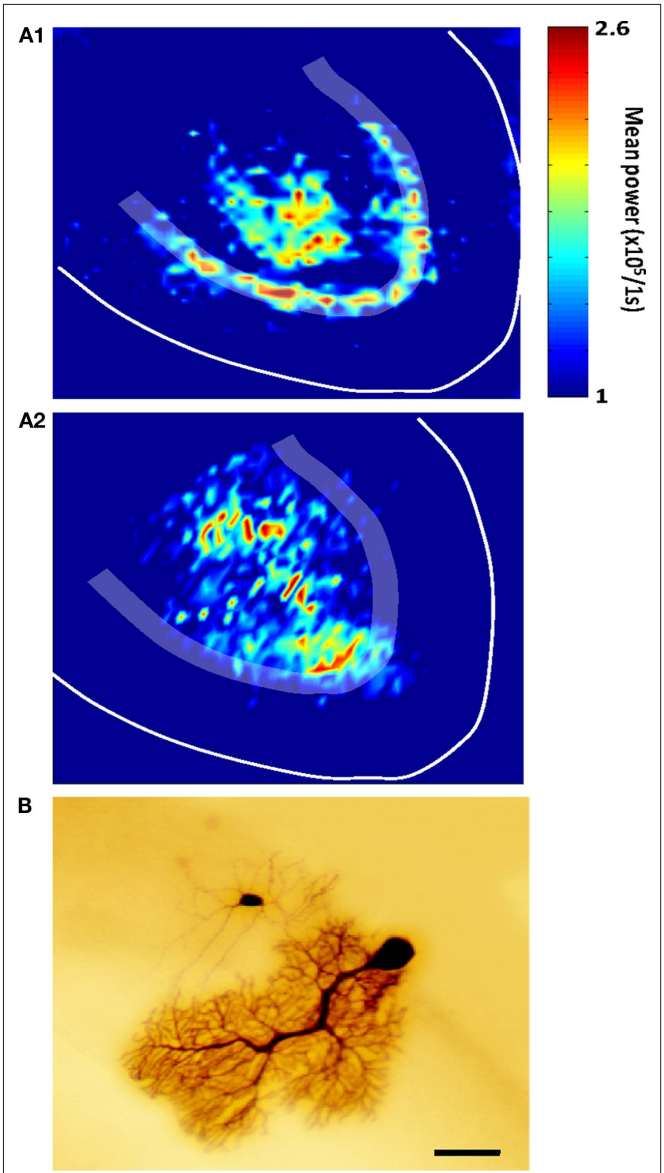

FIGURE 2 | Optical imaging of cerebellar high-frequency oscillations. (A1) Pooled peak power in the gamma band (20–60 Hz) from power spectra of optical data morphed onto an idealized cerebellar slice, with similar data shown for VFOs (80–160 Hz) shown in **(A2)** (n = 5, 1s epochs). Note that gamma frequency and very fast oscillations are predominant in different spatial locations, an observation confirmed by electrophysiological recordings. **(B)** An example of heterocellular dye-coupling between a Purkinje cell and an inhibitory interneuron. Note: biocytin was injected only into the Purkinje neuron during extracellular high frequency oscillations and is presumed to diffuse to the other cell via gap junctions. Taken from Middleton et al. (2008).

Given the laminar localization of VFOs in the optical signals together with pharmacological data with gap junction blockers, it was hypothesized that gap junctions between Purkinje cell axons may be responsible, or at least contribute to the VFOs. For this reason, a computational model based on these data was constructed to show that a network of Purkinje cells with gap junctions located on their proximal axons was sufficient to reproduce VFOs (Traub et al., 2008). Furthermore, predictions from the model, namely that the frequency of the VFOs was gated by sodium channel inactivation were subsequently proven experimentally by pharmacologically prolonging the corresponding inactivation time constant (Traub et al., 2008). Further examples where voltage sensitive dye data has been incorporated into computational models are detailed elsewhere (Sergio Solinas and Egidio D' Angelo, A realistic large-scale model of the cerebellum granular layer predicts circuit spatio-temporal dynamics, submitted; Jonathan Mapelli, Daniela Gandolfi and Egidio D' Angelo, High-pass filtering properties of granular to molecular layer transmission revealed by high-resolution voltage-sensitive dye imaging, submitted).

These studies demonstrate that whilst optical imaging with voltage sensitive dyes has not yet been exploited to its full potential, for understanding interactions macroscopically at the network level and in combination with computational approaches, it remains a powerful tool. Of course it remains that for most cases it would be more preferable to simultaneously monitor single cells, whilst also observing the network in which they are embedded. In order to make this feasible in terms of signal to noise and interpretation of the recorded signals, it would be preferable to have specific populations of cells labeled (i.e. only Purkinje cells). To overcome these issues, genetically encoded sensors (of either calcium or membrane potential) are preferable; these are discussed in detail below.

OPTICAL IMAGING USING GENETICALLY ENCODED PROBES

Ideally, computed cerebellar circuit dynamics could be directly matched with experimental data if recording methods existed that would allow recordings of large populations of identified neurons *in vivo*. Whilst, to date, this hasn't yet been achieved, imaging using genetically encoded probes could, at least in principle, make this possible. These nascent optogenetic approaches utilize fluorescent protein calcium or voltage sensors, with expression driven by cell type specific promoters, thus reporting activity from genetically defined cell populations (Knöpfel et al., 2006; Luo et al., 2008). Moreover, fluorescent protein-based probes can be constructed with multiple colors such that signals from "color tagged" cells or cell populations can be spectroscopically isolated even if single cells are not optically resolved. **Figure 3** illustrates genetic color tagging in a line of mice where green fluorescent protein is expressed in GABAergic cells (via the GAD 67 promoter) and yellow fluorescent protein is expressed in granule cells via the Kv3.1 promoter (Metzger et al., 2002; Tamamaki et al., 2003).

GENETICALLY ENCODED CALCIUM PROBES

Genetically-encoded calcium probes (GECPs) are proteins with engineered, calcium-sensitive fluorescence properties, as reviewed in (Knöpfel et al., 2006; Mank and Griesbeck, 2008). Within the cerebellar cortical network, cell-specific targeting of the calcium probe GCaMP2 to granule cells and Purkinje neurons was achieved by recombinant expression of GCaMP2 under control of the Kv3.1 potassium channel extended promoter (**Figure 4A1**) and the L7/pcp2 promoter (**Figure 4B1**), respectively, in transgenic mice (**Figures 4A2–4 and 4B2–4**) (Diez-Garcia et al., 2005). Furthermore, reportedly exclusive targeting of GCaMP2 to Bergmann glia was obtained after acute adenoviral infection of the cerebellar cortex with GCaMP2 under the cytomegalovirus immediate-early CMV promoter (Hoogland et al., 2009). The GCaMP2 probe permitted *in-vivo* recording of calcium transients from population activity of granule cells and Purkinje neurons, respectively (**Figures 4A5,6 and 4B5,6**). These results, together with data obtained for members of other families of protein probes in cells of the mouse cerebral cortex and hippocampus (Hasan et al., 2004; Heim et al., 2007; Mank et al., 2008; Wallace et al., 2008) provide a proof of principle for a cell-specific readout of network activity using GECPs. However, full exploitation of the potential of GECPs, requires further development. For instance, it still has to be shown that a sufficiently complete set of promoters/enhancers can be established to permit comprehensive dissection of the cerebellar circuitry. To expand the set of suitable promoters it appears advantageous to drive Cre recombinase by a cell type specific promoter and use this enzyme to activate the probe (Cre/lox system, for recent review see Bucholtz, 2008). The potential benefits include that transcription of the probe gene can be under the control of a strong promoter to drive high expression levels, while the protein is produced in only a subset of cells where the activator is present to switch on the probe gene. This allows the use of a weak, but highly specific promoter for the recombinase, with the combination resulting in a strong, highly

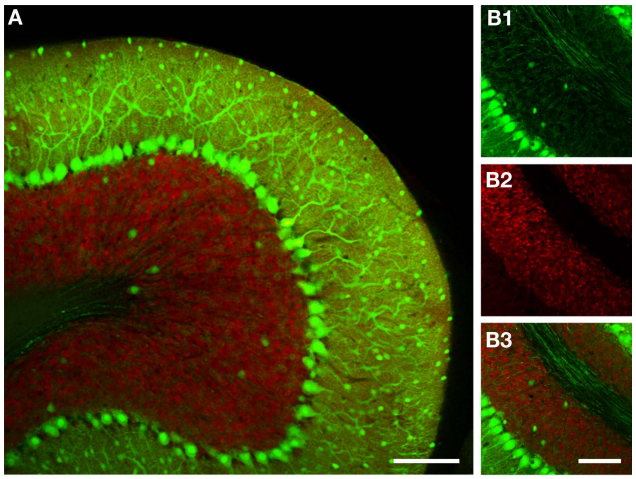

FIGURE 3 | The use of fluorescent protein color variants to genetically define multiple cell populations. (A) A confocal image of a cerebellar slice from a transgenic mouse expressing GFP and EYFP via the GAD 67 and Kv3.1 promoters respectively. Images were acquired with a 32-channel spectral resolution on a Nikon C1si system and deconvoluted with GFP and EYFP spectra. The resulting GFP and EYFP signals are shown in green, and red false colors to enhance contrast. In **(B)** are shown images with larger magnification of the separate channels demonstrating the very high resolution that can be achieved with genetic approaches (note individual Purkinje cell axons). **(B1)** shows only GFP fluorescence highlighting the dense axonal network formed by the Purkinje cells and interneurons, whilst in **(B2)** only EYFP is visible in the numerous small granule cells, finally **(B3)** shows both channels. Scale bar throughout: 100 μm.

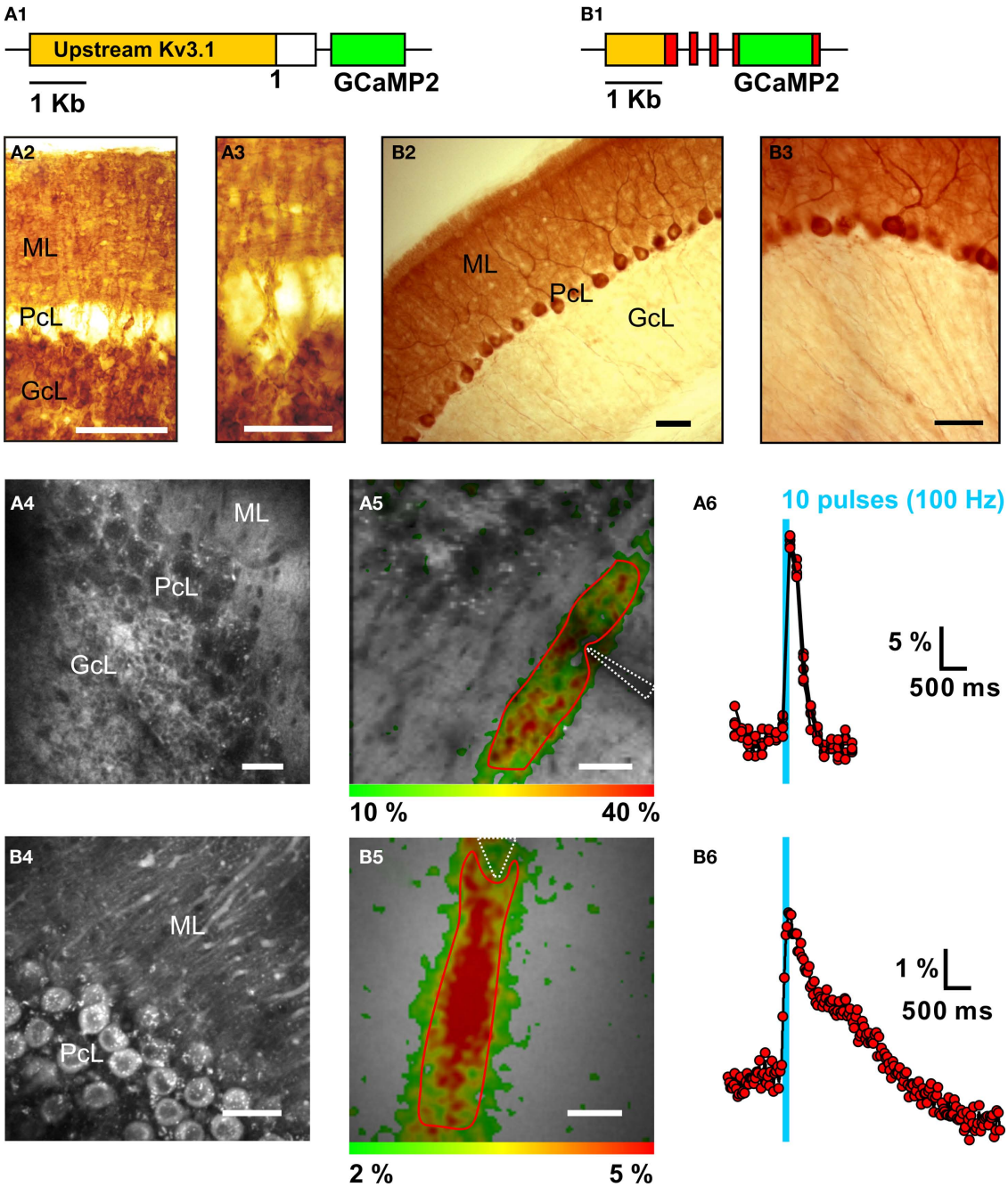

FIGURE 4 | Targeting of the genetically-encoded calcium probe GCaMP2 to granule cells and Purkinje neurons and *in-vivo* recording of calcium population transients in transgenic mice. (A1) Schematic of the pKv3.1-GCaMP2 gene construct consisting of the extended (~6 kb) promoter of the Kv3.1 potassium channel (orange) and GCaMP2 (green). **(A2)** Immunoreactivity against green fluorescent protein (GFP) in a coronal cerebellar section from a pKv3.1-GCaMP2-positive mouse showing the granule cell layer (GcL), Purkinje cell layer (PcL) and molecular layer (ML). Scale: 100 µm. Data from: (Diez-Garcia et al., 2005) **(A3)** Same as **(A2)**, but different field of view. Scale: 50 µm. **(A4)** Two-photon image of a craniotomized area (crus I/II; 190 µm below pia) of the cerebellum in a pKv3.1-GCaMP2-positive mouse *in-vivo*. Scale: 25 µm. **(A5)** *In-vivo* stimulation of a parallel fiber bundle using an external electrode (white dashed lines; 10 pulses; 100 Hz) with the GCaMP2 responses ($\Delta F/F$) coded according the color scale below. Scale: 50 µm. **(A6)** Time course of the fluorescence response ($\Delta F/F$) extracted from the region of interest (red) in **(A5)**. Duration of the stimulus indicated in blue. Data from (Diez-Garcia et al., 2007) **(B1)** Schematic of the pL7-GCaMP2 gene construct consisting of the L7(pcp2) (~1 kb) promoter (orange) and GCaMP2 (green) inserted into exon 4 of the L7(pcp2) gene. Natural translation initiation sites in L7(pcp2) exons (red) have been silenced. **(B2)** GFP immunoreactivity in a sagittal cerebellar section from a pL7-GCaMP2-positive mouse. Scale: 50 µm. **(B3)** Same as **(B2)** but different field of view. Scale: 50 µm. **(B4)** Two-photon image of a craniotomized area (crus I/II; 170 µm below pia) of the cerebellum in a pL7-GCaMP2-positive mouse *in-vivo*. Scale: 50 µm. **(B5)** *In-vivo* GCaMP2 response ($\Delta F/F$; coded according to the color scale below) in the molecular layer evoked by a local stimulation electrode (white dashed line; 10 pulse; 100 Hz) as obtained by single-photon fluorescence excitation (490 ± 10 nm). Scale: 50 µm. **(B6)** Time course of the fluorescence response ($\Delta F/F$) extracted from the region of interest (red) in **(B5)**.

specific protein expression. Furthermore cross-breeding of already available Cre mouse lines with probe mice, provides an efficient means to generate animals with GECPs targeting different components of the network. In the future virus-mediated gene delivery may eventually substitute for the need of transgenic animals carrying the probe gene while maintaining the power of the Cre/lox system (Atasoy et al., 2008). At present, conditional expression strategies have not yet been fully employed for optimizing GECP expression in specific neuron populations in experimental animals.

Apart from the need to specifically target individual cell types as a key requirement for complete mapping of the cerebellar circuit, another crucial aspect of currently available GECP-based imaging concerns the ability to resolve the temporal spike code of neurons in the network. The principal limitation of the GECP approach, as for calcium imaging of neuronal activity in general, derives from the intrinsic slowness of neuronal calcium transients (typical decay of spike triggered neuronal calcium events ~50–150 ms) as compared to action potentials (~0.4–2 ms). Using GECPs, the time resolution is further degraded because of the slow kinetics of calcium binding to GECPs (typical off binding time constants ~200–1500 ms) (Hendel et al., 2008; Hires et al., 2008).

From the point of view of their kinetic properties, GECPs are best suited to report electrical activity of cells that use sparse temporal codes (infrequent single spikes or action potential bursts at low incidence). Given that sparse activity is the rule rather than the exception in many brain circuits, e.g. (Kerr et al., 2005, 2007; Lee et al., 2006) the temporal filtering property of GECPs, is not expected to prevent recording of *in-vivo* neuronal activity patterns and, in fact, has the advantage to bestow these recordings with improved signal-to-noise ratios. In spite of the large dynamic range of spike-evoked elevation in intracellular calcium concentration, presently available GECPs do not, however, reliably report action potentials in all preparations (Hendel et al., 2008; Mank et al., 2008; Mao et al., 2008). In the case of GCaMP2, single spike sensitivity seems to be disfavored by a rather high calcium dissociation constant (1.2 μM) and Hill coefficient (2.5) (Hires et al., 2008; Pologruto et al., 2004). General problems that might reduce GECP performance in certain applications include: specific interactions of the calcium binding domain with intrinsic cytosolic proteins, GECP sequestration in intracellular compartments, and/or too low expression level. In the case of cameleons (Miyawaki et al., 1997) reengineering of the calmodulin binding interface yielded substantial improvement in the *in-vivo* performance of the probe (Palmer et al., 2006; Wallace et al., 2008). Furthermore, acute viral transfer of GECPs into neurons can elevate GECP expression to levels that enable reliable detection of single spikes from somatic calcium transients *in-vivo* (Wallace et al., 2008). Thus, virus-mediated gene transfer in combination with improved GECPs (Palmer et al., 2006; Souslova et al., 2007) is likely to overcome the technical limitations experienced in earlier studies (Diez-Garcia et al., 2007) and provide sufficient sensitivity to map the *in-vivo* activity of identified neurons. Using constitutive cell type specific GCaMP2 expression in transgenic mice, we have already succeeded to dissect the pre- and postsynaptic calcium responses evoked by compound activity of parallel fibers in the molecular layer of the cerebellum *in-vivo* (**Figure 4**). The postsynaptic response in Purkinje neurons, representing calcium signals from the Purkinje neuron dendrites, takes the form of a "beam-like" territory (**Figure 4B5**) indicating synaptic activation of Purkinje neurons along the direction of the parallel fibers (**Figure 4A5**). The ability to unambiguously discriminate and quantify pre- and postsynaptic events based on targeted GCaMP2 expression allowed the mechanism of presynaptic plasticity of the granule cell (Gc) to Purkinje neuron (PN) transmission upon repetitive 4 Hz (120 pulses) stimulation of parallel fibers (Qiu and Knöpfel, 2007), to be isolated *in vitro*. This protocol gives rise to a long-lasting potentiation (LTP) of Gc-PN synaptic efficacy with the presynaptic site of modification indicated by an associated increase of calcium influx into parallel fiber synaptic boutons. The observed plasticity required activation of protein kinase A, NMDA receptors and NO synthase in a presumably multi-synaptic pathway involving the activation of NMDA receptors on local interneurons (Qiu and Knöpfel, 2007). The Gc-PN presynaptic site was also susceptible to long-term synaptic depression (LTD), which was unmasked when presynaptic LTP at this synapse was pharmacologically inhibited (Qiu and Knöpfel, 2009). Thus, genetically targetable calcium probes provide a new experimental approach to trace synaptic mechanisms in neuronal circuits which, when extended to *in-vivo* preparations, can help address the relationship between molecular cellular events and behavior.

GENETICALLY ENCODED VOLTAGE PROBES

The kinetic limitations associated with genetically encoded calcium sensors can, in principle, be overcome by genetically encoded voltage probes. This theoretical advantage is important for structures such as the cerebellum where cells typically have very high spike rates, making GECPs impractical for resolving single spikes. There is no doubt that multisite cellular voltage signals are the type of data that can bridge cellular neurophysiology and circuit modeling, but as already outlined above, voltage sensitive dye imaging is technically more challenging than calcium imaging in terms of signal-to-noise ratio. This fact results from the smaller number of dye molecules that can be accommodated on the surface of cells when compared to cytosolic volume and a generally smaller dynamic range of optical voltage signals as compared to optical calcium signals. Attempts to generate fluorescent protein voltage probes started around the time calcium probes were being designed, but progress has been much slower. After failure of a first generation of such probes (Baker et al., 2007), a second generation proved much more promising. Currently the best available probes follow the original design of Sakai et al., termed VSFP1 (Sakai et al., 2001), but make use of a different voltage sensor domain (the part of the sensor that is voltage sensitive) (Dimitrov et al., 2007; Lundby et al., 2008; Mutoh et al., 2009). The third generation variants with the largest steady state voltage response are VSFP2.3, VSFP2.4 and Mermaid (Mutoh et al., 2009; Tsutsui et al., 2008) having dynamic ranges of around 12% ΔR/R in a side-by-side PC12 cell assay (Mutoh et al., 2009). Responses to transient electrical events in neurons are smaller, amounting in the best cases to 1–2% ΔR/R for slow potentials and 0.2–1% for action potentials or presumed action potential like voltage signals (Dimitrov et al., 2007; Tsutsui et al., 2008). The relatively small amplitudes of the optical signals induced by action potentials is a direct consequence of the intrinsic activation kinetics of VSFP which comprises a fast initial response and a subsequent relatively slow response (Mutoh et al., 2009). To explore the low-pass filter function imposed by these probes we used a combination of voltage

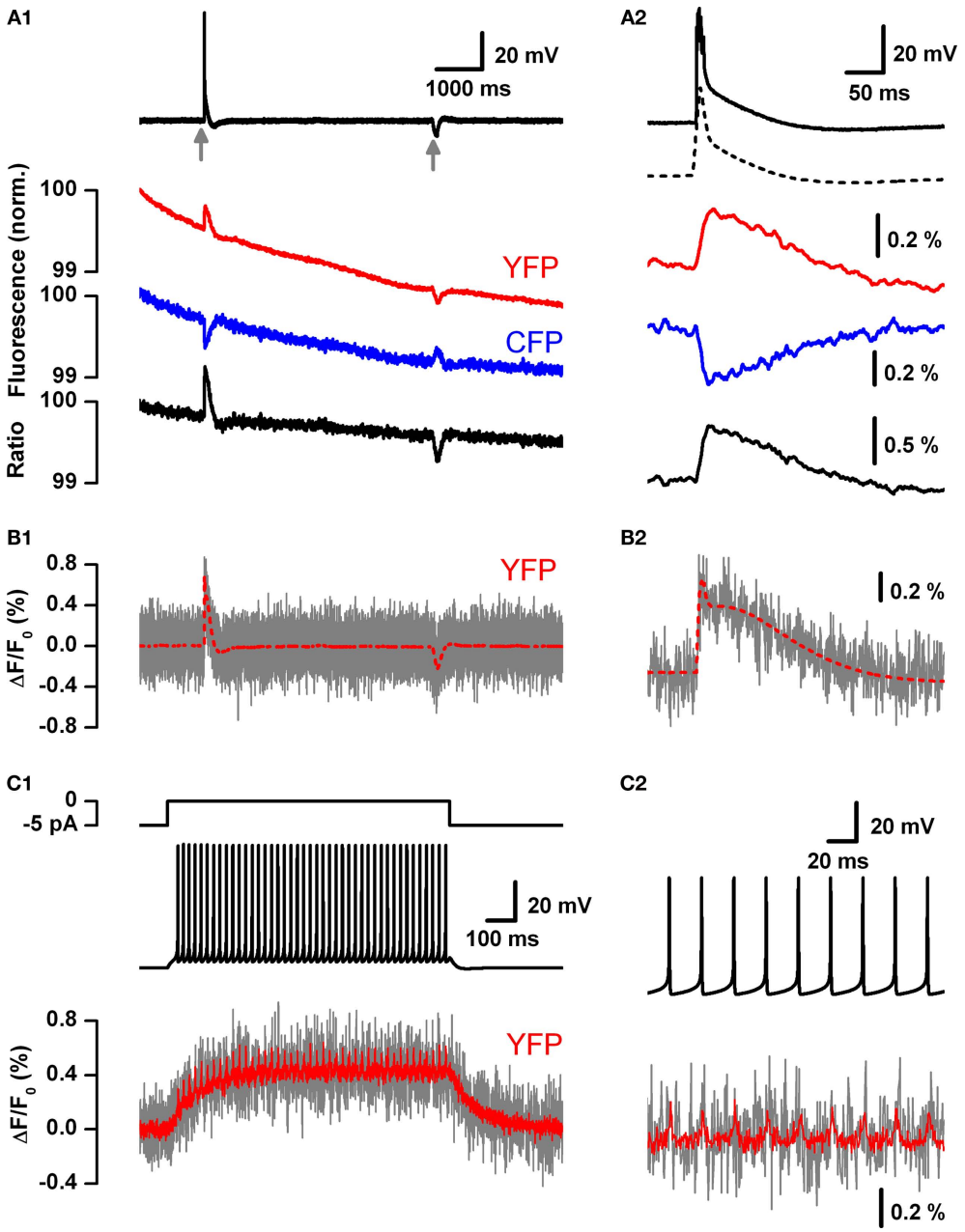

FIGURE 5| Estimation of the theoretical readout of simple and complex spikes from Purkinje neurons by voltage imaging using present generation VSFPs. (A1) A PC12 cell expressing VSFP2.1 was voltage-clamped with a voltage trace (top black trace) from a cerebellar Purkinje neuron during induction of a climbing fiber response (complex spike; marked by arrow) and during intracellular injection of a small hyperpolarizing current pulse (marked by a second arrow). Traces show membrane potential (top trace), yellow fluorescence (YFP; red trace), cyan fluorescence (CFP; blue trace) and the ratio of yellow and cyan fluorescence (bottom black trace). The voltage trace was recorded with 1 kHz cutoff frequency. Fluorescence signals were digitally low pass filtered (0.1 kHz), averaged over 20 consecutive sweeps and scaled in units of normalized absolute fluorescence. (Mutoh and Knöpfel, unpublished data, Methods as in Dimitrov et al., 2007). **(A2)** Same traces as in **(A1)** at expanded time scale. The black dotted trace is the low pass-filtered complex spike obtained from the upper voltage trace (black continuous line) by digital filtering with 0.1 kHz cutoff. The fluorescence traces are represented in units of the differential fluorescence change ($\Delta F/F_0$). **(B1)** Computer simulation of the fluorescence response of VSFP2.3 in a Purkinje cell body as evoked by the same voltage waveform as in (**A1**; top panel). The Purkinje soma is represented by a spherical membrane (25 µm diameter) containing VSFP2.3 at a surface density of 800 units per µm^2. VSFP2.3 was represented as a kinetic reaction model developed from experimental fluorescence data of this protein (Akemann et al., 2009). The traces show the simulated yellow (YFP) fluorescence response ($\Delta F\ F_0$) with (gray) and without (red line) photon quantum noise at 2 kHz sampling frequency (and otherwise unlimited bandwidth). **(B2)** Expanded view of **(B1)** in the range of the complex spike-evoked response. **(C1)** Simulated response of VSFP2.3 to Purkinje neuron simple spikes. A spiking model of a Purkinje cell body producing intrinsic action potentials (black trace) at 40 Hz (zero injected current; 37°C) was loaded with VSFP2.3 at 800 units per µm^2. The lower trace shows the VSFP2.3 fluorescence response (2 kHz sampling) in single trial (gray) and after averaging 20 trials (without jitter; red). **(C2)** View of **(C1)** at expanded time scale. For details regarding the simulations see Akemann et al. (2009).

clamped VSFP2.1 expressing PC12 cells together with computer simulations (**Figures 5A1,A2**).

VSFP2.1 when expressed in PC12 cells could clearly monitor (without averaging over sweeps) the slow component of the voltage transient associated with a climbing fiber response, however single action potentials were not resolved. Notably, this experiment was done with the early variant VSFP2.1 and improved signals are expected from newer variants, e.g. VSFP2.3 and VSFP2.4. With the aim to characterize the performance of VSFPs as indicators of Purkinje neuron electrical activity, we incorporated a Markov chain model of VSFP2.3 (where the sensor moves between different states in a voltage-dependent manner) into a previously established single compartment model of a Purkinje neuron (Akemann and Knöpfel, 2006). Consistent with the experimental results on the time course of VSFP2.1 signals (**Figures 5A1,A2**) the simulations predicted similar response shapes reported by VSFP2.3 but with a slightly larger amplitude (**Figures 5B1,B2**). In contrast to complex spikes, single simple spikes are predicted to be resolved only after averaging over >20 sweeps (**Figures 5C1,C2**). Attempts to generate faster (and possibly more sensitive) VSFP versions resulted in VSFP3s (Lundby et al., 2008). Although this new generation of VSFPs displays an optical response consisting of a very fast component which dominates over a slower one, the dynamic range of the fast component still needs to be extended to enable routine optical reading of fast electrical activity at the single neuron level in brain tissue (Akemann et al., 2009).

POTENTIAL DRAWBACKS ASSOCIATED WITH OPTICAL IMAGING METHODS

While this review does not aim to cover methodological aspects, we shall mention a few points of caution related to optical imaging. One of the key arguments for use of optical methods is that neuronal activity can be monitored non-invasively, giving an advantage over conventional microelectrode recording. Whilst this statement is true, illumination of tissue can also be associated with tissue damage. In particular it is established that photo-chemical reactions of certain dyes (in particular conventional voltage sensitive dyes) generate toxic by-products. Modern dyes are now available that have been optimized to minimize these effects. Furthermore voltage sensitive dyes (including fluorescent protein voltage sensors) add displaceable charges to the membrane, acting to increase the membrane capacitance. This "capacitance effect" has been recently investigated in detail (Akemann et al., 2009). Calcium indicators meanwhile suffer from the fact they directly bind calcium and thus act as calcium buffers, care must therefore be taken to ensure that calcium dynamics (and thus cellular properties) are not adversely altered. The problem becomes even more complicated with protein based calcium indicators which can potentially interact not only with Ca^{2+} but also other endogenous proteins (Wallace et al., 2008). One further point to note is the possibility of interference of the signal of interest (from the fluorescent reporter) with intrinsic fluorescence signals. A prominent case is the spectral overlap between green fluorescent protein-based sensors and flavoproteins (demonstrated and discussed in detail in Diez-Garcia et al., 2007). This issue can be resolved by using fluorescent proteins whose emission has a large spectral separation from the flavoprotein signal (e.g. Mutoh et al., 2009; Perron et al., 2009).

OUTLOOK

The aim of this review is to discuss and highlight the potential of optical imaging as a methodological platform that may serve as a link between cellular neurophysiology and circuit modeling. Clearly, realization of this potential has only begun. We anticipate that genetically encoded probes in combination with modern *in vivo* imaging techniques will allow gathering of data that can drive and validate large scale circuit models. At present, questions that address the responses of larger but genetically defined cell populations are difficult to answer using traditional electrophysiology. These include questions like the spatio-temporal interaction of different cell types during oscillatory activity, revisiting sensory receptive fields, and the spatial organization of signals related to motor commands. It is the hope that, in the near future, imaging circuit dynamics at the resolution of single genetically defined cells will help answer these questions and also shed light on the neuronal codes used in the cerebellum.

ACKNOWLEDGEMENTS

We thank all members of the Knöpfel laboratory for discussions and support. The work of this laboratory is supported by grants from RIKEN BSI (TK), the RIKEN BSI directors fund (TK), NIH grant NS057631 (under a sub award granted by Yale University to TK), and JSPS (Japanese Society for the Promotion of Science).

REFERENCES

Akemann, W., and Knöpfel, T. (2006). Interaction of Kv3 potassium channels and resurgent sodium current influences the rate of spontaneous firing of Purkinje neurons. *J. Neurosci.* 26, 4602–4612.

Akemann, W., Lundby, A., Mutoh, H., and Knöpfel, T. (2009). I effect of voltage sensitive fluorescent proteins on neuronal excitability. *Biophys. J.* 96, 3959–3976.

Atasoy, D., Aponte, Y., Su, H. H., and Sternson, S. M. (2008). A FLEX switch targets channelrhodopsin-2 to multiple cell types for imaging and long-range circuit mapping. *J. Neurosci.* 28, 7025–7030.

Baker, B. J., Lee, H., Pieribone, V. A., Cohen, L. B., Isacoff, E. Y., Knöpfel, T., and Kosmidis, E. K. (2007). Three fluorescent protein voltage sensors exhibit low plasma membrane expression in mammalian cells. *J. Neurosci. Methods* 161, 32–38.

Bucholtz, F. (2008). Principles of site-specific recombinase (SSR) technology. *J. Vis. Exp.* 15, doi: 10.3791/718.

Canolty, R. T., Edwards, E., Dalal, S. S., Soltani, M., Nagarajan, S. S., Kirsch, H. E., Berger, M. S., Barbaro, N. M., and Knight, R. T. (2006). High gamma power is phase-locked to theta oscillations in human neocortex. *Science* 313, 1626–1628.

Chance, B., Cohen, P., Jobsis, F., and Schoener, B. (1962). Localized fluorometry of oxidation-reduction states of intracellular pyridine nucleotide in brain and kidney cortex of the anesthetized rat. *Science* 136, 325.

Cohen, D., and Yarom, Y. (1998). Patches of synchronized activity in the cerebellar cortex evoked by mossy-fiber stimulation: questioning the role of parallel fibers. *Proc. Natl. Acad. Sci. U.S.A.* 95, 15032–15036.

Coutinho, V., Mutoh, H., and Knöpfel, T. (2004). Functional topology of the mossy fibre-granule cell – Purkinje cell system revealed by imaging of intrinsic fluorescence in mouse cerebellum. *Eur. J. Neurosci.* 20, 740–748.

De Schutter, E., and Bower, J. M. (1994a). An active membrane model of the cerebellar Purkinje cell II. Simulation of synaptic responses. *J. Neurophysiol.* 71, 401–419.

De Schutter, E., and Bower, J. M. (1994b). An active membrane model of the cerebellar Purkinje cell. I. Simulation of current clamps in slice. *J. Neurophysiol.* 71, 375–400.

Diez-Garcia, J., Akemann, W., and Knöpfel, T. (2007). In vivo calcium imaging from genetically specified target cells in mouse cerebellum. *Neuroimage* 34, 859–869.

Diez-Garcia, J., Matsushita, S., Mutoh, H., Nakai, J., Ohkura, M., Yokoyama, J., Dimitrov, D., and Knöpfel, T. (2005). Activation of cerebellar parallel fibers monitored in transgenic mice expressing a fluorescent Ca2+ indicator protein. *Eur. J. Neurosci.* 22, 627–635.

Dimitrov, D., He, Y., Mutoh, H., Baker, B. J., Cohen, L., Akemann, W., and Knöpfel, T. (2007). Engineering and characterization of an enhanced fluorescent protein voltage sensor. *PLoS ONE* 2, e440.

Diwakar, S., Magistretti, J., Goldfarb, M., Naldi, G., and D'Angelo, E. (2009). Axonal Na+ channels ensure fast spike activation and back-propagation in cerebellar granule cells. *J. Neurophysiol.* 101, 519–532.

Engelbrecht, C. J., Johnston, R. S., Seibel, E. J., and Helmchen, F. (2008). Ultra-compact fiber-optic two-photon microscope for functional fluorescence imaging in vivo. *Opt. Express* 16, 5556–5564.

Gall, D., Prestori, F., Sola, E., D'Errico, A., Roussel, C., Forti, L., Rossi, P., and D'Angelo, E. (2005). Intracellular calcium regulation by burst discharge determines bidirectional long-term synaptic plasticity at the cerebellum input stage. *J. Neurosci.* 25, 4813–4822.

Gao, W., Chen, G., Reinert, K. C., and Ebner, T. J. (2006). Cerebellar cortical molecular layer inhibition is organized in parasagittal zones. *J. Neurosci.* 26, 8377–8387.

Garaschuk, O., Milos, R. I., and Konnerth, A. (2006). Targeted bulk-loading of fluorescent indicators for two-photon brain imaging *in vivo*. *Nat. Protoc.* 1, 380–386.

Gray, C. M., Konig, P., Engel, A. K., and Singer, W. (1989). Oscillatory responses in cat visual cortex exhibit inter-columnar synchronization which reflects global stimulus properties. *Nature* 338, 334–337.

Hasan, M. T., Friedrich, R. W., Euler, T., Larkum, M. E., Giese, G., Both, M., Duebel, J., Waters, J., Bujard, H., Griesbeck, O., Tsien, R. Y., Nagai, T., Miyawaki, A., and Denk, W. (2004). Functional fluorescent Ca2+ indicator proteins in transgenic mice under TET control. *PLoS Biol* 2, e163.

Heim, N., Garaschuk, O., Friedrich, M. W., Mank, M., Milos, R. I., Kovalchuk, Y., Konnerth, A., and Griesbeck, O. (2007). Improved calcium imaging in transgenic mice expressing a troponin C-based biosensor. *Nat. Methods* 4, 127–129.

Hendel, T., Mank, M., Schnell, B., Griesbeck, O., Borst, A., and Reiff, D. F. (2008). Fluorescence changes of genetic calcium indicators and OGB-1 correlated with neural activity and calcium in vivo and in vitro. *J. Neurosci.* 28, 7399–7411.

Hires, S. A., Tian, L., and Looger, L. L. (2008). Reporting neural activity with genetically encoded calcium indicators. *Brain Cell Biol.* 36, 69–86.

Hoogland, T. M., Kuhn, B., Gobel, W., Huang, W., Nakai, J., Helmchen, F., Flint, J., and Wang, S. S. (2009). Radially expanding transglial calcium waves in the intact cerebellum. *Proc. Natl. Acad. Sci. U.S.A.* 106, 3496–3501.

Huang, C. M., Wang, L., and Huang, R. H. (2009). Cerebellar granule cell: ascending axon and parallel fiber. *Eur. J. Neurosci.* 23, 1731–1737.

Ikegaya, Y., Aaron, G., Cossart, R., Aronov, D., Lampl, I., Ferster, D., and Yuste, R. (2004). Synfire chains and cortical songs: temporal modules of cortical activity. *Science* 304, 559–564.

Kerr, J. N., de Kock, C. P., Greenberg, D. S., Bruno, R. M., Sakmann, B., and Helmchen, F. (2007). Spatial organization of neuronal population responses in layer 2/3 of rat barrel cortex. *J. Neurosci.* 27, 13316–13328.

Kerr, J. N., Greenberg, D., and Helmchen, F. (2005). Imaging input and output of neocortical networks in vivo. *Proc. Natl. Acad. Sci. U.S.A.* 102, 14063–14068.

Knöpfel, T., Diez-Garcia, J., and Akemann, W. (2006). Optical probing of neuronal circuit dynamics: genetically encoded versus classical fluorescent sensors. *Trends Neurosci.* 29, 160–166.

Knöpfel, T., Vranesic, I., Staub, C., and Gahwiler, B. H. (1991). Climbing fibre responses in olivo-cerebellar slice cultures. II. Dynamics of cytosolic calcium in purkinje cells. *Eur. J. Neurosci.* 3, 343–348.

Lee, A. K., Manns, I. D., Sakmann, B., and Brecht, M. (2006). Whole-cell recordings in freely moving rats. *Neuron* 51, 399–407.

Leznik, E., Makarenko, V., and Llinas, R. (2002). Electrotonically mediated oscillatory patterns in neuronal ensembles: an in vitro voltage-dependent dye-imaging study in the inferior olive. *J. Neurosci.* 22, 2804–2815.

Llinas, R., Leznik, E., and Makarenko, V. I. (2002). On the amazing olivocerebellar system. *Ann. N. Y. Acad. Sci.* 978, 258–272.

Lundby, A., Mutoh, H., Dimitrov, D., Akemann, W., and Knöpfel, T. (2008). Engineering of a genetically encodable fluorescent voltage sensor exploiting fast Ci-VSP voltage-sensing movements. *PLoS ONE* 3, e2514.

Luo, L., Callaway, E. M., and Svoboda, K. (2008). Genetic dissection of neural circuits. *Neuron* 57, 634–660.

Mank, M., and Griesbeck, O. (2008). Genetically encoded calcium indicators. *Chem. Rev.* 108, 1550–1564.

Mank, M., Santos, A. F., Direnberger, S., Mrsic-Flogel, T. D., Hofer, S. B., Stein, V., Hendel, T., Reiff, D. F., Levelt, C., Borst, A., Bonhoeffer, T., Hübener, M., and Griesbeck, O. (2008). A genetically encoded calcium indicator for chronic in vivo two-photon imaging. *Nat. Methods* 5, 805–811.

Mao, T., O'Connor, D. H., Scheuss, V., Nakai, J., and Svoboda, K. (2008). Characterization and subcellular targeting of GCaMP-type genetically-encoded calcium indicators. *PLoS ONE* 3, e1796.

Medina, J. F., and Mauk, M. D. (2000). Computer simulation of cerebellar information processing. *Nat. Neurosci.* 3, 1205–1211.

Metzger, F., Repunte-Canonigo, V., Matsushita, S., Akemann, W., Diez-Garcia, J., Ho, C. S., Iwasato, T., Grandes, P., Itohara, S., Joho, R. H., and Knöpfel, T. (2002). Transgenic mice expressing a pH and Cl- sensing yellow-fluorescent protein under the control of a potassium channel promoter. *Eur. J. Neurosci.* 15, 40–50.

Middleton, S. J., Racca, C., Cunningham, M. O., Traub, R. D., Monyer, H., Knöpfel, T., Schofield, I. S., Jenkins, A., and Whittington, M. A. (2008). High-frequency network oscillations in cerebellar cortex. *Neuron* 58, 763–774.

Miyawaki, A., Llopis, J., Heim, R., McCaffery, J. M., Adams, J. A., Ikura, M., and Tsien, R. Y. (1997). Fluorescent indicators for Ca2+ based on green fluorescent proteins and calmodulin. *Nature* 388, 882–887.

Muri, R., and Knöpfel, T. (1994). Activity induced elevations of intracellular calcium concentration in neurons of the deep cerebellar nuclei. *J. Neurophysiol.* 71, 420–428.

Mutoh, H., Perron, A., Dimitrov, D., Iwamoto, Y., Akemann, W., Chudakov, D. M., and Knöpfel, T. (2009). Spectrally-resolved response properties of the three most advanced FRET based fluorescent protein voltage probes. *PLoS ONE* 4, e4555.

Niedermeyer, E. (2004). The electrocerebellogram. *Clin. EEG Neurosci.* 35, 112–115.

Palmer, A. E., Giacomello, M., Kortemme, T., Hires, S. A., Lev-Ram, V., Baker, D., and Tsien, R. Y. (2006). Ca2+ indicators based on computationally redesigned calmodulin-peptide pairs. *Chem. Biol.* 13, 521–530.

Perron, A., Mutoh, H., Akemann, W., Gautam, S. G., Dimitrov, D., Iwamoto, Y., and Knöpfel, T. (2009). Second and third generation voltage-sensitive fluorescent proteins for monitoring membrane potential. *Front. Mol. Neurosci.* 2,5. doi: 10.3389/neuro.02.005.2009. [Epub ahead of print].

Pologruto, T. A., Yasuda, R., and Svoboda, K. (2004). Monitoring neural activity and $[Ca^{2+}]$ with genetically encoded Ca2+ indicators. *J. Neurosci.* 24, 9572–9579.

Qiu, D. L., and Knöpfel, T. (2007). An NMDA receptor/nitric oxide cascade in presynaptic parallel fiber-Purkinje neuron long-term potentiation. *J. Neurosci.* 27, 3408–3415.

Qiu, D. L., and Knöpfel, T. (2009). Presynaptically expressed long-term depression at cerebellar parallel fiber synapses. *Pflugers Arch* 457, 865–875.

Quadroni, R., and Knöpfel, T. (1994). Compartmental models of type A and type B guinea pig medial vestibular neurons. *J. Neurophysiol.* 72, 1911–1924.

Reinert, K. C., Dunbar, R. L., Gao, W., Chen, G., and Ebner, T. J. (2004). Flavoprotein autofluorescence imaging of neuronal activation in the cerebellar cortex in vivo. *J. Neurophysiol.* 92, 199–211.

Reinert, K. C., Gao, W., Chen, G., and Ebner, T. J. (2007). Flavoprotein autofluorescence imaging in the cerebellar cortex in vivo. *J. Neurosci. Res.* 85, 3221–3232.

Rossini, L., Rossini, P., and Chance, B. (1991). Continuous read-out of cytochrome-B, flavin and pyridine-nucleotide oxidoreduction processes in the perfused frog-heart and contracting skeletal-muscle. *Pharmacol. Res.* 23, 349–365.

Sacconi, L., Mapelli, J., Gandolfi, D., Lotti, J., O'Connor, R. P., D'Angelo, E. and Pavone, F. S. (2008). Optical recording of electrical activity in intact neuronal networks with random access second-harmonic generation microscopy. *Opt. Express* 16, 14910–14921.

Sakai, R., Repunte-Canonigo, V., Raj, C. D., and Knöpfel, T. (2001). Design and characterization of a DNA-encoded, voltage-sensitive fluorescent protein. *Eur. J. Neurosci.* 13, 2314–2318.

Soteropoulos, D. S., and Baker, S. N. (2006). Cortico-cerebellar coherence during a precision grip task in the monkey. *J. Neurophysiol.* 95, 1194–1206.

Souslova, E. A., Belousov, V. V., Lock, J. G., Strömblad, S., Kasparov, S., Bolshakov, A. P., Pinelis, V. G., Labas, Y. A., Lukyanov, S., Mayr, L. M., and Chudakov, D. M. (2007). Single fluorescent protein-based Ca2+ sensors with increased dynamic range. *BMC Biotechnol.* 7, 37, 1–10.

Staub, C., De, S. E., and Knöpfel, T. (1994). Voltage-imaging and simulation of effects of voltage- and agonist-activated conductances on soma-dendritic voltage coupling in cerebellar Purkinje cells. *J. Comput. Neurosci.* 1, 301–311.

Sullivan, M. R., Nimmerjahn, A., Sarkisov, D. V., Helmchen, F., and Wang, S. S. (2005). In vivo calcium imaging of circuit activity in cerebellar cortex. *J. Neurophysiol.* 94, 1636–1644.

Tamamaki, N., Yanagawa, Y., Tomioka, R., Miyazaki, J., Obata, K., and Kaneko, T. (2003). Green fluorescent protein expression and colocalization with calretinin, parvalbumin, and somatostatin in the GAD67-GFP knock-in mouse. *J. Comp. Neurol.* 467, 60–79.

Tank, D. W., Sugimori, M., Connor, J. A., and Llinas, R. R. (1988). Spatially resolved calcium dynamics of mammalian Purkinje cells in cerebellar slice. *Science* 242, 773–777.

Timofeev, I., and Steriade, M. (1997). Fast (mainly 30–100 Hz) oscillations in the cat cerebellothalamic pathway and their synchronization with cortical potentials. *J. Physiol.* 504(Pt 1), 153–168.

Traub, R. D., Middleton, S. J., Knöpfel, T., and Whittington, M. A. (2008). Model of very fast (>75 Hz) network oscillations generated by electrical coupling between the proximal axons of cerebellar Purkinje cells. *Eur. J. Neurosci.* 28, 1603–1616.

Tsutsui, H., Karasawa, S., Okamura, Y., and Miyawaki, A. (2008). Improving membrane voltage measurements using FRET with new fluorescent proteins. *Nat. Methods* 5, 683–685.

Vanzetta, I., Hildesheim, R., and Grinvald, A. (2005). Compartment-resolved imaging of activity-dependent dynamics of cortical blood volume and oximetry. *J. Neurosci.* 25, 2233–2244.

Vranesic, I., Iijima, T., Ichikawa, M., Matsumoto, G., and Knöpfel, T. (1994). Signal transmission in the parallel fiber-Purkinje cell system visualized by high-resolution imaging. *Proc. Natl. Acad. Sci. U.S.A.* 91, 13014–13017.

Wallace, D. J., Borgloh, S. M., Astori, S., Yang, Y., Bausen, M., Kugler, S., Palmer, A. E., Tsien, R. Y., Sprengel, R., Kerr, J. N., Denk, W., and Hasan, M. T. (2008). Single-spike detection in vitro and in vivo with a genetic Ca2+ sensor. *Nat Methods* 5, 797–804.

Womelsdorf, T., Schoffelen, J. M., Oostenveld, R., Singer, W., Desimone, R., Engel, A. K., and Fries, P. (2007). Modulation of neuronal interactions through neuronal synchronization. *Science* 316, 1609–1612.

Zhou, W. L., Yan, P., Wuskell, J. P., Loew, L. M., and Antic, S. D. (2008). Dynamics of action potential backpropagation in basal dendrites of prefrontal cortical pyramidal neurons. *Eur. J. Neurosci.* 27, 923–936.

Conflict of Interest Statement: The authors declare that the research was conducted in the absence of any commercial or financial relationships that could be construed as a potential conflict of interest.

Received: 23 April 2009; paper pending published: 07 May 2009; accepted: 30 June 2009; published online: 20 July 2009.
*Citation: Akemann W, Middleton SJ and Knöpfel T (2009) Optical imaging as a link between cellular neurophysiology and circuit modeling. Front. Cell. Neurosci. (2009) **3**:5. doi: 10.3389/neuro.03.005.2009*

frontiers in
CELLULAR NEUROSCIENCE

ORIGINAL RESEARCH ARTICLE
published: 20 July 2009
doi: 10.3389/neuro.03.006.2009

Synchronization in primate cerebellar granule cell layer local field potentials: basic anisotropy and dynamic changes during active expectancy

Richard Courtemanche[1]*, Pascal Chabaud[2] and Yves Lamarre[3]

[1] *FRSQ Groupe de Recherche en Neurobiologie Comportementale (CSBN), Concordia University, Canada*
[2] *Centre de Recherche en Sciences du Sport (EA 647), Université Claude Bernard-Lyon 1, France*
[3] *FRSQ Groupe de Recherche sur le Système Nerveux Central (GRSNC), Université de Montréal, Canada*

Edited by:
Egidio D'Angelo, University of Pavia, Italy

Reviewed by:
Alfredo Fontanini, Stony Brook University, USA
Stéphane Dieudonné, Ecole Normale Supérieure, France
Egidio D'Angelo, University of Pavia, Italy

***Correspondence:**
Richard Courtemanche, Center for Studies in Behavioral Neurobiology, Department of Exercise Science, SP-165-17, Richard J. Renaud Science Complex, 7141 Sherbrooke Street West, Concordia University, Montréal, QC, Canada H4B 1R6.
e-mail: rcourt@alcor.concordia.ca

The cerebellar cortex is remarkable for its organizational regularity, out of which task-related neural networks should emerge. In Purkinje cells, both complex and simple spike network patterns are evident in sensorimotor behavior. However, task-related patterns of activity in the granule cell layer (GCL) have been less studied. We recorded local field potential (LFP) activity simultaneously in pairs of GCL sites in monkeys performing an active expectancy (lever-press) task, in passive expectancy, and at rest. LFP sites were selected when they showed strong 10–25 Hz oscillations; pair orientation was in stereotaxic sagittal and coronal (mainly), and diagonal. As shown previously, LFP oscillations at each site were modulated during the lever-press task. Synchronization across LFP pairs showed an evident basic anisotropy at rest: sagittal pairs of LFPs were better synchronized (more than double the cross-correlation coefficients) than coronal pairs, and more than diagonal pairs. On the other hand, this basic anisotropy was modifiable: during the active expectancy condition, where sagittal and coronal orientations were tested, synchronization of LFP pairs would increase just preceding movement, most notably for the coronal pairs. This lateral extension of synchronization was not observed in passive expectancy. The basic pattern of synchronization at rest, favoring sagittal synchrony, thus seemed to adapt in a dynamic fashion, potentially extending laterally to include more cerebellar cortex elements. This dynamic anisotropy in LFP synchronization could underlie GCL network organization in the context of sensorimotor tasks.

Keywords: oscillations, cerebellar cortex, granule cell layer, synchronization, network activity, sensorimotor

INTRODUCTION

The structure of the cerebellar cortex is remarkably regular (Bloedel, 1992; Eccles et al., 1967), an organization out of which must ultimately emerge task-related cerebellar neural networks. Anatomical features such as afferent and efferent organization will partly determine the network organization, outlining the potential information processing units (Apps and Garwicz, 2005; Oscarsson, 1979; Voogd and Glickstein, 1998). In addition, methods for assessing neural network organization in physiological terms, such as the recording of local circuit activity at multiple sites will provide information about the way in which the different elements of the network are dynamically linked (Miller and Wilson, 2008). A preliminary evaluation of such dynamical networks can include the assessment of local field potential (LFP) activity and synchronization in identified areas (Buzsaki, 2006; Schnitzler and Gross, 2005; Singer et al., 1997). Focusing on cerebellar cortex 10–25 Hz LFP oscillations (Courtemanche et al., 2002; Pellerin and Lamarre, 1997) in the paramedian lobule, we measured the LFP synchronization occurring in the cerebro-cerebellar networks, and found task-dependent modulation of this activity in an active sensorimotor task (Courtemanche and Lamarre, 2005). An open question is how this activity is shaped within the cerebellar cortex.

In search of cerebellar cortex population activity, task-related multiple-electrode recordings have mostly focused on the Purkinje cell simple and complex spikes. For example, olivocerebellar activity is synchronized into parasagittal bands (Lang et al., 1999), and presents a population-level mosaic pattern in relation with movement (Welsh et al., 1995). Simple spikes also show population patterns of activity (Bell and Grimm, 1969; Shin and De Schutter, 2006), and a medio-lateral (on-beam) preferential synchrony pattern emerges during movement (Heck et al., 2007). Complex and simple spike population activity could interact in determining these network patterns (Schwarz and Welsh, 2001). Bearing some spatio-temporal similarities in signal to field potentials (Gao et al., 2003; Qiu et al., 2008; Rockni et al., 2007), neural activity-dependent imaging, such as in the use of activity-dependent fluorescent dyes to assess neural activity across tissue, also provides a window into network interactions. Applied to the cerebellar cortex, one of the main results was the physiological identification of parasagittal bands to the stimulation of the inferior olive or climbing fibers in the underlying white matter (Brown and Ariel, 2009; Gao et al., 2003; Rockni et al., 2007, 2008). Using pH-sensitive dyes, Gao et al. (2003) found that beams of parallel fiber stimulation could monitor the link between parasagittal bands via Purkinje cell postsynaptic

LTD, after conjunctive parallel fiber-climbing fiber stimulation. Rockni et al. (2007) identified parasagittal bands following climbing fiber stimulation, but also identified a patch-like activation through the stimulation of identified mossy fiber responses. Finally, parasagittal band zonation with inferior olive stimulation, and a relatively patchy response to granule cell layer stimulation using similar dyes was also emphasized in Brown and Ariel (2009), in the turtle cerebellar cortex. Using those methods, network interactions at the surface of the cerebellar cortex are starting to be documented.

Despite recent important advances in the understanding in the organization of the granule cell layer local circuit organization (D'Angelo, 2008; D'Angelo and de Zeeuw, 2009), multi-site task-related activity in the granule cell layer (GCL) has been less studied. Local circuit properties, such as the granule-Golgi cell interaction (De Schutter and Bjaalie, 2001; Geurts et al., 2003) have been investigated, but a more general organization of the granule cell layer based on the relations between distant local circuits has not been firmly established. Here we address the multi-site relationship in the primate GCL by focusing on the 10–25 Hz LFP oscillations present at rest, which are modulated during a motor task (Courtemanche et al., 2002; Pellerin and Lamarre, 1997). GCL oscillations have also been found in the resting rodent, strongest at ~7 Hz (Dugué et al., 2009; Hartmann and Bower, 1998; O'Connor et al., 2002). The goal of this study was to identify synchronization patterns, by recording simultaneous GCL LFP pairs oriented in a sagittal or coronal stereotaxic fashion, as monkeys were at rest or performed active and passive expectancy tasks. GCL LFP synchronization was anisotropic at rest, and dynamic during active expectancy, across our recording pairs: this LFP synchronization could represent inherent influences in cerebellar cortex cell population selection and task-related sensorimotor processing.

MATERIALS AND METHODS

ANIMALS

Three adult *Macaca mulatta*, one female (K, 4.7 kg) and two males (F, 7.8 kg and Z, 7.0 kg) were implanted with a recording chamber placed over the left posterior parietal cortex, to access the cerebellum, following known procedures (Lamarre et al., 1970). Animals were seated in a primate chair, unrestrained except for head fixation. All animal handling, care and surgical procedures were in accordance with the guidelines of the Canadian Council on Animal Care, and were approved by the Université de Montréal Institutional Animal Care and Use Committee.

RECORDINGS AND BEHAVIORAL CONDITIONS

An elaborate description of the basic recording procedures is given in Courtemanche et al. (2002). The main changes here are the modifications to permit simultaneous deep LFP recordings, which require a sturdy system to drive the microelectrodes through the dura and tentorium. Briefly, cerebellar cortex activity was recorded with two glass-coated tungsten microelectrodes (0.2–1 MΩ) lowered carefully to record primate GCL 10–25 Hz oscillations, aiming for the paramedian lobule (Pellerin and Lamarre, 1997). Electrode arrangements for monkeys F and Z were either sagittal or coronal, using a multi-electrode holder controlled digitally; this holder permitted an inter-electrode distance of 3 or 6 mm, and the plane of orientation could be aligned with either the stereotaxic sagittal or coronal plane. The depth of each microelectrode could be controlled independently. For monkey K, the two microelectrodes were held diagonally by two separate holders, before the multi-electrode holder had been designed; however, these holders' characteristics only permitted dual recordings in a 'diagonal' orientation. Signal was band-pass filtered at 3–70 Hz for LFPs (sampled at 1000 Hz) and 0.3–10 kHz for monitoring multi-unit activity, the latter used to locate the layers. The reference electrode was a copper wire located in a 0.9% saline solution filling the recording chamber. Upon reaching deep GCL activity corresponding to 10–25 Hz oscillations, recordings were made in three blocked conditions: (1) active expectancy (monkeys F and Z, with lever and juice pipette), (2) passive expectancy (monkeys F and Z, sitting quietly, no lever but with juice pipette) and (3) rest (all three monkeys, sitting quietly and attentive, for successive 5 s periods, no lever, no juice pipette). In the active expectancy condition, the monkeys pressed a lever with the left (ipsilateral) hand, after a delay of 1.1–1.5 s following a tone (400 Hz, 35 dB, duration 1.5 s), rewarded with drops of juice. In the passive expectancy condition, the monkey remained seated with the pipette available, but did not produce any stereotypical movement except readiness to receive juice. At rest, the monkey remained seated, and shifted the body occasionally. Monkeys were repeatedly exposed to the behavioral conditions, and following training, the monkeys adopted a stereotypical movement pattern in the active expectancy condition. The lever signal was sampled at 1000 Hz. For passive expectancy, the lever was removed and reward was given without any required action, in the same percentage of trials (70%) as the active condition, after a 1.1–1.5 s delay after stimulus onset.

ANALYSES

LFPs were analyzed using Fast Fourier Transforms (FFT) for rhythmicity, and the cross-correlation coefficient function for synchronization between the recording sites.

Rest

In the rest condition, we calculated the proportion of the signal within 10–25 Hz (Courtemanche et al., 2002) for consecutive 200-ms windows, overlapped by 50% to better catch oscillation episodes. To measure the relation between oscillatory spindle co-occurrence at both sites, which we called concomitance, we calculated the linear correlation between the 10–25 Hz rhythmicity at each site, over consecutive windows. This measure provides an estimate of the tightness of the relation in oscillatory content at the two electrodes in a stationary condition, i.e., 'if site 1 has strong oscillations, does site 2 also have the same?' (Courtemanche and Lamarre, 2005; Courtemanche et al., 2003). Measurements of the rhythmicity between the different orientations were compared with *t*-tests. Across the same time windows, we also calculated the cross-correlation coefficient (zero-lag value, which was appropriate for our LFP-LFP relations), providing a measure of the synchronization between the two LFPs (Courtemanche and Lamarre, 2005; Murthy and Fetz, 1996). In contrast to the quantification of the similarity in oscillatory profile, this is a measurement that evaluates the degree of simultaneous change in the signal (Gerstein and Nicolelis, 1999; Roelfsema et al., 1997). For statistical analysis,

t-tests compared the pairs across the different orientations, for all windows and each monkey (in one case, we used nonparametric tests, as the assumption of normality was violated, Kolmogorov–Smirnov $p > 0.05$). Thus, group values for synchronization and concomitance were compared across all windows, per pair orientation, per monkey.

Active and passive expectancy

In the active and passive conditions, rhythmicity was evaluated with the temporal spectral evolution (TSE) (Salmelin and Hari, 1994), which addresses the occurrence and amplitude of oscillations relative to the task. This consists in band-pass filtering (10–25 Hz) the LFPs, rectifying this filtered signal, and then averaging this new product across trials. For evaluation and illustration of the LFP-LFP synchronization, the cross-correlation coefficient was calculated similar to the rest condition, on 200-ms time windows shifted by 100 ms across the trial. In addition, for statistical analysis, TSE and cross-correlation coefficient values were determined over four different epochs: pre-stimulus (Ps), a 500-ms time window immediately preceding the onset of the stimulus, delay1 (Dl1), a 400-ms window starting 300 ms after stimulus onset, delay2 (Dl2), a 400-ms time window occurring 400 ms before the lever press up to the time of the press, and delay3 (Dl3), a 400-ms time window starting at 4000 ms after the stimulus. Multivariate analyses of variance were performed on the relative TSE values (Ps at 0% change) and on the cross-correlation values (same as Courtemanche and Lamarre, 2005), with each epoch as a repeated measure, and comparing the sagittal/coronal orientations, and the active/passive/rest conditions.

HISTOLOGY

In the last recording session, electrolytic lesions were made in the cerebellum at sites showing oscillatory activity. Two days later, monkeys were deeply anesthetized and perfused through the heart using a buffered 9% formaline–8% saline solution. Recording sites were controlled on 50-μm sagittal sections of the cerebellum stained with cresyl violet.

RESULTS

DATABASE

We recorded 15 sessions which had either stereotaxic sagittal or coronal electrode arrangements (monkeys F and Z), and for monkey K, diagonal electrode arrangements. A total of 27 recording pairs were recorded in the three monkeys. Raw LFP data were screened for removal of artifacts; for active and passive expectancy conditions, only the rewarded trials were kept. The average number of trials per session for each monkey, pooled for the active, passive, and rest conditions, were: monkey F (75 trials), Z (73 trials), and K (30 trials, rest only). The recording sites were principally localized, and aimed, to the paramedian lobule and caudal Crus II; in the case of coronal pairs, the medial site sometimes touched the lateral vermis.

OSCILLATIONS AND SYNCHRONIZATION DURING REST

Two LFP pairs, sagittal and coronal, are described first; the sagittal pair sites were both located in the paramedian lobule (**Figure 1A**), while for the coronal pairs, the medial site touched the caudal vermis, and the lateral site was in the paramedian lobule (**Figure 1B**). The recording pairs were separated by 6 mm, one following the stereotaxic sagittal plane (**Figure 1A**), and the others following the stereotaxic coronal plane (**Figure 1B**). Site localization was based on the reconstruction from the electrolytic lesions. The oscillations simultaneously waxed and waned on both microelectrodes, with periods of weak (yellow box), and strong oscillations (green box). During periods of strong oscillations, the LFP pairs would display a similar main peak frequency, evident for both the sagittal pair and the coronal pair (**Figures 1C,F**, ~17 Hz). Periods of strong oscillations would also be accompanied by an increased LFP synchronization, for both pairs, at zero lag (**Figures 1D,E**). In the presented example, the sagittal pair presented a stronger cross-correlation

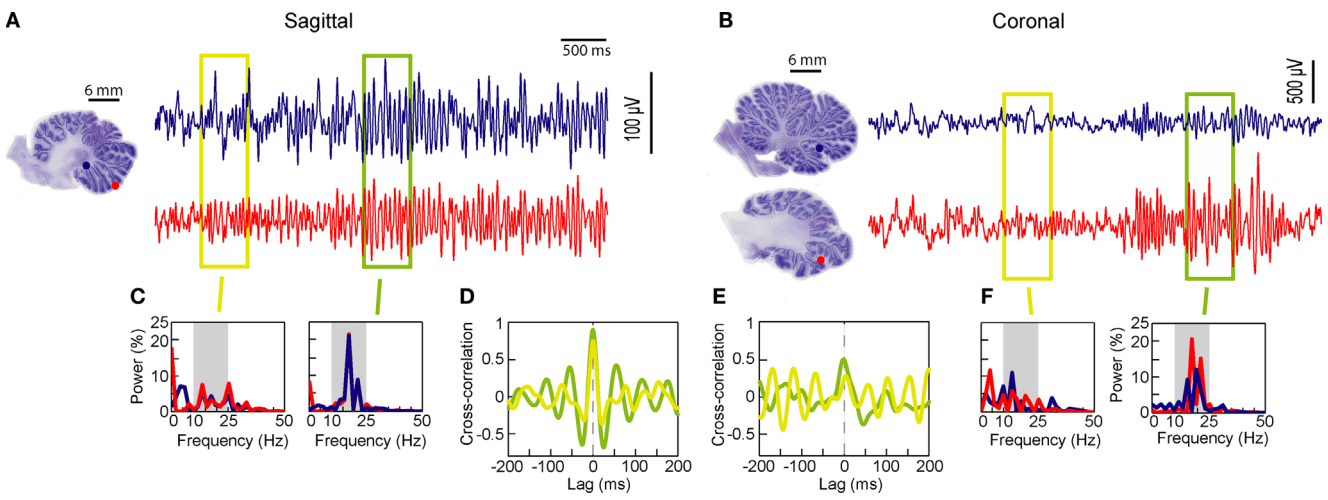

FIGURE 1 | Cerebellar cortex GCL simultaneous LFP recordings at rest, monkey F. (A,B) Simultaneous LFPs recorded sagittally or coronally. Estimated positions of the recording pairs shown, based on reconstruction from electrolytic lesions. Two periods are highlighted, one with low (yellow box) and one with strong (green box) oscillations. **(C,F)** Fast Fourier Transforms (FFT) for each recording site, for each selected period. **(D,E)** Cross-correlation for each selected period. Recording sites, field potential and FFT traces are color-matched.

coefficient (~0.9 at zero-lag) than the cross-correlation coefficient for the coronal pair (~0.4), a distinction that remained for both strong and weak oscillations.

During rest, to assess how oscillations would co-occur on both traces, we measured the 10–25 Hz relative power (%) at both sites, the 'concomitance'. **Figures 2A,B** shows the relative power for multiple windows ($n = 792$) between two simultaneously recorded LFPs in monkey F. The relationship shows a stronger linear correlation ('concomitance coefficient') between the 10–25 Hz content for the sagittal pair [$r = 0.71$, $F(1,790) = 798.79$, $p < 0.001$] than for the coronal pair [$r = 0.39$, $F(1,790) = 145.81$, $p < 0.001$]. As a control for chance simultaneity, comparing site 1 of the coronal pair with site 2 of the sagittal pair (thus on different days, disjointed in time) did not provide a significant linear correlation [$F(1,790) = 0.006$, $p = 0.87$]. When looking at a larger dataset, group measures on oscillation concomitance (10 pairs, 5 coronal, 3 sagittal, 2 diagonal, total of 13351 windows, in 3 monkeys), are shown in **Figure 2D**, for each monkey. Monkeys F and Z had stereotaxic sagittal and coronal pairs tested; we represent here the sagittal pairs with a lateral distance of zero, and coronal pairs were tested at a lateral distance of 6 mm in monkey F, and 3 mm in monkey Z. Sagittal distances were the same as for the coronal tests. These comparisons reveal a greater concomitance of 10–25 oscillations for sagittal pairs over coronal pairs, [monkey F, $t(82) = -5.32$, $p < 0.001$, monkey Z, $t(20) = -4.54$, $p < 0.001$], while concomitance for diagonal pairs in monkey K was not different when comparing a lateral distance of 2 and 6 mm [$t(20) = -1.08$, $p = 0.294$]. The sagittal pairs thus had a greater tendency to oscillate simultaneously than coronal, even if the effective distance separating the pair elements was the same.

For the same pairs, LFP cross-correlation coefficients across the same multiple 200-ms time windows were measured to evaluate synchronization (**Figures 2C,D**). The example shown for two pairs from monkey Z (**Figure 2C**, 1250 windows) present a greater sagittal than coronal synchronization, at zero lag, and regular across windows, as can be evaluated from the overlaid standard deviation. From the whole dataset, for monkeys F and Z, cross-correlation coefficient values for sagittal pairs (zero mm lateral distance on the abscissa) were twice as high as those of coronal pairs (3 or 6 mm lateral distance), as shown in **Figure 2D** [monkey F, Kruskal–Wallis test, H $t(1,245) = 116.81$, $p < 0.001$; monkey Z, $t(145) = -39.71$, $p < 0.01$]. In monkey K, with

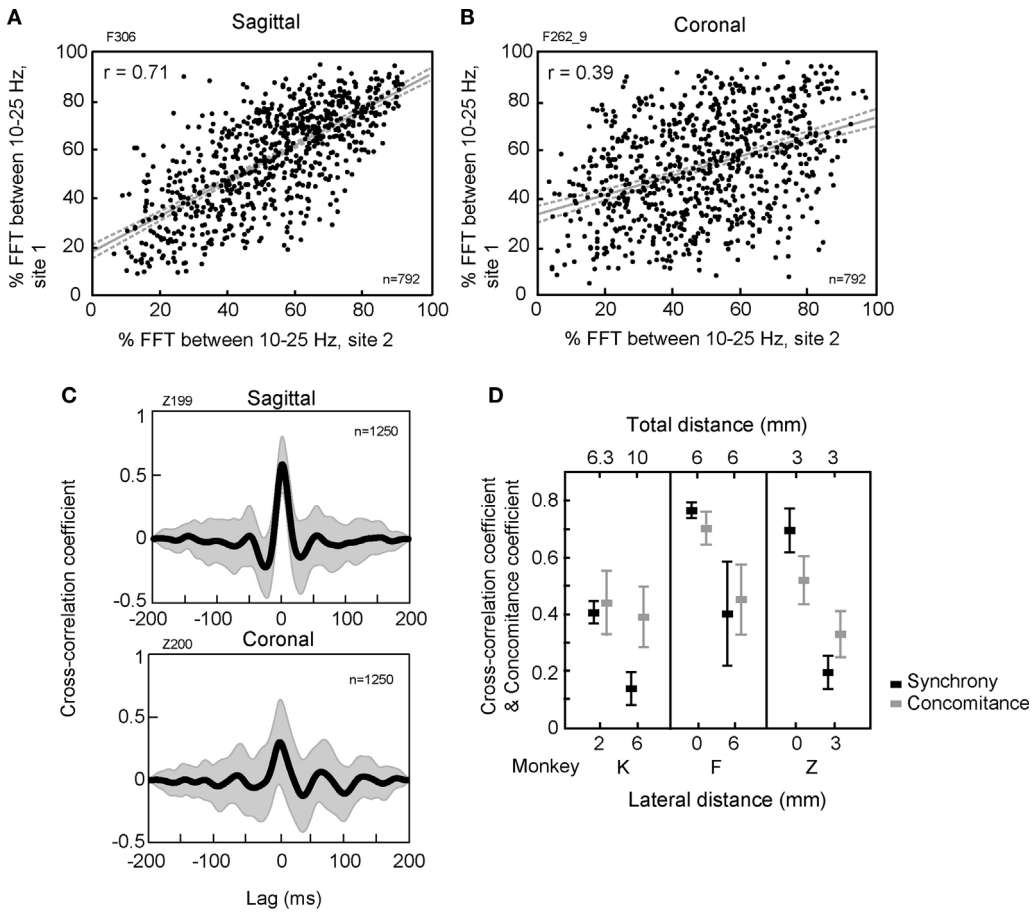

FIGURE 2 | Oscillation and synchronization properties of cerebellar GCL LFPs during rest. (A,B) Relationship between the 10–25 Hz oscillatory content (% of the LFP signal between 10–25 Hz) at both recording sites for a sagittal and a coronal pair in monkey F. Linear correlation value (r), regression line and 95% confidence interval indicated. **(C)** Averaged cross-correlograms (s.d., gray area) for multiple windows ($n = 1250$) for a sagittal and a coronal pair in monkey Z. **(D)** Mean and standard deviation for cross-correlation and concomitance coefficients in relation to both the lateral and the total distances between the two recorded sites for each monkey (K, F, and Z).

diagonally-oriented pairs, the cross-correlation coefficients were between the values of coronal and sagittal pairs [$t(96) = -27.03$, $p < 0.01$, higher for a lateral distance of 2 mm vs. 6 mm].

These concomitance and synchronization results provide evidence that LFP-LFP relations in the rest condition showed anisotropy, with greater similarities in the signals recorded at each site when the electrodes were arranged sagittally, in contrast to the other orientations. A striking feature here is that sagittal concomitance and cross-correlation were much higher than the coronal values, despite having the same effective distance separating the LFP recording sites.

OSCILLATIONS AND SYNCHRONIZATION DURING ACTIVE AND PASSIVE EXPECTANCY

The 10–25 Hz GCL LFP oscillations and synchronization between recorded sites were also evaluated during active expectancy (the lever-press task), and passive expectancy (free rewards). In active expectancy, the monkey had to wait until the appropriate time window to press the lever, while in passive expectancy, the lever was taken away, and the monkey did not have to move at all; in this condition, both monkeys (F and Z) remained immobile. Results are shown in **Figures 3A–F** (one experimental session in sagittal and

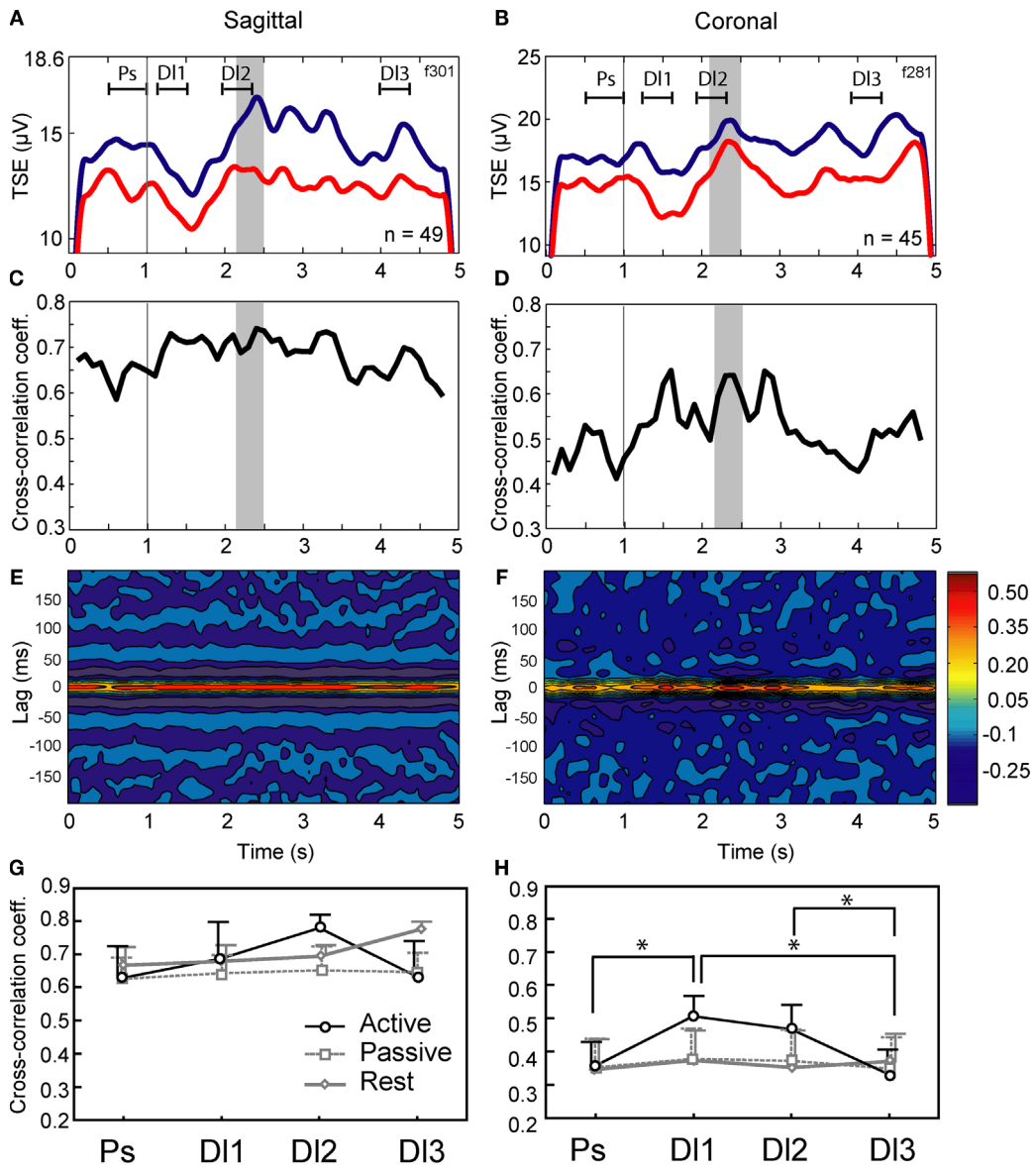

FIGURE 3 | Modulation of cerebellar LFP oscillations and synchronization of LFPs in the active condition, for a sagittal pair and a coronal pair. **(A,B)** Modulation of the 10–25 Hz oscillations across the trial, as shown by the temporal spectral evolution (TSE). Grey area: reward window, vertical line, stimulus onset. Line colors: A. blue-anterior, red-posterior; B. blue-medial, red-lateral. The different delays Ps, DI1, DI2, and DI3 are indicated. **(C,D)** Cross-correlation coefficients for the same experiments. **(E,F)** Cross-correlogram for the same experiments (abscissa: time in the trial; ordinate: lag; color: height in the correlogram). Parts A to F: typical results illustrated by data recorded in monkey F. **(G,H)** Cross-correlation of LFPs in all conditions (active, passive, and rest), for each delay (Ps, DI1, DI2, and DI3), for both monkeys F and K. Means and s.e.m. indicated; $*p < 0.05$ (Tukey *post-hoc*) of this value (active condition) vs. other active condition delays, and passive and rest conditions.

one in coronal for monkey F, and G,H group data, for monkeys F and Z). For both monkeys, LFP oscillations were modulated during the active task (see **Figures 3A,B** for a typical result obtained in monkey F): for most oscillatory sites, TSE values showed a decrease/re-increase pattern between stimulus onset and lever press, similar for both LFPs of either the sagittal or the coronal pairs. This mirrors the results showed in Courtemanche et al. (2002). The movements made by both monkeys to achieve the lever-press were stereotypical: in the time period leading to Dl2, the decrease in the LFP oscillations was related to the period when the hand position was most variable on the lever. The Dl2 period corresponds to the time when the monkey was generating the force to depress the lever. This is the same behavior as described by our group (Courtemanche and Lamarre, 2005; Courtemanche et al., 2002). For the synchronization values in-task, cross-correlation coefficients measured throughout the trials were greater for the sagittal pair than for the coronal pair (**Figures 3C,D**), as they were during rest. A dynamical aspect also appeared for the coronal pair, as cross-correlation coefficients clearly increased during the task (**Figure 3D**); coefficients during Dl1 and Dl2 increased to ~0.60 from initially ~0.47 during the Ps period. The 3-D color-coded correlograms in **Figures 3E,F** show that the maximal correlation was always at zero-lag.

LFP synchronization during the task was compared across the three experimental conditions, across multiple sessions (range 3–7 sessions per condition × orientation) in monkeys F and Z (**Figures 3G,H**). For monkey F, a MANOVA on the cross-correlation coefficients for the three conditions (active and passive expectancy, rest) × two orientations (sagittal and coronal) × four delays (Ps, Dl1, Dl2, Dl3) shows a main effect of electrode orientation [$F(1,12) = 10.86$, $p < 0.01$, sagittal > coronal], and a condition × delay interaction [$F(6,36) = 2.68$, $p < 0.05$]. For monkey Z, the MANOVA showed main effects of electrode orientation [$F(1,3) = 68.53$, $p < 0.01$, sagittal > coronal], delay [$F(3,9) = 9.61$, $p < 0.01$], condition × delay [$F(6,9) = 14.56$, $p < 0.001$], orientation × delay [$F(3,9) = 12.98$, $p < 0.01$], and condition × orientation × delay [$F(6,9) = 11.65$, $p < 0.001$] interactions. A MANOVA with the sessions from both monkeys showed a main effect of electrode orientation [$F(1,21) = 17.77$, $p < 0.001$, sagittal > coronal], of delay [$F(3,63) = 4.66$, $p < 0.01$], and a condition × delay interaction [$F(6,63) = 5.06$, $p < 0.001$]. **Figures 3G,H** shows the results of pairwise comparisons performed by *post-hoc* Tukey HSD on condition x orientation × delay interaction. In the active expectancy task, for coronal pairs (**Figure 3H**), the cross-correlations values was significantly superior in the Dl1 period compared to Ps and Dl3 ($p < 0.01$, Tukey HSD *post-hoc*) and also, significantly superior in the Dl2 period compared to Dl3 ($p < 0.05$). For the sagittal pairs, a weaker effect was observed (**Figure 3G**, Dl2 vs. Dl3, Tukey HSD *post-hoc*, $p = 0.096$). Overall, for both animals, (1) sagittally oriented pairs provided the greatest synchronization; (2) rest and passive expectancy did not show increased synchronization across the delays, both in sagittal and coronal (no statistical difference, Tukey HSD *post-hoc*); but (3) in active expectancy, a dynamic evolution of synchronization was observed during the task, strongly for coronal pairs: it increased from Ps to Dl1 then remained identical between Dl1 and Dl2, to decrease between Dl2 and Dl3.

The results show that, while the sagittal synchronization bias remains when the animals are in-task in comparison to rest, the task-related synchronization between LFPs shows a dynamic increase in LFP synchronization during active expectancy. This effect is especially noticeable for distant sites in the coronal plane, in view of their weaker LFP synchronization at the beginning of the task period.

DISCUSSION

We found anisotropy in the GCL synchronization patterns at rest, and dynamic changes during an active expectancy lever-press task. This network synchronization could represent a mechanism to define task-related network activity in the cerebellar cortex, complementing the dynamic task-related organization of the Purkinje cell complex spikes (Welsh et al., 1995), and simple spikes patterns (Heck et al., 2007).

OSCILLATION AND SYNCHRONIZATION AT REST

One of our main results was the high synchronization in pairs of sagittal GCL LFPs. This mirrors the sagittal bands found in the optical imaging signal following climbing fiber stimulation (Brown and Ariel, 2009; Gao et al., 2003; Rockni et al., 2007). However, what could be GCL-specific variables that could affect this synchronization pattern? Local circuit properties and afferent input patterns within the GCL could interact in creating this basic anisotropy. Considering initially intrinsic mechanisms, a first element of rhythmicity would be local circuit interaction through granule cell-Golgi cell loops. This putative oscillator comprises the necessary active elements: First, mossy fiber afferents contact both granule and Golgi cells, leading to feedforward and feedback loops (Llinás et al., 2004). Second, Golgi cells connect each granule cell with three to four inhibitory synapses through both the parallel fibers and the granule cell dendritic ending (Hámori and Somogyi, 1983; Jakab and Hámori, 1988). Last, Golgi cell dendrites obey a sagittal zonation (Sillitoe et al., 2008), and influence GCL discharge sagittally (Barmack and Yakhnitsa, 2008). These characteristics of Golgi cell connectivity within granule cell layer suggest how these neurons could play a substantial role both in generating beta oscillations and sagittal synchronization (for a review, see D'Angelo, 2008). Indeed, in realistic cerebellar network modeling, granule cells can generate a variety of temporal dynamics under inhibitory control of Golgi cells (Medina and Mauk, 2000), especially within the 10–50 Hz band (Maex and De Schutter, 1998, 2005). In addition, combining experiments and modeling, Dugué et al. (2009) show that gap-junction among Golgi cells play an important role in low-frequency oscillations (5–30 Hz) and resonance in the GCL. Cellular properties to resonance at targeted frequencies is seen within the GCL, in both granule cells (D'Angelo et al., 2001) and Golgi cells (Solinas et al., 2007). Taken together, these local circuits combined with the afferent input could bring the GCL to generate or at least maintain oscillatory activity, and have a preference for the sagittal orientation.

Additionally, extracerebellar influences could contribute to the sagittal basic rhythmicity. Afferents to the GCL, the mossy fiber input, terminate antero-posteriorly along the cerebellar cortex folia (Heckroth and Eisenman, 1988; Scheibel, 1977). Mossy fiber input coming from spino-cerebellar or cerebro-cerebellar sources could potentially influence the circuitry (Voogd and Glickstein, 1998). On the one hand, the influence could be rhythmic itself, and dictate the

internal rhythm; however, we have shown that under rest conditions, rhythms in certain cerebral areas are not optimally synchronous with rhythms in the paramedian lobule GCL (Courtemanche and Lamarre, 2005), so the influence is not direct. On the other hand, as Dugué et al. (2009) have shown, the Golgi cell oscillations *in vitro* are aided by a general increase in excitability; in the context of whole systems, such an increase could certainly be triggered via an input external to the GCL. However, this also shows that the external input does not specifically need to be a phasic rhythm to entrain the Golgi cells. An external tonic drive could be sufficient in triggering the local circuit to become oscillatory.

OSCILLATION AND SYNCHRONIZATION IN ACTIVE EXPECTANCY

Our second result in qualifying the LFP synchronization anisotropy was the increased LFP synchronization during active expectancy, more evident in the coronal pairs. This was different from passive expectancy and rest, and even though oscillations were sometimes present in rest and often present in passive expectancy (Courtemanche et al., 2002), these condition did not produce a steady increase in LFP synchronization. Thus, the mere fact that oscillations are present does not predict synchronization: however, when they are present, this does appear to facilitate synchronization (Buzsaki, 2006; Schnitzler and Gross, 2005).

With our setup, it would have been difficult to descend more than two electrodes in the monkey cerebellar cortex *in vivo* because it is so deep. Elements such as electrode holder strength and intracranial pressure were a consideration. However, given our results, the increased coronal LFP synchronization could possibly mean an expansion of the initial sagittal zones of GCL LFP synchronization. An intracerebellar mechanism for the coronal expansion could depend on parallel fibers, which course as much as 6 mm wide (Brand et al., 1976). Such a mechanism is reminiscent of the well-known cerebellar cortex beams (Eccles et al., 1967), shown during stimulation of the parallel fibers at the surface of the cerebellar cortex (Brown and Ariel, 2009; Gao et al., 2003; Qiu et al., 2008; Rockni et al., 2007). These parallel fibers contact Golgi cells, which can show coherent discharge along a transverse orientation (Volny-Luraghi et al., 2002). and their activity recorded *in vivo* shows 'loose synchrony' over hundreds of micrometers along the transverse axis (Maex et al., 2000; Volny-Luraghi et al., 2002; Vos et al., 1999). Our synchronization increase in the coronal orientation could be due to parallel fiber–mediated changes in connectivity, in the same way that beams of activity could unite parallel parasagittal modules (Rockni et al., 2008).

Additionally, the Lugaro cells could also sustain increased coronal synchrony, with axons that courses both coronally and sagittally (Lainé and Axelrad, 1996), potentially influencing GCL LFPs via an effect on Golgi cells and/or through an interaction with the serotonin afferent system (Dieudonné, 2001). Finally, extracerebellar circuits could also increase LFP synchronization in the coronal plane. For rat GCL 7-Hz oscillations, Hartmann and Bower (1998) found interhemispheric Crus IIa LFP synchronization, likely dependent on overall somatosensory circuit resonance. Synchronization variations we found here were within one hemisphere; interhemispheric relations in primate cerebellar GCL LFPs would have to be addressed.

The cerebellar multi-site LFP synchronization could highlight a functional process taking place. In addition to a contribution in preparation to action, there could be a direct role in the processing of task-related sensory information. In particular, the periods of increased synchronization in our task correspond to the time when the monkey's hand was in contact with the lever, as shown by Courtemanche and Lamarre (2005). Indeed, the period from start of Dl1 to the end of Dl2 corresponds to when the monkey rests the fingers on the lever, waiting for the proper time to press. There could be a direct somatosensory role for linking two coronal sites, as GCL activity has a definite relation with somatosensory processing (Courtemanche and Lamarre, 2005; Hartmann and Bower, 2001). In fact, the coronal LFP synchronization extension is in accord with the results of Volny-Luraghi et al. (2002), who showed that Golgi cells are synchronized in a coronal (beam-like) fashion with controlled stimulation of the whiskers. The equivalent has been found in modeling of cerebellar circuits: oscillatory activity in modeled GCL circuits can indeed serve to synchronize distinct patches of GCL (Franck et al., 2001). In this aspect, whether or not the LFP oscillations themselves carry any identifiable information, they can certainly contribute in bringing distant cerebellar sites together, relating together contextual information from distant sites (Nelson and Bower, 1990).

The synchronization in the cerebellum could also serve to bring together cerebro-cerebellar elements more efficiently. As an example, both cerebellum and neocortex receive input from the somatosensory system. Interaction between these regions has been proposed to underpin the correct selection and execution of motor commands. Population rhythms, especially in beta (15–30 Hz) and gamma (30–80 Hz) oscillations, common to these structures, could act as a common spatiotemporal code within which these cerebro-cerebellar interactions may occur (Salenius and Hari, 2003; Schnitzler and Gross, 2005). Indeed, cerebral cortex (mainly primary somatosensory, but also primary motor) and cerebellar cortex LFPs synchronize during the same active expectancy task described here (Courtemanche and Lamarre, 2005). In addition, during performance of a precision grip task in monkeys, Soteropoulos and Baker (2006) observed significant coherence between deep cerebellar nuclei units and primary motor cortex LFP oscillations bilaterally, at approximately 10–40 Hz. So, the increased coronal GCL LFP synchronization observed in our task, by extending the parts of cerebellum that potentially interact with networks in the sensorimotor cerebral cortex, could have functional importance in sensorimotor processing.

EXPERIMENTAL LIMITATIONS

Certain elements limit the interpretation of our results: (1) our electrodes were aligned relative to the stereotaxic sagittal plane (parallel or orthogonal), which could be misaligned with the mossy or Golgi 'sagittal' orientation, mainly when more lateral; however, such an error was minimized by our attempt at recording in the paramedian lobule proper. Our sagittal misalignment should be slight when within or close to the paramedian lobule (~4–13° from sagittal, estimated from Ozol and Hawkes, 1997). Also, (2) our sagittal and coronal intra-pair distance (3 and 6 mm) might have covered more than one lobule. These distances were bound by our electrode carrier, which had the rigidity needed to go deep to the paramedian lobule (Courtemanche et al., 2002). Interestingly, in **Figure 2D**, LFP synchronization was more related to lateral than total distance,

even if the latter could definitely influence lobule crossings; this provides support for a medio-lateral anisotropy. Additionally, our synchronization at the 3 mm lateral distance was lower than for the 6 mm distance (even if in different monkeys), the 3 mm distance certainly could have recorded sites within one lobule.

CEREBELLAR CORTEX MODULARITY

Our results complement electrophysiological and anatomical evidence for basic parasagittal modularity, such as in Purkinje cell complex spike synchrony patterns (Lang et al., 1999), and defined chemoarchitectonically and with molecular markers (Herrup and Kuemerle, 1997; Voogd and Glickstein, 1998). These bands are present across cerebellar cortex layers, including the posterior lobe GCL (Ozol and Hawkes, 1997), and are on the order of 0.5 mm wide in the primate (Hess and Voogd, 1986; Leclerc et al., 1990). These bands appear to represent a processing unit, as GCL-Purkinje cell relations seem to obey a privileged vertical organization (Lu et al., 2005). At rest, our GCL LFP pairs showed a good correlation for separations in the mm range: the difference could be due to the averaging nature of the LFP signal. During active expectancy, the increased coronal synchronization we found is in line with evidence where Purkinje cell simple spikes synchrony favors the coronal (beam-like) orientation during movement (Heck et al., 2007). As oscillatory phenomena would likely determine cerebellar cortex patterns of activity *in vivo* (de Solages et al., 2008; de Zeeuw et al., 2008), our results show a dynamic GCL anisotropy which is related to sensorimotor performance. Thus, part of the basic functional modularity in the cerebellar cortex, e.g., microzones (Apps and Garwicz, 2005; Oscarsson, 1979), could be shaped by the GCL activity patterns, but in a dynamic fashion.

ACKNOWLEDGMENTS

We gratefully thank Marie-Thérèse Parent, Michelle Yeates, Christian Valiquette, and Gaétan Richard for technical work; Elaine Chapman, Trevor Drew, Allan Smith, and Jean-Pierre Pellerin for help and discussions.

This project was supported by grants from the Canadian Institute for Health Research, Fonds pour les Chercheurs et l'Aide à la Recherche (Québec), and the National Alliance for Autism Research (USA) to YL. The work was also supported by fellowships and grants from the Natural Sciences and Engineering Research Council of Canada, the Fonds de Recherche en Santé du Québec-FCAR-Santé, and the National Alliance for Autism Research/Autism Speaks (USA) to RC.

REFERENCES

Apps, R., and Garwicz, M. (2005). Anatomical and physiological foundations of cerebellar information processing. *Nat. Rev. Neurosci.* 6, 297–311.

Barmack, N. H., and Yakhnitsa, V. (2008). Functions of interneurons in mouse cerebellum. *J. Neurosci.* 28, 1140–1152.

Bell, C. C., and Grimm, R. J. (1969). Discharge properties of Purkinje cells recorded on single and double microelectrodes. *J. Neurophysiol.* 32, 1044–1055.

Bloedel, J. R. (1992). Functional heterogeneity with structural homogeneity: how does the cerebellum operate? *Behav. Brain Sci.* 15, 666–678.

Brand, S., Dahl, A. L., and Mugnaini, E. (1976). The length of parallel fibers in the cat cerebellar cortex. An experimental light and electron microscopic study. *Exp. Brain Res.* 26, 39–58.

Brown, M. E., and Ariel, M. (2009). Topography and response timing of intact cerebellum stained with absorbance voltage-sensitive dye. *J. Neurophysiol.* 101, 474–490.

Buzsaki, G. (2006). Rhythms of the Brain. New York, Oxford University Press.

Courtemanche, R., Fujii, N., and Graybiel, A. M. (2003). Synchronous, focally modulated beta-band oscillations characterize local field potential activity in the striatum of awake behaving monkeys. *J. Neurosci.* 23, 11741–11752.

Courtemanche, R., and Lamarre, Y. (2005). Local field potential oscillations in primate cerebellar cortex: synchronization with cerebral cortex during active and passive expectancy. *J. Neurophysiol.* 93, 2039–2052.

Courtemanche, R., Pellerin, J. P., and Lamarre, Y. (2002). Local field potential oscillations in primate cerebellar cortex: modulation during active and passive expectancy. *J. Neurophysiol.* 88, 771–782.

D'Angelo, E. (2008). The critical role of Golgi cells in regulating spatio-temporal integration and plasticity at the cerebellum input stage. *Front. Neurosci.* 2, 35–46.

D'Angelo, E., and de Zeeuw, C. I. (2009). Timing and plasticity in the cerebellum: focus on the granular layer. *Trends Neurosci.* 32, 30–40.

D'Angelo, E., Nieus, T., Maffei, A., Armano, S., Rossi, P., Taglietti, V., Fontana, A., and Naldi, G. (2001). Theta-frequency bursting and resonance in cerebellar granule cells: experimental evidence and modeling of a slow k^+-dependent mechanism. *J. Neurosci.* 21, 759–770.

De Schutter, E., and Bjaalie, J. G. (2001). Coding in the granular layer of the cerebellum. *Prog. Brain Res.* 130, 279–296.

de Solages, C., Szapiro, G., Brunel, N., Hakim, V., Isope, P., Buisseret, P., Rousseau, C., Barbour, B., and Léna, C. (2008). High-frequency organization and synchrony of activity in the Purkinje cell layer of the cerebellum. *Neuron* 58, 775–788.

de Zeeuw, C. I., Hoebeek, F. E., and Schonewille, M. (2008). Causes and consequences of oscillations in the cerebellar cortex. *Neuron* 58, 655–658.

Dieudonné, S. (2001). Serotonergic neuromodulation in the cerebellar cortex: cellular, synaptic, and molecular basis. *The Neuroscientist* 7, 207–219.

Dugué, G. P., Brunel, N., Hakim, V., Schwartz, E., Chat, M., Lévesque, M., Courtemanche, R., Léna, C., and Dieudonné, S. (2009). Electrical coupling mediates tunable low-frequency oscillations and resonance in the cerebellar Golgi cell network. *Neuron* 61, 126–139.

Eccles, J. C., Ito, M., and Szentágothai, J. (1967). The Cerebellum as a Neuronal Machine. New York, Spinger-Verlag.

Franck, P., Maex, R., and De Schutter, E. (2001). Syncronization between patches of local excitation in a cerebellar granular layer model. *Neurocomputing* 38–40, 595–599.

Gao, W., Dunbar, R. L., Chen, G., Reinert, K. C., Oberdick, J., and Ebner, T. J. (2003). Optical imaging of long-term depression in the mouse cerebellar cortex in vivo. *J. Neurosci.* 23, 1859–1866.

Gerstein, G. L., and Nicolelis, M. A. L. (1999). Correlation-based analysis methods for neural ensemble data. In Methods for Neural Ensemble Recording, S. A. Simon, and M. A. L. Nicolelis, eds (Boca Raton FL, CRC Press), pp. 157–177.

Geurts, F. J., De Schutter, E., and Dieudonne, S. (2003). Unraveling the cerebellar cortex: cytology and cellular physiology of large-sized interneurons in the granular layer. *Cerebellum* 2, 290–299.

Hámori, J., and Somogyi, J. (1983). Differentiation of cerebellar mossy fiber synapses in the rat: a quantitative electron microscope study. *J. Comp. Neurol.* 220, 365–377.

Hartmann, M. J., and Bower, J. M. (1998). Oscillatory activity in the cerebellar hemispheres of unrestrained rats. *J. Neurophysiol.* 80, 1598–1604.

Hartmann, M. J., and Bower, J. M. (2001). Tactile responses in the granule cell layer of cerebellar folium crus IIa of freely behaving rats. *J. Neurosci.* 21, 3549–3563.

Heck, D. H., Thach, W. T., and Keating, J. G. (2007). On-beam synchrony in the cerebellum as the mechanism for the timing and coordination of movement. *Proc. Natl. Acad. Sci. U.S.A.* 104, 7658–7663.

Heckroth, J. A., and Eisenman, L. M. (1988). Parasagittal organization of mossy fiber collaterals in the cerebellum of the mouse. *J. Comp. Neurol.* 270, 385–394.

Herrup, K., and Kuemerle, B. (1997). The compartmentalization of the cerebellum. *Ann. Rev. Neurosci.* 20, 61–90.

Hess, D. T., and Voogd, J. (1986). Chemoarchitectonic zonation of the monkey cerebellum. *Brain Res.* 369, 383–387.

Jakab, R. L., and Hámori, J. (1988). Quantitative morphology and synaptology of cerebellar glomeruli in the rat. *Anat. Embryol.* 179, 81–88.

Lainé, J., and Axelrad, H. (1996). Morphology of the golgi-impregnated

Lugaro cell in the rat cerebellar cortex: a reappraisal with a description of its axon. *J. Comp. Neurol.* 375, 618–640.

Lamarre, Y., Joffroy, A. J., Filion, M., and Bouchoux, R. (1970). A stereotaxic method for repeated sessions of central unit recording in the paralyzed or moving animal. *Rev. Can. Biol.* 29, 371–376.

Lang, E. J., Sugihara, I., Welsh, J. P., and Llinás, R. (1999). Patterns of spontaneous Purkinje cell complex spike activity in the awake rat. *J. Neurosci.* 19, 2728–2739.

Leclerc, N., Dore, L., Parent, A., and Hawkes, R. (1990). The compartmentalization of the monkey and rat cerebellar cortex: zebrin I and cytochrome oxidase. *Brain Res.* 506, 70–78.

Llinás, R. R., Walton, K. D., and Lang, E. J. (2004). Cerebellum. In The Synaptic Organization of the Brain, G. M. Shepherd, ed (New York, NY, Oxford University Press), pp. 271–309.

Lu, H., Hartmann, M. J., and Bower, J. M. (2005). Correlations between Purkinje cell single unit activity and simultaneously recorded field potentials in the immediately underlying granule cell layer. *J. Neurophysiol.* 94, 1849–1860.

Maex, R., and De Schutter, E. (1998). Synchronization of Golgi and granule cell firing in a detailed network model of the cerebellar granule cell layer. *J. Neurophysiol.* 80, 2521–2537.

Maex, R., and De Schutter, E. (2005). Oscillations in the cerebellar cortex: a prediction of their frequency bands. *Prog. Brain Res.* 148, 181–188.

Maex, R., Vos, B. P., and De Schutter, E. (2000). Weak common parallel fibre synapses explain the loose synchrony observed between rat cerebellar Golgi cells. *J. Physiol.* 523, 175–192.

Medina, J. F., and Mauk, M. D. (2000). Computer simulation of cerebellar information processing. *Nat. Neurosci.* 3(Suppl), 1205–1211.

Miller, E. K., and Wilson, M. A. (2008). All my circuits: using multiple electrodes to understand functioning neural networks. *Neuron* 60, 483–488.

Murthy, V., and Fetz, E. E. (1996). Oscillatory activity in sensorimotor cortex of awake monkeys: synchronization of local field potentials and relation to behavior. *J. Neurophysiol.* 76, 3949–3967.

Nelson, M. E., and Bower, J. M. (1990). Brain maps and parallel computers. *Trends Neurosci.* 13, 403–408.

O'Connor, S., Berg, R. W., and Kleinfeld, D. (2002). Coherent electrical activity between vibrissa sensory areas of cerebellum and neocortex is enhanced during free whisking. *J. Neurophysiol.* 87, 2137–2148.

Oscarsson, O. (1979). Functional units of the cerebellum – sagittal zones and microzones. *Trends Neurosci.* 2, 143–145.

Ozol, K. O., and Hawkes, R. (1997). Compartmentation of the granular layer of the cerebellum. *Histol. Histopathol.* 12, 171–184.

Pellerin, J. P., and Lamarre, Y. (1997). Local field potential oscillations in primate cerebellar cortex during voluntary movement. *J. Neurophysiol.* 78, 3502–3507.

Qiu, D. L., Akemann, W., Chu, C. P., Araki, R., and Knopfel, T. (2008). Targeted optical probing of neuronal circuit dynamics using fluorescent protein sensors. *Neurosignals* 16, 289–299.

Rockni, D., Llinás, R., and Yarom, Y. (2007). Stars and stripes in the cerebellar cortex: a voltage sensitive dye study. *Front. Syst. Neurosci.* 1, 1–9.

Rockni, D., Llinás, R., and Yarom, Y. (2008). The morpho/functional discrepancy in the cerebellar cortex: looks alone are deceptive. *Front. Neurosci.* 2, 192–198.

Roelfsema, P. R., Engel, A. K., Kînig, P., and Singer, W. (1997). Visuomotor integration is associated with zero time-lag synchronization among cortical areas. *Nature* 385, 157–161.

Salenius, S., and Hari, R. (2003). Synchronous cortical oscillatory activity during motor action. *Curr. Opin. Neurobiol.* 13, 678–684.

Salmelin, R., and Hari, R. (1994). Spatiotemporal characteristics of sensorimotor neuromagnetic rhythms related to thumb movement. *Neuroscience* 60, 537–550.

Scheibel, A. (1977). Sagittal organization of mossy fiber terminal system in the cerebellum of the rat: a Golgi study. *Exp. Neurol.* 57, 1067–1070.

Schnitzler, A., and Gross, J. (2005). Normal and pathological oscillatory communication in the brain. *Nat. Rev. Neurosci.* 6, 285–296.

Schwarz, C., and Welsh, J. P. (2001). Dynamic modulation of mossy fiber system throughput by inferior olive synchrony: a multielectrode study of cerebellar cortex activated by motor cortex. *J. Neurophysiol.* 86, 2489–2504.

Shin, S. L., and De Schutter, E. (2006). Dynamic synchronization of Purkinje cell simple spikes. *J. Neurophysiol.* 96, 3485–3491.

Sillitoe, R. V., Chung, S. H., Fritschy, J. M., Hoy, M., and Hawkes, R. (2008). Golgi cell dendrites are restricted by Purkinje cell stripe boundaries in the adult mouse cerebellar cortex. *J. Neurosci.* 28, 2820–2826.

Singer, W., Engel, A. K., Kreiter, A. K., Munk, M. H. J., Neuenschwander, S., and Roelfsema, P. R. (1997). Neuronal assemblies: necessity, signature and detectability. *Trends Cogn. Sci.* 1, 252–261.

Solinas, S. Forti, L., Cesana, E., Mapelli, J., De Schutter, E., and D'Angelo, E. (2007). Fast-reset of pacemaking and theta-frequency resonance patterns in cerebellar Golgi cells: simulations of their impact in vivo. *Front. Cell. Neurosci.* 1, 4.

Soteropoulos, D. S., and Baker, S. N. (2006). Cortico-cerebellar coherence during a precision grip task in the monkey. *J. Neurophysiol.* 95, 1194–1206.

Volny-Luraghi, A., Maex, R., Vos, B., and De Schutter, E. (2002). Peripheral stimuli excite coronal beams of Golgi cells in rat cerebellar cortex. *Neuroscience* 113, 363–373.

Voogd, J., and Glickstein, M. (1998). The anatomy of the cerebellum. *Trends Neurosci.* 21, 370–375.

Vos, B. P., Maex, R., Volny-Luraghi, A., and De Schutter, E. (1999). Parallel fibers synchronize spontaneous activity in cerebellar Golgi cells. *J. Neurosci.* 19, RC6.

Welsh, J. P., Lang, E. J., Sugihara, I., and Llinás, R. (1995). Dynamic organization of motor control within the olivocerebellar system. *Nature* 374, 453–457.

Conflict of Interest Statement: The authors declare that the research was conducted in the absence of any commercial or financial relationships that could be construed as a potential conflict of interest.

Received: 01 May 2009; paper pending published: 15 May 2009; accepted: 09 July 2009; published online: 20 July 2009.

*Citation: Courtemanche R, Chabaud P and Lamarre Y (2009) Synchronization in primate cerebellar granule cell layer local field potentials: Basic anisotropy and dynamic changes during active expectancy. Front. Cell. Neurosci. (2009) **3**:6. doi: 10.3389/neuro.03.006.2009*

frontiers in
CELLULAR NEUROSCIENCE

REVIEW ARTICLE
published: 23 November 2009
doi: 10.3389/neuro.03.013.2009

Forward models and state estimation in compensatory eye movements

Maarten A. Frens[1] and Opher Donchin[2]*

[1] *Department of Neuroscience, Erasmus Medical Center, Rotterdam, The Netherlands*
[2] *Department of Biomedical Engineering, Ben Gurion University of the Negev, Be'er Sheva, Israel*

Edited by:
Egidio D'Angelo, University of Pavia, Italy

Reviewed by:
Stefano Ramat, Università degli Studi di Pavia, Italy
Nicolas Schweighofer, University of Southern California, USA

***Correspondence:**
Opher Donchin, Department of Biomedical Engineering, Ben Gurion University of the Negev, P.O. Box 635, Be'er Sheva 84105, Israel.
e-mail: donchin@bgu.ac.il

The compensatory eye movement (CEM) system maintains a stable retinal image, integrating information from different sensory modalities to compensate for head movements. Inspired by recent models of the physiology of limb movements, we suggest that CEM can be modeled as a control system with three essential building blocks: a forward model that predicts the effects of motor commands; a state estimator that integrates sensory feedback into this prediction; and, a feedback controller that translates a state estimate into motor commands. We propose a specific mapping of nuclei within the CEM system onto these control functions. Specifically, we suggest that the Flocculus is responsible for generating the forward model prediction and that the Vestibular Nuclei integrate sensory feedback to generate an estimate of current state. Finally, the brainstem motor nuclei – in the case of horizontal compensation this means the Abducens Nucleus and the Nucleus Prepositus Hypoglossi – implement a feedback controller, translating state into motor commands. While these efforts to understand the physiological control system as a feedback control system are in their infancy, there is the intriguing possibility that CEM and targeted voluntary movements use the same cerebellar circuitry in fundamentally different ways.

Keywords: cerebellum, model, control systems, vor, okr, vestibular nucleus, eye movements, forward model

COMPENSATORY EYE MOVEMENTS

Compensatory eye movements (CEM) is a general term for a number of different reflexes that keep an image fixed on the retina during movements of the body and the head (e.g. Delgado-Garcia, 2000). As such, these eye movements have a specific and well-defined goal: to prevent movement of the visual image on the retina, often called retinal slip, during fixation. The circuitry of the CEM system (**Figure 1**) is different from the circuitry for other eye movements such as saccades, although all the eye movement systems converge in the oculomotor nuclei of the brainstem (Buttner-Ennever and Buttner, 1992). For horizontal eye movements these are the abducens nucleus (Ab) and the nucleus prepositus hypoglossi (NPH). All CEM-related input to these brainstem structures comes from the Vestibular Nuclei (VN).

The optokinetic reflex (OKR) is a closed loop system that directly responds to retinal slip, generating eye movements with the direction and magnitude of measured retinal slip. Afferents from the retina project directly to the Accessory Optic System (AOS). The AOS, in turn projects to the VN and the cerebellum, through the Nucleus Reticularis Tegmenti Pontis (NRTP; Gerrits et al., 1984; Langer et al., 1985; Glickstein et al., 1994). The OKR has a response delay of about 80 ms (e.g Winkelman and Frens, 2006), mostly because of the inherent delay involved in visual processing (Graf et al., 1988). In keeping with this, the OKR is only responsive to low velocity stimuli.

For compensation of higher velocity stimuli, the CEM system depends on the vestibulo-ocular reflex (VOR) which uses vestibular input to estimate head movement and generate oppositely directed eye movements. Vestibular afferents from the labyrinth project directly to the VN. The two systems are complementary: the VOR compensates for higher frequencies while the OKR compensates for the lower velocities (Collewijn, 1989).

Both the VOR and OKR are adaptive, meaning that the mapping of stimulus to appropriate eye response can be tuned to match changing response properties of the eye and its supporting tissues (usually collectively called the "plant") or changes in the sensitivity of the sensory organs (Blazquez et al., 2004; Boyden et al., 2004; Andreescu et al., 2005; Gittis and du Lac, 2006). Changes in either plant response properties, sensory sensitivity, or environmental changes in the relationship of vision and vestibular input to movement will change the appropriate mapping from stimulus to response and thus the system must change the mapping so that retinal slip continues to be appropriately compensated. There is ample evidence that the flocculus, a small section of the cerebellar cortex is critical in this plasticity (e.g. Lisberger et al., 1984). The Purkinje cells (P-cells) of the flocculus project only to the VN. There are sites of plasticity both at the level of the parallel fibre synapses to these P-cells, as well as at the P-cell/VN synapses (Raymond et al., 1996; Boyden et al., 2004). In addition, the cerebellum has an important role in ongoing performance beyond its role in plasticity: the performance of the OKR decreases dramatically after floccular lesions (Takemori and Cohen, 1974; Zee et al., 1981), while the VOR is less affected (Waespe et al., 1983; Van Neerven et al., 1989).

THE STATE PREDICTING FEEDBACK CONTROLLER

There has been a long history of using models based on the principles of control theory to describe the control of eye movements generally and CEM in particular. Starting with the seminal work

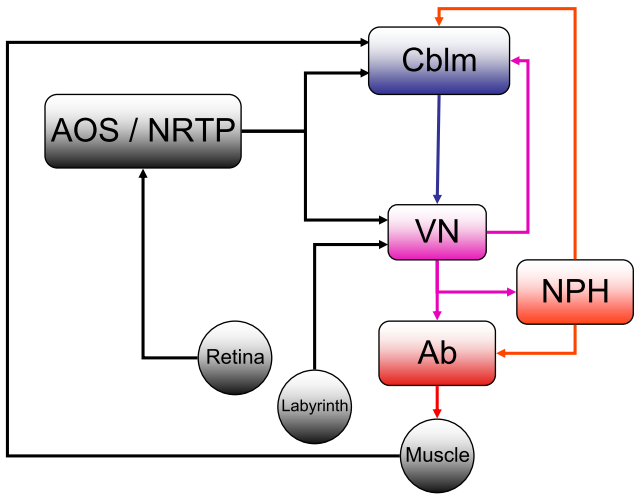

FIGURE 1 |The horizontal compensatory eye movement (CEM) system. Generally, this is described as two separate reflexes. The optokinetic reflex (OKR) uses visual input from the retina to stabilize the eye while the vestibulo-ocular reflex (OKR) responds to vestibular information from the labyrinth. This figure emphasizes the distinction between sensory feedback (black) and motor signals (red). Blue and purple represent central stages of processing, and are added for comparison with other figures. Cblm: cerebellar cortex; AOS/NRTP: accessory optic system and nucleus reticularis tegmentum pontis; VN: vestibular nucleus; NPH: neuclus prepositus hypoglossi; OMN/AB: oculomotor nucleus and abducens.

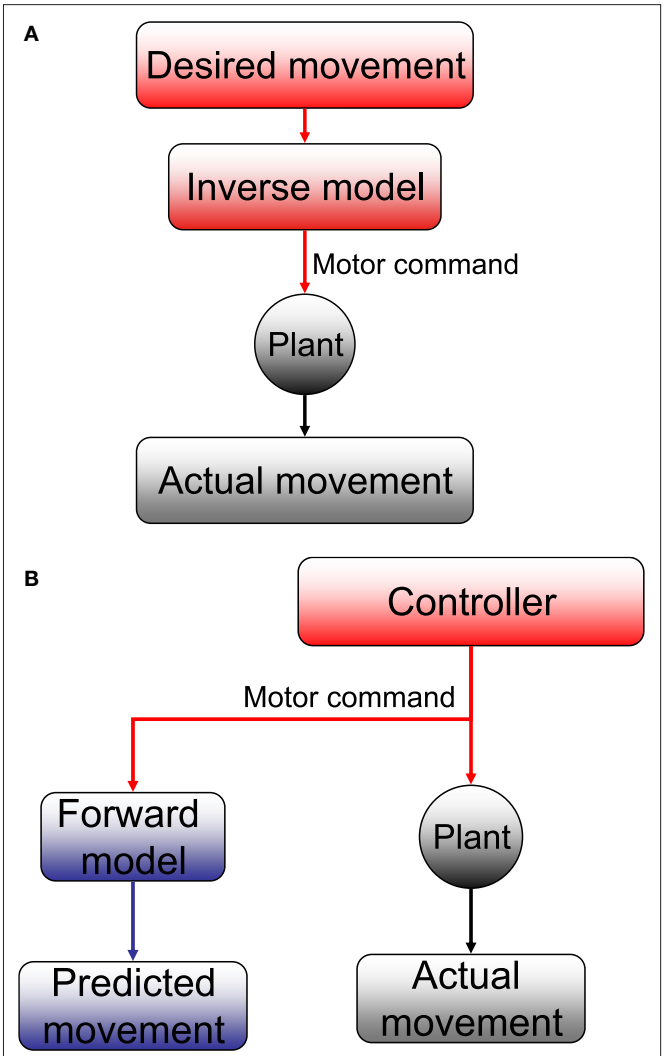

FIGURE 2 | (A) Inverse and **(B)** forward models. The plant takes motor commands and produces movement. The inverse model inverts this process, producing the motor commands that are appropriate for a given movement. A forward model mimics this process, estimating the movement that will be produced by the plant.

of David Robinson (for review Robinson, 1981), this tradition has generally posited a neural implementation of an inverse model that maps stimuli to command signals (Skavenski and Robinson, 1973). An inverse model, literally speaking, is a control process that inverts the plant; that is, the plant converts control signals into motion, so an inverse model converts desired motion into the appropriate control signals (Jordan and Rumelhart, 1992; **Figure 2A**).

The cerebellar floculus is thought by many to implement a form of inverse model (Kawato and Gomi, 1992, and see also Lisberger, 2009, for review of these ideas in relation to the smooth pursuit system). While this idea has many adherents, there are also alternative proposals. Perhaps most famously, Llinás (1988) proposed that the cerebellum is involved in adjusting movement timing to facilitate coordination, rather than in generating compensatory movement commands. Similar ideas have been put forward recently. Specifically, Jacobson et al. (2008) argued that synchrony and oscillatory activity in the inferior olive are compatible with a cerebellar timing mechanism driven by olivary harmonics. D'Angelo and De Zeeuw (2009) in contrast, focus on the temporal dynamics of the cerebellar granular layer. A somewhat more eclectic model that also focuses on timing is Braitenberg's model of the cerebellum as a system for generating sequences of movement in precise time relationship (Braitenberg et al., 1997). While each of these models can legitimately claim to explain important data, there is no doubt that the inverse model understanding of the cerebellum in CEM is the most widely accepted. We will not consider the other models in developing our own ideas below. The controversy about timing models and adaptation models of the cerebellum has been going on for a long time (Miles and Lisberger, 1981; Ivry and Keele, 1989; Simpson et al., 1996). There are those who believe the two different approaches are mutually compatible (Mauk et al., 2000). It is not our intention, in any case, to take on this issue.

The inverse model framework can be contrasted with a forward model (Wolpert and Miall, 1996; Todorov and Jordan, 2002; See **Figure 2B**) which simulates the activity of the plant: it converts the current state and the control signals into a prediction of what the plant will actually do. The bottom line is: inverse models output motor commands and forward models output estimates of state.

The focus on a neural inverse model of the oculomotor plant reflected a perspective that the central problem in oculomotor control is producing the appropriate motor commands once the goal is given. Researchers in other motor systems – notably arm movements – followed in the footsteps of the pioneering work in oculomotor research and focused on the inverse model problem and the question of how appropriate motor commands are generated, given

a particular desired movement. This approach was reinforced by the explanatory power of hypothesized desired trajectories (Flash and Hogan, 1985; Uno et al., 1989), and the apparent tendency of subjects to correct movements (Shadmehr and Mussa-Ivaldi, 1994; Donchin et al., 2003).

However, the possibility that a forward model also plays a role has been hypothesized for a long time (e.g. Wolpert and Miall, 1996; Kawato, 1999). One recent radical proposal has been that the system does not work with either a "desired trajectory" or an inverse model (Todorov, 2004). Under this approach, the problem of predicting the results of motor commands is no less central than the problem of generating those motor commands in the first place. The reason such state prediction is so important is because it allows stable feedback control. Feedback control is the use of the measured or predicted state of the system to generate ongoing motor commands. This form of control can be simpler and more flexible than open-loop control. However, control becomes unstable when it depends on delayed or noisy feedback. Since sensory systems are both slow and noisy, this is inevitably a problem in physiological motor control. A forward model can be faster and less noisy than the full sensory loop. However, predictions of the state must be combined with actual sensory feedback in order for the control loop to remain robust in the face of unpredicted perturbations.

Thus, the framework (which we will call the state-predicting feedback control, SPFC, framework) is built out of three essential building blocks (**Figure 3**; Todorov, 2004; Shadmehr and Krakauer, 2008). The *forward model* takes the current estimate of state and the motor commands and produces an initial prediction. The *state estimator* combines this prediction with actual sensory feedback to produce a better estimate of the current state. The *feedback controller* uses the current estimate of state in order to decide what motor commands to generate. It either replaces or incorporates the inverse model on which the tradition of Robinson had focused. We propose that this framework is an appropriate description of CEM control and that it can be mapped onto CEM physiology in a manner that is consistent with experimental evidence.

How could such a computational scheme be implemented in the known anatomy and physiology of CEM? The boxology of **Figure 3** doesn't necessarily reflect separate neural stages or nuclei. Nevertheless, Shadmehr and Krakauer (2008) have recently proposed that neural structures involved in the control of arm movements can, in fact, be mapped onto the control structure described by these boxes. They suggest that motor cortex, in combination with the basal ganglia, implements a feedback controller implementing a control policy that maximizes successful performance. They support this using data from patients with Parkinson's disease (Mazzoni et al., 2007), and hemiparesis (Raghavan et al., 2006). State estimation is hypothesized to occur in parietal cortex based on findings in patients with parietal lesions (Wolpert et al., 1998). Finally, on the basis of the cerebellar role in in-flight adjustment of saccades (Quaia et al., 2000) and anticipatory postural adjustments (Nowak et al., 2007), they claim the forward model is implemented in the cerebellum.

Since the CEM system is located in brain stem nuclei and the cerebellum, and neither motor cortex nor parietal cortex is instrumental, our effort to ascribe computational functions to physiological correlates in the CEM will necessarily produce different results. We will argue that, for CEM, the most suitable mapping would be that the oculomotor nuclei and integrators (Robinson's "inverse plant") combine to form a feedback controller. The cerebellar cortex (and not the whole cerebellum) generates a forward model, and the VN combine forward model output with current inputs to produce the state estimate.

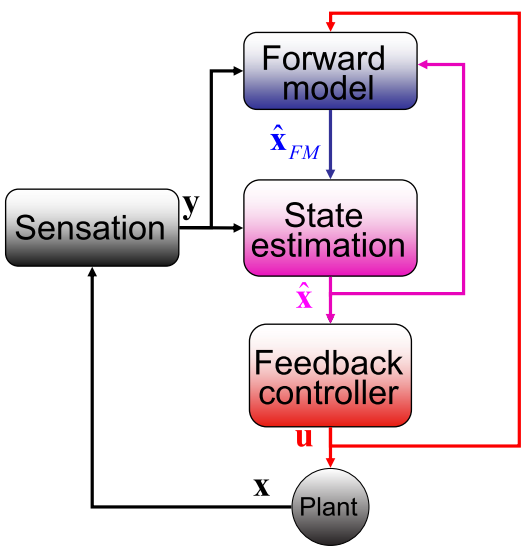

FIGURE 3 | The SPFC framework proposes that a feedback controller is optimized to produce motor commands that achieve task goals. In order to do this effectively, it uses an estimate of the current situation that is derived from a combination of feedback from the sensory system and forward model estimation that depends on efferent copy.

THE FEEDBACK CONTROLLER

The feedback controller maps current estimate of state onto the appropriate motor command. In the language of control system experts, this could be approximated as a transformation

$$\mathbf{u}_n = \mathbf{L}_n\left(\hat{\mathbf{x}}_n\right) \quad (1)$$

where $\mathbf{u}_n$ is a vector of length k_u describing the motor commands at the n^{th} time step. In our case, this would be the command driving the ocular musculature; each element of $\mathbf{u}_n$ represents the activation directed at a single muscle. $\hat{\mathbf{x}}_n$ is a vector of length k_x describing our current estimate of state; the elements of $\hat{\mathbf{x}}_n$ reflect variables like estimated eye position, eye velocity, and possibly include estimated head position and velocity and even desired eye position and velocity. Of course, both the state and the motor vectors could, in reality, be even more complicated. $\mathbf{L}_n$ is a function which maps each state onto the appropriate motor command. This mapping need not be linear or fixed in time. The point is that the feedback controller implements a function, **L**, that translates its input, an estimated state vector, $\hat{\mathbf{x}}$, into its output, the motor command vector, **u**.

By definition, the output of a controller is motor command so whatever produces the motor commands must necessarily be implementing a controller. In our case, motor command is the

activity that drives the muscles, and the motoneurons of the Abducens Nucleus are the output of the feedback controller, at least for horizontal motion. A subtler question regards whether any other related nuclei are also included.

In CEM, the controller must know the desired fixation point and it must receive an estimate of the current eye position. It calculates the vectorial difference between these two and generates motoneuron activity which will move the eye in the direction indicated by this vector. The brainstem circuit that traditionally constitutes the inverse plant meets these requirements (Buttner-Ennever and Buttner, 1992; Glasauer, 2007), even though there is debate on how the computation in the plant is achieved (see below). The issue of its input, a state estimate, will be discussed below.

The traditional view is that a displacement or velocity input is directly fed to the abducens output neurons that project to the eye muscles. In order to overcome the low-pass filter properties of the plant, an integrated version of this input is linearly added to the direct projection. The so-called oculomotor integrators are responsible for this indirect pathway (e.g. McFarland and Fuchs, 1992; Moschovakis, 1997). Recent work on the NPH, the putative horizontal integrator, undermines this view since neurons in the NPH are found to encode the whole motor command, **u**, rather than only the integrated part (Green et al., 2007; Ghasia et al., 2008), as shown in **Figure 4**. This makes the distinction between the NPH and the abducens unclear. One possibility, suggested by Green et al. is that NPH output serves feedback purposes. Indeed, on the basis of the finding that NPH feedback encodes "motor commands," Green et al. propose that the feedback is updating a cerebellar forward model (see **Figure 3**).

In both the Ab and the NPH, the CEM circuit is shared with the other eye movement systems (i.e. saccades and smooth pursuit). This fits the role of feedback controller, since the efference copy needed by the forward model should contain all oculomotor output in order to produce an optimal estimate of state (see below).

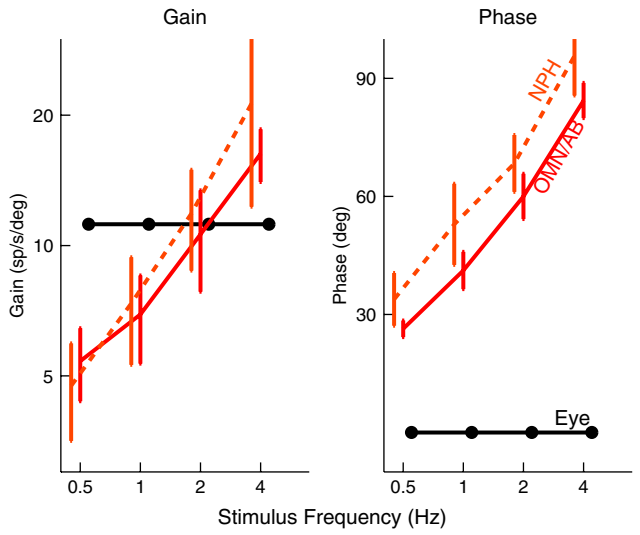

FIGURE 4 | NPH neurons (dashed, orange) behave like the motor command, represented by the solid, red curve. The black lines show the activity of a hypothetical neuron that would encode eye position, with a constant gain and phase. NPH and Ab activity were taken from (Green et al., 2007).

THE FORWARD MODEL

The Forward model updates our previous estimate of state. That is, we can use a forward model to generate an estimate about current state from our earlier estimate and our knowledge of system dynamics. We assume, for the purpose of simplicity, that the actual dynamics of the system can be described as linearly combining previous state and motor command:

$$\mathbf{x}_{n+1} = \mathbf{A}\mathbf{x}_n + \mathbf{B}\mathbf{u}_n + \boldsymbol{\varepsilon}_n \tag{2}$$

x is the actual state, whose estimate is discussed above ($\hat{\mathbf{x}}_n$). Both **x** and $\hat{\mathbf{x}}_n$ have the same size, but the latter is the brain's estimate and the former is the actual quantity. **A** is a $k_x \times k_x$ matrix, **B** is a $k_x \times k_u$ matrix, and $\boldsymbol{\varepsilon}_n$ is a noise term. Under this assumption, the forward model estimate would be generated from the previous estimate using a similar equation

$$\hat{\mathbf{x}}_{\mathrm{FM},n+1} = \hat{\mathbf{A}}\hat{\mathbf{x}}_n + \hat{\mathbf{B}}\mathbf{u}_n \tag{3}$$

where $\hat{\mathbf{A}}$ and $\hat{\mathbf{B}}$ represent the forward model's estimates of system dynamics. Notice that in this formulation, which is commonly used, the estimate of state used to calculate the forward model is not the same as the estimate produced by the forward model in the previous step. That is, we have $\hat{\mathbf{x}}_{\mathrm{FM},n+1}$ on the left side of the equation but $\hat{\mathbf{x}}_n$ on the right hand side. What we mean by this is that we may improve the estimate generated by the forward model (for instance, by incorporating information from sensory inputs) before we use it in the forward model's next step. This idea is demonstrated graphically in **Figure 3**.

One point requires clarification. The figure shows sensory input (black line) reaching the cerebellum in addition to the current estimates of state (purple) and efferent copy (red). This is drawn to reflect the realities described in **Figure 1**, which shows that sensory input does reach the cerebellar cortex. This includes retinal input from AOS (which is routed through the inferior olive and climbing fibers) and NRTP (which comes through mossy fibers). It also includes proprioceptive information. Part of the visual input, especially the part arriving through AOS, may play a role in adaptation processes discussed below. On the other hand, sensory input that has a direct effect on cerebellar activity is not entirely consistent with Eq. 3. It may nevertheless be consistent with the cerebellum producing a predictive estimate of state based on all the available information.

We assume that the forward model has no knowledge of the random fluctuations in the state represented by the noise term. However, we expect the forward model to be plastic. That is, if the state prediction of the forward model is consistently wrong the model should change. The cerebellar cortex appears to have all of these characteristics.

It has been amply demonstrated that the cerebellum receives efference copy from many motor systems. Specifically, the cortical area responsible for CEM, the flocculus, receives direct projections from the NPH (Sato et al., 1983; Langer et al., 1985; McCrea and Baker, 1985). Furthermore, it receives a strong input from the VN (Sato et al., 1983; Langer et al., 1985; Gerrits et al., 1989; Barmack et al., 1993), and we will argue later that this is the most likely candidate for a state estimator.

The key issue in claiming that cerebellar cortex produces a forward model is to show that the output uses efference copy to generate an estimate of state. This, we believe, is demonstrated by one important finding. **Figure 5** shows that spike triggered averaging (STA) of the eye velocity reveals that the neural activity does not predict or follow the movement with a large latency. Rather, the correlation peaks at a latency close to zero, or even slightly negative (Winkelman and Frens, 2007). Because the activity does not precede the eye movement, it cannot be causing it. Thus, floccular output is not part of the controller signal. Similarly, because it does not follow the eye movement, it cannot reflect purely sensory information. The flocculus thus processes efferent copy to produce an output that represents the current state faithfully, which is exactly what one expects from the forward model.

THE STATE ESTIMATOR

Ultimately, state estimation requires combining two sources of information about the current state. The first source of information is the forward model, and the second source is sensory input. In our case, the latter includes vestibular, visual and possibly also proprioceptive inputs.

We can formalize the relationship between state and sensory input using the equation

$$\mathbf{y}_n = \mathbf{H}(\mathbf{x}_n) + \boldsymbol{\eta}_n \tag{4}$$

$\mathbf{y}_n$ is a vector of length k_y whose components reflect all the different inputs from the head and eye. $\boldsymbol{\eta}_n$ is a noise term reflecting the fact that the activity in our sensory system is not a faithful representation of the state. The function $\mathbf{H}$ is meant to characterize the process of sensation.

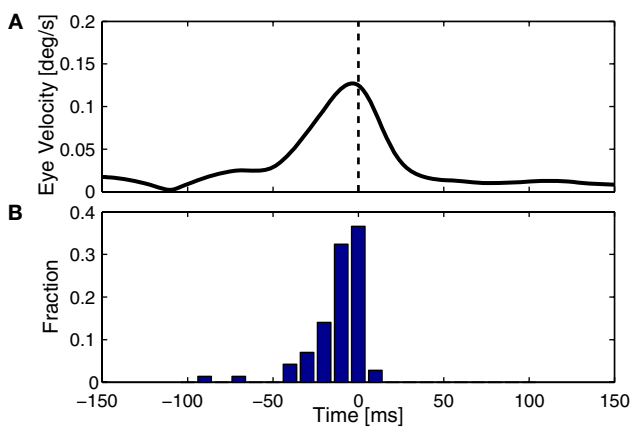

FIGURE 5 | Timing of cerebellar activity. (A) Shows a simple spike triggered average of eye velocity in response to white noise optokinetic stimulation. The white noise stimulus was provided by a panaromic projector system and consisted of a hexagonal matrix of green patches that were rotated coherently around the animal according to a three dimensional gaussian white noise process filtered through a 20-Hz low-pass filter. Note that the curve of this neuron peaks slightly before 0 ms, i.e. the P-cell is active slightly after the actual movement. **(B)** Summarizes the timing of the peak in 71 Purkinje cells, showing activity that more or less coincides with the movement (Winkelman and Frens, 2007).

In engineering applications, these two sources of information about state – the forward model and sensation or observation – are often combined using a Kalman filter

$$\hat{\mathbf{x}}_{n+1} = \hat{\mathbf{x}}_{\mathrm{FM},n+1} + \mathbf{K}_n\left[\mathbf{y}_n - \hat{\mathbf{H}}(\hat{\mathbf{x}}_n)\right] \tag{5}$$

The Kalman filter uses the forward model's estimate of the next state, $\hat{\mathbf{x}}_{\mathrm{FM},n+1}$, as a basis for the combined estimate. The forward model estimate is modified by the "sensory prediction error," $\mathrm{y}_n - \hat{\mathrm{H}}(\hat{\mathbf{x}}_n)$: the difference between the actual observation, $\mathbf{y}_n$, and the observation expected from our current estimate of state, $\hat{\mathbf{H}}(\hat{\mathbf{x}}_n)$. The matrix $\mathbf{K}_n$, of size $k_x \times k_y$, is called the Kalman gain and it quantifies both the way different sensors are relevant to different aspects of state and the relative reliability of sensation and forward model estimation.

In **Box 1**, we also explain how sensory delays lead to alternative formulations for state estimation. Whatever the details of the calculation by which state is estimated, a number of essential points can be made regarding its physiological and behavioral correlates. First, sensory estimation is a combination of internal predictions and currently available sensory information. Second, the way those two sources of information are combined should reflect their reliability: if sensory input is noisy, then the system should rely more on the forward model and vice versa. Third, the input/output relations of the system give us insight into the specific calculation being performed.

The state estimator receives input from the sensory organs and the forward model. Its output should be a state estimate that reflects more recent sensory input than the forward model.

If we accept that the flocculus generates a forward model, then the input requirements are met by the VN. All floccular output is directed to the VN, and sensory information about the head and eye converges here. As a matter of fact, the VN are quite inappropriately named. Vestibular information is just one of their many inputs.

One key study that has looked into the exact properties of the output of the VN is Stahl and Simpson (1995). The neurons of the VN can be divided into two groups. They first receive input from the flocculus (FTNs) while the rest, 80% of the neurons in the VN, do not (non-FTNs). The two groups of neurons have distinctly different behaviors, as seen in **Figure 6**. The firing of the non-FTNs predicts (with almost zero lead) the firing of the neurons in the Abducens Nucleus. This, in combination with the fact that all non-FTNs project to the Abducens Nucleus, suggests that the non-FTNs might be a good candidate for the estimate of state that actually drives the feedback controller. The relationship of the FTNs to sensory (vestibular) input, motor output (Abducens Nucleus) and actual eye movement is more complex. First, the FTNs lead the non-FTNs, suggesting that they are the first step in a two step computation, or perhaps an earlier step in a complex computation. Roughly 60% do not project to the midbrain Stahl and Simpson (1995). Second, the relationship of FTN activity to actual eye movement is better in the dark than in the light, consistent with the idea that FTN activity reflects the predictions of a forward model which has a greater influence on the controller when sensory input is compromised. This suggestion is reinforced by the fact that the difference between light and

BOX 1 | The Kalman filter and sensory delays

The Kalman filter model is popular in engineering applications in part because it is possible, in certain circumstances, to calculate the optimal value for the Kalman gain, $\mathbf{K}_n$, and, for this value, the estimate produced is as close as possible to the true value of the state. Indeed, properly speaking, Eq. 5 describes a Kalman filter only when the function $\mathbf{H}(\mathbf{x})$ is linear and the value of the gain is set to the Kalman gain. However, in the field of motor control the term is often used more loosely.

The Kalman filter updates the estimate of state produced by the forward model, $\hat{\mathbf{x}}_{FM}$, using the discrepancy between our prediction of sensory feedback, $\hat{\mathbf{H}}(\hat{\mathbf{x}})$, and the actual sensory feedback, $\mathbf{y}$. This discrepancy is often called the sensory prediction error. One concern in using the Kalman filter as a model of the activity of the VN is that there is no evidence that VN actually calculates anything like the sensory prediction error.

In Eq. 5, two different estimates of state are used, $\hat{\mathbf{x}}_{FM,n+1}$ and $\hat{\mathbf{x}}_n$. A true Kalman filter, uses only one of these estimates, $\hat{\mathbf{x}}_{FM,n+1}$. That is:

$$\hat{\mathbf{x}}_{n+1} = \hat{\mathbf{x}}_{FM,n+1} + \mathbf{K}_n\left(\mathbf{y}_{n+1} - \mathbf{H}\hat{\mathbf{x}}_{FM,n+1}\right) \quad (6)$$

This is because the true Kalman filter doesn't include sensory delay. In that case, the Kalman filter can be rewritten as a weighted average:

$$\hat{\mathbf{x}}_{n+1} = \left(\mathbf{I} - \mathbf{K}_n\hat{\mathbf{H}}\right)\hat{\mathbf{x}}_{FM,n+1} + \mathbf{K}_n\mathbf{y}_{n+1} \quad (7)$$

with $\mathbf{I}$ signifying the identity matrix. This version of the equation calculates a weighted average of prediction ($\hat{\mathbf{x}}_{FM,n+1}$) and sensation ($\mathbf{y}_{n+1}$) and does not calculate a sensory prediction error ($\mathbf{y}_{n+1} - \mathbf{H}\hat{\mathbf{x}}_{FM,n+1}$). This means that a network that calculates a state estimate based on optimal mixing for forward model prediction and noisy sensory data does not need to calculate a sensory prediction error. While this may not make any difference computationally, it does make a difference in terms of our physiological predictions. Eqs 6 and 7 imply a different sort of synaptic connectivity.

It is interesting to consider solutions to the delay problem. If feedback is delayed by d time steps, then $\mathbf{y}_{n-d} - \hat{\mathbf{H}}\hat{\mathbf{x}}_n$ would compare predictions about the current state with sensory information from a while ago (we assume for this discussion that sensation $\mathbf{H}$ is linear). One class of solutions which includes the Smith predictor (Wolpert and Miall, 1996) is to compare the delayed sensation, $\mathbf{y}_{n-d}$, to a delayed state estimate. In the brain, we do not have delay registers, but we can estimate the past state from the current one, or, for that matter from the output of the forward model, $\hat{\mathbf{x}}_{n-d} = \hat{\mathbf{R}}\hat{\mathbf{x}}_{FM,n+1}$, where $\hat{\mathbf{R}}$ performs backwards linear estimation of the state such as estimating previous position from current position and velocity. Since d is substantial (around 100 ms), the estimating backward using the current output of the state estimate, $\hat{\mathbf{x}}_n$, is relatively similar to using the current output of the forward model, $\hat{\mathbf{x}}_{FM,n+1}$, since both are relatively similar compared to $\hat{\mathbf{x}}_{n-d}$. This leads us to a modified Kalman filter

$$\hat{\mathbf{x}}_{n+1} = \hat{\mathbf{x}}_{FM,n+1} + \mathbf{K}_n\left(\mathbf{y}_{n-d} - \hat{\mathbf{H}}\hat{\mathbf{R}}'\hat{\mathbf{x}}_{FM,n+1}\right) \quad (8)$$

that can also be written as a weighted average

$$\hat{\mathbf{x}}_{n+1} = \left(\mathbf{I} - \hat{\mathbf{H}}\hat{\mathbf{R}}'\right)\hat{\mathbf{x}}_{FM,n+1} + \mathbf{K}_n\mathbf{y}_{n-d} \quad (9)$$

We have simulated this process using a Kalman filter tracking a particle driven by a sinusoidal force with a frequency of 2 Hz, using a time step of 10 ms. The "normal" filter receives the noisy sensory data with 0 delay; the "buffered" filter receives the sensory data with a 100 ms delay, but keeps track of the last 10 estimates of state and updates them as the delayed sensory information arrives; the "linear estimator" follows Eq. 8. It is clear from **Figure B1** that the linear estimator performs nearly as well as the buffered version in this case. The sum squared error of the buffered Kalman filter is 12 times greater than a filter without delay while that of the linear estimation filter is 15 times greater. This shows that a reasonable state estimator can be developed that is based primarily on weighted averages of the forward prediction and sensation, even in cases of significant delay. We suggest that the vestibular nucleus has the characteristics necessary for generating such an estimate.

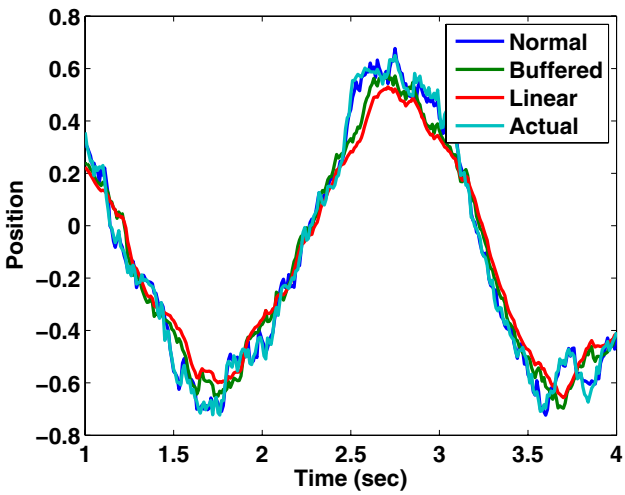

Estimated position and actual position as tracked by three different Kalman filters.

dark nearly disappears when target velocity and acceleration are increased (the target oscillates at a higher frequency) because in these situations, the vestibular input is much more reliable than visual input, and so the importance of the forward model would not be different in the light and the dark.

Finally, the notion that these neurons carry the full 3D properties of the eye movement, while the actual motor command itself does not, suggests that the VN carries an estimate of state rather than a motor command (Ghasia et al., 2008). This picture can be further complicated by a consideration of coordinate systems. Roy and Cullen (2004) show that activity of vestibular neurons – that normally reflects gaze shifts – is suppressed during gaze shifts involving active head movements. This is consistent with the idea that the vestibular nucleus activity reflects the activity of a forward model incorporating efferent copy of commands to the neck muscles. It also has important repercussions for the coordinate system of representation. Cancellation of

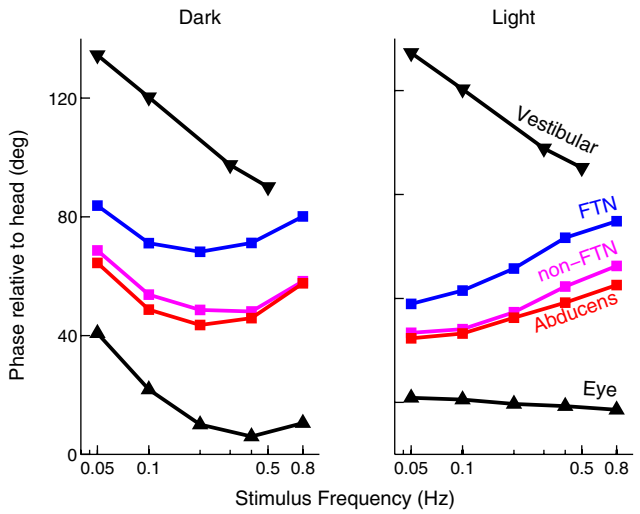

FIGURE 6 | Timing of activity of FTNs in the VN, compared to non-FTNs, Abducens nucleus, vestibular efferents, and the actual eye movement. All phases are given with respect to a vestibular stimulus that was either given in the dark (left panel), or in the light (right panel). Data from Stahl and Simpson (1995).

vestibular nucleus activity during active head movements suggests that vestibular nucleus activity reflects the position of the eyes in the head rather than the position of eyes in extrinsic space.

ADAPTATION

Only one more point needs to be made on the theoretical level. This concerns the issue of adaptation. In many control systems, the plant, the environment and the sensory system are not really fixed in time. For instance, in the case of eye movements, the physiological fluctuations in muscle strength change the effects of motor commands and putting on glasses (which change visual magnification and have different characteristics in different parts of visual space) or contact lenses (which change the weight of the eye) can change the way movements of the eye affect visual input. In such situations, the controller must adapt to changes in the plant. Generally, this may require adaptation of all three major components of the system. It is possible that the different forms of adaptation happen simultaneously: the forward model changes in response to sensory prediction error; the sensory prediction optimally re-weights sensation and prediction; the feedback controller adjusts the motor commands associated with the current state. Adaptation in nervous circuitry is generally supported by neural plasticity. Thus, we must be clear, when we discuss physiological correlates, to specify where we think plasticity may be taking place, and which neurons carry the signals that drive the plasticity and in what coordinates these signals are represented.

The mechanisms of plasticity of the cerebellar cortex have been well studied. The most widespread hypothesis is that climbing fibre (CF) projections (that produce Purkinje cell complex spikes) encode errors that modify the PF-PC synapses through LTD (Ito, 1986, 2006; Simpson et al., 1996). There is evidence for other forms of plasticity as well (Hansel et al., 2001; Coesmans et al., 2004). Nonetheless, many researchers accept the role of the CF as a teacher signal.

If we accept that CF activity carries some form of error signal that drives plasticity, we must face the question of what sort of error it really carries. Until recently, CF projection to the flocculus was thought to contain retinal slip signals. This would be appropriate if the flocculus was calculating an inverse model. On the other hand, such a signal is not optimal for modifying a forward model (FM). Adaptation in a forward model should reduce discrepancies between the estimated and the actual state; it should adapt in response to an error that reflects such discrepancies. Consequently the CF should report unexpected retinal slip rather than any retinal slip (See **Figure 7** for an example). Such signals have been found in the flocculus (Frens et al., 2001; Winkelman and Frens, 2006), as well as in the visual pathways projecting to the Inferior Olive (Ilg and Hoffmann, 1991, 1996).

Plasticity in the VN (Pugh and Raman, 2006, 2009), guided by the cerebellar projection may be the mechanism underlying the weighting required for the optimal state estimation proposed in **Box 1**. In a recent paper, Beraneck et al. (2008) showed that early recovery of the VOR from labyrinthectomy is cerebellar independent while later recovery is cerebellar dependent. Of course, this argues strongly for non-cerebellar mechanisms of plasticity in the CEM system. Additionally, it allows our model to make a prediction. Beraneck et al. suggest that the early, non-cerebellar recovery reflects plasticity in the vestibular nucleus. Our model suggests that this may result from a reweighting of the different inputs to the state estimator. Indeed, our model makes a strong prediction: the early stage of recovery from VOR will not depend on calculations related to the forward model while the later stage will have such a dependence.

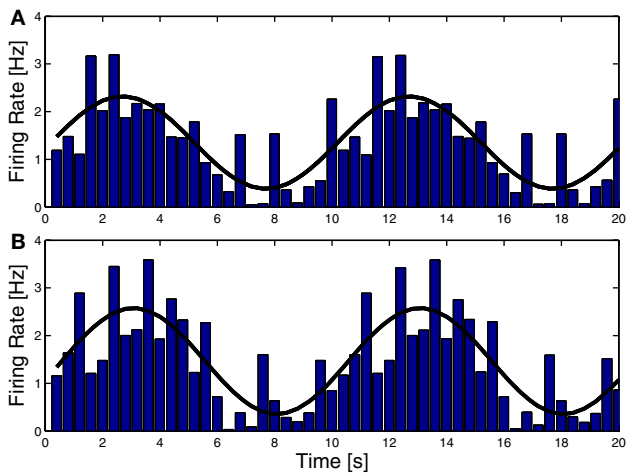

FIGURE 7 | Complex spike (CS) Modulation as a result of sinusoidal optokinetic stimulation. In **(A)** the stimulus was an oscillating pattern. In **(B)** the same pattern moved transparently over a static background. The behavior of the animal varied with the relative luminances of the moving and the static pattern. The frequency of the fitted sine wave equals the frequency of the stimulus (0.1 Hz). Note that the modulation in **(A)** and **(B)** is virtually identical, as are the CEM made by the animal (gain 0.60 and 0.58, respectively). Consequently the predicted slip (caused by the eye movement over the static pattern) is not reflected in the CS (Frens et al., 2001).

We were not able to find any studies of addressing the possibility of plasticity in the Ab or NPH. However, gaze stability is affected by VOR adaptation, and one reasonable explanation for this would be adaptation of the gain of the oculomotor integrator (Tiliket et al., 1994).

DISCUSSION

We propose that CEM are generated by a SPFC framework where specific functional roles can be ascribed to specific nuclei in the CEM circuitry. The strength of the SPFC framework has been demonstrated by many groups (Wolpert and Miall, 1996; Todorov and Jordan, 2002; Shadmehr and Krakauer, 2008). Recently, it has also been applied to describe eye movements (Glasauer, 2007; Ghasia et al., 2008). Because the physiology and anatomy underlying CEM is relatively well known, we are able to describe this mapping in more detail and with more precision than was possible in a similar attempt to describe the control of reaching movements (Shadmehr and Krakauer, 2008). The timing and nature of the signals that can be recorded in the flocculus, the VN, and the brainstem structures support our hypothesis. Also, plasticity in the flocculus and in the VN and the purported olivary error signals can be understood in terms of this framework.

Our model can be contrasted with the classical approach, where the output of the cerebellum is an inverse model (Kawato and Gomi, 1992). The difference in the role played in the cerebellar output is, perhaps, the most salient difference between the two approaches, but there are other differences as well. For instance, the classical approach does not explain the separate function of the three different areas – flocculus, vestibular nucleus, and brainstem motor nuclei – that generate a cascading series of motor commands. In contrast, the SPFC framework ascribes clear and distinct functions to each of these areas.

However, making an experimental distinction between the output of a forward model and the output of an inverse model can be quite difficult. Work by Kawato's group has shown that position, velocity and acceleration regress onto firing rate with a combined r^2 of above 0.7 (Shidara et al., 1993). This has been widely regarded as evidence that the cerebellum implements an inverse model. However, in follow up work, the Kawato group disavows this idea and claims that the floccular output cannot represent the main part of the motor command to the eyes (Gomi et al., 1998). Perhaps the two most convincing arguments in this respect come from our group and that of Dora Angelaki, as described above. Both of these lines of reasoning argue in favor of the forward model interpretation.

Our model enjoys a family resemblance with previously presented schemes, notably the Shadmehr and Krakauer (2008) model of reaching movement control and the Green et al. (2007) model for CEM. However, there are also key differences between our model and the others. Perhaps the most notable difference between our model and the Green et al. model is their suggestion that the vestibular nucleus implements an inverse model. One key issue in this regard is whether the output of the vestibular nucleus describes the upcoming motor command or the current estimate of state. Because CEM do not obey Listing's law, the use of the representation of violation of Listing's law (as was used to great effect in Ghasia et al., 2008) to separate motor commands from state estimates cannot be used in this system. Nevertheless, (1) Ghasia et al. (2008) do suggest that many neurons in the vestibular nucleus represent state, and (2) if the vestibular nucleus is implementing an inverse model and the flocculus is implementing a forward model, it is unclear where state and prediction should be combined.

Our model is also different from the one used by Shadmehr and Krakauer to describe reaching movements (Shadmehr and Krakauer, 2008). Shadmehr and Krakauer suggest that the output of the deep cerebellar nuclei (DCN) reflects the output of a forward model ($\hat{\mathbf{x}}_{FM}$). This is necessary in their scheme because they propose, based on evidence from errors in reaching movements, that the parietal cortex calculates an estimate of state, and thus they propose that the forward model output from the cerebellum should drive this estimate of state. One might say that the DCN is considered the output of the forward model because it more directly projects to the cortex, although the role of the ventrolateral thalamus – which relays the DCN projection to cortex – is not considered in their framework. In our system, the VN seem to be located appropriately to combine forward model prediction based on efferent feedback with delayed sensory information. The VN are analogues of the DCN. Thus, in our system, it is not the cerebellum but specifically the cerebellar cortex which generates a forward model prediction. This difference between our hypothesis and that of Shadmehr and Krakauer might arise for a number of reasons as both models are speculative. Shadmehr and Krakauer did not consider the cerebellar cortex and DCN separately or ascribe any role at all to the thalamus relay station. Our model is more comprehensive, primarily because we are considering a simpler system. However, it is possible that the computation carried out by the cerebellum in the two systems is different and both models are correct.

One important aspect of the Shadmehr and Krakauer analysis of the reaching movement system has to do with the role they ascribe to the basal ganglia in determining the mapping of estimated state to motor command. Their framework explicitly uses the language of optimal feedback control, popularized in our field by Todorov (2004). In optimal feedback control, the controller produces a command which will lead to the best possible combination of task success and energy conservation. In different tasks or with different weight attached to energy conservation, the controller will map states onto motor commands differently. In the scheme put forward by Shadmehr and Krakauer, the role of the basal ganglia is to work with the motor cortex to learn to produce such optimal motor commands. There is no equivalent of the basal ganglia in the CEM system, and it is quite possible that the CEM does not implement an optimal controller: the CEM system is a reflex system and the cost function may be very consistent relative to the costs associated with reaching movements in different tasks.

Another way in which our model differs from previous theories is that we explicitly reject the widespread hypothesis that state estimation is computed using a Kalman filter (see **Box 1**). Rather, it seems that the VN calculation of current state reflects a process with two or more stages, where floccular target neurons perform a first stage of estimation and are then integrated into the broader calculation. The use of a forward model is useful when sensory signals are either noisy or have a large delay. The latter is specifically the case for the retinal slip signals that drive the visual component of CEM (the OKR), which have a delay of 80 ms, whereas the vestibular afferents have a delay of

only a few ms. This may explain why lesions of the flocculus primarily affect the OKR, and only influence the plasticity of the VOR, but not its performance (Waespe et al., 1983; Van Neerven et al., 1989).

Although the CEM circuit is well studied, there are still many holes in our knowledge. For instance, the projections of the VN are only beginning to be understood. It is known that different VN neurons project to the brain stem and to the flocculus. Perhaps the VN calculates two different state estimates or perhaps its projection forward to the brain stem motor nuclei includes partial calculation of the motor command. Resolving this issue will need to wait until more data is available.

Also the finding that there are neurons at two levels of signal processing that strongly resemble the firing of the Abducens (the non-FTNs in the VN, Stahl and Simpson, 1995, and the cells in the NPH Green et al., 2007) requires further experimentation, for instance during eye movements that are mechanically perturbed.

Plasticity in the Abducens Nucleus or NPH is a key prediction of this model. An SPFC framework cannot successfully adapt to changes in the plant unless the feedback controller can adapt. Since recent findings have obscured the functional difference between Abducens Nucleus and NPH (Green et al., 2007; Ghasia et al., 2008), one tempting hypothesis is that NPH serves as the adaptive component of the feedback controller. However, this is only speculation until some data on plasticity in the two nuclei becomes available.

Similarly, the difference between foveate and afoveate species should be addressed. Foveate species have smooth pursuit, which they can use to voluntarily reduce retinal slip. In the afoveate rabbit, for instance, in an experimental paradigm, where the visual environment rotates along with a vestibular stimulus, the VN modulate only at high frequencies, along with the actual eye movement (Stahl and Simpson, 1995). In the (foveate) primate, this correlation is less robust (Miles, 1974; Waespe and Henn, 1978), since the smooth pursuit system can modify the eye movements. Thus, the VN appear to represent an estimate of the eye state faithfully in the rabbit (because CEM are the only eye movements present), but this relation is harder to study in primates, since CEM and SP are harder to distinguish.

In sum, we believe that the SPFC model for the CEM accounts for the available data on the anatomy and physiology of the brain areas involved. It solves important conundrums, especially the timing of the activity of P-cells involved in CEM. While the model remains speculative, it seems to us to be the most reasonable basis for continued exploration of the neural mechanisms involved in stabilizing the eye during fixation.

ACKNOWLEDGMENTS

Part of this work was funded by the Israeli Science Foundation, grant number 624/06 (Opher Donchin), and the NWO-VIDI program (Maarten A Frens).

REFERENCES

Andreescu, C. E., De Ruiter, M. M., De Zeeuw, C. I., and De Jeu, M. T. (2005). Otolith deprivation induces optokinetic compensation. *J. Neurophysiol.* 94, 3487–3496.

Barmack, N. H., Baughman, R. W., Errico, P., and Shojaku, H. (1993). Vestibular primary afferent projection to the cerebellum of the rabbit. *J. Comp. Neurol.* 327, 521–534.

Beraneck, M., McKee, J. L., Aleisa, M., and Cullen, K. E. (2008). Asymmetric recovery in cerebellar-deficient mice following unilateral labyrinthectomy. *J. Neurophysiol.* 100, 945–958.

Blazquez, P. M., Hirata, Y., and Highstein, S. M. (2004). The vestibulo-ocular reflex as a model system for motor learning: what is the role of the cerebellum? *Cerebellum* 3, 188–192.

Boyden, E. S., Katoh, A., and Raymond, J. L. (2004). Cerebellum-dependent learning: the role of multiple plasticity mechanisms. *Annu. Rev. Neurosci.* 27, 581–609.

Braitenberg, V., Heck, D., and Sultan, F. (1997)) The detection and generation of sequences as a key to cerebellar function: experiments and theory. *Behav. Brain Sci.* 20, 229–45.

Buttner-Ennever, J. A., and Buttner, U. (1992). Neuroanatomy of the ocular motor pathways. *Baillieres Clin. Neurol.* 1, 263–287.

Coesmans, M., Weber, J. T., De Zeeuw, C. I., and Hansel, C. (2004). Bidirectional parallel fiber plasticity in the cerebellum under climbing fiber control. *Neuron* 44, 691–700.

Collewijn, H. (1989). The vestibulo-ocular reflex: an outdated concept? *Prog. Brain Res.* 80, 197–209; discussion 171–192.

D'Angelo, E., and De Zeeuw, C. I. (2009). Timing and plasticity in the cerebellum: focus on the granular layer. *Trends Neurosci.* 32, 30–40.

Delgado-Garcia, J. M. (2000). Why move the eyes if we can move the head? *Brain Res. Bull.* 52, 475–482.

Donchin, O., Francis, J. T., and Shadmehr, R. (2003). Quantifying generalization from trial-by-trial behavior of adaptive systems that learn with basis functions: theory and experiments in human motor control. *J. Neurosci.* 23, 9032–9045.

Flash, T., and Hogan, N. (1985). The coordination of arm movements: an experimentally confirmed mathematical model. *J. Neurosci.* 5, 1688–1703.

Frens, M. A., Mathoera, A. L., and van der Steen, J. (2001). Floccular complex spike response to transparent retinal slip. *Neuron* 30, 795–801.

Gerrits, N. M., Epema, A. H., van Linge, A., and Dalm, E. (1989). The primary vestibulocerebellar projection in the rabbit: absence of primary afferents in the flocculus. *Neurosci. Lett.* 105, 27–33.

Gerrits, N. M., Epema, A. H., and Voogd, J. (1984). The mossy fiber projection of the nucleus reticularis tegmenti pontis to the flocculus and adjacent ventral paraflocculus in the cat. *Neuroscience* 11, 627–644.

Ghasia, F. F., Meng, H., and Angelaki, D. E. (2008). Neural correlates of forward and inverse models for eye movements: evidence from three-dimensional kinematics. *J. Neurosci.* 28, 5082–5087.

Gittis, A. H., and du Lac, S. (2006). Intrinsic and synaptic plasticity in the vestibular system. *Curr. Opin. Neurobiol.* 16, 385–390.

Glasauer, S. (2007). Current models of the ocular motor system. *Dev. Ophthalmol.* 40, 158–174.

Glickstein, M., Gerrits, N., Kralj-Hans, I., Mercier, B., Stein, J., and Voogd, J. (1994). Visual pontocerebellar projections in the macaque. *J. Comp. Neurol.* 349, 51–72.

Gomi, H., Shidara, M., Takemura, A., Inoue, Y., Kawano, K., and Kawato, M. (1998). Temporal firing patterns of Purkinje cells in the cerebellar ventral paraflocculus during ocular following responses in monkeys I. Simple spikes. *J. Neurophysiol.* 80, 818–831.

Graf, W., Simpson, J. I., and Leonard, C. S. (1988). Spatial organization of visual messages of the rabbit's cerebellar flocculus. II. Complex and simple spike responses of Purkinje cells. *J. Neurophysiol.* 60, 2091–2121.

Green, A. M., Meng, H., and Angelaki, D. E. (2007). A reevaluation of the inverse dynamic model for eye movements. *J. Neurosci.* 27, 1346–1355.

Hansel, C., Linden, D. J., and D'Angelo, E. (2001). Beyond parallel fiber LTD: the diversity of synaptic and non-synaptic plasticity in the cerebellum. *Nat. Neurosci.* 4, 467–475.

Ilg, U. J., and Hoffmann, K. P. (1991). Responses of monkey nucleus of the optic tract neurons during pursuit and fixation. *Neurosci. Res.* 12, 101–110.

Ilg, U. J., and Hoffmann, K. P. (1996). Responses of neurons of the nucleus of the optic tract and the dorsal terminal nucleus of the accessory optic tract in the awake monkey. *Eur. J. Neurosci.* 8, 92–105.

Ito, M. (1986). Long-term depression as a memory process in the cerebellum. *Neurosci. Res.* 3, 531–539.

Ito, M. (2006). Cerebellar circuitry as a neuronal machine. *Prog. Neurobiol.* 78, 272–303.

Ivry, R. B., and Keele, S. W. (1989). Timing functions of the cerebellum. *J. Cogn. Neurosci.* 1, 136–152.

Jacobson, G. A., Rokni, D., and Yarom, Y. (2008). A model of the olivo-cerebellar system as a temporal pattern generator. *Trends Neurosci.* 31, 617–625.

Jordan, M. I., and Rumelhart, D. E. (1992). Forward models: supervised learning with a distal teacher. *Cogn. Sci.* 16, 307–354.

Kawato, M. (1999). Internal models for motor control and trajectory planning. *Curr. Opin. Neurobiol.* 9, 718–727.

Kawato, M., and Gomi, H. (1992). The cerebellum and VOR/OKR learning models. *Trends Neurosci.* 15, 445–453.

Langer, T., Fuchs, A. F., Scudder, C. A., and Chubb, M. C. (1985). Afferents to the flocculus of the cerebellum in the rhesus macaque as revealed by retrograde transport of horseradish peroxidase. *J. Comp. Neurol.* 235, 1–25.

Lisberger, S. G. (2009). Internal models of eye movement in the floccular complex of the monkey cerebellum. *Neuroscience* 162, 763–776.

Lisberger, S. G., Miles, F. A., and Zee, D. S. (1984). Signals used to compute errors in monkey vestibuloocular reflex: possible role of flocculus. *J. Neurophysiol.* 52, 1140–1153.

Llinás, R. R. (1988). The intrinsic electrophysiological properties of mammalian neurons: insights into central nervous system function. *Science* 242, 1654–1664.

Mauk, M. D., Medina, J. F., Nores, W. L., and Ohyama, T. (2000). Cerebellar function: coordination, learning or timing? *Curr. Biol.* 10, R522–R525.

Mazzoni, P., Hristova, A., and Krakauer, J. W. (2007). Why don't we move faster? Parkinson's disease, movement vigor, and implicit motivation. *J. Neurosci.* 27, 7105–7116.

McCrea, R. A., and Baker, R. (1985). Anatomical connections of the nucleus prepositus of the cat. *J. Comp. Neurol.* 237, 377–407.

McFarland, J. L., and Fuchs, A. F. (1992). Discharge patterns in nucleus prepositus hypoglossi and adjacent medial vestibular nucleus during horizontal eye movement in behaving macaques. *J. Neurophysiol.* 68, 319–332.

Miles, F. A. (1974). Single unit firing patterns in the vestibular nuclei related to voluntary eye movements and passive body rotation in conscious monkeys. *Brain Res.* 71, 215–224.

Miles, F. A., and Lisberger, S. G. (1981). Plasticity in the vestibulo-ocular reflex: a new hypothesis. *Annu. Rev. Neurosci.* 4, 273–299.

Moschovakis, A. K. (1997). The neural integrators of the mammalian saccadic system. *Front. Biosci.* 2, d552–d577. PMID 9341239.

Nowak, D. A., Topka, H., Timmann, D., Boecker, H., and Hermsdorfer, J. (2007). The role of the cerebellum for predictive control of grasping. *Cerebellum* 6, 7–17.

Pugh, J. R., and Raman, I. M. (2006). Potentiation of mossy fiber EPSCs in the cerebellar nuclei by NMDA receptor activation followed by postinhibitory rebound current. *Neuron* 51, 113–123.

Pugh, J. R., and Raman, I. M. (2009). Nothing can be coincidence: synaptic inhibition and plasticity in the cerebellar nuclei. *Trends Neurosci.* 32, 170–177.

Quaia, C., Pare, M., Wurtz, R. H., and Optican, L. M. (2000). Extent of compensation for variations in monkey saccadic eye movements. *Exp. Brain Res.* 132, 39–51.

Raghavan, P., Krakauer, J. W., and Gordon, A. M. (2006). Impaired anticipatory control of fingertip forces in patients with a pure motor or sensorimotor lacunar syndrome. *Brain* 129, 1415–1425.

Raymond, J. L., Lisberger, S. G., and Mauk, M. D. (1996). The cerebellum: a neuronal learning machine? *Science* 272, 1126–1131.

Robinson, D. A. (1981). The use of control systems analysis in the neurophysiology of eye movements. *Annu. Rev. Neurosci.* 4, 463–503.

Roy, J. E., and Cullen, K. E. (2004). Dissociating self-generated from passively applied head motion: neural mechanisms in the vestibular nuclei. *J. Neurosci.* 24, 2102–2111.

Sato, Y., Kawasaki, T., and Ikarashi, K. (1983). Afferent projections from the brainstem to the three floccular zones in cats. II. Mossy fiber projections. *Brain Res.* 272, 37–48.

Shadmehr, R., and Krakauer, J. W. (2008). A computational neuroanatomy for motor control. *Exp. Brain Res.* 185, 359–381.

Shadmehr, R., and Mussa-Ivaldi, F. A. (1994). Adaptive representation of dynamics during learning of a motor task. *J. Neurosci.* 14, 3208–3224.

Shidara, M., Kawano, K., Gomi, H., and Kawato, M. (1993). Inverse-dynamics model eye movement control by Purkinje cells in the cerebellum. *Nature* 365, 50–52.

Simpson, J. I., Wylie, D. R., and De Zeeuw, C. I. (1996). On climbing fiber signals and their consequence(s). *Behav. Brain Sci.* 19, 368–383.

Skavenski, A. A., and Robinson, D. A. (1973). Role of abducens neurons in vestibuloocular reflex. *J. Neurophysiol.* 36, 724–738.

Stahl, J. S., and Simpson, J. I. (1995). Dynamics of rabbit vestibular nucleus neurons and the influence of the flocculus. *J. Neurophysiol.* 73, 1396–1413.

Takemori, S., and Cohen, B. (1974). Loss of visual suppression of vestibular nystagmus after flocculus lesions. *Brain Res.* 72, 213–224.

Tiliket, C., Shelhamer, M., Roberts, D., and Zee, D. S. (1994). Short-term vestibulo-ocular reflex adaptation in humans. I. Effect on the ocular motor velocity-to-position neural integrator. *Exp. Brain Res.* 100, 316–327.

Todorov, E. (2004). Optimality principles in sensorimotor control. *Nat. Neurosci.* 7, 907–915.

Todorov, E., and Jordan, M. I. (2002). Optimal feedback control as a theory of motor coordination. *Nat. Neurosci.* 5, 1226–1235.

Uno, Y., Kawato, M., and Suzuki, R. (1989). Formation and control of optimal trajectory in human multijoint arm movement. Minimum torque-change model. *Biol. Cybern.* 61, 89–101.

Van Neerven, J., Pompeiano, O., and Collewijn, H. (1989). Depression of the vestibulo-ocular and optokinetic responses by intrafloccular microinjection of GABA-A and GABA-B agonists in the rabbit. *Arch. Ital. Biol.* 127, 243–263.

Waespe, W., Cohen, B., and Raphan, T. (1983). Role of the flocculus and paraflocculus in optokinetic nystagmus and visual-vestibular interactions: effects of lesions. *Exp. Brain Res.* 50, 9–33.

Waespe, W., and Henn, V. (1978). Conflicting visual-vestibular stimulation and vestibular nucleus activity in alert monkeys. *Exp. Brain Res.* 33, 203–211.

Winkelman, B., and Frens, M. (2006). Motor coding in floccular climbing fibers. *J. Neurophysiol.* 95, 2342–2351.

Winkelman, B., and Frens, M. (2007). Three dimensional oculomotor tuning of complex and simple spikes in the cerebellar flocculus. Program No. 512.7. 2007 Meeting Planner. San Diego, CA: Society for Neuroscience.

Wolpert, D. M., Goodbody, S. J., and Husain, M. (1998). Maintaining internal representations: the role of the human superior parietal lobe. *Nat. Neurosci.* 1, 529–533.

Wolpert, D. M., and Miall, R. C. (1996). Forward Models for Physiological Motor Control. *Neural. Netw.* 9, 1265–1279.

Zee, D. S., Yamazaki, A., Butler, P. H., and Gucer, G. (1981). Effects of ablation of flocculus and paraflocculus of eye movements in primate. *J. Neurophysiol.* 46, 878–899.

Conflict of Interest Statement: The authors declare that the research was conducted in the absence of any commercial or financial relationships that could be construed as a potential conflict of interest.

Received: 25 May 2009; paper pending published: 09 July 2009; accepted: 06 November 2009; published online: 23 November 2009.

*Citation: Frens MA and Donchin O (2009) Forward models and state estimation in compensatory eye movements. Front. Cell. Neurosci. **3**:13. doi: 10.3389/neuro.03.013.2009*

frontiers in
CELLULAR NEUROSCIENCE

REVIEW ARTICLE
published: 20 November 2009
doi: 10.3389/neuro.03.014.2009

Implications of functional anatomy on information processing in the deep cerebellar nuclei

Yuval Baumel[1], Gilad A. Jacobson[2] and Dana Cohen[1,3]*

[1] *Gonda Interdisciplinary Brain Research Center, Bar Ilan University, Ramat Gan, Israel*
[2] *Friedrich Miescher Institute for Biomedical Research, Basel, Switzerland*
[3] *The Goodman Faculty of Life Sciences, Bar Ilan University, Ramat Gan, Israel*

Edited by:
Egidio D'Angelo, University of Pavia, Italy

Reviewed by:
Carlos D. Aizenman, Brown University, USA
Martha Bagnall, Salk Institute for Biological Studies, USA

****Correspondence:***
Dana Cohen, Gonda Interdisciplinary Brain Research Center, Bar Ilan University, Ramat Gan 52900, Israel.
e-mail: cohendan@biu.ac.il

The cerebellum has been implicated as a major player in producing temporal acuity. Theories of cerebellar timing typically emphasize the role of the cerebellar cortex while overlooking the role of the deep cerebellar nuclei (DCN) that provide the sole output of the cerebellum. Here we review anatomical and electrophysiological studies to shed light on the DCN's ability to support temporal pattern generation in the cerebellum. Specifically, we examine data on the structure of the DCN, the biophysical properties of DCN neurons and properties of the afferent systems to evaluate their contribution to DCN firing patterns. In addition, we manipulate one of the afferent structures, the inferior olive (IO), using systemic harmaline injection to test for a network effect on activity of single DCN neurons in freely moving animals. Harmaline induces a rhythmic firing pattern of short bursts on a quiescent background at about 8 Hz. Other neurons become quiescent for long periods (seconds to minutes). The observed patterns indicate that the major effect harmaline exerts on the DCN is carried indirectly by the inhibitory Purkinje cells (PCs) activated by the IO, rather than by direct olivary excitation. Moreover, we suggest that the DCN response profile is determined primarily by the number of concurrently active PCs, their firing rate and the level of synchrony occurring in their transitions between continuous firing and quiescence. We argue that DCN neurons faithfully transfer temporal patterns resulting from strong correlations in PCs state transitions, while largely ignoring the timing of simple spikes from individual PCs. Future research should aim at quantifying the contribution of PC state transitions to DCN activity, and the interplay between the different afferent systems that drive DCN activity.

Keywords: temporal patterns, rebound firing, short-term depression, harmaline, chronic recording, inferior olive, cerebellar nuclei

ANATOMY OF THE DEEP CEREBELLAR NUCLEI

TYPES OF NEURONS

The deep cerebellar nuclei (DCN) consist of three nuclei: the fastigial (medial) nucleus, the interposed nucleus and the dentate (lateral) nucleus. Together they form the sole output of the cerebellum. The total number of DCN neurons has been estimated at about 50–100,000 (Heidary, 1972; Beitz and Chan-Palay, 1979; Green et al., 2006). The neurons can be divided into three main sub-categories: excitatory projection neurons constituting approximately 50–60% of the population, that project to a variety of extra-cerebellar targets, including the cerebral cortex via the thalamus (Batini et al., 1992; Schwarz and Schmitz, 1997; Holdefer et al., 2000; Teune et al., 2000; Middleton and Strick, 2001; Dum and Strick, 2003; Kelly and Strick, 2003); inhibitory projection neurons constituting approximately 30–35% of the population, that project exclusively to the inferior olive (Tolbert et al., 1976; De Zeeuw et al., 1989; Fredette and Mugnaini, 1991); and local inhibitory interneurons constituting less than 10% of DCN neurons (Chan-Palay, 1977; Czubayko et al., 2001; Aizenman et al., 2003). These three subgroups are intermixed and spatially distributed heterogeneously throughout the DCN (Beitz and Chan-Palay, 1979; Kumoi et al., 1988; Batini et al., 1992). Recently, glycinergic projection neurons unique to the fastigial nuclei have been described (Bagnall et al., 2009). There are no reliable classifications of single cells into subgroups based solely on morphological features due to a considerable overlap in some of their features. For example, the soma size of the excitatory projection neurons ranges from 15 to 35 microns while that of the inhibitory ones ranges from 5 to 20 microns.

THE INPUT TO THE DCN

The DCN receive glutamatergic and GABAergic synaptic inputs, as well as a less-studied neuromodulatory input (see Gardette et al., 1987; Kitzman and Bishop, 1997; Saitow et al., 2009 for serotonergic innervations; and Jaarsma et al., 1997 for cholinergic innervations). The GABAergic input arises from PC axons. The glutamatergic input arises from the mossy fiber (mf) collaterals carrying information from the spinal cord, diverse areas in the cerebral cortex (via the dorsal pontine nuclei) and several brainstem areas, and the climbing fiber axon collaterals – the olivo-cerebellar (oc) fibers – which carry information from the IO (Kandel et al., 2000). Each type of input forms a different varicosity on DCN neurons, making it possible to sort synapses according to their origin. The largest portion of synaptic connections is formed by PCs [about 60–85% of synapses, depending on the species and method used for counting (Chan-Palay, 1973b; Mezey et al., 1977; Palkovits et al., 1977;

De Zeeuw and Berrebi, 1996)]. The oc fibers constitute about 5% of the DCN input (Chan-Palay, 1973b; Van der Want et al., 1989). The number of interneuron and mf synapses onto the projection neurons remains unclear (see e.g., Chan-Palay, 1973b; Wassef et al., 1986; De Zeeuw and Berrebi, 1995, 1996). The vast majority of axon terminals reaching the DCN form synaptic contacts on the glutamatergic projection neurons rather than on the GABAergic neurons (80% vs. 20%). This ratio is maintained regardless of origin (De Zeeuw and Berrebi, 1996).

The convergence–divergence ratio of different afferent inputs to the DCN has been estimated only for the PC-DCN pathway. A single PC is estimated to innervate approximately 30–40 DCN neurons and in turn, each DCN neuron, receives projections from about 600–900 PC (Chan-Palay, 1973a; Mezey et al., 1977; Palkovits et al., 1977). It is estimated that most of PC axons innervate both glutamatergic and GABAergic cells (De Zeeuw and Berrebi, 1995, 1996; Teune et al., 1998). Generally it has been suggested that mf collaterals show considerable ramification and a bilateral projection pattern in the nuclei (Shinoda et al., 1992, 2000; Wu et al., 1999) whereas the oc distribution is more local, generating a closed loop composed of the IO – cerebellar cortex – DCN – IO (Sugihara et al., 1999, 2001; Shinoda et al., 2000; Sugihara and Shinoda, 2004; Pijpers et al., 2005).

The dominance of the PC input onto the DCN seems to suggest that it plays a major role in modulating DCN activity compared to the other inputs. In the next section, we review electrophysiological evidence regarding the relative contribution of the different inputs to DCN output.

DCN ELECTROPHYSIOLOGY

Neurons in the DCN receive a wide array of inputs, both excitatory and inhibitory. A central question is to which extent can the different kinds of input shape DCN output, and whether the DCN is sensitive to specific interactions between co-occurring inputs from these different sources. Attaining such an understanding would be a significant step toward underpinning the DCN computation.

Several studies have monitored neuronal activity from DCN neurons during sensory stimuli and motor activity. Neurons in the DCN tend to fire spontaneously at rates >10 Hz, and can modulate their firing rates in complex ways in response to either sensory or motor activation (e.g., Thach, 1968, 1975; Eccles et al., 1974b,c; Strick, 1983; Rowland and Jaeger, 2005, 2008). Neurons exhibit increases and decreases in firing rate, suggesting that both excitatory and inhibitory inputs to the DCN play a significant role in shaping its output. It is difficult, though, to conclude from such works which afferent structures and synaptic conductances generated these responses. Rowland and Jaeger (2008) have tried to correlate DCN firing profile with the activity in different afferent structures. Their results suggest that IO output can substantially affect DCN output. Nonetheless, their olivary signal was limited to local field potential, and the complexity of the olivo-nuclear connection, which has both direct and indirect paths, further complicates the interpretation of such results.

Further insight into DCN processing comes from testing the influence of temporary modification of the afferent systems on animal behavior. Injection of both GABA agonists and antagonists to the DCN abolishes conditioned eye blink responses (Aksenov et al., 2004), while blockade of fast glutamate receptors in the DCN have a minor effect on conditioned responses (Aksenov et al., 2005). These results suggest that the expression of eye blink conditioning depends on intact GABAergic, and not glutamatergic, pathways to the DCN.

DCN processing depends not only on the properties of DCN afferent systems but also on the biophysics of DCN neurons. One major observation is that the PC-DCN synapse exhibits a strong short-term depression (STD). STD is shown in **Figure 1** in which a paired pulse protocol was used to stimulate the PC-DCN synapse. STD ranges from 30% for a 20-Hz input to 90% for rates >140 Hz (Telgkamp and Raman, 2002; Pedroarena and Schwarz, 2003). Thus, it seems that the massive PC-DCN projection is counteracted by a physiological mechanism, and may not be as dominant as indicated by anatomy. This may explain how neurons of

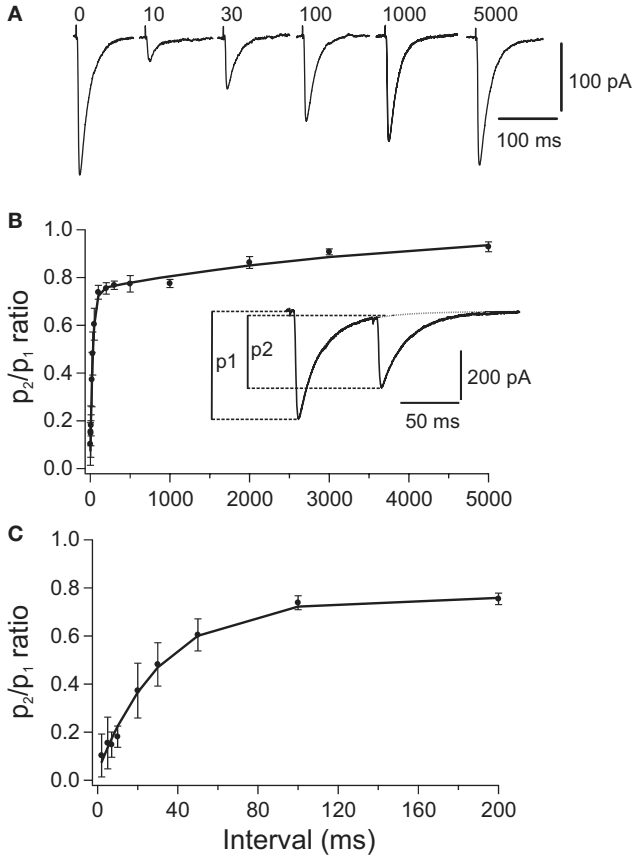

FIGURE 1 | Paired pulse depression (PPD) of compound PC-DCN IPSCs. **(A)** Representative example of IPSCs evoked by paired stimulation. Each trace illustrates the average of 25 single IPSCs evoked in a DCN by pairs of stimuli with different intervals applied to PC axons. Number above each trace indicates the interpulse interval in milliseconds. Traces corresponding to 10 and 30 ms were obtained after subtracting the response to the 1st stimulus (labeled with "0"). **(B,C)** Time course of recovery from PPD shown at two different time scales. Average peak amplitude ratio (p2/p1) was plotted against the interpulse interval (n = 24). The curves represent a double exponential expression fitted to the data. The peak amplitude of IPSCs was measured from the baseline to the peak of the respective IPSCs. Taken with permission from Pedroarena and Schwarz (2003).

the cerebellar nuclei maintain relatively high basal firing rates of 10–100 Hz (Thach, 1968; LeDoux et al., 1998; Rowland and Jaeger, 2005) despite the convergence of many PCs each firing at about 50 Hz. Nonetheless, direct stimulation of the inhibitory pathway at a rate above the presumed PC firing rate can lead to a further decline in DCN firing rate, demonstrating that changes in PC activity still have the capacity to modulate DCN activity (Telgkamp and Raman, 2002). Overall, PC-DCN synapses seem to exhibit larger sensitivity to dynamic than to steady PC activation; and despite the significant depression at the PC-DCN synapse, PCs can provide effective inhibition and shape DCN firing patterns (Telgkamp and Raman, 2002; Pedroarena and Schwarz, 2003).

Synaptic depression at the PC-DCN synapse has several computational implications. First, basal levels of asynchronous inhibition may keep DCN neurons within their dynamic range thus allowing them to respond to increases, as well as decreases, in PC firing rate (Thach, 1968; Jahnsen, 1986; Gauck and Jaeger, 2000; Telgkamp and Raman, 2002; Pedroarena and Schwarz, 2003). Second, the significant decline in PC-DCN synaptic strength suggests that although PC axons can transfer spike doublets when firing a complex spike (CS) (Khaliq and Raman, 2005; Monsivais et al., 2005), the DCN response to the second spike in the doublet will be strongly depressed. This supports the idea that DCN neurons can respond only to the first spike in the CS and thus cannot distinguish it from the arrival of SSs. If this is indeed the case, STD enables the IO to generate a complex spatiotemporal activation of the cerebellar cortex including induction of LTD/LTP and controlling pause duration (Mathy et al., 2009) without maintaining the tagging of CS activity when transferred downstream to the DCN. The impact of the direct IO-DCN excitatory pathway on DCN has still to be thoroughly investigated. Last, an important implication of the fast depression is that DCN neurons should be highly sensitive to *changes* in the rate of PC input, as elaborated in the section "Discussion".

Another observation is that DCN neurons respond to a hyperpolarizing current with a post-hyperpolarization rebound response, which plays a major part in many cerebellar theories (Medina et al., 2000; Kistler and De Zeeuw, 2003; Wetmore et al., 2008); after hyperpolarization, the membrane rapidly depolarizes and is capable of producing spikes at membrane potentials lower than prior to hyperpolarization (**Figure 2**). The strength of the rebound response increases with the amplitude (**Figures 2A–C**) and the duration (**Figures 2D–F**) of hyperpolarization (Jahnsen, 1986; Aizenman and Linden, 1999). This endows DCN neurons with the ability to respond to inhibitory inputs with a spiking output and also to respond differently to the same input depending on the history of synaptic input (**Figures 2G,H**). Thus, it is difficult to relate changes in firing rate to excitation/inhibition in a trivial way. The large temporal variability of about 50 ms in the onset of the rebound responses (Llinás and Muhlethaler, 1988) poses a problem for theories of cerebellar timing (Ivry and Keele, 1989; Mauk et al., 2000; Ivry and Spencer, 2004). This limitation may be

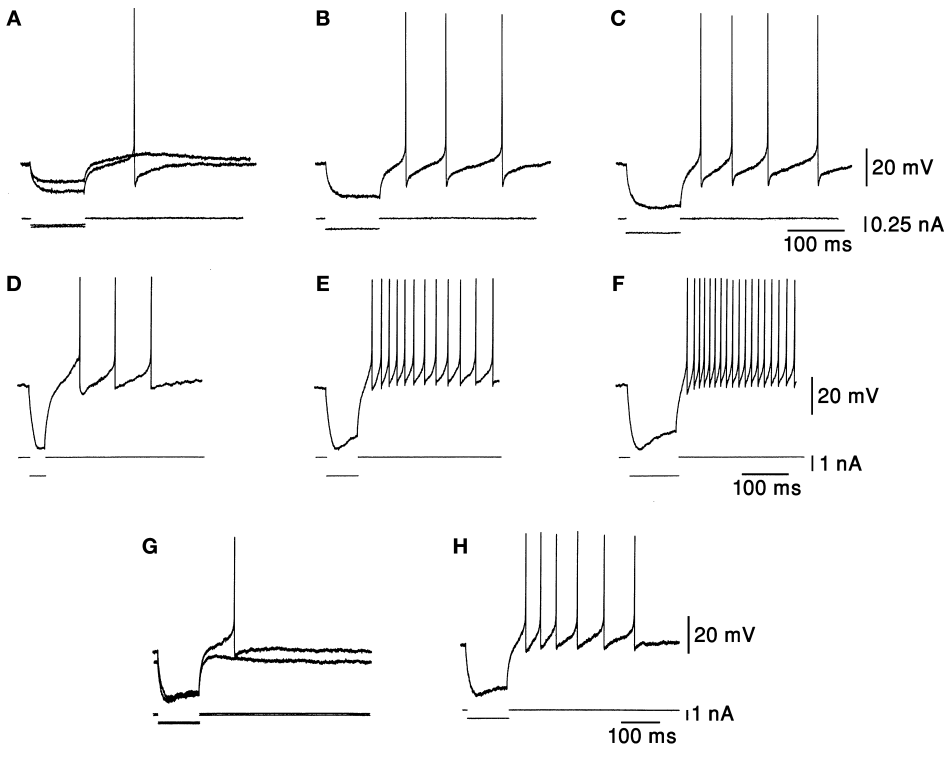

FIGURE 2 | Responses to hyperpolarizing current pulses. (A–C) Rebound responses were seen after hyperpolarizing current pulses. The smallest pulse produced only a subthreshold depolarization. As the stimulus increased in amplitude an increasing number of action potentials were generated. **(D–F)** The responses were dependent on the duration of preceding hyperpolarization. More spikes were seen after long hyperpolarizations. **(G,H)** The rebound response was dependent on the initial membrane potential. The response was larger when the membrane was depolarized. Taken with permission from Jahnsen (1986).

resolved if active depolarization occurs in these neurons instead of a mere return to resting potential, or by a strong, purely excitatory input component (e.g., Gauck and Jaeger, 2003; Rowland and Jaeger, 2005).

Different neuronal populations in the DCN may possess different biophysical machinery and firing properties. Attempts to correlate morphological features of DCN neurons such as soma size and shape, and dendritic arborization with electrophysiological properties have until recently not been conclusive, mainly because of the overlap in morphological properties of different DCN cell types. Recently, an *in vitro* study that allowed separating the inhibitory projection neurons from the non-inhibitory ones demonstrated that a reliable classification of DCN cells into subgroups can be achieved using a combination of several electrophysiological properties (Uusisaari et al., 2007). Specifically, compared to the excitatory projection neurons, the inhibitory projection neurons have a lower spontaneous firing rate and they do not reach as high firing frequencies during depolarizing current injections. Furthermore, these cells exhibit a longer-lasting rebound depolarization and associated spiking after a transient hyperpolarization. Increasing the temperature *in vitro* enhanced the difference in rebound firing between the excitatory and inhibitory neuronal populations. This would imply that under normal body temperature these differences will be further enhanced. In such a case, two outcomes could be expected: (1) the rather short lasting rebound firing in the excitatory projection neurons will be capable of reporting neuronal signals with higher temporal acuity; and (2) the long rebound firing in the inhibitory projection neurons will be capable of providing stable tonic GABAergic input to control the strength of gap junction coupling in IO neurons for long time periods (Jacobson et al., 2008).

To test the functional convergence of DCN afferents we used systemic injections of harmaline (10–15 mg/kg) to manipulate both the direct oc inputs to the DCN and the indirect PC input converging on the DCN (Llinás and Volkind, 1973). Harmaline, which serves as an animal model for essential tremor, accentuates IO subthreshold oscillations, thus increasing cf firing rate to about 10 Hz (De Montigny and Lamarre, 1973; Llinás et al., 1974). This massive CS activity, which occurs synchronously in PCs, significantly decreases SS firing in many PCs (Lamarre et al., 1971; Llinás and Volkind, 1973; Llinás and Muhlethaler, 1988). We recorded DCN activity in freely moving rats ($n = 3$) using chronically implanted electrodes (for methods see the **Figure 3** and Cohen and Nicolelis, 2004; Jacobson et al., 2009). Preliminary results show that harmaline induced a transition from stochastic firing to long periods of quiescence (7/12 cells) or to an ON/OFF firing pattern in which activity alternated between short bursts of action potentials and long quiescence periods (5/12 cells). This ON/OFF pattern repeated every 100–130 ms which is typical of IO interspike intervals following harmaline application (Llinás and Volkind, 1973; Jacobson et al., 2009). Neurons could alternate between the ON/OFF pattern and the prolonged quiescence. In 3/12 cells, a variety of firing patterns was observed, including an increase in firing rate and a stable firing rate. Examples of two cells recorded prior to and after harmaline injection are shown in **Figure 3**. Similar firing patterns have previously been described in an isolated brain stem-cerebellar preparation under different levels of hyperpolarization (Llinás and Muhlethaler, 1988). In that work, harmaline injection resulted in a repeating synaptic input pattern consisting of a short lasting (10–12 ms) excitatory post synaptic potential (EPSP) followed by a long lasting (80–100 ms) inhibitory post synaptic potential (IPSP). Occasionally DCN neurons exhibited only IPSPs, suggesting that the distribution of inhibitory potentials over the cerebellar nucleus is broader than that of the excitatory oc potentials (Llinás and Muhlethaler, 1988). This in turn suggests that the direct effect of IO on DCN via oc collaterals is probably more restricted than the IO broad effect via PCs. The extent and conditions under which direct oc input can induce an excitatory response in DCN neurons remain to be determined.

DISCUSSION

Information processing depends on structural anatomy, intrinsic properties of the neuronal elements and network dynamics. In this review, we summarize the major points relating to these aspects of DCN processing and further provide initial results relating to DCN network performance by examining harmaline-induced changes in DCN activity in freely moving animals.

At first glance, it seems likely that as a result of the increase in IO firing induced by harmaline (Lamarre et al., 1971; Llinás and Volkind, 1973; Llinás and Muhlethaler, 1988) activity in the DCN would be enhanced significantly via two different pathways: (1) excessive activation of oc collaterals is expected to excite DCN neurons and (2) cf activation of PC, which decreases significantly the firing of SS (Lamarre et al., 1971; Llinás and Volkind, 1973; Llinás and Muhlethaler, 1988), is expected to decrease PC firing rate and thus indirectly disinhibit the DCN. Our results, however, suggest that the effect of the IO on DCN firing is not as trivial. Instead of increasing their firing rate after harmaline application, 75% of the recorded the DCN neurons became quiescent or exhibited rhythmic ON/OFF firing patterns entrained to IO firing. Two neural mechanisms that are not mutually exclusive can induce the ON response: (1) direct activation of synchronous oc collaterals, and (2) rebound firing in the DCN. Evidence for a role for rebound firing in shaping the ON response comes from Llinás and Muhlethaler (1988), showing that the duration of the ON response is significantly longer than that of the IO mediated EPSP and that strong phasic firing occurs following hyperpolarizing current injection. On the other hand, rebound firing has been questioned *in vivo* (Alvina et al., 2008) and there exists evidence for direct IO-DCN excitation (Eccles et al., 1974a,b; Rowland and Jaeger, 2005). The physiological conditions under which rebound firing manifests itself and the degree to which direct IO excitation can drive DCN neurons remain to be elucidated.

The paradoxical silencing of DCN neurons by harmaline can be attributed to several mechanisms: (1) inhibition exerted by cf-activated PCs; (2) effective recruitment of local DCN interneurons; or (3) depolarization block resulting from the reduction in PC firing. There is currently no clear evidence for any of these options. Local interneurons constitute a small group of DCN neurons, and their role so far remains unknown. Depolarization block has been reported only incidentally (Pugh and Raman, 2009), and the conditions under which it would manifest itself are yet to be determined. As for the inhibition exerted by cf-activated PCs, it is possible that the infrequent complex spikes produced by PCs on a silent background allow the PC-DCN inhibitory synapses to

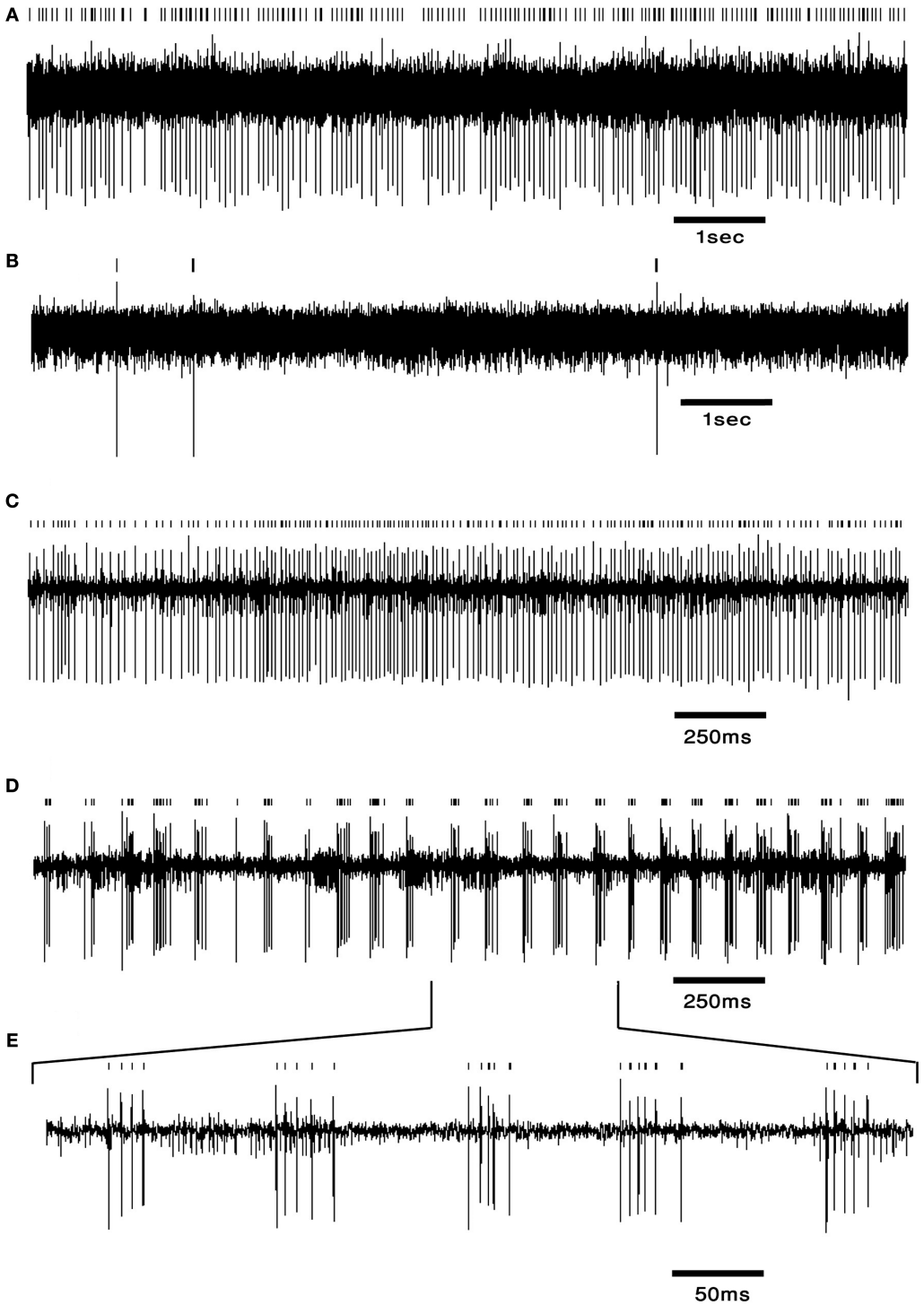

FIGURE 3 | DCN neurons exhibit typical firing patterns following harmaline injection. (A,B) An example of a tonically firing neuron **(A)** that became almost completely quiescent after harmaline injection **(B)**. **(C,D)** An example of a tonically firing neuron **(C)** that exhibited an ON/OFF firing pattern after harmaline injection **(D)**. **(E)** Time expansion of the marked section in **(D)** showing the typical cycle of the ON/OFF pattern. Small bars above the trace mark the sorted spikes. The surgical procedure has been described in detail (Cohen and Nicolelis, 2004; Jacobson et al., 2009). In brief, adult Long Evans male rats weighing 350–500 g (Harlan, Indianapolis, IN, USA) were initially sedated by 5% isoflurane and then injected i.m. with ketamine HCl and xylazine HCl (100 and 10 mg/kg, respectively). Supplementary injections of ketamine and xylazine were given as required. The skull surface was exposed and a craniotomy, slightly larger than the electrode array, was performed above the medial and interposed nuclei. Center of implant was at –11.3 mm posterior to bregma, 1.5 mm lateral to the midline (coordinates taken from Paxinos and Watson, 1998). Arrays of 16 electrodes were lowered 4 mm from the surface of the brain and fixed using dental cement. Rats were allowed at least 2 weeks of recovery prior to recording. Electrode location was verified using histology.

recover and exert a stronger inhibitory effect. This recovery by itself may not be enough, as *in vitro* studies have shown that inhibition grows with PC rate, despite STD. However, if complemented by harmaline induced recruitment of PCs that are normally silent, PC-DCN release-from-depression by CS activity may turn out to be highly effective.

What generates the heterogeneity in DCN responses to harmaline injection? The quiescent and rhythmic DCN neurons under harmaline (see **Figure 3**) may differ in the degree of synchronicity between the PCs that drive them, or simply in the number of rhythmic PCs impinging upon them at a given time. If the CS signals reach the DCN almost simultaneously, inhibition strength may wear off before the next CS, thus allowing for a rebound response. If on the other hand, CS signals arrive asynchronously throughout IO cycle, the inhibitory time-course will be smoothed, preventing rebound firing throughout the oscillatory cycle. Both zero lag (synchronous) and non-zero lags (asynchronous) IO activity correlations have been reported *in vivo* (Sugihara et al., 1993, 1995; Lang, 2001, 2002; Jacobson et al., 2009), providing a substrate for these two firing patterns. Alternatively, DCN neurons that receive less inhibition may be able to respond to the direct IO-DCN excitatory input, while strongly inhibited neurons may not.

What interplay between DCN afferents and biophysical properties would best account for the firing patterns observed in the absence of harmaline? The firing patterns observed in DCN *in vivo* suggest that the properties of the different afferent inputs and the biophysics of DCN neurons interact in complex ways to form the DCN output. Evidence exists for the involvement of all afferent structures in shaping DCN output (Thach, 1968; Eccles et al., 1974a,b; Strick, 1983; Rowland and Jaeger, 2005, 2008; Ohyama et al., 2006). The contribution of PCs to DCN firing is particularly interesting because PCs participate in the feedback loops involving both excitatory cerebellar afferents. Our results may indicate that normal cerebellar activation involves strong PC activation that in turn can bidirectionally modulate DCN firing.

To efficiently activate phasic firing in DCN neurons, converging PCs must start at a high firing rate to evoke hyperpolarization and cease firing synchronously to instantly remove inhibition and evoke a rebound response. Interestingly, increased synchrony has been reported in PCs following sensory stimulation (Schultz et al., 2009). Although the precise numbers are hard to pin down, we suggest that the firing patterns in DCN are controlled primarily by the number of concurrently active PCs, their firing rate and level of synchrony in the transition from continuous firing to quiescence.

Two plausible mechanisms may underlie synchronized intermissions lasting tens of milliseconds to seconds in PCs: (1) transition between states in bistable PCs imposed by synchronized IO activity (Loewenstein et al., 2005; Jacobson et al., 2008; Yartsev et al., 2009), and (2) generation of pauses in SS firing in several PCs simultaneously by synchronized activation of molecular layer interneurons forming an efficient inhibitory network via gap junction (Mann-Metzer and Yarom, 1999; Mittmann et al., 2005). Analysis of SS activity in anesthetized animals reveals high synchrony prior to the occurrence of a pause (Shin and De Schutter, 2006; De Schutter and Steuber, 2009). This short lasting synchrony indicates that many PCs undergo an intermission in firing at the same time, thus generating an accurate timing signal marking the imminent removal of the sustained PC inhibition from DCN neurons.

The two mechanisms proposed for DCN disinhibition – SS pauses and PC bistability – differ in their duration. Short, pause-induced intermissions may disinhibit DCN neurons just enough to generate a short burst of activity, while longer, state-transition intermissions may enable prolonged DCN firing which in turn can decouple IO neurons and reselect functional subgroups within it (Llinás, 1974; Llinás et al., 1974; De Zeeuw et al., 1989, 1993, 1997; Llinás and Sasaki, 1989; Lang et al., 1996; Placantonakis et al., 2006).

FUTURE DIRECTIONS

Despite significant advances in the last decades, the current understanding of DCN function is partial, and lags behind the research of the cerebellar cortex. Considering the crucial position of the DCN as the output station of the entire cerebellar circuit, improving our understanding of DCN function should be a central goal of cerebellar research.

Filling in the gaps in anatomical and physiological knowledge of the DCN is an important task but we believe that good hypotheses are necessary in order to interpret the data and design experiments that easily distinguish between different hypotheses.

We suggest two experiments that directly arise from our hypothesis that PC state transitions determine DCN output. The first is to monitor the activity of a DCN neuron simultaneously with its afferent PCs, and test the relationship between state transitions and DCN firing. The other is to study the effect of IO decoupling on DCN output. We expect IO decoupling to desynchronize state transitions in neighboring PCs leading to a smoothing of firing patterns in the DCN. We believe that in the upcoming decade, the DCN may stop stuttering and start telling a story.

ACKNOWLEDGMENTS

Dana Cohen was supported by grant SENSOPAC (FP6-IST028056) from the European Commission. Gilad A. Jacobson is supported by an EMBO long-term fellowship.

REFERENCES

Aizenman, C. D., Huang, E. J., and Linden, D. J. (2003). Morphological correlates of intrinsic electrical excitability in neurons of the deep cerebellar nuclei. *J. Neurophysiol.* 89, 1738–1747.

Aizenman, C. D., and Linden, D. J. (1999). Regulation of the rebound depolarization and spontaneous firing patterns of deep nuclear neurons in slices of rat cerebellum. *J. Neurophysiol.* 82, 1697–1709.

Aksenov, D., Serdyukova, N., Irwin, K., and Bracha, V. (2004). GABA neurotransmission in the cerebellar interposed nuclei: involvement in classically conditioned eyeblinks and neuronal activity. *J. Neurophysiol.* 91, 719–727.

Aksenov, D. P., Serdyukova, N. A., Bloedel, J. R., and Bracha, V. (2005). Glutamate neurotransmission in the cerebellar interposed nuclei: involvement in classically conditioned eyeblinks and neuronal activity. *J. Neurophysiol.* 93, 44–52.

Alvina, K., Walter, J. T., Kohn, A., Ellis-Davies, G., and Khodakhah, K. (2008). Questioning the role of rebound firing in the cerebellum. *Nat. Neurosci.* 11, 1256–1258.

Bagnall, M. W., Zingg, B., Sakatos, A., Moghadam, S. H., Zeilhofer, H. U., and du Lac, S. (2009). Glycinergic projection neurons of the cerebellum. *J. Neurosci.* 29, 10104–10110.

Batini, C., Compoint, C., Buisseret-Delmas, C., Daniel, H., and Guegan, M. (1992). Cerebellar nuclei and the nucleocortical projections in the rat: retrograde tracing coupled to GABA

and glutamate immunohistochemistry. *J. Comp. Neurol.* 315, 74–84.

Beitz, A. J., and Chan-Palay, V. (1979). The medial cerebellar nucleus in the rat: nuclear volume, cell number, density and orientation. *Neuroscience* 4, 31–45.

Chan-Palay, V. (1973a). Afferent axons and their relations with neurons in the nucleus lateralis of the cerebellum: a light microscopic study. *Z. Anat. Entwicklungsgesch.* 142, 1–21.

Chan-Palay, V. (1973b). On the identification of the afferent axon terminals in the nucleus lateralis of the cerebellum. An electron microscope study. *Z. Anat. Entwicklungsgesch.* 142, 149–186.

Chan-Palay, V. (1977). Cerebellar Dentate Nucleus; Organization, Cytology and Transmitters. Berlin, Springer-Verlag.

Cohen, D., and Nicolelis, M. A. (2004). Reduction of single-neuron firing uncertainty by cortical ensembles during motor skill learning. *J. Neurosci.* 24, 3574–3582.

Czubayko, U., Sultan, F., Thier, P., and Schwarz, C. (2001). Two types of neurons in the rat cerebellar nuclei as distinguished by membrane potentials and intracellular fillings. *J. Neurophysiol.* 85, 2017–2029.

De Montigny, C., and Lamarre, Y. (1973). Rhythmic activity induced by harmaline in the olivo-cerebello-bulbar system of the cat. *Brain Res.* 53, 81–95.

De Schutter, E., and Steuber, V. (2009). Patterns and pauses in Purkinje cell simple spike trains: experiments, modeling and theory. *Neuroscience.* 162, 816–826.

De Zeeuw, C. I., and Berrebi, A. S. (1995). Postsynaptic targets of Purkinje cell terminals in the cerebellar and vestibular nuclei of the rat. *Eur. J. Neurosci.* 7, 2322–2333.

De Zeeuw, C. I., and Berrebi, A. S. (1996). Individual Purkinje cell axons terminate on both inhibitory and excitatory neurons in the cerebellar and vestibular nuclei. *Ann. N. Y. Acad. Sci.* 781, 607–610.

De Zeeuw, C. I., Holstege, J. C., Ruigrok, T. J., and Voogd, J. (1989). Ultrastructural study of the GABAergic, cerebellar, and mesodiencephalic innervation of the cat medial accessory olive: anterograde tracing combined with immunocytochemistry. *J. Comp. Neurol.* 284, 12–35.

De Zeeuw, C. I., Van Alphen, A. M., Hawkins, R. K., and Ruigrok, T. J. H. (1997). Climbing fibre collaterals contact neurons in the cerebellar nuclei that provide a GABAergic feedback to the inferior olive. *Neuroscience* 80, 981–986.

De Zeeuw, C. I., Wentzel, P., and Mugnaini, E. (1993). Fine structure of the dorsal cap of the inferior olive and its GABAergic and non-GABAergic input from the nucleus prepositus hypoglossi in rat and rabbit. *J. Comp. Neurol.* 327, 63–82.

Dum, R. P., and Strick, P. L. (2003). An unfolded map of the cerebellar dentate nucleus and its projections to the cerebral cortex. *J. Neurophysiol.* 89, 634–639.

Eccles, J. C., Rantucci, T., Sabah, N. H., and Taborikova, H. (1974a). Somatotopic studies on cerebellar fastigial cells. *Exp. Brain Res.* 19, 100–118.

Eccles, J. C., Sabah, N. H., and Taborikova, H. (1974b). Excitatory and inhibitory responses of neurones of the cerebellar fastigial nucleus. *Exp. Brain Res.* 19, 61–77.

Eccles, J. C., Sabah, N. H., and Taborikova, H. (1974c). The pathways responsible for excitation and inhibition of fastigial neurones. *Exp. Brain Res.* 19, 78–99.

Fredette, B. J., and Mugnaini, E. (1991). The GABAergic cerebello-olivary projection in the rat. *Anat. Embryol. (Berl.)* 184, 225–243.

Gardette, R., Krupa, M., and Crepel, F. (1987). Differential effects of serotonin on the spontaneous discharge and on the excitatory amino acid-induced responses of deep cerebellar nuclei neurons in rat cerebellar slices. *Neuroscience* 23, 491–500.

Gauck, V., and Jaeger, D. (2000). The control of rate and timing of spikes in the deep cerebellar nuclei by inhibition. *J. Neurosci.* 20, 3006–3016.

Gauck, V., and Jaeger, D. (2003). The contribution of NMDA and AMPA conductances to the control of spiking in neurons of the deep cerebellar nuclei. *J. Neurosci.* 23, 8109–8118.

Green, J. T., Arenos, J. D., and Dillon, C. J. (2006). The effects of moderate neonatal ethanol exposure on eyeblink conditioning and deep cerebellar nuclei neuron numbers in the rat. *Alcohol* 39, 135–150.

Heidary, H. (1972). Neuron populations in the cerebellum of the cat. *Experientia* 28, 313–314.

Holdefer, R. N., Miller, L. E., Chen, L. L., and Houk, J. C. (2000). Functional connectivity between cerebellum and primary motor cortex in the awake monkey. *J. Neurophysiol.* 84, 585–590.

Ivry, R., and Keele, S. (1989). Timing functions of the cerebellum. *J. Cogn. Neurosci.* 1, 136–152.

Ivry, R. B., and Spencer, R. M. C. (2004). The neural representation of time. *Curr. Opin. Neurobiol.* 14, 225–232.

Jaarsma, D., Ruigrok, T. J., Caffe, R., Cozzari, C., Levey, A. I., Mugnaini, E., and Voogd, J. (1997). Cholinergic innervation and receptors in the cerebellum. *Prog. Brain Res.* 114, 67–96.

Jacobson, G. A., Lev, I., Yarom, Y., and Cohen, D. (2009). Invariant phase structure of olivo-cerebellar oscillations and its putative role in temporal pattern generation. *Proc. Natl. Acad. Sci. U.S.A.* 106, 3579–3584.

Jacobson, G. A., Rokni, D., and Yarom, Y. (2008). A model of the olivo-cerebellar system as a temporal pattern generator. *Trends Neurosci.* 31, 617–625.

Jahnsen, H. (1986). Electrophysiological characteristics of neurones in the guinea-pig deep cerebellar nuclei in vitro. *J. Physiol.* 372, 129–147.

Kandel, E. R., Schwartz, J. H., and Jessell, T. M. (eds). (2000). Principles of Neural Science. New York, McGraw-Hill.

Kelly, R. M., and Strick, P. L. (2003). Cerebellar loops with motor cortex and prefrontal cortex of a nonhuman primate. *J. Neurosci.* 23, 8432–8444.

Khaliq, Z. M., and Raman, I. M. (2005). Axonal propagation of simple and complex spikes in cerebellar Purkinje neurons. *J. Neurosci.* 25, 454–463.

Kistler, W. M., and De Zeeuw, C. I. (2003). Time windows and reverberating loops: a reverse-engineering approach to cerebellar function. *Cerebellum* 2, 44–54.

Kitzman, P. H., and Bishop, G. A. (1997). The physiological effects of serotonin on spontaneous and amino acid-induced activation of cerebellar nuclear cells: an in vivo study in the cat. *Prog. Brain Res.* 114, 209–223.

Kumoi, K., Saito, N., Kuno, T., and Tanaka, C. (1988). Immunohistochemical localization of gamma-aminobutyric acid- and aspartate-containing neurons in the rat deep cerebellar nuclei. *Brain Res.* 439, 302–310.

Lamarre, Y., de Montigny, C., Dumont, M., and Weiss, M. (1971). Harmaline-induced rhythmic activity of cerebellar and lower brain stem neurons. *Brain Res.* 32, 246–250.

Lang, E. J. (2001). Organization of olivocerebellar activity in the absence of excitatory glutamatergic input. *J. Neurosci.* 21, 1663–1675.

Lang, E. J. (2002). GABAergic and glutamatergic modulation of spontaneous and motor-cortex-evoked complex spike activity. *J. Neurophysiol.* 87, 1993–2008.

Lang, E. J., Sugihara, I., and Llinás, R. (1996). GABAergic modulation of complex spike activity by the cerebellar nucleoolivary pathway in rat. *J. Neurophysiol.* 76, 255–275.

LeDoux, M. S., Hurst, D. C., and Lorden, J. F. (1998). Single-unit activity of cerebellar nuclear cells in the awake genetically dystonic rat. *Neuroscience* 86, 533–545.

Llinás, R. (1974). Eighteenth Bowditch lecture. Motor aspects of cerebellar control. *Physiologist* 17, 19–46.

Llinás, R., Baker, R., and Sotelo, C. (1974). Electrotonic coupling between neurons in cat inferior olive. *J Neurophysiol* 37, 560–571.

Llinás, R., and Muhlethaler, M. (1988). Electrophysiology of guinea-pig cerebellar nuclear cells in the in vitro brain stem-cerebellar preparation. *J. Physiol.* 404, 241–258.

Llinás, R., and Sasaki, K. (1989). The functional organization of the olivo-cerebellar system as examined by multiple Purkinje cell recordings. *Eur. J. Neurosci.* 1, 587–602.

Llinás, R., and Volkind, R. A. (1973). The olivo-cerebellar system: functional properties as revealed by harmaline-induced tremor. *Exp. Brain Res.* 18, 69–87.

Loewenstein, Y., Mahon, S., Chadderton, P., Kitamura, K., Sompolinsky, H., Yarom, Y., and Hausser, M. (2005). Bistability of cerebellar Purkinje cells modulated by sensory stimulation. *Nat. Neurosci.* 8, 202–211.

Mann-Metzer, P., and Yarom, Y. (1999). Electrotonic coupling interacts with intrinsic properties to generate synchronized activity in cerebellar networks of inhibitory interneurons. *J. Neurosci.* 19, 3298–3306.

Mathy, A., Ho, S. S., Davie, J. T., Duguid, I. C., Clark, B. A., and Hausser, M. (2009). Encoding of oscillations by axonal bursts in inferior olive neurons. *Neuron* 62, 388–399.

Mauk, M. D., Medina, J. F., Nores, W. L., and Ohyama, T. (2000). Cerebellar function: coordination, learning or timing?' *Curr. Biol.* 10, R522–R525.

Medina, J. F., Nores, W. L., Ohyama, T., and Mauk, M. D. (2000). Mechanisms of cerebellar learning suggested by eyelid conditioning. *Curr. Opin. Neurobiol.* 10, 717–724.

Mezey, E., Palkovits, M., Hamori, J., and Szentagothai, J. (1977). Quantitative cytology and electron microscopy of the cerebellar nuclei in the cat. *Verh. Anat. Ges.* 71, 171–176.

Middleton, F. A., and Strick, P. L. (2001). Cerebellar projections to the prefrontal cortex of the primate. *J. Neurosci.* 21, 700–712.

Mittmann, W., Koch, U., and Hausser, M. (2005). Feed-forward inhibition shapes the spike output of cerebellar Purkinje cells. *J. Physiol.* 563, 369–378.

Monsivais, P., Clark, B. A., Roth, A., and Hausser, M. (2005). Determinants of action potential propagation in cerebellar Purkinje cell axons. *J. Neurosci.* 25, 464–472.

Ohyama, T., Nores, W. L., Medina, J. F., Riusech, F. A., and Mauk, M. D. (2006). Learning-induced plasticity in deep cerebellar nucleus. *J. Neurosci.* 26, 12656–12663.

Palkovits, M., Mezey, E., Hamori, J., and Szentagothai, J. (1977). Quantitative histological analysis of the cerebellar nuclei in the cat. I. Numerical data on cells and on synapses. *Exp. Brain Res.* 28, 189–209.

Paxinos, G., and Watson, C. (1998). *The rat brain in stereotaxic coordinates.* San Diego: Academic press.

Pedroarena, C. M., and Schwarz, C. (2003). Efficacy and short-term plasticity at GABAergic synapses between Purkinje and cerebellar nuclei neurons. *J. Neurophysiol.* 89, 704–715.

Pijpers, A., Voogd, J., and Ruigrok, T. J. (2005). Topography of olivo-corticonuclear modules in the intermediate cerebellum of the rat. *J. Comp. Neurol.* 492, 193–213.

Placantonakis, D. G., Bukovsky, A. A., Aicher, S. A., Kiem, H.-P., and Welsh, J. P. (2006). Continuous electrical oscillations emerge from a coupled network: a study of the inferior olive using lentiviral knockdown of connexin36. *J. Neurosci.* 26, 5008–5016.

Pugh, J. R., and Raman, I. M. (2009). Nothing can be coincidence: synaptic inhibition and plasticity in the cerebellar nuclei. *Trends Neurosci.* 32, 170–177.

Rowland, N. C., and Jaeger, D. (2005). Coding of tactile response properties in the rat deep cerebellar nuclei. *J. Neurophysiol.* 94, 1236–1251.

Rowland, N. C., and Jaeger, D. (2008). Responses to tactile stimulation in deep cerebellar nucleus neurons result from recurrent activation in multiple pathways. *J. Neurophysiol.* 99, 704–717.

Saitow, F., Murano, M., and Suzuki, H. (2009). Modulatory effects of serotonin on GABAergic synaptic transmission and membrane properties in the deep cerebellar nuclei. *J. Neurophysiol.* 101, 1361–1374.

Schultz, S. R., Kitamura, K., Post-Uiterweer, A., Krupic, J., and Hausser, M. (2009). Spatial pattern coding of sensory information by climbing fiber-evoked calcium signals in networks of neighboring cerebellar Purkinje cells. *J. Neurosci.* 29, 8005–8015.

Schwarz, C., and Schmitz, Y. (1997). Projection from the cerebellar lateral nucleus to precerebellar nuclei in the mossy fiber pathway is glutamatergic: a study combining anterograde tracing with immunogold labeling in the rat. *J. Comp. Neurol.* 381, 320–334.

Shin, S.-L., and De Schutter, E. (2006). Dynamic synchronization of Purkinje cell simple spikes. *J. Neurophysiol.* 96, 3485–3491.

Shinoda, Y., Sugihara, I., Wu, H. S., and Sugiuchi, Y. (2000). The entire trajectory of single climbing and mossy fibers in the cerebellar nuclei and cortex. *Prog. Brain Res.* 124, 173–186.

Shinoda, Y., Sugiuchi, Y., Futami, T., and Izawa, R. (1992). Axon collaterals of mossy fibers from the pontine nucleus in the cerebellar dentate nucleus. *J. Neurophysiol.* 67, 547–560.

Strick, P. L. (1983). The influence of motor preparation on the response of cerebellar neurons to limb displacements. *J. Neurosci.* 3, 2007–2020.

Sugihara, I., Lang, E. J., and Llinás, R. (1993). Uniform olivocerebellar conduction time underlies Purkinje cell complex spike synchronicity in the rat cerebellum. *J. Physiol.* 470, 243–271.

Sugihara, I., Lang, E. J., and Llinás, R. (1995). Serotonin modulation of inferior olivary oscillations and synchronicity: a multiple-electrode study in the rat cerebellum. *Eur. J. Neurosci.* 7, 521–534.

Sugihara, I., and Shinoda, Y. (2004). Molecular, topographic, and functional organization of the cerebellar cortex: a study with combined aldolase C and olivocerebellar labeling. *J. Neurosci.* 24, 8771–8785.

Sugihara, I., Wu, H., and Shinoda, Y. (1999). Morphology of single olivocerebellar axons labeled with biotinylated dextran amine in the rat. *J. Comp. Neurol.* 414, 131–148.

Sugihara, I., Wu, H. S., and Shinoda, Y. (2001). The entire trajectories of single olivocerebellar axons in the cerebellar cortex and their contribution to cerebellar compartmentalization. *J. Neurosci.* 21, 7715–7723.

Telgkamp, P., and Raman, I. M. (2002). Depression of inhibitory synaptic transmission between Purkinje cells and neurons of the cerebellar nuclei. *J. Neurosci.* 22, 8447–8457.

Teune, T. M., van der Burg, J., De Zeeuw, C. I., Voogd, J., and Ruigrok, T. J. (1998). Single Purkinje cell can innervate multiple classes of projection neurons in the cerebellar nuclei of the rat: a light microscopic and ultrastructural triple-tracer study in the rat. *J. Comp. Neurol.* 392, 164–178.

Teune, T. M., van der Burg, J., van der Moer, J., Voogd, J., and Ruigrok, T. J. (2000). Topography of cerebellar nuclear projections to the brain stem in the rat. *Prog. Brain Res.* 124, 141–172.

Thach, W. T. (1968). Discharge of Purkinje and cerebellar nuclear neurons during rapidly alternating arm movements in the monkey. *J. Neurophysiol.* 31, 785–797.

Thach, W. T. (1975). Timing of activity in cerebellar dentate nucleus and cerebral motor cortex during prompt volitional movement. *Brain Res.* 88, 233–241.

Tolbert, D. L., Massopust, L. C., Murphy, M. G., and Young, P. A. (1976). The anatomical organization of the cerebello-olivary projection in the cat. *J. Comp. Neurol.* 170, 525–544.

Uusisaari, M., Obata, K., and Knopfel, T. (2007). Morphological and electrophysiological properties of GABAergic and non-GABAergic cells in the deep cerebellar nuclei. *J. Neurophysiol.* 97, 901–911.

Van der Want, J. J., Wiklund, L., Guegan, M., Ruigrok, T., and Voogd, J. (1989). Anterograde tracing of the rat olivocerebellar system with *Phaseolus vulgaris* leucoagglutinin (PHA-L). Demonstration of climbing fiber collateral innervation of the cerebellar nuclei. *J. Comp. Neurol.* 288, 1–18.

Wassef, M., Simons, J., Tappaz, M. L., and Sotelo, C. (1986). Non-Purkinje cell GABAergic innervation of the deep cerebellar nuclei: a quantitative immunocytochemical study in C57BL and in Purkinje cell degeneration mutant mice. *Brain Res.* 399, 125–135.

Wetmore, D. Z., Mukamel, E. A., and Schnitzer, M. J. (2008). Lock-and-key mechanisms of cerebellar memory recall based on rebound currents. *J. Neurophysiol.* 100, 2328–2347.

Wu, H. S., Sugihara, I., and Shinoda, Y. (1999). Projection patterns of single mossy fibers originating from the lateral reticular nucleus in the rat cerebellar cortex and nuclei. *J. Comp. Neurol.* 411, 97–118.

Yartsev, M. M., Givon-Mayo, R., Maller, M., and Donchin, O. (2009). Pausing Purkinje cells in the cerebellum of the awake cat. *Front. Syst. Neurosci.* 3, 2. doi:10.3389/neuro.06.002.2009

Conflict of Interest Statement: The authors declare that the research was conducted in the absence of any commercial or financial relationships that could be construed as a potential conflict of interest.

Received: 23 June 2009; paper pending published: 13 July 2009; accepted: 08 November 2009; published online: 20 November 2009.

*Citation: Baumel Y, Jacobson GA and Cohen D (2009) Implications of functional anatomy on information processing in the deep cerebellar nuclei. Front. Cell. Neurosci. **3**:14. doi: 10.3389/neuro.03.014.2009*

frontiers in
CELLULAR NEUROSCIENCE

REVIEW ARTICLE
published: 09 November 2009
doi: 10.3389/neuro.03.012.2009

Regularity, variability and bi-stability in the activity of cerebellar Purkinje cells

Dan Rokni, Zohar Tal, Hananel Byk and Yosef Yarom*

Department of Neurobiology, Institute of Life Sciences, and Interdisciplinary Center for Neural Computation, Hebrew University, Jerusalem, Israel

Edited by:
Egidio D'Angelo,
University of Pavia, Italy

Reviewed by:
Alain Marty, Université Paris Descartes, France
Eric J. Lang, New York University, USA

****Correspondence:***
Yosef Yarom, Department of Neurobiology, Institute for Life Science, and Interdisciplinary Center for Neural Computation, The Hebrew University, Jerusalem, Israel.
e-mail: yarom@vms.huji.ac.il

Recent studies have demonstrated that the membrane potential of Purkinje cells is bi-stable and that this phenomenon underlies bi-modal simple spike firing. Membrane potential alternates between a depolarized state, that is associated with spontaneous simple spike firing (up state), and a quiescent hyperpolarized state (down state). A controversy has emerged regarding the relevance of bi-stability to the awake animal, yet recordings made from behaving cat Purkinje cells have demonstrated that at least 50% of the cells exhibit bi-modal firing. The robustness of the phenomenon *in vitro* or in anaesthetized systems on the one hand, and the controversy regarding its expression in behaving animals on the other hand suggest that state transitions are under neuronal control. Indeed, we have recently demonstrated that synaptic inputs can induce transitions between the states and suggested that the role of granule cell input is to control the states of Purkinje cells rather than increase or decrease firing rate gradually. We have also shown that the state of a Purkinje cell does not only affect its firing but also the waveform of climbing fiber-driven complex spikes and the associated calcium influx. These findings call for a reconsideration of the role of Purkinje cells in cerebellar function. In this manuscript we review the recent findings on Purkinje cell bi-stability and add some analyses of its effect on the regularity and variability of Purkinje cell activity.

Keywords: simple spike, climbing fiber, mossy fiber, complex spike, Ca imaging, firing state

INTRODUCTION

Like most neurons, Purkinje cells (PCs) are classically described as stable electrical elements where the resting potential is continuously interrupted by synaptic potentials. Once the synaptic potentials reach a certain threshold, an action potential is generated. This somewhat simplistic description implies that the firing rate of a cell mirrors its synaptic input. This view of PCs has recently been challenged by the finding that they operate as bi-stable elements. PCs seem to have two stable levels of membrane potential: a hyperpolarized state that is devoid of simple spike firing (down state), and a depolarized state in which the cell spontaneously fires at high frequencies even in the absence of any synaptic input (up state) (Williams et al., 2002; Loewenstein et al., 2005; Fernandez et al., 2007). Hence, PC firing rate does not reflect a simple summation of its inputs. This alternative view of PCs is not commonly accepted. De Zeeuw and colleagues reported that although bimodal distributions of firing rate are frequently encountered in anesthetized animals, PCs switch to a continuous firing mode once the anesthesia is removed (Schonewille et al., 2006). Conversely, recordings from awake, restrained cats demonstrated that ~50% of the cells exhibit bi-modal firing dynamics (Yartsev et al., 2009), and preliminary results also documented bi-modal firing of Purkinje cells in freely moving rats (Lev et al., 2006). One way to reconcile these contradictory reports is to assume that the balance between continuous and bi-modal firing is modulated by the behavioral state of the animal such as exploration, stress or alertness. In the following we describe the phenomenon of bi-stability and its effect on the responses of PCs to synaptic inputs.

PURKINJE CELL BI-STABILITY

PC bi-stability is readily observed in intra- and extra-cellular recordings in both *in vitro* and *in vivo* preparations. In slice preparations it is occasionally periodic, where the state durations are on a time scale of seconds (**Figure 1A**). An epoch of up state (**Figure 1A** lower trace) starts with a slow membrane depolarization that upon reaching threshold elicits a prolonged firing period characterized by initial fast rate that slowly settles to a steady state firing frequency with different degrees of regularity (see below). The firing epoch terminates abruptly where the membrane potential is rapidly hyperpolarized below the original level. The membrane potential (after omitting action potentials) attains two distinct levels. In the example shown in **Figure 1A** an average value of −57 mV was observed during the down state, whereas the depolarized up state was ~−47 mV (**Figure 1B**). Similar behavior can be observed when the activity of a single PC is extracellularly monitored (**Figure 1C**). The alternation between firing and quiescent epochs on time scales of seconds is a robust feature of the activity. As with the intracellular recording, a firing epoch starts abruptly with a high firing rate that quickly settled to a somewhat lower frequency of various regularities. In contrast to the intracellular recording, here the bi-stability is quantified by calculating the instantaneous firing frequency. The distribution of the frequencies (**Figure 1D**) shows that almost half of the time the cell is quiescent, whereas when it is active, it tends to fire at 20–30 Hz. Several lines of evidence support the intrinsic origin of PC bi-stability. First, brief intracellular current injections are sufficient to induce state transitions (see **Figure 3**). Second, a dc current

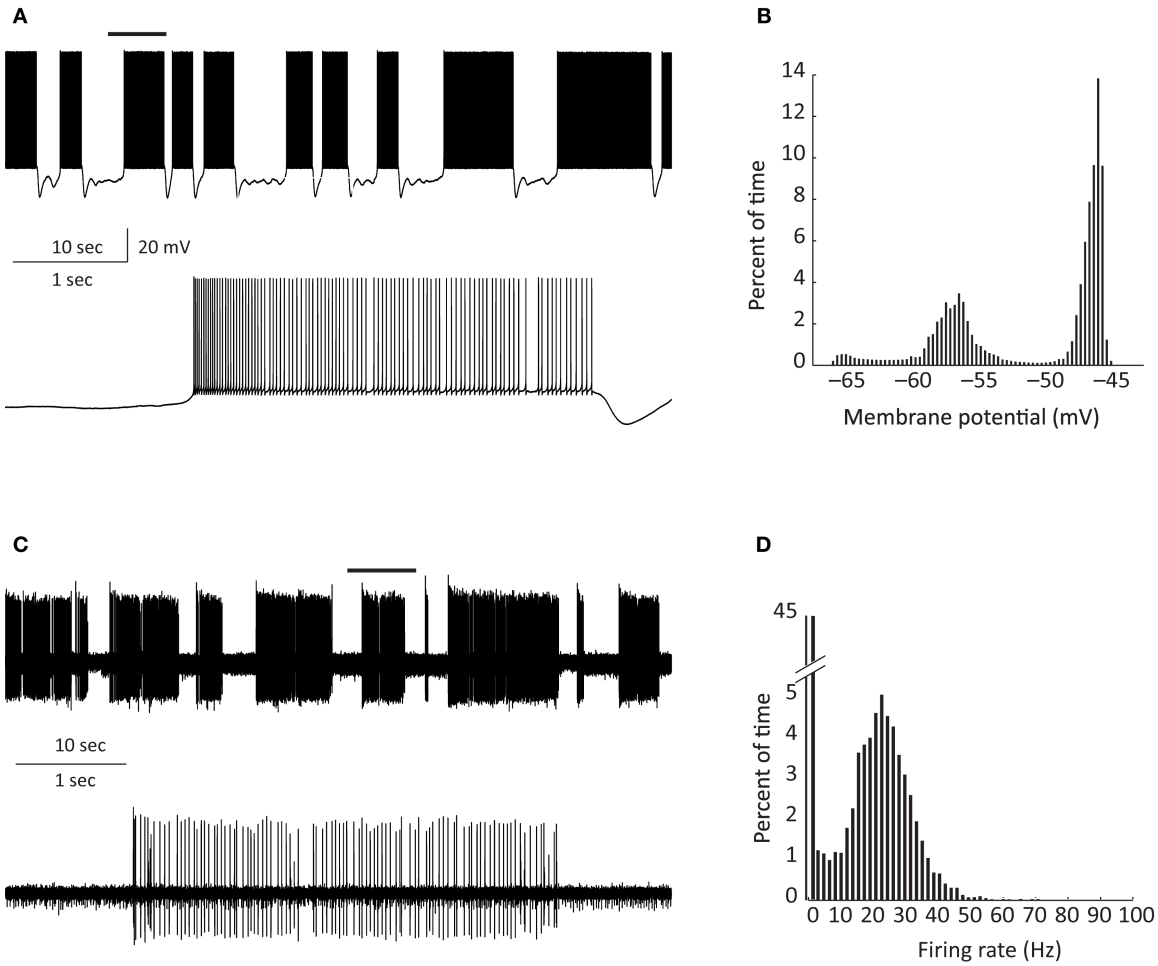

FIGURE 1 | PC bi stability recorded intracellularly in a cerebellar slice (A) and extracellularly in a ketamine anesthetized rat (C) (see Tal et al., 2008 for methods). An epoch of up state (marked by horizontal bars in the upper traces) is displayed on an extended time scale in the lower traces in **(A)** and **(C)**. **(B,D)** Show the percentage of time spent in each membrane potential **(B)** and instantaneous frequency **(D)**.

injection that hyperpolarizes the membrane potential maintains the cell in the down state and does not reveal any bi-modal inputs (Loewenstein et al., 2005), and third, the spontaneous firing rate of PCs is not altered by synaptic blockers (Cerminara and Rawson, 2004). Yet, synaptic inputs may still affect the timing of spikes. As intrinsic firing is expected to be regular, we estimated the firing regularity during up states using CV_2 analysis (Holt et al., 1996). As shown in **Figure 2**, simple spike firing is rather regular both *in vitro* (**Figure 2A**) and *in vivo* (**Figure 2C**). The mean CV_2 value *in vitro* was 0.25 ± 0.03, indistinguishable from the CV_2 values obtained *in vivo* (0.26 ± 0.03, $p > 0.5$; **Figure 2D**). The regularity of firing was also examined by plotting the relationship between consecutive ISIs (**Figure 2A1**). Most of the ISIs were in the range of 20–40 ms however occasional prolonged ISIs were observed. These prolonged ISIs were accompanied by hyperpolarizations, suggesting the involvement of spontaneous IPSPs (see inset in **Figure 2A**). To test this possibility we measured the effect of gabazine (0.5 μM) on firing regularity. Although the maximal firing frequency was not affected by gabazine, a significant increase in firing regularity was observed (Hausser and Clark, 1997). In the example shown in **Figure 2** the prolonged ISIs and the accompanied hyperpolarizations (**Figure 2A**) were absent in the presence of GABAzine (**Figure 2B**), and accordingly the CV_2 value was reduced from 0.45 to 0.19. These observations lead to the conclusion that the firing during the up state *in vitro* is intrinsically generated and can be modulated by inhibitory synaptic potentials.

STATE TRANSITIONS

The intrinsic bi-modality of simple spikes implies that PC inputs to the cerebellar nuclei (CN) are binary signals and therefore can report the PC state but not individual synaptic events. Nonetheless, for these signals to be meaningful, the transitions between the states should be governed by synaptic inputs. Indeed, a variety of input signals are extremely efficient in inducing state transitions (**Figure 3**). Interestingly, most of these signals can induce both upward and downward shifts. For example, a brief hyper- or depolarizing current injection during a down state will shift the membrane potential to an up state whereas the same current during an up state will shift the cell to a down state (**Figures 3A,B**). Similarly, climbing fiber (CF) inputs can induce bi-directional state

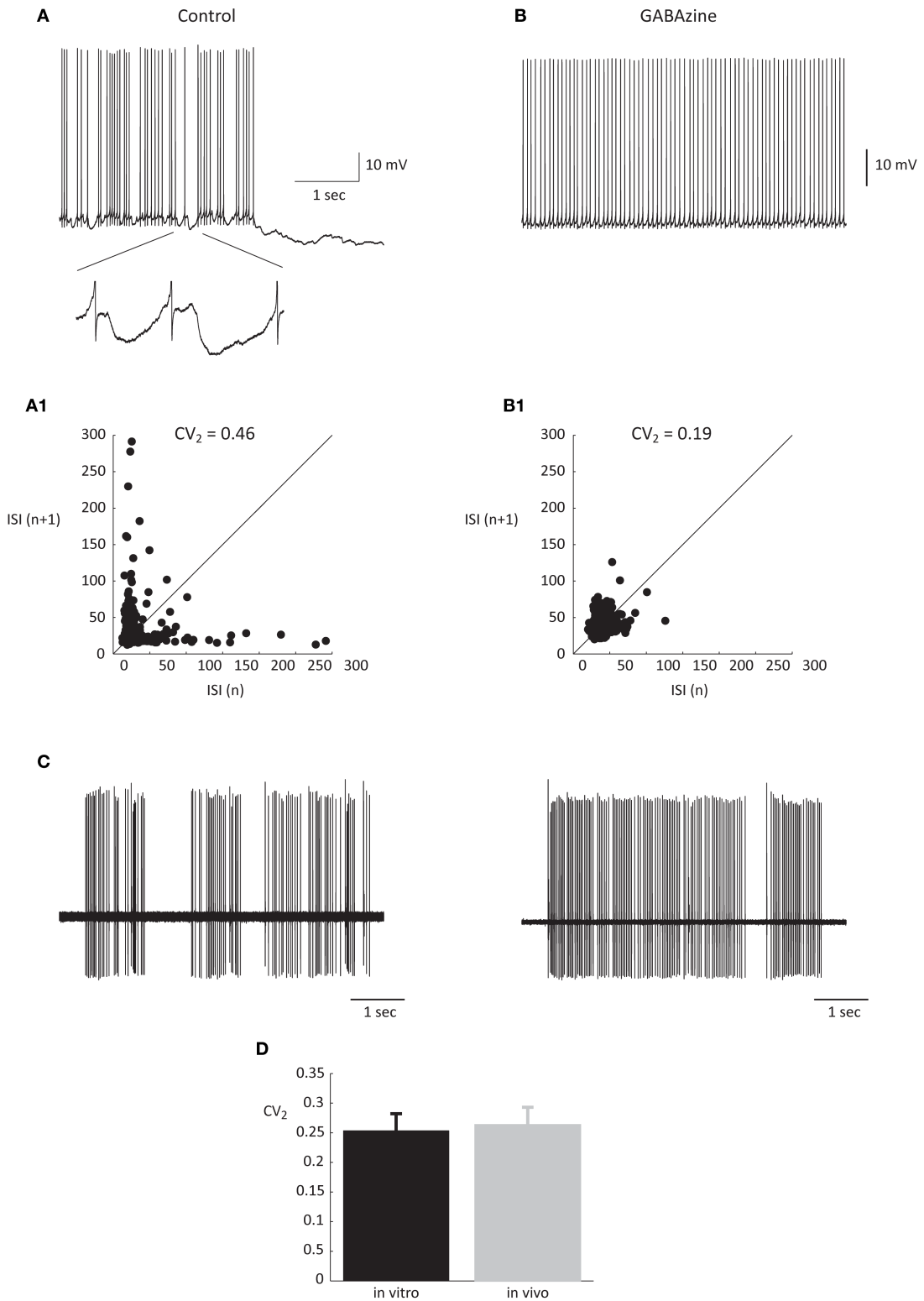

FIGURE 2 | The regularity of PC firing during upstate. (A,B) Traces showing the up state firing of a PC in a slice preparation (see Tal et al., 2008 for methods) before **(A)** and after **(B)** application of GABAzine (0.5 μM). Inset in **(A)** shows examples of the IPSPs in the original trace in an expanded scale. **(A1,B1)** the relations between consecutive ISIs before **(A1)** and after **(B1)** GABAzine application constructed from 2 min of recordings of the same cells as in **(A)** and **(B)**. **(C)** Two extreme examples of the most non-regular (left) and the most regular (right) units that were recorded in an anesthetized rat *in vivo*. **(D)** The average CV_2 values obtained *in vitro* and *in vivo* n = 12 and 6, respectively.

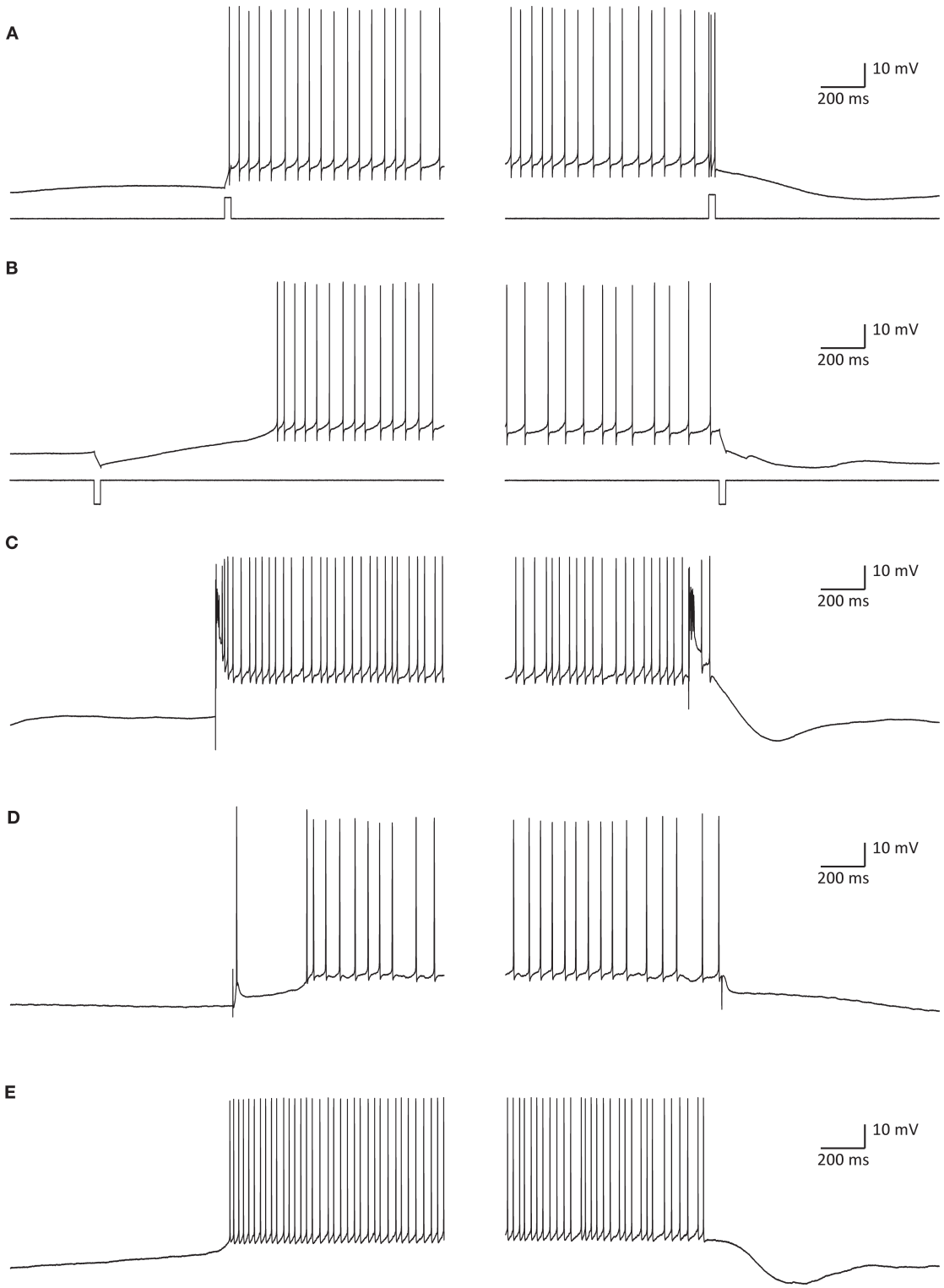

FIGURE 3 | State transitions can be induced by current injections (A,B) synaptic inputs (C,D) or can occur spontaneously (E). (A) A 35-ms depolarizing current pulse of 100 pA induced a transition to an up state (left) and to a down state (right). **(B)** The same as in **(A)** for a hyperpolarizing current pulse. **(C)** Transitions induced by CSs that were evoked by stimulating the white matter just below the recorded PC. **(D)** State transitions induced by stimulating the granule cells (left) and the molecular layer interneurons (MLIs; right). For granule cells activation the stimulating electrode was placed at the granular layer just below the recorded PC and for activation of the MLIs the electrode was placed either in the molecular layer or in the granular layer laterally to the recorded PC. **(E)** Spontaneous transitions. All traces were obtained with whole cell recordings in slice preparations (see Tal et al., 2008 for methods).

transitions (**Figure 3C**). In fact transitions are so easily induced that they occasional occur spontaneously (**Figure 3E**). In a recent study we showed that the mossy fiber – granule cell input can also induce bi-directional transitions (Jacobson et al., 2008). Transitions from a down to an up state occurred when an excitatory granule cell input was activated, while transitions from an up to a down state occurred when the molecular layer interneurons were activated (**Figure 3D**). We found that the probability of transitions induced by granule cell inputs is tightly linked to EPSP amplitude. At high stimulation intensity that generated an EPSP of ~15 mV and usually elicited an action potential, transitions from down state to up state occurred at 74% and transitions from up state to down state at 62%. At low stimulation intensity that generated an EPSP of ~8 mV and only occasionally an action potential, transitions from down state to up state occurred at 19% and transitions from up state to down state at 3%. It is important to note that transitions were not limited to stimulations that directly triggered an action potential.

There is ample evidence to support the idea that a significant excitatory input to PCs is organized along the ascending branch of the granule cell axons whereas the inhibitory input, presumably activated by the same mossy fibers, are likely to be most effective at the perimeter of the excitatory input (Cohen and Yarom, 1998; Isope and Barbour, 2002; Sims and Hartell, 2005, 2006; Rokni et al., 2007; Lu et al., 2009; Walter et al., 2009). Thus, a mossy fiber input can, theoretically, generate a spatially organized patch of PCs in their up state. It follows that the role of the mossy fibers input onto PCs is to induce state transitions rather than control their firing rate or spike timing.

STATE DEPENDENCE OF COMPLEX SPIKE WAVEFORM

As described above the climbing fiber (CF) input into PCs can induce state transitions. This is not surprising since this unique input is one of the most powerful synapses in the nervous system. Activation of the CF input results in an all-or-none response known as a complex spike (CS) (Eccles et al., 1966). In contrast to the brief simple spike, the complex spike consists of a large initial spike followed by a train of secondary spikes or wavelets. This complex response, which occasionally appears in the form of a voltage ripple, is triggered by an enormous synaptic potential generated by the activation of hundreds of synaptic releasing sites (Rossi et al., 1993). The exceptionally high quantal content of this synapse ensures very small variations in the amplitude of the synaptic current triggered by a single pre-synaptic action potential. Nevertheless, as shown in **Figure 4A** the response is state dependent, being longer at the

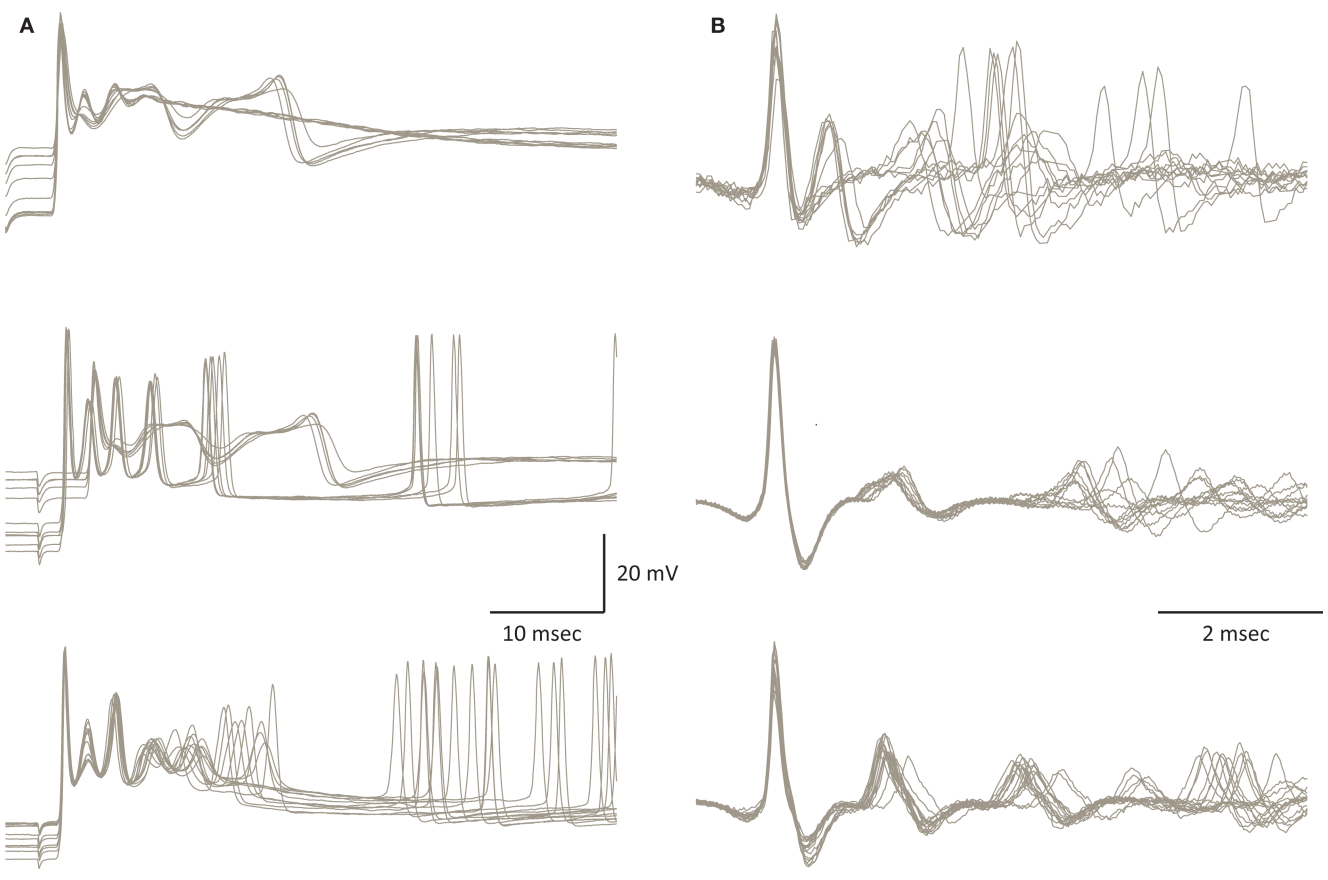

FIGURE 4 | Variability of the CS waveform. (A) Examples of CSs recorded from 3 PCs in slice preparation. The superimposed traces represent CSs that were elicited by stimulating the white matter below the recorded PC. Note the variable waveform and the changes in the resting potential just before the onset of the CSs. **(B)** Examples of spontaneously occurring CSs recorded from 3 PC in anesthetized rats. Note the limited variability of the initial part of the waveform as opposed to the extensive variations in the late wavelets (figure modified from Tal et al., 2008).

depolarized state. The trial by trial changes in the CS waveform, despite the invariability of the underlying synaptic potential, suggests that it is governed by the cell's current excitability state. Similar variation in the CS waveform has been observed in *in-vivo* extracellular recordings (**Figure 4B**). These variations, which have been previously reported (Gilbert and Thach, 1977; Llinas and Sugimori, 1980; Callaway et al., 1995; Hansel and Linden, 2000; Servais et al., 2004; Khaliq and Raman, 2005; Loewenstein et al., 2005; Sacconi et al., 2008; Zagha et al., 2008) may reflect the effect of the PC state on the response. However, under *in vivo* conditions other parameters contribute to these variations. For example it has been recently demonstrated that the prolonged olivary action potential generates a short burst of action potentials that propagates all the way to the cerebellar cortex. The number of action potentials will undoubtedly change the CS waveform although this effect will be diminished due to synaptic depression (Eccles et al., 1966; Dittman and Regehr, 1998). Nevertheless the state of the PC is bound to exert its modulatory effect on the response whether it is evoked by a single spike or a burst of spikes. Furthermore, it is likely that long term changes in the synaptic potential such as different levels of potentiation or depression of the CF–PC synapses contribute to alterations of the CS waveform on a longer time scale (Hashimoto and Kano, 1998; Hansel and Linden, 2000; Weber et al., 2003).

The variability in CS waveform is demonstrated in **Figure 4** for intracellular recordings in slice preparation (**Figure 4A**) and extracellular recordings in anesthetized rats (**Figure 4B**). Significant variation in the waveform duration was observed in both modes of recordings. The variability in duration is due to variability in both the number of wavelets and their duration. In a recent study (Tal et al., 2008), we explored whether bi-stability could account for the variability in CS waveform. We found that indeed there is a significant difference between the CSs generated during the up state and those generated during the down state. The difference between these groups lies in the amplitude of the initial overshooting action potential and the amplitude and dynamics of the subsequent train of wavelets (Tal et al., 2008). Following this study we concluded that indeed the CS waveform is state dependent but the characteristics of this dependence are cell specific.

STATE DEPENDENT CA^{++} SIGNALING

The rather long durations of the up state, suggest that the dynamics of calcium current and intracellular calcium concentration ($[Ca^{++}]$), may be involved in the mechanism underlying the formation of the state as well as the state transitions. $[Ca^{++}]$ is a multifunctional parameter that participates in a variety of processes including synaptic release (Simon and Llinas, 1985; Mulkey and Zucker, 1993), direct activation of K currents (Meech and Standen, 1974; Yarom et al., 1985), and long term modulation of synaptic efficacy (Christie et al., 1996; Ito, 2001; Sjostrom and Nelson, 2002). Therefore we have recently examined the dynamics of $[Ca^{++}]$ in the two states and the effect of these states on synaptically evoked Ca^{++} influx (Rokni and Yarom, 2009). Using Ca^{++} imaging to record the changes in $[Ca^{++}]$, we found that epochs of up states are associated with a somatic increase in $[Ca^{++}]$, resembling the increase in $[Ca^{++}]$ induced by intracellularly evoked bursts of Na^{+}-spikes (Lev-Ram et al., 1992). We further demonstrated that the Ca^{++} signal associated with CSs is state dependent. At the somatic level the Ca^{++} signals during the up state were smaller than those occurring during the down state. In contrast, the Ca^{++} signals at the dendritic level were larger in the up state than in the down state.

Here, we examined the trial by trial variability of the Ca^{++} waveform. Generally speaking, Ca^{++} signals covaried in different areas of the dendritic tree. However there were some exceptions. One of these is shown in **Figure 5**. This PC had two dendrites emerging from the cell body (**Figure 5A**). Fluorescence was averaged in each dendritic region of interest (ROI) (**Figure 5A**) to generate the transients shown in **Figures 5B,C**. Comparing the amplitudes of these transients in the two dendrites (**Figure 5D**) revealed that: (a) There are significant trial by trial changes in the amount of Ca^{++} influx, and (b) The variations occurred independently in the two branches of the dendritic tree; and (c) Although most of the variability in the right dendrite could be attributed to noise, variability in the left dendrite clearly exceeded the noise level. This spatial specificity is most likely determined by interneuron activity (Callaway et al., 1995). We concluded that the variability in the Ca^{++} signal can only partially account for the variability of the CS waveform and that the mechanisms underlying the variations in CS waveforms differ from the mechanisms that induce variation in the dendritic Ca^{++} signals (see Callaway et al., 1995; Davie et al., 2008).

CONCLUSIONS

THE CONTROVERSY OVER PURKINJE CELL BI-STABILITY

Although it has become widely accepted that PCs fire intrinsically and do not reflect granule cell inputs in a simple manner, the exact nature of PC firing is a matter of controversy. This controversy cannot be attributed only to differences in preparations, conditions or anesthesia, as even in slices the descriptions of PC firing range from tonic firing (Williams et al., 2002; Schonewille et al., 2006), through bi-stable (Loewenstein et al., 2005; Tal et al., 2008), to tri-stablel (Womack and Khodakhah, 2002). These differences are partially due to terminology or the investigators point of view. For example, bi-modal firing of PCs has been described already by Bell and Grimm (1969) in the late 1960s, and later again by Llinas and Sugimori (1980) and yet these authors have not used the term bi-stability. In addition to these technicalities that may generate an apparent controversy, real differences in physiological observations have been reported. These differences can be attributed to a different state of the system. For example different levels of neuromodulators may either induce a bi-stable state or alternatively abolish it. Indeed Williams et al. (2002) show that serotonin transforms tonic firing PCs *in vitro* to bi-stable cells. In our hands PCs can be transformed from bi-stable to tonic firing and back by application of small dc currents. Further investigations are needed in order to unravel how the modulation of intrinsic firing of PCs serves behavior.

FUNCTIONAL IMPLICATIONS OF PC BI-STABILITY

The involvement of the cerebellum in temporal coordination of motor tasks as well as in a variety of behavioral paradigms is well documented (Ivry et al., 1988; Timmann et al., 1999, 2001; Zackowski et al., 2002; Ackermann, 2008; O'Reilly et al., 2008). These paradigms typically require representation of temporal information in timescales of tens to hundreds of milliseconds. The capacity of PCs to attain prolonged firing states endows the system

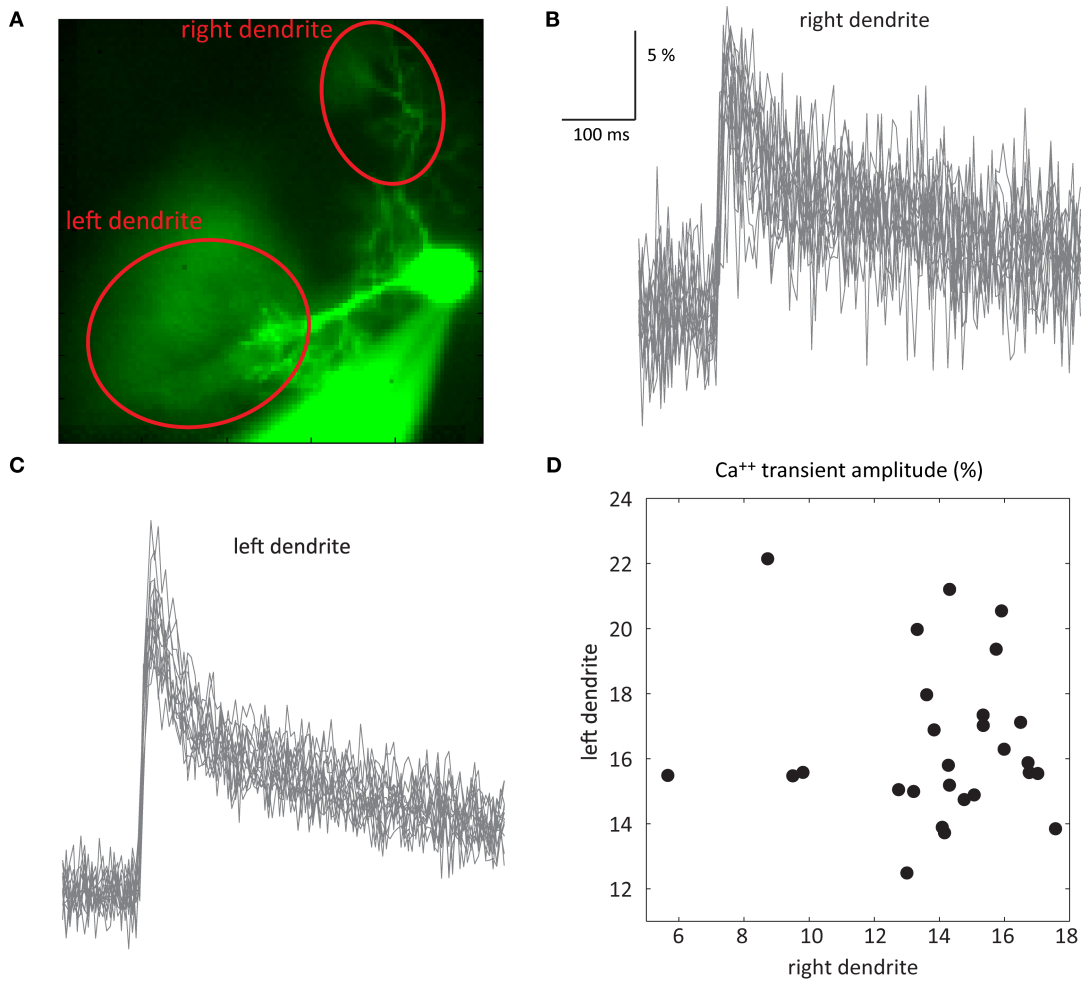

FIGURE 5 | Independence of Ca^{++} transients in two dendrites. (A) An image of a PC with two dendrites emerging directly from the soma. **(B,C)** 27 superimposed Ca^{++} transients recorded at 2.5 ms/frame at the right **(B)** and left **(C)** dendrites (ROIs marked by the red ovals in **(A)**; see Rokni and Yarom, 2009 for methods). **(D)** A scatter plot of the relationship between the amplitudes of the Ca^{++} transients at the right and left dendrites.

with intrinsically generated prolonged timescales without the need for a continuous synaptic input. We showed that the firing during these states has a certain degree of irregularity. This irregularity has recently been suggested to encode meaningful information (Steuber et al., 2007; De Schutter and Steuber, 2009). However, the ability of the PC-CN synapse to reliably transmit this information is an open question. A partial answer to this question can be found in numerous reports on the properties of the PC-CN synapse (Aizenman et al., 2000; Kreiner and Jaeger, 2004; Telgkamp et al., 2004). This synapse is characterized by the rapid depression of its efficacy upon high frequency stimulation. Thus it is expected that during PC up states the amplitude of the PC-CN synaptic potential will decrease to about 50% of its original value (Telgkamp and Raman, 2002; Pedroarena and Schwarz, 2003). Furthermore, because of the massive convergence of hundreds of PC axons onto each CN neuron, the ability of this synapse to transmit the information encoded in the inter spike intervals (ISIs) of PC simple spikes firing, is severely limited. Since there is no indication for tight correlation in simple spike timing in neighboring PCs, we conclude that if the irregularity encodes information it cannot be read by CN neurons. The massive convergence of PC axons in the CN also raises doubts about the ability of CN neurons to resolve changes in PC firing within the up states. This issue has been discussed by Jacobson et al. (2008).

We have recently suggested a conceptual framework in which the olivo-cerebellar system serves as a generator of temporal patterns. These patterns, which are needed to perform specific behavioral tasks, are the product of the oscillatory activity in the inferior olive and the bi-stability of PC firing (Jacobson et al., 2008). Accordingly, the onset and duration of the oscillatory activity in the inferior olive is administrated by the firing states of the PCs. The spatial arrangement of the firing states, which is organized by mossy fiber inputs, governs olivary activity via the GABAergic projection neurons of the CN. According to this framework the information delivered by PCs is the onset and duration of the firing states rather than the irregularities of the inter-spike intervals.

STATE TRANSITIONS

The induction of state transitions by a variety of input signals indicates that indeed PC states are under strict neuronal control and therefore likely to contain valuable information. The most

interesting mode of control is that of the mossy fibers. Here the direct excitatory input, via the granule cells, can shift the PCs to their up state, while the indirect inhibitory input via the MLI can shift the cells to their down state or alternatively prevent the shift to an up state. The spatial organization of these two inputs to the cerebellar cortex as well as their temporal relationships will undoubtedly generate a specific spatial organization of the PC states. This spatial organization will be determined by the efficacy of the parallel fiber input. The well documented long term plasticity of the parallel fibers input into PCs offers an additional possibility to this scheme. It implies that the specific spatial organization is a dynamic feature that is molded by experience. Plasticity at the mossy fiber granular cell synapse (Mapelli and D'Angelo, 2007) can contribute to the dynamic control of the spatial organization of PC states. These possibilities are in line with the commonly accepted notion that the cerebellum is the site of learning and storage of motor skills. The spatial and temporal distributions of the firing states of PCs that are formed by the CF input, have completely different properties. The isochronic organization along the parasagittal plane is a rather rigid organization. The effectiveness of this input in upswing shifts renders this input a somewhat different role. A tempting possibility is that the shifts induced by the CF input serve in emergency situations where rigid, fast and instinctive measures are to be implemented.

It is interesting to note that all types of synaptic inputs can operate as toggle switches, inducing bi-directional transitions. It follows that the response of a PC to synaptic input (the direction of state transition) depends on the current state. For example the response of a quiescent PC to a CF input would be a transition to the up state and prolonged firing. Conversely, in the up state the same PC may respond to the CF input by seizing fire. Hence to reach a particular spatial organization of firing states the input has to be designed according to the current situation. In other words the 'designer' of the input should know the current state of the cells. Such knowledge is most unlikely. An alternative possibility is that the efficiency of an input to shift the state of the neuron depends on its state. The slow processes that are responsible for the spontaneous transitions suggest that the threshold for transitions decreases with time and thus the state itself may determine the threshold. This is supported by the observation that the ability to shift state, depends on the time of the input relative to the onset of the state. Thus, a depolarizing input from down state that shifts to an up state is more efficient the longer the cell has been in the down state. The ease in which each input shifts PCs between states needs a thorough examination and characterization.

THE STABILITY OF THE INPUT SIGNAL

As stated above, in order to reach a particular spatial organization of firing states, the response to a specific input has to be state dependent. In previous work we demonstrated that the response to a CF input is state dependent. During a depolarizing state complex spikes tend to be prolonged (Tal et al., 2008) and are associated with differential changes in the calcium influx (Rokni and Yarom, 2009). A dendritic increase in calcium influx was observed during the up state whereas a decrease was observed at the soma. Here we further investigated the calcium influx associated with the response to CF inputs. First we demonstrated that there is a trial by trial variability in the amount of calcium influx that seems to be independent of the variability in the voltage responses. Second, we presented a specific example of the independent variability of calcium influx that occurred in two dendrites of the same PC. Together these observations suggest that the calcium influx in response to CF inputs is modulated by both, the inhibitory network of the molecular layer interneurons and the PC's membrane potential. These two modes of modulation of the calcium influx, can furnish the system with the ability to organize the spatial distribution of the firing state independently of the current states.

REFERENCES

Ackermann, H. (2008). Cerebellar contributions to speech production and speech perception: psycholinguistic and neurobiological perspectives. *Trends Neurosci.* 31, 265–272.

Aizenman, C. D., Huang, E. J., Manis, P. B., and Linden, D. J. (2000). Use-dependent changes in synaptic strength at the Purkinje cell to deep nuclear synapse. *Prog. Brain Res.* 124, 257–273.

Bell, C. C., and Grimm, R. J. (1969). Discharge properties of Purkinje cells recorded on single and double microelectrodes. *J. Neurophysiol.* 32, 1044–1055.

Callaway, J. C., Lasser-Ross, N., and Ross, W. N. (1995). IPSPs strongly inhibit climbing fiber-activated [Ca2+]i increases in the dendrites of cerebellar Purkinje neurons. *J. Neurosci.* 15, 2777–2787.

Cerminara, N. L., and Rawson, J. A. (2004). Evidence that climbing fibers control an intrinsic spike generator in cerebellar Purkinje cells. *J. Neurosci.* 24, 4510–4517.

Christie, B. R., Magee, J. C., and Johnston, D. (1996). Dendritic calcium channels and hippocampal long-term depression. *Hippocampus* 6, 17–23.

Cohen, D., and Yarom, Y. (1998). Patches of synchronized activity in the cerebellar cortex evoked by mossy-fiber stimulation: questioning the role of parallel fibers. *Proc. Natl. Acad. Sci. U.S.A.* 95, 15032–15036.

Davie, J. T., Clark, B. A., and Hausser, M. (2008). The origin of the complex spike in cerebellar Purkinje cells. *J. Neurosci.* 28, 7599–7609.

De Schutter, E., and Steuber, V. (2009). Patterns and pauses in Purkinje cell simple spike trains: experiments, modeling and theory. *Neuroscience* 162, 816–826.

Dittman, J. S., and Regehr, W. G. (1998). Calcium dependence and recovery kinetics of presynaptic depression at the climbing fiber to Purkinje cell synapse. *J. Neurosci.* 18, 6147–6162.

Eccles, J. C., Llinas, R., and Sasaki, K. (1966). The excitatory synaptic action of climbing fibres on the purinje cells of the cerebellum. *J. Physiol. (Lond.)* 182, 268–296.

Fernandez, F. R., Engbers, J. D., and Turner, R. W. (2007). Firing dynamics of cerebellar purkinje cells. *J. Neurophysiol.* 98, 278–294.

Gilbert, P. F., and Thach, W. T. (1977). Purkinje cell activity during motor learning. *Brain Res.* 128, 309–328.

Hansel, C., and Linden, D. J. (2000). Long-term depression of the cerebellar climbing fiber – Purkinje neuron synapse. *Neuron* 26, 473–482.

Hashimoto, K., and Kano, M. (1998). Presynaptic origin of paired-pulse depression at climbing fibre-Purkinje cell synapses in the rat cerebellum. *J. Physiol. (Lond.)* 506(Pt 2), 391–405.

Hausser, M., and Clark, B. A. (1997). Tonic synaptic inhibition modulates neuronal output pattern and spatiotemporal synaptic integration. *Neuron* 19, 665–678.

Holt, G. R., Softky, W. R., Koch, C., and Douglas, R. J. (1996). Comparison of discharge variability in vitro and in vivo in cat visual cortex neurons. *J. Neurophysiol.* 75, 1806–1814.

Isope, P., and Barbour, B. (2002). Properties of unitary granule cell – >Purkinje cell synapses in adult rat cerebellar slices. *J. Neurosci.* 22, 9668–9678.

Ito, M. (2001). Cerebellar long-term depression: characterization, signal transduction, and functional roles. *Physiol. Rev.* 81, 1143–1195.

Ivry, R. B., Keele, S. W., and Diener, H. C. (1988). Dissociation of the lateral and medial cerebellum in movement timing and movement execution. *Exp. Brain Res.* 73, 167–180.

Jacobson, G. A., Rokni, D., and Yarom, Y. (2008). A model of the olivo-cerebellar system as a temporal pattern generator. *Trends Neurosci.* 31, 617–625.

Khaliq, Z. M., and Raman, I. M. (2005). Axonal propagation of simple and complex spikes in cerebellar Purkinje neurons. *J. Neurosci.* 25, 454–463.

Kreiner, L., and Jaeger, D. (2004). Synaptic shunting by a baseline of synaptic conductances modulates responses to inhibitory input volleys in cerebellar Purkinje cells. *Cerebellum* 3, 112–125.

Lev, I., Jacobson, G. A., Yarom, Y., and Cohen, D. (2006). Bistable behavior of cerebellar neurons revealed by chronic recordings of neural activity in freely moving rats. *Society for Neuroscience Abstract*.

Lev-Ram, V., Miyakawa, H., Lasser-Ross, N., and Ross, W. N. (1992). Calcium transients in cerebellar Purkinje neurons evoked by intracellular stimulation. *J. Neurophysiol.* 68, 1167–1177.

Llinas, R., and Sugimori, M. (1980). Electrophysiological properties of in vitro Purkinje cell somata in mammalian cerebellar slices. *J. Physiol. (Lond.)* 305, 171–195.

Loewenstein, Y., Mahon, S., Chadderton, P., Kitamura, K., Sompolinsky, H., Yarom, Y., and Hausser, M. (2005). Bistability of cerebellar Purkinje cells modulated by sensory stimulation. *Nat. Neurosci.* 8, 202–211.

Lu, H., Esquivel, A. V., and Bower, J. M. (2009). 3D electron microscopic reconstruction of segments of rat cerebellar Purkinje cell dendrites receiving ascending and parallel fiber granule cell synaptic inputs. *J. Comp. Neurol.* 514, 583–594.

Mapelli, J., and D'Angelo, E. (2007). The spatial organization of long-term synaptic plasticity at the input stage of cerebellum. *J. Neurosci.* 27, 1285–1296.

Meech, R. W., and Standen, N. B. (1974). Calcium-mediated potassium activation in Helix neurones. *J. Physiol. (Lond.)* 237, 43P–44P.

Mulkey, R. M., and Zucker, R. S. (1993). Calcium released by photolysis of DM-nitrophen triggers transmitter release at the crayfish neuromuscular junction. *J. Physiol. (Lond.)* 462, 243–260.

O'Reilly, J. X., Mesulam, M. M., and Nobre, A. C. (2008). The cerebellum predicts the timing of perceptual events. *J. Neurosci.* 28, 2252–2260.

Pedroarena, C. M., and Schwarz, C. (2003). Efficacy and short-term plasticity at GABAergic synapses between Purkinje and cerebellar nuclei neurons. *J. Neurophysiol.* 89, 704–715.

Rokni, D., Llinas, R., and Yarom, Y. (2007). Stars and stripes in the cerebellar cortex: a voltage sensitive dye study. *Front. Syst. Neurosci.* 1, 1. doi: 10.3389/neuro.06.001.2007.

Rokni, D., and Yarom, Y. (2009). State-dependence of climbing fiber-driven calcium transients in purkinje cells. *Neuroscience* 162, 694–701.

Rossi, F., Borsello, T., Vaudano, E., and Strata, P. (1993). Regressive modifications of climbing fibres following Purkinje cell degeneration in the cerebellar cortex of the adult rat. *Neuroscience* 53, 759–778.

Sacconi, L., Mapelli, J., Gandolfi, D., Lotti, J., O'Connor, R. P., D'Angelo, E., and Pavone, F. S. (2008). Optical recording of electrical activity in intact neuronal networks with random access second-harmonic generation microscopy. *Opt. Express* 16, 14910–14921.

Schonewille, M., Khosrovani, S., Winkelman, B. H., Hoebeek, F. E., De Jeu, M. T., Larsen, I. M., Van der Burg, J., Schmolesky, M. T., Frens, M. A., and De Zeeuw, C. I. (2006). Purkinje cells in awake behaving animals operate at the upstate membrane potential. *Nat. Neurosci.* 9:459–461; author reply 461.

Servais, L., Bearzatto, B., Hourez, R., Dan, B., Schiffmann, S. N., and Cheron, G. (2004). Effect of simple spike firing mode on complex spike firing rate and waveform in cerebellar Purkinje cells in non-anesthetized mice. *Neurosci. Lett.* 367, 171–176.

Simon, S. M., and Llinas, R. R. (1985). Compartmentalization of the submembrane calcium activity during calcium influx and its significance in transmitter release. *Biophys. J.* 48, 485–498.

Sims, R. E., and Hartell, N. A. (2005). Differences in transmission properties and susceptibility to long-term depression reveal functional specialization of ascending axon and parallel fiber synapses to Purkinje cells. *J. Neurosci.* 25, 3246–3257.

Sims, R. E., and Hartell, N. A. (2006). Differential susceptibility to synaptic plasticity reveals a functional specialization of ascending axon and parallel fiber synapses to cerebellar Purkinje cells. *J. Neurosci.* 26, 5153–5159.

Sjostrom, P. J., and Nelson, S. B. (2002). Spike timing, calcium signals and synaptic plasticity. *Curr. Opin. Neurobiol.* 12, 305–314.

Steuber, V., Mittmann, W., Hoebeek, F. E., Silver, R. A., De Zeeuw, C. I., Hausser, M., and De Schutter, E. (2007). Cerebellar LTD and pattern recognition by Purkinje cells. *Neuron* 54, 121–136.

Tal, Z., Chorev, E., and Yarom, Y. (2008). State-dependent modification of complex spike waveforms in the cerebellar cortex. *Cerebellum* 7, 577–582.

Telgkamp, P., Padgett, D. E., Ledoux, V. A., Woolley, C. S., and Raman, I. M. (2004). Maintenance of high-frequency transmission at purkinje to cerebellar nuclear synapses by spillover from boutons with multiple release sites. *Neuron* 41, 113–126.

Telgkamp, P., and Raman, I. M. (2002). Depression of inhibitory synaptic transmission between Purkinje cells and neurons of the cerebellar nuclei. *J. Neurosci.* 22, 8447–8457.

Timmann, D., Citron, R., Watts, S., and Hore, J. (2001). Increased variability in finger position occurs throughout overarm throws made by cerebellar and unskilled subjects. *J. Neurophysiol.* 86, 2690–2702.

Timmann, D., Watts, S., and Hore, J. (1999). Failure of cerebellar patients to time finger opening precisely causes ball high-low inaccuracy in overarm throws. *J. Neurophysiol.* 82, 103–114.

Walter, J. T., Dizon, M. J., and Khodakhah, K. (2009). The functional equivalence of ascending and parallel fiber inputs in cerebellar computation. *J. Neurosci.* 29, 8462–8473.

Weber, J. T., De Zeeuw, C. I., Linden, D. J., and Hansel, C. (2003). Long-term depression of climbing fiber-evoked calcium transients in Purkinje cell dendrites. *Proc. Natl. Acad. Sci. U.S.A.* 100, 2878–2883.

Williams, S. R., Christensen, S. R., Stuart, G. J., and Hausser, M. (2002). Membrane potential bistability is controlled by the hyperpolarization-activated current I(H) in rat cerebellar Purkinje neurons in vitro. *J. Physiol. (Lond.)* 539, 469–483.

Womack, M., and Khodakhah, K. (2002). Active contribution of dendrites to the tonic and trimodal patterns of activity in cerebellar Purkinje neurons. *J. Neurosci.* 22, 10603–10612.

Yarom, Y., Sugimori, M., and Llinas, R. (1985). Ionic currents and firing patterns of mammalian vagal motoneurons in vitro. *Neuroscience* 16, 719–737.

Yartsev, M. M., Givon-Mayo, R., Maller, M., and Donchin, O. (2009). Pausing purkinje cells in the cerebellum of the awake cat. *Front. Syst. Neurosci.* 3, 2. doi: 10.3389/neuro.06.002.2009.

Zackowski, K. M., Thach, W. T., Jr., and Bastian, A. J. (2002). Cerebellar subjects show impaired coupling of reach and grasp movements. *Exp. Brain Res.* 146, 511–522.

Zagha, E., Lang, E. J., and Rudy, B. (2008). Kv3.3 channels at the Purkinje cell soma are necessary for generation of the classical complex spike waveform. *J. Neurosci.* 28, 1291–1300.

Conflict of Interest Statement: The authors declare that the research was conducted in the absence of any commercial or financial relationships that could be construed as a potential conflict of interest.

Received: 01 July 2009; paper pending published: 03 September 2009; accepted: 16 October 2009; published online: 09 November 2009.

Citation: Rokni D, Tal Z, Byk H and Yarom Y (2009) Regularity, variability and bi-stability in the activity of cerebellar Purkinje cells. Front. Cell. Neurosci. ***3****:12. doi: 10.3389/neuro.03.012.2009*

frontiers in
CELLULAR NEUROSCIENCE

REVIEW ARTICLE
published: 04 January 2010
doi: 10.3389/neuro.03.019.2009

Cerebellar and extracerebellar involvement in mouse eyeblink conditioning: the ACDC model

Henk-Jan Boele[1†], Sebastiaan K. E. Koekkoek[1†] and Chris I. De Zeeuw[1,2*†]

[1] *Department of Neuroscience, Erasmus Medical Center, Rotterdam, The Netherlands*
[2] *Netherlands Institute for Neuroscience, Royal Academy of Arts and Sciences, Amsterdam, The Netherlands*

Edited by:
Egidio D'Angelo, University of Pavia, Italy

Reviewed by:
Yosef Yarom, Hebrew University, Israel
Egidio D'Angelo, University of Pavia, Italy

****Correspondence:***
Chris I. De Zeeuw, Department of Neuroscience, Erasmus Medical Center, Dr. Molewaterplein 50, P.O. box 1738, 3000 DR Rotterdam, The Netherlands.
e-mail: c.dezeeuw@erasmusmc.nl

[†]Henk-Jan Boele, Sebastiaan K. E. Koekkoek and Chris I. De Zeeuw have contributed equally to this work.

Over the past decade the advent of mouse transgenics has generated new perspectives on the study of cerebellar molecular mechanisms that are essential for eyeblink conditioning. However, it also appears that results from eyeblink conditioning experiments done in mice differ in some aspects from results previously obtained in other mammals. In this review article we will, based on studies using (cell-specific) mouse mutants and region-specific lesions, re-examine the general eyeblink behavior in mice and the neuro-anatomical circuits that might contribute to the different peaks in the conditioned eyeblink trace. We conclude that the learning process in mice has at least two stages: An early stage, which includes short-latency responses that are at least partly controlled by extracerebellar structures such as the amygdala, and a later stage, which is represented by well-timed conditioned responses that are mainly controlled by the pontocerebellar and olivocerebellar systems. We refer to this overall concept as the Amygdala-Cerebellum-Dynamic-Conditioning Model (ACDC model).

Keywords: eyeblink conditioning, cued fear conditioning, mouse, amygdala, cerebellum, ACDC model

INTRODUCTION

Ever since Ivan Pavlov described the phenomenon of classical conditioning at the beginning of the 20th century (Pavlov, 1927), it has been widely used as a formalized training paradigm to study learning and memory formation. The simplicity of the paradigm is attractive: during training a behaviorally neutral stimulus, the conditioned stimulus (CS), is repeatedly followed by an unconditioned stimulus (US) that evokes a particular reflex, the unconditioned response (UR). This paired presentation of stimuli during training sessions gradually leads to the development of a conditioned response (CR), which is the reflex in response to the previously neutral CS. The pairings of the CS and US can occur in a delay or a trace conditioning paradigm. In a delay paradigm the CS precedes the US several hundred milliseconds and the stimuli temporally overlap and co-terminate. In a trace paradigm the CS is followed by a stimulus free interval before the US is presented (Pavlov, 1927).

One extensively studied form of classical conditioning is delay eyeblink conditioning. Work done in cats, rabbits, ferrets, and rats indicates that the cerebellum plays an essential role in eyeblink conditioning (see Eyeblink conditioning). The advent of mouse transgenics has opened up the possibility to further investigate the molecular and network mechanisms underlying eyeblink conditioning in a reproducible, conditional, and cell-specific fashion. Developments in transgenics have been particularly advantageous for cerebellar research because both the granule cells and the Purkinje cells can be manipulated with cell-specific promotors such as those for the GABA alpha6-subunit receptor (Luddens et al., 1990; McLean et al., 2000) and L7 (Oberdick et al., 1990; Barski et al., 2000). However, during more than 15 years of eyeblink conditioning in mice, it also appeared that several features of the conditioning process in mice differ from those in other mammals. Especially auditory startle reflexes and learned aspecific fear responses seem to be more prominent in the mouse eyeblink trace than in those of the other mammals. Until now these startle and fear responses seem to be neglected and are poorly described. However, before we can evaluate the contribution of specific cerebellar molecular mechanisms to the eyeblink conditioning learning process, a systematic description and unambiguous interpretation of these different peaks in the mouse eyeblink trace is required. In this review we will first evaluate the main studies that have identified the underlying circuitries of conditioned eyelid responses, auditory startle reflexes, and conditioned cued fear responses in mammals other than the mouse (part Neural Circuitries Underlying Delay Eyeblink Conditioning, Auditory Startle Reflexes, and Cued Fear Conditioning in Non-Murine Animals). Then, based on the characteristics of the responses in mice (parts Eyeblink Conditioning in Mice, Auditory Startle Reflexes in Mice and the Optimal CS for Eyeblink Conditioning, Cued Fear Conditioning in Mice and Similarities with Eyeblink Conditioning), we will propose how different networks, including the thalamo-amygdalar, pontocerebellar, and olivocerebellar systems, can contribute in an integrated fashion to different peaks in the conditioned mouse eyeblink trace (part The ACDC model: An Integrated Hypothesis of Eyeblink Conditioning in Mice).

NEURAL CIRCUITRIES UNDERLYING DELAY EYEBLINK CONDITIONING, AUDITORY STARTLE REFLEXES, AND CUED FEAR CONDITIONING IN NON-MURINE ANIMALS

EYEBLINK CONDITIONING

During classical conditioning of the eyeblink and/or nictitating membrane response[1] the CS is usually provided by an auditory tone and the US by a periocular electrical stimulation (Gormezano et al.,

[1] To enhance readability the term 'eyeblink conditioning' is used for both conditioning of the external eyelid response and nictitating membrane response.

1962). In operant eyeblink conditioning the US is formed by a corneal air puff, which elicits a defensive eyeblink response. Repeated pairings of the tone and the electrical stimulation or corneal air puff will gradually result in a well-timed eyelid closure in response to the tone. Converging lines of evidence obtained in cats, rabbits, ferrets, and rats suggest a major role for the cerebellum in delay eyeblink conditioning (McCormick et al., 1981, 1982; Mauk et al., 1986; Yeo and Hardiman, 1992; Hesslow, 1994; Rasmussen et al., 2008). Briefly, the main neurocircuitries involved in mediating the CS and US include the pontocerebellar and olivocerebellar input systems, respectively (**Figure 1A**). The auditory CS signals are relayed via mossy fiber – parallel fiber projections from the lateral parts of the pontine nuclei to the Purkinje cells in the cerebellar cortex (Steinmetz et al., 1986, 1987; Tracy et al., 1998; Freeman and Rabinak, 2004; Cicirata et al., 2005), and to a lesser extent via mossy fiber collaterals to the interposed cerebellar nuclei (Dietrichs et al., 1983; Brodal et al., 1986; Parenti et al., 2002; Cicirata et al., 2005). The sensory trigeminal US signals on the other hand are relayed by climbing fibers from mainly the dorsal accessory inferior olive to the Purkinje cells and via climbing fiber collaterals to the interposed nuclei (McCormick et al., 1985; Yeo et al., 1985; Mauk et al., 1986; Gould et al., 1993; Ruigrok and Voogd, 2000). The CR-pathway is formed by the interposed nuclei projections via the red nucleus to the brainstem nuclei that innervate the eyelid muscles. These nuclei include the facial nucleus, which activates the orbicularis oculi muscle (Morcuende et al., 2002), and the oculomotor nucleus, which simultaneously deactivates the levator palpebrae muscle (Trigo et al., 1999; Delgado-Garcia and Gruart, 2002, 2005). The eyelid UR usually has two components: One (R1) is mediated by the short loop from the trigeminal nerve and nucleus to the facial nucleus, while the other one (R2) is mediated by a superimposed loop through the reticular formation and/or cervical spinal cord (Holstege et al., 1986; Pellegrini et al., 1995; van Ham and Yeo, 1996a, b).

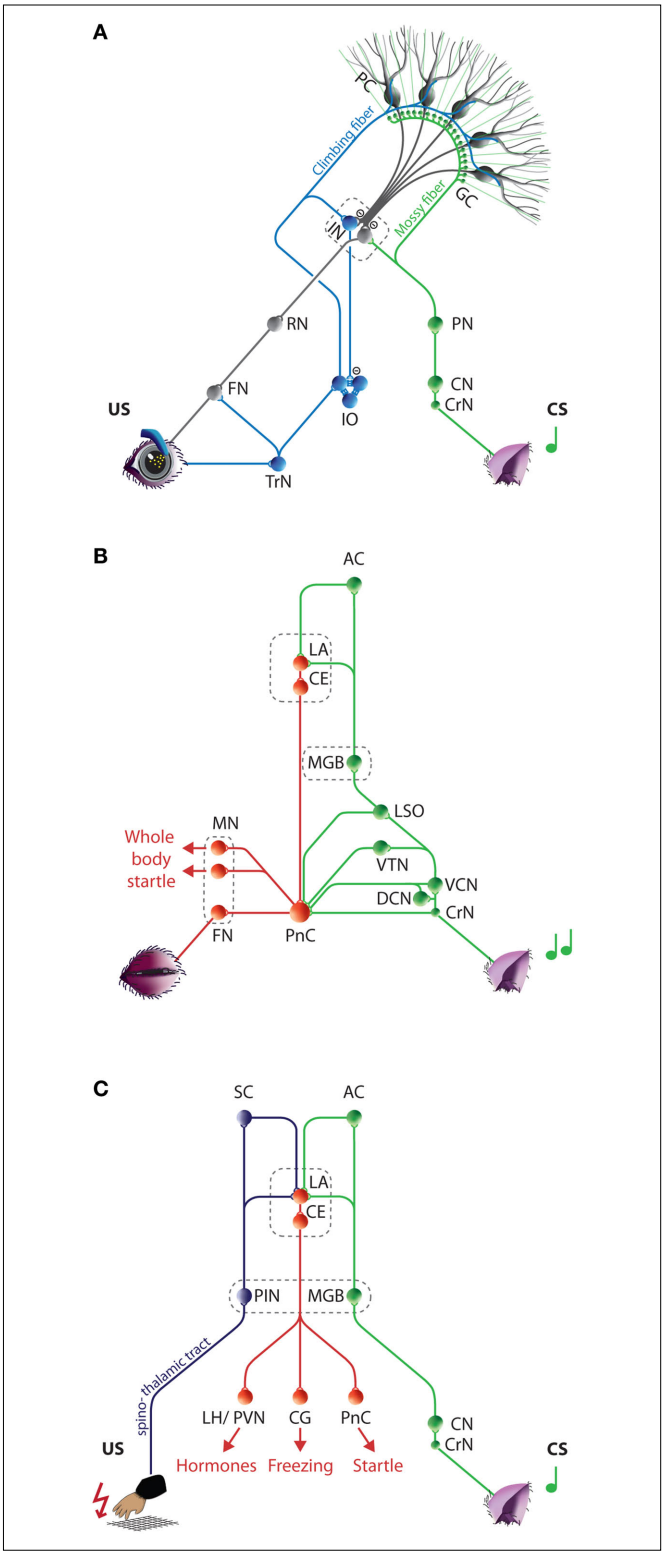

FIGURE 1 | Neurocircuitries underlying eyeblink conditioning, auditory startle reflexes, and cued fear conditioning. (A) Neural circuits engaged during eyeblink conditioning. The mossy fiber CS-pathway (green) and climbing fiber US-pathway (blue) converge at the PCs in the cerebellar cortex and to a much lesser extent at the IN neurons. The CR-pathway (gray) is formed by the cerebellar output neurons and relayed via the RN to the FN and OMN, which innervate the eyelid muscles. (For simplicity only the eyelid innervation by the FN is depicted, see text for more details.) Conditioned induced plasticity at the PC and possibly also in the IN gradually leads to the establishment of an adequate CR. **(B)** Neural circuits engaged during auditory startle reflexes. The fastest route for transmission of acoustic input into motor output is from the CrN via the PnC to the motor neurons, including the FN. In addition, multiple afferent systems including the LSO, VTN, DCN, and VCN excitate the giant PnC neurons. Amygdala activity directly controls the expression of the startle reflex by its projections to the PnC. **(C)** Neural circuits engaged during cued fear conditioning. The tone (CS) and electric foot shock (US) are relayed to the LA from thalamic and cortical regions of the auditory (green) and somatosensory (purple) systems, respectively. The LA directly and indirectly projects to the CE, which efferents (red) control the expression of the different aspects of the fear reaction. One or two paired trials induces efficient plasticity in the LA resulting in typical fear CRs including freezing, tachycardia, tachypneu, and facial responses. AC, Auditory cortex; CE, Central amygdala; CG, Central gray; CN, Cochlear nucleus; CrN, Cochlear root nucleus; CS, Conditioned stimulus; DCN, Dorsal cochlear nucleus; FN, Facial nucleus; GC, Granule cell; IN, Interposed nuclei; IO, Inferior olive; LA, Lateral amygdala; LH, Lateral hypothalamus; LSO, Lateral superior olive; MGB, Medial geniculate body of the thalamus; MN, Motor neurons; OMN Oculomotor Nucleus, PC, Purkinje cell; PIN, Posterior intralaminar nucleus of the thalamus; PN, Pontine nuclei; PnC, Caudal pontine reticular nucleus; PVN, Paraventricular hypothalamic nucleus ; RN, Red nucleus; SC, Somatosensory cortex; TrN, Trigeminal nerve nucleus; US, Unconditioned stimulus; VCN, Ventral cochlear nucleus; VTN, Ventrolateral tegmental nucleus.

Even though the essential neuro-anatomical circuits underlying eyeblink conditioning are relatively well-described, the crucial plasticity mechanisms involved in the conditioning process are a matter in dispute. The classical site for plasticity is the cerebellar cortex (Marr, 1969; Albus, 1971; Ito et al., 1982). In cats, rabbits, and ferrets eyeblink controlling areas in the cerebellar cortex are clustered in lobule HVI, HVII, and the paramedian lobe (Yeo et al., 1985; Hesslow, 1994; Gruart et al., 1997; Yeo and Hesslow, 1998; Villarreal and Steinmetz, 2005; Svensson et al., 2006). Purkinje cell recordings in the C3 zone of lobule HVI in decerebrated ferrets during paired CS-US presentations clearly show the gradual development of a perfectly timed pause response in Purkinje cell simple spike and complex spike firing (Jirenhed et al., 2007; Rasmussen et al., 2008). This Purkinje cell pause disappears during extinction and reappears rapidly during reacquisition training. The plasticity processes at the Purkinje cell that causes this pause are still unknown. It seems unlikely that long-term depression (LTD) at the parallel fiber to Purkinje cell synapse is the sole underlying mechanism, because this mechanism is unable to explain the almost perfect timing of the Purkinje cell pause while varying the CS duration and thereby the CS-US co-termination. Even if the CS outlasts the used interstimulus interval (ISI) by several hundred milliseconds the Purkinje cell pause stops just after the expected US (Hesslow, personal communication). In line with this finding, Welsh et al. (2005) showed that pharmaceutical blockage of LTD in the rat cerebellar cortex does not prevent adaptation of the eyeblink CR timing after an ISI switch.

Lesions of the rabbit cerebellar cortex including all eyeblink controlling areas cannot completely abolish the expression of previously learned CRs. The timing, however, of the postlesion CRs is severely affected: Both onset and peak amplitude have a remarkable short latency (Perrett et al., 1993; Ohyama and Mauk, 2001; Ohyama et al., 2006). These postlesion CRs suggest additional sites of plasticity. One of these sites could be the cerebellar nuclei, because eyeblink conditioning induced plasticity in the interposed nuclei has been reported at both the systems physiological and morphological level (Perrett et al., 1993; Kleim et al., 2002; Ohyama et al., 2006; Weeks et al., 2007). The essential condition for this plasticity is convergence of the US and CS signals by climbing fibers and mossy fibers, respectively (**Figure 1A**). Climbing fibers originating from the dorsal accessory inferior olive indeed provide collaterals to the interposed nuclei (Ruigrok and Voogd, 2000). In contrast, mossy fiber projections from the pontine nuclei to the interposed nuclei are extremely sparse (Dietrichs et al., 1983; Brodal et al., 1986; Parenti et al., 2002; Cicirata et al., 2005). Therefore, their formation might be necessary to establish convergence of the CS and US in the interposed nuclei to support associative memory formation (Kleim et al., 2002; Ohyama et al., 2006). Interestingly, Delgado-Garcia and co-workers have demonstrated in freely moving cats that (posterior) interposed nuclei neurons (type A) start firing about 20 ms after CR onset. These data suggest that neuronal activity of the interposed nuclei cannot be causally related to the initiation of the CR. The main function of the cerebellum in eyeblink conditioning should be to establish a perfectly timed eyeblink CR by reinforcing the motor command and dampening the oscillations in the eyelid movement (Delgado-Garcia and Gruart, 2002, 2006). Instead, extracerebellar regions like the motor cortex or striatum might initiate the CRs (Aou et al., 1992; Gruart et al., 2000). Taken together, plasticity in the cerebellar cortex and nuclei seems to be responsible for different aspects of the learning process. According to the 'trigger-and-storage' model the initial encoding during training occurs in the Purkinje cells while the subsequent long-term memory is stored in the interposed nuclei (Medina et al., 2002). Others suggest that the cerebellar cortex influences the timing and amplitude of the CR, whereas the interposed nuclei are essential for the expression of CRs (Ohyama and Mauk, 2001).

Apart from the cerebellum, the hippocampus and amygdala are probably also involved in delay eyeblink conditioning. In rabbits, hippocampal pyramidal cells display learning related firing patterns that model the eyeblink CR (Berger and Thompson, 1978; Blankenship et al., 2005). The hippocampal neurons seem to encode more abstract aspects of the learning process like contextual and temporal information (Hoehler and Thompson, 1980; Kim and Fanselow, 1992; Lee and Kim, 2004). Interestingly, lesions of the hippocampus cannot abolish previously learned CRs and even seem to facilitate the learning in a delay eyeblink conditioning paradigm, which might be explained by a removal of hippocampal interference with the CS-US association in the cerebellum (Schmaltz and Theios, 1972; Lee and Kim, 2004).

The amygdala may serve to enhance the effectiveness of the CS and to influence the arousal during training. Weisz et al. (1992) demonstrated that in rabbits amygdala lesions mildly impair the rate of conditioning. The effect of these amygdala lesions was stronger in a paradigm with a relatively low intensity CS (65 dB), which elicits only submaximal CR acquisition. In line with this effect, stimulation of the rabbit amygdala enhances the amplitude of the nictitating membrane response (Whalen and Kapp, 1991). Interestingly, the role of the amygdala in eyeblink conditioning seems to be more prominent in rats than in rabbits (Mintz and Wang-Ninio, 2001; Neufeld and Mintz, 2001; Lee and Kim, 2004; Blankenship et al., 2005). Both permanent and reversible lesions of the rat amygdala before conditioning robustly impair the acquisition of CRs. During the first five training sessions the impact of these lesions on the level of conditioning is just as detrimental as cerebellar nuclei lesions (**Figures 3B1–B3;** Lee and Kim, 2004). At later stages, however, the impact of cerebellar lesions is greater. This segregation in two stages may reflect the 'two-process model of conditioning' (Rescorla and Solomon, 1967; Lennartz, 1992; Lee and Kim, 2004), which predicts that nonspecific emotional fear responses, such as increased heart rate, blood pressure and respiration, emerge after only a few CS-US pairings, whereas the development of specific motor CRs requires a greater number of pairings. The initial emotional CRs could facilitate the subsequent acquisition of well-timed motor CRs.

Anatomical and electrophysiological data indicate that the amygdala may indeed facilitate the learning during eyeblink conditioning. The lateral amygdala receives convergent input from both the auditory CS and somatosensory US modalities (for details see "Cued Fear Conditioning" and **Figure 1C**) (Burton and Craig, 1979; Ledoux et al., 1987; LeDoux et al., 1990; Whalen and Kapp, 1991; Weisz et al., 1992). The lateral amygdala in turn sends its output to the central amygdala, which directly projects to the pontine nuclei that provide the mossy fibers to lobules HVI, HVII, and the paramedian lobule (Mihailoff et al., 1989), thereby

modulating the effectiveness of the CS signals to the cerebellum. Electrophysiological recordings of the amygdala in rabbits that were aimed at detecting CS and US activities during eyeblink conditioning show that about 60% of the neurons respond to the CS and more than 70% to the US. Surprisingly, only a few neurons show enhanced responsiveness to the CS alone after CS-US pairings (Richardson and Thompson, 1984). This finding might partly be explained by the relatively small contribution of the amygdala in rabbit eyeblink conditioning, but possibly also by the phenomenon of 'neuronal competition' in the lateral amygdala during memory formation (see also "Cued Fear Conditioning in Mice and Similarities with Eyeblink Conditioning").

Conclusively, the cerebellum is essential and sufficient for eyeblink conditioning, but the hippocampus and even more so the amygdala also seem to contribute to the memory formation, suggesting that in normal biological circumstances multiple brain memory systems in fact have to interact to establish the adequate CR.

AUDITORY STARTLE REFLEXES

A sudden and intense auditory stimulus elicits a fast bodily startle reflex, which includes a rapid eyelid closure and a contraction of facial, neck, and skeletal muscles (Davis et al., 1982; Yeomans and Frankland, 1995; Koch, 1999). This startle reflex has an extremely short latency to onset. Measurements of rats done with ballistic chambers sensing whole-body movements reveal a latency to onset and latency to peak amplitude of about 15 ms and 30 ms, respectively (Pilz et al., 1988; Koch, 1999). More sensitive are electromyographical (EMG) recordings of face-, neck-, and limb muscles, showing that the startle reflex typically starts in the face and spreads down from there to the neck and body (Caeser et al., 1989). In the EMG trace one can distinguish several peaks within the 30 ms after stimulus onset (Pilz et al., 1988; Caeser et al., 1989). Both the latency to onset and the peak amplitude of the startle reflex correlate with the stimulus intensity: Increased sound pressure decreases the latency to onset and increases the peak amplitude (Pilz et al., 1987, 1988; Caeser et al., 1989). One component of the facial startle reflex is the eyelid reflex (Koch, 1999). This eyelid startle reflex can also be seen in cat and rat eyeblink conditioning experiments using a relatively mild auditory stimulus (70 dB click or 2.8 kHz 82 dB tone, respectively) (Skelton, 1988; Woody and Aou, 1999).

The extremely short latency to onset of eyelid and body startle reflexes indicates that the circuitry underlying these reflexes must involve only a few synaptic connections. As illustrated in **Figure 1B** the basic auditory startle circuit is formed by only three central neurons, including the cochlear root nuclei, the giant neurons in the caudal pontine reticular nucleus (PnC), and the motoneurons in the brainstem or spinal cord (Davis et al., 1982, 1993; Lingenhohl and Friauf, 1994; Koch, 1999; Fendt et al., 2001). Blockage of glutamate receptors in the PnC prevents both the expression of the head and whole-body startle reflex (Krase et al., 1993). Since the PnC receives excitatory inputs from multiple afferent systems in the lower brainstem including not only the dorsal and ventral cochlear nucleus, but also the lateral superior olive and ventrolateral tegmental nucleus (connections at the bottom of **Figure 1B**), it is not surprising that PnC neurons demonstrate, just like the peaks in the EMG trace, multiple peaks in their EPSP activity at particular latencies (Lingenhohl and Friauf, 1994; Koch, 1999). In addition to these simple circuits, direct and indirect projections from the central amygdala to the PnC control the expression of the startle reflex (connections shown at the top of **Figure 1B**). Increased activity in the amygdala enhances the responsiveness of giant PnC neurons to auditory stimuli and thereby also the startle behavior (Rosen et al., 1991; Davis et al., 1993) indicating that fear potentiation of the startle reflex is under control of plasticity processes in the amygdala (Davis, 1992).

CUED FEAR CONDITIONING

During a typical cued fear conditioning experiment a tone (CS) is paired with an aversive foot shock (US). After a few CS-US pairings the previously behaviorally neutral tone elicits a wide range of defensive responses (LeDoux, 2000; Pare et al., 2004). These responses include gross reactions of the skeletal musculature resulting in typical freezing behavior, facial contractions, increased respiration, increased blood pressure and heart rate, and pupillary dilations (Lennartz, 1992). Damage to the lateral amygdala, in particular the dorsal subregion, strongly interferes with both the acquisition and expression of these fear CRs indicating that at least an essential part of the convergence of the CS and US occurs in the lateral amygdala (LeDoux et al., 1990; Campeau and Davis, 1995; Fanselow and LeDoux, 1999). The auditory CS signals are mainly relayed from the cochlear nucleus via the inferior colliculus and medial geniculate body of the thalamus to the lateral amygdala (LeDoux et al., 1990). In addition, there is an extra auditory loop via the auditory cortex (**Figure 1C**). The electrical US signals from the foot shock also terminate in the lateral amygdala; they are relayed via the spino-thalamic tract and the lateral intralaminar nucleus of the thalamus (Shi and Davis, 1999; LeDoux, 2000). The lateral amygdala exerts its main action on the fear CR via the central amygdala, which projects directly to several brainstem nuclei including the hypothalamus, peri-aqueductal gray matter, bed nucleus of the stria terminalis, and PnC. Each of these structures contributes to a particular aspect of the general fear reaction (**Figure 1C**) (Killcross et al., 1997; Pitkanen et al., 1997; Pare et al., 2004).

Plasticity in the amygdala during fear conditioning has been extensively described (Quirk et al., 1995; Rogan et al., 1997; Bauer et al., 2001; Blair et al., 2001; Rumpel et al., 2005; Won and Silva, 2008). Neurons in the dorsal part of the lateral amygdala in rats show increased tone-evoked firing rates due to long-term potentiation (LTP) induced by fear conditioning. The latency of the earliest responses of these neurons is about 20 ms following the tone onset in a fear conditioning trial (Quirk et al., 1995). Neurons in the basolateral and ventral areas of the lateral amygdala also demonstrate clear responses, but at latencies of about 40 and 50 ms, respectively (Muramoto et al., 1993; Quirk et al., 1995). Interestingly, after destruction of the amygdala, fear CRs can be reacquired. This reacquisition only occurs if the animals are trained before the amygdala is lesioned (Kim and Davis, 1993). This finding suggests that extra-amygdalar regions also play a role in memory storage during fear conditioning. One of these regions could in fact be the cerebellum, because lesions of the cerebellar vermis

severely disrupt fear memory (Supple and Leaton, 1990), and LTP at inhibitory synapses in the cerebellar vermis can be related to associative processes during fear learning (Sacchetti et al., 2005, 2009; Scelfo et al., 2008). Taken together, during cued fear conditioning the amygdala and cerebellum closely seem to interact to establish the fear CR, mediated by indirect anatomical projections between the two structures.

EYEBLINK CONDITIONING IN MICE

In contrast to detailed neuro-anatomical studies done in cats, rabbits, ferrets, and rats, the fundamental anatomical knowledge underlying eyeblink conditioning in mice is limited up to now. Most work done in mice was aimed to investigate cerebellar molecular mechanisms underlying eyeblink conditioning by using transgenic mice, thereby assuming that in mice the contributions of the cerebellar cortex and cerebellar nuclei to eyeblink conditioning are similar to those of other mammals. Studies on Purkinje cell plasticity processes underlying eyeblink conditioning reported disturbed CR acquisition in mGluR1 mutant mice (Aiba et al., 1994), Purkinje cell degenerative (pcd) mice (Chen et al., 1996), GluRδ2-deficient mice (Kishimoto et al., 2001b), phospholipase C β4 mutant mice (Miyata et al., 2001), Purkinje cell-specific protein kinase C inhibitor overexpressing mice (Koekkoek et al., 2003), and Fmr1 knockout mice (Koekkoek et al., 2005). In line with these findings Purkinje cell-specific mGluR1-rescue mice show normal learning in a delay eyeblink conditioning paradigm (Kishimoto et al., 2002). Mice lacking electrical coupling among their olivary neurons that provide the climbing fibers to the cerebellar cortex show disturbed timing of their CRs. This phenotype might be due to the fact that the balance between LTD and LTP induction in Purkinje cells is disturbed (Koekkoek et al., 2003; Van Der Giessen et al., 2008). First attempts to define the eyeblink controlling regions in the cerebellar cortex in mice indicate that corneal air puff responding Purkinje cells are located at least in the simplex lobule and adjacent parts of lobule HVI (Van Der Giessen et al., 2008), which is in agreement with findings previously obtained from other mammals (see Eyeblink Conditioning). Synaptic processes in the interposed nuclei also seem to be crucial during mouse eyeblink conditioning. First, bilateral infusions of both GABAa receptor agonists and antagonist in the cerebellar nuclei impair acquisition of eyeblink CRs (Sakamoto and Endo, 2008). Second, Wada et al. (2007) reported normal acquisition when granule cell transmission was selectively blocked, suggesting that convergent information at the interposed nuclei is sufficient for the acquisition of eyeblink CRs. Still the CRs in this study are only expressed after removal of the blockage. Thus, different from rabbits (Lavond and Steinmetz, 1989; Perrett et al., 1993; Ohyama et al., 2006), in mice the granule cell network may be required for CR expression. Taken together, results from eyeblink studies done in mutant mice show trends that are similar to those that can be seen in functional anatomical and pharmacological studies done in larger mammals. Yet, if one looks at the rate of conditioning, the topographical characteristics of the eyeblink CR, and the technical approaches, several issues in mice differ from other mammals. Below we will discuss these differences and focus on parallels and similarities with cued fear conditioning in order to conclude with a new model on the relative contribution of the amygdala and the cerebellum in mouse eyeblink conditioning.

RATE OF CONDITIONING

The average percentage CRs in mice usually saturates asymptotically at 50 to 70 after 5 days of training (Chen et al., 1996; Qiao et al., 1998; Kishimoto et al., 2001a; Miyata et al., 2001; Wada et al., 2007; Sakamoto and Endo, 2008). In addition, reported learning curves in mice show an immense variation. For instance, Vogel et al. (2002) reported an average CR percentage of 70 for the first training session while Lee et al. (2009) reported a percentage of less than 40 even after 7 days of training. Averaged eyeblink conditioning learning curves in rabbits and ferrets, in contrast, appear rather consistent. Usually they begin to exhibit first CRs on the second day of training and attain an average CR percentage of 80 to 100 within 5 days of training (Steinmetz et al., 1987; Welsh and Harvey, 1989; Yeo and Hardiman, 1992; Bracha and Bloedel, 1996; Ivarsson and Svensson, 2000; Ohyama and Mauk, 2001; Villarreal and Steinmetz, 2005). The lower average percentage of CRs in mice might be partly due to the typical experimental design when using mice (i.e. group comparison of eyeblink conditioning rates of knockout mice versus their wild-type littermates) that does not allow exclusion of animals that do not reach a certain criterion such as a minimum CR percentage after a particular training period. The variation in reported learning curves in mice could partly be explained by the use of mice with different backgrounds and ages (Paylor and Crawley, 1997; Kishimoto et al., 2001a; Vogel et al., 2002). However, it probably also reflects multiple inconsistencies in the experimental paradigms including different stimulation and recording methodologies and different exclusion and inclusion criteria for CR identification. Due to these inconsistencies comparisons of results from different studies using mice are difficult to make.

TOPOGRAPHICAL CHARACTERISTICS OF THE CONDITIONED EYEBLINK TRACES IN MICE

The topographical characteristics of eyeblink responses during conditioning in mice seem to differ from those in other mammals. EMG traces in several studies show that mice respond to the CS with a rapid robust eyelid closure whereby the eyelid remains closed during the rest of the ISI (see for instance EMG traces in Kishimoto et al., 2001b, 2002; Sakamoto and Endo, 2008). These responses have a latency to onset of about 60–80 ms and a latency to peak amplitude of about 100 ms (Kishimoto et al., 2001b, 2002; Wada et al., 2007; Sakamoto and Endo, 2008), and thereby stand in marked contrast to those of rabbits and ferrets, which show a gradual closing of the eyelid in the CS-US interval with the peak amplitude perfectly coinciding with the US onset (Perrett et al., 1993; Ivarsson and Svensson, 2000; Aksenov et al., 2004). The rapid eyelid response in mice seems to reflect a motoneuronal burst activity and one might doubt the cerebellar origin of this type of eyelid response. Further, the small startle reflex within 50 ms after CS onset, which has also been described for cats and rats (Skelton, 1988; Woody and Aou, 1999), seems to be more prominently present in the mouse conditioned eyeblink trace.

When measured with the Magnetic Distance Measurement Technique (MDMT) one can usually distinguish two different peaks between the startle reflex and the UR. These two peaks include a short-latency response (SLR) and a CR (**Figure 2A**) (Koekkoek et al., 2003, 2005). The SLR was first mentioned in a pioneering mouse eyeblink conditioning study done by Tonegawa's laboratory

(Aiba et al., 1994) and later confirmed by others (Vogel et al., 2002). In the MDMT signal a typical SLR has a peak amplitude of about 0.4 mm, a latency to onset of 50–70 ms, a latency to peak amplitude of 115 ms, and a duration that extends over the ISI (**Figures 2A,E**). Both latency to onset and latency to peak amplitude are relatively fixed, i.e. they are independent of the ISI and they do not shift in the eyeblink trace during consecutive training sessions. The shape of these SLRs is similar to the rapid eyelid responses measured with EMG as described above. In contrast to startle reflexes, SLRs increase in number over especially the first training sessions and they occur relatively infrequently in unpaired trials when a behaviorally neutral tone is used (Aiba et al., 1994; Vogel et al., 2002). This suggests that SLRs are learned and associative. Vogel et al. (2002) reported that only a few CS–US pairings can already establish SLRs, a finding that is also confirmed by our lab. Due to their magnitude and duration SLRs might lead to misinterpretations of the real cerebellar CR. The characteristics of SLRs also differ from those of CRs, which occur later in the ISI and which require more paired trials to become clearly apparent. Moreover, during the consecutive training sessions also in mice the CR peak amplitude usually increases and shifts towards US onset (Aiba et al., 1994; Miyata et al., 2001; Sakamoto and Endo, 2008). Thus, SLRs appear to be rather early, aspecific, learned eyelid responses, whereas CRs occur, as expected, at the time of the US. The fact that SLRs require only a few CS–US pairings raises the question whether they are, like conditioned fear responses, also originating from the amygdala.

Further evidence for the hypothesis that SLRs in mice have an extracerebellar origin comes from studies demonstrating that, in contrast to other mammals, lesions of the interposed nuclei in mice do not fully abolish previously learned eyelid responses to the CS (Koekkoek et al., 2003, 2005; Sakamoto and Endo, 2008). For several reasons it is unlikely that the remaining eyelid responses in these studies were the result of incompleteness of the lesions. First, the interposed nuclei lesions made by Koekkoek et al. (2003, 2005) were bilateral, and silver staining of the efferent fibers from the nuclei showed that the lesions resulted in degeneration of fibers in all the relevant output tracts (**Figures 3A1,A2**). Second, the lesions did not affect only the percentage of CRs, but they also affected the overall shape of the eyelid response in that well-timed CRs disappeared, while the remaining responses had the typical shape of SLRs as described above (**Figure 3A3**). Third, compara-

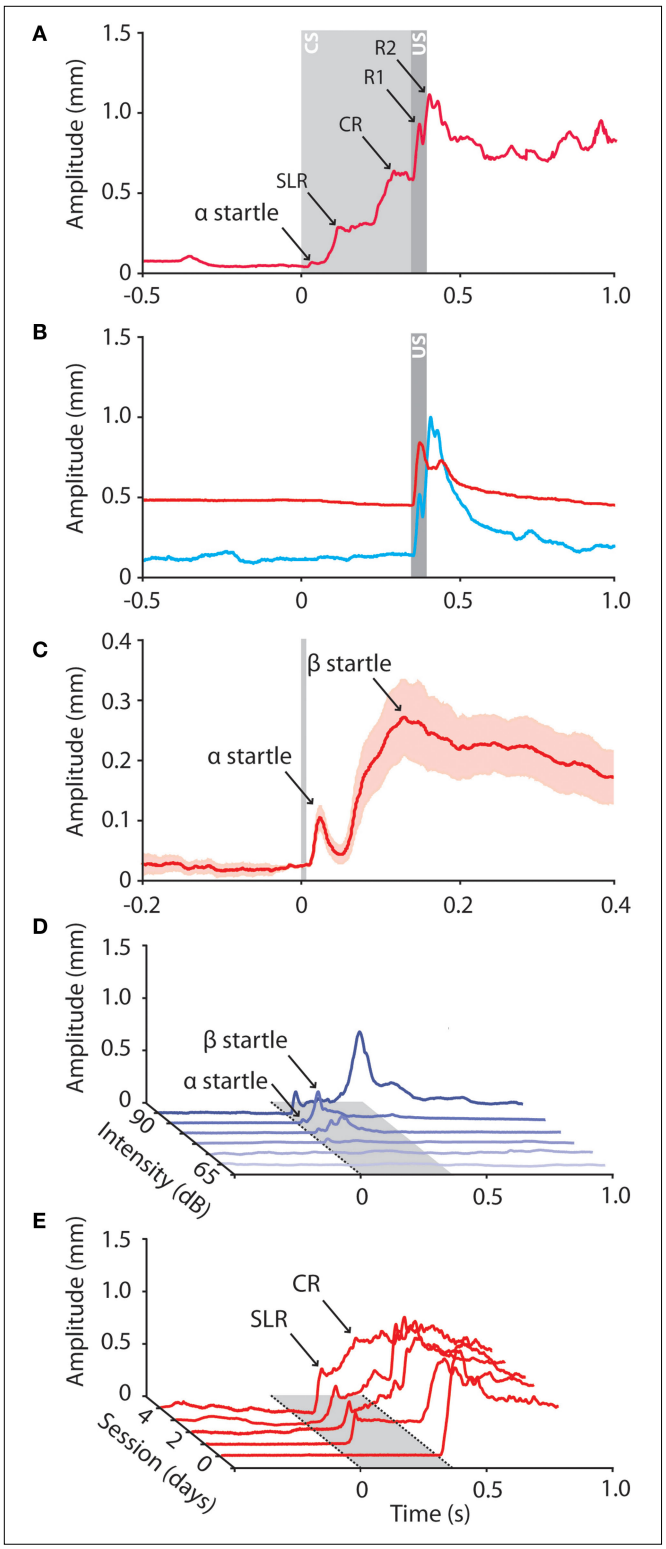

FIGURE 2 | Raw data traces obtained from mice during eyeblink conditioning and auditory startle reflexes. (A) Different peaks can be distinguished in the conditioned eyeblink trace, including a small startle peak, a short-latency response (SLR), a conditioned response (CR), and two or more unconditioned response peaks (R1 and R2). In all panels: tone onset at $t = 0$; puff onset at $t = 350$; CS duration 380 ms; US duration 30 ms; ISI 350 ms; at amplitude = 0 mm the eyelid is maximum opened, at 1 mm the eyelid is fully closed. **(B)** Raw data traces of a reflexive eyeblink response of a mouse when awake behaving (blue) and during 'quiet wakefulness' (red). When behaving the eyelid is fully open and the oscillatory properties of the eyelid motor system are clearly visible in the eyeblink response. During quiet wakefulness the mouse sits very quiet, the eyelid is half closed, the baseline is completely flat, and there is a virtual absence of the normal oscillations of the eyelid response. **(C)** Mean (±SEM) of 20 raw data traces of eyelid startle reflexes in response to a loud auditory tone (90 dB, 10 kHz). Note that, when presented such a loud tone, two startle peaks (α and β) can be distinguished in the raw data traces. **(D)** The amplitude of the auditory startle reflex correlates with the intensity of the auditory stimulus. First small α responses emerge, whereas β responses appear when the tone intensity is increased. **(E)** Example raw data traces of a mouse over the consecutive training sessions. During habituation session (T-0) the behaviorally neutral CS does not elicit eyelid responses. During the first paired training sessions SLRs emerge whereas prolonged training results in well-timed CRs.

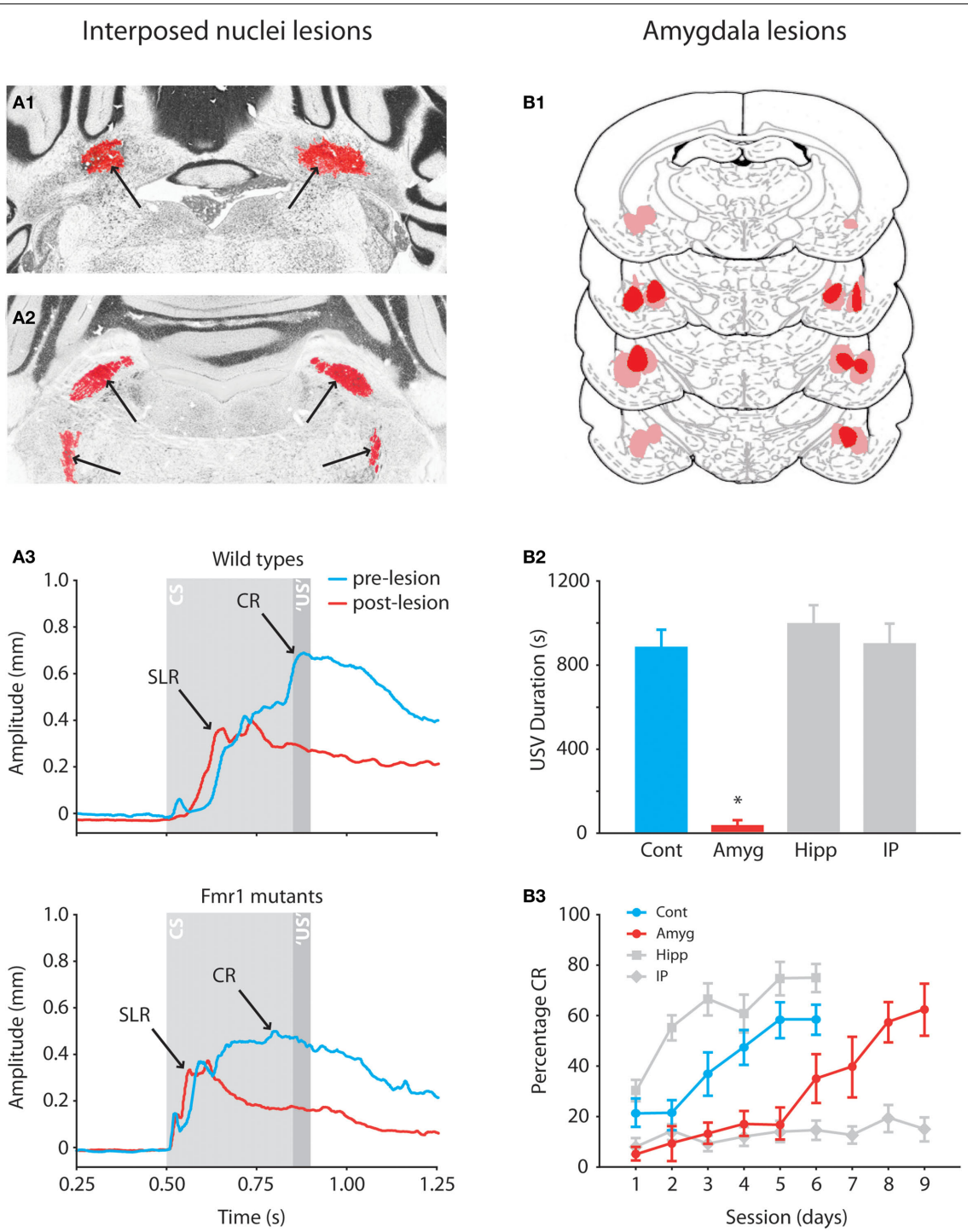

FIGURE 3 | Effects of anterior interposed nucleus lesions in mice and amygdala lesions in rats on eyeblink conditioning. (A1) Example of bilateral lesion (arrows) of anterior interposed nucleus in Nissl-stained section of Fmr1 mutant. **(A2)** Example of degenerated axonal fibers (silver staining is indicated by arrows) in the superior cerebellar peduncle and ipsilateral descending tracts. **(A3)** Eyeblink traces showing the average amplitudes of the CRs in wild-type and Fmr1 mutants before (blue) and after (red) the lesions. In both mutants and wild-types lesions of the anterior interposed nucleus abolish well-timed cerebellar CRs, whereas startle reflexes and SLRs are still present in the eyeblink trace. Reproduced with permission from Koekkoek et al. (2005). **(B1)** Histological reconstructions of amygdala lesion sites in rats. Numbers indicate distance in millimeters posterior to Bregma. **(B2)** Mean ultrasonic vocalization (USV) during day 6 of the training sessions. The USV duration is a valid model of anxiety in rats (Sanchez, 2003), and a reduced USV duration behaviorally confirms the lesions of the amygdala. **(B3)** Mean percentage of CR (±SEM) during daily training sessions from control (n = 9), interposed nuclei lesioned (n = 9), amygdala lesioned (n = 9), and hippocampus lesioned (n = 10) rats. Lesions of the amygdala robustly slowed down the acquisition of eyeblink CRs indicating that the amygdala modulates the eyeblink conditioning process. Reproduced with permission from Lee and Kim (2004).

ble lesions made by Sakamoto and Endo (2008) with a reversible approach (i.e. muscimol and picrotoxin infusions) also could not completely abolish previously learned eyelid CRs. They even found an increase of the responses for the training sessions after infusions. In contrast to Koekkoek et al. (2003, 2005), Sakamoto and Endo did not report any change in latency to onset or latency to peak amplitude of the residual responses.

In cats, rabbits, and ferrets, one can also observe different peaks in their conditioned eyeblink trace. Ivarsson and Svensson (2000) reported two distinctive components in the conditioned eyeblink trace of ferrets and rabbits. However, mean latency to onset of the first peak (CR1) is about 150 ms, which is not compatible with the short latency to onset of SLRs in mice. Further, as mentioned above, SLR with similar shapes have also been described in rabbits after cerebellar cortex lesions. If sufficiently large, these lesions can induce responses with a latency to onset of about 60–80 ms and a latency to peak amplitude of 115–130 ms (Perrett et al., 1993), which are in line with the SLRs in mice (Koekkoek et al., 2003, 2005). In cats, one can distinguish at least four different peaks in the eyeblink trace (Woody and Aou, 1999). When we compare the latencies of these four peaks two of them, α_2 and early β responses, seem to resemble the latencies of SLRs in mice. Both of these responses can also be observed occasionally before training, but their occurrence frequency increases during eyeblink conditioning, suggesting that they have both associative and non-associative properties.

Conclusively, mice show at least two peaks in their conditioned eyeblink traces: an SLR and a CR and these peaks may well have their counterparts in larger mammals. The SLRs form a concern for mouse eyeblink conditioning, because they might lead, due to their magnitude and duration, to misinterpretations of cerebellar CRs. Since each response has different characteristics of the association process, they may originate, at least in part, from different sources.

TECHNICAL CONSIDERATIONS

The data described above show that both qualitatively and quantitatively several features of the conditioned eyeblink behavior in mice differ from those in other mammals. Below we will consider the impact of the various technical approaches on the outcome of conditioning in mice. Apart from the impact of the precise type of CS, which will be discussed in "Auditory Startle Reflexes in Mice and the Optimal CS for Eyeblink Conditioning", the relevant differences in these approaches include the used US intensities, the specific methods for recording the eyeblink responses, and the control of the level of alertness.

US intensities for eliciting CRs in mice

In order to evoke sufficient CRs in mice the US usually is provided at a high intensity level. Whereas a relatively mild corneal air puff is enough to obtain a significant amount of CRs in rabbits (Welsh and Harvey, 1989), in mice (but also in rats) a comparably mild US induces a low level of conditioning (Skelton, 1988; Aiba et al., 1994). Therefore, most conditioning paradigms in mice use a strong aversive US, the intensity of which is often increased over the consecutive training sessions. Such a US does not only elicit a robust eyeblink, but often also a rapid head jerk away from the site of stimulation (Chen et al., 1996; Kishimoto et al., 2002; Sakamoto and Endo, 2008; Lee et al., 2009). This approach may make it hard to rely on EMG for recording eyeblink responses in mice, because it will be difficult to distinguish the actual movements of the eyelid from those of other surrounding facial muscles (see also below). Moreover, especially in mice such strong aversive stimuli form a fearful trigger, which can be expected to evoke various defensive behavioral responses involving activities in multiple brain regions. Thus, the requirements for an appropriate US in mice present challenges both for the technical recording methodology and for the interpretation of the regional brain activities involved in eliciting the CRs.

Recording technology for eyeblink responses

The advent in mouse transgenics has triggered innovative modifications of the physiological recording technologies that were originally designed for larger mammals. For example, EMG, which is a feasible method for measuring eyeblink responses in rabbits (Gormezano et al., 1962; Welsh, 1992; Yeo and Hardiman, 1992), turned out to be too indirect and too sensitive to record selectively eyelid movements in mice (Koekkoek et al., 2002; Vogel et al., 2002). To avoid picking up false positive signals from other facial muscles Koekkoek and colleagues developed MDMT. This technology takes advantage of magnet-sensitive chips and allows direct and precise detection of the actual eyelid movements at a high spatiotemporal resolution, which can be used for quantifying the characteristics of eyeblink responses in mice (Koekkoek et al., 2002).

Controlling the level of alertness

One explanation for the lower percentage of CRs in mice compared to other mammals might be the relatively high occurrence of periods of 'quiet wakefulness' during the eyeblink conditioning experiment. The state of quiet wakefulness is characterized by the mouse sitting quietly with its eyes half closed, which does not reflect freezing behavior due to anxiety. In the MDMT eyeblink trace quiet wakefulness is represented by a flat and elevated baseline, which, as a consequence, results in a reduced UR amplitude. In addition, there is a virtual absence of the oscillations (≈25 Hz) that are prominently present in the alert state during both the CRs and the URs (**Figure 2B**) (Trigo et al., 1999; Koekkoek et al., 2002; Delgado-Garcia and Gruart, 2006). During the state of quiet wakefulness even a well-conditioned mouse will not demonstrate CRs. However, the CRs reappear when the animal 'wakes up'. The occurrence of those periods of quiet wakefulness and the tools used to avoid them or to awaken the mouse (e.g. a sudden loud noise) can strongly influence the outcome of the learning process. Interestingly, different internal brain states may well depend upon changes in oscillatory electrical brain activity (Poulet and Petersen, 2008). During periods of quiet wakefulness mice show synchronous, slow large-amplitude oscillations (1–5 Hz) in the electroencephalogram (EEG) as well as in the single unit recordings of their layer 2/3 pyramidal cells, whereas during a high level of alertness faster low-amplitude oscillations are replacing the slow oscillations. This internal brain state forms a key determinant in attention, expectation, sensorimotor coordination and learning (Gilbert and Sigman, 2007). Probably, the observed reduced oscillations in the eyelid movement in mice during quiet wakefulness reflect the eyelid component of this general internal brain state. Because the state of alertness will

have a great influence on the rate of eyeblink conditioning in mice, one might consider to deliver mild auditory startle pulses based upon the oscillations in the MDMT signal.

AUDITORY STARTLE REFLEXES IN MICE AND THE OPTIMAL CS FOR EYEBLINK CONDITIONING

Using a relatively mild auditory tone (10 kHz, 70 dB) the auditory startle reflex in mice is represented in the MDMT eyeblink trace by a single peak with an amplitude of ca 0.1 mm, a latency to onset of about 15 ms, and a latency to peak amplitude of 25 ms (**Figures 2A,C**). We call this peak, in line with this component in cats, the α-startle peak (Woody and Aou, 1999). Our values in mice correspond to those obtained from facial and head EMG recordings in rats at similar sound intensities (Caeser et al., 1989). However, in mice we can frequently observe additional and more complex eyelid responses (β-startle peaks) with a much longer latency and a bigger amplitude (**Figure 2C**). We assume that the α-startle peak in mice, as in larger mammals, is formed by the three synapse circuit including the cochlear complex, PnC, and facial nucleus, while the β-startle reflex is mediated by the longer loop superimposed upon the PnC and cochlear complex (**Figure 1B**) (Fendt et al., 1996; Koch, 1999). Interestingly, the β-startle reflex in mice resembles the topographical characteristics of their associative SLRs during eyeblink conditioning, suggesting that the underlying neurocircuitry is similar (compare traces in **Figures 2A,C**).

In general α responses in mice emerge at lower sound intensities than β responses, but the latency to onset, the amplitude and the duration of both the α and β eyelid startle reflexes are, similar to those of the whole-body startle reflex, influenced by the intensity of the tone (**Figure 2D**). The threshold to elicit startle reflexes differs among mice of different backgrounds and age. For example, at 8 kHz, 129P3/J and CBA/CaJ mice (male, 15–72 weeks) have a hearing threshold of 70 dB and 20 dB, respectively (JAX® Mice). In C57Bl/6 mice (12–20 weeks) the threshold to elicit β-startle reflexes is usually around 75 dB at 10 kHz, but some animals display them already at levels less than 70 dB (**Figure 2D**). In addition, the stimulus thresholds to elicit α and β startle reflexes in mice show relatively big fluctuations over time in individual animals similar to those described for rats (Pilz et al., 1988). Moreover, in mice auditory stimuli just above hearing threshold already can elicit startle reflexes, indicating that the bandwith between behaviorally neutral and non-neutral auditory stimuli is very narrow. For eyeblink conditioning, in which the auditory stimulus initially serves as a behaviorally neutral CS, this narrow bandwith forms a serious concern. This problem does not pertain so much to the α startle reflexes, which usually diminish over the training sessions (Koekkoek et al., 2005) and can be easily distinguished from CRs, but it holds particularly true for the β startle reflexes, which are often topographically indistinguishable from associative SLRs and sometimes even resemble CRs. The occurrence of β-startle reflexes cq non-associative SLRs in mice may be influenced by the frequency of the auditory CS, but this topic is still subject to debate. Some studies say that they can be reduced by low frequency stimulation at 1 kHz (Lee et al., 2009), but the vast majority of peak latencies of the CRs in these studies still occurs between 85 ms and 140 ms, which corresponds well to the timing of SLRs. On the contrary, others indicate that low frequency tones at 2 kHz can elicit a large number of startle and non-associative freezing responses at the latency of SLRs (Smith et al., 2007). In our hands a tone frequency at 5 or 10 kHz with a rise/fall time of 25 ms and a 68 dB background white-noise is the optimal CS, which elicits minimal startle and non-associative blink reflexes, and supports optimal conditioning. The sound pressure level of a neutral CS differs among mice. Therefore, it is crucial to make a behavioral audiogram for each individual mouse during habituation sessions before the paired training sessions start so as to identify its behaviorally neutral dB. However, despite all efforts to minimize and control both startle reflexes and non-associative SLRs, both do remain present during eyeblink conditioning experiments in mice, indicating that a behaviorally neutral CS is almost elusive.

CUED FEAR CONDITIONING IN MICE AND SIMILARITIES WITH EYEBLINK CONDITIONING

The advent of mouse transgenics has also been advantageous for elucidating some of the mechanisms in the amygdala that underlie cued fear conditioning. For example, LTP induction at thalamic inputs to the lateral amygdala projection neurons and the glutamatergic synapses in the basal amygdala is absent in GluR1, but normal in GluR3 mutant mice (Humeau et al., 2007). As a consequence GluR1 mutant mice do not display conditioned freezing in response to an auditory CS, whereas GluR3 knockouts on the other hand show normal learning in a cued fear conditioning paradigm (Humeau et al., 2007). Mice that express α calcium-calmodulin-dependent kinase II (αCaMKII) that cannot undergo inhibitory phosphorylation have lower thresholds for LTP and a high level of freezing before and after tone onset in a cued conditioning paradigm (Elgersma et al., 2002). In addition, mouse transgenic studies have allowed us to examine 'neuronal competition' in the lateral amygdala during memory formation (Han et al., 2007). Although 70% of the lateral amygdala neurons receive convergent input of the foot shock US and tone CS, only 25% of them exhibit cued fear conditioning induced plasticity. This relatively low percentage could possibly explain why earlier recordings in the amygdala of rabbits that were aimed at detecting CS and US activities during eyeblink conditioning showed only a few amygdala neurons with enhanced responsiveness to the CS after CS-US pairings (Richardson and Thompson, 1984). As mentioned above, the cerebellum is also involved in cued fear conditioning. The ionotropic glutamate receptor delta2 subunit (GluRδ2) is specifically expressed at the postsynaptic site of the parallel fiber to Purkinje cell synapse (Araki et al., 1993; Yuzaki, 2003). Mice that lack this GluRδ2 show impaired acquisition in a delay eyeblink conditioning paradigm (Kishimoto et al., 2001b). However, these mice also have short- and long-term memory impairments in a cued fear conditioning paradigm (Sacchetti et al., 2004). This finding suggests that the cerebellum also participates in the neural circuitry subserving emotional fear responses.

Interestingly, when aversive US intensities are used, as is typical in eyeblink experiments with mice, the main difference between fear and non-fear (i.e. eyeblink) conditioning may well disappear. Too rigid implementation of theoretical categorizations of fear versus non-fear conditioning can thus easily lead to an overly restrictive consideration of the underlying neural processes.

THE ACDC MODEL: AN INTEGRATED HYPOTHESIS OF EYEBLINK CONDITIONING IN MICE

As explained above, the magnitude and duration of the SLRs in mice might lead to misinterpretation of the origin and the percentage of CRs. We hypothesize that the associative properties of SLRs have an extracerebellar origin, most likely the amygdala, which is known to be central in the control of conditioned fear responses. It has been shown that the relative contribution of the amygdala to the eyeblink conditioning process differs among animals. Whereas its role seems to be minimal in rabbits, in rats the amygdala plays an important role in modulating the eyeblink conditioning process by enhancing the effectiveness of the CS and the arousal of the animal. The amygdala is in a good position to modulate the CS input to the cerebellum, because it projects directly to the pontine nuclei neurons that provide the mossy fibers (**Figure 4**) (Mihailoff et al., 1989). In mice the role of the amygdala during eyeblink conditioning has not been investigated yet. As in rats, the amygdala might be important for enhancing the effectiveness of the CS and the arousal of the animal. Further, we hypothesize that especially in mice the amygdalar contribution is directly resembled by an SLR in the eyeblink trace.

Thus, the Amygdala-Cerebellum-Dynamic-Conditioning Model predicts that the amygdala contributes to the early associative SLR that occurs rather rapidly in the beginning of training, while the cerebellum is mainly involved in controlling the later, well-timed CR that coincides with the onset of the US and that slowly emerges as the training proceeds (**Figure 2E**). Both the amygdala and the cerebellum can contribute to the various associative components when the following three conditions are met: (i) both CS and US inputs converge upon the same neurons; (ii) these neurons serve as an output to exert motor control; and (iii) learning induced plasticity creates an adequate novel output (i.e. the CR). Both systems meet these conditions. Auditory CS and somatosensory US inputs converge in the lateral amygdala. While the cochlear nucleus relays the auditory CS to the medial geniculate body of the thalamus and from there to the lateral amygdala, the trigeminal nucleus mediates the peri-orbital US signals via the posterior intralaminar nucleus of the thalamus to the lateral amygdala (**Figure 4**) (Burton and Craig, 1979; Ledoux et al., 1987; Whalen and Kapp, 1991). Presumably because of convergent activities during fear conditioning, LTP can be induced in neurons of the lateral amygdala, and as a consequence the auditory responses of these neurons can be enhanced (Rumpel et al., 2005; Humeau et al., 2007). Since these neuronal responses occur at latencies between 20 ms and 50 ms (Quirk et al., 1995), and since the lateral amygdala sends it output via the central amygdala and PnC to the facial nucleus, these neuronal latencies are in line with the latency to onset (about 50–70 ms) of the eyelid SLRs in mice during eyeblink conditioning. For the cerebellum, it is clear that the auditory CS is mediated by the cochlear and pontine neurons to the granule cells in the cerebellar cortex, and that their parallel fibers converge on Purkinje cells with the US

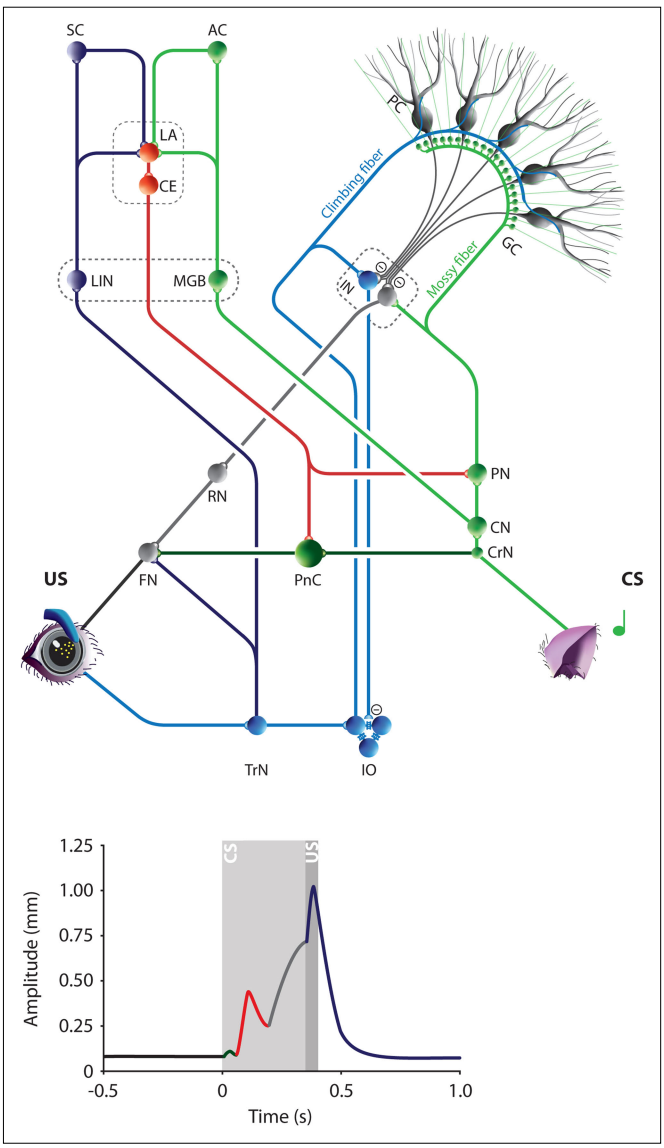

FIGURE 4 | The Amygdala-Cerebellum-Dynamic-Conditioning Model. An integrated model to explain the different phases in the mouse eyeblink conditioning learning process and the different peaks in the individual eyeblink traces. The colors in the model eyeblink trace represent the anatomical afferents to the FN or PnC. During eyeblink conditioning the tone (CS) and corneal air puff (US) converge at least in the amygdala and cerebellum. They are relayed to the LA from thalamic and cortical regions of the auditory (green) and somatosensory (purple) systems. Pontocerebellar (green) and olivocerebellar (blue) systems mediate the convergence of CS and US on Purkinje cells in the cerebellar cortex and to a lesser extent on the IN neurons. Amygdala and cerebellum control the FN activity via PnC (red) and RN (gray), respectively. During the first learning phase in eyeblink conditioning very efficient plasticity in the LA results in mild conditioned fear responses, including rapid facial responses such as an eyelid closure. This is represented in the eyeblink trace by an SLR (red). A few CS-US pairings are enough to obtain clear SLRs in mice. Prolonged training will induce cerebellar learning, which behaviorally is represented by a perfectly timed eyelid closure (gray). In addition, direct projections from the amygdala to the PN might contribute directly to the CS input of the cerebellum. Thus, the ACDC model assumes that neuronal mechanism in different brain regions contribute to the establishment of an adequate CR. AC, Auditory cortex; CE, Central amygdala; CN, Cochlear nucleus; CrN, Cochlear root nucleus; CS, Conditioned stimulus; FN, Facial nucleus; GC, Granule cell; IN, Interposed nuclei; IO, Inferior olive; LA, Lateral amygdala; MGB, Medial geniculate body of the thalamus; MN, Motor neurons; PC, Purkinje cell; PIN, Posterior intralaminar nucleus of the thalamus; PN, Pontine nuclei; PnC, Caudal pontine reticular nucleus; RN, Red nucleus; SC, Somatosensory cortex; TrN, Trigeminal nerve nucleus; US, Unconditioned stimulus.

signals that are mediated by the climbing fiber system (Yeo et al., 1985; Steinmetz et al., 1989). The Purkinje cells in turn can well provide the output that is required to modulate the interposed nuclei neurons that control the red nucleus and thereby the facial and oculomotor nucleus motor neurons (Morcuende et al., 2002; Jirenhed et al., 2007). It is still under debate which cellular mechanisms are induced during convergent, associative eyeblink activity in the cerebellum (Kishimoto et al., 2001b; Koekkoek et al., 2003; Welsh et al., 2005). Both the simple spike and complex spike activity of Purkinje cells are reduced during the acquisition process (Jirenhed et al., 2007). Thus, during eyeblink conditioning using an auditory CS and a peri-orbital US convergence of stimuli does occur both in the lateral amygdala and in the cerebellum, these systems both have a central output that exerts motor control of the eyelid muscles, and learning induced plasticity takes place in both systems. In addition, the amygdala and cerebellum may interact with each other. Thus, the ACDC model can explain several unique features of eyeblink conditioning in mice, like the occurrence of the typical SLRs during normal acquisition training, which cannot be abolished by lesions of the cerebellar nuclei. Further validation of the ACDC model awaits. It will be interesting to find out if SLRs and CRs can be produced independently in mice. In principle, one should be able to bypass the contribution of the amygdala proper by electrically stimulating the pontine nuclei, thereby removing the SLRs that occur with eyeblink conditioning using auditory stimulation. This type of experiment, together with those in which the mouse amygdala is lesioned, should show whether the ACDC model is correct.

ACKNOWLEDGMENTS

This work was supported by the Dutch Organisation for Medical Sciences (ZON-MW), Life Sciences (NWO-ALW), Senter (Neuro-Bsik), Prinses Beatrix Fonds, and the European Community (EEC; SENSOPAC).

REFERENCES

Aiba, A., Kano, M., Chen, C., Stanton, M. E., Fox, G. D., Herrup, K., Zwingman, T. A., and Tonegawa, S. (1994). Deficient cerebellar long-term depression and impaired motor learning in mGluR1 mutant mice. *Cell* 79, 377–388.

Aksenov, D., Serdyukova, N., Irwin, K., and Bracha, V. (2004). GABA neurotransmission in the cerebellar interposed nuclei: involvement in classically conditioned eyeblinks and neuronal activity. *J. Neurophysiol.* 91, 719–727.

Albus, J. S. (1971). A theory of cerebellar function. *Math. Biosci.* 10, 25–61.

Aou, S., Woody, C. D., and Birt, D. (1992). Changes in the activity of units of the cat motor cortex with rapid conditioning and extinction of a compound eye blink movement. *J. Neurosci.* 12, 549–559.

Araki, K., Meguro, H., Kushiya, E., Takayama, C., Inoue, Y., and Mishina, M. (1993). Selective expression of the glutamate receptor channel delta 2 subunit in cerebellar Purkinje cells. *Biochem. Biophys. Res. Commun.* 197, 1267–1276.

Barski, J. J., Dethleffsen, K., and Meyer, M. (2000). Cre recombinase expression in cerebellar Purkinje cells. *Genesis* 28, 93–98.

Bauer, E. P., LeDoux, J. E., and Nader, K. (2001). Fear conditioning and LTP in the lateral amygdala are sensitive to the same stimulus contingencies. *Nat. Neurosci.* 4, 687–688.

Berger, T. W., and Thompson, R. F. (1978). Neuronal plasticity in the limbic system during classical conditioning of the rabbit nictitating membrane response. I. The hippocampus. *Brain Res.* 145, 323–346.

Blair, H. T., Schafe, G. E., Bauer, E. P., Rodrigues, S. M., and LeDoux, J. E. (2001). Synaptic plasticity in the lateral amygdala: a cellular hypothesis of fear conditioning. *Learn. Mem.* 8, 229–242.

Blankenship, M. R., Huckfeldt, R., Steinmetz, J. J., and Steinmetz, J. E. (2005). The effects of amygdala lesions on hippocampal activity and classical eyeblink conditioning in rats. *Brain Res.* 1035, 120–130.

Bracha, V., and BIoedel, J. R. (1996). The multiple-pathway model of circuits subserving the classical conditioning of withdrawal reflexes. In Acquisition of Motor Behavior in Vertebrates, J. R. Bloedel, T. Ebner and S. Wise, eds (Cambridge, MA, MIT Press), pp. 175–204.

Burton, H., and Craig, A. D. Jr. (1979). Distribution of trigeminothalamic projection cells in cat and monkey. *Brain Res.* 161, 515–521.

Caeser, M., Ostwald, J., and Pilz, P. K. (1989). Startle responses measured in muscles innervated by facial and trigeminal nerves show common modulation. *Behav. Neurosci.* 103, 1075–1081.

Campeau, S., and Davis, M. (1995). Involvement of subcortical and cortical afferents to the lateral nucleus of the amygdala in fear conditioning measured with fear-potentiated startle in rats trained concurrently with auditory and visual conditioned stimuli. *J. Neurosci.* 15, 2312–2327.

Chen, L., Bao, S., Lockard, J. M., Kim, J. K., and Thompson, R. F. (1996). Impaired classical eyeblink conditioning in cerebellar-lesioned and Purkinje cell degeneration (pcd) mutant mice. *J. Neurosci.* 16, 2829–2838.

Cicirata, F., Zappala, A., Serapide, M. F., Parenti, R., Panto, M. R., and Paz, C. (2005). Different pontine projections to the two sides of the cerebellum. *Brain Res. Brain Res. Rev.* 49, 280–294.

Davis, M. (1992). The role of the amygdala in fear and anxiety. *Annu. Rev. Neurosci.* 15, 353–375.

Davis, M., Falls, W. A., Campeau, S., and Kim, M. (1993). Fear-potentiated startle: a neural and pharmacological analysis. *Behav. Brain Res.* 58, 175–198.

Davis, M., Gendelman, D. S., Tischler, M. D., and Gendelman, P. M. (1982). A primary acoustic startle circuit: lesion and stimulation studies. *J. Neurosci.* 2, 791–805.

Delgado-Garcia, J. M., and Gruart, A. (2002). The role of interpositus nucleus in eyelid conditioned responses. *Cerebellum* 1, 289–308.

Delgadoz-Garcia, J. M., and Gruart, A. (2005). Firing activities of identified posterior interpositus nucleus neurons during associative learning in behaving cats. *Brain Res. Brain Res. Rev.* 49, 367–376.

Delgado-Garcia, J. M., and Gruart, A. (2006). Building new motor responses: eyelid conditioning revisited. *Trends Neurosci.* 29, 330–338.

Dietrichs, E., Bjaalie, J. G., and Brodal, P. (1983). Do pontocerebellar fibers send collaterals to the cerebellar nuclei? *Brain Res.* 259, 127–131.

Elgersma, Y., Fedorov, N. B., Ikonen, S., Choi, E. S., Elgersma, M., Carvalho, O. M., Giese, K. P., and Silva, A. J. (2002). Inhibitory autophosphorylation of CaMKII controls PSD association, plasticity, and learning. *Neuron* 36, 493–505.

Fanselow, M. S., and LeDoux, J. E. (1999). Why we think plasticity underlying Pavlovian fear conditioning occurs in the basolateral amygdala. *Neuron* 23, 229–232.

Fendt, M., Koch, M., and Schnitzler, H. U. (1996). Somatostatin in the pontine reticular formation modulates fear potentiation of the acoustic startle response: an anatomical, electrophysiological, and behavioral study. *J. Neurosci.* 16, 3097–3103.

Fendt, M., Li, L., and Yeomans, J. S. (2001). Brain stem circuits mediating prepulse inhibition of the startle reflex. *Psychopharmacology (Berl.)* 156, 216–224.

Freeman, J. H. Jr., and Rabinak, C. A. (2004). Eyeblink conditioning in rats using pontine stimulation as a conditioned stimulus. *Integr. Physiol. Behav. Sci.* 39, 180–191.

Gilbert, C. D., and Sigman, M. (2007). Brain states: top-down influences in sensory processing. *Neuron* 54, 677–696.

Gormezano, I., Schneiderman, N., Deaux, E., and Fuentes, I. (1962). Nictitating membrane: classical conditioning and extinction in the albino rabbit. *Science* 138, 33–34.

Gould, T. J., Sears, L. L., and Steinmetz, J. E. (1993). Possible CS and US pathways for rabbit classical eyelid conditioning: electrophysiological evidence for projections from the pontine nuclei and inferior olive to cerebellar cortex and nuclei. *Behav. Neural Biol.* 60, 172–185.

Gruart, A., Guillazo-Blanch, G., Fernandez-Mas, R., Jimenez-Diaz, L., and Delgado-Garcia, J. M. (2000). Cerebellar posterior interpositus nucleus as an enhancer of classically conditioned eyelid responses in alert cats. *J. Neurophysiol.* 84, 2680–2690.

Gruart, A., Pastor, A. M., Armengol, J. A., and Delgado-Garcia, J. M. (1997). Involvement of cerebellar cortex and nuclei in the genesis and control of unconditioned and conditioned eyelid motor responses. *Prog. Brain Res.* 114, 511–528.

Han, J. H., Kushner, S. A., Yiu, A. P., Cole, C. J., Matynia, A., Brown, R. A., Neve, R. L., Guzowski, J. F., Silva, A. J., and Josselyn, S. A. (2007). Neuronal competition and selection during memory formation. *Science* 316, 457–460.

Hesslow, G. (1994). Correspondence between climbing fibre input and motor output in eyeblink-related areas in cat cerebellar cortex. *J. Physiol. (Lond.)* 476, 229–244.

Hoehler, F. K., and Thompson, R. F. (1980). Effect of the interstimulus (CS-UCS) interval on hippocampal unit activity during classical conditioning of the nictitating membrane response of the rabbit (*Oryctolagus cuniculus*). *J. Comp. Physiol. Psychol.* 94, 201–215.

Holstege, G., van Ham, J. J., and Tan, J. (1986). Afferent projections to the orbicularis oculi motoneuronal cell group. An autoradiographical tracing study in the cat. *Brain Res.* 374, 306–320.

Humeau, Y., Reisel, D., Johnson, A. W., Borchardt, T., Jensen, V., Gebhardt, C., Bosch, V., Gass, P., Bannerman, D. M., Good, M. A., Hvalby, O., Sprengel, R., and Luthi, A. (2007). A pathway-specific function for different AMPA receptor subunits in amygdala long-term potentiation and fear conditioning. *J. Neurosci.* 27, 10947–10956.

Ito, M., Sakurai, M., and Tongroach, P. (1982). Climbing fibre induced depression of both mossy fibre responsiveness and glutamate sensitivity of cerebellar Purkinje cells. *J. Physiol.* 324, 113–134.

Ivarsson, M., and Svensson, P. (2000). Conditioned eyeblink response consists of two distinct components. *J. Neurophysiol.* 83, 796–807.

Jirenhed, D. A., Bengtsson, F., and Hesslow, G. (2007). Acquisition, extinction, and reacquisition of a cerebellar cortical memory trace. *J. Neurosci.* 27, 2493–2502.

Killcross, S., Robbins, T. W., and Everitt, B. J. (1997). Different types of fear-conditioned behaviour mediated by separate nuclei within amygdala. *Nature* 388, 377–380.

Kim, J. J., and Fanselow, M. S. (1992). Modality-specific retrograde amnesia of fear. *Science* 256, 675–677.

Kim, M., and Davis, M. (1993). Electrolytic lesions of the amygdala block acquisition and expression of fear-potentiated startle even with extensive training but do not prevent reacquisition. *Behav. Neurosci.* 107, 580–595.

Kishimoto, Y., Suzuki, M., Kawahara, S., and Kirino, Y. (2001a). Age-dependent impairment of delay and trace eyeblink conditioning in mice. *Neuroreport* 12, 3349–3352.

Kishimoto, Y., Kawahara, S., Fujimichi, R., Mori, H., Mishina, M., and Kirino, Y. (2001b). Impairment of eyeblink conditioning in GluRdelta2-mutant mice depends on the temporal overlap between conditioned and unconditioned stimuli. *Eur. J. Neurosci.* 14, 1515–1521.

Kishimoto, Y., Fujimichi, R., Araishi, K., Kawahara, S., Kano, M., Aiba, A., and Kirino, Y. (2002). mGluR1 in cerebellar Purkinje cells is required for normal association of temporally contiguous stimuli in classical conditioning. *Eur. J. Neurosci.* 16, 2416–2424.

Kleim, J. A., Freeman, J. H. Jr., Bruneau, R., Nolan, B. C., Cooper, N. R., Zook, A., and Walters, D. (2002). Synapse formation is associated with memory storage in the cerebellum. *Proc. Natl. Acad. Sci. U.S.A.* 99, 13228–13231.

Koch, M. (1999). The neurobiology of startle. *Prog. Neurobiol.* 59, 107–128.

Koekkoek, S. K., Hulscher, H. C., Dortland, B. R., Hensbroek, R. A., Elgersma, Y., Ruigrok, T. J., and De Zeeuw, C. I. (2003). Cerebellar LTD and learning-dependent timing of conditioned eyelid responses. *Science* 301, 1736–1739.

Koekkoek, S. K., Yamaguchi, K., Milojkovic, B. A., Dortland, B. R., Ruigrok, T. J., Maex, R., De Graaf, W., Smit, A. E., VanderWerf, F., Bakker, C. E., Willemsen, R., Ikeda, T., Kakizawa, S., Onodera, K., Nelson, D. L., Mientjes, E., Joosten, M., De Schutter, E., Oostra, B. A., Ito, M., and De Zeeuw, C. I. (2005). Deletion of FMR1 in Purkinje cells enhances parallel fiber LTD, enlarges spines, and attenuates cerebellar eyelid conditioning in Fragile X syndrome. *Neuron* 47, 339–352.

Koekkoek, S. K. E., Den Ouden, W. L., Perry, G., Highstein, S. M., and De Zeeuw, C. I. (2002). Monitoring kinetic and frequency-domain properties of eyelid responses in mice with magnetic distance measurement technique. *J. Neurophysiol.* 88, 2124–2133.

Krase, W., Koch, M., and Schnitzler, H. U. (1993). Glutamate antagonists in the reticular formation reduce the acoustic startle response. *Neuroreport* 4, 13–16.

Lavond, D. G., and Steinmetz, J. E. (1989). Acquisition of classical conditioning without cerebellar cortex. *Behav. Brain Res.* 33:113–164.

LeDoux, J. E. (2000). Emotion circuits in the brain. *Annu. Rev. Neurosci.* 23, 155–184.

LeDoux, J. E., Cicchetti, P., Xagoraris, A., and Romanski, L. M. (1990). The lateral amygdaloid nucleus: sensory interface of the amygdala in fear conditioning. *J. Neurosci.* 10, 1062–1069.

Ledoux, J. E., Ruggiero, D. A., Forest, R., Stornetta, R., and Reis, D. J. (1987). Topographic organization of convergent projections to the thalamus from the inferior colliculus and spinal cord in the rat. *J. Comp. Neurol.* 264, 123–146.

Lee, K. H., Chatila, T. A., Ram, R. A., and Thompson, R. F. (2009). Impaired memory of eyeblink conditioning in CaMKIV KO mice. *Behav. Neurosci.* 123, 438–442.

Lee, T., and Kim, J. J. (2004). Differential effects of cerebellar, amygdalar, and hippocampal lesions on classical eyeblink conditioning in rats. *J. Neurosci.* 24, 3242–3250.

Lennartz, W. (1992). Analysis of response systems in Pavlovian conditioning reveals rapidly versus slowly acquired conditioned responses: Support for two factors, implications for behavior and neurobiology. *Psychobiology* 20, 93–119.

Lingenhohl, K., and Friauf, E. (1994). Giant neurons in the rat reticular formation: a sensorimotor interface in the elementary acoustic startle circuit? *J. Neurosci.* 14, 1176–1194.

Luddens, H., Pritchett, D. B., Kohler, M., Killisch, I., Keinanen, K., Monyer, H., Sprengel, R., and Seeburg, P. H. (1990). Cerebellar GABAA receptor selective for a behavioural alcohol antagonist. *Nature* 346, 648–651.

Marr, D. (1969). A theory of cerebellar cortex. *J. Physiol.* 202, 437–470.

Mauk, M. D., Steinmetz, J. E., and Thompson, R. F. (1986). Classical conditioning using stimulation of the inferior olive as the unconditioned stimulus. *Proc. Natl. Acad. Sci. U.S.A.* 83, 5349–5353.

McCormick, D. A., Clark, G. A., Lavond, D. G., and Thompson, R. F. (1982). Initial localization of the memory trace for a basic form of learning. *Proc. Natl. Acad. Sci. U.S.A.* 79, 2731–2735.

McCormick, D. A., Lavond, D. G., Clark, G. A., Kettner, R. E., Rising, C. E., and Thompson, R. F. (1981). The engram found? Role of the cerebellum in classical conditioning of nictitating membrane and eyelid responses. *Bull. Psychon. Soc.* 18, 103–105.

McCormick, D. A., Steinmetz, J. E., and Thompson, R. F. (1985). Lesions of the inferior olivary complex cause extinction of the classically conditioned eyeblink response. *Brain Res.* 359, 120–130.

McLean, P. J., Shpektor, D., Bandyopadhyay, S., Russek, S. J., and Farb, D. H. (2000). A minimal promoter for the GABA(A) receptor alpha6-subunit gene controls tissue specificity. *J. Neurochem.* 74, 1858–1869.

Medina, J. F., Christopher Repa, J., Mauk, M. D., and LeDoux, J. E. (2002). Parallels between cerebellum- and amygdala-dependent conditioning. *Nat. Rev. Neurosci.* 3, 122–131.

Mihailoff, G. A., Kosinski, R. J., Azizi, S. A., and Border, B. G. (1989). Survey of noncortical afferent projections to the basilar pontine nuclei: a retrograde tracing study in the rat. *J. Comp. Neurol.* 282, 617–643.

Mintz, M., and Wang-Ninio, Y. (2001). Two-stage theory of conditioning: involvement of the cerebellum and the amygdala. *Brain Res.* 897, 150–156.

Miyata, M., Kim, H. T., Hashimoto, K., Lee, T. K., Cho, S. Y., Jiang, H., Wu, Y., Jun, K., Wu, D., Kano, M., and Shin, H. S. (2001). Deficient long-term synaptic depression in the rostral cerebellum correlated with impaired motor learning in phospholipase C beta4 mutant mice. *Eur. J. Neurosci.* 13, 1945–1954.

Morcuende, S., Delgado-Garcia, J. M., and Ugolini, G. (2002). Neuronal premotor networks involved in eyelid responses: retrograde transneuronal tracing with rabies virus from the orbicularis oculi muscle in the rat. *J. Neurosci.* 22, 8808–8818.

Muramoto, K., Ono, T., Nishijo, H., and Fukuda, M. (1993). Rat amygdaloid neuron responses during auditory discrimination. *Neuroscience* 52, 621–636.

Neufeld, M., and Mintz, M. (2001). Involvement of the amygdala in classical conditioning of eyeblink response in the rat. *Brain Res.* 889, 112–117.

Oberdick, J., Smeyne, R. J., Mann, J. R., Zackson, S., and Morgan, J. I. (1990). A promoter that drives transgene expression in cerebellar Purkinje and retinal bipolar neurons. *Science* 248, 223–226.

Ohyama, T., and Mauk, M. (2001). Latent acquisition of timed responses in cerebellar cortex. *J. Neurosci.* 21, 682–690.

Ohyama, T., Nores, W. L., Medina, J. F., Riusech, F. A., and Mauk, M. D. (2006). Learning-induced plasticity in deep cerebellar nucleus. *J. Neurosci.* 26, 12656–12663.

Pare, D., Quirk, G. J., and Ledoux, J. E. (2004). New vistas on amygdala networks in conditioned fear. *J. Neurophysiol.* 92, 1–9.

Parenti, R., Zappala, A., Serapide, M. F., Panto, M. R., and Cicirata, F. (2002). Projections of the basilar pontine nuclei and nucleus reticularis tegmenti pontis to the cerebellar nuclei of the rat. *J. Comp. Neurol.* 452, 115–127.

Pavlov, I. P. (1927). Conditioned Reflexes, An investigation of the physiological activity of the cerebral cortex, Translated and edited by G. V. Anrep, New York, Dover Publications.

Paylor, R., and Crawley, J. N. (1997). Inbred strain differences in prepulse inhibition of the mouse startle response. *Psychopharmacology (Berl.)* 132, 169–180.

Pellegrini, J. J., Horn, A. K., and Evinger, C. (1995). The trigeminally evoked blink reflex. I. Neuronal circuits. *Exp. Brain Res.* 107, 166–180.

Perrett, S. P., Ruiz, B. P., and Mauk, M. D. (1993). Cerebellar cortex lesions disrupt learning-dependent timing of conditioned eyelid responses. *J. Neurosci.* 13, 1708–1718.

Pilz, P. K., Caeser, M., and Ostwald, J. (1988). Comparative threshold studies of the acoustic pinna, jaw and startle reflex in the rat. *Physiol. Behav.* 43, 411–415.

Pilz, P. K., Schnitzler, H. U., and Menne, D. (1987). Acoustic startle threshold of the albino rat (*Rattus norvegicus*). *J. Comp. Psychol.* 101, 67–72.

Pitkanen, A., Savander, V., and LeDoux, J. E. (1997). Organization of intra-amygdaloid circuitries in the rat: an emerging framework for understanding functions of the amygdala. *Trends Neurosci.* 20, 517–523.

Poulet, J. F., and Petersen, C. C. (2008). Internal brain state regulates membrane potential synchrony in barrel cortex of behaving mice. *Nature* 454, 881–885.

Qiao, X., Chen, L., Gao, H., Bao, S., Hefti, F., Thompson, R. F., and Knusel, B. (1998). Cerebellar brain-derived neurotrophic factor-TrkB defect associated with impairment of eyeblink conditioning in Stargazer mutant mice. *J. Neurosci.* 18, 6990–6999.

Quirk, G. J., Repa, C., and LeDoux, J. E. (1995). Fear conditioning enhances short-latency auditory responses of lateral amygdala neurons: parallel recordings in the freely behaving rat. *Neuron* 15, 1029–1039.

Rasmussen, A., Jirenhed, D. A., and Hesslow, G. (2008). Simple and complex spike firing patterns in purkinje cells during classical conditioning. *Cerebellum* 7, 563–566.

Rescorla, R. A., and Solomon, R. L. (1967). Two-process learning theory: relationships between Pavlovian conditioning and instrumental learning. *Psychol. Rev.* 74, 151–182.

Richardson, R. T., and Thompson, R. F. (1984). Amygdaloid unit activity during classical conditioning of the nictitating membrane response in rabbit. *Physiol. Behav.* 32, 527–539.

Rogan, M. T., Staubli, U. V., and LeDoux, J. E. (1997). Fear conditioning induces associative long-term potentiation in the amygdala. *Nature* 390, 604–607.

Rosen, J. B., Hitchcock, J. M., Sananes, C. B., Miserendino, M. J., and Davis, M. (1991). A direct projection from the central nucleus of the amygdala to the acoustic startle pathway: anterograde and retrograde tracing studies. *Behav. Neurosci.* 105, 817–825.

Ruigrok, T. J., and Voogd, J. (2000). Organization of projections from the inferior olive to the cerebellar nuclei in the rat. *J. Comp. Neurol.* 426, 209–228.

Rumpel, S., LeDoux, J., Zador, A., and Malinow, R. (2005). Postsynaptic receptor trafficking underlying a form of associative learning. *Science* 308, 83–88.

Sacchetti, B., Scelfo, B., and Strata, P. (2005). The cerebellum: synaptic changes and fear conditioning. *Neuroscientist.* 11, 217–227.

Sacchetti, B., Scelfo, B., and Strata, P. (2009). Cerebellum and emotional behaviour. *Neuroscience* 162, 756–762.

Sacchetti, B., Scelfo, B., Tempia, F., and Strata, P. (2004). Long-term synaptic changes induced in the cerebellar cortex by fear conditioning. *Neuron* 42, 973–982.

Sakamoto, T., and Endo, S. (2008). GABAA receptors in deep cerebellar nuclei play important roles in mouse eyeblink conditioning. *Brain Res.* 1230, 125–137.

Sanchez, C. (2003). Stress-induced vocalisation in adult animals. A valid model of anxiety? *Eur. J. Pharmacol.* 463, 133–143.

Scelfo, B., Sacchetti, B., and Strata, P. (2008). Learning-related long-term potentiation of inhibitory synapses in the cerebellar cortex. *Proc. Natl. Acad. Sci. U.S.A.* 105, 769–774.

Schmaltz, L. W., and Theios, J. (1972). Acquisition and extinction of a classically conditioned response in hippocampectomized rabbits (*Oryctolagus cuniculus*). *J. Comp. Physiol. Psychol.* 79, 328–333.

Shi, C., and Davis, M. (1999). Pain pathways involved in fear conditioning measured with fear-potentiated startle: lesion studies. *J. Neurosci.* 19, 420–430.

Skelton, R. W. (1988). Bilateral cerebellar lesions disrupt conditioned eyelid responses in unrestrained rats. *Behav. Neurosci.* 102, 586–590.

Smith, D. R., Gallagher, M., and Stanton, M. E. (2007). Genetic background differences and nonassociative effects in mouse trace fear conditioning. *Learn. Mem.* 14, 597–605.

Steinmetz, J. E., Lavond, D. G., and Thompson, R. F. (1989). Classical conditioning in rabbits using pontine nucleus stimulation as a conditioned stimulus and inferior olive stimulation as an unconditioned stimulus. *Synapse* 3, 225–233.

Steinmetz, J. E., Logan, C. G., Rosen, D. J., Thompson, J. K., Lavond, D. G., and Thompson, R. F. (1987). Initial localization of the acoustic conditioned stimulus projection system to the cerebellum essential for classical eyelid conditioning. *Proc. Natl. Acad. Sci. U.S.A.* 84, 3531–3535.

Steinmetz, J. E., Rosen, D. J., Chapman, P. F., Lavond, D. G., and Thompson, R. F. (1986). Classical conditioning of the rabbit eyelid response with a mossy-fiber stimulation CS: I. Pontine nuclei and middle cerebellar peduncle stimulation. *Behav. Neurosci.* 100, 878–887.

Supple, W. F. Jr., and Leaton, R. N. (1990). Lesions of the cerebellar vermis and cerebellar hemispheres: effects on heart rate conditioning in rats. *Behav. Neurosci.* 104, 934–947.

Svensson, P., Bengtsson, F., and Hesslow, G. (2006). Cerebellar inhibition of inferior olivary transmission in the decerebrate ferret. *Exp. Brain Res.* 168, 241–253.

Tracy, J. A., Thompson, J. K., Krupa, D. J., and Thompson, R. F. (1998). Evidence of plasticity in the pontocerebellar conditioned stimulus pathway during classical conditioning of the eyeblink response in the rabbit. *Behav. Neurosci.* 112, 267–285.

Trigo, J. A., Gruart, A., and Delgado-Garcia, J. M. (1999). Discharge profiles of abducens, accessory abducens, and orbicularis oculi motoneurons during reflex and conditioned blinks in alert cats. *J. Neurophysiol.* 81, 1666–1684.

Van Der Giessen, R. S., Koekkoek, S. K., van Dorp, S., De Gruijl, J. R., Cupido, A., Khosrovani, S., Dortland, B., Wellershaus, K., Degen, J., Deuchars, J., Fuchs, E. C., Monyer, H., Willecke, K., De Jeu, M. T., and De Zeeuw, C. I. (2008). Role of olivary electrical coupling in cerebellar motor learning. *Neuron* 58, 599–612.

van Ham, J. J., and Yeo, C. H. (1996a). The central distribution of primary afferents from the external eyelids, conjunctiva, and cornea in the rabbit, studied using WGA-HRP and B-HRP as transganglionic tracers. *Exp. Neurol.* 142, 217–225.

van Ham, J. J., and Yeo, C. H. (1996b). Trigeminal inputs to eyeblink motoneurons in the rabbit. *Exp. Neurol.* 142, 244–257.

Villarreal, R. P., and Steinmetz, J. E. (2005). Neuroscience and learning: lessons from studying the involvement of a region of cerebellar cortex in eyeblink classical conditioning. *J. Exp. Anal. Behav.* 84, 631–652.

Vogel, R. W., Ewers, M., Ross, C., Gould, T. J., and Woodruff-Pak, D. S. (2002). Age-related impairment in the 250-millisecond delay eyeblink classical conditioning procedure in C57BL/6 mice. *Learn. Mem.* 9, 321–336.

Wada, N., Kishimoto, Y., Watanabe, D., Kano, M., Hirano, T., Funabiki, K., and Nakanishi, S. (2007). Conditioned eyeblink learning is formed and stored without cerebellar granule cell transmission. *Proc. Natl. Acad. Sci. U.S.A.* 104, 16690–16695.

Weeks, A. C., Connor, S., Hinchcliff, R., LeBoutillier, J. C., Thompson, R. F., and Petit, T. L. (2007). Eye-blink conditioning is associated with changes in synaptic ultrastructure in the rabbit interpositus nuclei. *Learn. Mem.* 14, 385–389.

Weisz, D. J., Harden, D. G., and Xiang, Z. (1992). Effects of amygdala lesions on reflex facilitation and conditioned response acquisition during nictitating membrane response conditioning in rabbit. *Behav. Neurosci.* 106, 262–273.

Welsh, J. P. (1992). Changes in the motor pattern of learned and unlearned responses following cerebellar lesions: a kinematic analysis of the nictitating membrane reflex. *Neuroscience* 47, 1–19.

Welsh, J. P., and Harvey, J. A. (1989). Cerebellar lesions and the nictitating membrane reflex: performance deficits of the conditioned and unconditioned response. *J. Neurosci.* 9, 299–311.

Welsh, J. P., Yamaguchi, H., Zeng, X. H., Kojo, M., Nakada, Y., Takagi, A., Sugimori, M., and Llinas, R. R. (2005). Normal motor learning during pharmacological prevention of Purkinje cell long-term depression. *Proc. Natl. Acad. Sci. U.S.A.* 102, 17166–17171.

Whalen, P. J., and Kapp, B. S. (1991). Contributions of the amygdaloid central nucleus to the modulation of the nictitating membrane reflex in the rabbit. *Behav. Neurosci.* 105, 141–153.

Won, J., and Silva, A. J. (2008). Molecular and cellular mechanisms of memory allocation in neuronetworks. *Neurobiol Learn Mem* 89, 285–292.

Woody, C. D., and Aou, S. (1999). Identification of differently timed motor components of conditioned blink responses. *Brain Res.* 836, 79–89.

Yeo, C. H., and Hardiman, M. J. (1992). Cerebellar cortex and eyeblink conditioning: a reexamination. *Exp. Brain Res.* 88, 623–638.

Yeo, C. H., Hardiman, M. J., and Glickstein, M. (1985). Classical conditioning of the nictitating membrane response of the rabbit. III. Connections of cerebellar lobule HVI. *Exp. Brain Res.* 60, 114–126.

Yeo, C. H., and Hesslow, G. (1998). Cerebellum and conditioned reflexes. *Trends Cogn. Sci.* 2, 322–330.

Yeomans, J. S., and Frankland, P. W. (1995). The acoustic startle reflex: neurons and connections. *Brain Res. Brain Res. Rev.* 21, 301–314.

Yuzaki, M. (2003). The delta2 glutamate receptor: 10 years later. *Neurosci. Res.* 46, 11–22.

Conflict of Interest Statement: The authors declare that the research was conducted in the absence of any commercial or financial relationships that could be construed as a potential conflict of interest.

Received: 21 July 2009; paper pending published: 21 August 2009; accepted: 29 November 2009; published online: 04 January 2010.

Citation: Boele HJ, Koekkoek SKE and De Zeeuw CI (2010) Cerebellar and extracerebellar involvement in mouse eyeblink conditioning: the ACDC model. Front. Cell. Neurosci. ***3****:19. doi: 10.3389/neuro.03.019.2009*

frontiers in
CELLULAR NEUROSCIENCE

ORIGINAL RESEARCH ARTICLE
published: 14 May 2010
doi: 10.3389/fncel.2010.00012

A realistic large-scale model of the cerebellum granular layer predicts circuit spatio-temporal filtering properties

Sergio Solinas[1,2], Thierry Nieus[3] and Egidio D'Angelo[1,2]*

[1] *Department of Physiology, University of Pavia and Consorzio Nazionale Interuniversitario per le Scienze Fisiche della Materia, Pavia, Italy*
[2] *Brain Connectivity Center, Istituto Neurologico IRCCS fondazione C. Mondino, Pavia, Italy*
[3] *Neuroscience and Brain Technology, Italian Institute of Technology, Genova, Italy*

Edited by:
James M. Bower, University of Texas at San Antonio, USA

Reviewed by:
Fidel Santamaria, University of Texas at San Antonio, USA
James M. Bower, University of Texas at San Antonio, USA

****Correspondence:***
Egidio D'Angelo, Department of Physiology, University of Pavia, Via Forlanini 6, 27100 Pavia, Italy.
e-mail: dangelo@unipv.it

The way the cerebellar granular layer transforms incoming mossy fiber signals into new spike patterns to be related to Purkinje cells is not yet clear. Here, a realistic computational model of the granular layer was developed and used to address four main functional hypotheses: center-surround organization, time-windowing, high-pass filtering in responses to spike bursts and coherent oscillations in response to diffuse random activity. The model network was activated using patterns inspired by those recorded *in vivo*. Burst stimulation of a small mossy fiber bundle resulted in granule cell bursts delimited in time (time windowing) and space (center-surround) by network inhibition. This burst–burst transmission showed marked frequency-dependence configuring a high-pass filter with cut-off frequency around 100 Hz. The contrast between center and surround properties was regulated by the excitatory–inhibitory balance. The stronger excitation made the center more responsive to 10–50 Hz input frequencies and enhanced the granule cell output (with spikes occurring earlier and with higher frequency and number) compared to the surround. Finally, over a certain level of mossy fiber background activity, the circuit generated coherent oscillations in the theta-frequency band. All these processes were fine-tuned by NMDA and GABA-A receptor activation and neurotransmitter vesicle cycling in the cerebellar glomeruli. This model shows that available knowledge on cellular mechanisms is sufficient to unify the main functional hypotheses on the cerebellum granular layer and suggests that this network can behave as an adaptable spatio-temporal filter coordinated by theta-frequency oscillations.

Keywords: spatio-temporal dynamics, cerebellar cortex, neural networks, granular layer, electrophysiological modeling, NMDA receptors, GABA receptors

INTRODUCTION

The cerebellum, owing to its regular structure, has inspired several theoretical models emphasizing the combinatorial properties of the network (Marr, 1969; Albus, 1971; Tyrrell and Willshaw, 1992; Dean et al., 2010). More recently, simplified spiking models have also been developed (Maex and De Schutter, 1998; Medina and Mauk, 2000). Here, by taking advantage of recent advances in single cell and granular layer circuit physiology, a new computational model is developed that incorporates a much higher level of realism than previously possible. The model has then been used to investigate granular layer spatio-temporal dynamics and evaluate the main functional hypotheses suggested by biological investigations.

In brain slices, intracellular recordings have provided a detailed understanding of membrane and synaptic properties of single neurons (among others D'Angelo et al., 1995; Dieudonné, 1998; Forti et al., 2006; see also below), while multi-electrode array (MEA) and voltage-sensitive-dye imaging (VSD) recordings have revealed relevant aspects of ensemble granular layer activities (Mapelli and D'Angelo, 2007; D'Angelo et al., 2009; Mapelli et al., 2010a,b). Recordings *in vivo* have shown the behavior of single granular layer neurons (Vos et al., 1999; Chadderton et al., 2004; Jörntell and Ekerot, 2006; Rancz et al., 2007) and their collective activity (Roggeri et al., 2008; Courtemanche et al., 2009) in response to natural stimuli. These results have supported in turn four main functional hypotheses. (1) The granular layer response to mossy fiber bursts should be spatially organized in a center-surround pattern, where the excitatory–inhibitory balance is dominated by excitation in the center and by inhibition in the surrounding areas. (2) The granular layer should generate a time-window effect limiting the duration and intensity of the GrC output (D'Angelo and De Zeeuw, 2009). (3) The granular layer should behave as a high-pass filter allowing patterns over 50 Hz to be optimally transmitted (Mapelli et al., 2010). Finally, (4) sparse GrC random activity should be able to sustain coherent low-frequency oscillations of granular layer activity (Maex and De Schutter, 1998). However, whether and how these aspects integrate into a coherent functional framework has remained unclear.

Among the properties that may contribute to determine the granular layer function, some appear especially relevant. The cardinal structural properties include the glomerular organization of the mossy fiber inputs (Rossi and Hamann, 1998; Mapelli et al., 2009) and feed-forward, feed-back and lateral inhibition (Mapelli and D'Angelo, 2007; Kanichay and Silver, 2008). At

Abbreviations: GrC, granule cell; GoC, Golgi cell; SC/BC, stellate cell/basket cell; MLI, molecular layer interneuron; mf, mossy fiber; pf, parallel fiber.

the molecular level, special importance has been attributed to NMDA and GABA-A (α1 and α6 subunit-containing) receptors (D'Angelo et al., 1995; Cull-Candy et al., 1998; Farrant and Nusser, 2005). These are highly sensitive to neurotransmitter spillover and are suitable to set the appropriate time constants for signal processing in the cerebellar glomerulus. Finally, neurotransmitter release probability at the mf-GrC synapse, which can be tuned by long-term synaptic plasticity (D'Errico et al., 2009), regulates the time course of EPSP temporal summation and spike emission. Thus, these factors need to be taken into account to appropriately simulate granular layer dynamics in the spatial, temporal and frequency domains.

The computational reconstruction of the granular layer reported in this work was based on biophysically realistic models of granule cells (GrCs: D'Angelo et al., 2001; Diwakar et al., 2009) and Golgi cells (GoCs: Solinas et al., 2007a,b) and of their synapses (Nieus et al., 2006; Mapelli et al., 2009). The network, stimulated with patterns inspired to those observed in the mossy fibers (mfs) *in vivo*, generated center-surround, time-windowing, high-pass filtering and theta-frequency oscillations regulated by neurotransmitter release and NMDA and GABA-A synaptic receptors. Interestingly, the center-surround structure was capable of fine-tuning the delay, number, and frequency of spikes generated by GrCs suggesting that the cerebellum granular layer behaves as a complex spatio-temporal filter, which can be adapted through long-term synaptic plasticity and coordinated by coherent oscillations.

MATERIALS AND METHODS

The granular layer network structure was generated on the basis of detailed anatomical and functional information (Eccles et al., 1967; Palkovits et al., 1971, 1972; Hámori and Somogyi, 1983; Jakab and Hámori, 1988; Harvey and Napper, 1991; Korbo et al., 1993; Sultan, 2001; Barmack and Yakhnitsa, 2008) and using models of neurons and synapses including biophysical representations of membrane ionic channels and receptors (D'Angelo et al., 2001; Nieus et al., 2006; Solinas et al., 2007a,b; Diwakar et al., 2009). These neuronal and synaptic models have been extensively validated in previous works using electrophysiological and imaging data. Therefore, we have been able to develop a "realistic network model", in which the large number of parameters is constrained to biology. In this "bottom-up" approach, the functional properties of the network emerge from the properties of constitutive elements and from their synaptic organization (e.g. see Druckmann et al., 2007; Gleeson et al., 2007; Izhikevich and Edelman, 2008). The appropriateness of network responses was assessed by comparison with MEA and VSD recordings of network activity, which have recently become available for the cerebellum granular layer. Moreover, the availability of input spike patterns and neuronal responses *in vivo* (Vos et al., 1999; Chadderton et al., 2004; Jörntell and Ekerot, 2006; Rancz et al., 2007; Roggeri et al., 2008) has allowed to simulate granular layer network dynamics under conditions representative of natural activity states.

GENERAL PROPERTIES OF THE GRANULAR LAYER MODEL

The network had a size sufficient to reproduce a functionally relevant portion of the cerebellar granular layer, i.e. a cube with 100 μm edge length (**Table 1** and **Figure 1**). The model included 315 mfs, 4393 neurons (4096 GrCs, 27 GoCs and 270 SCs/BCs) and more than 40000 synapses. The number of cells and synapses was large enough to maintain realistic convergence/divergence ratios (Eccles et al., 1967). On this scale, mf branching was not implemented (see Sultan and Heck, 2003). Moreover, to achieve inhibitory control over GoCs, a partial representation of the SC/BC was also included.

Network connections were constructed using precise rules, yet allowing the number of connections and synaptic weights to show statistical variability (Gaussian distribution: mean = 1, s.d. = 0.4; see Medina and Mauk, 2000). No systematic differences were observed using different seeds for parameter randomization, so that in several cases the same network configuration was used to facilitate data

Table 1 | The constitutive elements of the granular layer network.

	Num.	Div.	Conv.	Transmitter	Receptors	Spillover	Previous models
Glomeruli	315						
GrC	4096						Nieus et al., 2006
GoC	27						Solinas et al., 2007a,b
SC/BC	270						
mf→GrC		1:53	4:1	Glutamate	AMPA, NMDA	Yes	Nieus et al., 2006
mf→GoC		1:3.6	50:1	Glutamate	AMPA, NMDA	Yes	This paper – Cesana et al., 2009
GrC→GoC (pf)		1:1.9	100:1	Glutamate	AMPA	No	This paper – from literature data
					NMDA	Yes	
					kainite	Yes	
GoC→GrC		1:600	4:1	GABA	GABA-A (a1, a6)	Yes	Mapelli et al., 2009
SC/BC→GoC		1:1	6–50:1	GABA	α-function	–	This paper

The table reports the number of elements in the network, the convergence and divergence ratios of connections, the transmitters and receptors involved, the presence of spillover and the references to previous models. All the corresponding mechanisms have been taken from the literature and are therefore not free parameters but rather constitutive elements of the network.

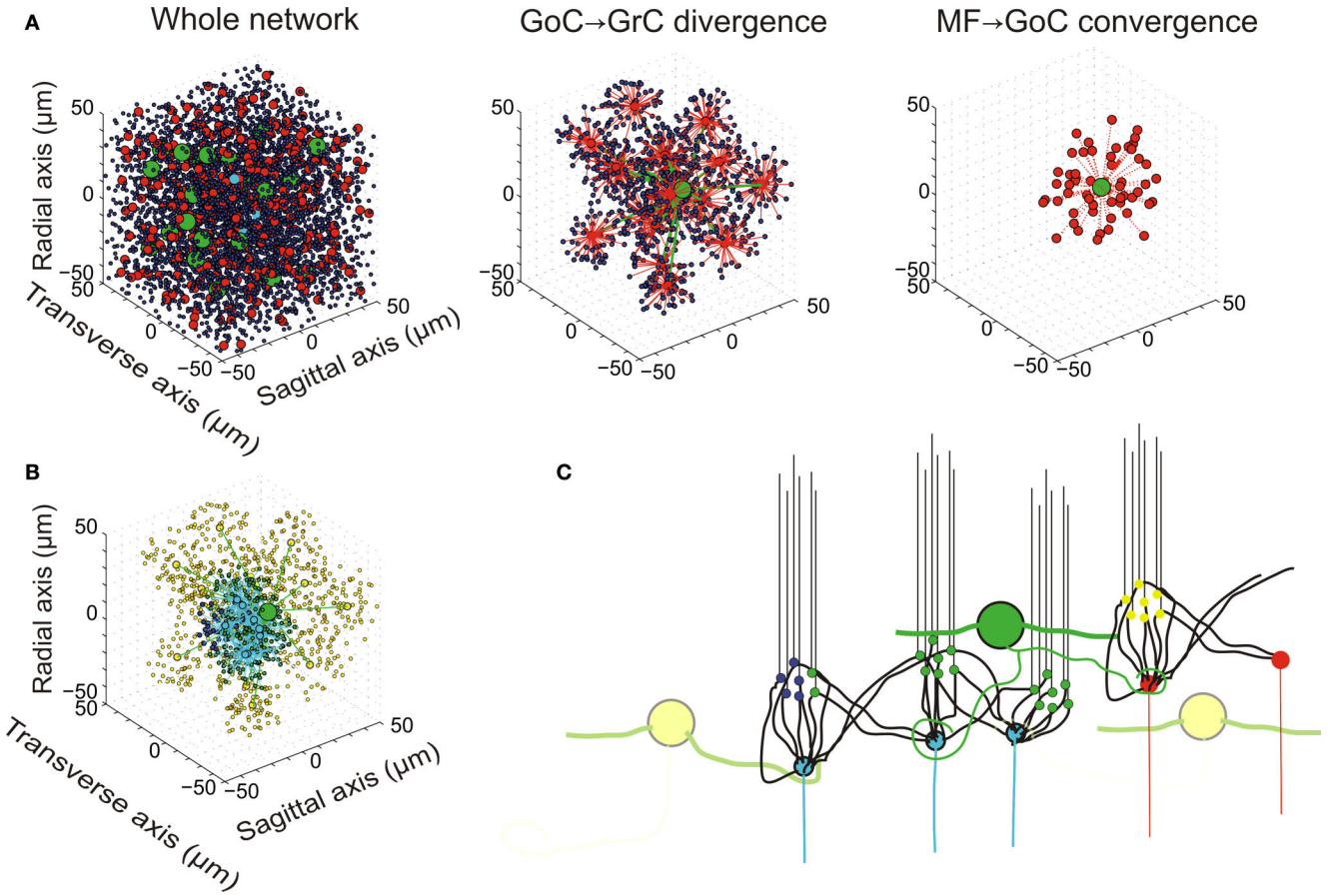

FIGURE 1 | Network topology. (A) Elements of the network. **(i)** *The whole network*: the granular layer network was simulated as a cube with edge length 100 μm. It contained 4096 GrCs (blue dots), 27 GoCs (green spheres), and 315 glomeruli (red and cyan dots). The meaning of the eight glomeruli indicated with cyan dots is explained in **(B)**. **(ii)** *GoC–GrC divergence*: the panel shows the glomeruli reached by a single GoC axon and GrCs inhibited therein. **(iii)** *Mf–GoC convergence*: The panel shows the glomeruli reaching a single GoC. Note that *GoC–GrC divergence* is wider than mf–GoC convergence, setting the basis for lateral inhibition. **(B)** Neurons responding to an input burst delivered to a small mf bundle. In this example, which is drawn from the network shown in **(A)**, eight glomeruli represented with cyan dots were supposed to delivered a burst (five spike at 500 Hz) to the network. One of the GoCs excited by the burst [the same as in **(ii)**] is indicated with a large green dot. The GrCs are indicated with small dots: GrCs that are only inhibited are yellow, GrCs that are only excited are blue, GrCs that are both excited and inhibited are green. Note that excitation is concentrated in the center and inhibition in the surround. **(C)** Schematic drawing of network connectivity [same color code as in **(B)**].

comparison. Background noise in the network was generated by random spike patterns in mfs and pacemaking in GoCs and SC/BCs (see e.g. Häusser and Clark, 1997; Chadderton et al., 2004; Rancz et al., 2007). Neurons and synapses were endowed with multiple receptor and ionic channel-based mechanisms, allowing an accurate representation of neuronal firing. The synapses were endowed with neurotransmitter diffusion mechanisms and with a representation of vesicle cycling, generating spillover and developing short-term facilitation and depression. However, no molecular noise (e.g. from ionic diffusion, channel gating or receptor binding) or synaptic noise (e.g. from stochastic vesicle fusion) were introduced.

The model was written with NEURON-7.1. The simulation of 3 s of activity required about 20 h on a Pentium-5 dual-core but just 30 min using 80 CPUS on the CASPUR parallel cluster (http://www.caspur.it/en/). A graphical interface was written to represent the data as in MEA and VSD experiments.

SPECIAL PROPERTIES OF INHIBITORY CONNECTIVITY

The most relevant aspects of granular layer network organization depend on the inhibitory connections, which are therefore considered in detail. Lateral inhibition, as in other brain areas (Buzsáki, 2006), is an important structural property of the circuit. This has been reported since early anatomical investigations (e.g. see Eccles et al., 1967) and has recently been substantiated by electrophysiological recordings (Mapelli and D'Angelo, 2007). Lateral inhibition descended from the disproportionate extension of the GoC axon compared to its dendritic afferent field (i.e., the mossy fibers excited an area including GrC and GoC basal dendrites, but then the GoC axon redistributed inhibition over a much larger area). Two relevant aspects of the inhibitory connections, which have recently been reported in experimental investigations, have been taken into account in the model (**Figure 1C**).

First, ultrastructural measurements have revealed that each GrC receives on average three GoC inhibitory synapses (Hámori and Somogyi, 1983), but has left open the problem on whether these synapses originated from the same or from different GoCs. Typically, GrC IPSCs can be recruited by raising stimulation intensity (Mapelli et al., 2009), suggesting that three to four independent GoCs are indeed connected. Recordings from GoC-GrC pairs further support this connectivity by showing that the size of the GoC-GrC IPSCs is equivalent to the minimal response generated by single fiber stimulation (Mapelli et al., 2009).

Secondly, since glomeruli receive about 50 dendrites from as many different GrCs, the additional issue is whether a GoC innervates all the GrCs impinging on the same glomerulus. Even minimal stimulation (i.e. one that activates a single synaptic contact) can elicit a direct and an indirect spillover-mediated component in GrC IPSCs (Mapelli et al., 2009). Since spillover is a sign of release on neighboring synapses in the glomerulus (Rossi and Hamann, 1998), a GoC axon should inhibit numerous (if not all) GrC dendrites in the same glomerulus.

Therefore, in addition to lateral inhibition, the GoC-GrC connections were implemented with these topological rules: a GoC was not allowed to innervate a GrC more than once (and therefore did not innervate adjacent glomeruli) and each glomerulus was fully innervated by a single GoC. In fact these rules are a simplification, since do not separate direct from indirect inhibition. An explicit representation of the glomerulus with internal diffusion allowing for independent generation of direct and indirect IPSCs may further improve this description.

NETWORK ARCHITECTURE AND GENERATION OF NETWORK CONNECTIONS

The generation of the model network occurred in three steps: (1) calculating the number of constitutive elements, (2) distributing the elements in space, and (3) connecting the elements.

(1) Starting from a GrC density of $4 \times 10^6/\text{mm}^3$, the density of GoCs was calculated to be ~$9000/\text{mm}^3$ to respect the ratio 1:430 reported by Korbo et al. (1993). The density of glomeruli was calculated from the convergence/divergence ratio of the mf-GrC connections. Each glomerulus includes a mean of 53 dendrites from different GrCs and each GrC emits on average four dendrites (Jakab and Hámori, 1988). The density of glomeruli was calculated as $(4 \times 10^6/\text{mm}^3 \times 4$ dendrites$)/(53$ dendrites/glomerulus$) \approx 3 \times 10^5/\text{mm}^3$. Although in this network there is space for just 9 GoCs, their number was increased to 27 to compensate for the inhibitory connections that should occur in GrCs (a total of $4096 \times 4 = 16384$ inhibitory connections) but cannot be generated by the nine internal GoCs (providing only $600 \times 9 = 5400$ inhibitory connections). The missing 10984 inhibitory connections were generated by 18 additional GoCs ($10984/600 = 18$) located outside the network but projecting their axons inside it.

(2) After having calculated the number of constitutive elements (GrCs, glomeruli and GoCs and their synapses), these were placed into the network volume with coordinates drawn from a uniform random distribution. The next step was to connect these elements together.

(3) The network connections were generated by applying simple rules, most of which can be directly extracted from original works on cerebellar architecture (e.g. see Eccles et al., 1967). (a) The GrC dendrites could not reach glomeruli farther than 40 μm (mean dendritic length 13.6 μm). (b) A single GrC was not allowed to project more than one dendrite inside the same glomerulus. (c) Only one GoC axon was allowed to enter a glomerulus forming inhibitory synapses on all the afferent GrC dendrites. (d) A GoC axon entering into one glomerulus was prevented from accessing the neighboring glomeruli sharing GrCs with the first glomerulus. This prevented a GrC from being inhibited twice through the same GoC, a case that does not seem to hold experimentally (see Mapelli et al., 2009). (e) Each GoC was allowed to access at most 40 glomeruli resulting in a maximum ~2000 GrCs inhibited by the same GoC. (f) GoCs received excitation from 50 glomeruli and 100 GrCs through parallel fibers (pfs) randomly selected within the network. These approximate numbers conform to existing estimates (Ito, 2006). (g) Each GoC was provided with an inhibitory input from SC/BC comprising two categories. One, equivalent to 6 SC/BC, provided a background rhythmic inhibition at 18.5 Hz (Häusser and Clark, 1997). The inhibitory SC/BC background activity was calibrated to balance the mf background activity in GoCs. The other, equivalent to 50 SC/BCs, provided dynamic inhibition through GrCs and pfs, implementing a dis-inhibitory loop. The dis-inhibitory loop was activated only to investigate network oscillations in **Figure 8E** and its intensity was regulated over various values.

In order to test the impact of the connectivity rules, in some modeling experiments a "mesh" configuration was used. The "mesh" was built after removing the connectivity rules *3c* and *3d* reported above, so that GoCs were connected to GrC distributed all over the network. Nonetheless, each GrC still received the same number of excitatory and inhibitory synapses. A competitive growth algorithm would be desirable in the future.

IMPLEMENTATION OF NETWORK DYNAMICS

The neuron (GrC and GoC) models derived from previous models, which had been carefully tested against available experimental results *in slices* (D'Angelo et al., 2001; Nieus et al., 2006; Solinas et al., 2007a,b). These models were able to reproduce all the details of spike shape, timing and frequency in response to current injection and synaptic stimulation. The synaptic models were adapted from the original scheme reported by Nieus et al. (2006) and were able to reproduce the kinetics and size of the EPSCs and IPSCs during repetitive synaptic transmission at the different synapses. These models accounted for vesicular dynamics, neurotransmitter spillover and receptor gating (including multiple closed, desensitized and open states) but not for quantal release mechanisms. The dynamics of synaptic responses were fully determined by the kinetic constants of synaptic and neuronal models. Given the short distances traveled by the spikes, axonal conduction times were considered negligible. Transmission delay was 1 ms for all the synapses.

In order to conform to *in vivo* conditions, all models had to be adapted from their original temperature T_{orig} to T_{sim} = 37°C using the correction factor $Q_{10}^{(Tsim-Torig)/10}$ (Gutfreund et al., 1995; see also Traub and Llinas, 1979; Traub et al., 1991; Vanier and Bower, 1999). We have used: Q_{10} = 3 for ionic channel gating, Q_{10} = 2.4 for receptor gating, Q_{10} = 1.5 for ionic channel permeation, Q_{10} = 1.3 for neurotransmitter diffusion, Q_{10} = 3 for Ca^{2+} pumps and buffers, Q_{10} = 1.3 (GrC) or 1.7 (GrC) for intracellular Ca^{2+} diffusion. Following adaptation at 37°C, the models were in matching with recordings at this same temperature (data not shown). The basic properties of GrCs and GoCs embedded into the granular layer network are shown in **Figures 2–4**.

SINGLE CELL AND SYNAPTIC MODELS

The GrC model was adapted from Nieus et al. (2006) by applying appropriate Q_{10} corrections. In addition, the GABA leakage conductance was increased by two times (60 μS/cm²), the Inward rectifier K^+ conductance was increase by 1.5 times (1350 μS/cm²) and the leakage reversal potential was adjusted to restoring resting potential to −70 mV (see D'Angelo et al., 2001). With this asset, the GrC model properly reproduced responses to current injection at 37°C (data not shown) and spike trains observed *in vivo* (Chadderton et al., 2004; Jörntell and Ekerot, 2006) reaching maximum firing rates as high as 500 Hz (see **Figure 2B$_1$**).

The GoC model was adapted from Solinas et al. (2007a,b) by applying appropriate Q_{10} corrections.

Without needing any further change, the GoC model properly reproduced responses to peripheral stimulation observed *in vivo* (Vos et al., 1999) and could reach a maximum firing rate of 350 Hz (see **Figure 2B$_2$**).

The SC/BC models, in the absence of detailed computational representations, were designed as random spike generators with a basal firing of 18.5 Hz (Armstrong and Rawson, 1969; Häusser and Clark, 1997).

The mf-GrC synapses take part to the formation of the cerebellar glomerulus, are glutamatergic and activate AMPA and NMDA receptors. The release, diffusion and ionic receptor mechanisms were the same reported by Nieus et al. (2006). Using a probability of release of 0.6, the model was able to faithfully reproduce postsynaptic currents recorded at 37°C *in vitro* (Saviane and Silver, 2006) and *in vivo* (Chadderton et al., 2004; Rancz et al., 2007). The time constant of the recovery from depression, τ_{REC} = 8 ms, was derived from *in vivo* measurements (Jörntell and Ekerot, 2006) and allowed to reproduce natural dynamics of short-term plasticity (the time constants of presynaptic facilitation and vesicle inactivation were set to τ_{facil} = 5 ms and τ_I = 1 ms, respectively).

The mf-GoC synapses are similar in several respects to the mf-GrC synapses. They are also located within the cerebellar glomerulus (Eccles et al., 1967) and are glutamatergic activating both AMPA and NMDA receptors (Kanichay and Silver, 2008; Cesana et al., 2009). The mf-GoC synapse was adapted from the mf-GrC synapse model (see above) to reproduce a peak postsynaptic current of −66 pA (Cesana et al., 2009; see **Figures 2–5**). Release probability and vesicle cycling parameters were set at the same values as at the mf-GrC synapse.

The GrC-GoC synapses are formed by pfs onto GoC apical dendrites in the molecular layer (Palay and Chan-Palay, 1974). These glutamatergic synapses activate AMPA, NMDA and Kainate-receptors (Dieudonné, 1998; Bureau et al., 2000; Misra et al., 2000). During repetitive stimulation, the AMPA current shows synaptic depression while the Kainate and NMDA currents show slow temporal summation. AMPA and NMDA currents were taken from the mf-GrC synapses and the kainate receptor current was modified from the AMPA kinetic scheme. Release probability was 0.1 and vesicle cycling parameters were set at the same values as at the mf-GrC synapse.

The *GoC-GrC synapses* are GABAergic and impinge on GrC dendrites within the glomeruli. GABAergic neurotransmission was modeled based on Mapelli et al. (2009). The GABA-A receptor schemes comprised channels with fast (α1) and slow (α6) kinetics and GABA spillover generating the transient and sustained components of inhibition observed experimentally. In order to account for experimental results (Mapelli et al., 2009), the parameters describing presynaptic dynamics were: release probability = 0.35, τ_{REC} = 36 ms, τ_{facil} = 58.5 ms and τ_I = 0.1 ms, respectively (Mapelli et al., 2009).

The *SC/BC-GoC synapses* are GABAergic and impinge on the GrC apical dendrites in the molecular layer. The postsynaptic current resulting from a single spike was described by a double-exponential function with τ_1 = 0.26 ms, τ_2 = 15 ms, and 1370 pS maximum conductance, similar to synapses made by the same neurons onto Purkinje cells (see Jaeger et al., 1997).

PATTERNS OF ACTIVITY

The granular layer shows a background activity state, over which the mf inputs generate evoked responses. In brain slice recordings, mfs and GrCs are silent, GoCs show rhythmic spontaneous activity at around 6 Hz (Dieudonné, 1998; Forti et al., 2006) and SC/BCs show rhythmic spontaneous activity at around 18.5 Hz (Häusser and Clark, 1997). Evoked activity occurs in GrC clusters of about 30 μm diameter (Mapelli et al., 2010a), which may represent granular layer functional units (Sultan and Heck, 2003). In the anesthetized rat *in vivo*, the mfs show a low basal activity (<1 Hz), GrCs generate sporadic spikes (<0.1 Hz) (Chadderton et al., 2004; Rancz et al., 2007), GoCs show a basal activity at 1–18 Hz (mean = 8.42, numeric cv = 0.43; Vos et al., 1999) and SC/BCs show a basal activity at 47 ± 17 Hz (Wang et al., 2009). Following punctuate sensory stimulation, mfs convey high-frequency bursts and GrCs and GoCs respond after short delay generating themselves short bursts at 200–300 Hz (Vos et al., 1999, 2000; Chadderton et al., 2004; Jörntell and Ekerot, 2006; Rancz et al., 2007). These responses are clustered in small areas and can be detected by measuring the corresponding local field potentials (Roggeri et al., 2008).

Spontaneous activity

Background activity in the model was generated by the following mechanisms. (i) The mfs were activated with a random spiking activity. Spike timing was drawn from a Poisson distribution (mean = 1 Hz, cv_2 = 0.9; see below for cv_2 definition). (ii) GoCs were spontaneously active and their spike frequency and cv_2 matched the range reported *in vivo* once mfs and SC/BC were made active them-

selves. (iii) SC/BCs were endowed with a random spiking activity drawn from a Poisson distribution (mean = 18.5 Hz, cv2 = 0.9). It should be noted that SC/BC functions were critical to control the basal activity state of GoCs. When the SC/BC random activity was turned off, the GoCs showed an unnaturally high firing frequency and blocked granular layer signal processing (unpublished observations).

Evoked activity

The mf bursts generated by punctuate tactile stimulation are composed of 5–10 spikes with an average frequency around 100 Hz and instantaneous frequencies as high as 700 Hz in the anesthetized rat (Chadderton et al., 2004; Rancz et al., 2007). More protracted stimuli have been reported to generate longer bursts with frequencies modulated between a few Hz and 500 Hz in the behaving monkey (Kase et al., 1980) and up to 1000 Hz in the decerebrated cat (Jörntell and Ekerot, 2006). Evoked activity was simulated by stimulating eight contiguous unbranched mfs in the middle of the network (see **Figure 1**), which activated ~30 μm large GrC clusters. The stimuli consisted in spike bursts of different frequencies and duration, as indicated in the specific result sections (**Figures 2–7**), overriding the ongoing background activity.

DATA ANALYSIS

Simulation results were stored for offline analysis and processed using customized MATLAB programs (The MathWorks, Natick, MA, USA).

Single cell activities were analyzed as in ordinary patch-clamp experiments (averages of up to 150 simulations were required to overcome the irregularity generated by background network activity). The auto- and cross-correlograms (e.g. see **Figure 8**) were generated using data from 3-s long simulations. In order to display the average firing rate of an individual cell, the histograms were normalized by the total number of cells, by the number of stimulation spikes and by the bin width (1 ms).

Spatially organized activity was analyzed as in VSD experiments. Activity images (e.g. see **Figure 5A**) were reconstructed from the membrane potential of individual GrCs generating an average response within a volume. The peak of the cumulative depolarization of GrCs contained within the given volume was in fact a function of spike synchrony and frequency (see Mapelli et al., 2010b). To keep into account image blurring due to light diffraction in VSD imaging recordings (Mapelli et al., 2010b), simulated images were constructed from GrCs located within ±10 μm from the focal plane. The spatial profile of responses to focal mf stimulation was constructed by computing the mean depolarization of GrCs located within spherical shells with radius between 5 and 35 μm from the core of excitation. The gain of transmission of mf bursts was evaluated by measuring the granular layer output at a given frequency relative to the single-pulse response (**Figure 7**).

In order to quantify the excitatory–inhibitory balance (E-I balance), the reconstructed VSD images were analyzed as in MEA experiments. The network was stimulated to make a doublet of spikes. The intensity of excitation was measured at the peak of the first spike in control conditions. The intensity of inhibition was estimated by the changes in the second spike caused by GABA receptor blockage (see Mapelli and D'Angelo, 2007; see **Figure 5**).

In this work three definitions of the coefficient of variation were used for consistency with different experimental works: cv = SD/mean, numeric cv = MAD/median, cv_2 = mean $[2 \times |ISI_{n+1} - ISI_n|/(ISI_{n+1} + ISI_n)]$ (Holt et al., 1996).

RESULTS

RESPONSE OF SINGLE GrCs AND GoCs EMBEDDED INTO THE GRANULAR LAYER NETWORK

Once embedded into the network, single neurons receive a continuous barrage of excitatory and inhibitory synaptic inputs driven by network-dependent activity. This can alter short-term facilitation and depression and the threshold and precision of spike firing (Dobrunz and Stevens, 1999; Klyachko and Stevens, 2006). The intrinsic responsiveness and synaptic activation of single GrCs and GoCs was assessed in model neurons embedded into the simulated granular layer network (**Figures 2–4**), which generated a continuous background activity (see Materials and Methods). Intrinsic responsiveness was assessed through intracellular current injection and synaptic responses were elicited by delivering a 100-Hz burst composed of five impulses over a small bundle of eight adjacent and unbranched mfs. With this stimulus, the response occupied a surface of about 30 μm diameter reflecting the spots observed with VSD recordings in slices (Mapelli et al., 2010a,b) and matching the granular layer functional units reported by Sultan and Heck (2003) (the spatial aspects of the response are considered in detail below, see **Figures 5 and 6**).

The *GrC* model (**Figure 2A1**) background activity comprised EPSPs generated by mfs and IPSPs generated by GoCs, while spontaneous firing was almost absent. The GrC model properly reproduced responses to current injection (**Figure 2B1**; D'Angelo et al., 1995, 2001). Most salient properties were non-sagging inward rectification in the subthreshold range and regular firing with almost no adaptation during depolarization, with maximum frequencies as high as 500 Hz (**Figure 2B1**). In response to a brief mf burst, the GrC model showed various responses depending on the number of active excitatory synapses and on the number and timing of IPSPs received through the mf-GoC-GrC (feed-forward) and mf-GrC-GoC-GrC (feed-back) loops (**Figure 2C1**). In response to a short mf spike burst, the GrC model generated EPSPs showing short-term depression of the transient component and temporal summation of the protracted component, which could lead to brief spike bursts. The background and evoked activity of GrCs faithfully reproduced patch-clamp recordings *in vivo* (Eccles et al., 1967; Chadderton et al., 2004; Jörntell and Ekerot, 2006; Rancz et al., 2007).

The *GoC* model (**Figure 2A2**) showed spontaneous activity determined by its pacemaker properties (Dieudonné, 1998; Forti et al., 2006) and modulated by mf, pf and SC/BC synaptic inputs. The GoC maintained a firing rate of 8.4 Hz with cv_2 = 0.44, consistent with recordings *in vivo* (Vos et al., 1999; Solinas et al., 2007b). Upon current injection (**Figure 2A2**), the GoC model showed the complex repertoire of dynamic rebounds observed in recordings in slices, including firing with adaptation during depolarization, sagging inward rectification during hyperpolarization, rebound excitation on return to the resting state from

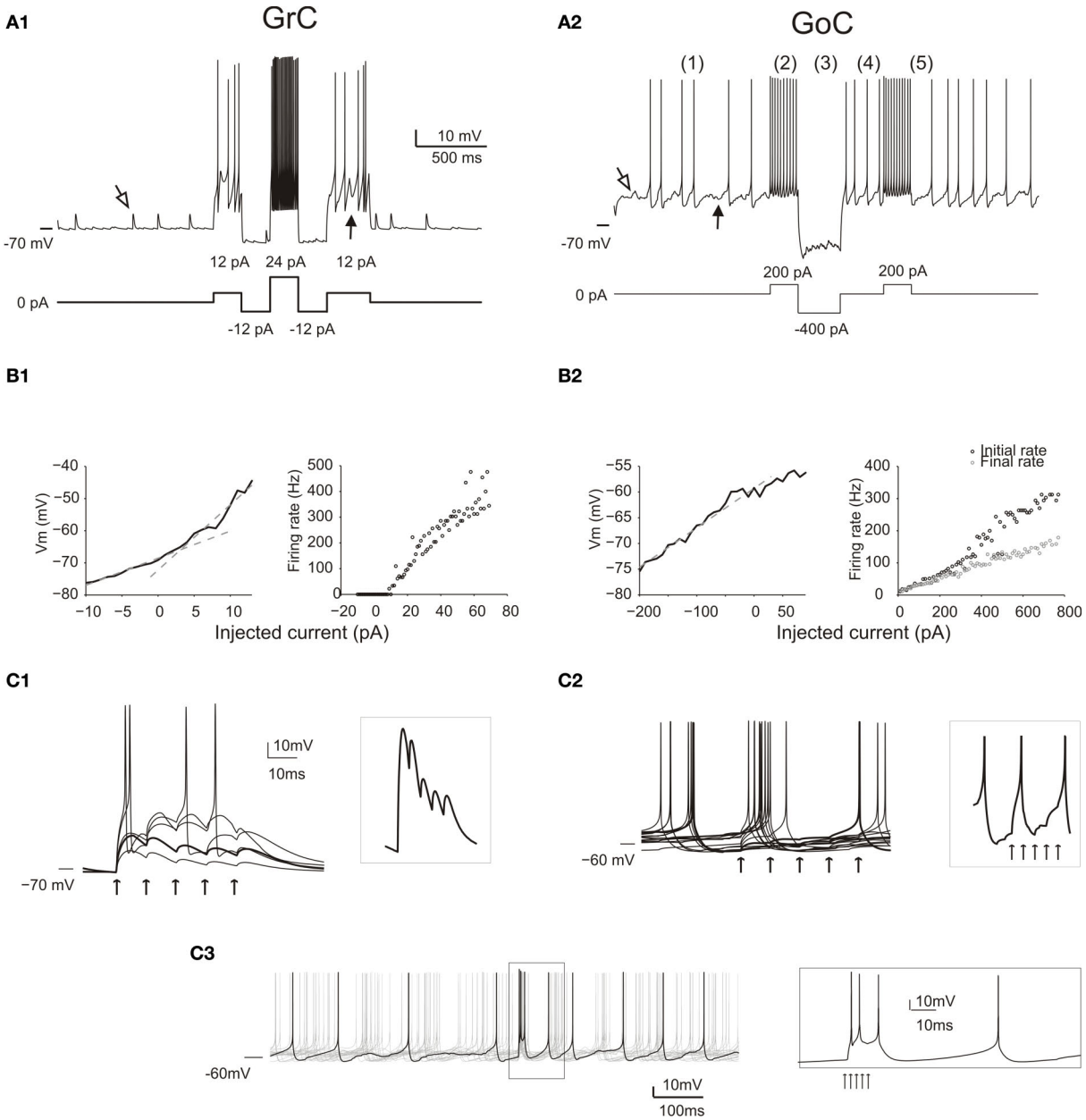

FIGURE 2 | Responses of GrCs and GoCs in the network. (A) The response of a GrC **(A1)** and a GoC **(A2)** to current injection. As in all the following simulations, the neurons are affected by background activity. The GrCs show EPSPs (open arrow) caused by mf activity and IPSPs (filled arrow) caused by GoC activity (the IPSPs are only visible when the neuron is depolarized, since GABA-A receptor Cl^- reversal potential is almost coincident with resting potential). The GoC shows a low-amplitude synaptic noise, caused by mf and pf EPSPs (open arrow) and by SC/BC IPSPs (filled arrow), and low-frequency spiking due to intrinsic pacemaking. Both the GrC and the GoC maintain their characteristic discharge patterns previously described in slice preparations. The GrC shows a discharge proportional to injected current. The GoC shows (1) pacemaking, (2) spike frequency adaptation during depolarization, (3) sagging inward rectification, (4) rebound excitation following hyperpolarization, (5) phase reset after a high-frequency burst. **(B)** Input–output relationships for a GrC **(B1)** and a GoC **(B2)** in response to current injection. The GrC shows fast inward rectification (the V/I curve is fitted with two straight lines, with slope corresponding to input resistance of 842 MOhm and 2 GOhm, respectively). The GrC shows an almost linear spike frequency increase up to 500 Hz. The GoC does not show fast inward rectification (the V/I curve is fitted with a single straight lines, with slope corresponding to input resistance 80 MOhm). The GrC shows an almost linear spike frequency increase up to 300 Hz and a rapid adaptation nearly halving the firing frequency. **(C)** The effect of an input spike burst (five spikes at 100 Hz on eight contiguous mfs) on GrCs **(C1)** and GoCs **(C2, C3)**. Examples are taken from neurons receiving a variable number of mf inputs. The GrCs **(C1)** receive from one to five active inputs. With weak activation EPSP short-term depression is visible (thick trace also enlarged in the inset), while with strong activation the GrCs emit short spike bursts. When the GoC receives eight active mf inputs **(C2)**, the different traces show a single spike occurring at different phases of the pacemaking cycle followed by phase reset. Individual EPSPs are small and barely visible (thick trace also enlarged in the inset). When the GoC receives 45 mf inputs (5 spikes at 500 Hz) **(C3)**, the traces show a short burst of two to three spikes at high frequency followed by phase-reset. The spikes in the burst (see inset) arise in 1.5 ms after the stimulus and then occur after 3.3, 7.6 and 47.2 ms.

hyperpolarization and phase-reset on return to the resting state from burst firing (Solinas et al., 2007a,b). The GoC model reached firing rates as high as 350 Hz (**Figure 2B2**). In response to a brief mf burst (**Figure 2C2**), the GoC model generated EPSPs determined by direct mf-GoC activation and by propagation of activity through the mf-GrC-GoC loop (Cesana et al., 2009). With a weak input (8 mfs) the GoC generated a single spike and phase reset the pacemaker. With a strong input (45 mfs) the GoC generated a brief burst composed of two to three spikes followed by phase reset (**Figure 2C$_3$**, inset) as observed following punctuate stimulation *in vivo* (Vos et al., 1999; Solinas et al., 2007b). The spikes were generated in 1.5 ms and the burst reached an initial frequency of over 300 Hz (cf. Kanichay and Silver, 2008). The background and evoked activity of GoCs as well as their firing patterns are in keeping with extracellular recordings *in vivo* (for review and other references see D'Angelo, 2008).

These simulations show that the GrC and GoC models [for GrCs: D'Angelo et al. (2001), Nieus et al. (2006), Diwakar et al., (2009); for GoCs: Solinas et al. (2007a,b)] adapted to 37°C and subjected to background and stimulated network activity, were able to reproduce the typical response patterns observed *in vivo* [for GrC: Chadderton et al. (2004), Jörntell and Ekerot (2006), Rancz et al. (2007); for GoC: Vos et al. (1999)].

SUBCELLULAR MECHANISMS DETERMINE TIMING OF GrC AND GoC RESPONSES IN THE NETWORK

While neuronal responses in slices look stereotyped, the responses of GrCs and GoCs embedded into the network show a remarkable variability. This is due to random background activity, to variations in the number and strength of synaptic contacts and to the assortment of excitatory and inhibitory fibers impinging on a given cell. **Figure 3** shows the cell-specific contribution of glutamate and GABA-A receptors to dendritic responses of GrCs and GoCs.

Fast excitatory transmission was ensured through AMPA receptor-mediated currents, which showed short-term depression at the mf-GrC and mf-GoC synapses and short-term facilitation at the pf-GoC synapses. Slow excitation was sustained by the NMDA and the kainate receptor-mediated currents, the former being most evident at the mf-GrC synapse and the latter being specifically expressed at the pf-GoC synapse (Dieudonné, 1998; Bureau et al., 2000; Misra et al., 2000; Kanichay and Silver, 2008; Cesana et al., 2009). Thus, whereas all excitatory synapse could efficiently react to spike bursts, only the mf-GrC synapse was sensitive to fast transitions in firing rate. Inhibition was mediated by GABA-A currents both at the GoC-GrC and at the SC/BC-GoC synapses. At the GoC-GrC synapses, GABAergic currents were protracted by the slow kinetics of GABA-A α6 receptors (see below; D'Angelo et al., 1995; Rossi and Hamann, 1998; Mapelli et al., 2009). Therefore, potentially, the network could implement the time-window mechanism (requiring fast GrC responses and delayed GoC reaction through the mf-GoC-GrC or feed-forward inhibitory loop; D'Angelo and De Zeeuw, 2009), high pass filtering (requiring frequency-dependent build-up of the burst response through NMDA currents at the mf-GrC relay), and slow oscillations (through the pf-GoC-GrC or feed-back inhibitory loop). These properties are considered below.

GLOMERULAR TRANSMISSION: POSTSYNAPTIC RECEPTOR ACTIVATION AND RELEASE PROBABILITY

Among the processes controlling the GrC response, there are some that merit specific mention, since they are thought to confer the GrC with specific integration properties: the regulation of synaptic excitation by NMDA and GABA-A receptors and the regulation of neurotransmission by mf-GrC release probability (**Figure 4A**). In addition to AMPA receptors, GrCs have the most prominent expression of NMDA receptors in the cerebellum (Cull-Candy et al., 1998) and, unique in the brain, express the α6 subunit of GABA-A receptors (Farrant and Nusser, 2005). Both NMDA and GABA-A α6 receptors have slow kinetics and are highly sensitive to neurotransmitter spillover (see also **Figure 3**).

In these simulations, blocking the NMDA receptors markedly reduced EPSP temporal summation delaying and curtailing the GrC response, while blocking GABA-A α1 and GABA-A α6 receptors sorted the opposite effect. The time of occurrence for the 1st, 2nd, 3rd, 4th spikes was 6.5 ± 1.1 ($n = 20$), 14.1 ± 1.3 ($n = 5$), 24.6 ± 1.3 ($n = 4$), 36.4 ± 1.6 ($n = 4$) ms in control; 5.4 ± 0.4 ($n = 34$), 16.0 ± 2.0 ($n = 35$), 24.4 ± 1.6 ($n = 37$), 34.5 ± 1.9 ($n = 21$) ms with α6 receptor block; 5.3 ± 0.5 ($n = 36$), 13.3 ± 1.0 ($n = 106$), 23.6 ± 0.8 ($n = 34$), 33.4 ± 0.6 ($n = 64$) ms with α1 and α6 receptor block. Thus, both α1- and α6-containing GABA-A receptors controlled the number and the regularity of GrC spike discharge.

Mf-GrC release probability can be tuned by long-term synaptic plasticity (Sola et al., 2004; D'Errico et al., 2009) and regulate the rate of short-term depression and EPSP temporal summation (Nieus et al., 2006). In the model, GrC spikes at low release probability were delayed and less numerous compared to those at high release probability (**Figure 4A**), confirming the experimental observations obtained during LTP and LTD recordings in slices and *in vivo* (Nieus et al., 2006; Roggeri et al., 2008).

Once considering the whole GrC-GoC circuit, the relative timing of GrC and GoC activity became evident (**Figure 4B**). In response to an input burst, the GrCs and GoCs coactived by the same mf set fired almost at the same time (it should be noted that the reaction time of GrCs and GoCs conforms to experimental measurements: D'Angelo et al., 1995; Kanichay and Silver, 2008; Cesana et al., 2009). An additional delay was due to the time spent at the GoC-GrC synapse for GABA release and for the opening of GABA channels. This allowed the GrCs to generate a short spike burst before being inhibited.

These observations indicate that the mechanisms and reaction times of the circuit are appropriate to implement spatio-temporal filtering according to the time-window hypothesis (see also **Figures 2 and 3**; D'Angelo and De Zeeuw, 2009).

LATERAL INHIBITION AND CENTER-SURROUND ORGANIZATION OF THE GRANULAR LAYER RESPONSE

A main organizing principle deriving from MEA (Mapelli and D'Angelo, 2007) and VSD (Mapelli et al., 2010a,b) experiments is that activation of the mf bundle generates alternated areas of excitation and inhibition, which, on average, are organized in a center-surround manner. The origin of this effect has been attributed to the larger extension of the GoC inhibitory field compared to the GoC input through the basal dendrites, but a single center-surround structure was experimentally hard to

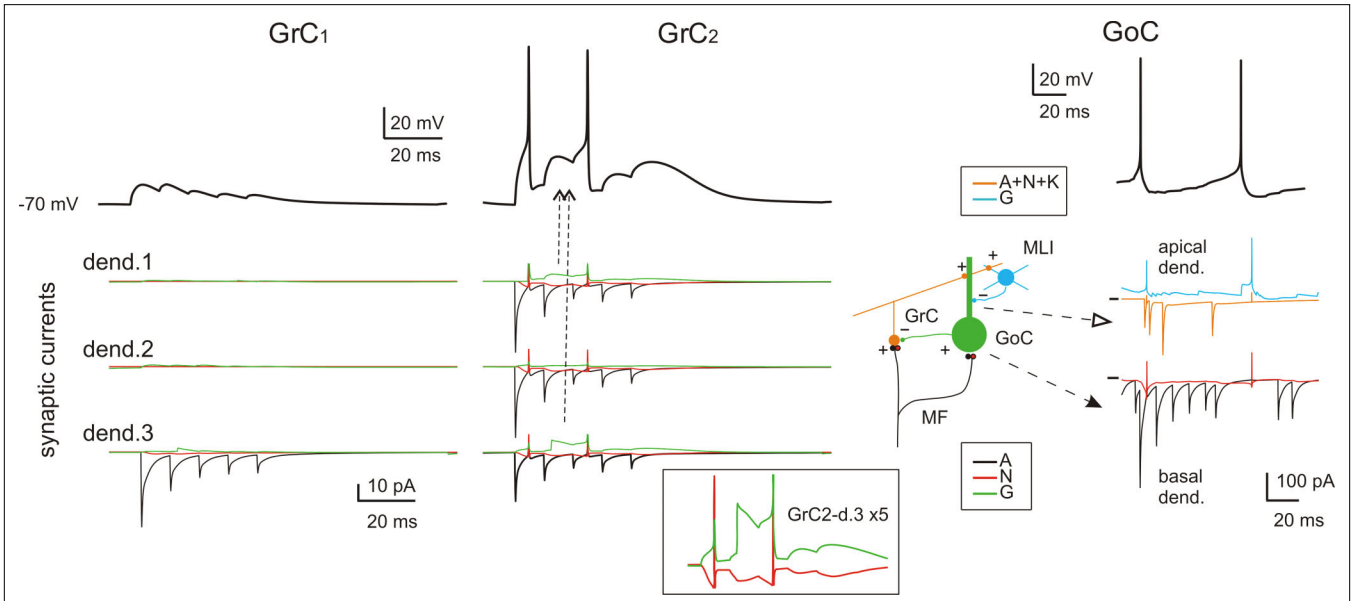

FIGURE 3 | Subcellular mechanisms of GrC and GoC responses. Response of two exemplar GrCs and one GoC activated by a mf burst (five spikes at 500 Hz on eight contiguous mfs). The top traces show intracellular membrane potential while the bottom traces show the synaptic membrane currents. All glutamate receptor-dependent currents (A = AMPA, N = NMDA, K = kainate) are downward while the GABA-A receptor-mediated currents (G = GABA-A: α1 and α6 receptor-mediated currents together) are upward, except when changes in the driving force invert the current sign (glutamate reversal potential = 0 mV and GABA reversal potential = –65 mV). GrC_1 receives only 1 mf input, GrC_2 receives 3 mf inputs and 2 GoC inputs. Note inhibition of spike generation by evoked IPSCs in GrC_2 (arrow). In contrast to AMPA current short-term depression, the inset shows the NMDA and GABA-A currents build-up up on enlarged scale (vertical axis ×5). In GoCs, several pf and mf synapses contribute to generate the glutamatergic inputs on apical and basal dendrites, respectively. The pf input involves activation of AMPA, NMDA and kainate receptors, while the mf input activates AMPA and NMDA receptors. The inhibitory input from molecular layer interneurons (MLI) occurs on the apical dendrites. Note generation of a spike doublet by the EPSCs occurring through the feed-forward (filled arrow) and feed-back (open arrow) loops. The pf EPSCs occur with some delay compared to mf EPSCs, accounting for the time required for GrC excitation and pf-GrC transmission, and are interrupted by GoC inhibition of GrCs. MLIs intensify their action just after GrC discharge contributing to terminate GoC inhibition on GrCs.

isolate. To test the center-surround hypothesis, the model was activated through eight neighboring unbranched mfs with 500-Hz bursts composed of just two spikes (similar results were also obtained with longer bursts, data not shown). Mf stimulation caused a doublet of spikes forming a spot of activity that degraded around the core. Then, blocking inhibition increased the intensity and extension of the response. As explained in our previous paper (Mapelli and D'Angelo, 2007), the difference between the response before and after inhibition allowed to quantify the excitatory–inhibitory balance (E-I balance) (**Figure 5A**, right). The E-I balance was evaluated using the first peak to estimate excitation and the changes of the second peak caused by GABA receptor blockage to estimate inhibition (see Mapelli and D'Angelo, 2007, Materials and Methods and **Figure 5B**). The spatial profile of the E-I balance revealed a Mexican-hat profile indicative of *center-surround* organization, in which inhibition overcomes excitation around the core (**Figure 5C**).

THE IMPACT OF CENTER-SURROUND ORGANIZATION ON SPIKE TRANSMISSION

The center surround organization bore consequences for the way spikes were transmitted through the granular layer. In the center, where the E-I balance is higher, the depolarization was faster and the inhibitory window closed more slowly, so that the GrCs emitted spike bursts with shorter delay, higher rate and longer duration than in the surround. This effect was particularly evident by comparing the PSTH generated by two exemplar GrCs, one in the center and the other in the surround (**Figure 6A**).

Inhibition in the model respected two rules derived from experimental observations. Just one GoC axon was allowed to enter into a glomerulus and to form inhibitory synapses on all the GrC dendrites therein. Moreover, a GoC axon entering a glomerulus was prevented from accessing the neighboring glomeruli, which shared GrCs with the first glomerulus. This prevented a GrC from being inhibited twice through the same GoC (see Mapelli et al., 2009) and clustered inhibitory synapse belonging to closed mf-GrC-GoC-GrC and mf-GoC-GrC loops. The extent to which the center-surround organization depended on this synaptic organization of inhibition was assessed by comparison with a mesh-like GoC-GrC connectivity merely based on statistics. In the mesh configuration, late spikes were more common and the time-window effect was less pronounced (**Figure 6B**). The core remained more excited after the first spike, while the surround appeared less affected (**Figure 6C**). Thus, time-window and the center-surround effects generated by the feed-forward inhibitory loop were enhanced by the specific topology of inhibitory connections.

These simulations suggest that the center-surround organization benefits of the specific connectivity of the inhibitory synapses and allows for a selective control of spike transfer through the core, as further considered below.

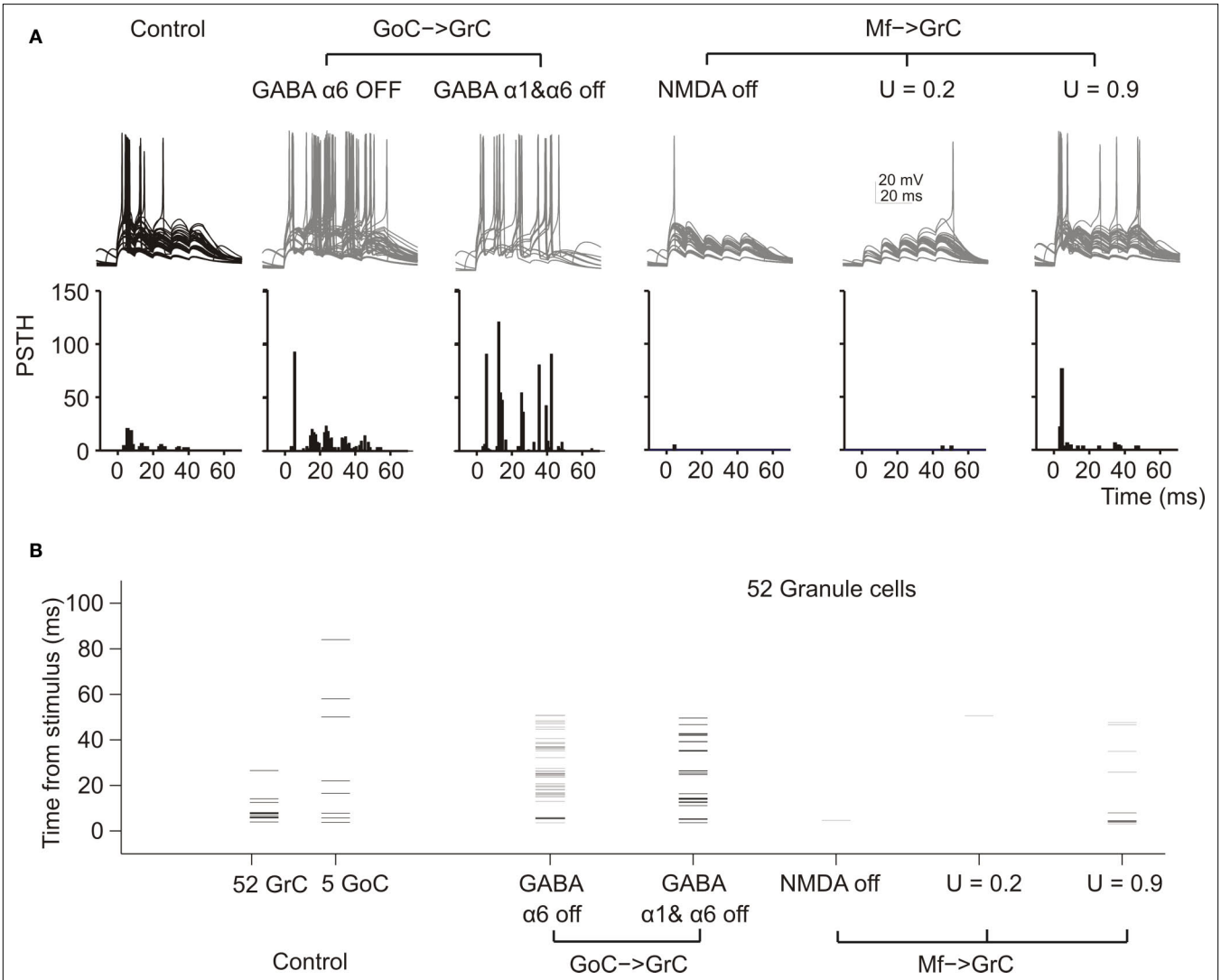

FIGURE 4 |The impact of molecular/cellular mechanisms on GrC synaptic excitation in the network. (A) Response of GrCs activated by a mf burst (five spikes at 100 Hz on eight contiguous mfs). Each group of traces corresponds to the same 52 GrCs sharing a common bursting mf. The underlying PSTH reports the probability of spike occurrence in 1-ms bins for all (250) GrCs responding to the mf burst. Note that the switch-off of GABA-A α6 receptors and even more of GABA-A α1 + GABA-A α6 receptors, which control the fast and slow components of inhibition, considerably enhances spike generation protracting the duration of the output burst. Blocking the NMDA receptors prevents EPSP temporal summation reducing the GrC response. Decreasing release probability slows down temporal summation while increasing release probability accelerates temporal summation, with opposite effects on the rate of the GrC resposne. **(B)** The raster-plot shows the timing of individual spikes in different conditions for the same 52 GrCs shown in **(A)** and for 5 GoC. Note that GoCs, through GABA-A α1 and α6 receptors, regulate the duration of the time window for GrC discharge, which normally lasts 5–10 ms from the stimulus. Repetitive GrC firing is prevented by the block of NMDA receptors and by a low release probability.

FREQUENCY-DEPENDENCE OF GRANULAR LAYER TRANSMISSION AND PREDICTIONS ON ITS REGULATION

The mfs can discharge at different frequencies (Kase et al., 1980; Van Kan et al., 1993, 1994; Arenz et al., 2008). In the model, the network was stimulated using bursts of five impulses activating eight neighboring mfs repeated at frequencies between 5 and 500 Hz (**Figure 7A**; see Materials and Methods). Raising stimulation frequency from 5 to 500 Hz increased temporal summation (**Figure 7B**) and spike generation in GrCs. As a consequence, the response increased following a sigmoidal gain curve with cut-off frequency around 100 Hz (**Figure 7C**). The frequency-dependent enhancement of excitation matched the high-pass filtering properties of the granular layer observed experimentally (Mapelli et al., 2010b).

The granular layer transmission properties strictly depended on specific synaptic receptors (**Figure 7C**). When NMDA receptors were blocked, the transmission curve was selectively depressed at low-frequency (below 20 Hz, where EPSP temporal summation was more critically dependent on NMDA receptors; cf. D'Angelo et al., 1995) but the high-pass filtering properties were maintained. When GABA-A α6 receptors were blocked, the transmission curve was enhanced especially at low frequency,

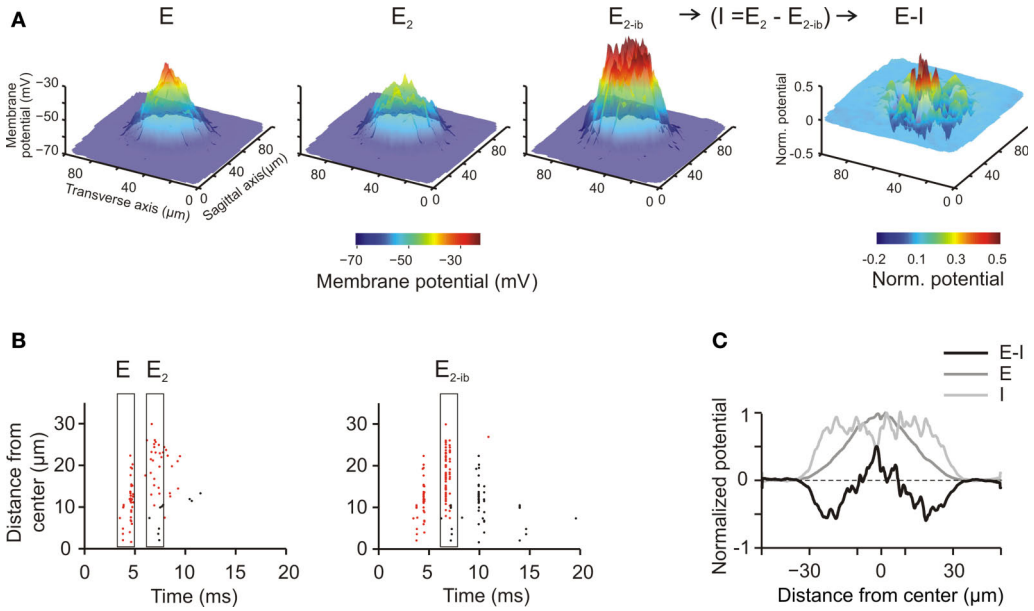

FIGURE 5 | Center surround organization and lateral inhibition. (A) Spatial pattern of GrC responses to a short mf burst (two spikes at 500 Hz on eight contiguous mfs) at the time of the first spike (E) and of the second spike (E_2). E_{2-bi} indicates the response at the time of the second spike when inhibition is blocked. Since inhibition arises after excitation, it is does not affect generation of the first spike but markedly reduces generation of the second and following spikes. Thus, the influence of inhibition on the GrC response was obtained as ($I = E–E_{2-bi}$). The difference between excitation and inhibition (E–I) reveals that inhibition is especially effective in reducing excitation around the core, generating a Mexican hat profile. The plots were the average of 10 simulations using different random seeds for synaptic connectivity. **(B)** Spikegrams for all active GrCs ordered from center to periphery [data from one of the simulation used to make **(A)**]. The first spikes are indicated by red dots, the second and following spikes by black dots. In the center the first spike occurs about 5 ms after the stimulus, whereas in the surround it tends to occur later. The second spike, which is quite rare in control, becomes well evident when inhibition is blocked. **(C)** The spatial profile of inhibition (I) was subtracted from the profile of excitation (E) to obtain the E-I balance (E-I) along a section passing through the core of the corresponding plot in **(A)** (average data obtained from 10 simulations with different random seeds for synaptic connectivity). The larger extension of inhibition compared to excitation and the Mexican-hat profile of the E-I balance are evident.

consistent with the slow time constant of these receptors. When both GABA-A α6 and GABA-A α1 receptors were blocked the transmission curve was enhanced at all frequencies and high-pass filtering was strongly reduced. These results, which are in keeping with experimental observations obtained with VSD imaging (Mapelli et al., 2010b), indicate that the high-pass filtering properties of granular layer depend on phasic GABA-A receptor-dependent transmission (no further changes were obtained by blocking the tonic GABA-A receptor-mediated current, not shown).

The granular layer transmission properties also depended on glutamate release probability at the mf-GrC synapse (**Figure 7C**). Reducing release probability from the control value 0.6 to 0.2 depressed temporal summation yielding an effect similar to blocking NMDA receptors. Raising release probability to 0.9 enhanced transmission at low-frequency but not at high-frequency (probably because EPSP short-term depression became so strong that temporal summation was prevented).

The frequency dependence of the granular layer response changed moving from the center to the surround of the responding area (**Figure 7D**). In the center, the high-pass filtering curve arose at lower frequencies and attained a higher maximum gain than in the surround. Moreover, the gain difference between center and surround was more pronounced at high than low input frequency (the ratio between gain measured at 10 and 25 μm from the core was 3 at 300 Hz, 2.3 at 100 Hz and 1.5 at 50 Hz; **Figure 7E**). Thus, the center-surround is predicted to generate complex transformations of incoming mf signals.

THE EMERGENCE OF OSCILLATION AND PREDICTIONS ON THEIR REGULATION

In vivo, GrCs show rare spontaneous activity (Chadderton et al., 2004; Jörntell and Ekerot, 2006; Rancz et al., 2007). However, in certain circumstances, the ensemble activity generated by the granular layer can take the form of coherent oscillations [7 Hz in the rat (Hartmann and Bower, 1998) and 7–25 Hz in the monkey (Pellerin and Lamarre, 1997; Courtemanche et al., 2009)]. It was not clear if this sparse GrC background activity could sustain the coherent oscillations.

In these simulations, the model was driven by random mf activity at different frequencies (see Materials and Methods) generating a sparse low-frequency discharge of GrCs (<1 Hz/cell; **Figure 8A**) reflecting the basal GrC activity recorded in the anesthetized rat (Chadderton et al., 2004; Rancz et al., 2007) and in the decerebrated cat (Jörntell and Ekerot, 2006). When basal mf activity was low (10 Hz) ensemble activity was barely detectable but when basal mf activity was higher (20–40 Hz) the granular layer generated coherent oscillations at 7–15 Hz. Coherent oscillations were never easily resolved in single GrCs, which maintained a sparse activity, but clearly emerged as a population activity in the spikegrams.

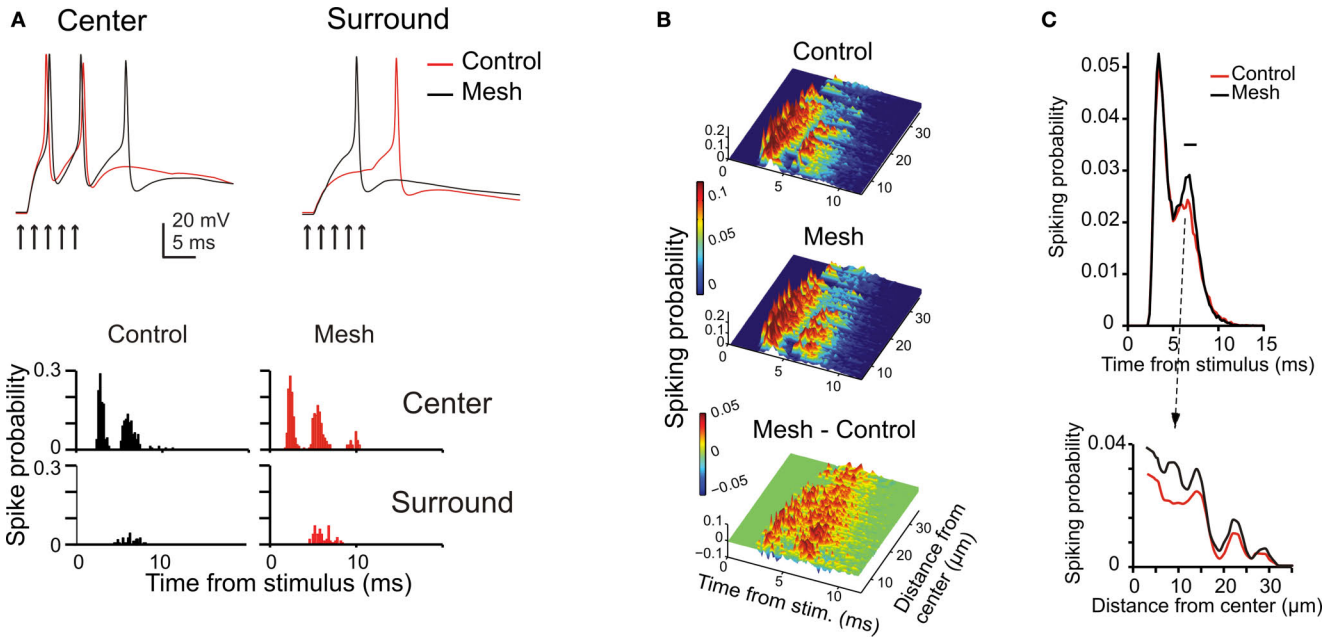

FIGURE 6 | The impact of network topology on granular layer responses. Granular layer response elicited by a mf burst (five spikes at 500 Hz on eight contiguous mfs) using the control or the mesh-like network configurations (see Materials and Methods). **(A)** The traces show that responses in the center have shorter latency and higher number of spikes than in the surround of the activated area (exemplar traces are taken at 10 and 32 μm from the core; arrows mark the time of stimulation). The PSTHs (bin width 0.5 ms) were normalized by the number of simulations. The mesh-like configuration reduces the overall level of inhibition, with a more evident effect in the surround, so that the PSTH of peripheral cells shows a remarkable increase in the second/third spike firing probability. **(B)** The PSTHs of responding GrCs were ordered according to GrC distance from the stimulus center and color coded. In the control network configuration, most neurons fire a high frequency spike doublet with short latency which, in some cases, is followed by a late spike with lower time precision. Some neurons in the periphery fire just a single late spike. The mesh network configuration shows differences in the timing of the first and second spikes and an enhanced probability of third spikes. The mesh-control plot shows sharp peaks in the early response phase due to differences in spike timing and wider peaks in the late response phase due to increase firing probability. **(C)** Time and space response profiles with control and mesh network configurations. The *upper plot* shows the mean response of all GrCs. The two curves show a significant difference at the time of the second spike. The point of maximum difference is at 7.2 ms after the stimulus and the difference is significant in the range indicated by the black bar ($p < 0.007$, *t*-test). The *lower plot* illustrates the spatial profile of control and mesh responses at the time of their maximal difference.

A measure of rhythmicity was provided by the autocorrelograms of groups of GrCs and GoCs, which showed firing at regular periods over hundreds of milliseconds. The cross-correlograms between GrCs and GoCs cells (**Figure 8B**) also showed coherent oscillations, indicating that activity in the two cell populations were correlated. The coherent granular layer oscillations followed those of GoCs with a 5- to 10-ms lag due to the time spent in the feed-back inhibitory loop.

The granular layer oscillation assumed a frequency correlated with that in the mf input, as revealed by power spectrum analysis (**Figure 8C**). The output frequency was typically in the 7–15 Hz range remaining lower than the input frequency. The oscillation was regulated by several synaptic mechanisms operating in the cerebellar glomerulus (**Figure 8Di**; cf. **Figure 4**). Blocking GrC NMDA receptors strongly reduced the PSD peak amplitude, while blocking GrC GABA-A α6 receptors markedly increased the PSD peak amplitude, reflecting opposite regulation on the feed-back (GrC-GoC-GrC) loop. Blocking both GrC GABA-A α6 and GABA-A α1 interrupted the feed-back loop and flattened the PSD curve. Another remarkable effect was generated by altering mf-GrC release probability and therefore EPSP temporal summation. Decreasing mf-GrC release probability ($p = 0.2$) reduced the PSD peak amplitude, while increasing mf-GrC release probability ($p = 0.9$) increased the PSD peak amplitude, again reflecting opposite regulation on the feed-back loop. Moreover, (**Figure 8Dii**), when the feed-back loop was enhanced (GABA-A α6 receptor block or $p = 0.9$) the PSD peak frequency was increased, while the opposite occurred when the loop was weakened. Therefore, synaptic mechanisms allowed to fine-tune the intensity and frequency of oscillations.

It should be noted that increasing the strength of the mf-GoC synapse (**Figure 8Ei**) and of the SC/BC-GoC synapse (**Figure 8Eii**) progressively reduced the PSD of oscillations. Thus, oscillations were critically dependent on circuit components that controlled the feed-back inhibitory loop.

DISCUSSION

This computational investigation provides a formal demonstration that available knowledge on cellular properties and circuit connectivity can explain center-surround and time-window effects during burst transmission and that sparse GrC random activity can sustain coherent low-frequency oscillations (D'Angelo and De Zeeuw, 2009; D'Angelo et al., 2009). The model predicts differential transmission through the center-surround structure reflecting the balance between NMDA and GABA-A receptor activation.

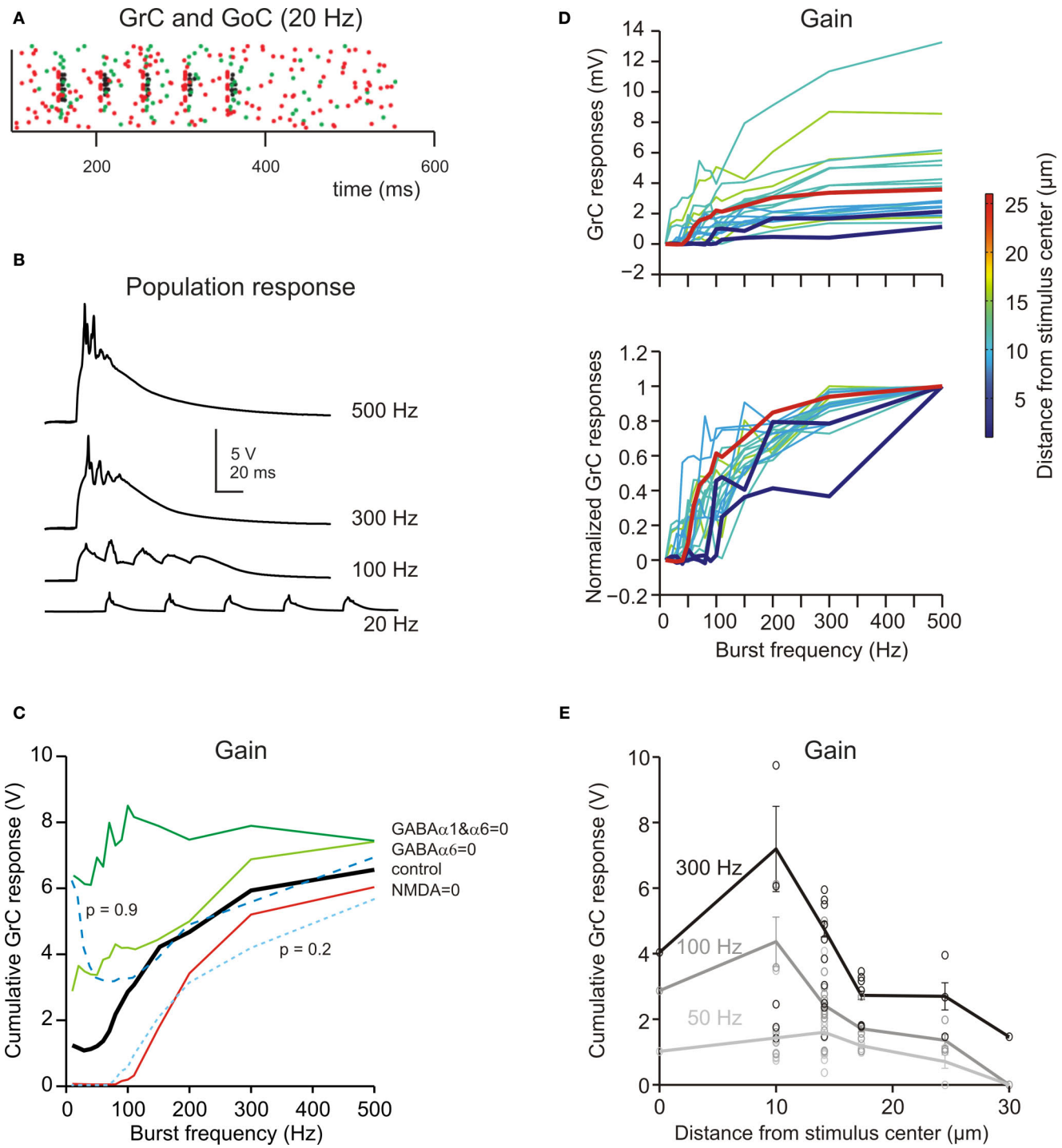

FIGURE 7 | Frequency-dependence of granular layer responses. (A) The raster plot shows the response of all GrCs (blue dots) and GoCs (green dots) to a bursts (five spikes at 20 Hz) on eight contiguous mfs (red dots). **(B)** The GrC membrane potential (traces are the sum over all active GrCs) shows poor temporal summation at low stimulation frequency (20 Hz) but marked temporal summation at high frequencies (>100 Hz). **(C)** The gain function showed a steep increase above 50 Hz. By blocking the NMDA receptors, the responses were depressed with a specific loss of transmission at low frequency. By blocking GABA receptors, the responses were enhanced with a more marked increase of transmission at low frequency. Reducing release probability ($p = 0.2$) depressed the gain curve at all frequencies, while raising release probability ($p = 0.9$) enhanced the gain curve specifically at low frequency. **(D)** The gain curve changed from the center to surround of the excited area. In the center the gain curve arose at lower frequencies and attained higher gain than in the surround. **(i)** shows absolute gain curves, **(ii)** shows normalized gain curves. Each gain trace is from a different GrC. **(E)** Gain as a function of distance from the center of the active areas. The points are measures in responding spots located along different radii (mean ± sd indicate the values along the whole circumference at the given distance; see Materials and Methods for details). The difference between center and surround in terms of gain was more pronounced at high than low input frequency.

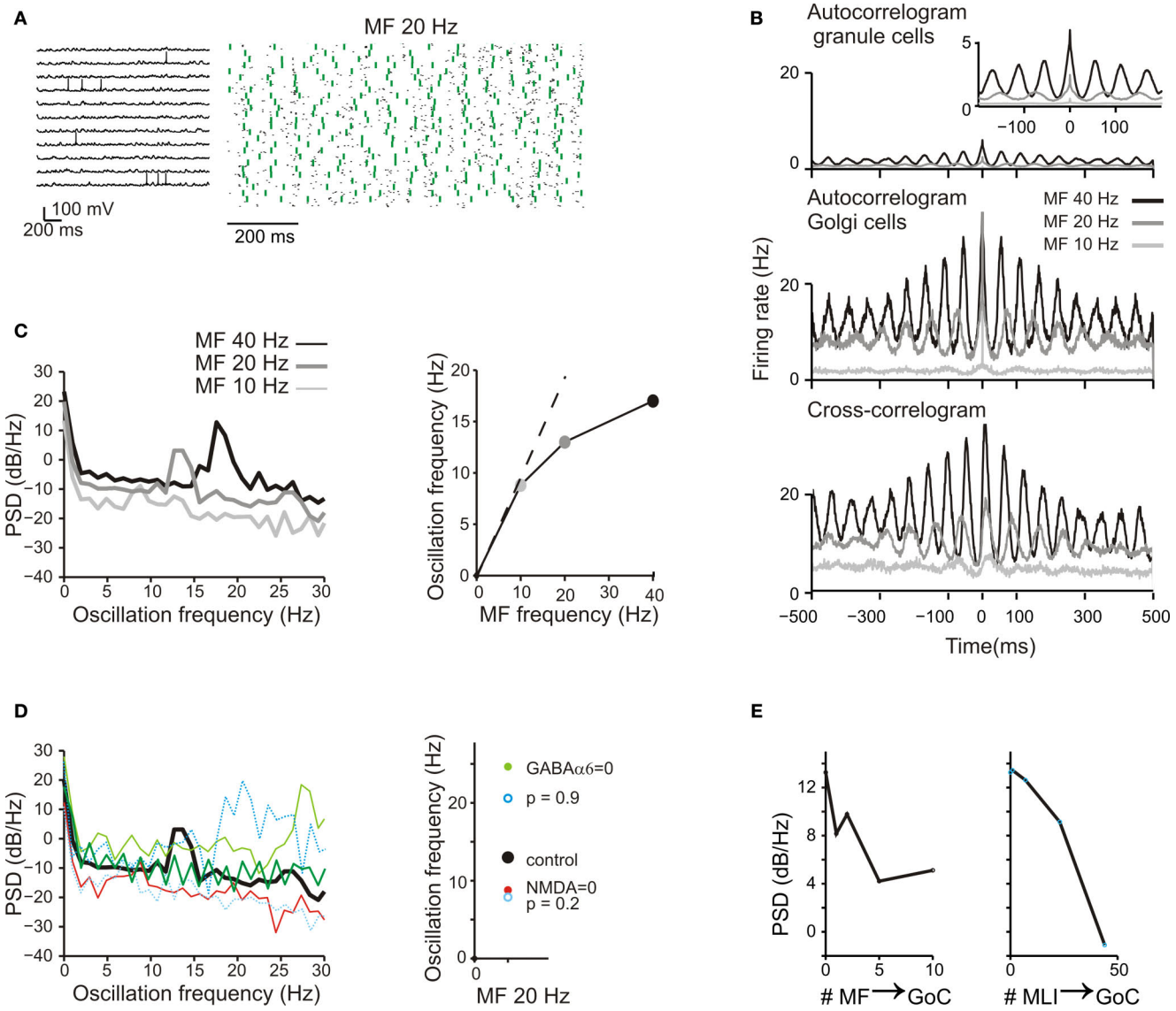

FIGURE 8 | Background activity and oscillations. (A) The response of GrCs and GoCs to a 20-Hz mf random activity. Activity of individual GrCs was sparse and appeared to occur at random and uncorrelated times [membrane potential traces, **(i)**]. However, when represented in a raster plot **(ii)**, GrC (blue dots) and GoC (green dots) activity appeared organized in a repetitive coherent pattern. **(B)** Autocorrelograms of GrC and GoC population activity at three different frequencies of the random input (10 Hz, 20 Hz, 40 Hz; **(i,ii)**). The autocorrelogram of GrCs is enlarged in the inset. The cross-correlogram shows the mean activity of the GoCs in relation to spikes fired by GrCs **(iii)**. **(C)** The power spectrum density (PSD) of the GrC population activity shows a peak between 7 and 20 Hz at the three different input frequencies [**(i)**: 10 Hz, 20 Hz, 40 Hz]. These peaks are represented as a function of the input frequency in **(ii)**. **(D)** The effect of altering neurotransmission mechanisms on the GrC power spectral density generated with a 20-Hz mf random activity. Blocking NMDA receptors reduced the PSD peak frequency, while blocking GABA-A receptors increased the PSD peak frequency. Decreasing mf-GrC release probability ($p = 0.2$) reduced the PSD peak frequency, while increasing mf-GrC release probability ($p = 0.9$) increased the PSD peak frequency. **(E)** The effect of altering the strength of GoC excitation through the mfs and of GoC inhibition through MLI on the GrC power spectral density generated with a 20-Hz mf random activity. The oscillatory effect, revealed by the intensity of the GrC PSD, tends to vanish as the intensity of the feed-forward inhibitory loop is increased and as the intensity of the feed-back dis-inhibitory loop is increased.

The center had a lower cut-off for input signals and generated spike bursts at higher frequency and with shorter delay than the surround. In the center the time–window closed less effectively and contained more spikes than in the surround. The higher mf-GrC release probability in the center than in the surround due to long-term synaptic plasticity (Mapelli and D'Angelo, 2007) would further enhance the contrast between adjacent network areas. The main prediction of the model is therefore that the granular layer circuit behaves as a spatio-temporal filter, whose local properties can be adapted through long-term plasticity and different areas can be synchronized through low-frequency oscillations. It can be envisioned that distributed inputs generate a continuum

of center-surround structures performing a complex time- and frequency-dependent transformation of input signals (e.g. Mapelli et al., 2010a) to be relayed to Purkinje cells. These results support the concept that input mossy fiber bursts are first separated and transformed in granular layer sub-circuits and then relayed to Purkinje cells for subsequent integration and pattern recognition (Dean et al., 2010).

The major innovation in this model is that membrane mechanisms are reproduced using Hodgkin–Huxley gating schemes and synaptic transmission using synaptic vesicle cycling schemes, which are based on extended electrophysiological experiments and biophysical analysis in slices (D'Angelo et al., 2001; Nieus et al., 2006; Solinas et al., 2007a,b; Diwakar et al., 2009 and references therein). Moreover, circuit structure is reproduced beyond statistical connectivity, accounting for a sophisticated arrangement of neuronal and synaptic elements (see Mapelli and D'Angelo, 2007; D'Angelo, 2008; D'Angelo and De Zeeuw, 2009; D'Angelo et al., 2009; Mapelli et al., 2009, 2010a). Finally, the simulations accounted for granular layer responses to three major mf discharge patterns inspired by *in vivo* recordings: localized bursting, frequency-modulated activity and diffused random activity (Kase et al., 1980; Chadderton et al., 2004; Jörntell and Ekerot, 2006; Rancz et al., 2007). In response to single input bursts, the model showed center–surround responses and time windowing (D'Angelo and De Zeeuw, 2009). In response to input trains at different frequencies, the granular layer behaved as a high-pass filter with a rapid growth of the response between 50 and 100 Hz, as observed in VSD recordings (Mapelli et al., 2010b). In response to continuous random stimuli, the model generated synchronous oscillations in the theta band (Pellerin and Lamarre, 1997; Hartmann and Bower, 1998; Maex and De Schutter, 1998; Courtemanche et al., 2009).

The model, by being reconstructed from a detailed description of its constitutive elements, could account for the multiple dynamics of granular layer activity observed *in vitro* and *in vivo*. The individual GrCs and GoCs showed responses to mf burst stimulation compatible with those elicited *in vivo* following punctuate stimulation of the whisker pad (Vos et al., 1999; Chadderton et al., 2004; Rancz et al., 2007) or following more prolonged touching on the limbs (Jörntell and Ekerot, 2006). The specific firing patterns depended on the blend of local excitation and inhibition. Moreover, the neurons, although individually maintaining a low and irregular firing rate, could be entrained into coherent oscillatory activity. Therefore, the model, in addition to demonstrate that biophysical properties *in vitro* are sufficient to reproduce multiple activity patterns *in vivo*, provides the basis for investigating the contribution of single neurons to network activity and, conversely, network's influence on single neurons (Buzsáki, 2006; Izhikevich and Edelman, 2008).

Previous models [originally the theoretical models of Marr (1969), Albus (1971), Tyrrell and Willshaw (1992), Dean et al. (2010) but also the computational model of Maex and De Schutter (1998), Medina and Mauk (2000)] were based on the statistical properties of the granular layer connectivity. Here we have faced the problem of how GoCs contact GrCs in the glomeruli by using the following rules: a GoC inhibits all the dendrites in a glomerulus and cannot inhibit a GrC more than once. As a corollary, each GrC is inhibited by different (up to 5 with a mean of 4) GoCs and all GrCs sending their dendrites in the same glomerulus have at least one GoC in common. This organization, by increasing the efficiency of feed-forward loops and concentrating inhibition into certain cell subgroups, enhanced center-surround transmission and time windowing. These rules are compatible with original Golgi staining images (Golgi, 1883; Ramón y Cajal, 1887, 1889, 1904; Eccles et al., 1967; Palay and Chan-Palay, 1974) but would require further refinement of the glomerular representation in the model to improve generation of direct and indirect GABAergic responses (Rossi and Hamann, 1998; Mapelli et al., 2009) and to implement glomerular crosstalk (Mitchell and Silver, 2000a,b). It should also be noted that network topologies were not fully resolved in the model, because mf and GoC axon branching on the sagittal plane and pf long-range connections on the transverse plane could not be implemented on the scale of this network (see Wu et al., 1999; Sultan, 2001; Barmack and Yakhnitsa, 2008; D'Angelo, 2008).

The model identified different roles for the main components of inhibition. Lateral inhibition was critical to determine the center-surround effect, feed-forward inhibition to determine the time-windowing effect and feed-back inhibition to determine coherent oscillations. In fact, in the model, the generation of oscillatory activity in response to random mf bursts decreased with the strength of the feed-forward loop, which, in turn, was essential to generate time-windowing in response to localized mf activity. Since the relative strength of the feed-forward and feed-back loops is unknown, different mechanism can be envisaged: (i) the relative strength of feed-back and feed-forward loops is dynamically balanced through the intervention of SC/BC-GoC inhibition (Dumoulin et al., 2001) or through glomerular mechanisms (Mitchell and Silver, 2000a,b, 2003; Mapelli et al., 2009); (ii) the feed-forward loop is independently regulated through pfs originating from GrCs located outside the active beam; (iii) oscillating activity is conveyed into the cerebellum in pre-organized patterns. Although these mechanisms may coexist, the latter is especially interesting since both GrCs and GoCs have resonant properties in the theta-band (D'Angelo et al., 2001; Solinas et al., 2007a,b; D'Angelo and De Zeeuw, 2009). It is therefore possible that theta patterns at the input (around 7 Hz in rodents; Hartmann and Bower, 1998) are particularly efficient in generating granular layer responses (Ros et al., 2009).

The model appropriately reproduced the high-pass filtering properties of the granular layer, so that burst patterns over 50 Hz were efficiently transmitted while those at lower frequencies were not (Mapelli et al., 2010b). This is in keeping with the proposal that GrCs receive and retransmit high-frequency bursts (Chadderton et al., 2004; Rancz et al., 2007). The higher cut-off observed in the surround than in the center suggests that a frequency-code is spatially implemented through the center-surround structure. The gain control mechanisms based on stochastic resonance (Mitchell and Silver, 2003) may overlay with those considered here and account for the frequency-dependent modulation of incoming signals observed in certain functional conditions (Arenz et al., 2008).

In the model, generation of appropriate spatio-temporal patterns of activity of the cerebellum granular layer required a detailed description of cellular and synaptic properties. The time course of vesicle cycling regulated temporal summation during repetitive neurotransmission (see **Figures 2 and 4**) and filtering at the mf-GrC relay (see **Figure 7**). Transmission at low frequency was

enhanced by the slow time constant of excitation introduced by the NMDA receptors and was reduced by the slow time constant of inhibition introduced by GABA-A α-6 receptors (see **Figure 7**), suggesting that the balance of the two is critical to regulate circuit functioning. These same mechanisms also helped maintaining network oscillations in the theta-frequency band (see **Figure 8**; D'Angelo et al., 2001; Solinas et al., 2007b). It should be noted that, with unconstrained parameterization, a previous model generated 40 Hz oscillations, which are probably non-physiological (Maex and De Schutter, 1998).

In order to assess the hypothesis that the granular layer behaves as an adaptable spatio-temporal filter coordinated by low-frequency oscillations, experimental tests may be combined with further computational investigations. First, the implementation of rules for long-term synaptic plasticity in the model of the mf-GrC synapse (D'Errico et al., 2009) could allow investigating the impact of adaptation on network filtering and pattern recognition. Secondly, the ability of the circuit of generating theta-frequency oscillations in response to repetitive bursting (which would be naturally conveyed by the cerebral cortex; Ros et al., 2009) could be investigated by modulating the resonant properties of GrCs and GoCs models (D'Angelo et al., 2001; Solinas et al., 2007b). Thirdly, the observation that tonic inhibition can control granular layer gain (Mitchell and Silver, 2003) could be assessed by introducing quantal mechanisms of neurotransmitter release in the model of the mf-GrC synapse (Arleo et al., 2010). The integration of the current model into larger modules including the molecular layer and deep cerebellar nuclei will eventually provide a tool for investigating the spatio-temporal filtering hypothesis of the entire cerebellar network (Dean et al., 2010).

ACKNOWLEDGMENTS

This work was supported by projects SENSOPAC (FP6-IST 028056) and CYBERRAT (Bio-ICT convergence 216528) of the European Commission and by NEUROIMAGE of CNISM (Consorzio Interuniversitario per le Scienze Fisiche della Materia) to E.D. The computational facility for the most intensive simulations was provided by the parallel cluster CASPUR (Consorzio Interuniversitario per le Applicazioni di Supercalcolo per Università e Ricerca). We thank Dr. S. Masoli for his contribution to parallelization of the model.

REFERENCES

Albus, J. S. (1971). A theory of cerebellar function. *Math. Biosci.* 10, 25–61.

Arenz, A., Silver, R. A., Schaefer, A. T., and Margrie, T. W. (2008). The contribution of single synapses to sensory representation in vivo. *Science* 321, 977–980.

Arleo, A., Nieus, T., Bezzi, M., Derrico, A., D'Angelo, E., and Coenen, S. O. (2010). How synaptic release probability shapes neuronal transmission: information theoretic analysis in a cerebellar granule cell. *Neural Comp.* 22, 1113–1148.

Armstrong, D. M., and Rawson, J. A. (1969). Activity patterns of cerebellar cortical neurones and climbing fibre afferents in the awake cat. *J. Physiol. (Lond.)* 289, 425–448.

Barmack, N. H., and Yakhnitsa, V. (2008). Functions of interneurons in mouse cerebellum. *J. Neurosci.* 28, 1140–1152.

Bureau, I., Dieudonné, S., Coussen, F., and Mulle, C. (2000). Kainate receptor-mediated synaptic currents in cerebellar Golgi cells are not shaped by diffusion of glutamate. *Proc. Natl. Acad. Sci. U.S.A.* 97, 6838–6843.

Buzsáki, G. (2006). *Rhythms of the Brain*. New York: Oxford University Press.

Cesana, E., Dieudonné, S., Isope, P., Bidoret, C., D'Angelo, E., and Forti, L. (2009). Excitatory inputs to cerebellar Golgi cells in the cerebellum. *SfN Abstract* 367.17.

Chadderton, P., Margrie, T. W., and Häusser, M. (2004). Integration of quanta in cerebellar granule cells during sensory processing. *Nature* 428, 856–860.

Courtemanche, R., Chabaud, P, and Lamarre, Y. (2009). Synchronization in primate cerebellar granule cell layer local field potentials: basic anisotropy and dynamic changes during active expectancy. *Front. Cell. Neurosci.* 3:6. doi: 10.3389/neuro.03.006.2009.

Cull-Candy, S. G., Brickley, S. G., Misra, C., Feldmeyer, D., Momiyama, A., and Farrant, M. (1998). NMDA receptor diversity in the cerebellum: identification of subunits contributing to functional receptors. *Neuropharmacology* 37, 1369–1380.

D'Angelo, E. (2008). The critical role of Golgi cells in regulating spatio-temporal integration and plasticity at the cerebellum input stage. *Front. Neurosci.* 2:1, 35–46. doi: 10.3389/neuro.01.008.2008.

D'Angelo, E., De Filippi, G., Rossi, P., and Taglietti, V. (1995). Synaptic excitation of individual rat cerebellar granule cells in situ: evidence for the role of NMDA receptors. *J. Physiol. (Lond.)* 484, 397–413.

D'Angelo, E., and De Zeeuw, C. I. (2009). Timing and plasticity in the cerebellum: focus on the granular layer. *Trends Neurosci.* 32, 30–40.

D'Angelo, E., Koekkoek, S. K. E., Lombardo, P., Solinas, S., Ros, E., Garrido, J., Schonewille, M., and De Zeeuw, C. I. (2009). Timing in the cerebellum: oscillations and resonance in the granular layer. *Neuroscience* 162, 805–815.

D'Angelo, E., Nieus, T., Maffei, A., Armano, S., Rossi, P., Taglietti, V., Fontana, A., and Naldi, G. (2001). Theta-frequency bursting and resonance in cerebellar granule cells: experimental evidence and modeling of a slow K^+-dependent mechanism. *J. Neurosci.* 21, 759–770.

D'Errico, A., Prestori, F., and D'Angelo, E. (2009). Differential induction of bidirectional long-term changes in neurotransmitter release by frequency-coded patterns at the cerebellar input. *J. Physiol. (Lond.)* 587, 5843–5857.

Dean, P., Porrill, J., Ekerot, C.-F., and Jörntell, H. (2010). The cerebellar microcircuit as anadaptive filter: experimental and computational evidence. *Nat. Neurosci. Rev.* 11, 30–43.

Dieudonné, S. (1998). Submillisecond kinetics and low efficacy of parallel fibre-Golgi cell synaptic currents in the rat cerebellum. *J. Physiol. (Lond.)* 510, 845–866.

Diwakar, S., Magistretti, J., Goldfarb, M., Naldi, G., and D'Angelo, E. (2009). Axonal Na+ channels ensure fast spike activation and back-propagation in cerebellar granule cells. *J. Neurophysiol.* 101, 519–532.

Dobrunz, L. E., and Stevens, C. F. (1999). Response of hippocampal synapses to natural stimulation patterns. *Neuron* 22, 157–166.

Druckmann, S., Banitt, Y., Gidon, A., Schürmann, F., Markram, H., and Segev, I. (2007). A novel multiple objective optimization framework for constraining conductance-based neuron models by experimental data. *Front. Neurosci.* 1:1, 7–18. doi: 10.3389/neuro.01.1.1.001.2007.

Dumoulin, A., Triller, A., and Dieudonné, S. (2001). IPSC kinetics at identified GABAergic and mixed GABAergic and glycinergic synapses onto cerebellar Golgi cells. *J. Neurosci.* 21, 6045–6057.

Eccles, J. C., Ito, M., and Szentagothai, J. (1967). *The Cerebellum as a Neuronal Machine*. Berlin: Springer.

Farrant, M., and Nusser, Z. (2005). Variations on an inhibitory theme: phasic and tonic activation of GABAA receptors. *Nat. Rev. Neurosci.* 6, 215–229.

Forti, L., Cesana, E., Mapelli, J., and D'Angelo, E. (2006). Ionic mechanisms of autorhythmic firing in rat cerebellar Golgi cells. *J. Physiol. (Lond.)* 574, 711–729.

Gleeson, P., Steuber, V., and Silver, R. A. (2007). neuroConstruct: a tool for modeling networks of neurons in 3D space. *Neuron* 54, 219–235.

Golgi, C. (1883). Sulla fina anatomia degli organi centrali del sistema nervoso IV. Sulla fina anatomia delle circonvoluzioni cerebellari. *Riv. Sper. Freniatr. Med. Leg. Alien. Ment.* 9, 1–17.

Gutfreund, Y., Yarom, Y., and Segev, I. (1995). Subthreshold oscillations and resonant frequency in guinea-pig cortical neurons: physiology and modelling. *J. Physiol. (Lond.)* 483(Pt 3), 621–640.

Hámori, J., and Somogyi, J. (1983). Differentiation of cerebellar mossy fiber synapses in the rat: a quantitative electron microscope study. *J. Comp. Neurol.* 220, 365–377.

Hartmann, M. J., and Bower, J. M. (1998). Oscillatory activity in the cerebellar hemispheres of unrestrained rats. *J. Neurophysiol.* 80, 1598–1604.

Harvey, R. J., and Napper, R. M. A. (1991). Quantitative studies of the mammalian cerebellum. *Prog. Neurobiol.* 36, 437–463.

Häusser, M., and Clark, B. A. (1997). Tonic synaptic inhibition modulates neuronal output pattern and spatiotemporal synaptic integration. *Neuron* 19, 665–678.

Holt, G. R., Softky, W. R., Koch, C., and Douglas, R. J. (1996). Comparison of discharge variability in vitro and in vivo in cat visual cortex neurons. *J. Neurophysiol.* 75, 1806–1814.

Ito, M. (2006). Cerebellar circuitry as a neuronal machine. *Prog. Neurobiol.* 78, 272–303.

Izhikevich, E. M., and Edelman, G. M. (2008). Large-scale model of mammalian thalamocortical systems. *Proc. Natl. Acad. Sci. U.S.A.* 105, 3593–3598.

Jaeger, D., De Schutter, E., and Bower, J. M. (1997). The role of synaptic and voltage-gated currents in the control of Purkinje cell spiking: a modeling study. *J. Neurosci.* 17, 91–106.

Jakab, R. L., and Hámori, J. (1988). Quantitative morphology and synaptology of cerebellar glomeruli in the rat. *Anat. Embryol.* 179, 81–88.

Jörntell, H., and Ekerot, C. F. (2006). Properties of somatosensory synaptic integration in cerebellar granule cells in vivo. *J. Neurosci.* 26, 11786–11797.

Kanichay, R. T., and Silver, R. A. (2008). Synaptic and cellular properties of the feedforward inhibitory circuit within the input layer of the cerebellar cortex. *J. Neurosci.* 28, 8955–8967.

Kase, M., Miller, D. C., and Noda, H. (1980). Discharges of Purkinje cells and mossy fibres in the cerebellar vermis of the monkey during saccadic eye movements and fixation. *J. Physiol. (Lond.)* 300, 539–555.

Klyachko, V. A., and Stevens, C. F. (2006). Excitatory and feed-forward inhibitory hippocampal synapses work synergistically as an adaptive filter of natural spike trains. *PLoS Biol.* 4, e207. doi:10.1371/journal.pbio.0040207.

Korbo, L., Andersen, B. B., Ladefoged, O., and Møller, A. (1993). Total numbers of various cell types in rat cerebellar cortex estimated using an unbiased stereological method. *Brain Res.* 609, 262–268.

Maex, R., and De Schutter, E. (1998). Synchronization of Golgi and granule cell firing in a detailed network model of the cerebellar granule cell layer. *J. Neurophysiol.* 80, 2521–2537.

Mapelli, J., and D'Angelo, E. (2007). The spatial organization of long-term synaptic plasticity at the input stage of cerebellum. *J. Neurosci.* 27, 1285–1296.

Mapelli, J., Gandolfi, D., and D'Angelo, E. (2010a). Combinatorial responses controlled by synaptic inhibition in the cerebellum granular layer. *J. Neurophysiol.* 103, 250–261.

Mapelli, J., Gandolfi, D., and D'Angelo, E. (2010b). High-pass filtering and dynamic gain regulation enhance vertical bursts transmission along the mossy fiber pathway of cerebellum. *Front. Cell. Neurosci.* 4:14. doi:10.3389/fncel.2010.00014

Mapelli, L., Rossi, P., Nieus, T., and D'Angelo, E. (2009). Tonic activation of GABAB receptors reduces release probability at inhibitory connections in the cerebellar glomerulus. *J. Neurophysiol.* 101, 3089–3099.

Marr, D. (1969). A theory of cerebellar cortex. *J. Physiol. (Lond.)* 202, 437–470.

Medina, J. F., and Mauk, M. D. (2000). Computer simulation of cerebellar information processing. *Nat. Neurosci.* 3, 1205–1211.

Misra, C., Brickley, S. G., Farrant, M., and Cull-Candy, S. G. (2000). Identification of subunits contributing to synaptic and extrasynaptic NMDA receptors in Golgi cells of the rat cerebellum. *J. Physiol. (Lond.)* 524, 147–162.

Mitchell, S. J., and Silver, R. A. (2000a). Glutamate spillover suppresses inhibition by activating presynaptic mGluRs. *Nature* 404, 498–502.

Mitchell, S. J., and Silver, R. A. (2000b). GABA spillover from single inhibitory axons suppresses low-frequency excitatory transmission at the cerebellar glomerulus. *J. Neurosci.* 20, 8651–8658.

Mitchell, S. J., and Silver, R. A. (2003). Shunting inhibition modulates neuronal gain during synaptic excitation. *Neuron* 38, 433–445.

Nieus, T., Sola, E., Mapelli, J., Saftenku, E., Rossi, P., and D'Angelo, E. (2006). LTP regulates burst initiation and frequency at mossy fiber-granule cell synapses of rat cerebellum: experimental observations and theoretical predictions. *J. Neurophysiol.* 95, 686–699.

Palay, S. L., and Chan-Palay, V. (1974). *Cerebellar Cortex*. New York: Springer-Verlag.

Palkovits, M., Magyar, P., and Szentàgothai, J. (1971). Quantitative histological analysis of the cerebellar cortex in the cat. II. Cell numbers and densities in the granular layer. *Brain Res.* 32, 15–30.

Palkovits, M., Magyar, P., and Szentágothai, J. (1972). Quantitative histological analysis of the cerebellar cortex in the cat. IV. Mossy fiber-Purkinje cell numerical transfer. *Brain Res.* 45, 15–29.

Pellerin, J. P., and Lamarre, Y. (1997). Local field potential oscillations in primate cerebellar cortex during voluntary movement. *J. Neurophysiol.* 78, 3502–3507.

Ramón y Cajal, S. (1887, 1889, 1904). *Textura del sistema nervioso del hombre y de los vertebrados (3 volumenes)*. Madrid: Imprenta y Librería de Nicolás Moya.

Rancz, E. A., Ishikawa, T., Duguid, I., Chadderton, P., Mahon, S., and Häusser, M. (2007). High-fidelity transmission of sensory information by single cerebellar mossy fibre boutons. *Nature* 450, 1245–1248.

Roggeri, L., Rivieccio, B., Rossi, P., and D'Angelo, E. (2008). Tactile stimulation evokes long-term synaptic plasticity in the granular layer of cerebellum. *J. Neurosci.* 28, 6354–6359.

Ros, H., Sachdev, R. N., Yu, Y., Sestan, N., and McCormick, D. A. (2009). Neocortical networks entrain neuronal circuits in cerebellar cortex. *J. Neurosci.* 29, 10309–10320.

Rossi, D. J., and Hamann, M. (1998). Spillover-mediated transmission at inhibitory synapses promoted by high affinity alpha6 subunit GABAA receptors and glomerular geometry. *Neuron* 20, 783–795.

Saviane, C., and Silver, R. A. (2006). Fast vesicle reloading and a large pool sustain high bandwidth transmission at a central synapse. *Nature* 439, 983–987.

Sola, E., Prestori, F., Rossi, P., Taglietti, V., and D'Angelo, E. (2004). Increased neurotransmitter release during long-term potentiation at mossy fibre-granule cell synapses in rat cerebellum. *J. Physiol. (Lond.)* 2004 557, 843–861.

Solinas, S., Forti, L., Cesana, E., Mapelli, J., De Schutter, E, and D'Angelo, E. (2007a). Computational reconstruction of pacemaking and intrinsic electroresponsiveness in cerebellar golgi cells. *Front. Cell. Neurosci.* 1:2. doi: 10.3389/neuro.03.002.2007.

Solinas, S., Forti, L., Cesana, E., Mapelli, J., De Schutter, E, and D'Angelo, E. (2007b). Fast-reset of pacemaking and theta-frequency resonance patterns in cerebellar golgi cells: simulations of their impact in vivo. *Front. Cell. Neurosci.* 1:4. doi: 10.3389/neuro.03.004.2007.

Sultan, F. (2001). Distribution of mossy fiber rosettes in the cerebellum of cat and mice: evidence for a parasagittal organization at the single fiber level. *Eur. J. Neurosci.* 13, 2123–2130.

Sultan, F., and Heck, D. (2003). Detection of sequences in the cerebellar cortex: numerical estimate of the possible number of tidal-wave inducing sequences represented. *J. Physiol. (Paris)* 97, 591–600.

Traub, R. D., and Llinas, R. (1979). Hippocampal pyramidal cells: significance of dendritic ionic conductances for neuronal function and epileptogenesis. *J. Neurophysiol.* 42, 476–496.

Traub, R. D., Wong, R. K., Miles, R., and Michelson, H. (1991). A model of a CA3 hippocampal pyramidal neuron incorporating voltage-clamp data on intrinsic conductances. *J. Neurophysiol.* 66, 635–650.

Tyrrell, T., and Willshaw, D. (1992). Cerebellar cortex: its simulation and the relevance of Marr's theory. *Philos. Trans. R. Soc. Lond., B,* 336, 239–257.

Van Kan, P. L., Horn, K. M., and Gibson, A. R. (1994). The importance of hand use to discharge of interpositus neurones of the monkey. *J. Physiol. (Lond.)* 480, 171–190.

Van Kan, P. L., Houk, J. C., and Gibson, A. R. (1993). Output organization of intermediate cerebellum of the monkey. *J. Neurophysiol.* 69, 57–73.

Vanier, M. C., and Bower, J. M. (1999). A comparative survey of automated parameter-search methods for compartmental neural models. *J. Comput. Neurosci.* 7, 149–171.

Vos, B. P., Volny-Luraghi, A., and De Schutter, E. (1999). Cerebellar Golgi cells in the rat: receptive fields and timing of responses to facial stimulation. *Eur. J. Neurosci.* 11, 2621–2634.

Vos, B. P., Volny-Luraghi, A., Maex, R., and De Schutter, E. (2000). Precise spike timing of tactile-evoked cerebellar Golgi cell responses: a reflection of combined mossy fiber and parallel fiber activation? *Prog. Brain Res.* 124, 95–106.

Wang, X., Chen, G., Gao, W., and Ebner, T. J. (2009). Parasagittal organization of cerebellar cortex, parallel fibers and synaptic plasticity. *SfN Abstract* 319.10.

Wu, H. S., Sugihara, I., and Shinoda, Y. (1999). Projection patterns of single mossy fibers originating from the lateral reticular nucleus in the rat cerebellar cortex and nuclei. *J. Comp. Neurol.* 411, 97–118.

Conflict of Interest Statement: The authors declare that the research was conducted in the absence of any commercial or financial relationships that could be construed as a potential conflict of interest.

Received: 01 August 2009; paper pending published: 13 November 2009; accepted: 18 March 2010; published online: 14 May 2010.

Citation: Solinas S, Nieus T and D'Angelo E (2010) A realistic large-scale model of the cerebellum granular layer predicts circuit spatio-temporal filtering properties. Front. Cell. Neurosci. ***4****:12. doi: 10.3389/fncel.2010.00012*

frontiers in
CELLULAR NEUROSCIENCE

HYPOTHESIS AND THEORY ARTICLE
published: 27 August 2010
doi: 10.3389/fncel.2010.00027

Model-founded explorations of the roles of molecular layer inhibition in regulating Purkinje cell responses in cerebellar cortex: more trouble for the beam hypothesis

James M. Bower*

Research Imaging Center, University of Texas Health Science Center, San Antonio, TX, USA

Edited by:
Egidio D'Angelo, University of Pavia, Italy

Reviewed by:
Yosef Yarom, Hebrew University, Israel
Michael Hausser, University College London, UK

****Correspondence:***
James M. Bower, Research Imaging Center, 7703 Floyd Curl Drive, San Antonio, TX 78229-3900, USA.
e-mail: bower@uthscsa.edu

For most of the last 50 years, the functional interpretation for inhibition in cerebellar cortical circuitry has been dominated by the relatively simple notion that excitatory and inhibitory dendritic inputs sum, and if that sum crosses threshold at the soma the Purkinje cell generates an action potential. Thus, inhibition has traditionally been relegated to a role of sculpting, restricting, or blocking excitation. At the level of networks, this relatively simply notion is manifest in mechanisms like "surround inhibition" which is purported to "shape" or "tune" excitatory neuronal responses. In the cerebellum, where all cell types except one (the granule cell) are inhibitory, these assumptions regarding the role of inhibition continue to dominate. Based on our recent series of modeling and experimental studies, we now suspect that inhibition may play a much more complex, subtle, and central role in the physiological and functional organization of cerebellar cortex. This paper outlines how model-based studies are changing our thinking about the role of feed-forward molecular layer inhibition in the cerebellar cortex. The results not only have important implications for continuing efforts to understand what the cerebellum computes, but might also reveal important features of the evolution of this large and quintessentially vertebrate brain structure.

Keywords: modeling, evolution

THE CLASSICAL VIEW OF CEREBELLAR MOLECULAR LAYER INHIBITION

For most of the last 50 years, the functional interpretation of cerebellar inhibitory circuits in general, and molecular layer inhibition in particular, has been dominated by the relatively straight forward hypothesis that inhibitory and excitatory synaptic inputs sum spatially and temporally to determine whether Purkinje cells reach threshold and consequently generate an action potential (Andersen, 2006). This "integrate and fire" framework continues to provide the basis for most models and theories of cerebellar function today (Medina and Mauk, 2000; Mauk and Ohyama, 2004; Carrillo et al., 2008; Dean et al., 2010), and in fact for the role of inhibition in brain function as a whole (Andersen, 2006). Consistent with the traditional integrate and fire model of neuronal function, the role of inhibition in the cerebellum has traditionally been described in terms of "sculpting," blocking, or canceling excitatory effects on neuronal output (Bell and Grimm, 1969; Andersen, 2006; Gao et al., 2006; Shin and De Schutter, 2006; McKay et al., 2007; de Gruijl et al., 2009; Wisden et al., 2009; Wulff et al., 2009; Dean et al., 2010), a role that was originally codified in what has come to be known as "the cerebellar beam hypothesis" (Eccles et al., 1967). Originally proposed by Braitenberg and Atwood (1958) based on the unique geometrical relationship between the parallel fibers of the granule cells and the Purkinje cell, the beam hypothesis holds that computation in cerebellar cortical circuitry is fundamentally organized around the propagation of excitatory parallel fiber activity along "beams," sequentially activating cerebellar Purkinje cells (Eccles et al., 1967; Heck et al., 2007). Molecular layer inhibition was assumed to sculpt and sharpen these excitatory "on-beam" Purkinje cell responses by producing an "off-beam" inhibitory area transversely flanking each side of the core beam (Cohen and Yarom, 2000; Gao et al., 2006; Heck et al., 2007; Rokni et al., 2007, 2009).

ARE THERE NATURALLY OCCURRING PARALLEL FIBER INDUCED PURKINJE CELL BEAMS?

While the assumption of strong parallel fiber inputs on Purkinje cells and inhibition as a sculpting lateral mechanism continues to dominate modern cerebellar theories (Mauk and Ohyama, 2004; Hong and Optican, 2008), there is actually little experimental evidence that natural patterns of afferent cortical activation actually produce beam-like patterns of either excited or inhibited Purkinje cells (Bell and Grimm, 1969; Eccles et al., 1972; Bower and Woolston, 1983; Kolb et al., 1997; Cohen and Yarom, 1998; De Jaeger and Proteau, 2003; Holtzman et al., 2006; Heck et al., 2007; Rokni et al., 2007; de Solages et al., 2008). Instead Purkinje cells either activated or inhibited by peripheral stimuli are found in patches, not beams (Eccles et al., 1972; Bower and Woolston, 1983; Gao et al., 2006) whose locations, when measured, are found to be in close proximity to activated regions of the granule cell layer (Bower and Woolston, 1983; Kolb et al., 1997; Cohen and Yarom, 1998; De Jaeger and Proteau, 2003; Lu et al., 2005; Rokni et al., 2007; Brown and Ariel, 2009). Those few *in vivo* reports claiming to demonstrate the presence of beams either mapped Purkinje cell responses without reference to activity in the granule cell layer (Garwicz and Andersson, 1992; Jorntell and Ekerot, 2002; Heck et al., 2007), employed electrical rather than natural forms

of afferent stimulation (Jorntell and Ekerot, 2002), or drew their conclusions based on patterns of activity obtained in completely different animals (Jorntell and Ekerot, 2002, 2006). For additional discussion of these methodological concerns see Bower (2002).

Figure 1, reproduced from Bower and Woolston, 1983, shows the pattern of Purkinje cell excitatory and inhibitory activity induced in cerebellar folium Crus IIA following stimulation of the ipsilateral upper lip in an anesthetized rat. **Figure 1A** shows the spatial distribution of granule cell layer activity induced by the peripheral tactile stimulus, while **Figure 1B** shows the resulting activity produced in Purkinje cells. It can be seen that those Purkinje cells responding with short-latency increases in spike output (indicated by black histogram bins in **Figure 1B**) were not found along beams, but instead were restricted to the region directly overlying the activated granule cell layer (dotted area in both **Figures 1A,B**). Similarly, Purkinje cells showing a reduction in firing were also not found along a beam, but instead were located above as well as adjacent to the activated region of the granule cell layer (stippled histogram bins in **Figure 1B**). While this apparent inhibitory influence does extend slightly beyond the activated region of the granule cell layer, at no point were reductions in Purkinje cell firing seen at a distance greater than 200 microns, even though parallel fibers in the rat can extend for up to a 2.5 mm in both directions from the site of granule cell layer activation (Houk and Walsh, 1971; Harvey and Napper, 1991; Barmack and Yakhnitsa, 2008a). In other words, just as there was no "beam" of activated Purkinje cells extending

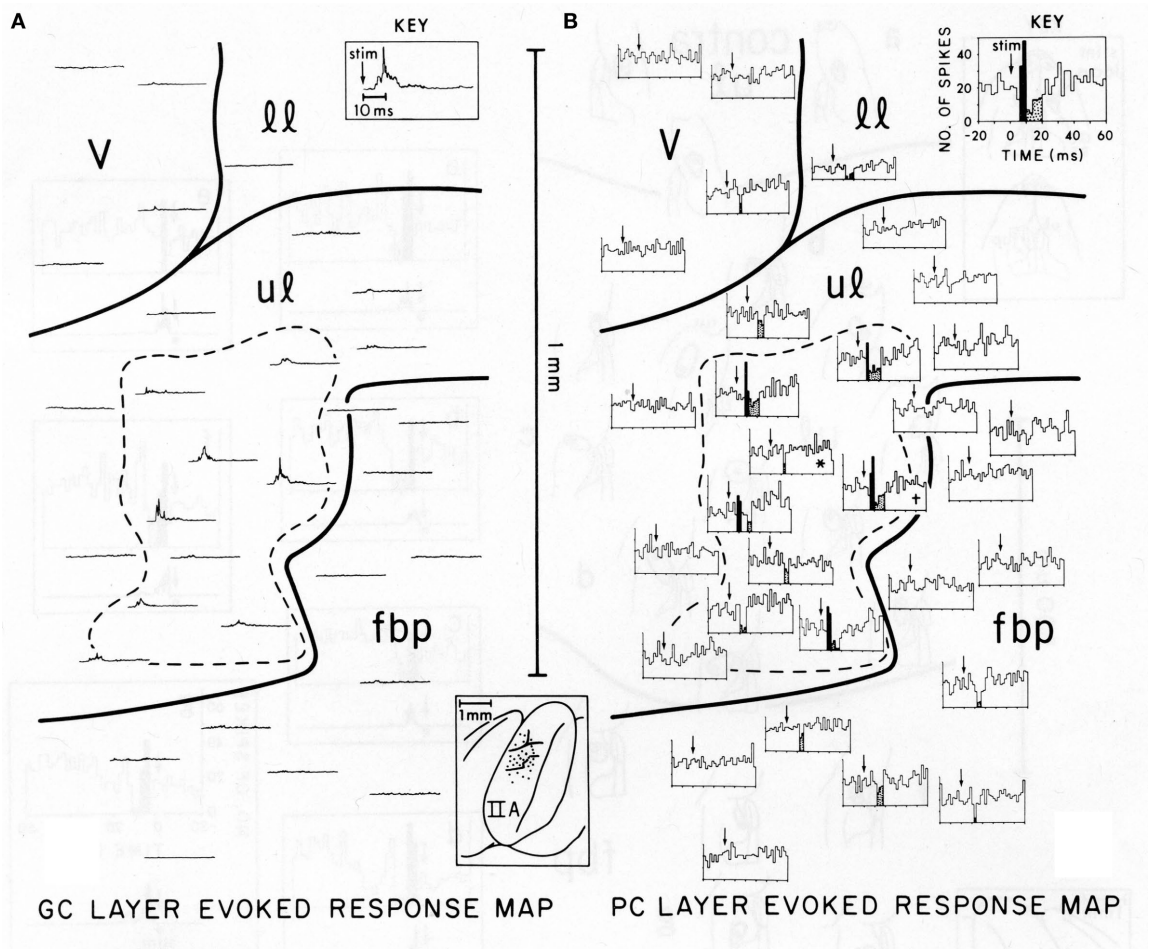

FIGURE 1 | Comparison of the spatial distribution of granule cell and Purkinje cell layer responses in Crus IIA of the rat, evoked by stimulation of a single upper lip locus. Parallel fibers run from the top of the figure (medial) to the bottom (lateral). **(A)** Granule cell layer evoked-response map. This map illustrates the spatial distribution of activity evoked by mechanical stimulation of the single ipsilateral upper lip locus. Each rectified, averaged GC layer response (30 trials) is centered over the electrode puncture location from which the response was recorded (see brain diagram of Crus IIA at bottom center). The largest GC layer responses were recorded within the area enclosed by the dashed line. The time scale and stimulus onset (arrow) for all traces are shown in the key at top right. **(B)** Purkinje cell layer evoked-response map. This map illustrates the spatial distribution of PC layer activity evoked by the same peripheral stimulus that evoked the GC layer response in **(A)**. Each PST histogram represents responses of a different Purkinje cell recorded from the same 19 electrode punctures as the GC layer responses shown in **(A)**. Statistically significant short-latency increases in PC activity are indicated in black with decreases stippled. Both these maps are oriented so that the course of the GC parallel fibers is from the top of the figure to the bottom, i.e., along the axis of the folium (see brain diagram at lower center). In each PST histogram, the arrow indicates the onset of the stimulus. The key at top right indicates the scale for the x and y axes for all histograms. v, vibrissae; 11, lower lip; ul, upper lip; fbp, furry buccal pad.

down the folium, there is also no evidence for an "off-beam" inhibitory band extending along the parallel fibers. The original beam hypothesis also did not predict inhibitory effects within the ("on-beam") area of Purkinje cell excitation (Eccles et al., 1967). In the data shown in **Figure 1** and elsewhere (Cohen and Yarom, 2000), short duration excitatory Purkinje cell responses are almost always followed by a decrease in spiking, presumably due to inhibitory effects. It should also be noted that this decrease in firing occurs at the same latency whether preceded by excitation or not, and regardless of whether the Purkinje cell is above or adjacent to the area of granule cell layer activation.

MODELING PURKINJE CELL RESPONSES TO FOCAL ACTIVATION OF THE GRANULE CELL LAYER

Over the last several years we have constructed realistic models of cerebellar Purkinje cells (Deschutter and Bower, 1994a,b,c; Jaeger et al., 1997; Santamaria and Bower, 2005) and the cerebellar cortical network (Santamaria et al., 2007) to try to better understand, among other things, why focal activation of the granule cell layer does not produce beams of Purkinje cell excitation or inhibition. These modeling efforts were designed to test a specific hypothesis, first formulated by Llinas (1982), that the focal activation of Purkinje cells was due to synaptic input from synapses on the ascending segment of the granule cell axon before it bifurcated into two parallel fibers (Mugnaini, 1972). Llinas suggested that these ascending segment synapses had a more powerful influence on Purkinje cells because they provided a more synchronous input than did parallel fibers contacting Purkinje cells further down the folium (Llinas, 1982). Confirming the first component of this hypothesis, we have obtained direct anatomical evidence that Purkinje cells do receive excitatory synaptic projections from ascending granule cell axons (Gundappa-Sulur et al., 1999; Lu et al., 2009), and experimental evidence is mounting that these inputs drive strong excitatory responses in Purkinje cells (Jaeger and Bower, 1994, 1999; Cohen and Yarom, 1998; Gundappa-Sulur et al., 1999; Isope and Barbour, 2002; Lu et al., 2005; Sims and Hartell, 2005, 2006; Rokni et al., 2008; Brown and Ariel, 2009; Lu et al., 2009; Walter et al., 2009).

While ascending granule cell inputs likely account for Purkinje cell activation directly above an activated region of the granule cell layer, until recently, the other component of the Llinas hypothesis, that the lack of Purkinje cell responses along a beam is due to the relative desynchronization of parallel fibers has not been examined directly. However, several known anatomical and physiological features of the parallel fiber system are consistent with this proposal. First, while it has been known for some time that individual parallel fibers make one synapse per Purkinje cell (Harvey and Napper, 1991), recent evidence in mammals suggests that there may be approximately twice as many granule cell synapses per unit length on ascending as compared to parallel fiber segments of the granule cell axon (Pichitpornchai et al., 1994) a result also found in turtles (Tolbert et al., 2004). With respect to parallel fiber desynchronization, it has been known for a long time that parallel fibers are quite variable in their conduction velocities (Eccles et al., 1966). However, in addition, the structure of the molecular layer itself would seem to assure a more desynchronized parallel fiber volley down the molecular layer. Specifically, action potentials initiated in parallel fiber volley down the folium must first traverse the entire height of the molecular layer before reaching the parallel fiber branch point, while action potentials in deeper parallel fibers start propagating almost immediately (see **Figure 2**). Thus the geometry of the cortex itself appears to contribute to the desynchronization of parallel fibers. Interestingly, this initial desynchronization due to the branching pattern geometry of granule cell axons in the molecular layer appears to be further enhanced by the fact that the intrinsic conduction velocities of deeper parallel fibers can be twice as fast as those found more superficial in the molecular layer (Vranesic

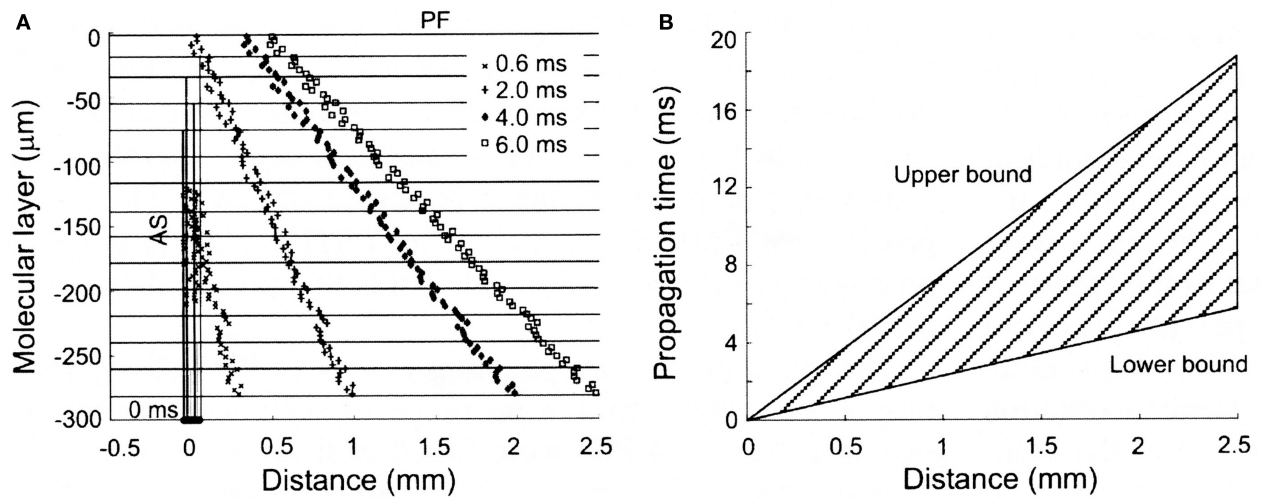

FIGURE 2 | Spatial and temporal patterns of action potential propagation along granule cell axons. (A) Calculated synaptic distributions following a synchronously activated patch of granule cells, consisting of 80 cells distributed over 50 square microns along the X-axis. Note the increasingly desynchronized volley of parallel fiber activity with distance from the activated region. **(B)** Range of propagation times for action potentials converging at different distances from the site of granule cell activation. The upper and lower bounds are calculated using the slowest (0.15 m/s) and fastest (0.50 m/s) published propagation velocities for parallel fiber action potentials. Reproduced with permission from Santamaria et al., 2007.

et al., 1994). **Figure 2** shows the predicted spatial and temporal range of parallel fiber activity following focal granule cell layer activation when these anatomical and physiological constraints are taken into account.

In order to test whether these properties of the parallel fiber system alone could account for the lack of Purkinje cell beams, we constructed a biologically realistic model of the cerebellar granule cell to Purkinje cell pathway (Santamaria et al., 2007). When the spatial and temporal patterns of parallel fiber activity shown in **Figure 2** were applied to modeled Purkinje cells, the results, shown in **Figure 3**, were unexpected. In **Figure 3**, the top four histograms (A–D) are physiological data obtained *in vivo* following focal activation of the granule cell layer under the Purkinje cell whose response is labeled A. As in our original report (Bower and Woolston, 1983) and as shown in **Figure 1**, only the Purkinje cell overlying the activated region of the granule cell layer responded with short-latency excitation. The second set of histograms (E–H) were obtained when the spatial temporal pattern of granule cell inputs shown in **Figure 2** were applied to Purkinje cell models positioned at the same distances from simulated granule cell activation as in A–D. Despite an intentional choice of (biologically plausible) parameters minimizing the number of parallel fiber inputs and maximizing their degree of asynchrony (see Santamaria et al., 2007 for details), the model surprisingly still produced beams of activated Purkinje cells. Thus, while the desynchronization of parallel fibers resulted in progressively broader Purkinje cell excitatory responses with distance, the model produced simulated beam-like excitatory responses not seen experimentally. Based on these modeling results we concluded that the original parallel fiber desynchronization mechanism proposed by Llinas (1982) was not sufficient to account for the experimental data.

Looking more closely at the responses shown in **Figures 3A–D** and **Figures 3E–H**, beyond the existence of beam-like activation, the most striking difference between the real and simulated results is the excessive activation of the simulated Purkinje cells. Comparing **Figures 3A and E** for example, it is clear that stimulation in the model produced a much more dramatic and prolonged excitatory response than is seen *in vivo*. Accordingly, it seemed likely that more realistic responses would likely be obtained after adding molecular layer inhibition which had not to that point been included in the model. When molecular layer inhibition was added to the network model (Santamaria et al., 2007), while changing no other model parameters, the simulated responses (**Figures 3I–L**) were remarkably similar to those recorded *in vivo* (**Figures 3A–D**). For example, after adding molecular layer inhibition, Purkinje cell responses above the activated region of the granule cell layer included both excitatory and following inhibitory responses (**Figure 3I**), while Purkinje cells not directly overlying the activated granule cell layer but nearby showed decreases in spiking (**Figure 3J**). Further, and importantly, the beam-like activity recorded in the model without inhibition (**Figures 3F–H**) was completely absent.

MOLECULAR LAYER INHIBITION SUPPRESSES THE BEAM

The most general prediction of the modeling effort just described is that feed-forward molecular layer inhibition plays a critical, but here-to-fore unrecognized role in regulating the responses of Purkinje cells to excitatory granule cell input, an in particular in suppressing the "beam." Instead of laterally sculpting excitatory Purkinje cell beams as predicted by the beam hypothesis and assumed in many models and interpretations of cerebellar cortical function (Bell and Grimm, 1969; Mauk and Ohyama, 2004; Gao et al., 2006; Shin and De Schutter, 2006; Steuber et al., 2007; Hong and Optican, 2008), molecular layer inhibition instead appears to prevent excitatory Purkinje cell beams from occurring. In support of this basic model prediction, we subsequently showed experimentally that blocking molecular layer inhibition *in vivo*, results in the emergence of beam-like patterns of Purkinje cell activity that are remarkably similar to those seen in the model lacking feed-forward molecular layer inhibition (Santamaria et al., 2007). A similar result has recently been reported by Walter et al. (2009).

While the reader is referred to Santamaria et al. (2007), for a full description of the network modeling parameters, responses to parameter variations, and other specific model-based explanations for the influence of molecular layer interneurons, there are several aspects of the modeling results that are worthy of specific mention here. As with many realistic modeling efforts (Bower, 1990), one of the most valuable contributions this type of model can make is in shedding new light on the functional consequences of well known anatomical features. Through most of the history of neuroscience, function has simply been inferred from a fairly straightforward interpretation of the anatomy, the beam hypothesis itself being an excellent example. Accordingly, the most obvious interpretation of the anatomical arrangement between parallel fibers and Purkinje cells has been that parallel fiber activity would result in a successive spatial activation of Purkinje cells, an interpretation bolstered by experimental studies using direct electrical stimulation techniques (Eccles et al., 1966), essentially designed on the assumption that this was how the system worked. It has taken careful experimental investigations using natural peripheral stimuli (Bower and Woolston, 1983; Santamaria et al., 2007), combined with realistic modeling, to understand why this is not the case. Similarly, the laterally inhibitory role for molecular layer interneurons in the beam hypothesis derives from a simple interpretation of the fact that the axons of these neurons course in a direction perpendicular to the parallel fibers (Sultan and Bower, 1998). Considering the anatomy alone, it seems perfectly rational to assume simple lateral inhibitory effects, while it has never been previously proposed that laterally projecting axons would counterbalance progressive parallel fiber excitation down the folium. The model however, demonstrates such counterbalancing as a consequence of a combination of the relatively rapid induction of inhibitory inputs, the desynchronization of parallel fiber volleys, and the intrinsic electrical properties of the Purkinje cell dendrite. None of these dynamic effects can be inferred from looking at the anatomy of axonal projections alone.

Never-the-less, the anatomical fact that molecular layer axons project perpendicular to the course of the parallel fibers (Sultan and Bower, 1998), almost certainly has some functional significance. In the context of the counterbalancing role for molecular layer inhibition, this perpendicular project pattern could be interpreted as suggesting that there is a close relationship between the specific parallel fibers synapses made on a particular Purkinje cell dendritic tree and the feed-forward inhibitory synapses projecting onto that same tree. Further anatomical studies would be necessary to confirm the possibility, but it would be entirely consistent with the counterbalancing effect of inhibition proposed here if the same parallel fibers synapsing on a particular Purkinje cell, also activated nearby molecular layer interneurons whose orthogonal

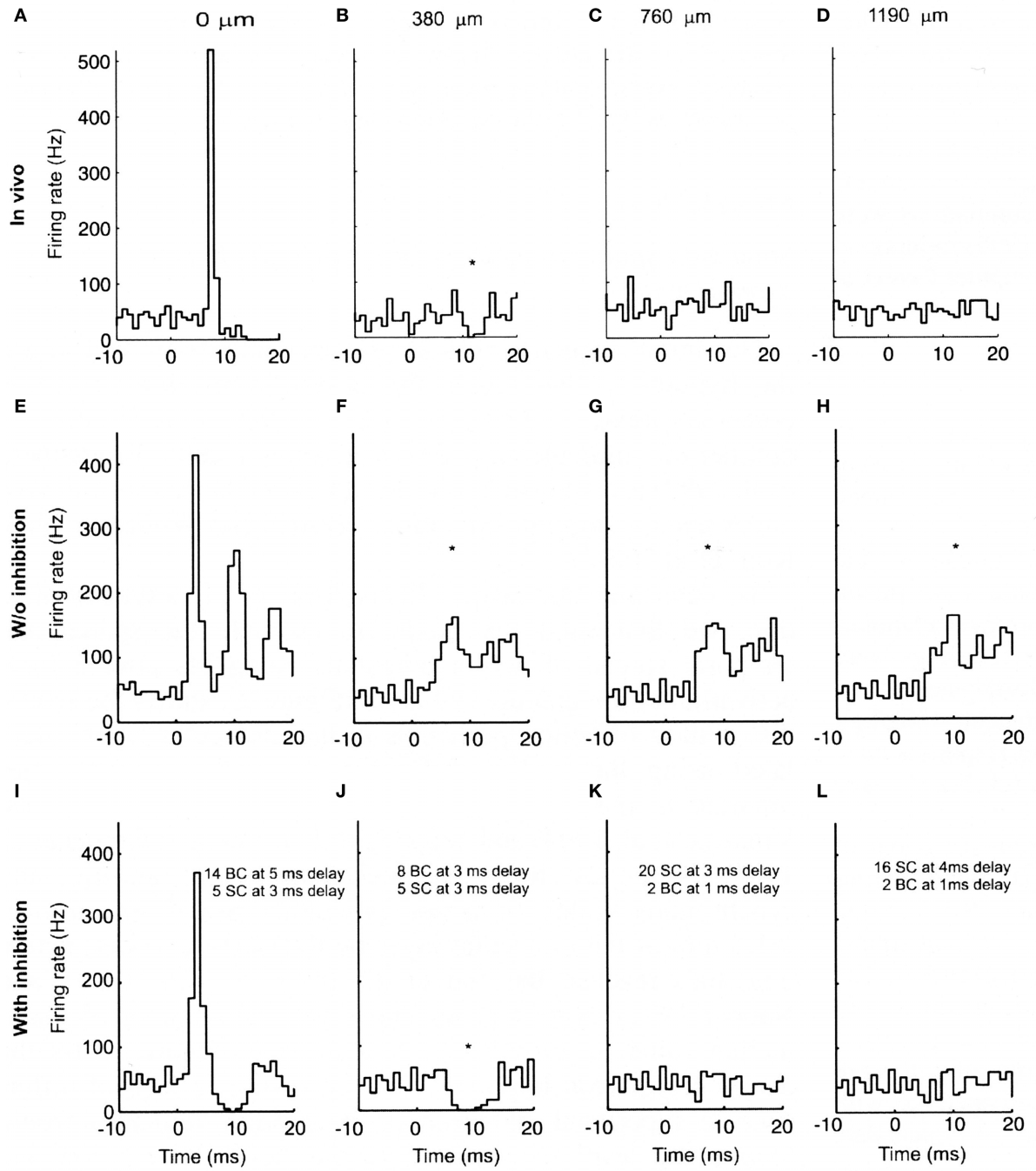

FIGURE 3 | Experimental and modeled granule cell effects on PCs. (A–D) PSTHs (300 trials) of simultaneously recorded PCs evoked by tactile stimulation of the ipsilateral upper lip *in vivo*. **(A)** PC immediately above the stimulated region of granule cells. **(B–D)** PCs recorded along the path of the parallel fibers at the indicated distances. **(E–H)** PSTHs (256 trials) from network simulations using the largest range of parallel fiber conduction velocities (0.15 top, 0.5 m/s bottom), and 4% of granule cells activated. **(I–L)** Similar simulations as **(E–H)** with feed-forward inhibition added to the model. **(E)** and **(I)** received the same total amount of excitatory input, split between ascending and parallel fiber synapses. The notations indicate the inhibitory conduction delays as well as the number of basket (BC) and stellate cell (SC) synapses converging on the corresponding PCs. All simulated Purkinje cells received randomly activated excitatory and inhibitory synapses resulting in an average spontaneous firing frequency of 40 Hz. The difference in the delay in the excitatory onset latency in the *in vivo* **(A)** and modeled (**E** and **I**) PCs is due to the additional conduction delays from the stimulated skin to the cerebellum *in vivo*, which for simplicity were not included in the model. The * denotes statistically significant difference from background activity (T-test, $p < 0.05$). Reproduced with permission from Santamaria et al., 2007.

axonal project patterns assured a restricted influence on the same Purkinje cell. The project patterns of molecular layer interneurons also suggest that the dynamical state of the dendrite of parasagittal rows of Purkinje cells might also be coordinated, perhaps reflecting the known parasaggital orientation of projections to the deep cerebellar nuclei (Ruigrok, 2010). Whatever the functional

significance of the branching pattern of inhibitory axons, for certain their effects are more complex than the simple flanking inhibition assumed by the beam hypothesis.

While our (Santamaria et al., 2007) and Walter's et al. (2009) *in vivo* studies provide experimental support for the general role of inhibition in suppressing Purkinje cell beams, a recent report by Yarom based on an *in vitro* whole cerebellar preparation purports to find no evidence for such an inhibitory effect (Rokni et al., 2007, 2008). While these authors do interpret their data to suggest that granule cell input does not produce beams, they report no additional lateral spread of Purkinje cell activity after the topical application of agents that block inhibition (Rokni et al., 2007, 2008). There are several possible explanations for the failure to see, in this preparation, the emergence of beam-like activity we and others have reported after blocking inhibition *in vivo* (Santamaria et al., 2007; Walter et al., 2009). As these authors acknowledge, the interpretation of optical recordings can be difficult, with optical signals likely dominated by dendritic processes, with little contribution from the somatic spike. This is especially the case in Purkinje cells where somatic spikes do not propagate into the dendrite (Llinas and Sugimori, 1980). This is also a concern with the recent report on the effects of cortical inhibition by Gao et al., 2006. Therefore, it seems likely that the optical imaging methods used in these studies would not detect changes in somatic Purkinje cell spiking and therefore would not necessarily be expected to reveal the beam-like behavior recorded at the single cell level when inhibition is blocked (Santamaria et al., 2007; Walter et al., 2009). That said, it should be noted that a close inspection of the published data (Figure 6, Rokni et al., 2007) does appear to demonstrate a subtle increased spreading of activity along the direction of the parallel fibers when inhibition is blocked, possibly including a region (to the right of the figure) outside the optically sampled area.

A second concern about the optical imaging data involves the likely plane of section being sampled. In our modeling results, most of the change in dendritic currents associated with blocking inhibition were localized in the bottom third of the molecular layer. If the optical imaging results principally reflect activity in upper levels, then they might be transparent to the results we report. It should be noted that even in the presence of inhibition, our network model indicates robust synaptic effects in Purkinje cells along the parallel fibers (**Figure 4B**) which never-the-less do not result in Purkinje cell somatic firing (**Figure 4G**).

Finally, if the lack of parallel fiber induced beams is not a consequence of the molecular layer inhibitory circuitry, one is left to argue that there is some fundamental difference in the strength of synaptic effects between ascending and parallel fiber synapses (c.f. Rokni et al., 2007, 2008). While there is evidence for morphological and physiological differences in the plastic properties of these synapses (Gundappa-Sulur et al., 1999; Sims and Hartell, 2005, 2006), there is good evidence that these synapses don't differ in their average synaptic strength (Isope and Barbour, 2002; Walter et al., 2009). It should be noted that, the synaptic strengths of parallel fiber and ascending segment inputs in our models were the same. Therefore, an equally important prediction of the modeling results is that functional differences between ascending and parallel fiber synapses are NOT based on differences in their average synaptic strengths, but instead on the temporal organization of cortical patterns of synaptic activity and in particular the relative timing of inhibition. Thus, while Walter et al., 2009, have interpreted the similarity in synaptic strengths between parallel fiber and ascending segment synapses to suggest a "computationally equivalence," computational significance is determined by the circuitry in which synapses are embedded. In other words, the influence of both types of synapses on Purkinje cell behavior is strongly influenced by the larger dynamical structure of the network in which the Purkinje cell is embedded. It should also be noted that the claim of computational equivalence by Walter et al. (2009), would seem to depend on some mechanism to globally block molecular layer inhibition, as it was only under those artificial conditions that they (and we) found parallel fibers could drive Purkinje cell output *in vivo*.

NEW ROLE(S) FOR MOLECULAR LAYER INHIBITION

Beyond the more general conclusions just discussed, as is often the case with realistic models, the model makes a number of more detailed predications regarding the organization and function of cortical inhibitory mechanisms. In particular the model suggests different roles for the dendritic and somatic inhibition onto Purkinje cells provided by molecular layer interneurons. Traditionally, these two types of inhibition have been attributed to distinctly different cell types, the so-called "stellate cells" whose soma's are found high in the molecular layer and which provide inhibitory input directly to the Purkinje cell dendrite, and "basket cells" whose somas are found deep in the molecular layer and which provide a strong inhibitory input directly to the Purkinje cells soma (Palay and Chan, 1974; O'Donoghue et al., 1989; Castejon et al., 2001a; Donato et al., 2008; Wisden et al., 2009). However, our recent quantitative anatomical study of molecular layer interneurons suggests that these cells are, in fact, one homogenous population, whose probability of providing an inhibitory input directly to the soma simply goes up as the soma is deeper in the molecular layer (Sultan and Bower, 1998). Consistent with a single population of neurons, molecular layer interneurons with somas in the middle regions of the molecular layer provide both types of inputs. In this paper we will therefore distinguish between "stellate-like" dendritic and "basket-like" somatic inhibition rather than referring to stellate and basket-type cells.

While on the one hand our anatomical and modeling results suggests that molecular layer interneurons are one population of cells, our models predict that dendritic and somatic inhibition play different functional roles. While all molecular layer neurons receive input from the excitatory granule cell axons (Stell et al., 2007) it is known that these two types of inhibition have distinctly different postsynaptic effects on Purkinje cells. For example, dendritic (stellate-type) inputs have, at best, weak effects on the Purkinje cell soma (Vincent and Marty, 1996) while basket-type inputs are very effective in controlling Purkinje cell somatic spiking (Vincent and Marty, 1996). However, beyond these general descriptions, the functional or computational similarities and differences between these two types of molecular layer inhibition are not well understood (Kreiner and Jaeger, 2004; Barmack and Yakhnitsa, 2008b).

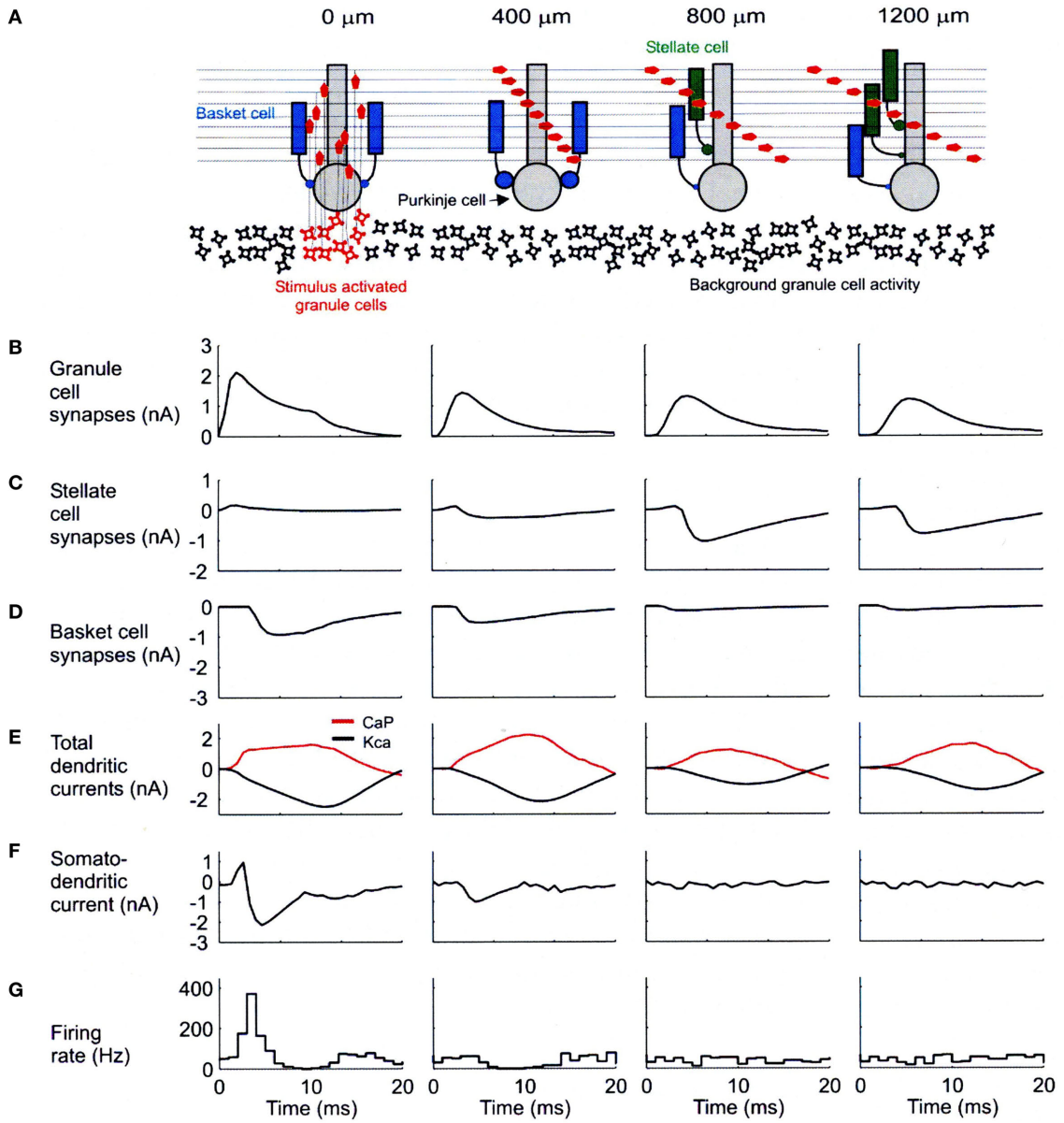

FIGURE 4 | Biophysical mechanisms underlying excitatory and inhibitory relationships in the network model. (A) Schematic diagram showing synaptic influences on PCs at different distances from the site of granule cell layer activation. Activated granule cells and predicted patterns of parallel fiber desynchronization are shown in red. Basket- and stellate-type inhibition represented as blue and green, respectively. **(B)** Total excitatory currents from granule cell synaptic inputs on PCs. The PC at 0 m received only ascending segment synapses. **(C)** Total inhibitory synaptic currents from stellate-type synapses. Although feed-forward stellate-type synapses are not activated at 0 and 400 m the background activated synapses shunt the excitatory depolarization from granule cells. **(D)** Total basket cell synaptic currents. **(E)** Total dendritic calcium P currents (CaP, red) and calcium activated potassium currents (Kca, black) with respect to basal levels of activity after synaptic stimulation. **(F)** Net somato-dendritic current regulating the firing rate of the PC. **(G)** PSTH showing the resulting somatic response. All plots correspond to PCs at distances indicated in the schematic diagram at the top of the figure. Positive current is inwards in **(B–E)** and toward the soma in **(F)**. Averages calculated from 64 simulations in **(B–E)** and 256 in **(F)**. Reproduced with permission from Santamaria et al., 2007.

As shown in **Figure 4**, our network models have resulted in specific predictions regarding the effects and potential functional roles of dendritic and somatic molecular layer inhibition. The diagram at the top of this figure (**Figure 4A**) shows the simulated spatial/temporal pattern of granule cell synaptic input converging on modeled Purkinje cells located above (far left) and at the indicated distances from a region of simulated granule cell layer excitation. The charts and graphs below each of these Purkinje cells (B–F) shown the relationships between several important modeling parameters reflecting the influence of molecular layer inhibition. The histograms at the bottom of this figure (G) again show simulated responses for Purkinje cells at each distance.

Space does not allow a complete description of the mechanisms underlying these relationships or, for example, the important analysis of parameter variations. For additional discussion as well as additional figures explaining model behavior, the reader is referred to Santamaria et al. (2007). Instead, the following discussion summarizes several predictions regarding the role of these two types of inhibition in cerebellar cortical networks. Each section will also consider independent supporting and contradictory evidence:

Feed-forward dendritic (stellate-type) inhibition specifically serves to counterbalance parallel fiber excitation in local regions of the Purkinje cell dendrite. The model specifically predicts that the lack of beam like activation of Purkinje cell along the parallel fibers is due to an effective balance established by the geometry of the network itself between dendritic (stellate-type) inhibition and parallel fiber excitation. This balance is manifest at the level of local dendritic segments, where feed-forward inhibition and parallel fiber excitation effectively produce a local clamp on the membrane voltage (Jaeger et al., 1997; Jaeger and Bower, 1999). This local voltage control, in turn, influences the activation balance between the much larger intrinsic voltage dependent calcium and potassium conductances in the Purkinje cell dendrite. Specifically, in the case of inhibition, allowing dendritic potassium currents to more effectively compensate for increasing voltage dependent calcium conductances. This in turn, results in no net flow of somatic/dendritic current following an increase in parallel fiber activity, and therefore no effect of parallel fibers on the intrinsic spiking of the Purkinje cell (**Figure 4F**). Our models (Jaeger et al., 1997) as well as experimental results (Jaeger and Bower, 1999), suggest that this balance between parallel fiber excitation and molecular layer dendritic inhibition is key to the normal function of the Purkinje cell dendrite (Kreiner and Jaeger, 2004) and normal patterns of Purkinje cell somatic activity. In keeping with the general influence of dendritic inhibition on parallel fiber excitation predicted here, recent biophysical studies on the post synaptic responses of PC dendrites show that intra-dendritic excitatory responses are powerfully restricted in amplitude and duration by molecular layer inhibition (Brunel et al., 2004; Mittmann et al., 2005).

It may be important to point out explicitly that this influence of parallel fiber excitation and molecular layer inhibition on the dendrite of the Purkinje cell is very different in kind from the "integrate and fire" type functionality that dominates many existing models of Purkinje cell behavior (Medina and Mauk, 2000; Mauk and Ohyama, 2004; Carrillo et al., 2008). While the local dendritic influence of these two types of synapses could be considered to be a kind of local summing, our previous modeling results have shown that the "firing" of the Purkinje cell is under the secondary influence of the large voltage dependent conductances in the Purkinje cell dendrite and soma (Jaeger and Bower, 1999) and not the result of a simple sum of parallel fiber excitation and molecular layer inhibition. The interaction of the synaptic and intrinsic voltage dependent ionic conductances is far more complex than assumed in integrate and fire models. It is even likely that the local dendritic influences of parallel fiber excitation and molecular layer inhibition may be more complicated than simple summing, an issue we are currently addressing by constructed models based on serial EM reconstructions of local regions of the Purkinje cell dendrite (Lu et al., 2009).

Regardless of the local biophysical interaction of excitation and inhibition, in principle, the existence of an additional synapse in the feed-forward inhibitory pathway might at first seem to pose a problem for such a counterbalancing mechanism. However, a more detailed analysis of the network model indicates that the balancing effect emerges from the geometric and temporal structure of cerebellar cortical circuitry itself. First, the model suggests that the network derived desynchronization of parallel fiber volleys does, in fact, have an important consequence as it assures that Purkinje cells more distant from the site of granule cell layer activation do not receive an overwhelmingly large simultaneous excitatory synaptic parallel fiber excitatory input. Second, molecular layer interneurons are known to be electrically compact with very large input resistances (Hausser and Clark, 1997) assuring that they respond rapidly to granule cell synaptic input (Clark and Cull-Candy, 2002; Chavas and Marty, 2003; Suter and Jaeger, 2004; Crowley et al., 2007). It has even been suggested that activation by a single granule cell input is sufficient to produce a spike output from a molecular layer interneuron (Barbour, 1993). It is also now known that activation of molecular layer interneurons results in a rapid onset of inhibitory postsynaptic currents in Purkinje cells (Brunel et al., 2004; Steuber et al., 2007). There is even evidence for electrical synapses between molecular layer interneurons (Sotelo and Llinas, 1972; Mann-Metzer and Yarom, 2000) which could serve to speed or spread the establishment of dendritic inhibition. It should also be noted, however, that ascending segment synaptic activation occurs too rapidly and synchronously to be regulated by stellate type inhibition. Thus an equally important conclusion of this analysis is that ascending segment synapses influence Purkinje cells before dendritic inhibition can be established. In addition, ascending segment synaptic input projects onto a different part of the Purkinje cell dendrite than do the parallel fibers of the Purkinje cell dendrite (Gundappa-Sulur et al., 1999; Lu et al., 2009).

The effects of Feed-forward somatic (basket type) inhibition are profound and local. The previous sections described the model-derived prediction that the lack of Purkinje cell excitation at a distance following granule cell layer activation involves a dendritic level interaction between Stellate-type inhibition and parallel fiber activation resulting in no direct influence on Purkinje cell spiking output (Santamaria et al., 2007). In contrast, the model predicts that the influence of Basket-type somatic inhibition is restricted to Purkinje cells above and adjacent to the area of granule cell layer activation, and results in a direct effect on spiking output. As shown in **Figure 4G** and consistent with experimental data (**Figures 1 and 3**), Purkinje cells in these relative positions respond with a clear reduction in firing, which for Purkinje cells immediately overlying the activated granule cell region, usually follows the stimulus related increase in firing (Rokni et al., 2007). As illustrated by the currents shown in **Figure 4D**, the model predicts that, in both cases, this reduction in firing is due to the direct influence of a powerful and rapid basket-type inhibitory input on the soma and initial segment of the Purkinje cell.

There are several lines of experimental evidence that support model predictions regarding basket-type inhibition. First, it is well known that basket-type inhibition on Purkinje cells is rapid and profound (Vincent and Marty, 1996; Donato et al., 2008; Sakaba, 2008). Second, the prediction that basket-type influence is restricted to a region local to the site of granule cell layer activation

is consistent with experimental data showing that molecular layer interneurons whose soma's are deep in the molecular layer have receptive fields similar to those of nearby and not distant regions of the granule cell layer (Ekerot and Jorntell, 2003; Jorntell and Ekerot, 2003; Barmack and Yakhnitsa, 2008b). While these restricted receptive fields have previously been attributed to a parallel fiber selection process (Ekerot and Jorntell, 2003; Jorntell and Ekerot, 2003; Dean et al., 2010), we believe that it is more likely that these interneurons may be specific targets for ascending granule cell axon bundles (Gundappa-Sulur et al., 1999; Lu et al., 2009). This suggestion is consistent with the observations that these cell's dendrites rise higher in the molecular layer than those of more superficial molecular layer interneurons making stellate-type connections (O'Donoghue et al., 1989; Sultan and Bower, 1998; Castejon et al., 2001a,b; Barmack and Yakhnitsa, 2008b) making them potential targets for ascending granule cell axons.

Recent optical imaging studies performed using an *in vitro* isolated cerebellar preparation have also shown the induction of likely inhibition overlying and immediately adjacent to a focal activation of the granule cell layer (Cohen and Yarom, 2000; Rokni et al., 2007). However, these authors attributed only the lateralized inhibitory optical signals (so called "off beam") to molecular layer inhibition, suggesting that the signals observed "on-beam" reflected the activity of Golgi cells within the granule cell layer (Cohen and Yarom, 2000). As already described, our models suggest that all nearby suppression of Purkinje cell firing is due to the large and power effects of basket-type inputs on the Purkinje cell soma, a result that would appear to be supported by more recent intracellular recordings by this group demonstrating that this "on-beam" optical signal is associated with actual membrane hyperpolarization in Purkinje cells (Rokni et al., 2007).

FUNCTIONAL IMPLICATIONS

Most modern models and theories of cerebellar cortex exclude molecular layer inhibition altogether (Ohyama et al., 2003; Yamazaki and Tanaka, 2007; Carrillo et al., 2008; Dean and Porrill, 2008; Traub et al., 2008; de Gruijl et al., 2009; Dean et al., 2010), and those in which it is included, have not distinguished between dendritic and somatic types of molecular layer inhibition (Chauvet and Chauvet, 1999; Medina et al., 2000; Silkis, 2000; De Jaeger and Proteau, 2003; Mauk and Ohyama, 2004; Steuber et al., 2007; Hong and Optican, 2008; Wulff et al., 2009). The model-based studies here suggest that although both forms of molecular layer inhibition are involved in controlling Purkinje cell responses to parallel fiber input, stellate (dendritic), and basket (somatic)-type inhibition are organized quite differently, with different spatial, temporal, and physiological effects and consequences.

DENDRITIC INHIBITION AND PARALLEL FIBER EXCITATION CONTROL THE "STATE" OF THE PURKINJE CELL DENDRITE

With the evidence continuing to accumulate that parallel fiber inputs do not activate Purkinje cells along a beam (see above), those who continue to believe that parallel fibers can and do directly drive Purkinje cell output have generally suggested that the lack of beams is due to a synaptic learning based selection process that leaves many if not most of the parallel fibers biophysically silent (Isope and Barbour, 2002; Jorntell and Ekerot, 2002; Ekerot and Jorntell, 2003; Jorntell and Ekerot, 2003; Apps and Garwicz, 2005; Heck et al., 2007; Dean et al., 2010). Our results, however, suggest the alternate view that parallel fiber inputs are active, but under the control of feed-forward stellate-type molecular layer inhibition and are not intended to drive Purkinje cell output directly. This revised way of thinking about the influence of parallel fibers on Purkinje cells has important algorithmic implications for cerebellar cortical function (for further discussion: Bower, 2002). Instead of supporting a parallel fiber driven cerebellar learning function (Marr, 1969; Albus, 1971; Mauk and Ohyama, 2004; Ito, 2006; Thompson and Steinmetz, 2009), feed-forward dendritic stellate-type inhibition and parallel fiber excitation together are proposed to regulate the local dynamics of the Purkinje cell dendrite (Jaeger et al., 1997) with the large dendritic Ca and K dendritic currents providing most of the direct influence on Purkinje cell somatic spiking (Deschutter and Bower, 1994c; Sugimori et al., 1994; Jaeger et al., 1997; Womack and Khodakhah, 2003). In support of this idea, it has been pointed out by Mann-Metzer and Yarom (2002) and colleagues that the relatively "jittery" spiking response of molecular layer neurons to synaptic input with a duration that is independent of the strength of that input, is not consistent with a role in precise temporal coding. This behavior is consistent with a modulatory function however.

Algorithmically, our models and physiological data have suggested that this modulatory regulation of the dynamic balance between the large voltage dependent membrane condutances directly influences the response of the Purkinje cell to input from the ascending branch (Santamaria and Bower, 2005). Specifically, because the synapses of the ascending synapses contact only the smallest spiny branchlets of the Purkinje cell (Gundappa-Sulur et al., 1999; Lu et al., 2009), their voltage effects traverse regions of the dendrite under voltage clamp control of parallel fibers and feed-forward inhibition. We have interpreted this geometrical arrangement to suggest that the local parallel fiber/feed-forward voltage clamp mechanism serves functionally to modulate inputs from the ascending segment axons. Consistent with this prediction, we have shown using simultaneous granule cell layer and Purkinje cell recordings that any single activation of the granule cell layer does not necessarily result in a response from its overlying Purkinje cell (Lu et al., 2005).

BASKET CELLS AND PARALLEL FIBERS

One elegance of the arrangement between parallel fiber excitation and molecular layer dendritic (stellate) inhibition is that any activation of the granule cell layer produces both a strong influence on overlying Purkinje cells as well as a modulatory influence on more distant Purkinje cells [for more detail on this theory see Bower (2002)]. It is easy to see how such an algorithmic structure could extend seamlessly across the large extent of cerebellar cortex. However, what role does this leave for the basket-type somatic inhibition. Our modeling results predict that this type of inhibition is also specifically involved in controlling the influence of parallel fibers on Purkinje cell spiking output, however, not in as subtle or perhaps even as elegant a fashion as dendritic inhibition. Specifically, analysis of our network models predicts that basket-type input occurs at precisely the time that, otherwise, parallel fiber activity generated by local activation of the granule cell layer would otherwise directly influence the output of the Purkinje cell soma. In other words, the

model suggests that the profound somatic inhibition generated by the basket-type input, in effect, assures that this locally generated parallel fiber input DOES NOT result in Purkinje cell output (Huang et al., 2006). In the absence of this inhibitory influence, Purkinje cells above and nearby activated regions of the granule cell layer produce uncharacteristically large and prolonged responses in the model (Santamaria et al., 2007) and *in vivo* (Mittmann et al., 2005; Rokni et al., 2007; Santamaria et al., 2007).

On the surface, this proposed inhibitory function of basket-type inputs might seem more akin to the traditional inhibitory role of sculpting or shaping excitatory responses (Bell and Grimm, 1969; Cohen and Yarom, 2000; Gao et al., 2006; Shin and De Schutter, 2006; Heck et al., 2007; Rokni et al., 2007; Barmack and Yakhnitsa, 2008b; Wisden et al., 2009). However, analysis of the model suggests instead, that basket-type inhibition is present to maintain the computational integrity of cortical processing. In other words, if the functional role of parallel fibers is to modulate the state of the dendrite and not provide a direct excitatory drive on Purkinje cell output, then some mechanism should exist to compensate for conditions in which parallel fibers might be able to directly drive somatic firing. While at a distance, the excitatory effect of parallel fibers can be counterbalanced by stellate-dendritic type inhibition, our models and physiological results suggest that this is not the case near the point of parallel fiber bifurcation. In these locations and with a sufficiently large activation of the granule cell layer, there is a risk that parallel fibers will directly drive Purkinje cell somatic output (Huang et al., 2006). Our models predicts that it is precisely in these regions that Basket-type inhibition can effectively shut down somatic Purkinje cell spiking. Further experimental evidence that this might be case is presented in **Figure 5**.

Originally intended to determine whether Purkinje cell beams might emerge with appropriately timed sequences of granule cell layer activations as subsequently suggested by (Heck, 1999), this figure shows Purkinje cell responses following stimulation of two different peripheral locations activating two different, but nearby, regions of the granule cell layer (from Bower and Woolston, 1983). **Figure 5A** shows the location of the two tactile stimuli used, in this case the ipsilateral and contralateral upper lip, while **Figure 5B** shows the corresponding two activated regions of the granule cell layer. **Figure 5C** shows responses recorded from a single Purkinje cell (location shown by the arrow in **Figure 5B**), resulting from stimulation of either peripheral locus alone (top and bottom), or stimulation of the two peripheral locations at different times (middle three histograms). It can be seen that this Purkinje cell which is located over the area of the granule cell layer activated by contralateral upper lip stimulation, as expected responds to stimulation of the contralateral upper lip with an increase in firing followed by a decrease in firing (top histogram). As also expected, this same Purkinje cell, which is adjacent to the region of the granule cell layer responding to ipsilateral stimulation, only responded with a decrease in spiking to ipsilateral stimulation (bottom histogram). When, however, the timing of both stimuli was adjusted so that the suppression of firing induced by ipsilateral stimulation temporally overlapped the increase in firing due to contralateral stimulation (middle histogram), the excitatory response even to the underlying granule cell layer input was suppressed. We suggest that the significance of this result is not that the excitatory response was being sculpted by surround inhibition, but that the basket-type somatic input was assuring that parallel fiber inputs did not influence the output of the cell. Based on the conduction velocity of parallel fibers, inhibition occurs at precisely the time that parallel fiber inputs resulting from activation of the contralateral stimulus would be converging on this Purkinje cell. Instead of summing with the ascending input to provide a more robust Purkinje cell output (Huang et al., 2006) as has been proposed for example by Huang et al. (2006), the response of the Purkinje cell is instead suppressed.

In summary, our studies suggest that basket-type molecular layer somatic inhibition may provide a mechanism to enforce what we are suggesting is a core computational feature of cerebellar cortical circuitry, that parallel fibers are modulatory and don't directly drive Purkinje cell somatic spiking. Obviously, this possibility further distances cerebellar function from the beam hypothesis and most current models and theories of cerebellar function (Dean et al., 2010), as it suggests that mechanisms specifically exist to assure that parallel fibers NEVER directly drive Purkinje cell output, regardless of the strength or pattern of granule cell layer activation, or any presumed plastic modification of synaptic strength driven by climbing fiber inputs (Dean et al., 2010). Previously, Braitenberg et al. (1997) have specifically suggested that Purkinje cell beams might emerge under special "tidal wave" conditions of granule cell layer activation. However, to date the only experimental support for this hypothesis has been generated in *in vitro* slice preparations under conditions in which cortical inhibition was blocked pharmacologically (Heck, 1995). As already discussed in and shown in **Figure 5**, our own efforts to look at "tidal wave effects" now almost 25 years ago, failed to find any such effects, *in vivo* specifically because of inhibitory mechanisms.

Of course, as always, it remains an open question how these experiments conducted in anesthetized preparations with one or at most two peripheral stimuli will illuminate cerebellar behavior in awake behaving preparations. Recordings in our laboratory from tactile regions of the cerebellum in awake behaving animals reveal that real behavior results in much more complex peripheral activation patterns producing much more complex patterns of granule cell layer activity (Hartmann and Bower, 1998, 2001). Future modeling efforts applying more realistic patterns of granule cell layer activity to the network model should, in principle, allow us to more rigorously test the basket-inhibition regulatory hypothesis under many different and more natural stimulus conditions.

ALTERNATIVE VIEWS OF THE FUNCTION OF MOLECULAR LAYER INHIBITION

As many neurobiologists are aware, cerebellar physiologists, anatomists, and theorists have been engaged in a long and complex debate regarding the role of synaptic plasticity in cerebellar cortical function (Ito, 2006). In part as a way to explain the contrast between the large number of parallel fibers as compared to a single climbing fibers converging on each Purkinje cell, Marr (1969) and Albus (1971) independently speculated that the climbing fiber determined (or instructed) which of the 10s of thousands of parallel fibers influenced the output of a particular Purkinje cell. Underlying this assertion was the assumption that it was unlikely that Purkinje cell function could depend on a range of active parallel fibers from tens to hundreds of thousands synaptic inputs. One of the more inter-

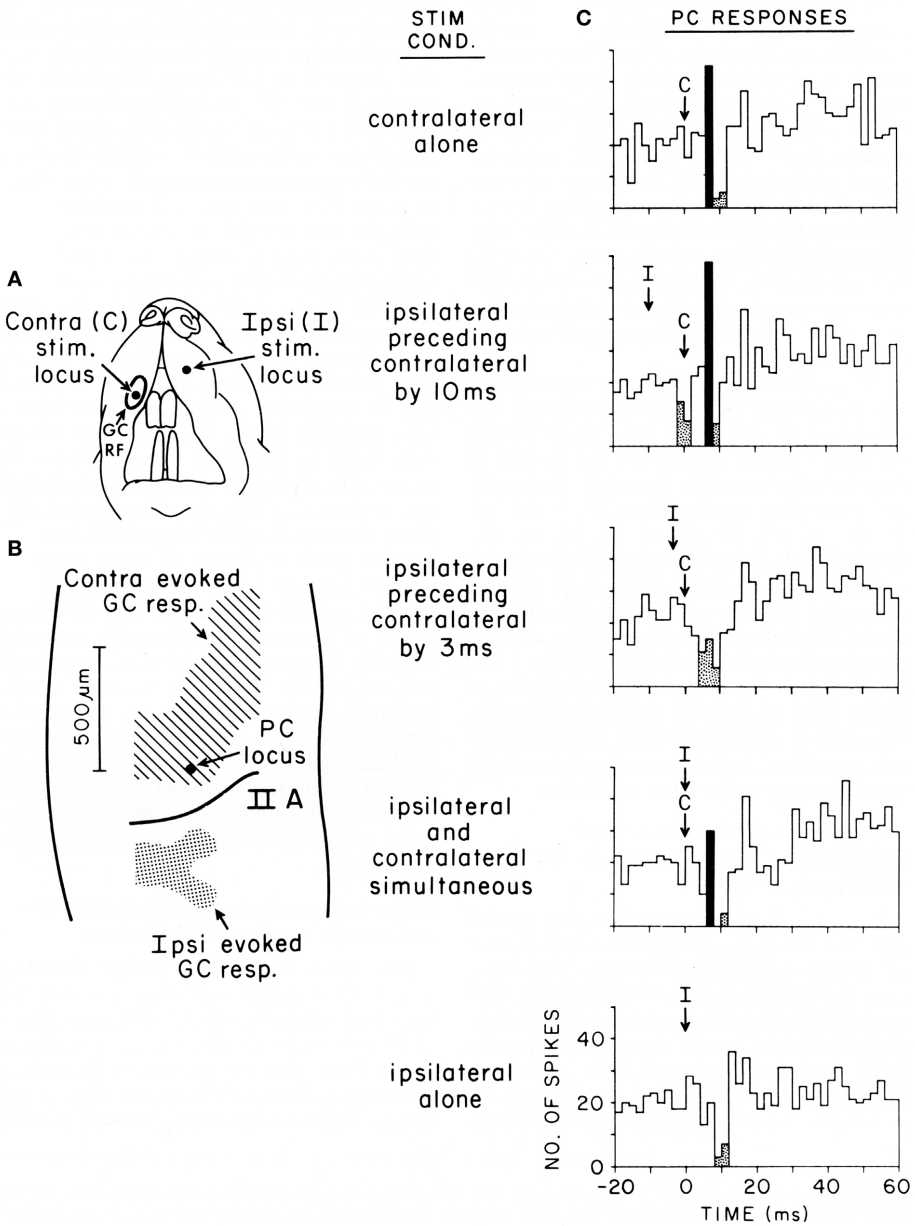

FIGURE 5 | Purkinje cell responses to cotemporaneous peripheral stimuli activating two adjacent regions of the granule cell layer in Crus IIA of the rat. (A) This figurine shows the location of the contralateral (C) and ipsilateral (I) upper lip foci stimulated in this experiment. **(B)** Shows the areas of the granule cell layers that responded to stimulation of each location. This figure also shows the location of the Purkinje cell whose responses to stimulation of different temporal sequences of the two peripheral stimuli are shown in **(C)**. **(C)** Five peri-stimulus time histograms representing the responses of the same Purkinje cell to stimulation of the two peripheral stimuli in different temporal sequences. Statistically significant increases in spiking activity are shown in black, while statistically significant decreased spiking is shown stippled. For analysis of results see text. Reproduced with permission from Bower and Woolston, 1983.

esting consequences of the modulatory relationship we propose between parallel fiber and stellate-type inputs, is that the feed-forward nature of stellate-type inhibition, driven itself by parallel fibers, may very well result in a natural scaling between the amount of parallel fiber excitation and stellate-type inhibition. Thus, the local voltage clamp mechanism should be viable whether hundreds or tens of thousands of parallel fibers are active. This, of course, is a question for further realistic modeling.

The debate about cerebellum learning has also been strongly framed around the more specific question regarding the role of synaptic plasticity in cerebellar function. Physiological studies reporting plastic changes in parallel fiber synapses and more recently, plastic changes in synapses associated with molecular layer inhibition (Scelfo et al., 2008) have been central to the debate about cerebellar learning in general (Ito, 2006). Space does not allow a complete discussion of the many experiments supporting

and questioning the role of synaptic plasticity in cortical function, however, there is one fundamental and important consequence of the view of the cerebellum emerging from our models that is relevant to this debate. Our results suggest that essential features of the connectivity and therefore the function of cortical networks in general and Purkinje cells and molecular layer interneurons in particular are determined in a fixed way by the spatial relationships between neuronal components. Thus, the receptive fields of Purkinje cells are determined by the receptive fields of granule cells in the underlying granule cell layer (Bower and Woolston, 1983) via synapses on the ascending segment of the granule cell axon, and not by a synaptic plasticity rule or the climbing fiber system (Dean et al., 2010). Similarly, our models predict that the receptive fields of molecular layer interneurons are determined by their spatial location relative to activity in the granule cell layer, not by some plasticity synaptic mechanism (Dean et al., 2010). This is not to say that synapses are not plastic, all synapses are plastic, it is to suggest that the fundamental relationships between neurons in the cerebellum are determined spatially and are not "learned."

Experimental evidence purporting to show that receptive fields of both Purkinje cells and now molecular layer interneurons are "learned" have not directly compared the responses of either type of neuron directly to the receptive field properties of the underlying granule cell layer in the same animals (Dean et al., 2010). While there are regularities in the afferent input maps to the granule cell layer in the cerebellum (Bower and Kassel, 1990), these patterns are not regular enough to allow receptive field relationships to be understood by aggregating data across multiple animals (Jorntell and Ekerot, 2003). While we have previously shown by direct comparison in the same animals, that Purkinje cell receptive fields are determined by the receptive fields of the underlying granule cell layer (Bower and Woolston, 1983), based on the studies presented here, we would predict that molecular layer interneurons whose soma's are deep in the molecular layer (and therefore making basket-type connections) would have receptive fields similar to those of the underlying granule cell layer. On the other hand, more superficial molecular layer interneurons should have broader receptive fields reflecting the multiple afferent inputs typically seen in larger regions of the granule cell layer (Bower and Kassel, 1990). In fact, those receptive fields should specifically reflect the origins of the parallel fibers running in their region of the cerebellum. Intermediate depth molecular layer interneurons should be intermediate. As a corollary, we also predict that molecular layer interneurons in the deeper layers of the molecular layer would receive their predominant granule cell synaptic input from ascending granule cell axons, while more superficial molecular layer interneurons would receive a larger proportion of their inputs from parallel fibers. This prediction is consistent with the ratio of these two different types of synapses in the deep and superficial regions of the granule cell layer (Gundappa-Sulur et al., 1999) as well as with the vertically elongated shape of the dendrites of deep molecular layer interneurons (O'Donoghue et al., 1989; Sultan and Bower, 1998; Castejon et al., 2001a,b; Barmack and Yakhnitsa, 2008b). Both these anatomical and physiological experiments are doable, but have not yet been done.

The results presented here may also have important implications for the more general issue of information coding in Purkinje cell spike trains. Recently, it has been suggested that decreases in Purkinje cell spiking, at least in part associated with cortical inhibitory mechanisms, either reflect changes in coding state (Rokni et al., 2009) or may even themselves be part of the Purkinje cell neural code (De Schutter and Steuber, 2009). With respect to coding state, there is some evidence, mostly *in vitro* (Rokni et al., 2009), but also in awake preparations (Yartsev et al., 2009), that Purkinje cells may be "bistable" exhibiting "upstates" and "downstates." These states are proposed to change the way in which Purkinje cells respond to synaptic input including inhibition (Rokni et al., 2009). But it has also been suggested that synaptic inputs from parallel fibers and molecular layer inhibitory neurons might be involved in switching between these states (Rokni et al., 2009). We have previously shown that the general level of background synaptic activity provided by parallel fibers and stellate-type inputs can have a profound effect on the firing behavior of Purkinje cells (Jaeger et al., 1997) and a principle conclusion of our work to date is that the primary role of parallel fiber excitation and molecular layer inhibition is to modulate the dynamical state of the Purkinje cell dendrite (Bower, 2002). In principle, the role for dendritic inhibition proposed here is consistent with a role in such "state changes" although we also suspect that the climbing fiber input is involves as well.

In addition to these longer time scale "state" modulations of Purkinje cell spiking, it has also recently been suggested that intermediate duration pauses in spiking, on the order of 10's to 100's of milliseconds might be a mechanism for coding specific forms of information for transfer to the deep cerebellar nuclei (De Schutter and Steuber, 2009) (Kreiner and Jaeger, 2004; Jaeger, 2007). It has further been suggested that a principle role for cerebellar LTP is in regulating the duration of these pauses in spiking (De Schutter and Steuber, 2009). In the cerebellum, this argument is related to a long tradition of speculations regarding Purkinje cell output (Eccles et al., 1967), that effective excitation in the deep cerebellar nuclei can be achieved by inhibiting the inhibitory output of Purkinje cells (Jaeger, 2007; De Schutter and Steuber, 2009).

While these are interesting ideas, and some are based on models efforts (De Schutter and Steuber, 2009), the question with respect to the current paper is what role molecular layer inhibition might play in the short term pausing mechanism (Jaeger, 2007). As is generally the case with Purkinje cells, the answer to this question is made more complicated by the large intrinsic voltage dependent conductances found in the Purkinje cell dendrites and soma. Evidence suggests that the interplay of these conductances all by themselves can result in pauses in spiking activity in the absence of inhibitory synaptic influence (Steuber et al., 2007; De Schutter and Steuber, 2009). With respect to inhibition, it has recently been proposed that the role of cortical inhibitory circuits is more in coordinating, or synchronizing pauses between nearby Purkinje cells than in generating the pauses *per se* (De Schutter and Steuber, 2009). Our predictions that basket-type inhibition is mostly a local effect, close to a region of granule cell activation is compatible with such a coordinating mechanism. Unfortunately, however, as is typical for theories of the role of molecular layer inhibition in general, current speculations don't distinguish between stellate and basket forms of inhibition (De Schutter and Steuber, 2009). In previous modeling studies, we have shown that while rapid increases in overall stellate-type dendritic inhibitory input can influence the timing of individual Purkinje cell spikes generated in the soma (Jaeger et al., 1997), these influences occur over millisecond times scales not the 10s or 100s of milliseconds assumed associated with information coding (Steuber et al., 2007;

De Schutter and Steuber, 2009). Further, in the absence of perhaps artificially rapid increases in dendritic inhibition, we would predict that this type of inhibition only influences cell spiking very indirectly through subtle changes in local dendritic voltage. Thus, it seems unlikely that stellate-type inhibition would have much of a direct effect on spike coding reflected in pauses in spiking.

EVOLUTIONARY CONSIDERATION

Finally, there is another likely important consideration with respect to a direct role of especially basket-type molecular layer inhibition in neural coding mechanisms, and that is that this type of synaptic connection is only found in mammals and birds (Llinas and Hillman, 1969; Larsell, 1972; Larsell and Jansen, 1972). Anatomical studies have shown that the cerebellar cortex of most fish (Waks and Westerman, 1970), amphibians (Midtgaard, 1992) and some reptiles (Llinas et al., 1969) lack basket-type connections altogether. In those fish, amphibians, and reptiles whose Purkinje cell soma's do receive inhibitory projections from molecular layer interneurons they are of the more traditional "en passant" rather than the specialized basket-type (Llinas et al., 1969; Waks and Westerman, 1970; Midtgaard, 1992).

The fact that only mammals and birds have been shown to have true Basket-type connections would seem to produce additional difficulties for an information coding mechanism based on pauses due to this type of inhibitory input. Presumably, principles of Purkinje cell coding and cerebellar function are not significantly different in non-mammalian and non-avian species. Instead, we would suggest that the limited comparative distribution of basket-type connections is more consistent with the idea that these inputs restrict parallel fiber synaptic influences on Purkinje cell outputs, making sure that Purkinje cells don't spike to this type of input.

Reexamining our network modeling results from more of an evolutionary perspective, there are two features of mammalian cerebellar cortex that make basket-cell type inputs necessary: very large numbers of parallel fiber inputs per Purkinje cell, and Purkinje cell dendrites that are electronically compact. It follows that we would predict that species lacking basket-type inhibitory connections should either have significantly fewer parallel fibers per Purkinje cell and/or have significantly less electrotonically compact dendrites. To test these predictions, we are currently engaged in a comparative study of multiple vertebrate species to determine both the ratio of granule cells to Purkinje cells and the passive electrical properties of those Purkinje cells. Preliminary results suggest that, in fact, mammals and birds generally have the highest ratio of granule cells per Purkinje cells and also have the most electrotonically compact Purkinje cells (Cornelis et al., 2007; Wilcox et al., 2009). The mormyrid fish may be an exception, but interestingly enough, there is some evidence that they may also have a more basket-like inhibitory connection (Grant et al., 1998).

While these experiments are still underway, the results to date are consistent with the suggestion that Basket-type inhibition is an evolutionary adaptation to changes in cortical properties influencing the convergence of parallel fiber inputs on Purkinje cells. The idea that a significant structural component of the mammalian cerebellar cortical network may be an adaptation to control an unwanted consequence of the evolutionary development of the cerebellum is novel. However, these types of adaptations are increasingly being reported in the study of gene regulatory networks, for example, where one can argue that both the function and structure of a complex biological regulatory mechanism are more accessible (Bolouri, 2008).

THE ROLE OF MODELING IN UNDERSTANDING BRAIN BIOPHYSICS AND FUNCTION

Finally, as the interest in molecular layer inhibition has continued to rise, so do speculations regarding both the physiology and function of this important component of cerebellar cortex. As part of this new trend, a recent paper recording cerebellar neuronal responses to vestibular stimulation in the mouse, Barmack and Yakhnitsa (2008a) interpreted physiological recordings obtained from randomly sampled mossy fiber afferents, granule cells, Purkinje cells and climbing fibers to suggest that it is climbing fibers and not granule cells that provide the primary drive on molecular layer interneurons. Without distinguishing the morphological and physiological differences between stellate and basket-type inhibition, and without carefully quantifying the spatial relationships between the recorded neurons, perhaps the most remarkable aspect of this speculation is that the authors themselves acknowledge that there is no anatomical evidence for direct climbing fiber input to molecular layer interneurons. In effect, the authors simply assumed that correlation is strong evidence for causation, even in the absence of a possible anatomical mechanism. Perhaps the principle take home message from the current paper, and our modeling studies to date, is that teasing out the actual causal relationships between neurons in even a structure as generally uniform as the cerebellar cortex requires tools that allow complex forms of causality to be discovered, explored, and tested. While our new interpretation for the role of molecular layer inhibition in the cerebellum will likely be controversial, it is slowly becoming apparent in numerous other brain regions, in part due to modeling, that traditional relatively simple interpretations of the interaction of synaptic excitation and inhibition in brain circuitry may not apply (Chance et al., 2002; Kreiner and Jaeger, 2004; Scelfo et al., 2008). Further, the causal speculations made here are quantified in the form of a biophysically realistic model, available to anyone to download and critique. It is our view that real progress in understanding structure/function relationships in neuronal circuits will increasingly depend on the use and sharing of such biophysically based models.

ACKNOWLEDGMENTS

This work was supported by a grant from the National Science Foundation.

REFERENCES

Albus, J. S. (1971). A theory of cerebellar function. *Math. Biosci.* 10, 25–61.

Andersen, P. (2006). Inhibitory circuits in the thalamus and hippocampus – an appraisal after 40 years. *Prog. Neurobiol.* 78, 264–271.

Apps, R., and Garwicz, M. (2005). Anatomical and physiological foundations of cerebellar information processing. *Nat. Rev. Neurosci.* 6, 297–311.

Barbour, B. (1993). Synaptic currents evoked in Purkinje cells by stimulating individual granule cells. *Neuron* 11, 759–769.

Barmack, N. H., and Yakhnitsa, V. (2008a). Distribution of granule cells projecting to focal Purkinje cells in mouse uvula-nodulus. *Neuroscience* 156, 216–221.

Barmack, N. H., and Yakhnitsa, V. (2008b). Functions of Interneurons in Mouse cerebellum. *J. Neurosci.* 28, 1140–1152.

Bell, C., and Grimm, R. (1969). Discharge properties of Purkinje cells recorded on single and double

microelectrodes. *J. Neurophysiol.* 32, 1044–1055.

Bolouri, H. (2008). *Computational Modeling of Gene Regulatory Networks – A Primer*. London: Imperial College Press.

Bower, J. M. (1990). "Reverse engineering the nervous system: an anatomical, physiological, and computer based approach," in *An Introduction to Neural and Electronic Networks*, eds S. Zornetzer, J. Davis and C. Lau (New York: Academic Press), pp. 3–24.

Bower, J. M. (2002). The organization of cerebellar cortical circuitry revisited: implications for function. *Ann. N. Y. Acad. Sci.* 978, 135–155.

Bower, J. M., and Kassel, J. (1990). Variability in tactile projection patterns to cerebellar folia crus IIA of the Norway rat. *J. Comp. Neurol.* 302, 768–778.

Bower, J. M., and Woolston, D. C. (1983). Congruence of spatial organization of tactile projections to granule cell and Purkinje cell layers of cerebellar hemispheres of the albino rat: vertical organization of cerebellar cortex. *J. Neurophysiol.* 49, 745–766.

Braitenberg, V., and Atwood, R. P. (1958). Morphological observations in the cerebellar cortex. *J. Comp. Neurol.* 109, 1–34.

Braitenberg, V., Heck, D., and Sultan, F. (1997). The detection and generation of sequences as a key to cerebellar function: experiments and theory. *Behav. Brain Sci.* 20, 229–277.

Brown, M. E., and Ariel, M. (2009). Topography and response timing of intact cerebellum stained with absorbance voltage-sensitive dye. *J. Neurophysiol.* 101, 474–490.

Brunel, N., Hakim, V., Isope, P., Nadal, J. P., and Barbour, B. (2004). Optimal information storage and the distribution of synaptic weights: perceptron versus Purkinje cell. *Neuron* 43, 745–757.

Carrillo, R. R., Ros, E., Boucheny, C., and Coenen, O. J. (2008). A real-time spiking cerebellum model for learning robot control. *BioSystems* 94, 18–27.

Castejon, O., Castejon, H., and sims, P. (2001a). Light microscopy, confocal laser scanning microscopy, scanning and transmission electron microscopy of cerebellar basket cells. *J. Submicrosc. Cytol. Pathol.* 33, 23–32.

Castejon, O. J., Castejon, H. V., and Sims, P. (2001b). Light microscopy, confocal laser scanning microscopy, scanning and transmission electron microscopy of cerebellar basket cells. *J. Submicrosc. Cytol. Pathol.* 33, 23–32.

Chance, F. S., Abbott, L. F., and Reyes, A. D. (2002). Gain modulation from background synaptic input. *Neuron* 35, 773–782.

Chauvet, P., and Chauvet, G. A. (1999). Purkinje local circuits with delays: mathematical conditions of stability for learning and retrieval. *Neural Netw.* 12, 59–77.

Chavas, J., and Marty, A. (2003). Coexistence of excitatory and inhibitory GABA synapses in the cerebellar interneuron network. *J. Neurosci.* 23, 2019–2031.

Clark, B. A., and Cull-Candy, S. G. (2002). Activity-dependent recruitment of extrasynaptic NMDA receptor activation at an AMPA receptor-only synapse. *J. Neurosci.* 22, 4428–4436.

Cohen, D., and Yarom, Y. (1998). Patches of synchronized activity in the cerebellar cortex evoked by mossy-fiber stimulation: questioning the role of parallel fibers. *Proc. Natl. Acad. Sci. U.S.A.* 95, 15032–15036.

Cohen, D., and Yarom, Y. (2000). Cerebellar on-beam and lateral inhibition: two functionally distinct circuits. *J. Neurophysiol.* 83, 1932–1940.

Cornelis, H., Lu, H., Georgi, J. S., and Bower, J. M. (2007). Comparative computational study of cerebellar Purkinje cell form and function. *Abstr. Soc. Neurosci.* 33 409.21.

Crowley, J. J., Carter, A. G., and Regehr, W. G. (2007). Fast vesicle replenishment and rapid recovery from desensitization at a single synaptic release site. *J. Neurosci.* 27, 5448–5460.

de Gruijl, J. R., van der Smagt, P., and De Zeeuw, C. I. (2009). Anticipatory grip force control using a cerebellar model. *Neuroscience* 162, 777–786.

De Jaeger, D., and Proteau, L. (2003). The relative efficacy of different forms of knowledge of results for the learning of a new relative timing pattern. *Q. J. Exp. Psychol. A.* 56, 621–640.

De Schutter, E., and Steuber, V. (2009). Patterns and pauses in Purkinje cell simple spike trains: experiments modeling and theory. *Neuroscience* 162, 816–826.

de Solages, C., Szapiro, G., Brunel, N., Hakim, V., and Isope, P. (2008). High-frequency organization and synchrony of activity in the purkinje cell layer of the cerebellum. *Neuron* 58, 775–788.

Dean, P., and Porrill, J. (2008). Adaptive-filter models of the cerebellum: computational analysis. *Cerebellum* 7, 567–571.

Dean, P., Porrill, J., Ekerot, C.-F., and Jorntell, H. (2010). The cerebellar microcircuit as an adaptive filter: experimental and computational evidence. *Nat. Rev. Neurosci.* 11, 30–40.

Deschutter, E., and Bower, J. (1994a). An active membrane model of the cerebellar Purkinje-cell.1. Simulation of current clamps in slice. *J. Neurophysiol.* 71, 375–400.

Deschutter, E., and Bower, J. (1994b). An active membrane model of the cerebellar purkinje-cell.2. Simulation of synaptic responses. *J. Neurophysiol.* 71, 401–419.

Deschutter, E., and Bower, J. (1994c). Simulated responses of cerebellar purkinje-cells are independent of the dendritic location of granule cell synaptic inputs. *Proc. Natl. Acad. Sci. USA* 91, 4736–4740.

Donato, R., Rodrigues, R. J., Takahashi, M., Tsai, M. C., and Soto, D. (2008). GABA release by basket cells onto Purkinje cells, in rat cerebellar slices, is directly controlled by presynaptic purinergic receptors, modulating Ca2+ influx. *Cell Calcium* 44, 521–532.

Eccles, J. C., Ito, M., and Szentagothai, J. (1967). *The Cerebellum as a Neuronal Machine*. Berlin: Springer.

Eccles, J. C., Llinas, R., and Sasaki, K. (1966). Parallel fibre stimulation and the responses induced thereby in the Purkinje cells of the cerebellum. *Exp. Brain Res.* 1, 17–29.

Eccles, J. C., Sabah, N. H., Scmidt, R. F., and Taborikova, H. (1972). Cutaneous mechanoreceptors influencing impulse discharges in cerebellar cortex. I. In mossy fibers. *Exp. Brain Res.* 15, 245–260.

Ekerot, C. F., and Jorntell, H. (2003). Parallel fiber receptive fields: a key to understanding cerebellar operation and learning. *Cerebellum* 2, 101–109.

Gao, W., Chen, G., Reinert, C., and Ebner, T. J. (2006). Cerebellar cortical molecular layer inhibition is organized in parasagittal zones. *J. Neurosci.* 26, 8377–8387.

Garwicz, M., and Andersson, G. (1992). Spread of synaptic activity along parallel fibers in cat cerebellar anterior lobe. *Exp. Brain Res.* 88, 615–622.

Grant, K., Sugawara, Y., Gomez, L., Han, V. Z., and Bell, C. C. (1998). The mormyrid electrosensory lobe in vitro: physiology and pharmacology of cells and circuits. *J. Neurosci.* 18, 6009–6025.

Gundappa-Sulur, G., De Schutter, E., and Bower, J. M. (1999). The ascending branch of the granule cell axon: a significant component in cerebellar cortical circuitry. *J. Comp. Neurosci.* 406, 580–596.

Hartmann, M., and Bower, J. M. (1998). Oscillatory activity (spindling) in the cerebellum of unrestrained rats. *J. Neurophysiol.* 80, 1598–1604.

Hartmann, M., and Bower, J. M. (2001). Tactile responses in the granule cell layer of cerebellar folium Crus Iia of freely behaving rats. *J. Neurosci.* 28, 3549–3563.

Harvey, R. J., and Napper, R. M. A. (1991). Quantitative studies of the mammalian cerebellum. *Prog. Neurobiol.* 36, 437–463.

Hausser, M., and Clark, B. A. (1997). Tonic synaptic inhibition modulates neuronal output pattern and spatiotemporal synaptic integration. *Neuron* 19, 665–678.

Heck, D. (1995). Sequential stimulation of guinea-pig cerebellar cortex in-vitro strongly affects Purkinje-cells via parallel fibers. *Naturwissenschaften* 82, 201–203.

Heck, D. (1999). Sequential stimulation of rat and guinea pig cerebellar granular cells in vitro leads to increasing population activity in parallel fibers. *Neurosci. Lett.* 263, 137–140.

Heck, D. H., Thach, W. T., and Keating, J. G. (2007). On-beam synchrony in the cerebellum as the mechanism for the timing and coordination of movement. *Proc. Natl. Acad. Sci. U.S.A.* 104, 7658–7663.

Holtzman, T., Rajapaksa, T., Mostofi, A., and Edgley, S. A. (2006). Different responses of rat cerebellar Purkinje cells and Golgi cells evoked by widespread convergent sensory inputs. *J. Physiol. (Lond)* 574, 491–507.

Hong, S., and Optican, L. M. (2008). Interaction between Purkinje cells and inhibitory interneurons may create adjustable output waveforms to generate timed cerebellar output. *PLoS ONE* 3, e(2770). doi:10.1371/journal.pone.0002770

Houk, J. C., and Walsh, J. V. (1971). The length and organization of parallel fibers. *Proc. Int. Congr. Phy. Sci.* 9, 776.

Huang, C., Wang, L., and Huang, R. H. (2006). Cerebellar granule cell: ascending axon and parallel fiber. *Eur. J. Neurosci.* 23, 1731–1737.

Isope, P., and Barbour, B. (2002). Properties of unitary granule cell – Purkinje cell synapses in adult rat cerebellar slices. *J. Neurosci.* 22, 9668–9678.

Ito, M. (2006). Cerebellar circuitry as a neuronal machine. *Prog. Neurobiol.* 78, 272–303.

Jaeger, D. (2007). Pauses as neural code in the cerebellum. *Neuron* 54, 9–10.

Jaeger, D., and Bower, J. M. (1994). Prolonged responses in rat cerebellar Purkinje cells following activation of the granule cell layer: an intracellular in vitro and in vivo investigation. *Exp. Brain Res.* 100, 200–214.

Jaeger, D., and Bower, J. M. (1999). Synaptic control of spiking in cerebellar Purkinje cells: dynamic current clamp based on model conductances. *J. Neurosci.* 19, 6090–6101.

Jaeger, D., De Schutter, E., and Bower, J. M. (1997). The role of synaptic and voltage-gated currents in the control of Purkinje cell spiking: a modeling study. *J. Neurosci.* 17, 91–106.

Jorntell, H., and Ekerot, C. F. (2002). Reciprocal bidirectional plasticity of parallel fiber receptive fields in cerebellar Purkinje cells and their afferent interneurons. *Neuron* 34, 797–806.

Jorntell, H., and Ekerot, C. F. (2003). Receptive field plasticity profoundly alters the cutaneous parallel fiber synaptic input to cerebellar interneurons in vivo. *J. Neurosci.* 23, 9620–9631.

Jorntell, H., and Ekerot, C.-F. (2006). Properties of somatosensory synaptic integration in cerebellar granule cells in vivo. *J. Neurosci.* 26, 11786–11797.

Kolb, F. P., Arnold, G., Lerch, R., Straka, H., and Buttner-Ennerver, J. (1997). Spatial distribution of field potential profiles in the cat cerebellar cortex evoked by peripheral and central inputs. *Neuroscience* 81, 1155–1181.

Kreiner, L., and Jaeger, D. (2004). Synaptic shunting by a baseline of synaptic conductances modulates responses to inhibitory input volleys in cerebellar Purkinje cells. *Cerebellum* 3, 112–125.

Larsell, O. (1972). *The Comparitive Anatomy and Histology of the Cerebellum from Monotremes through Apes*. Minneapolis: University of Minnesotta Press.

Larsell, O., and Jansen, J. (1972). *The Comparitive Anatomy and Histology of the Cerebellum: the Human Cerebellum, Cerebellar Connections, and Cerebellar Cortex*. Minneapolis: University of Minnesotta Press.

Llinas, R. (1982). "General discussion: radial connectivity in the cerebellar cortex: a novel view regarding the functional organization of the molecular layer," in *The Cerebellum: New Vistas (Exp. Brain Res. Suppl. Vol. 6)*, eds S. L. Palay and V. Chan-Palay (New York: Springer Verlag), pp. 189–194.

Llinas, R., Bloedel, J. R., and Hillman, D. E. (1969). Functional characterization of neuronal circuitry of frog cerebellar cortex. *J. Neurophysiol.* 32, 847–870.

Llinas, R., and Hillman, D. E. (1969). "Physiological and morphological organization of cerebellar circuits in various vertebrates," in *Neurobiology of Cerebellar Evolution and Development*, ed. R Llinas (Chicago: American Medical Association), pp. 43–76.

Llinas, R., and Sugimori, M. (1980). Electrophysiological properties of in vitro Purkinje cell dendrites in mammalian cerebellar slices. *J. Physiol.* 305, 197–213.

Lu, H., Esquivel, A. V., and Bower, J. M. (2009). 3D electron microscopic reconstruction of segments of rat cerebellar purkinje cell dendrites receiving ascending and parallel fiber granule cell synaptic inputs. *J. Comp. Neurol.* 514, 583–594.

Lu, H., Hartmann, M. J., and Bower, J. M. (2005). Correlations between purkinje cell single-unit activity and simultaneously recorded field potentials in the immediately underlying granule cell layer. *J. Neurophysiol.* 94, 1849–1860.

Mann-Metzer, P., and Yarom, Y. (2000). Electrotonic Coupling Synchronizes Interneuron Activity in the Cerebellar Cortex. *Prog. Brain Res.* 124, 115–122.

Mann-Metzer, P., and Yarom, Y. (2002). Jittery trains induced by synaptic-like current in cerebellar inhibitory interneurons. *J. Neurophysiol.* 87, 149–186.

Marr, D. (1969). A theory of cerebellar cortex. *J. Physiol. (Lond.)* 202, 437–471.

Mauk, M. D., and Ohyama, T. (2004). Extinction as new learning versus unlearning: considerations from a computer simulation of the cerebellum. *Learn. Mem.* 11, 566–571.

McKay, B. E., Engbers, J. D. T., Mehaffey, W. H., Gordon, G. R. J., and Molineux, M. L., (2007). Climbing fiber discharge regulates cerebellar functions by controlling the intrinsic characteristics of Purkinje cell output. *J. Neurophysiol.* 97, 2590–2604.

Medina, J. F., Garcia, K. S., Nores, W. L., Taylor, N. M., and Mauk, M. D. (2000). Timing mechanisms in the cerebellum: testing predictions of a large-scale computer simulation. *J. Neurosci.* 20, 5516–5525.

Medina, J. F., and Mauk, M. D. (2000). Computer simulation of cerebellar information processing. *Nat. Neurosci.* 3(Suppl.), 1205–1211.

Midtgaard, J. (1992). Stellate cell inhibition of Purkinje cells in the turtle cerebellum in vitro. *J. Physiol. (Lond.)* 457, 355–367.

Mittmann, W., Koch, U., and Hausser, M. (2005). Feed-forward inhibition shapes the spike output of cerebellar Purkinje cells. *J. Physiol. (Lond.)* 563, 369–378.

Mugnaini, E. (1972). "The histology and cytology of the cerebellar cortex." in *The Comparitive Anatomy and Histology of the Cerebellum: The Human Cerebellum, Cerebellar Connections, and Cerebellar Cortex.*, eds O. Larsell and J. Jansen (Minneapolis: University of Minnesota Press), pp. 201–262.

O'Donoghue, D. L., King, J. S., and Bishop, G. A. (1989). Physiological and anatomical studies of the interactions between Purkinje cells and basket cells in the cat's cerebellar cortex: evidence for a unitary relationship. *J. Neurosci.* 9, 2141–2150.

Ohyama, T., Nores, W. L., Murphy, M., and Mauk, M. D. (2003). What the cerebellum computes. *Trends Neurosci.* 26, 222–227.

Palay, S. L., and Chan, P. V. (1974). *Cerebellar Cortex: Cytology and Organization*. Berlin: Springer.

Pichitpornchai, C., Rawson, J. A., and Rees, S. (1994). Morphology of parallel fibres in the cerebellar cortex of the rat: an experimental light and electron microscopic study with biocytin. *J. Comp. Neurol.* 342, 206–220.

Rokni, D., Llinas, R., and Yarom, Y. (2007). Stars and stripes in the cerebellar cortex: a voltage sensitive dye study. *Front. Syst. Neurosci.* 1, 1.

Rokni, D., Llinas, R., and Yarom, Y. (2008). The morpho/functional discrepancy in the cerebellar cortex: looks alone are deceptive. *Front. Neurosci.* 2, 192–198.

Rokni, D., Tal, Z., Byk, H., and Yarom, Y. (2009). Regularity, variability and bi-stability in the activity of cerebellar Purkinje cells. *Front. Cell. Neurosci.* 3, 1–9.

Ruigrok, T. J. (2010). Ins and outs of cerebellar modules. *Cerebellum*. doi: 10.1007/s12311-010-0164-y

Sakaba, T. (2008). Two Ca(2+)-dependent steps controlling synaptic vesicle fusion and replenishment at the cerebellar basket cell terminal. *Neuron* 57, 406–419.

Santamaria, F., and Bower, J. M. (2005). Background synaptic activity modulates the response of a modeled purkinje cell to paired afferent input. *J. Neurophysiol.* 93, 237–250.

Santamaria, F., Tripp, P. G., and Bower, J. M. (2007). Feedforward inhibition controls the spread of granule cell-induced Purkinje cell activity in the cerebellar cortex. *J. Neurophysiol.* 97, 248–263.

Scelfo, B., Sacchetti, B., and Strata, P. (2008). Learning-related long-term potentiation of inhibitory synapses in the cerebellar cortex. *Proc. Natl. Acad. Sci. U.S.A.* 105, 769–774.

Shin, S. L., and De Schutter, E. (2006). Dynamic synchronization of Purkinje cell simple spikes. *J. Neurophysiol.* 96, 3485–3491.

Silkis, I. (2000). Interrelated modification of excitatory and inhibitory synapses in three-layer olivary-cerebellar neural network. *BioSystems* 54, 141–149.

Sims, R. E., and Hartell, N. A. (2005). Differences in transmission properties and susceptibility to long-term depression reveal functional specialization of ascending axon and parallel fiber synapses to Purkinje cells. *J. Neurosci.* 25, 3246–3257.

Sims, R. E., and Hartell, N. A. (2006). Differential susceptibility to synaptic plasticity reveals a functional specialization of ascending axon and parallel fiber synapses to cerebellar Purkinje cells. *J. Neurosci.* 26, 5153–5159.

Sotelo, C., and Llinas, R. (1972). Specialized membrane junctions between neurons in the vertebrate cerebellar cortex. *J. Cell Biol.* 53, 271–289.

Stell, B. M., Rastaing, P., Triller, A., and Marty, A. (2007). Activation of presynaptic GABAA receptors induces glutamate release from parallel fiber synapses. *J. Neurosci.* 27, 9022–9031.

Steuber, V., Mittmann, W., Hoebeek, F. E., Silver, R. A., and De Zeeuw, C. I. (2007). Cerebellar LTD and pattern recognition by Purkinje cells. *Neuron* 54, 121–136.

Sugimori, M., Kay, A. R., and Llinas, R. (1994). The persistent Na + current in cerebellar Purkinje cells has a single channel conductance distinct from the inactivating current. *Abstr. Soc. Neurosci.* 20(Pt 1), 63.

Sultan, F., and Bower, J. M. (1998). Quantitative Golgi study of the rat cerebellar molecular layer interneurons using principal component analysis. *J. Comp. Neurol.* 393, 353–373.

Suter, K. J., and Jaeger, D. (2004). Reliable control of spike rate and spike timing by rapid input transients in cerebellar stellate cells. *Neuroscience* 124, 305–317.

Thompson, R. F., and Steinmetz, J. E. (2009). The role of the cerebellum in classical conditioning of discrete behavioral responses. *Neuroscience* 162, 732–755.

Tolbert, D. L., Conoyer, B., and Ariel, M. (2004). Quantitative analysis of granule cell axons and climbing fiber afferents in the turtle cerebellar cortex. *Anat. Embryol. (Berl).* 209, 49–58.

Traub, R. D., Middleton, S. J., Knopfel, T., and Whittington, M. A. (2008). Model of very fast (> 75 Hz) network oscillations generated by electrical coupling between the proximal axons of cerebellar Purkinje cells. *Eur. J. Neurosci.* 28, 1603–1616.

Vincent, P., and Marty, A. (1996). Fluctuations of inhibitory postsynaptic currents in Purkinje cells from rat cerebellar slices. *J. Physiol.* 494 (Pt 1), 183–199.

Vranesic, I., Iijima, T., Ichikawa, M., Matsumoto, G., and Knopfel, T. (1994). Signal transmission in the parallel fiber Purkinje-cell system visualized by high-resolution imaging. *Proc. Natl. Acad. Sci. U.S.A.* 91, 13014–13017.

Waks, M. D., and Westerman, R. A. (1970). Inhibition of Purkinje cells in the cerebellum of the teleost Salmo gairdneri Richardson. *Comp. Biochem. Physiol.* 33, 465–469.

Walter, J. T., Dizon, M. -. J., and Khodakhah, K. (2009). The functional equivalence of ascending and parallel fiber inputs in cerebellar computation. *J. Neurosci.* 29, 8462–8473.

Wilcox, R. N., Herculano-Houzel, S., and Bower, J. M. (2009). Proportionality of cerebellar Purkinje and granule cells across vertebrate species. *Abstr. Soc. Neurosci.* 34, 464.2.

Wisden, W., Murray, A. J., McClure, C., and Wulff, P. (2009). Studying cerebellar circuits by remote control of selected neuronal types with GABA(A) receptors. *Front. Mol. Neurosci.* 2, 29. doi: 10.3389/neuro.02.029.2009.

Womack, M., and Khodakhah, K. (2003). Somatic and dendritic small-conductance calcium-activated potasium channels regulate the output of cerebellar Purkinje cells. *J. Neurosci.* 23, 2600–2607.

Wulff, P., Shonewille, M., Renzi, M., Viltono, L., and Sassoe-Pognetto, M., (2009). Synaptic inhibition of Purkinje cells mediates consolidation of vistibulo-cerebellar motor learning. *Nat. Neurosci.* 12, 1042–1051.

Yamazaki, T., and Tanaka, S. (2007). A spiking network model for passage-of-time representation in the cerebellum. *Eur. J. Neurosci.* 26, 2279–2292.

Yartsev, M. M., Givon-Mayo, R., Maller, M., and Donchin, O. (2009). Pausing purkinje cells in the cerebellum of the awake cat. *Front. Syst. Neurosci.* 3, 2. doi: 10.3389/neuro.06.002.2009.

Conflict of Interest Statement: The authors declare that the research was conducted in the absence of any commercial or financial relationships that could be construed as a potential conflict of interest.

Received: 30 January 2010; paper pending published: 23 March 2010; accepted: 04 July 2010; published online: 27 August 2010.

Citation: Bower JM (2010) Model-founded explorations of the roles of molecular layer inhibition in regulating Purkinje cell responses in cerebellar cortex: more trouble for the beam hypothesis. Front. Cell. Neurosci. ***4****:27. doi: 10.3389/fncel.2010.00027*

frontiers in
CELLULAR NEUROSCIENCE

ORIGINAL RESEARCH ARTICLE
published: 28 May 2010
doi: 10.3389/fncel.2010.00014

High-pass filtering and dynamic gain regulation enhance vertical bursts transmission along the mossy fiber pathway of cerebellum

Jonathan Mapelli[1,2]*†, Daniela Gandolfi[1,2†] and Egidio D'Angelo[1,3]*

[1] *Department of Physiology, University of Pavia, Pavia, Italy*
[2] *Consorzio Interuniversitario per le Scienze Fisiche della Materia, Pavia, Italy*
[3] *Brain Connectivity Center, Istituto Neurologico IRCCS fondazione C. Mondino, Pavia, Italy*

Edited by:
James M. Bower, University of Texas at San Antonio, USA

Reviewed by:
Michael Hausser, University College London, UK
Dieter Jaeger, Emory University, USA

***Correspondence:**
Egidio D'Angelo and Jonathan Mapelli, Department of Physiology, University of Pavia, Via Forlanini 6, I-27100 Pavia, Italy.
e-mail: dangelo@unipv.it; jonathan.mapelli@unipv.it

†*Jonathan Mapelli and Daniela Gandolfi have equally contributed to this paper.*

Signal elaboration in the cerebellum mossy fiber input pathway presents controversial aspects, especially concerning gain regulation and the spot-like (rather than beam-like) appearance of granular to molecular layer transmission. By using voltage-sensitive dye imaging in rat cerebellar slices (Mapelli et al., 2010), we found that mossy fiber bursts optimally excited the granular layer above ~50 Hz and the overlaying molecular layer above ~100 Hz, thus generating a cascade of high-pass filters. NMDA receptors enhanced transmission in the granular, while GABA-A receptors depressed transmission in both the granular and molecular layer. Burst transmission gain was controlled through a dynamic frequency-dependent involvement of these receptors. Moreover, while high-frequency transmission was enhanced along vertical lines connecting the granular to molecular layer, no high-frequency enhancement was observed along the parallel fiber axis in the molecular layer. This was probably due to the stronger effect of Purkinje cell GABA-A receptor-mediated inhibition occurring along the parallel fibers than along the granule cell axon ascending branch. The consequent amplification of burst responses along vertical transmission lines could explain the spot-like activation of Purkinje cells observed following punctuate stimulation *in vivo*.

Keywords: cerebellum, gain control, GABA-A receptors, NMDA receptors, voltage-sensitive dye, imaging

INTRODUCTION

In the cerebellar cortex, mossy fiber signals are first processed in the granular layer before being conveyed toward the Purkinje cells and other molecular layer interneurons. Theories have predicted that the cerebellar cortex controls transmission gain and behaves as an adaptable filter (Marr, 1969; Albus, 1971; Fujita, 1982; recently considered by D'Angelo and De Zeeuw, 2009 and carefully reviewed by Dean et al., 2010), but the existence and functional mechanisms of these operations are still object of debate.

Since brain circuits elaborate spike sequences, understanding signal processing requires a careful analysis of the consequences of specific spike patterns on neuronal responses. The mossy fibers generate spike bursts following punctuate sensory stimulation (Chadderton et al., 2004; Jörntell and Eckerot, 2006; Rancz et al., 2007). Given the presence of numerous synaptic mechanisms with differentiated kinetics, it may be expected that burst transmission along the mossy fiber pathway of cerebellum is sensitive to spike frequency. However, the mechanism proposed to regulate the gain at the mossy fiber – granule cell relay is based on tonic inhibition (Mitchell and Silver, 2003; Arenz et al., 2008), which may not be sensitive to rapid frequency changes during bursts. A related issue is how granular layer bursts are retransmitted to the molecular layer. Punctuate stimulation causes a prominent vertical activation of Purkinje cells overlaying the active granular layer areas (Bower and Woolstone, 1983; Cohen and Yarom, 1998; Rokni et al., 2008). However, the "beam theory" (Eccles et al., 1967) predicted that mossy fiber activity would generate parallel fiber beams, which are indeed observed using parallel fiber stimulation (e.g. see Vranesic et al., 1994; Baginskas et al., 2009). A possible explanation was that vertical activation could reflect differential synaptic density or strength along the ascending granule cell axon compared to parallel fiber synapses (Sims and Hartell, 2005, 2006), but the demonstration of the functional equivalence of the two inputs has reopened the dispute (Walter et al., 2009). Alternatively, differential properties of synaptic inhibition could be critical, as indicated by experimental (Cohen and Yarom, 1998) and computational analysis (Santamaria et al., 2007).

Here, by using voltage-sensitive dye (VSD) imaging in sagittal and coronal slices (Mapelli et al., 2010), we have investigated granular to molecular layer transmission using mossy fiber bursts at different frequencies. We found that optimal responses occurred in the granular layer over ~50 Hz and in the overlaying Purkinje cells over ~100 Hz, while Purkinje cell excitation along the parallel fibers was not frequency-dependent. The gain of burst transmission was dynamically regulated by GABA-A and NMDA receptor-dependent mechanisms without requiring tonic inhibition. The efficacy of GABA-A receptor-dependent inhibition with respect to excitation increased passing from the granular to molecular layer and explained the frequency-dependent behaviors in these subcircuits. These results suggest that high-pass filtering and dynamic gain regulation could enhance vertical transmission of high-frequency bursts along the mossy fiber pathway of cerebellum.

MATERIALS AND METHODS

EXPERIMENTAL TECHNIQUES

Acute cerebellar slices were obtained from 18- to 25-day-old Wistar rats as previously reported (D'Angelo et al., 1995, 1999). Briefly, rats were anesthetized with halotane (SIGMA; 0.5 ml in 2 dm^3 for 1–2 min) before being killed by decapitation. The cerebellum was gently removed, the vermis was isolated, fixed on a plastic support with cyano-acrilic glue, and immersed in cold (2–3°C) cutting solution. Slices (220-μm thick) were cut either in the sagittal or coronal plane. The cutting solution contained (Dugué et al., 2005; in mM): K-Gluconate 130, KCl 15, EGTA 0.2, Hepes 20, Glucose 10 (pH 7.4 with NaOH). Slices were incubated for about 1 h before recordings at 31°C in oxygenated Krebs solution containing (mM): NaCl 120, KCl 2, $MgSO_4$ 1.2, $NaHCO_3$ 26, KH_2PO_4 1.2, $CaCl_2$ 2, glucose 11 (pH 7.4 when equilibrated with 95% O_2–5% CO_2). When needed, the extracellular solution was added with the GABA-A receptor blocker, 10 μM gabazine (SR-95531, Tocris Cookson), or the NMDA and AMPA receptor blockers, 50 μM D-APV (Tocris Cookson) and 10 μM NBQX (Tocris Cookson). The dye (Di-4-ANEPPS, Molecular Probes) was dissolved and stocked in Krebs with 50% ethanol (SIGMA) and 5% Cremophor EL (a Castor oil derivative, SIGMA). Slices for optical recordings were incubated for 30 min in oxygenated Krebs solution added with 3% Di-4-ANEPPS stock solution mixed with 50% fetal Bovine Serum (Molecular Probes).

Slices were gently positioned in the recording chamber and immobilized with a nylon mesh attached to a platinum Ω-wire. Perfusion of standard extracellular solution (2–3 ml/min) maintained at 32°C with a feed-back temperature controller (Thermostat HC2, Multi Channel Systems, Reutlingen, Germany) was performed during the recording session. The mossy fibers were stimulated with square voltage pulses (±4–8 V; 100 μs) delivered either individually or in trains (five pulses at 10, 20, 50, 100, 200 or 500 Hz). Voltage pulses were usually applied through couples of MEA electrodes (MEA 60 MultiChannel Systems, see Mapelli and D'Angelo, 2007 for further details) or through a bipolar tungsten electrode connected to a commercial stimulator (STG 1008, Multi channel systems).

VSD RECORDINGS

The recording chamber was installed on an upright epifluorescence microscope (BX51WI, Olympus, Europa Gmbh, Hamburg, Germany), equipped with a 10X (UM Plan FL 0.3 NA) or 40X (XLUM Plan FL, 0.95 NA) objective (see Tominaga et al., 2000). The light generated by a halogen lamp (150W, MHF-G150LR, MORITEX Corp., Tokyo, Japan) was controlled by an electronic shutter (model0, Copal, Co., Tokyo, Japan) and then passed through an excitation filter ($\lambda = 530 \pm 10$ nm), projected onto a dichroic mirror ($\lambda = 565$ nm) and reflected toward the objective lens to illuminate the specimen. Fluorescence generated by the tissue was transmitted through an absorption filter ($\lambda > 590$ nm) to the CCD camera (MICAM Ultima, Scimedia, Brainvision, Tokyo, Japan). The whole imaging system was connected through an I/O interface (Brainvision) to a PC controlling illumination, stimulation and data acquisition. The final pixel size was 10 μm with 10X and 2.5 μm with 40X objectives. Full-frame image acquisition was performed at 1 kHz. Data were acquired and displayed by Brainvision software and signals were analyzed using routines written in MATLAB (Mathworks, Natick, USA).

At the beginning of recordings, a calibration procedure was adopted to ensure homogeneity across experiments. The dynamic range of the CCD camera was calibrated by measuring background fluorescence and setting the average light intensity in the absence of stimulation to 50% of the saturation level. The background fluorescence was sampled for 50 ms before triggering electrical stimulation and was used to measure the initial fluorescence intensity (F_0). The relative fluorescence change ($\Delta F/F_0$) was then calculated for each time frame. With standard stimulation intensities (4–8 V; see Mapelli and D'Angelo, 2007) the maximum granular layer response measured 0.5–1% $\Delta F/F_0$.

A potential draw-back of linear optical methods is that each focal plane contains also out-of-focus light causing blurring. In order to estimate the optical distortion occurring in our preparations, empirical point spread functions (PSF) were generated by collecting light at different depths (in 0.8 μm steps) from fluorescent beads (0.04-μm diameter) injected into the granular and molecular layer in sagittal and coronal cerebellar slices (Yae et al., 1992) and processing signals off-line (Image-J). In the granular layer, which is almost isotropic, PSF analysis showed that light signals vanished in ~10 μm both vertically and horizontally. In the molecular layer, the orientation of parallel fibers generated anisotropic light scattering so that signals vanished in ~25 μm along the parallel fiber axis and in ~15 μm on the orthogonal axis (data not shown). This effect was therefore negligible on the scale of our analysis.

The signal-to-noise ratio was improved by averaging 16 consecutive sweeps at the stimulus repetition frequency of 0.2 Hz. Given maximal $\Delta F/F_0 \approx 1\%$ and noise SEM $\approx \pm 0.1\%$ ($n = 12$ slices), the signal-to-noise (S/N) ratio was about 10 times ensuring a reliable measurement of peak response amplitude.

ON THE ORIGIN OF VSD SIGNALS

The VSD fluorescence depends on the relative surface and density of the electrogenic elements of the granular layer (Eccles et al., 1967; Palkovits et al., 1971; Palay and Chan-Palay, 1974; Ito, 1984; Harvey and Napper, 1991; Sultan, 2001). The granule cell-Golgi cell ratio is 500:1 for cell number and 3:50 for cell surface, so that the estimated total membrane area of granule cells is about 30 times larger than that of Golgi cells. Since the amplitude of optical signal is correlated with the membrane surface, the major contribution to the optical signal in the granular layer should be generated by granule cells. In the molecular layer, stellate cells are sixteen times and basket cells are six times more abundant than Purkinje cells, while on average Purkinje cells are about 85 times larger than stellate and basket interneurons. The estimated total membrane area of Purkinje cells is about four times larger than that of stellate and basket cells. The optical signal in the molecular layer should therefore to arise mainly from Purkinje cells.

EPSPs and EPSP-spike complexes correlated with granule cells and Purkinje cell activity were recorded using patch-clamp recordings. In both cases, VSD imaging detected more effectively EPSPs than spikes. This was probably due to a series of factors, including the limited sampling frequency (1 kHz) and the time scattering of spikes in different acquisitions. Given the di-synaptic activation of Purkinje cells by mossy fiber stimulation, time scattering was probably even more influential than in granule cells (cf. Figure 2B Mapelli et al., 2010). It should also be noted that, while VSD

responses from the somatic and dendritic areas of Purkinje cells were quite similar at low stimulus intensity, the somatic became ~30% larger than the dendritic response at high intensity (see **Figure 2B**). This probably reflected the fact that PC spikes, which do not back-propagate significantly, do not even contribute much to dendritic depolarization.

It should be noted that the VSD signal was collected from numerous granule cells, was averaged over several acquisitions and was sampled at 1 frame/ms. Therefore, although sensitive to the presence of spikes (Mapelli et al., 2010), the VSD signal could not reveal the precise shape of the action potential. The VSD signal was modulated by the contribution of the excitatory glutamate NMDA and AMPA receptors and by the inhibitory $GABA_A$ receptor (see **Figure 3A** for details), revealing its sensitivity to subthreshold integration of synaptic inputs.

PATCH-CLAMP RECORDINGS

Whole-cell patch-clamp recordings were performed from Purkinje cells using pipettes containing the following intracellular solution (mM); K-gluconate 135, KCl 5, Hepes 10, EGTA 0.2, $MGCl_2$ 4.6, ATP-Na_2 4, GTP-Na 0.4 (pH 7.35). With this solution, the pipette resistance was 3–4 MΩ. Signals were sampled at 20 kHz and low-pass filtered at 2 kHz. Recordings were obtained by using a Multiclamp 700B amplifier (Molecular Devices) and signals were digitally converted with a Digidata 1440A (Molecular Devices). All Purkinje cells showed spontaneous firing in cell attached (13.1 ± 4.9 Hz, $n = 4$) as well as after passing into the whole-cell recording configuration in current clamp mode (14.8 ± 3.0 Hz, $n = 4$). The stimulation of the white matter in the granular layer generated EPSP, IPSPs as well as simple and complex spikes depending on the stimulation intensity and on the position of the stimulating electrode (data not shown). Data used for correlating intracellular membrane depolarization with the VSD signal were taken after moving the cell out of the spontaneous firing region (−39.6 ± 1.4 mV, $n = 4$) by negative current injection (≤−200 pA).

DATA ANALYSIS

A quantitative analysis of the VSD signal was performed in regions of interest (ROIs), which showed a clear response in the granular layer and molecular layer. In each ROI, the peak intensity of signals was normalized to the response to a single control pulse taken at the beginning of the recordings session in the granular layer. The ROIs usually had a size of 20×20 μm^2 (2×2 pixels), thus ideally collecting the fluorescence variations generated by a layer containing ~15 granule cells or one Purkinje cell. Because of light scattering (see above), these numbers represent a lower limit.

For coronal slice recordings, an automatic procedure was written in MATLAB allowing to identify two separate stripes (80-μm large) of activation running in parallel through the granular and the molecular layer. All responses were normalized to the maximum granular layer response. Data obtained from different slices were averaged by aligning the corresponding stripes with their origin located in correspondence of the orthogonal projection of the electrode tip into the molecular layer.

In order to quantify the size of activated areas, a threshold was set at 70% of the maximum normalized response (see Mapelli et al., 2010). An automatic analysis allowed to isolate active pixels so that the extension of activated areas could be compared in different experimental conditions. The EPSP delay was detected at a threshold set at 0.2% $\Delta F/F_0$ (given noise SEM ≈ ± 0.1%).

Gain curves $g(f)$ were fitted with a sigmoidal-shaped function of input frequency (f) of the form:

$$g(f) = (A_1 - A_2)/(1 + (f/f_c)^p) + A_2 \quad (1)$$

where A_1 and A_2 are the initial and final amplitude, f_c is the cut-off frequency and p is the order of the function (ORIGIN, Microcal Software Inc.).

Statistics are reported as mean ± standard error of the mean (SEM).

RESULTS

VSD RESPONSES OF THE GRANULAR AND MOLECULAR LAYER FOLLOWING WHITE MATTER STIMULATION

In sagittal slices of the cerebellar vermis, stimulation of the white matter generated VSD signals involving the mossy fiber – granule cell – PC pathway and the climbing fiber – PC pathway (**Figure 1**). Activation in the two pathways could be distinguished considering three properties (Eccles et al., 1967; Llinas and Sugymori, 1980a,b; Ito, 1984): (i) the latency of PC responses should be longer for the mossy fiber pathway, which is di-synaptic, (ii) the PC responses should follow granular layer responses with mossy fiber but not with climbing fiber stimulation, and (iii) the time course of PC responses should be EPSP-like for mossy fiber stimulation, while resembling a complex spike with climbing fiber stimulation.

In the majority of recordings (17 of 23 slices, 74%), mossy fiber were activated exciting the granular layer and causing a depolarization peaking in 5.2 ± 0.2 ms ($n = 17$ slices; **Figure 1A**). Then, in some of these recordings activation propagated into the adjacent molecular layer causing a depolarization peaking in 12.4 ± 1.7 ms ($n = 5$; **Figure 1A**). The additional delay was probably determined by the time required for synaptic transmission at the mossy fiber – granule cell and parallel fiber – Purkinje cell synapses and by the time needed for the Purkinje cells to respond (activation of granule cells ascending axons and transmission along the parallel fibers were probably negligible; Diwakar et al., 2009). In a minor number of recordings (6 of 23 slices; 26%), climbing fibers were also activated causing a fast molecular layer response peaking in 2.9 ± 0.2 ms (**Figure 1B**; $n = 6$ slices), which thus anticipated the granular layer response. The molecular layer response was composed of a peak followed by a repolarization and by a long lasting depolarizing hump (lasting more than 100 ms; **Figure 1B**), which were presumably related to generation of complex spikes in the Purkinje cells. The continuation of the present paper considers only results obtained by analyzing molecular layer signals generated through mossy fibers activation.

COMBINED VSD AND PATCH-CLAMP RECORDINGS FROM PURKINJE CELLS

It has been shown that VSD signals generated in the granular layer are correlated to the average depolarization of granule cells (see Figure 2 Mapelli et al., 2010). In order to assess the activity state of neurons contributing to generate the molecular layer VSD signals, whole-cell recordings were performed from Purkinje cells. These are the largest neurons of the molecular layer and extend their

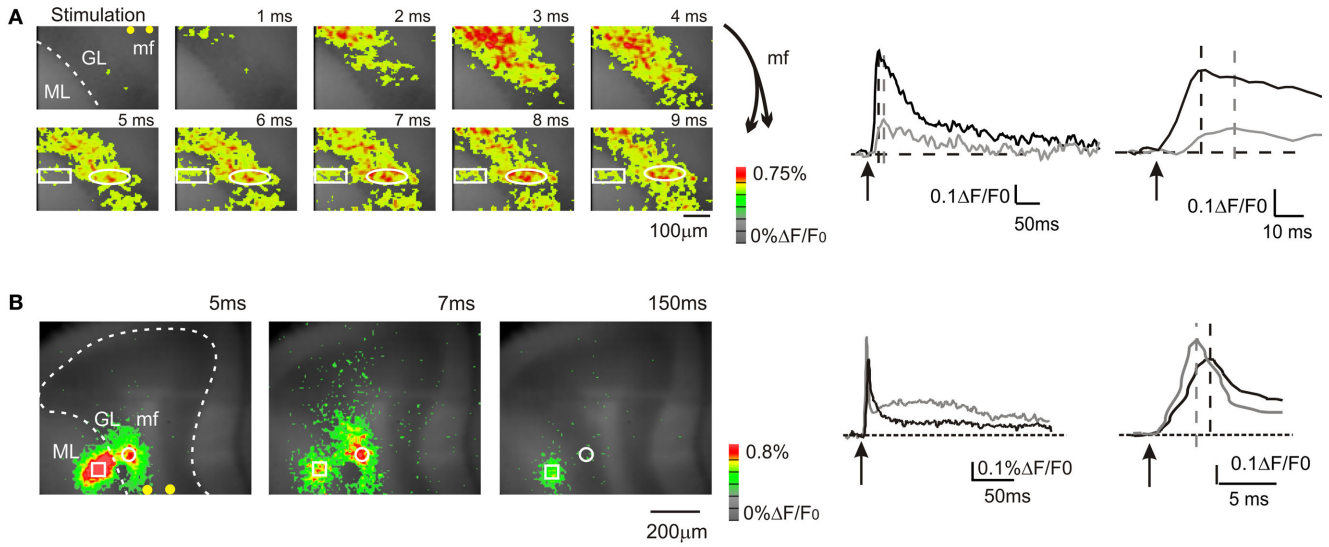

FIGURE 1 | Mossy fiber and climbing fiber responses to white matter stimulation. VSD imaging in parasagittal slices of the cerebellar vermis. In this and in the following figures: mf, mossy fiber; GL, granular layer; PC, Purkinje cell layer, ML, molecular layer, pf, parallel fiber. In this and the following figures, yellow dots indicate stimulation electrodes. **(A)** Optical maps of responses evoked by a single stimulus delivered to the white matter (arrowhead), illustrating the sequence of granular to molecular layer activation through the mossy fibers. Maps show the temporal evolution of granular and molecular layer activation with a time resolution of 1 ms. In the granular layer, the optical signal rapidly propagates from the stimulation site with short delay (2–3 ms) and peaks in 5–6 ms. The activity propagates in a restricted region of the molecular layer (rectangle) with a further delay of 3 ms compared to the corresponding granular layer activation (circle). The traces illustrate the time course of granular layer (black trace) and molecular layer (grey trace) activation following white matter stimulation in the same ROIs indicated on the left. Molecular layer activation is slower and smaller than granular layer activation (magnified in the inset). The schematics on the right illustrate the orientation of mossy fibers branching. **(B)** Optical maps of responses evoked by a single stimulus delivered to the white matter, illustrating direct Purkinje cell activation through the climbing fibers. An intense molecular layer response peaks in 3–5 ms anticipating a slower granular layer response peaking in 7–8 ms. The traces illustrate the time course of granular layer (black trace) and molecular layer (grey trace) activation following white matter stimulation in the same ROIs indicated on the left. Molecular layer activation is faster and larger than granular layer activation (magnified in the inset). The response time relative to stimulation is are indicated for each map.

dendritic arborization in the sagittal plane. WCR were performed from Purkinje cells generating simple spikes (but not complex spikes; cf. Sacconi et al., 2008; Rokni et al., 2009) in response to white matter stimulation in the granular layer. In these neurons, EPSPs arose in 7.1 ± 0.2 ms and peaked in 12.1 ± 0.3 ms ($n = 4$), compatible with a di-synaptic pathway. When the cells were depolarized above about −50 mV, the EPSPs were usually followed by a hyperpolarization probably reflecting intrinsic repolarizing currents and IPSPs caused by molecular layer interneurons (not shown in the figure).

The intracellular electrical activity was compared with VSD responses taken from ROIs corresponding to the soma and to the dendritic tree of recorded Purkinje cells (**Figure 2A**). In response to a single impulse, Purkinje cells showed EPSPs and EPSP-spike complexes in variable proportions depending on the stimulation intensity (Llinas and Sugymori, 1980a,b). At low intensity, both somatic and dendritic VSD signals were a close scaled version of the EPSPs recorded intracellularly (**Figure 2B**). At higher intensity, the VSD response increased along with the number of EPSP-spike complexes but remained slower and proportionately smaller than the average electrical response. Thus both in the somatic and dendritic region, the VSD signal reflected the intracellular electrical activity of Purkinje cells.

PHARMACOLOGICAL PROPERTIES OF THE INHIBITORY AND EXCITATORY CIRCUITS

Granular layer responses are regulated by the inhibitory circuit (Mapelli and D'Angelo, 2007; Mapelli et al., 2009). VSD signals were increased by 10-μM gabazine, which could act both by blocking GABAergic synapses between Golgi cells and granule cells as well as those between molecular layer interneurons and their targets, the Golgi cells and the Purkinje cells. During gabazine application, in the granular layer, both peak amplitude and the late phase of the response increased (at peak, +51.9 ± 11.6%; $n = 4$, $p < 10^{-5}$, paired t-test; at 50 ms, +110.4 ± 28.8%, $n = 4$; $p < 0.01$, paired t-test). Also in the molecular layer the VSD signal was enhanced by the application of 10-μM gabazine (at peak, +40.9 ± 12.2%; $n = 4$, $p < 0.05$, paired t-test; at 50 ms, + 243.8 ± 53.2%; $n = 4$, $p < 10^{-4}$, paired t-test) (**Figure 3A**). Furthermore, blocking the GABAergic synapses increased the extension of the granular (+157.8 ± 35.7%; $n = 4$, $p < 0.03$, paired t-test) and molecular layer responses (+187.5 ± 40.6%; $n = 4$, $p < 0.05$, paired t-test).

The other major synaptic mechanism regulating granular layer excitation and transmission toward the molecular layer is based on the NMDA receptors (Kinney and Slater, 1993; D'Angelo et al., 1995), which are primarily expressed at the mossy fiber – granule cell

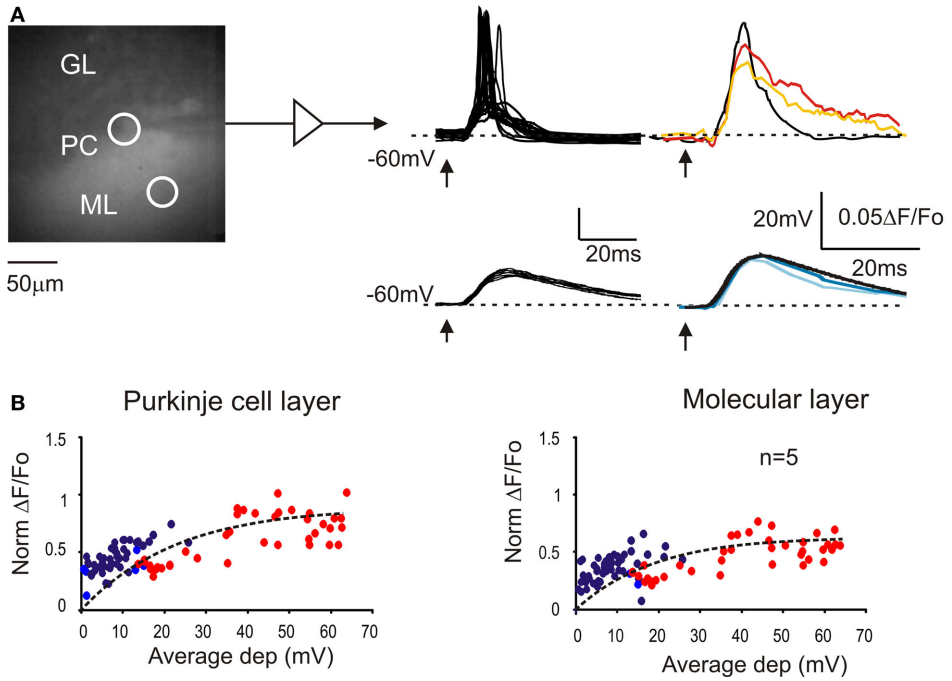

FIGURE 2 | The relationship between VSD signals and Purkinje cell activity. **(A)** Image of a stained cerebellar slice obtained by collecting background epifluorescence showing Granular layer, Purkinje cell layer and Molecular layer during a whole-cell recording from a Purkinje cell. The patch pipette appears as a shadow (since is not filled with dye molecules). Red and orange circles indicate the ROIs corresponding to the recorded PC and its dendritic arborization, from which the VSD signals were measured. Excitatory postsynaptic potential (EPSPs) and EPSP-spike complexes were obtained at low and high stimulation intensity, respectively (arrows indicate the stimulus time). Average electrical signals (black traces) are compared with average fluorescence changes from the PC layer (red and dark blue) and from molecular layer (orange and light blue). **(B)** Correlation between average membrane depolarization and average fluorescence change from ROIs in the Purkinje cell layer and in the molecular layer. The intensity of fluorescence changes is normalized to the corresponding granular layer response. The dotted lines correspond to fittings performed with an exponential function, $y = y_0 + A_1[1\text{-}\exp(-x/\tau)]$ ($y_0 = 0$, $A_1 = 0.9$, $\tau = 22.6$ for Purkinje cell layer; $y_0 = 0$, $A_1 = 0.6$, $\tau = 18.7$ for molecular layer). Red and orange circles indicate Purkinje cells responding with spikes to at least half of the stimuli. Data points are taken from five different cells.

synapse (Garthwaite and Brodbelt, 1989; Cull-Candy et al., 1998). The block of NMDA currents decreased peak response amplitude in the granular layer (−28.8 ± 12%; $n = 4$, $p = < 0.01$, paired t-test) as well the late phase of the response (at 50 ms −59.7 ± 10.7%; $n = 4$, $p < 0.005$, paired t-test). Furthermore, blocking NMDA receptors reduced the extension of the granular layer (−34.1 ± 7.3%; $n = 4$, $p < 0.05$, paired t-test) and of the molecular layer response (−53.3 ± 7.5%; $n = 4$, $p < 10^{-3}$, paired t-test). Finally, blocking the NMDA receptors almost completely blocked the transmission toward the molecular layer (−85.3 ± 4.8%; $n = 4$, $p < 10^{-11}$, paired t-test) (**Figure 3B**).

These experiments show that the VSD signal was sensitive to the major regulatory systems of the cerebellar circuit potentially able to control signal transmission along the mossy fiber pathway.

FREQUENCY-DEPENDENCE OF GRANULAR LAYER – MOLECULAR LAYER TRANSMISSION

Mossy fibers usually convey bursts of frequency-modulated discharges to the granular layer (Kase et al., 1980; Chadderton et al., 2004; Jörntell and Ekerot, 2006; Rancz et al., 2007; Arenz et al., 2008). To address the impact of these patterns we have investigated granular layer activation in response to trains of stimuli delivered to the mossy fiber bundle at different frequencies.

The stimulation of the mossy fiber bundle with a train of five impulses at different frequencies induced characteristic activation patterns in the granular layer (**Figure 4**). The stimulation at 10 Hz induced similar responses at each pulse. However, increasing the stimulation frequency revealed a considerable temporal summation. As a whole, granular layer responses became more extended (e.g. +6.9 ± 4.3% at 10 Hz vs +127.3 ± 20.8% at 500 Hz) and intense as the input train frequency was increased (**Figures 4A,B**). In the granular layer, temporal summation became remarkable over 50 Hz, while in the molecular layer the frequency sensitivity was shifted, so that only inputs at frequencies higher than 100 Hz could be reliably transmitted (**Figure 4C**). At the highest frequencies (200–500 Hz), no further improvement in maximal transmission was observed but the maximal response occurred earlier during the train (e.g. on the 4th pulse at 100 Hz and on the 3rd pulse at 500 Hz). Finally, it should be noted that a post-burst response (measured 50 ms after the train) became also more evident as the frequency was increased.

The frequency-dependence of transmission from mossy fiber to granular and to molecular layer was represented as the change in maximal response amplitude (gain) and delay (lag) compared to low-frequency stimulation (**Figure 4D**). The gain curves showed a sigmoidal increase while the lag showed a decrease with

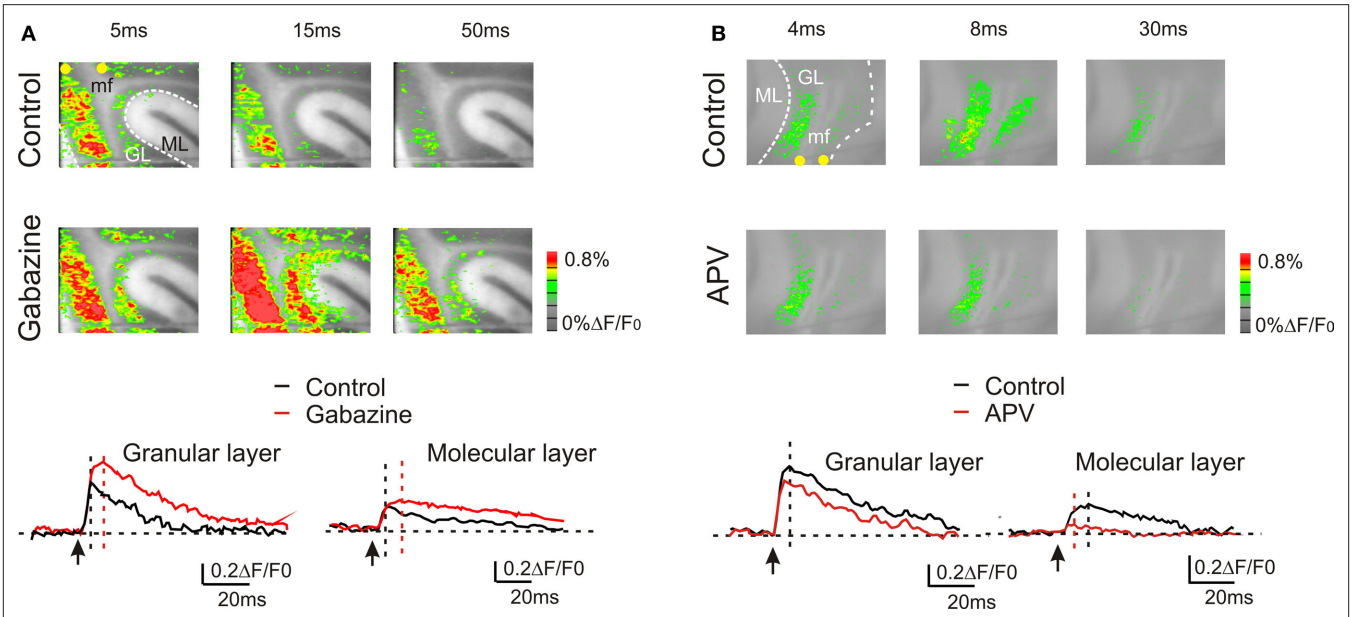

FIGURE 3 | GABA-A and NMDA receptor-dependent regulation of transmission along the mossy fiber pathway. (A) The effect of the GABA-A receptor blocker 10-μM gabazine in response to a single pulse in the white matter. Gabazine enhanced the granular layer response and facilitated transmission toward the molecular layer. The traces show the time course of the effect both in the granular and molecular layer. **(B)** The effect of the NMDA receptor blocker 50-μM APV in response to a single pulse in the white matter. APV reduced the granular layer response and markedly depressed transmission toward the molecular layer. The traces show the time course of the effect both in the granular and molecular layer.

frequency (**Figure 4D**), reflecting enhanced temporal summation and instantiating two high-pass filters. As expected, granular layer excitation occurred with shorter delay and at lower frequencies than molecular layer excitation, so that the two filters appeared to work in cascade. The gain curves were fitted with a sigmoidal-shaped function relative to low-frequency responses (Eq. 1) yielding the following values of cut-off frequency (f_c), initial amplitude (A_1) and final amplitude (A_2): in the granular layer, best fitting required a 2nd order function with $f_c = 20.9$ Hz, $A_1 = 1.11$, $A_2 = 1.46$, and $(A_2–A_1)/A_1 = 31.5\%$; in the molecular layer, best fitting required a 5th order function with $f_c = 170$ Hz, initial amplitude $A_1 = 0.44$, final amplitude $A_2 = 0.99$, and $(A_2–A_1)/A_1 = +125\%$. Thus, the gain function of the molecular layer was right-shifted compared to that of the granular layer. These data suggest that the information conveyed through the mossy fibers is optimally transmitted with high-frequency bursts while low-frequency bursts may not pass the threshold for effective molecular and Purkinje cell activation.

REGULATION OF GRANULAR AND MOLECULAR LAYER FILTERING BY GABA-A AND NMDA RECEPTORS

The frequency-dependence of granular – molecular layer transmission has to reside into the specific properties of their receptors, channels and circuits. Among these, two systems have the potential of regulating transmission in a frequency-dependent manner, the GABAergic inhibitory system and the excitatory mechanism involving NMDA receptors.

The application of 10-μM gabazine had major effects on granular – molecular layer communication during repetitive neurotransmission (**Figure 5A**). The extension of activated areas increased at all frequencies: for instance, with a 500-Hz train, the increase was +182.6 ± 30.9% ($n = 4$, $p < 0.006$, paired t-test) in the granular layer and +216.5 ± 57.8% ($n = 4$, $p < 0.004$, paired t-test) in the molecular layer. Moreover, temporal summation, gain and lag varied compared to control conditions. (i) Temporal summation did not saturate even at the highest tested frequencies either in the granular or in the molecular layer (**Figure 5B**), revealing the absence of feed-forward and feed-back inhibition (D'Angelo and De Zeeuw, 2009). Likewise, the post-burst response was markedly enhanced. (ii) The frequency-dependence of the gain function in the molecular layer became similar to that in the granular layer (**Figure 5B**). In the granular layer, best fitting required 2nd order with $f_c = 32.0$ Hz, $A_1 = 1.3$, $A_2 = 2.2$, and $(A_2–A_1)/A_1 = +69.2\%$; in the molecular layer, best fitting required 2nd order with $f_c = 23.9$ Hz, initial amplitude $A_1 = 0.56$, final amplitude $A_2 = 1.29$, and $(A_2–A_1)/A_1 = +130.3\%$. (iii) After blocking synaptic inhibition, the lag to maximal response was between the 4th and 5th pulse at all frequencies both in the granular and in the molecular layer remaining higher that in control and indicating a continued temporal summation no longer limited by inhibition.

The application of 50-μM APV had also major effects on granular – molecular layer communication during repetitive neurotransmission (**Figure 6**), which appeared nearly opposite to those of gabazine. The extension of activated areas decreased at all frequencies: for instance, with a 500-Hz train, the variation was −37.4 ± 7.7% ($n = 4$, $p < 0.01$, paired t-test) in the granular layer and −45.5 ± 4.5% ($n = 4$, $p < 0.05$, paired t-test) in the molecular layer. Moreover, temporal summation, gain and lag varied compared to control conditions. (i) Temporal summation tended to saturate at all frequencies (except for the 500-Hz burst; **Figure 6B**) revealing the absence of NMDA receptor-dependent temporal

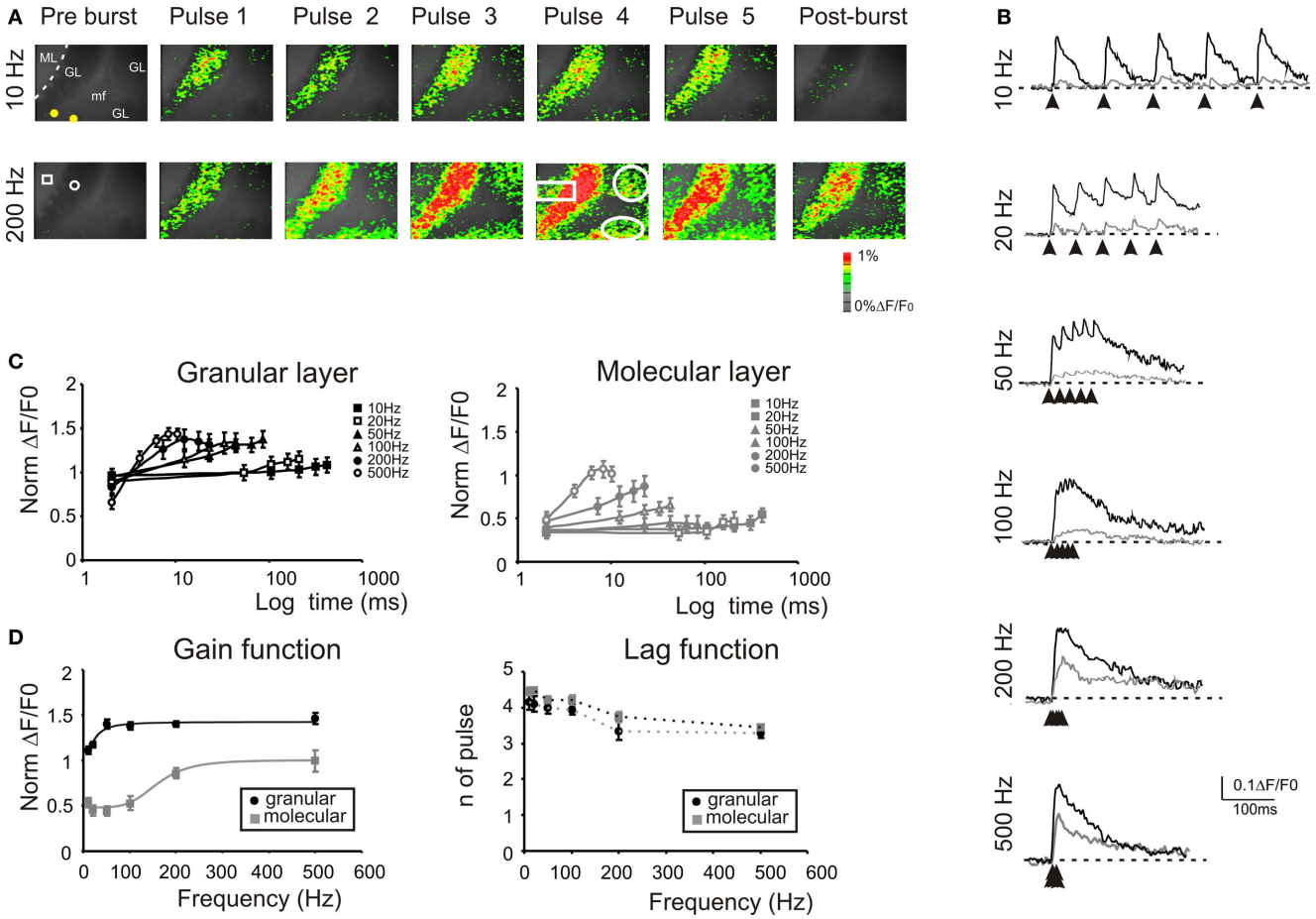

FIGURE 4 | Frequency-dependence of responses to repetitive stimulation. **(A)** Optical maps were obtained at the peak of responses in 5-pulse bursts delivered to the white matter for two significant frequencies (10 and 200 Hz). Passing from 10 Hz to 200 Hz, there is a progressive intensification of temporal summation in the granular layer which lead to a progressive activation of new recruited areas (white circles). Moreover, the increased stimulation frequency progressively activated the molecular layer (white rectangle) at each pulse of the burst. The post-burst maps were taken 50 ms after the end of the burst where with low-frequency stimulation the activity is almost abolished while, with high frequency there is a persistent signals throughout the granular layer. **(B)** Traces on the right illustrate the time course of the response in ROIs located in adjacent responding regions of the granular (black) and molecular layer (gray). Note the much stronger molecular layer response at higher frequencies and the consistent temporal summation of all signals. **(C)** Maximum response amplitudes were measured for each of the five pulses of bursts delivered at different frequencies in the granular (black; $n = 8$ slices, $n = 32$ ROIs for each frequency) and in the molecular layer (gray; $n = 8$ slices, $n = 28$ ROIs for each frequency). Points are reported as mean ± SEM. **(D)** Gain and lag curves for granular (black; $n = 8$ slices, $n = 32$ ROIs for each frequency) and molecular layer (gray; $n = 8$ slices, $n = 28$ ROIs for each frequency) responses. Gain is the maximum response obtained at a certain frequency and lag is the number of pulses needed to achieve the maximal response. The gain curves were fitted a sigmoidal function (Eq.1). Points are reported as mean ± SEM.

summation during the train (D'Angelo et al., 1995). Likewise, the post-burst response was markedly depressed. (ii) The frequency-dependence of the gain function in the granular layer (but not in the molecular layer) varied significantly. The gain curve of the granular layer did not show increase below 200 Hz due to lack of NMDA receptor-dependent integration, but then increased steeply at 500 Hz exploiting residual AMPA receptor-dependent summation (**Figure 6B**). Fittings used to reveal the impact of NMDA receptors were performed assuming the presence of a plateau after 500 Hz: in the granular layer, best fitting required 2nd order with $f_c = 257$ Hz, $A_1 = 0.87$, $A_2 = 1.1$, and $(A_2–A_1)/A_1 = +26.4\%$; in the molecular layer, best fitting required 2nd order with $f_c = 264$ Hz, initial amplitude $A_1 = 0.45$, final amplitude $A_2 = 0.7$, and $(A_2–A_1)/A_1 = +55.5\%$. (iii) The lag to maximal response tended to increase slightly, according to the facilitating effect of NMDA receptors on temporal summation.

Therefore, the GABAergic inhibitory system and the excitatory NMDA receptor-dependent systems had opposite effects on the filtering properties of the granular and molecular layer.

SIGNAL TRANSMISSION ALONG THE PARALLEL FIBERS

The ascending branch of the granule cell axon contacts the overlaying Purkinje cells and then bifurcates to form the parallel fibers traveling on the longitudinal plane. In order to understand how the frequency-dependence of signal transmission from granular to molecular layer reverberates into the parallel

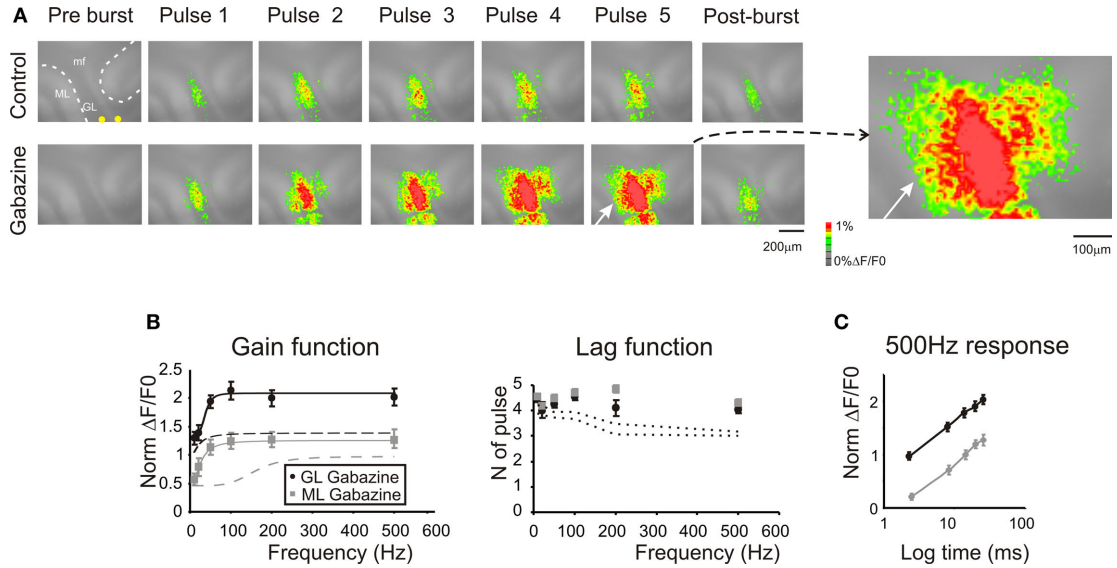

FIGURE 5 | Regulation of frequency-dependence by GABA-A receptors. (A) Optical maps were obtained at the peak of responses in 5-pulse 100 Hz bursts delivered to the white matter. Application of 10-μM gabazine markedly enhanced amplitude and extension of responses in the granular and molecular layer, and the effect increased during and after the burst (50 ms after the end of the burst). It should be noted the marked response summation in the presence of gabazine. The enlarged map evidences the activation of the molecular layer (white arrow) following the application of 10-μM gabazine. **(B)** Maximum response amplitudes were measured for each of the five pulses of bursts delivered at different frequencies both in the granular and molecular layer (n = 4 slices, n = 16 ROIs for each frequency). Gain and lag curves for granular (black) and molecular layer (gray) responses show that gain increased and the shape of curves changed compared to control (dashed lines). The gain curves were fitted with a sigmoidal function (Eq.1). Lag remained over control values (dashed lines) at all frequencies. **(C)** The time course peak amplitude increase at 500 Hz, was taken to demonstrate for a representative frequency (the maximum tested) the non-saturating nature of the response in the presence of 10-μM gabazine (cfr **Figure 4C**). Points are reported as mean ± SEM.

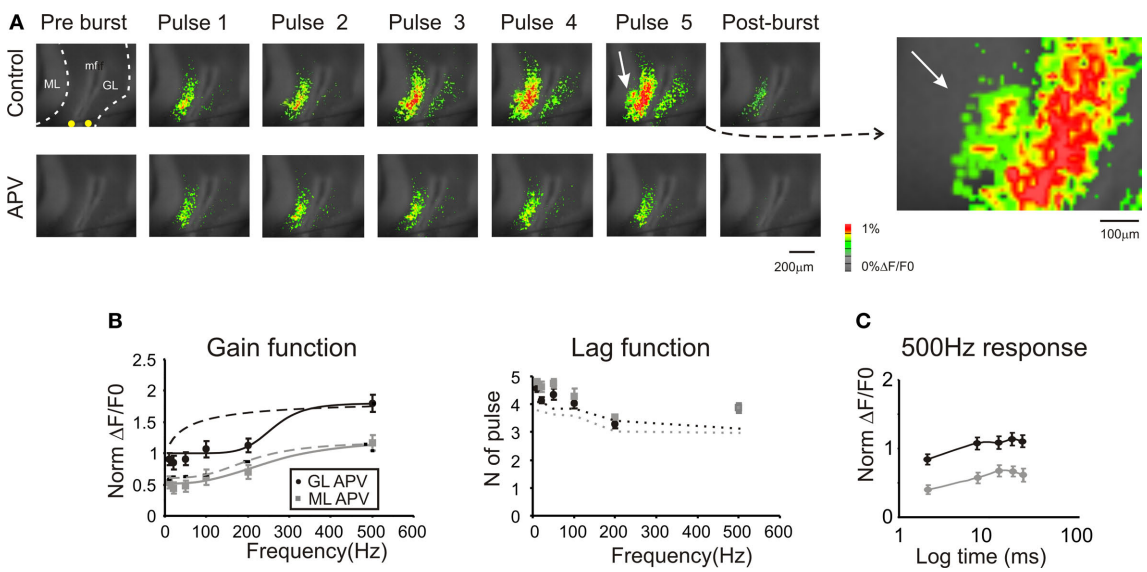

FIGURE 6 | Regulation of frequency-dependence by NMDA receptors. (A) Optical maps were obtained at the peak of responses in five-pulse 200 Hz bursts delivered to the white matter. Application of 50-μM APV markedly reduced amplitude and extension of responses in the granular and molecular layer, and the response remained stationary during the bursts. After the end of the burst (50 ms) APV reduced the remaining part of the response which was probably generated by the summation of NMDA dependent currents. The enlarged map evidences the molecular layer region (white arrow) which was activated in control condition. **(B)** Maximum response amplitudes were measured for each of the five pulses of bursts delivered at different frequencies both in the granular and molecular layer (n = 4 slices, n = 16 ROIs for each frequency). Gain and lag curves for granular (black) and molecular layer (gray) responses show that gain decreased and the shape of the curve changed compared to control (dashed lines). The gain curves were fitted with a sigmoidal function (Eq.1). Lag remained around control values (dashed lines) at all frequencies. **(C)** The time course peak amplitude increase at 500 Hz, was taken to demonstrate for a representative frequency the saturating nature of the response in the presence of 50-μM APV (cfr **Figure 4C**). Points are reported as mean ± SEM.

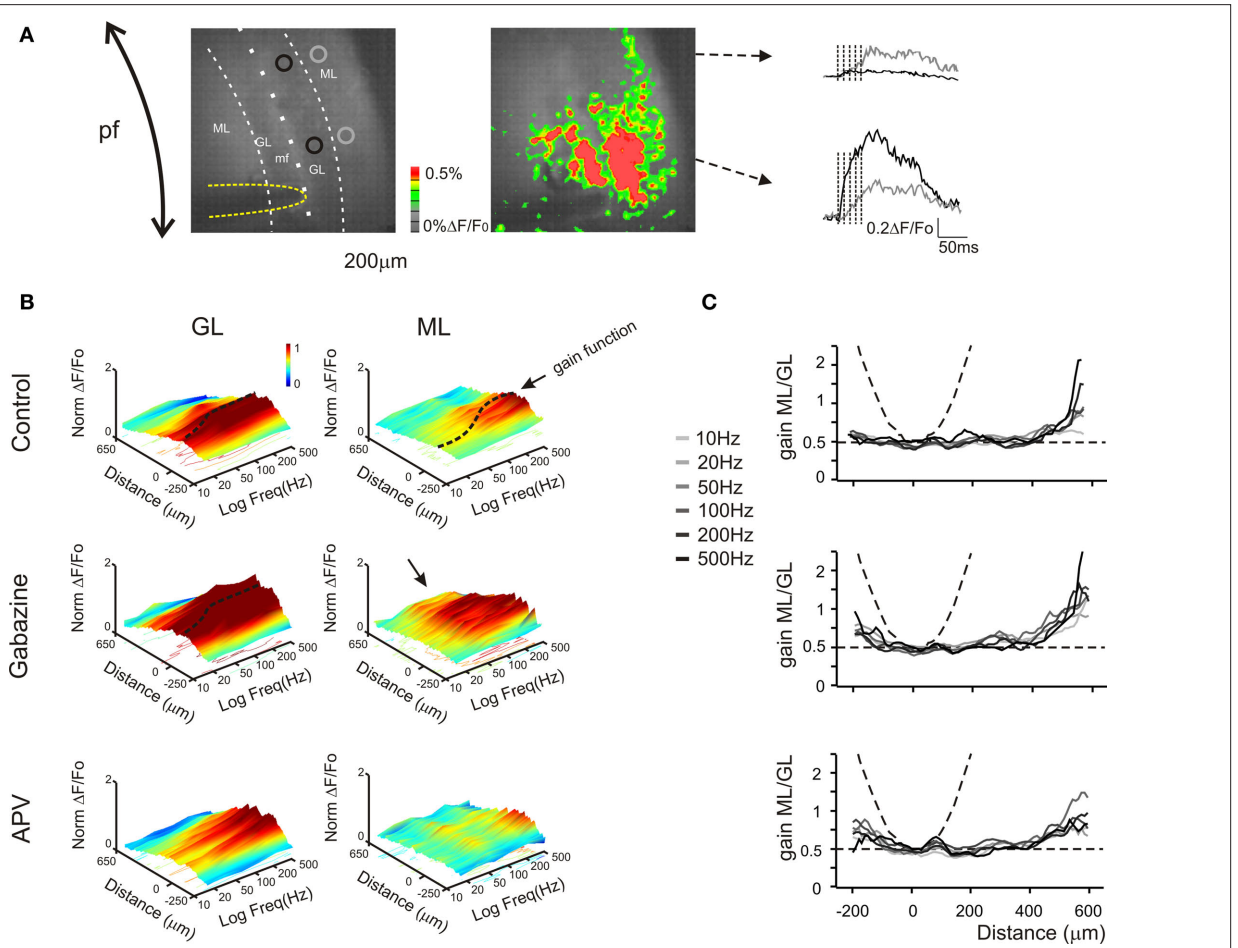

FIGURE 7 | Granular and molecular layer activation in coronal slices. (A) Optical maps obtained at the peak of responses in five pulses 100 Hz burst delivered to the white matter (yellow line surrounds the stimulation electrode), in coronal slices. The molecular layer signal propagates beyond the corresponding granular layer activated area, activating distal areas of the molecular layer The traces illustrate the time course of different regions (black and gray circles) of the granular (black trace) and molecular layer (grey trace). Note that the molecular layer response proximal to the core of the granular layer activation is slower and smaller than the corresponding granular layer response, while in distal regions the molecular layer signal overcomes the almost absent granular layer response (as evidenced from the optical map). **(B)** The spatial profile of gain was measured for different frequencies burst both in the granular and in the molecular layer (n = 4 slices, for each frequency). 3D maps show the spatial distribution of gain functions in different experimental conditions (Control, Gabazine and APV), evidencing the space (x) and frequency (y) dependence of granular and molecular layer activation (z). Dashed lines indicate gain functions in the core of the granular and molecular layer activation (cfr **Figures 4–6**). The spatial profile (x-axis) of the granular layer activation is narrow around the stimulating electrode (0 reference) and decays in distal regions, maintaining this profile even increasing the stimulation frequency. Conversely the excitation profile of the molecular layer shows the activation of the periphery for all tested frequency, while the core of excitation shows a strong dependence on the stimulation frequency. The application of Gabazine enhances the granular layer excitation without significantly affecting its spatial profile and gain curve. Differently, the molecular layer excitation shows a homogeneous increase of the activation above 50 Hz. Moreover the most evident effect of the block of GABAergic synapses was to enlarge the spatial profile so that there is a massive spread of activation in distal regions (black arrow) most probably generated by to the block of the molecular layer interneurons inhibition. The application of APV decreases the excitation of both granular and molecular layer without significantly affecting its spatial profile. Nevertheless the granular layer response increases above 100–200 Hz, thus disabling the signal transmission to the molecular layer. 3D Maps were generated by using average spatial profiles with SEM values ranging from 0.0001 to 0.001 $\Delta F/F_0$. **(C)** The contribution of parallel fibers activation to molecular layer responses could be isolated by evaluating the spatial profile of the ratio between the molecular and granular layer gain values for different frequencies and in different experimental conditions. In control condition the gain ratio in the core of activation is similar to the case of sagittal slices (~ 0.5). In the periphery the molecular layer overcomes the granular layer gain suggesting the signal propagation through the parallel fibers (cfr **B**). Dashed lines indicate the limit cases of maximum (parable) and no contribution (straight line) of parallel fiber to the molecular layer activity. The application of 10-μM gabazine increases the gain ratio spatial profiles for all frequencies. Conversely the block of NMDA receptor by the application of 50-μM APV poorly modulates the gain ratio profiles.

fibers, we used repetitive mossy fiber stimulation in coronal slices (**Figure 7A**). The application of 10–500 Hz bursts activated the granular layer and, as in the case of sagittal slices, signals reached the overlaying molecular layer. Interestingly, the molecular layer showed activation also in areas distant from the stimulation site, where no evident responses in the granular layer could be observed suggesting longitudinal transmission along the parallel fiber bundle.

The delay between the focus of excitation along the vertical axis and the distal part of the parallel fibers (at 500 μm distance) was 11.3 ± 1.8 ms ($n = 4$) in control and 5.6 ± 1.1 ms ($n = 4$) in the presence of gabazine. The time at which signals became detectable (20% over noise) was therefore protracted by molecular layer circuit inhibition, consistent with the observation that molecular layer signals are largely generated by Purkinje cell responses. These delays, by including postsynaptic signal processes, yield a lower limit of ~50 μm/ms for the conduction velocity along the parallel fibers.

The spatial profile of excitation was reconstructed at different frequencies (**Figure 7B**). Not unexpectedly, excitation of the granular layer and transmission toward the molecular layer were much more evident at high frequency (typically above 50–100 Hz, as observed in sagittal sections). The granular layer responded in a limited area without remarkable lateral propagation. This most probably reflects the fact that mossy fibers ramify in the sagittal plane and cannot therefore contribute to lateral signal diffusion in coronal sections. The granular layer signals were transmitted forward to the overlaying molecular layer and then propagated along the parallel fibers. The application of 10-μM gabazine enhanced while that of 50-μM APV reduced the overall pathway response.

To determine the effectiveness of parallel fiber–mediated excitation, the ratio between molecular and granular layer activity was computed along the transverse axis (**Figure 7C**). This ratio ($Gain_{molecular}/Gain_{granular}$) takes a parabolic shape around the maximum activity point if there is transversal transmission, while it becomes flat if there is pure vertical transmission. The upward concavity of the plots confirms that transmission takes place along the parallel fibers independent from direct signal transmission from the granular layer. Moreover, the plots indicate that transversal transmission occurs in control, is maintained in the presence of APV, and is enhanced in the presence of bicuculline.

THE SEQUENCE OF FREQUENCY-DEPENDENT EFFECTS

The results reported above indicate that there are specific mechanisms of frequency-dependent transmission of the maximum response to mossy fiber bursts in the granular and in the overlaying molecular layer. To complete the investigation of transmission, the retransmission of mossy fiber burst along the parallel fibers was analyzed at different stimulation frequencies (**Figure 8**). Surprisingly, activation along the parallel fiber beams (~500 μm from the vertical transmission point) was not frequency-dependent, neither changes were observed after application of APV. However, after applying gabazine, a frequency-dependence similar to that of the molecular layer in the vertical transmission point was observed. Thus, improved transmission of high-frequency bursts occurred along the vertical axis but not along the parallel fiber beams.

Finally, the frequency-dependence of transmission of the post-burst response was considered. In control, the post-burst response increased markedly above 50–100 Hz in the granular and in the molecular layer along the vertical transmission line, but showed no frequency-dependence along the parallel fibers. Moreover, the post-burst response was nearly doubled by GABA-A receptor blockage, which also reconstituted frequency-dependence along the parallel fiber beams. In these aspects the post-burst response was similar to the maximum burst response. However, the post-burst response was almost completely suppressed by NMDA receptor blockage at all frequencies, indicating that the NMDA receptor system was able to protract the effect of high-frequency bursts for tens of ms after their termination.

DISCUSSION

This paper shows that excitation generated by mossy fibers, after invading the granular layer, propagates vertically into the molecular layer and then transversally along the parallel fibers. The central finding is that transmission of mossy fiber bursts through the granular and molecular layer is markedly frequency-dependent implementing a cascade of two high-pass filters regulated by NMDA and GABA-A receptors. Eventually, retransmission of bursts above ~100 Hz is amplified along vertical transmission lines but not along the parallel fibers. This difference in frequency-dependent gain in the two subcircuits could cause the spot-like activation patterns of the molecular layer observed in response to punctuate stimulation *in vivo* (Bower and Woolston, 1983) and substantiate the adaptable spatio-temporal filter hypothesis predicted on theoretical grounds (Dean et al., 2010).

VSD SIGNALS AND THE SPREAD OF EXCITATION ALONG THE MOSSY FIBER – PARALLEL FIBER PATHWAY

VSD signal generation was correlated with the activity of granule and Purkinje cells (cf. Mapelli et al., 2010 and see Materials and Methods and **Figure 2**), which are by far the major excitable elements of the granular and molecular layer (see also Cohen and Yarom, 1998; Jacobson et al., 2008). The activation delays from granular to molecular layer were consistent with those observed using either VSD imaging or field potential recordings in other papers (e.g. see Vranesic et al., 1994; Baginskas et al., 2009; Walter et al., 2009). Moreover, the impact of GABA-A and NMDA receptor blockers on the spatio-temporal kinetics of the response was similar to that observed with MEA and patch-clamp recordings (D'Angelo et al., 1995; Mapelli and D'Angelo, 2007). Therefore, although Di-4-ANEPPS has been shown to enhance GABAergic responses in some cases (Mennerick et al., 2010), it did not substantially alter critical parameters of granular and molecular layer activation in cerebellar slice recordings. It should also be noted that Purkinje cells showed similar basal frequency with and without the dye (data not shown), further suggesting the maintenance of a correct excitatory-inhibitory balance.

The propagation of signals followed the anatomical organization of cerebellar fibers (Sultan, 2001). In the granular layer, mossy fibers and Golgi cell axons generate multiple ramifications in the sagittal plane and granule cells project their axons vertically toward the molecular layer. Accordingly, in sagittal slices, activation spread beside the mossy fiber bundle and then ascended vertically into the molecular layer. In coronal slices, the molecular layer showed strong activation just over the responding granular layer area, and then activation propagated longitudinally along the parallel fibers.

At low frequency, the response along the parallel fibers was comparable to that along vertical transmission lines, in keeping with the functional equivalence of the two inputs to Purkinje cells recently reported by Walter et al. (2009). However, at high frequency, vertical was much stronger than parallel fiber transmission. This may explain why, *in vivo*, when high-frequency burst are generated by mossy fibers in response to punctuate stimulation, Purkinje cell

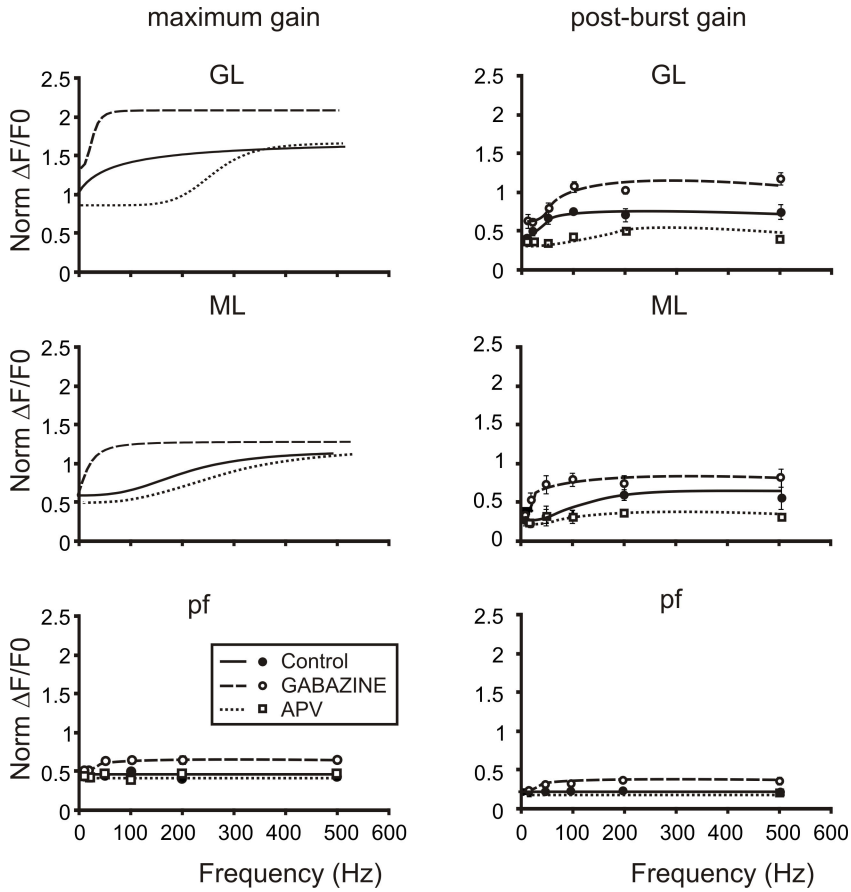

FIGURE 8 |The cascade of filters from mossy to parallel fibers. Plots summarize the cascade filters generated from the mossy fiber to the parallel fibers. Signals conveyed through mossy fibers are primarily high-pass filtered by the granular layer. This first high-pass filter cuts signals below 50 Hz mainly through the activation of NMDA currents, in fact the application of APV (empty squares and dotted lines) shifts the cut-off frequencies of both gain and post-burst curves above 100 Hz. Moreover granule cell axons convey signals at the first Purkinje cells synaptic stage. Here a second filter cuts very high-frequency signals (100–200 Hz) mainly through the action of the inhibitory system. Note that gain and post-burst curves are poorly modified by the application of APV while the application of Gabazine (empty circles and dashed lines) significantly enhances gain and post-burst values decreasing the cut-off frequencies (20–50 Hz). Traveling throughout granule cell axons, signals could be conveyed to parallel fibers and then reach the second Purkinje cell synaptic stage. Here signals appear to be linearly modulated by the incoming frequency. Only the block of the inhibitory system unmasks the same frequency-dependence encountered in the other stages. This could be due to the strong action of interneurons on Purkinje cells preventing them to depolarize. Post-burst gain values were calculated 50 ms after the end of bursts both for sagittal and coronal slices ($n = 4$). Maximum gain and post-burst gain for parallel fibers were calculated by taking the average of 10 pixels (100 μ) in the distal part of coronal slices.

activation occurs in spots with a prevalent vertical organization (Bower and Woolston, 1983; Cohen and Yarom, 1998; Jacobson et al., 2008; Lu et al., 2009).

PHASIC SYNAPTIC MECHANISMS DETERMINE FREQUENCY-DEPENDENT GAIN REGULATION IN THE GRANULAR LAYER

In the granular layer, the normalized gain increase observed after GABA-A receptor blockage was 86% at high- frequency but just 14% at low-frequency [cf. $(A_2–A_1)/A_1$ to A_1 values in **Figures 4–5**]. Since GABA-A receptor-dependent effect at high frequency reflected the response to 3–5 impulses in short-sequence, while at low frequency it reflected the steady-state background inhibition, the gain considered here depended on dynamic inhibitory loops rather than on tonic inhibition (Mitchell and Silver, 2003). Therefore, gain control of burst transmission in the granular layer depends on the dynamical activation of inhibitory circuits, as originally envisaged by Marr (1969), Albus (1971) and Fujita (1982).

In the granular layer, GABA-A receptor activation through the Golgi cell loops reduces EPSP temporal summation in granule cells (Armano et al., 2000; Kanichay and Silver, 2008; for review see D'Angelo, 2008; D'Angelo and De Zeeuw, 2009). The GABAergic system caused both a global transmission decrease over the whole-frequency range and a specific transmission decrease at frequencies lower than 50 Hz, possibly involving the differential kinetic properties of α6-and α1-receptor-mediated mechanisms (Mapelli et al., 2009).

In the granular layer, gain was also regulated by NMDA receptors but in the opposite direction: after blocking NMDA receptors, the normalized gain change at intermediate input frequencies was

–25% after. NMDA receptors, by exploiting their slow kinetic time constants, boosted EPSP temporal summation and sustained a protracted post-burst responses (cf. D'Angelo et al., 1995) in the 10–200 Hz range. AMPA receptors, which have kinetic time constants in the 1–2 ms range, allowed temporal summation at very high frequencies (500 Hz). Thus, the combination of the two receptor-dependent mechanisms allowed to amplifying transmission over a broad frequency range covering the natural range of mossy fiber discharge (Chadderton et al., 2004; Eckerot and Jorntell, 2006). It should also be noted that NMDA receptors tuned the persistence of granule cell responses after mossy fiber burst termination.

DIFFERENTIAL GAIN CONTROL IN THE GRANULAR AND MOLECULAR LAYER

In the molecular layer, gain was regulated by GABAergic mechanisms but not by NMDA receptor-dependent mechanisms, in agreement with the prominent localization of NMDA receptors in the granular layer. In the molecular layer, the impact of GABA-A receptors became progressively stronger: GABA-A receptors depressed transmission below ~100 Hz along vertical transmission lines and over the whole-frequency range along the parallel fibers. Among factors explaining the progressive shift of inhibitory control toward higher frequencies along the mossy fiber – parallel fiber pathway, one could be that GABAergic inhibition is especially effective in controlling NMDA receptor-dependent depolarization in the granular layer (Mapelli and D'Angelo, 2007). Another factor could be that, in the cerebellar glomerulus, inhibition is specifically depressed at high frequency due to presynaptic crosstalk and activation of metabotropic glutamate receptors (Mitchell and Silver, 2000a,b). A third aspect is that the center-surround structures formed by the granular layer following activation of a mossy fiber bundle, have complex transmission properties: compared to the surround, the center detects burst on a broader band and emits bursts with shorter lag, higher frequency and longer duration (Solinas et al., 2010). This could favor activation of overlaying Purkinje cells and, at the same time, enhance inhibition around them. Thus, preprocessing and spatial organization of signal in the granular layer could play a relevant role for generating the spot-like organization of molecular layer responses *in vivo*. In addition, the inhibitory circuits of the molecular layer could have themselves specific organization and transmission properties favoring spot-like responses rather than beam formation (Cohen and Yarom, 1998; Santamaria et al., 2007).

CONCLUSIONS

In conclusion, in cerebellar slices, mossy fibers signals can reach the molecular layer and then travel along the parallel fibers. However, signal transmission is regulated by synaptic mechanisms implementing a cascade of high-pass filters. Only activity over 50 Hz is retransmitted to the molecular layer. Then, the Purkinje cells placed over the excited granular layer area respond maximally when mossy fiber bursts have a frequency higher than 100 Hz. This high-frequency enhancement is lost along the parallel fibers. Thus, a high-frequency burst in a mossy fiber bundle excites quite strongly the overlying Purkinje cells but much more poorly those aligned along the parallel fibers. This same spatial organization was also evident for the post-burst, which prolonged the duration of granular and molecular layer responses. These effects would favor the emergence of spots while preventing efficient beam formation, as indeed observed following punctuate stimulation *in vivo* when mossy fibers generate bursts with frequencies over 100 Hz (Bower and Woolston, 1983). As a corollary, parallel fibers may be specialized to determine a low-gain frequency-independent background excitation along the beam.

ACKNOWLEDGMENTS

This work was supported by grants SENSOPAC (FP6-IST028056) of the European Commission and by NEUROIMAGE of CNISM (Consorzio Interuniversitario per le Scienze Fisiche della Materia) to Egidio D'Angelo.

REFERENCES

Albus, J. S. (1971). A theory of cerebellar function. *Math. Biosci.* 10, 25–61.

Arenz, A., Silver, R. A., Schaefer, A. T., and Margrie, T. W. (2008). The contribution of single synapses to sensory representation *in vivo*. *Science* 321, 977–980.

Armano, S., Rossi, P., Taglietti, V., and D'Angelo, E. (2000). Long-term potentiation of intrinsic excitability at the mossy fiber – granule cell synapse of rat cerebellum. *J. Neurosci.* 20, 5208–5216.

Baginskas, A., Palani, D., Chiu, K., and Raastad, M. (2009). The H-current secures action potential transmission at high frequencies in rat cerebellar parallel fibers. *Eur. J. Neurosci.* 29, 87–96.

Bower, J. M., and Woolston, D. C. (1983). Congruence of spatial organization of tactile projections to granule cell and Purkinje cell layers of cerebellar hemispheres of the albino rat: vertical organization of cerebellar cortex. *J. Neurophysiol.* 49, 745–766.

Chadderton, P., Margrie, T. W., and Hausser, M. (2004). Integration of quanta in cerebellar granule cells during sensory processing. *Nature* 428, 856–860.

Cohen, D., and Yarom, Y. (1998). Patches of synchronized activity in the cerebellar cortex evoked by mossy-fiber stimulation: questioning the role of parallel fibers. *Proc. Natl. Acad. Sci. U.S.A.* 95, 15032–15036.

Cull-Candy, S. G., Brickley, S. G., Misra, C., Feldmeyer, D., Momiyama, A., and Farrant, M. (1998). NMDA receptor diversity in the cerebellum: identification of subunits contributing to functional receptors. *Neuropharmacology* 37, 1369–1380.

D'Angelo, E. (2008). The critical role of Golgi cells in regulating spatio-temporal integration and plasticity at the cerebellum input stage. *Front. Neurosci.* 2, 35–46.

D'Angelo, E., De Filippi, G., Rossi, P., and Taglietti, V. (1995). Synaptic excitation of individual rat cerebellar granule cells in situ: evidence for the role of NMDA receptors. *J. Physiol. (Lond.)* 484, 397–413.

D'Angelo, E., and De Zeeuw, C. I. (2009). Timing and plasticity in the cerebellum: focus on the granular layer. *Trends Neurosci.* 32, 30–40.

D'Angelo, E., Rossi, P., Armano, S., and Taglietti, V. (1999). Evidence for NMDA and mGlu receptor-dependent long-term potentiation of mossy fibre – granule cell transmission in rat cerebellum. *J. Neurophysiol.* 81, 277–287.

Dean, P., Porrill, J., Ekerot, C. F., and Jörntell, H. (2010). The cerebellar circuit as an adaptive filter: experimental and computational evidence. *Nat. Rev. Neurosci.* 11, 30–43.

Diwakar, S., Magistretti, J., Goldfarb, M., Naldi, G., and D'Angelo, E. (2009). Axonal Na^+ channels ensure fast spike activation and back-propagation in cerebellar granule cells. *J. Neurophysiology* 101, 519–532.

Dugué, G. P., Dumoulin, A., Triller, A., and Dieudonné, S. (2005). Target-dependent use of co-released inhibitory transmitters at central synapses. *J. Neurosci.* 23, 6490–6498.

Eccles, J. C., Ito, M., and Szentagothai, J. (1967). *The Cerebellum as a Neuronal Machine*. Berlin: Springer Verlag.

Fujita, M. (1982). Adaptive filter model of the cerebellum. *Biol. Cybern.* 45, 195–206.

Garthwaite, J., and Brodbelt, A. R. (1989). Synaptic activation of N-methyl-D-aspartate and non-N-methyl-D-aspartate receptors in the mossy fibre pathway in adult and immature rat cerebellar slices. *Neuroscience* 29, 401–412.

Harvey, R. J., and Napper, R. M. (1991). Quantitative studies on mammalian cerebellum. *Prog. Neurobiol.* 36, 437–463.

Ito, M. (1984). *The Cerebellum and Neural Control*. New York: Raven publishing.

Jacobson, G. A., Rokni, D., and Yarom, Y. (2008). A model of the olivo-cerebellar system as a temporal pattern generator. *Trends Neurosci.* 31, 617–625.

Jörntell, H., and Ekerot, C. F. (2006). Properties of somatosensory synaptic integration in cerebellar granule cells *in vivo*. *J. Neurosci.* 26;11786–11797.

Kanichay, R. T., and Silver, R. A. (2008). Synaptic and cellular properties of the feedforward inhibitory circuit within the input layer of the cerebellar cortex. *J. Neurosci.* 28, 8955–8967.

Kase, M., Miller, D. C., and Noda, H. (1980). Discharges of Purkinje cells and mossy fibres in the cerebellar vermis of the monkey during saccadic eye movements and fixation. *J. Physiol. (Lond.)* 300, 445–453.

Kinney, G. A., and Slater, N. T. (1993). Potentiation of NMDA receptor-mediated transmission in turtle cerebellar granule cells by activation of metabotropic glutamate receptors. *J. Neurophysiol.* 69, 585–594.

Llinas, R., and Sugimori, M. (1980a). Electrophysiological properties of *in vitro* Purkinje cell dendrites in mammalian cerebellar slices. *J. Physiol. (Lond.)* 305, 197–213.

Llinas, R., and Sugimori, M. (1980b). Electrophysiological properties of *in vitro* Purkinje cell somata in mammalian cerebellar slices. *J. Physiol. (Lond.)* 305, 171–195.

Lu, H., Esquivel, A. V., and Bower, J. M. (2009). 3D electron microscopic reconstruction of segments of rat cerebellar Purkinje cell dendrites receiving ascending and parallel fiber granule cell synaptic inputs. *J. Comp. Neurol.* 514, 583–594.

Mapelli, J., and D'Angelo, E. (2007). The spatial organization of long-term synaptic plasticity at the input stage of the cerebellum. *J. Neurosci.* 27, 1285–1296.

Mapelli, J., Gandolfi, D., and D'Angelo, E. (2010). Combinatorial responses controlled by synaptic inhibition in the cerebellum granular layer. *J. Neurophys.* 103, 250–261.

Mapelli, L., Rossi, P., Nieus, T., and D'Angelo, E. (2009). Tonic activation of GABA-B receptors reduces release probability at inhibitory connections in the cerebellar glomerulus. *J. Neurophysiol.* 101, 3089–3099.

Marr, D. A. (1969). Theory of the cerebellar cortex. *J. Physiol. (Lond.)* 202, 437–470.

Mennerick, S., Chisari, M., Shu, H. J., Taylor, A., Vasek, M., Eisenman, L. N., and Zorumski, C. F. (2010). Diverse voltage-sensitive dyes modulate GABAA receptor function. *J. Neurosci.* 30, 2871–2879.

Mitchell, S. J., and Silver, R. A. (2000a). Glutamate spillover suppresses inhibition by activating presynaptic mGluRs. *Nature* 404, 498–502.

Mitchell, S. J., and Silver, R. A. (2000b). GABA spillover from single inhibitory axons suppresses low-frequency excitatory transmission at the cerebellar glomerulus. *J. Neurosci.* 20, 8651–8658.

Mitchell, S. J., and Silver, R. A. (2003). Shunting inhibition modulates neuronal gain during synaptic excitation. *Neuron* 38; 433–445.

Palay, S. L., and Chan-Palay, V. (1974). *Cerebellar Cortex*. New York: Springer-Verlag.

Palkovits, M., Magyar, P., and Szentàgothai, J. (1971). Quantitative histological analysis of the cerebellar cortex in the cat. II. Cell numbers and densities in the granular layer. *Brain Res.* 32, 15–30.

Rancz, E. A., Ishikawa, T., Duguid, I., Chadderton, P., Mahon, S., and Hausser, M. (2007). High-fidelity transmission of sensory information by single cerebellar mossy fibre boutons. *Nature* 450, 1245–1249.

Rokni, D., Llinas, R., and Yarom, Y. (2008). The morpho/functional discrepancy in the cerebellar cortex: looks alone are deceptive. *Front Neurosci.* 2, 192–198.

Rokni, D., Tal, Z., Byk, H., and Yarom, Y. (2009). Regularity, variability and bi-stability in the activity of cerebellar purkinje cells. *Front. Cell. Neurosci.* 3:12. doi:10.3389/neuro.03.012.2009.

Sacconi, L., Mapelli, J., Gandolfi, D., Lotti, J., O'Connor, R. P., D'Angelo, E., and Pavone, F. S. (2008). Optical recording of electrical activity in intact neuronal networks with random access second-harmonic generation microscopy. *Opt. Express* 16, 14910–14921.

Santamaria, F., Tripp, P. G., and Bower, J. M. (2007). Feedforward inhibition controls the spread of granule cell-induced Purkinje cell activity in the cerebellar cortex. *J. Neurophysiol.* 97, 248–263.

Sims, R. E., and Hartell, N. A. (2005). Differences in transmission properties and susceptibility to long-term depression reveal functional specialization of ascending axon and parallel fiber synapses to Purkinje cells. *J. Neurosci.* 23, 3246–3257.

Sims, R. E., and Hartell, N. A. (2006). Differential susceptibility to synaptic plasticity reveals a functional specialization of ascending axon and parallel fiber synapses to cerebellar Purkinje cells. *J. Neurosci.* 26, 5153–5159.

Solinas, S., Nieus, T., and D'Angelo, E. (2010). A realistic large-scale model of the cerebellum granular layer predicts circuit spatio-temporal filtering properties. *Front. cell. Neurosci.* 4:12. doi: 10.3389/fncel.2010.00012.

Sultan, F. (2001). Distribution of mossy fiber rosettes in the cerebellum of cat and mice: evidence for a parasagittal organization at the single fiber level. *Eur. J. Neurosci.* 13, 2123–2130.

Tominaga, T., Tominaga, Y., Yamada, H., Matsumoto, G., and Ichikawa, M. (2000). Quantification of optical signals with electrophysiological signals in neural activities of Di-4-Anepps stained rat hippocampal slices. *J. Neurosci. Methods* 102, 11–23.

Vranesic, I., Iijima, T., Ichikawa, M., Matsumoto, G., and Knöpfel, T. (1994). Signal transmission in the parallel fiber-Purkinje cell system visualized by high-resolution imaging. *Proc. Natl. Acad. Sci. U.S.A.* 20, 13014–13017.

Walter, J. T., Dizon, M. J., and Khodakhah, K. (2009). The functional equivalence of ascending and parallel fiber inputs in cerebellar computation. *J. Neurosci.* 29, 8462–8473.

Yae, H., Elias, S. A., and Ebner, T. J. (1992). Deblurring of 3-dimensional patterns of evoked rat cerebellar cortical activity: a study using voltage-sensitive dyes and optical sectioning. *J. Neurosci. Methods* 42, 195–209.

Conflict of Interest Statement: The authors declare that the research was conducted in the absence of any commercial or financial relationships that could be construed as a potential conflict of interest.

Received: 07 August 2009; paper pending published: 09 November 2009; accepted: 16 April 2010; published online: 28 May 2010. Citation: Mapelli J, Gandolfi D and D'Angelo E (2010) High-pass filtering and dynamic gain regulation enhance vertical bursts transmission along the mossy fiber pathway of cerebellum. Front. Cell. Neurosci. ***4****:14. doi: 10.3389/fncel.2010.00014*